

From adaptation to motion: In-depth characterization of γ -proteobacteria under acid or hormone stress

Dissertation

Zur Erlangung des Doktorgrades

der Naturwissenschaften

(Dr. rer. nat.)



der Fakultät für Biologie

der Ludwig-Maximilians-Universität München

vorgelegt von

Kilian Schumacher

aus Wasserburg am Inn

München, 2024

Diese Dissertation wurde angefertigt
unter der Leitung von Prof. Dr. Kirsten Jung
im Bereich der Fakultät für Biologie
an der Ludwig-Maximilians-Universität München

Gutachter:

1. Prof. Dr. Kirsten Jung
2. Prof. Dr. Thomas Nägele

Datum der Abgabe: 04.07.2024

Tag der mündlichen Prüfung: 09.10.2024

Eidesstattliche Erklärung

Ich versichere hiermit an Eides statt, dass die vorgelegte Dissertation von mir selbstständig und ohne unerlaubte Hilfe angefertigt wurde. Des Weiteren erkläre ich, dass ich nicht anderweitig ohne Erfolg versucht habe, eine Dissertation einzureichen oder mich der Doktorprüfung zu unterziehen. Die folgende Dissertation liegt weder ganz, noch in wesentlichen Teilen einer anderen Prüfungskommission vor.

Kilian Schumacher, München 04.07.2024

Statutory Declaration

I declare that I have authored this thesis independently, that I have not used other than the declared sources/resources. As well I declare, that I have not submitted a dissertation without success and not passed the oral exam. The present dissertation (neither the entire dissertation nor parts) has not been presented to another examination board.

Kilian Schumacher, Munich 04.07.2024

Contents

Eidesstattliche Erklärung	III
Statutory Declaration	III
Contents	IV
Nomenclature	VI
Abbreviations	VII
List of publications	IX
Declaration of contributions	X
Summary	XII
Zusammenfassung	XIII
1 Introduction	1
1.1 Overview of acidic environments	1
1.2 Bacterial acid stress response mechanisms	3
1.3 pH-induced chemotaxis and motility	5
1.4 Bacterial exposure to eukaryotic stress hormones	7
1.5 Heterogeneous stress responses	8
1.6 Previous and current approaches to systematically study acid stress	10
1.6.1 Detection of transcriptional regulation using RNA-Seq	11
1.6.2 Assessment of protein synthesis rates using Ribo-Seq	12
1.6.3 Unravelling novel sORFs through Ribo-Seq	12
1.7 Scope of this thesis	13
2 Results	14
2.1 Ribosome profiling reveals the fine-tuned response of <i>Escherichia coli</i> to mild and severe acid stress	14
2.2 Motility-activating mutations upstream of <i>flhDC</i> reduce acid shock survival of <i>Escherichia coli</i>	49

2.3 Eukaryotic catecholamine hormones influence the chemotactic control of <i>Vibrio campbellii</i> by binding to the coupling protein CheW	67
2.4 Division of labor and collective functionality in <i>Escherichia coli</i> under acid stress	78
2.5 Bacterial battle against acidity	93
2.6 Bacterial acid stress response: from cellular changes to antibiotic tolerance and phenotypic heterogeneity	121
3 Concluding discussion.....	132
3.1 Novel adaptations of <i>Escherichia coli</i> to acid stress uncovered by Ribo-Seq....	133
3.1.1 Differential synthesis of membrane proteins and putatively altered membrane fluidity	133
3.1.2 Restriction of cellular metabolism	135
3.1.3 Induction of siderophore and iron uptake	136
3.1.4 Discovery of sORFs that are exclusively detectable under acid stress conditions.....	137
3.2 Stress-dependent adaptations of chemotaxis and motility.....	138
3.2.1 pH-dependent differential expression of motility genes	138
3.2.2 Insertion sequence element-controlled regulation of motility.....	139
3.2.3 Binding of stress hormones to the motility machinery	141
3.3 Phenotypic heterogeneity under consecutively increasing acid stress	143
3.4 Conclusions and outlook	145
References for Chapters 1 and 3	148
Supplemental information – Chapter 2.1	169
Supplemental information – Chapter 2.2	176
Supplemental information – Chapter 2.3	183
Supplemental information – Chapter 2.4	227
Acknowledgements	235
Curriculum Vitae	237

Nomenclature

Proteins are numbered according to the first methionine/valine in the wild-type amino acid sequence designated as '1'. N- or C-terminal affinity tags are indicated corresponding to their position (e.g. sORF15:3xFLAG).

Gene deletions are indicated by the 'Δ' symbol, e.g., $\Delta mhpR$.

'P' indicates a promoter, e.g., P_{mhpR} .

Abbreviations

ARs	acid resistance systems
ATP	adenosine triphosphate
bp	base pair
cDNA	complementary DNA
CFAs	cyclopropane fatty acids
Co-IP	co-immunoprecipitation
DNA	deoxyribonucleic acid
DNase	deoxyribonuclease
EHEC	enterohemorrhagic <i>Escherichia coli</i>
EPI	epinephrine
EtOH	ethanol
G3P	glycerol 3-phosphate
GABA	gamma-aminobutyric acid
GO	gene ontology
GSEA	gene set enrichment analysis
HK	histidine kinase
IS	insertion sequence
LAB	labetalol
LB	lysogeny broth
LC-MS	liquid chromatography-mass spectrometry
MALDI-TOF	matrix-assisted laser desorption/ionization - time of flight
MCPs	methyl-accepting chemotaxis proteins
MNase	micrococcal nuclease
mRNA	messenger RNA
MST	microscale thermophoresis

NE	norepinephrine
NGS	next generation sequencing
nt	nucleotide
OD ₆₀₀	optical density at 600 nanometer
OMP	outer membrane protein
PE	phenylephrine
qRT-PCR	quantitative real-time PCR
RNA	ribonucleic acid
RNA-Seq	RNA sequencing
ROS	reactive oxygen species
RPFs	ribosome-protected fragments
RR	response regulator
rRNA	ribosomal RNA
SCFAs	short-chain fatty acids
scRNA-Seq	single-cell RNA sequencing
sORF	small open reading frame
sRNA	small RNA
UTR	untranslated region
UV light	ultraviolet light
w/v	weight per volume

List of publications:

Chapter 2.1:

Schumacher, K., Gelhausen, R., Kion-Crosby, W., Barquist, L., Backofen, R., and Jung, K. (2023). Ribosome profiling reveals the fine-tuned response of *Escherichia coli* to mild and severe acid stress. *mSystems*.10.1128/msystems.01037-23.

Chapter 2.2:

Schumacher, K., Braun, D., Kleigrew, K. and Jung, K. (2024). Motility-activating mutations upstream of *flhDC* reduce acid shock survival of *Escherichia coli*. *Microbiol Spectr*. 12:e0054424.

Chapter 2.3:

Muñoz, A.W., Hoyer, E., Schumacher, K., Grognot, M., Taute, K.M., Hacker, S.M., Sieber, S.A., and Jung, K. (2022). Eukaryotic catecholamine hormones influence the chemotactic control of *Vibrio campbellii* by binding to the coupling protein CheW. *Proc. Natl. Acad. Sci. U. S. A.* 119. 10.1073/pnas.2118227119.

Chapter 2.4:

Brameyer, S., Schumacher, K., Kuppermann, S., and Jung, K. (2022). Division of labor and collective functionality in *Escherichia coli* under acid stress. *Commun. Biol.* 5, 1–14. 10.1038/s42003-022-03281-4.

Chapter 2.5:

Schwarz, J.*, Schumacher, K.*, Brameyer, S., and Jung, K. (2022). Bacterial battle against acidity. *FEMS Microbiol. Rev.* 46. 10.1093/femsre/fuac037.

* These authors contributed equally

Chapter 2.6:

Schumacher, K., Brameyer, S., and Jung, K. (2023). Bacterial acid stress response: from cellular changes to antibiotic tolerance and phenotypic heterogeneity. *Curr. Opin. Microbiol.* 75:102367.10.1016/j.mib.2023.102367

Declaration of contributions

Chapter 2.1:

KS and KJ initiated and designed the study. KS performed all *in vivo* experiments and created all strains and plasmids. Ribo-Seq and RNA-Seq data analysis using the HRIBO pipeline was performed by RG with input from KS. Gene set enrichment analysis and novel sORF detection were performed by KS and RG. The identification of novel transcription factors involved in the acid stress response of *E. coli* was performed by KS. The autoencoder analysis to differentiate the acid stress and general stress responses was conducted by WKC with input from KS. KS designed the figures, and KS and KJ wrote the manuscript with input from RG, WKC, LB, and RB. KS was assisted by the research students Pol Bannasch and Annika Krimmel.

Chapter 2.2:

KS and KJ initiated and designed the study. KS performed all *in vivo* experiments and created all strains and plasmids. DB assisted KS with strain- and plasmid construction, promoter activity assays, and acid shock experiments. KG conducted LC-MS and analyzed the respective data. KS and KJ wrote the manuscript with input from all authors.

Chapter 2.3:

SAS and KJ initiated and designed the study. AWM conducted the synthesis of tailored probes for chemical proteomic experiments, photoaffinity labeling, and Co-IP. EH performed soft agar colony expansion assays. EH and KS performed protein purification, MST experiments, and growth assays. KS conducted chemotaxis capillary assays. MG and KT performed 3D chemotaxis assays. AWM, EH, KS, MG, and SMH analyzed data. AWM, SAS, and KJ wrote the manuscript with input from all authors.

Chapter 2.4:

SB and KJ initiated and designed the study. SB and KS performed fluorescence microscopy and data analysis. SB and KS constructed all strains and plasmids. KS verified the functionality of fluorescent antiporter hybrids by western blot. SK performed phylogenetic analysis. SB and KJ wrote the manuscript with input from KS and SK.

Chapter 2.5:

KJ initiated and designed the study. JS summarized the literature and wrote the text for the following chapters: 'Enzyme-based H⁺-consuming acid stress resistance systems', 'Acid-resistance system 1 (AR1)', Arginine-dependent AR (Adi) system (AR3)', 'Lysine-dependent AR (Cad) system (AR4)', 'Ornithine-dependent AR (Orn) system (AR5)', 'Deiminase and deaminase systems', 'ToxR-like receptor CadC', and 'Transcriptional regulator AphB'. KS summarized the literature and wrote the text for the following chapters: 'pH homeostasis and ion transport', 'Acid-dependent chemotaxis', 'Glutamate-dependent AR (Gad) system (AR2)', 'Synthesis of acid-shock proteins', 'Urease', 'Hybrid HK EvgS', 'HK PhoQ', 'Chemoreceptors Tar and Tsr', and 'Chemoreceptor TlpB'. SB summarized the literature and wrote the text for the following chapters: 'Phylogenetic occurrence of the Gad, Adi, Cad, and Orn systems in the bacterial kingdom', 'HK SsrA', 'HK ArsS', and 'Functional diversification of bacterial populations under acid stress'. KJ summarized the literature and wrote the text for the following chapters: 'Introduction', 'Synthesis of acid-shock proteins', 'Synthesis of chaperones', 'Modifications of the cytoplasmic membrane', 'HK PmrB', 'Functional diversification of bacterial populations under acid stress', and 'Concluding remarks'. Above mentioned chapters were corrected and modified with input from all authors. SB and KJ designed the figures with input from all authors.

Chapter 2.6:

KJ initiated and designed the study. KS summarized the literature and wrote the text for the chapter 'Acid stress-dependent alterations of the transcriptome and proteome of various bacteria'. SB summarized the literature and wrote the text for the chapter 'Acid stress and antibiotic tolerance'. KJ summarized the literature and wrote the text for the chapters 'Introduction', 'The heterogeneous acid stress response', and 'Conclusions and perspectives'. Above mentioned chapters were corrected and modified with input from all authors. KS and SB designed the figures with input from KJ.

We hereby confirm the above statements:

Kilian Schumacher

Kirsten Jung

Summary

Sensing and responding to acidity is crucial for bacteria to survive in a variety of habitats, such as the gastrointestinal tracts of vertebrates. However, previous approaches to systematically study the response of bacteria to acid stress have been restricted to methods with significant drawbacks involving proteomics and microarrays or were limited to mildly acidic conditions. In this thesis, the advantages of ribosome profiling (Ribo-Seq) were leveraged and combined with RNA-Seq to study genome-wide adaptations of *Escherichia coli* to mild (pH 5.8) and severe near-lethal acidic conditions (pH 4.4). The obtained findings included novel strategies of *E. coli* to gain acid tolerance, such as reduction of membrane protein synthesis and global metabolism, as well as the induction of iron uptake and siderophore synthesis. Moreover, Ribo-Seq uncovered novel small proteins that were exclusively detectable under acid stress, and acid-specific adaptations were distinguished from other stressors using autoencoder-based machine learning.

Ribo-Seq and RNA-Seq also revealed an induction of motility genes at pH 5.8 but not at pH 4.4, indicating that flagella biosynthesis is dependent on the degree of acid stress. Follow-up studies were conducted focusing on stress-dependent alterations of chemotaxis and motility. These revealed that motility-activating mutations upstream of the master regulatory genes *flhDC* compromised the survival of *E. coli* under acid shock. Accordingly, an inverse correlation between motility and shock survival was demonstrated, suggesting a differentiation of *E. coli* into a motile and an acid-tolerant subpopulation. This trade-off between motility and the ability to tolerate acid shock periods was found to depend on the differential integration of insertion sequence elements in the promoter region of *flhDC*. In another study, stress-dependent adaptations of chemotaxis in the marine pathogen *Vibrio campbellii* were highlighted. Stress hormones such as eukaryotic epinephrine bound to the chemotaxis coupling protein CheW and affected the sensing of chemoattractants. Finally, the use of a triple-fluorescent reporter strain demonstrated that the three major acid-resistance systems are heterogeneously activated in an *E. coli* population. These results indicated a 'bet-hedging' strategy and division of labor under acid stress conditions.

Overall, the results obtained in this thesis shed new light on bacterial stress adaptations and provide new starting points for future research, such as an in-depth characterization of novel acid-induced small proteins, the analysis of subpopulations with different acid tolerance, and the search for further stress-dependent mechanisms of chemotaxis and motility.

Zusammenfassung

Das Wahrnehmen und Reagieren auf Säurestress ist essentiell für das Überleben von Bakterien in Lebensräumen wie dem Verdauungstrakt von Wirbeltieren. Frühere Versuche die Reaktion von Bakterien auf Säurestress systematisch zu analysieren beschränkten sich jedoch auf Methoden wie Proteomics und Microarrays, oder auf milden Säurestress. In dieser Arbeit wurden die Vorteile von Ribo-Seq genutzt und mit RNA-Seq kombiniert um die Anpassungen von *Escherichia coli* an milden (pH 5.8) und starken, fast tödlichen, Säurestress (pH 4.4) aufzuzeigen. Die Ergebnisse beinhalteten neue Säuretoleranzstrategien wie die reduzierte Synthese von Membranproteinen, einen minimierten Stoffwechsel und die Induktion der Eisenaufnahme und Siderophorsynthese. Zudem wurden neue kleine Proteine durch Ribo-Seq entdeckt, welche nur unter Säurestress detektierbar waren. Außerdem wurden durch den Einsatz von Autoencoder-basiertem maschinellen Lernen säurestressspezifische Anpassungen von anderen Stressoren abgegrenzt.

Die Ribo-Seq und RNA-Seq Ergebnisse zeigten auch eine erhöhte Expression von Motilitätsgenen bei pH 5.8, nicht aber bei pH 4.4, was auf eine Regulation der Flagellensynthese in Abhängigkeit der Stressintensität hindeutete. Daher wurden weitere Studien zu säurestressabhängigen Änderungen der Chemotaxis und Beweglichkeit durchgeführt. Dabei wurde gezeigt, dass Mutationen nahe der Masterregulatorengene *flhDC*, welche die Beweglichkeit erhöhen, das Überleben von *E. coli* unter Säureschockbedingungen verringern. Gleichzeitig wurde eine inverse Korrelation zwischen der Motilität und dem Überleben unter Säureschock festgestellt, was eine Differenzierung von *E. coli* in eine bewegliche und eine säuretolerante Subpopulation unter Säurestress nahelegte. Es konnte schließlich gezeigt werden, dass der Kompromiss zwischen Beweglichkeit und dem Überleben unter Säureschock von der unterschiedlichen Integration von Insertionssequenzelementen in der Promotorregion von *flhDC* abhängig ist. In einer weiteren Studie wurde die stressabhängige Anpassung der Chemotaxis im marinen Pathogen *Vibrio campbellii* demonstriert. Stresshormone wie das eukaryotische Adrenalin banden an das chemotaktische Kopplungsprotein CheW und beeinflussten das Wahrnehmen von Lockstoffen. Schließlich konnte mit Hilfe eines fluoreszierenden Reporterstamms die heterogene Aktivierung der drei hauptsächlich Säureresistenzsysteme innerhalb einer *E. coli* Population gezeigt werden. Diese Ergebnisse weisen auf eine funktionelle Arbeitsteilung unter Stressbedingungen hin.

Zusammenfassend werfen die Ergebnisse dieser Doktorarbeit neues Licht auf bakterielle Stressanpassungen und bieten viele neue Ansatzpunkte für zukünftige Forschungsprojekte, wie z.B. die Charakterisierung von neuen säureinduzierten kleinen Proteinen, die Analyse von Subpopulationen mit unterschiedlicher Säuretoleranz, sowie die Suche nach weiteren stressabhängigen Anpassungen der Beweglichkeit und Chemotaxis.

1 Introduction

1.1 Overview of acidic environments

pH is defined as the 'power of hydrogen' and measures the acidity or basicity of an aqueous solution (1). It is calculated by taking the negative logarithm of hydrogen ion concentration and ranges from 1 to 14. By definition, solutions with $\text{pH} < 7$ are acidic, $\text{pH} > 7$ are basic, and solutions with a pH of exactly 7 are neutral at 25 °C (2). The pH varies significantly in different environmental habitats and can range from less than 2 in acid mine drainage to a pH of 10 to 11 in soda lakes (3, 4).

This thesis focuses on γ -proteobacteria exposed to acidic environments such as gastrointestinal tracts, macrophage phagosomes, acidic soils, peat bogs, industrial fermentation tanks, or biomining sites (Figure 1). Bacteria within the gastrointestinal tract of humans and animals encounter varying levels of acidity which is crucial for digestion and immune defense (5). The stomach possesses an exceptionally low pH ranging from 1.5 to 3.5 due to the presence of hydrochloric acid secreted by gastric glands (6). Correspondingly, the stomach constitutes the major bactericidal barrier of the gastrointestinal tract for pathogens (7). It is important to note that the capacity of microbes for tolerating the acidity of the stomach varies significantly and results in infective doses that differ by several orders of magnitude (Chapter 2.5). For instance, *Escherichia* and *Shigella* spp. are highly tolerant towards acidity and have low infective doses whereas *Vibrio cholerae* requires $\sim 10^8$ ingested cells to conduct an infection (8–10). Mildly acidic conditions are present in the duodenum which is in direct contact with the stomach and exhibits a pH of ~ 6 (11, 12). Moving further along the tract, bacteria that survived the stomach acidity are also confronted with mild acidity in the proximal colon including the cecum (12, 13). In this environment, short-chain fatty acids (SCFAs) are produced by anaerobic fermenting bacteria resulting in a pH of 6.4 or lower (14). In a medical context, acidic conditions can be faced in macrophage phagosomes (Figure 1) (15), where intracellular pathogens including *Salmonella*, *Legionella*, and *Mycobacterium* are exposed to acidity as a consequence of the activity of vacuolar-type proton ATPases (V-ATPases) and Na^+/H^+ antiporters (16).

Acidic environments are also found to large extents in soil (Figure 1). In these surroundings, acidification can be triggered by carbonic acid (H_2CO_3) formation as a consequence of the combination of carbon dioxide (CO_2) emissions with atmospheric water (17). Additionally, burning fossil fuels releases sulfur and nitrogen oxides, which, upon reacting with water, form sulfuric and nitric acids. These acidic compounds accumulate in the soil through acidic rain (18). Furthermore, root respiration and the breakdown of organic matter by microorganisms release CO_2 , elevating H_2CO_3 levels in the soil (19). This process triggers cation

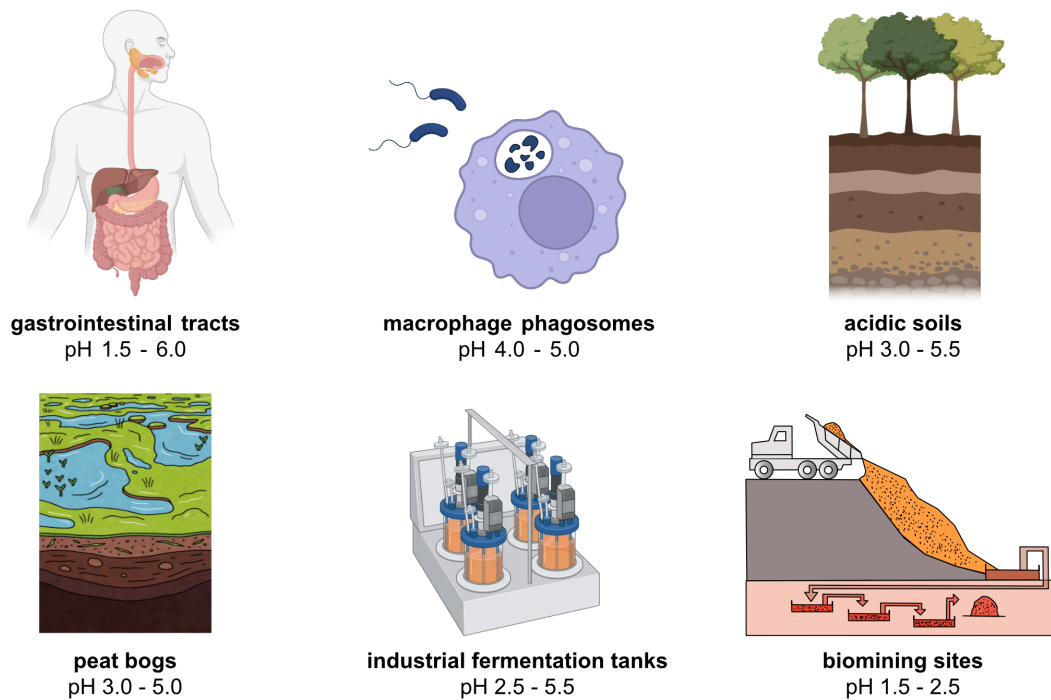


Figure 1: Schematic illustration of habitats where acidophilic and neutralophilic bacteria can be exposed to acidity.

exchange, leading to the leaching of base cations such as Ca^{2+} and Mg^{2+} from the soil, consequently increasing the proportion of Al^{3+} and H^+ ions (20). Overall, acidic soils account for 30% of the global ice-free land with pH values of as low as < 3.5 (21). Additionally, low pH can be encountered by bacteria in peat bogs (Figure 1). *Sphagnum*-dominated acidic peat bogs account for ~3% of the terrestrial surface on earth and are characterized by a pH between 3 and 5 (22). In these habitats, which are usually mineral nutrient deprived, methanotrophic communities are commonly encountered (22–24).

Acidity also holds significant importance for the food industry (Figure 1). Predominantly found in dairy products, homofermentative and heterofermentative lactic acid bacteria along with propionic bacteria prompt the generation of lactic acid, propionic acid, EtOH, and CO_2 . These compounds contribute to improved flavor, digestibility, nutritional qualities, and preservation of the products (25, 26). Consequently, bacteria encounter the acidity resulting from their own fermentation activities and are commonly exposed to a pH between 4.0 and 5.5 (27). Another industry relying on acid-tolerant microbes is the biomining industry (Figure 1), which is specialized in recovering valuable metals from reduced sulfides present in ores and concentrates (28). In this process, metal ions undergo oxidation which leads to the production of acid mine drainage, consisting mainly of sulfuric acid and causing ambient pH values below 1.5 (29).

In summary, the significance of acid tolerance spans several domains impacting public health, industrial sectors, and ecological landscapes which are characterized by different levels of acidity.

1.2 Bacterial acid stress response mechanisms

Bacteria evolved a magnitude of sophisticated stress response mechanisms to survive in environments with fluctuating pH. For instance, the intrinsic buffering capacity of the cytoplasm is essential in habitats with high proton concentrations. In particular, biological macromolecules including amino-acid side chains, polyamines, polyphosphates, and inorganic phosphate, can be protonated (30). Thus, fluctuating H^+ concentrations can be balanced through the sequestration of pH-titratable cellular components.

Upon exposure to acidity, the cytoplasmic membrane serves as the primary barrier for protons and limits intrusion into the cell. However, H^+ can still permeate into the cytoplasm via ion channels, water chains, or damaged membranes (31). To prevent the latter, modifications of the cytoplasmic membrane which alter the lipid composition, integrity, or fluidity, occur in bacteria. One common adaptation of this kind is incorporating cyclopropane fatty acids (CFAs) into the membrane (Figure 2). CFAs are synthesized from unsaturated fatty acids by adding a methyl group from S-adenosine-methionine to a double bond and CFA-enriched membranes were demonstrated to be less permeable for protons (32). Notably, an *E. coli* mutant lacking the CFA synthase gene was more sensitive to acid stress (32, 33). Furthermore, the proportion of saturated to unsaturated fatty acids in the membrane can increase in low-pH environments (34). Besides fatty acids also lipid types are modified upon acidification. Such adaptations involve the presence of aminoacylated derivatives of phosphatidylglycerol, the formation of hopanoids and sphingolipids, and the increase of ornithine lipids (35).

In addition to the restriction of H^+ uptake, proton export constitutively occurs in bacteria via proton-cation antiporters, or proton pumps associated with the respiratory chain (Figure 2). Nevertheless, the activity of these pumps depends on the generation of the proton motive force (36). Under mildly acidic conditions, *E. coli* restricts the production of the F_0F_1 ATPase to limit proton re-entry (37, 38). Conversely, the F_0F_1 -ATPase synthase was also shown to actively pump protons out of the cell in an ATP-dependent manner in several species under severe acid stress (38–41).

Alongside constitutive response mechanisms, inducible defense strategies against acidity exist in γ -proteobacteria. Such responses are commonly initiated by acid sensors which are responsible for the detection of cytoplasmic and external proton concentrations. Acid sensors can be implemented in bacterial cells in different forms such as HKs of two-component systems, one-component-systems, or cytoplasmic transcription factors (Chapter 2.5). In many cases, H^+ are sensed via the protonation of single amino acid residues or patches of amino acids, and conformational changes are triggered which propagate the signal (42–44). Examples of bacterial acid stress sensors include ArsS, EvgS, PhoQ, PmrB, SsrA, CadC, and AphB, which are reviewed in Chapter 2.5.

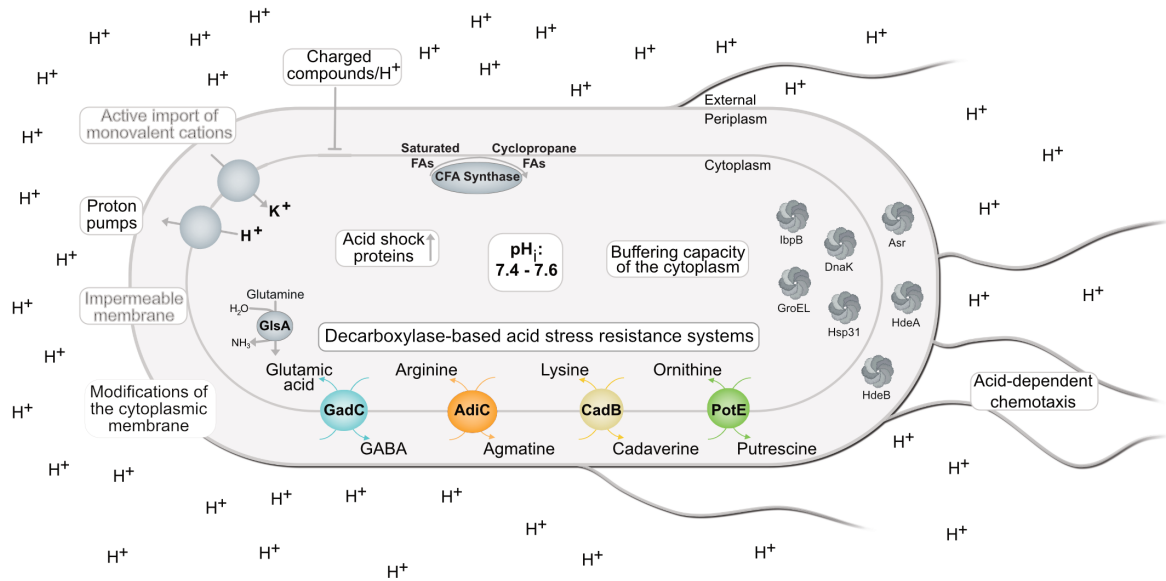


Figure 2: Summary of acid stress response mechanisms in γ -proteobacteria. This figure was adapted from Schwarz and Schumacher *et al.* 2022 (Chapter 2.5).

A prime example of inducible acid defense mechanisms are so-called enzyme-based H^+ -consuming acid resistance systems (ARs). These systems elevate the pH via amino acid decarboxylases and the more alkaline reaction products, which are exported by antiporters in exchange for amino acid substrates (Figure 2). ARs were mostly studied in *E. coli*, which is equipped with four main ARs including the glutamate decarboxylase (Gad, AR2), arginine decarboxylase (Adi, AR3), lysine decarboxylase (Cad, AR4), and ornithine decarboxylase (Orn, AR5) systems. Each system is comprised of an H^+ -consuming decarboxylase (GadA/GadB, AdiA, CadA, SpeF) and a corresponding antiporter (GadC, AdiC, CadB, PotE) (43–45). Gene regulation of AR components and the exact mechanisms of acid stress relief have been reviewed by Foster 2004, de Biase and Pennacchietti 2012, Kanjee and Houry 2013, Lund *et al.* 2014, Guan and Liu 2020, and Arcari *et al.* 2020 (see also Chapter 2.5) (42–47).

In brief, AR systems simultaneously increase the internal and external pH by proton consumption via decarboxylation of the respective amino acids (glutamate, arginine, lysine, or ornithine) and export of the more alkaline reaction products (GABA, agmatine, cadaverine, or putrescine) (Figure 2). Importantly, each AR is activated at a distinct pH range and growth phase (43–45). While the Cad, Adi, and Orn systems entirely depend on the presence of the respective amino acids (48–50), the Gad system is activated in the stationary phase irrespective of the presence of glutamate (51, 52). Moreover, transcriptional regulation of *gadA* and *gadBC* constitutes one of the most complex mechanisms known in prokaryotes (46). On the other hand, *cadBA*, *adiA*, and *adiC* expression is controlled by a single regulator, *AdiY* or *CadC* respectively (50, 53). Regulators involved in transcriptional regulation of *speF* and *potE*

of the Orn system are currently unknown. In addition to the four systems mentioned above, *E. coli* is equipped with another unexplored system referred to as AR1. In contrast to AR2-5, AR1 is not dependent on the uptake of external amino acids but relies on the consumption of internally derived glutamate using the decarboxylating enzymes of the Gad system (54).

Inducible chaperones and acid shock proteins also confer acid resistance to bacteria. Periplasmic chaperones such as HdeA and HdeB restrict protein aggregation in the periplasm and are essential for survival considering that acidification triggers protein damage, denaturation, and unfolding (55). HdeA and HdeB show maximal activity at pH < 4 and bind proteins unfolded at low pH to prevent them from aggregation (56, 57). Another protective periplasmic chaperone is Asr, which is annotated as an 'acid shock protein'. Asr is induced in a pH range of 3-4 and knockout mutants are highly vulnerable to acid shock (58). Recently, the molecular mechanism of Asr-mediated acid protection was unraveled. Asr acts as an intrinsically disordered chaperone which guarantees outer membrane integrity by preventing aggregation of proteins carrying positive net charges (59). Besides the periplasmic examples mentioned above, other protective chaperones act in the cytoplasm. These involve GroEL, DnaK, IbpB, and Hsp31 (*hchA*) (Figure 2).

Moreover, multidrug efflux pumps such as MdtEF are induced by acidity (60, 61). In addition to their role in drug extrusion, efflux pumps can export protons and consequently relieve acid stress (62). Importantly, several lines of evidence for facilitated development of antibiotic resistance as a consequence of induced acid defense mechanisms exist (63–65). This overlap between acid stress and antibiotic stress responses is summarized in Chapter 2.6.

1.3 pH-induced chemotaxis and motility

Bacteria can detect chemical gradients, enabling them to move toward or away from specific stimuli. This process involves specialized structures such as flagella, allowing the bacteria to swim and navigate to favorable environments or away from harmful substances (66, 67).

Considering acidity, the chemoreceptors Tar and Tsr are essential for navigating *E. coli* to habitats with desired pH levels. These receptors are methyl-accepting chemotaxis proteins (MCPs) and form clusters in the cell membrane which associate with the HK CheA and the adaptor protein CheW (Figure 3) (68–70). Both MCPs can sense the external and cytoplasmic pH and induce a signal transduction cascade, ultimately resulting in control of the flagellar motor (Figure 3) (71, 72). Adaptive receptor methylation in both Tar and Tsr fine-tunes the pH response and a 'push-pull' mode of action has been noted (73). Another crucial receptor for pH taxis is TlpB of *Helicobacter pylori* (Figure 3). Notably, *tlpB* knockout mutants have been characterized as pH non-responsive (74, 75).

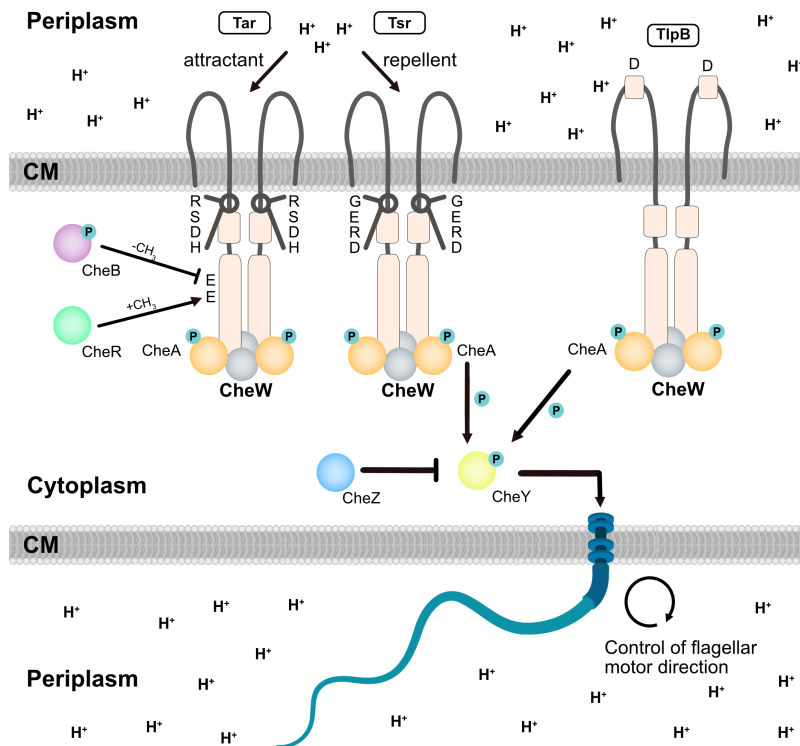


Figure 3: Control of bacterial chemotaxis and flagellar movement in response to acid stress. Amino acid residues are marked in single letter code when described to be important for pH-sensing. CM, cytoplasmic membrane.

Upon signal propagation from chemoreceptors, the kinase CheA is phosphorylated while CheW serves as an adaptor protein. Subsequently, activated CheA transfers its phosphoryl group to the RR CheY, converting it into its active, phosphorylated form (CheY-P). CheY-P is essential for controlling the flagellar motor rotation as it binds and interacts with the motor switch complex (Figure 3). When CheY-P dissociates, the flagellar motor resumes its normal spinning motion, propelling the bacterium forward in a straight run. CheY-P can also be dephosphorylated by the phosphatase CheZ, and CheB as well as CheR proteins are involved in adaptation (Figure 3). CheR methylates the receptors, while CheB demethylates them (66, 67).

Besides alterations in chemotactic behaviors, differential expression of flagellar components has been observed under acidity. For instance, flagellar genes were differentially expressed in *E. coli* at pH 5.0 (37) and similar observations were made in *Brucella suis*, *Listeria monocytogenes*, and *Campylobacter jejuni* (see Chapter 2.6), suggesting a universal phenomenon in motile bacteria. It is worth noting, that motility and chemotaxis appear to be strictly dependent on the degree of acid stress, considering that taxis towards aspartate was reported to be abolished at pH <5 and bacteria were demonstrated to be non-motile at pH 4 (76). Moreover, flagellar excision and rapid shedding of flagella upon sudden drops to pH 4 have been noted (77, 78). This suggests, that bacteria when exposed to acidity aim to migrate to habitats with lower H⁺ concentrations only under mildly acidic conditions.

1.4 Bacterial exposure to eukaryotic stress hormones

Besides acid stress, bacteria can encounter a variety of other stressors in their environments such as temperature fluctuations, nutrient scarcity, toxic chemicals, oxidative stress, or antibiotic stress (79). Another stressor which gained increasing attention over the last years in the field of bacteriology are eukaryotic stress hormones. For instance, catecholamine hormones such as epinephrine (EPI), phenylephrine (PE), norepinephrine (NE), labetalol (LAB), or dopamine, are present in a wide range of hosts such as animals and humans where they function as neurotransmitters and stress hormones (80). These compounds harbor side-chain amines and a catechol motif (Figure 4).

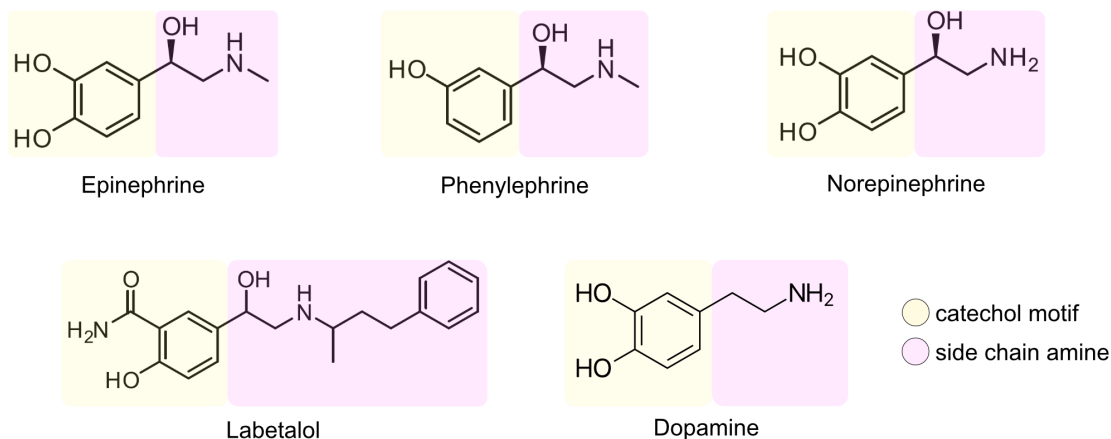


Figure 4: Chemical structures of a selection of eukaryotic catecholamine hormones. Catechol motifs and side chain amines are colored yellow and purple.

It was previously indicated that pathogenic infections of mammalian hosts were facilitated when the host organism was stressed (81, 82). Along this line, catecholamine hormones induced the growth of several bacterial species due to the iron-sequestering properties of the catechol siderophore (83). Importantly, catecholamine hormones can also affect biofilm formation, virulence, siderophore production, and the invasion of epithelial cells (82, 84–87). Hence, certain pathogens may use these compounds produced under stress as cues for recognition of the eukaryotic environment with the ultimate purpose of occupying a specific niche within the host (88). This hypothesis is further supported as bacterial chemotaxis was impacted by stress hormones. For example, NE was reported to act either as an attractant or a repellent for *E. coli*, depending on the concentration (89). Moreover, stress hormones can increase bacterial horizontal gene transfer efficiencies, enhance the expression of pili as well as the attachment to gut tissue, and activate type II secretion systems (90–92).

In eukaryotes, the binding of catecholamines to G protein-coupled receptors is well known (93, 94). Based on the effects in bacteria described above, it appears plausible that catecholamine receptors may have also evolved in prokaryotes. Indeed, a former study in EHEC indicated the

binding of NE and EPI to the HKs QseE and QseC (95, 96). Nevertheless, knockout mutants lacking the above mentioned genes still responded to eukaryotic stress hormones in *V. cholerae* and *Salmonella* (87, 97, 98). This suggests, that further yet unknown receptors exist in bacteria. For the marine pathogen *Vibrio campbellii*, NE and dopamine simultaneously increased growth, siderophore production, motility, as well as the expression of virulence genes (86). Notably, while α -adrenoreceptor antagonists like LAB inhibited the effect of NE on motility, β -adrenoreceptor antagonists such as propranolol (PRO) did not exhibit any effect. This indicates, that catecholamines likely act through a specific receptor in *V. campbellii* (86).

V. campbellii, formerly known as *V. harveyi*, is an important model organism for the study of quorum sensing (99, 100). This marine bacterium belongs to the γ -proteobacteria class, exhibits motility and bioluminescence, and is an opportunistic pathogen for marine species such as fish, shrimp, squid, and other marine invertebrates (101). To detect the potential receptor of catecholamine hormones in *V. campbellii*, or other target proteins, chemical proteomics shall be applied (see Chapter 1.7). Chemical proteomics involves synthesizing chemical probes containing an alkyne handle suitable for target protein enrichment via affinity-based protein profiling, followed by mass spectrometry (MS)-based proteome profiling (102, 103). This approach successfully identified target proteins of diverse chemicals in various bacteria (104–106). Thus, it represents a promising approach for gaining further insights into the interplay of eukaryotic catecholamine hormones and target proteins in prokaryotes.

1.5 Heterogeneous stress responses

Heterogeneous stress responses in bacteria refer to the varied and non-uniform reactions and gene expression levels of individual cells within a population to environmental or physiological stressors (107, 108). Unlike multicellular organisms, where heterogeneity can occur at different levels (cellular, tissue, organismal), the variability in bacteria is observed at the level of individual cells (109). Heterogeneity arises from internal factors including the cellular physiological state and stochastic gene expression, often referred to as 'noise', but can be influenced by external factors such as stressors, nutrient availability, and cell density (110, 111). Thereby, risks associated with unpredictable environments can be mitigated due to diversification, a strategy referred to as 'bet-hedging' (112, 113). It is important to note that phenotypic heterogeneity refers to the presence of diverse phenotypes within a genetically identical population, whereas homogeneous populations are characterized by uniform gene expression levels (Figure 5). In the field of bacteriology, both fluorescence microscopy (Chapter 2.4) and single-cell RNA sequencing (scRNA-Seq) are commonly used to study heterogeneous expression levels of genes and pathways (114).

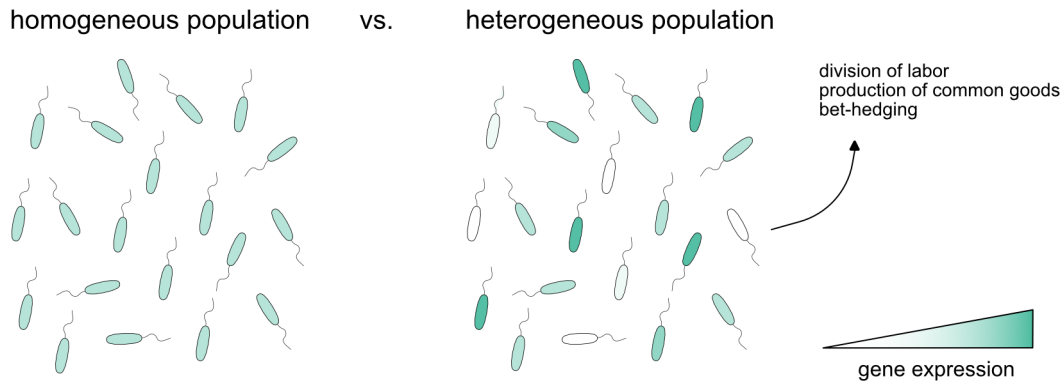


Figure 5: Schematic illustration of homogeneous and heterogeneous bacterial populations. Differential gene expression levels among individual cells are indicated using green and white colors.

This work focuses on heterogeneous responses under acid stress. Nevertheless, division of labor and bet-hedging have previously been observed upon exposure of bacteria to other stressors. For instance, cell-to-cell variability was noted upon exposure of *E. coli* to oxidative stress. In this case, supplementation of H_2O_2 triggered heterogeneity which was dependent on the ROS levels within the immediate environment of single cells and was affected by cell-cell interactions (115). Moreover, *Bacillus cereus* exhibited high-level heterogeneity during the adaptive salt stress response (116). Phenotypic heterogeneity under antibiotic stress is also a well-known phenomenon and was summarized in several literature reviews (see also Chapter 2.6) (117–119). In terms of acid stress, cell-to-cell variability was indicated in *Salmonella* which is confronted with acidity in vacuoles of macrophages (120). In *E. coli*, GadE, the master regulator of the Gad system, is heterogeneously expressed irrespective of the stress intensity. This results in a preemptive split into subpopulations with different acid tolerance among an isogenic population (121).

Further, the Cad system is heterogeneously activated among single cells in *E. coli*, but not in *V. campbellii*. Fluorescence microscopy revealed around 70% ON cells and 30% OFF cells in terms of CadB-eGFP expression. The underlying reason for this was reported to be a ribosome stalling motif which is present in the transcriptional activator CadC in *E. coli*, but missing in the *Vibrionaceae* family. This polyproline motif causes low CadC copy numbers (≤ 4 molecules per cell) which in turn lead to noisy gene expression of the target *cadBA* operon. This design of the signaling system represents an example of heterogeneity caused by the stochastic distribution of regulators among the population (122).

The ON/OFF behavior of the *E. coli* population in activating the Cad system raises the question of whether cells that do not express the Cad system induce the Adi and/or Gad system, which would indicate a division of labor under acid stress. To address this question, a comprehensive analysis of the distribution of the three major ARs in *E. coli* under consecutively increasing acid stress is provided in Chapter 2.4.

1.6 Previous and current approaches to systematically study acid stress

Next generation sequencing (NGS), also known as high-throughput sequencing, refers to a set of advanced sequencing technologies that enable rapid and parallel sequencing of millions of nucleic acid fragments. These advances revolutionized the field of genomics by providing the possibility to quickly and cost-effectively analyze large amounts of genetic information (123, 124). Before the availability of NGS, bacterial transcriptomes were mainly studied using microarrays (Figure 6) (125). A microarray constitutes a solid surface onto which DNA or RNA probes can be attached in a spatially defined manner. Probes are designed as complementary to specific genes or transcripts of interest and abundance is measured based on the emission of fluorescently-labeled cDNA binding to immobilized probes (126, 127). While microarrays are a cost-effective option, they are less sensitive compared to NGS-based methods, have limited genome coverage, and have a fixed content due to probe design which limits the detection of novel transcripts (128). In the context of bacterial acid stress resistance, a selected part of the *E. coli* transcriptome was studied via a microarray at pH 7.0 and 5.0 (37).

Beforehand, global adaptations of *E. coli* to acidity were also captured on the protein level by two-dimensional gel electrophoresis (Figure 6), separating proteins based on their isoelectric point and molecular weight (129, 130). With this approach, abundant proteins at pH 4.4, pH 4.9, and pH 6.0 were identified via excision from gels, followed by N-terminal sequence analysis (129), or MALDI-TOF (130). In recent years, the adaptations to acidity of a wide range of bacterial species have been studied using RNA-Seq and/or proteomics (summarized in Chapter 2.6).

Proteomics is defined as the large-scale study of proteins to characterize the entire protein content of a cell, which is usually based on liquid chromatography-mass spectrometry (LC-MS) (Figure 6) (131, 132). Nevertheless, the percentage of detected proteins in proteomics relative to total protein abundance remains in many cases limited due to issues based on aggregation or precipitation of membrane proteins. On average, membrane proteins constitute 30% of a proteome and target residues for tryptic cleavage are to a large extent absent in transmembrane helices and rather found in hydrophilic areas (133).

A powerful strategy to overcome the above mentioned limitations is to combine RNA-Seq with ribosome profiling (Ribo-Seq). This approach enables simultaneous detection of genome-wide mRNA levels and protein synthesis rates.

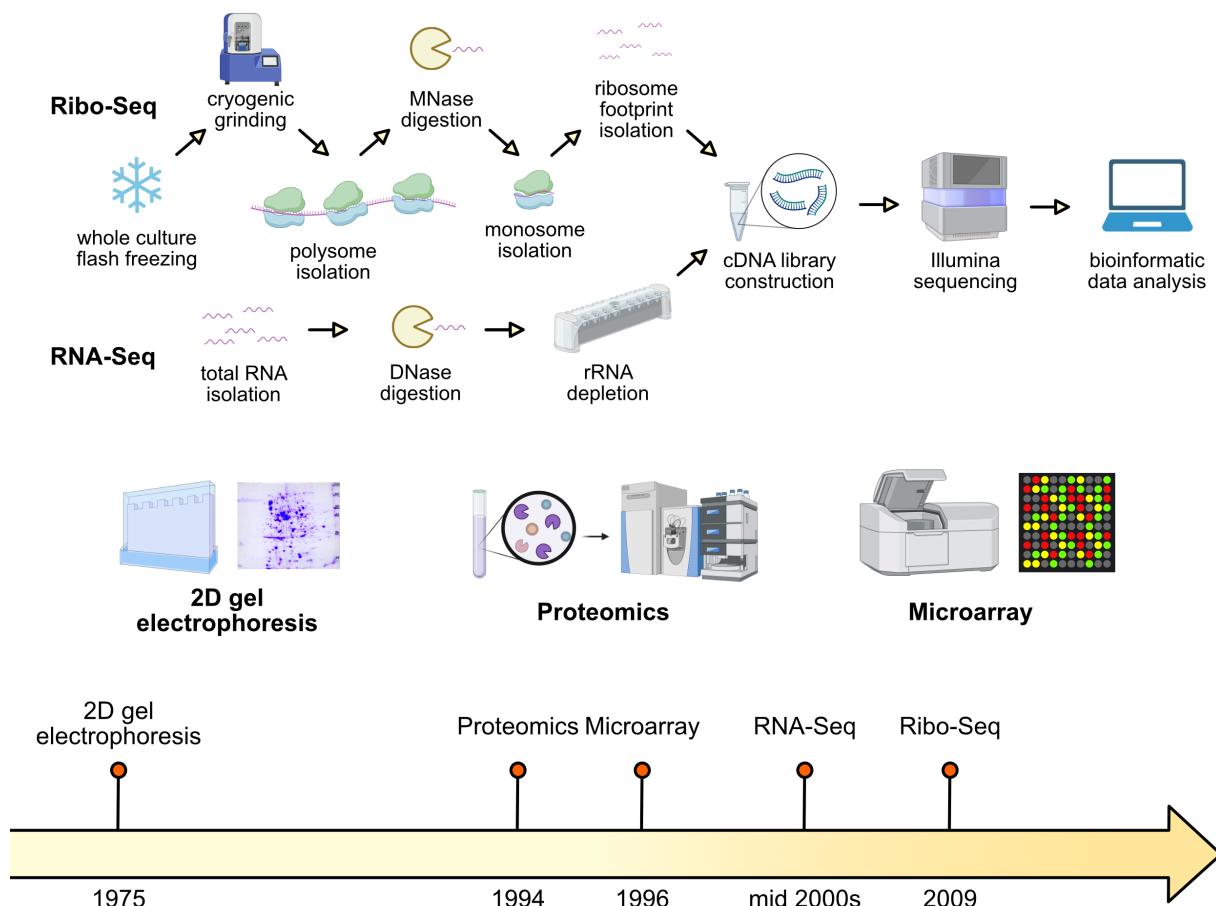


Figure 6: Schematic overview of methods for detection of genome-wide alterations in RNA and protein levels. The timeline indicates the year in which the respective methods were first described in the literature (134–139). Parts of this figure were created using BioRender.com.

1.6.1 Detection of transcriptional regulation using RNA-Seq

RNA-seq is a high-throughput sequencing technique that enables the genome-wide quantification and profiling of RNA and the comparison of transcriptomic responses in different experimental conditions. RNA-Seq workflows involve RNA extraction, DNase digestion, rRNA depletion, cDNA library construction, high-throughput sequencing, and bioinformatic analysis (Figure 6) (140, 141). RNA isolation is frequently conducted by commercially available kits or phenol-chloroform extraction (142). Subsequently, genomic DNA contaminations are removed by DNase digestion. Considering that rRNA accounts for the vast majority of bacterial transcripts, rRNA is depleted to enrich mRNA transcripts, for instance via hybridization to magnetic bead-linked complementary oligonucleotides (143). Finally, mRNA is converted to cDNA via random hexamer-primed reverse transcription, and adaptors, as well as unique indices, are ligated to cDNA fragments (140). Overall, the introduction of RNA-Seq has enabled the detection of numerous novel coding sequences, non-coding RNAs, and transcriptional start sites in bacteria (140, 141).

1.6.2 Assessment of protein synthesis rates using Ribo-Seq

RNA-Seq combined with Ribo-Seq enables simultaneous assessment of genome-wide mRNA levels and protein synthesis rates and allows the calculation of global translation efficiencies (139, 144). Protein synthesis is measured via Ribo-Seq by detection of transcripts which are protected from nuclease digestion by ribosome coverage. Therefore, in contrast to RNA-Seq, not the whole mRNA fraction is converted to cDNA but only RNA fragments shielded by ribosomes at the moment of sample collection. This allows genome-wide mapping of ribosome positions with single-nucleotide resolution. Ribosome-protected fragments (RPFs) are also referred to as ribosome footprints and are obtained by nuclease digestion of non-ribosome-covered RNA (139, 144–146). In eukaryotes, RNaseI is commonly used for digestion, which is however inactivated by bacterial ribosomes (147). To this end, MNase obtained from *Staphylococcus aureus* is commonly used for bacterial Ribo-Seq (148–151). In contrast to eukaryotes where RPFs display a uniform length of 28 nt, bacterial ribosome footprints range from 15 to 45 nt (139, 150, 152). Before MNase digestion, cells are commonly harvested by flash-freezing and lysed through cryogenic grinding. Bacterial polysomes are then isolated and converted to monosomes upon nuclease addition (Figure 6). Subsequently, RNA is isolated and enriched for RPFs via size selection and the remaining ribosome footprints are converted to cDNA (145, 150, 151, 153). In terms of stress conditions, Ribo-Seq combined with RNA-Seq has so far only been conducted in *E. coli* under heat stress (45 °C) (154).

1.6.3 Unravelling novel sORFs through Ribo-Seq

sORFs are open reading frames that are defined by their short length. However, the definition is inconsistent across literature and ranges from < 50 aa, to <70 aa, and < 100 aa (155–158). To a large extent, sORFs were previously overlooked due to technical limitations and were thus lacking in bacterial genome annotations. Beyond their size, small proteins are characterized by hydrophobicity and sometimes nonexistent charge which complicates their detection and the characterization of molecular functions (155–160). Furthermore, small proteins oftentimes harbor alpha-helical structures and are incorporated, or associated with the bacterial membrane (161, 162). Considering genomic locations, sORFs can be encoded independently in intergenic regions, antisense, nested (in the same or alternative frame) relative to known ORFs, or in the 5'- or 3' UTR of annotated genes. Moreover, sRNAs that encode a small peptide are considered dual-function RNAs, and small proteins can also be obtained by protease cleavage of a larger peptide (155, 157).

In recent years, Ribo-Seq and mass spectrometry-based approaches optimized for small proteins (peptidomics) have revealed a large reservoir of sORFs in a variety of bacterial species. Detection of sORFs through Ribo-Seq is commonly assisted by the supplementation of translation-arresting drugs before sample collection. Trapping ribosomes at the translation

initiation site (TIS) or translation termination site (TTS) is especially important for detecting sORFs encoded nested on the same strand within known sORFs (156, 163–165). The immense potential of novel sORF detection by Ribo-Seq was illustrated in various bacterial and archaeal species (157). Specifically, using mainly TIS- and TTS-Seq, 139 novel candidate sORFs have been identified in *Salmonella* (166), 47 in *H. volcanii* (167), and 37 in *S. meliloti* (168). Nevertheless, experiments for the detection of novel sORFs in various organisms have so far been restricted to standard growth conditions. Thus, it will be of intriguing interest to conduct Ribo-Seq under various experimental setups, such as under stress conditions (see Chapter 2.1).

1.7 Scope of this thesis

Adaptations to acid stress are crucial for the survival of γ -proteobacteria throughout the passage of gastrointestinal tracts. In recent decades, various studies have been conducted to describe global systematic acid stress responses. Nevertheless, these investigations were mainly limited due to technical constraints and/or were conducted only under mildly acidic conditions. Within this thesis, the advantages of NGS, in particular Ribo-Seq, shall be leveraged to discover genome-wide adaptations of *E. coli* to mild (pH 5.8) and near-lethal (pH 4.4) acid stress, as well as to find novel differentially expressed biological pathways and key transcriptional regulators. These large-scale datasets can subsequently be mined to reveal novel sORFs exclusively expressed under acidity, and used to highlight acid-specific adaptations guided by autoencoder-based machine learning (see Chapter 2.1).

Moreover, alterations in flagella and chemotaxis gene expression were previously indicated to be crucial for bacterial acid stress responses. To further explore this relationship, a strain from the single-gene knockout Keio collection (BW25113 *mhpR::km*) shall be analyzed in terms of acid shock survival rates and motility. This mutant is characterized by an IS insertion in the promoter region of the chemotaxis and motility master regulatory genes *flhDC* and is thus hypermotile and suitable for exploring a potential correlation between motility and the survival of acid shock periods (see Chapter 2.2). Potential adaptations of γ -proteobacterial chemotactic signaling are further investigated in Chapter 2.3 by studying the response of the marine pathogen *Vibrio campbellii* to eukaryotic stress hormones. This study aims to discover protein targets of catecholamine hormones through chemical proteomics including photoaffinity labeling.

Finally, the three main inducible ARs of *E. coli* shall be analyzed in-depth concerning potential heterogeneous activation among single cells. By constructing a triple reporter strain and conducting fluorescence microscopy under consecutively increasing acid stress, potential bet-hedging strategies and division of labor in *E. coli* are investigated (Chapter 2.4).

2 Results

2.1 Ribosome profiling reveals the fine-tuned response of *Escherichia coli* to mild and severe acid stress

Schumacher, K., Gelhausen, R., Kion-Crosby, W., Barquist, L., Backofen, R., and Jung, K. (2023). Ribosome profiling reveals the fine-tuned response of *Escherichia coli* to mild and severe acid stress. mSystems.10.1128/msystems.01037-23.

Available online at:

<https://pubmed.ncbi.nlm.nih.gov/37909716/>

Ribosome profiling reveals the fine-tuned response of *Escherichia coli* to mild and severe acid stress

Kilian Schumacher,¹ Rick Gelhausen,² Willow Kion-Crosby,^{3,4} Lars Barquist,^{3,4} Rolf Backofen,^{2,5} Kirsten Jung¹

AUTHOR AFFILIATIONS See affiliation list on p. 29.

ABSTRACT The ability to respond to acidic environments is crucial for neutralophilic bacteria. *Escherichia coli* has a well-characterized regulatory network that triggers a multitude of defense mechanisms to counteract excess protons. Nevertheless, systemic studies of the transcriptional and translational reprogramming of *E. coli* to different degrees of acid stress have not yet been performed. Here, we used ribosome profiling and RNA sequencing to compare the response of *E. coli* (pH 7.6) to sudden mild (pH 5.8) and severe near-lethal acid stress (pH 4.4) conditions that mimic passage through the gastrointestinal tract. We uncovered new differentially regulated genes and pathways, key transcriptional regulators, and 18 novel acid-induced candidate small open reading frames. By using machine learning and leveraging large compendia of publicly available *E. coli* expression data, we were able to distinguish between the response to acid stress and general stress. These results expand the acid resistance network and provide new insights into the fine-tuned response of *E. coli* to mild and severe acid stress.

IMPORTANCE Bacteria react very differently to survive in acidic environments, such as the human gastrointestinal tract. *Escherichia coli* is one of the extremely acid-resistant bacteria and has a variety of acid-defense mechanisms. Here, we provide the first genome-wide overview of the adaptations of *E. coli* K-12 to mild and severe acid stress at both the transcriptional and translational levels. Using ribosome profiling and RNA sequencing, we uncover novel adaptations to different degrees of acidity, including previously hidden stress-induced small proteins and novel key transcription factors for acid defense, and report mRNAs with pH-dependent differential translation efficiency. In addition, we distinguish between acid-specific adaptations and general stress response mechanisms using denoising autoencoders. This workflow represents a powerful approach that takes advantage of next-generation sequencing techniques and machine learning to systematically analyze bacterial stress responses.

KEYWORDS acid resistance, small proteins, transcription factor, ribosome profiling, RNA-Seq, machine learning

The infective dose of enteropathogens varies significantly among bacterial genera and is dependent on the number and complexity of acid resistance mechanisms (1). *Escherichia coli* is equipped with a high number of defense mechanisms to survive the acidity of the stomach and, correspondingly, can have an infective dose as low as less than 50 cells (2). Enterobacteria that survive the stomach also confront mild acid stress in the colon due to the presence of short-chain fatty acids produced by obligate anaerobes (3). Other neutralophilic bacteria encounter low pH environments in a variety of settings, such as acidic soils, fermented food, or phagosomes within macrophages (1).

The cytoplasmic membrane represents a primary barrier for protons (H⁺). Nevertheless, at low pH, H⁺ can permeate into the cytoplasm via protonated water chains, ion channels, or damaged membranes (4). Upon acidification, the cytoplasmic pH transiently

Editor Ákos T. Kovács, Universiteit Leiden, Leiden, the Netherlands

Address correspondence to Kirsten Jung, jung@imu.de.

The authors declare no conflict of interest.

See the funding table on p. 29.

Received 26 September 2023

Accepted 28 September 2023

Published 1 November 2023

Copyright © 2023 Schumacher et al. This is an open-access article distributed under the terms of the [Creative Commons Attribution 4.0 International license](https://creativecommons.org/licenses/by/4.0/).

decreases but returns to neutral within short time intervals. For example, a reduction in external pH to 5.5 causes a temporary decline in internal pH to ~6.0 (5). Intracellular acidification leads to the protonation of biological molecules, ultimately altering their charge and structure. This, in turn, may lead to protein unfolding, denaturation, and reduced enzymatic activities (6). Furthermore, acidification causes membrane and DNA damage (7, 8).

To maintain a constant internal pH and balance fluctuations in H^+ concentrations, the intrinsic buffering capacity of the cytoplasm is crucial, as protons can be sequestered by side-chains of proteins, inorganic phosphates, polyphosphates, or polyamines (9). Additional protective mechanisms that counteract acid stress and ensure survival in low pH habitats involve proton pumps, membrane remodeling, acid-dependent chemotaxis, chaperones, acid shock proteins, and the induction of enzyme-based H^+ -consuming acid resistance (AR) systems (10, 11).

E. coli is equipped with four different AR systems, namely, the glutamate decarboxylase (Gad, AR2), arginine decarboxylase (Adi, AR3), lysine decarboxylase (Cad, AR4), and ornithine decarboxylase (Orn, AR5) systems (12, 13). Each AR system consists of an H^+ -consuming amino acid decarboxylase (GadA/GadB, AdiA, CadA, SpeF) and a corresponding antiporter (GadC, AdiC, CadB, PotE), which serves to uptake the amino acid and export the more alkaline reaction product into the surrounding medium. This strategy ensures a simultaneous increase in intracellular and extracellular pH (7, 13, 14). Notably, each AR system is activated at different external pH values and growth phases (7, 15). We have previously found that individual *E. coli* cells exposed to consecutively increasing acid stress activate the Gad, Adi, and Cad systems heterogeneously, resulting in functional diversification and enhanced population fitness (15, 16). The regulatory network of the Gad system is highly complex and involves more than 10 regulatory elements (17), whereas the Adi and Cad systems are each regulated by a single transcriptional regulator, AdiY and CadC, respectively (15). Nevertheless, additional regulatory elements seem to exist that not only link these three ARs in individual cells but also contribute to a fine-tuned response of *E. coli* to different levels of acid stress (15).

Previous systematic studies to determine genome-wide adaptations within the acid stress response of *E. coli* have either been restricted to microarrays (18), two-dimensional gel electrophoresis (19, 20), or have only been performed under mild acidic conditions (pH 5.0–6.0) (21–23). Here, we present the first systemic study of global adaptations to different intensities of acid stress in *E. coli* at both the transcriptional and translational levels. Specifically, we compare gene expression and translation at pH 5.8 and pH 4.4 with pH 7.6, using RNA sequencing (RNA-Seq) and ribosome profiling (Ribo-Seq). Ribo-Seq allows deep-sequencing of ribosome-protected mRNA fragments (RPFs) (24, 25), which are obtained by nuclease digestion of non-ribosome-covered RNA, and has significantly advanced the current understanding of translational regulation (26). The applications of Ribo-Seq are manifold and include monitoring protein synthesis rates across the proteome, the identification of novel small open reading frames (sORFs), as well as determining protein copy numbers per cell during steady-state growth (27, 28). In contrast to mass spectrometry-based approaches, ribosome profiling is independent of protein biochemistry and allows detection of small proteins with less than 50 amino acids in length (29). In recent years, substantial advances in understanding translational events have been made through the utilization of Ribo-Seq, not only in various bacterial species but also in archaea, bacteriophages, and microbiomes (28, 30–35).

Our results reveal hundreds of differentially transcribed and translated genes of *E. coli* K-12 at pH 5.8 and 4.4, as well as examples of pH-dependent changes in translation efficiency. We identified previously undiscovered biological processes in response to acidity, including increased siderophore synthesis, glycerol catabolism, copper efflux, nucleotide biosynthesis, and spermidine/multidrug export, as well as decreased membrane transport and metabolic activities. In addition, we have identified new transcription factors (TFs) as key players during low pH exposure and 18 novel candidate sORFs involved in the response to acid stress. Finally, we differentiated

acid-specific transcriptional adaptations by using machine learning to compare the low pH response to that of other stressors.

RESULTS AND DISCUSSION

Examination of alterations in the translome and transcriptome of *E. coli* in response to varying degrees of acid stress

To mimic natural stress conditions, such as the passage of *E. coli* through the gastrointestinal tract, we established the following protocol involving a sudden change to low pH, detection of a rapid response, and severe, near-lethal acid stress. Specifically, *E. coli* K-12 MG1655 was cultivated in unbuffered lysogeny broth (LB) medium at pH 7.6 until the exponential growth phase ($OD_{600} = 0.5$). Then, 5 M hydrochloric acid was added directly to expose the cells to a pH of 5.8 or stepwise to a pH of 4.4, corresponding to mild and severe acid stress (Fig. 1A). The final optical densities were comparable (pH 7.6: $OD_{600} =$

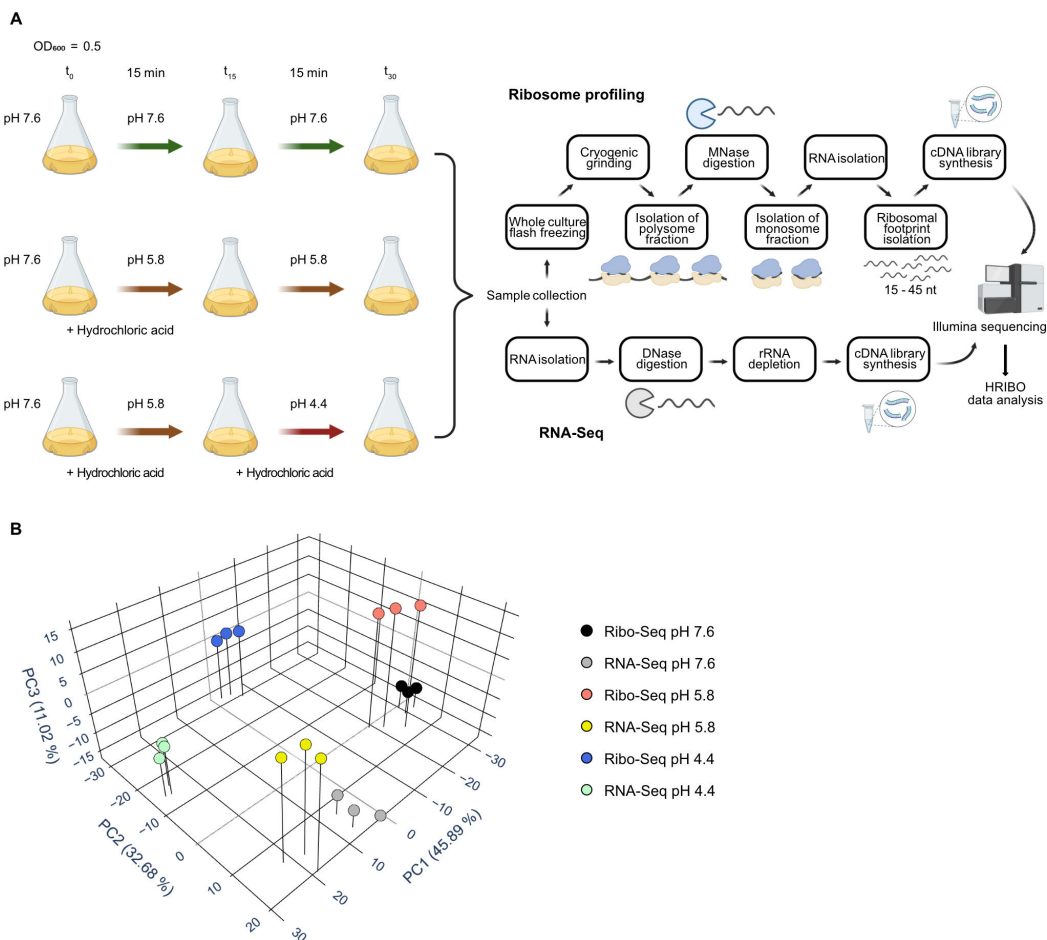


FIG 1 A schematic overview of culture conditions, pH-shift procedures, and the Ribo-Seq and RNA-Seq workflows. (A) Biological triplicates of *E. coli* MG1655 cells were grown in unbuffered LB medium (pH 7.6) to an OD_{600} of 0.5 (t_0). Subsequently, the cultures were either grown for an additional 30 min at pH 7.6, shifted for 30 min to pH 5.8, or shifted first for 15 min to pH 5.8 (t_{15}) and then to pH 4.4 (t_{30}). pH shifts were initiated by the direct addition of 5 M HCl to the cultures. At t_{30} , samples were collected. For RNA-Seq, total RNA was isolated, DNase digested, and ribosomal RNA was depleted prior to cDNA library preparation. For Ribo-Seq, whole cultures were flash-frozen in liquid nitrogen and cryogenically grinded using a freezer mill. Polysome fractions were isolated, and non-ribosome-protected RNA was digested using MNase. Ribosomal footprints were purified from the monosome fraction using a size selection gel and converted to cDNA libraries. Upon Illumina sequencing, the data were analyzed using the HRIBO pipeline (37). (B) Principal component analysis of median-of-ratios normalized and regularized log-transformed (rlog) read count values for *E. coli* Ribo-Seq and RNA-Seq triplicate data at pH 4.4, 5.8, and 7.6. Panel (A) was created with [BioRender.com](https://www.biorender.com).

~1.1; pH 4.4: $OD_{600} = \sim 0.7$) (Table S1), and the pH values hardly changed compared to t_0 (Fig. 1A; Table S2). To investigate whether a 15-min exposure to pH 4.4 was sufficient to induce cellular adaptation to severe acid stress, we examined the temporal dynamics of *adiA* expression by quantitative reverse transcription PCR (RT-qPCR). We detected an increase in *adiA* mRNA levels as early as 15 min after the shift to pH 4.4 and no substantial further increase after 30 or 60 min (Fig. S1). Additionally, we evaluated cell viability at the final experimental time points using propidium iodide (PI) staining (36) and examined colony-forming units (CFUs). The average percentage of dead cells detected by PI staining was less than 1% at pH 7.6, 5% at pH 5.8, and 18% at pH 4.4 (Fig. S2A). A positive control (5-min heat treatment at 80°C) resulted in an average of 97.2% non-viable cells, as determined by PI staining. The CFU count results underline that at least 2×10^8 viable cells were collected irrespective of pH at the moment of sample collection for Ribo- and RNA-Seq (Fig. S2B).

Cells were harvested and lysed as previously described by whole-culture flash freezing and cryogenic grinding in a freezer mill to avoid bias from translation-arresting drugs and filtering (38). The subsequent steps of our ribosome profiling protocol were a combination of methodologies reported by Latif and colleagues (39) and Mohammad and Buskirk (40) (see Materials and Methods for details). Strand-specific Illumina sequencing yielded an average of approximately 30 million cDNA reads per sample for Ribo-Seq and 5–10 million for RNA-Seq. The next-generation sequencing data were analyzed using an extended version of the high-throughput HRIBO data analysis pipeline (37). All samples achieved sufficient coverage with over two million reads, each mapping uniquely to the coding regions. The rRNA contamination was higher in the pH 4.4 Ribo-Seq samples than in other conditions but accounted for less than 15% in all cDNA libraries (Fig. S3). The length distribution of the generated RPFs was broad, ranging from 15 to 45 nucleotides (Fig. S4), consistent with previous observations in other prokaryotic ribosome profiling analyses (38, 39). We did not detect stress-induced increased relative ribosome occupancy in the initiation region of ORFs under acid stress compared to neutral pH. This is in contrast to previous observations in *E. coli* under heat stress (41) and in yeast under oxidative stress (42), which reported increased relative ribosome accumulation at start codons in stressed cells. In fact, ribosome occupancy in the translation initiation regions was slightly reduced at pH 4.4 and 5.8 compared with physiological pH (Fig. S5). This could be explained due to diminished ribosome-RNA complex stability and increased ribosome drop-off under acidic conditions. The biological triplicates for each experimental condition clustered on the first three principal components in a principle component analysis (PCA) plot (Fig. 1B). Notably, the global gene expression profiles were highly distinct at pH 4.4 compared with both pH 5.8 and 7.6.

Coordinated regulation of transcription and translation in response to acid stress

The tool *deltaTE* (43) was used to assess transcriptional and translational changes (i.e., differential expression and differential translation efficiency) in response to mild and severe acid stress. Low-expression transcripts were filtered out, and we focused our analysis on 3,654 genes with mean reads per kilobase per million reads mapped (rpkm) values ≥ 5 across all investigated conditions. Our findings reveal that 702 transcripts were significantly altered at pH 5.8 compared with physiological pH [absolute mRNA \log_2 fold change (FC) ≥ 1 and false discovery rate (FDR) adjusted $P \leq 0.05$], and 1,030 genes showed significant differences in mRNA levels at pH 4.4 (Fig. 2A). These results suggest that extensive transcriptional reprogramming occurred, which was influenced by the degree of acid stress. As illustrated by the Venn diagram overlaps (Fig. 2), a large number of adaptations occurred regardless of the degree of acid stress. Nonetheless, several hundred genes were differentially expressed exclusively at pH 5.8 or 4.4 (Fig. 2A). This suggests that in addition to universal adaptations at low pH, specific adaptations for mild and severe acid stress occur. We further determined the number of genes with

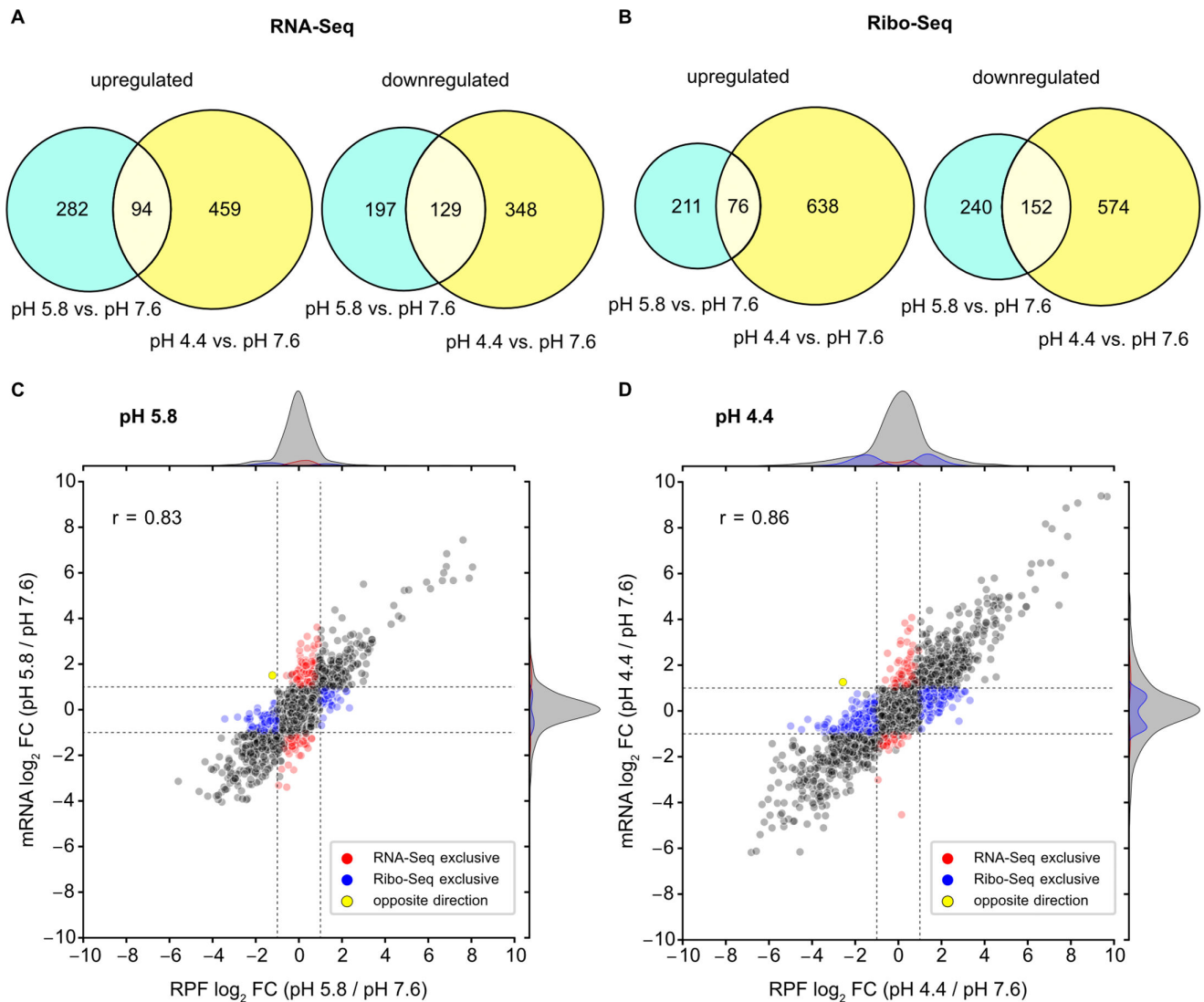


FIG 2 Genome-wide adaptations correlate at the transcriptional and translational levels in *E. coli* under acid stress. Weighted Venn diagrams show the total number and overlap of genes with significant FCs (absolute \log_2 FC ≥ 1 and P -adjust ≤ 0.05) determined by (A) RNA-Seq or (B) Ribo-Seq for cells exposed to pH 5.8 or pH 4.4, compared to the control (pH 7.6). (C) Comparison of global RPF and mRNA \log_2 FC values for pH 5.8, or (D) pH 4.4 vs pH 7.6. Dashed lines indicate \log_2 fold change values of +1 or -1. Hundreds of genes exhibited differential expression (absolute \log_2 FC ≥ 1 and P -adjust ≤ 0.05) at both the transcriptional and translational levels, whereas others were exclusively detected by either RNA-Seq (red dots) or Ribo-Seq (blue dots) or had significant changes in opposite directions (yellow dots). Values of the Pearson correlation coefficient (r) are indicated.

stress-dependent alterations in RPF counts to be 679 at pH 5.8 and 1,440 at pH 4.4 (absolute RPF \log_2 FC ≥ 1 and FDR adjusted $P \leq 0.05$), which was in a similar range compared with the RNA-Seq data (Fig. 2A and B). Accordingly, the global FC values for mRNA and RPF levels showed a high Pearson correlation coefficient (r) under both conditions (Fig. 2C and D, gray dots). This indicates that transcriptional regulation of these genes is the predominant response to acid stress. However, a subset of genes exhibited exclusive and significant regulation at either the transcriptional (red dots) or translational (blue dots) level.

Specifically, at pH 5.8, 193 genes were detected to be significantly regulated exclusively by RNA-Seq, while 216 genes were exclusively affected in the Ribo-Seq data (Fig. 2C; Table S3). At pH 4.4, 127 differentially regulated genes were found exclusively by RNA-Seq and 570 genes by Ribo-Seq (Fig. 2D; Table S3). Notably, for *fruA* at pH 5.8 and *yechH* at pH 4.4, opposite changes were observed at the transcriptional and translational

levels (Fig. 2C and D, yellow dots). FruA is the fructose permease of the phosphoenolpyruvate-dependent sugar phosphotransferase system (44), whereas the function of YecH remains unknown.

Next, we investigated translation efficiency (TE) to identify genes that undergo translational regulation in response to acidic conditions. TE provides information regarding ribosome counts per mRNA and is calculated as the ratio of RPFs over transcript counts within a gene's coding sequence normalized to mRNA abundance (43). We identified 22 genes at pH 5.8 and 89 genes at pH 4.4, which displayed significantly altered TEs (absolute \log_2 TE fold change ≥ 1 and P -adjust ≤ 0.05) (Table S4). The highest increase in TE at pH 4.4 was found for the KpLE2 phage-like element (*topAI*), a hydroxyethylthiazole kinase (*thiM*), and a palmitoleoyl acyltransferase (*lpxP*). In contrast, *yecH* and *yjbE*, both encoding uncharacterized proteins, and *malM* of the maltose regulon showed the most prominent decrease in TE at pH 4.4 (Table S4). At pH 5.8, we noted the largest increase in TE for a ferredoxin-type protein encoded by *napF*, an iron transport protein (*feoA*), and a tagaturonate reductase (*uxaB*). Conversely, the largest decrease was observed for a protein of the fructose-specific phosphotransferase system (*fruA*), a tripartite efflux pump membrane fusion protein (*emrK*), and an HTH-type transcriptional regulator (*ydeO*) (Table S4).

In summary, besides extensive transcriptional reprogramming, dozens of genes exhibit significant FCs either at the transcriptional or translational level in response to acid stress. This underlines that transcription and translation are not always coupled in bacteria. Similar findings were reported by Zhang and colleagues (41), who conducted Ribo-Seq and RNA-Seq analyses for *E. coli* under heat stress (41). Overall, such differential regulation can be explained, for example, by delayed translation relative to transcript synthesis, selective recruitment or release of ribosomes, or regulation during translation initiation, elongation, or ribosome biogenesis (45–49), which could be beneficial under stress conditions.

Functional implications of genes with differential mRNA and RPF levels under mild acid stress

To obtain a more profound understanding of the fine-tuned response of *E. coli* to different degrees of acid stress, we first analyzed all genes with differential mRNA and ribosome coverage levels during mild acid stress (pH 5.8). Under this condition, the top candidates with the highest FC values for mRNA and RPF are as follows: (i) the *cad* operon, encoding the core components of the Cad AR system (see also below); (ii) the *glp* regulon, responsible for glycerol and *sn*-glycerol 3-phosphate uptake and catabolism (50); (iii) the *mdtJI* operon, encoding a heterodimeric multidrug/spermidine exporter (51); and (iv) genes encoding proteins involved in motility and flagella biosynthesis (Table 1). A comprehensive list of normalized read counts, mRNA and RPF FCs, and TEs for all *E. coli* genes is provided in Table S5. We tested a representative selection of differentially expressed genes by RT-qPCR. In all cases, the detected changes in mRNA levels were consistent with the data gathered by RNA-Seq (Fig. S6A). Both *recA* and *secA* were chosen as reference genes for RT-qPCR because their rpkM counts were relatively constant under the conditions tested (Table S5; Fig. S6B).

Next, we performed gene set enrichment analysis (GSEA) using *clusterProfiler* (52) to identify biological processes associated with differentially expressed genes at pH 5.8. Among the most enriched Gene Ontology (GO) terms for biological processes at pH 5.8 was “spermidine transmembrane transport” (Fig. 3), which corresponds to the induction of *mdtJI* (Table 1) and a polyamine ABC transporter encoded by *potABCD* (Table S5). Polyamines are crucial for survival under acid stress, as they reduce membrane permeability by blocking OmpF and OmpC porins (53–55). External spermidine supplementation also improved acid resistance in *Streptococcus pyogenes* (56). On the other hand, overaccumulation of polyamines can be toxic and potentially lethal for *E. coli* (51, 57). Therefore, precise transmembrane transport of polyamines in acidic environments is critical and contributes to survival in acidic conditions.

TABLE 1 Top 20 genes with increased RPF levels at pH 5.8 compared to pH 7.6, sorted in descending order by Ribo-Seq log₂ FC values^a

Gene name	Log ₂ FC (Ribo)	P-adjust (Ribo)	Log ₂ FC (RNA)	P-adjust (RNA)	Cellular location	Annotation
<i>glpA</i>	8.05	1 × 10 ⁻¹⁵⁹	6.26	2 × 10 ⁻³⁸	C	Anaerobic glycerol-3-phosphate dehydrogenase subunit A
<i>glpB</i>	7.89	2 × 10 ⁻¹⁴¹	5.77	6 × 10 ⁻²⁹	C	Anaerobic glycerol-3-phosphate dehydrogenase subunit B
<i>cadA</i>	7.61	2 × 10 ⁻¹⁴⁴	7.44	3 × 10 ⁻⁵⁷	C	Lysine decarboxylase 1
<i>glpC</i>	7.16	5 × 10 ⁻⁸⁹	5.67	4 × 10 ⁻³⁵	C, IM	Anaerobic glycerol-3-phosphate dehydrogenase subunit C
<i>cadB</i>	6.86	8 × 10 ⁻⁹⁶	6.85	5 × 10 ⁻³⁵	IM	Lysine:cadaverine antiporter
<i>glpT</i>	6.84	2 × 10 ⁻¹⁰⁵	6.28	2 × 10 ⁻³⁹	IM	sn-Glycerol 3-phosphate:phosphate antiporter
<i>glpD</i>	6.72	4 × 10 ⁻¹²⁶	6.00	2 × 10 ⁻⁵²	C, IM	Aerobic glycerol 3-phosphate dehydrogenase
<i>mdtJ</i>	6.65	2 × 10 ⁻⁶⁷	5.67	6 × 10 ⁻³⁶	IM	Multidrug/spermidine efflux pump membrane subunit MdtJ
<i>glpQ</i>	6.11	2 × 10 ⁻⁸⁹	5.31	2 × 10 ⁻²⁹	P	Glycerophosphoryl diester phosphodiesterase
<i>mdtI</i>	5.93	3 × 10 ⁻⁴⁹	5.60	9 × 10 ⁻³⁴	IM	Multidrug/spermidine efflux pump membrane subunit MdtI
<i>glpF</i>	5.10	7 × 10 ⁻⁶⁴	5.26	1 × 10 ⁻¹⁹	IM	Glycerol facilitator
<i>yfdX</i>	4.89	2 × 10 ⁻²⁴	5.23	4 × 10 ⁻²⁵	P	Protein YfdX
<i>frc</i>	4.78	1 × 10 ⁻³⁶	4.01	2 × 10 ⁻¹⁵	C	Formyl-CoA transferase
<i>glpK</i>	4.62	9 × 10 ⁻⁵⁴	4.10	1 × 10 ⁻²⁵	C	Glycerol kinase
<i>yfdV</i>	4.40	3 × 10 ⁻¹⁸	4.58	1 × 10 ⁻¹²	IM	Putative transport protein YfdV
<i>oxc</i>	4.28	2 × 10 ⁻²⁸	3.75	1 × 10 ⁻¹⁴	C	Xalyl-CoA decarboxylase
<i>figC</i>	3.41	3 × 10 ⁻²²	2.95	3 × 10 ⁻⁹	P	Flagellar basal-body rod protein FigC
<i>figB</i>	3.40	1 × 10 ⁻²⁴	3.09	1 × 10 ⁻¹⁰	P	Flagellar basal-body rod protein FigB
<i>dhaL</i>	3.39	9 × 10 ⁻¹³	3.08	1 × 10 ⁻¹⁰	C	Dihydroxyacetone kinase subunit L
<i>figD</i>	3.33	7 × 10 ⁻²⁵	2.90	5 × 10 ⁻⁹	C	Flagellar biosynthesis, initiation of hook assembly

^aC, cytosol; P, periplasm; IM, inner membrane.

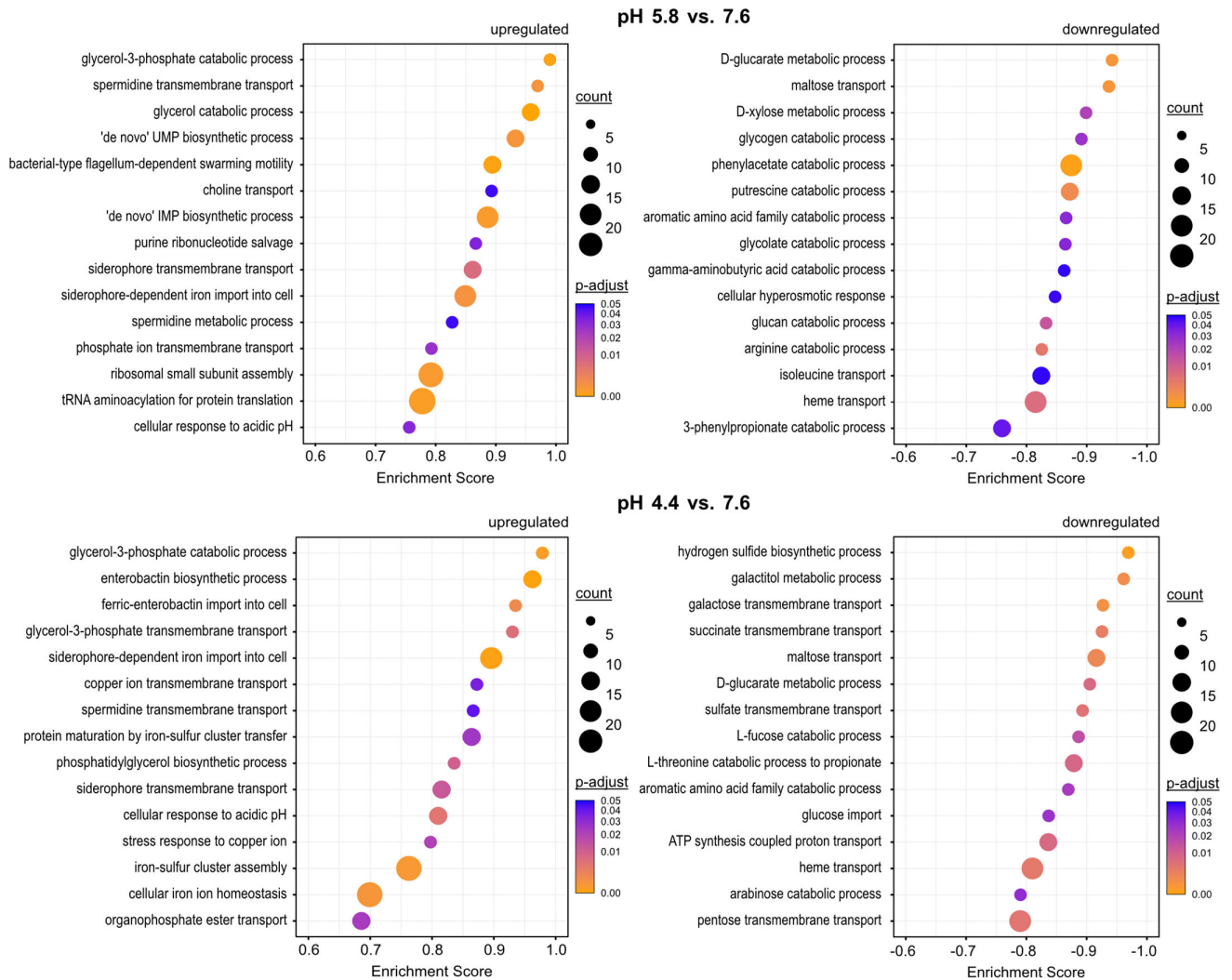


FIG 3 Up- and downregulated biological processes in *E. coli* at pH 5.8 and 4.4. GSEA was conducted using the *gseGO* function in the *clusterProfiler* package (52) with the ribosome profiling differential expression data sorted by \log_2 fold change values as input. GO terms were considered up- or downregulated if *P*-adjust values were ≤ 0.05 . The top 15 non-redundant GO terms were sorted in descending order by the *clusterProfiler* enrichment score and are shown for pH 5.8 vs 7.6 and pH 4.4 vs 7.6. The dot size represents the number of genes associated with each GO term, and the dot color represents adjusted *P*-values corrected for the false discovery rate.

The enrichment of the GO terms “glycerol-3-phosphate catabolic process” and “glycerol catabolic process” at pH 5.8 (Fig. 3) has not yet been associated with acid stress to our knowledge. Notably, of the 14 genes with the largest increase in RPF counts at pH 5.8, 7 belong to the *glp* regulon (Table 1). This regulon is required for the uptake and catabolism of glycerol and *sn*-glycerol 3-phosphate (G3P) (50). In this pathway, G3P is converted to dihydroxyacetone phosphate by membrane-bound dehydrogenases, either aerobically via GlpD or anaerobically by the GlpABC complex (58, 59). Alternatively, dihydroxyacetone phosphate can be produced directly from glycerol by GldA and the protein products of the *dhaKLM* operon (60). The *dhaKLM* operon was also induced at pH 5.8 (Table S5). It remains unclear whether glycerol and G3P catabolism directly contribute to acid tolerance or whether the *glp* regulon is activated as a consequence of other low pH adjustments. Expression of *glp* genes is regulated by the repressor GlpR, which is inactivated upon binding of glycerol or G3P (61). We hypothesize that changes in phospholipid composition under acid stress conditions (62) may release G3P, which in

turn induces the *glp* regulon. Accordingly, the GO term “phosphatidylglycerol biosynthetic process” was enriched under acid stress (Fig. 3).

Another observation is the upregulation of *de novo* biosynthesis pathways for pyrimidine and purine nucleotides at pH 5.8 (Fig. 3). The induction of a large proportion of the PurR-dependent regulon involved in *de novo* nucleotide synthesis (Fig. 3; Table S5) suggests that *E. coli* requires additional nucleotides to cope with the extensive transcriptional reprogramming. Besides, intracellular acidification can lead to DNA damage, such as depurination (63), making enhanced nucleotide biosynthesis a critical compensatory mechanism. Recently, *Oenococcus oeni* was reported to experience a decrease in the abundance of both purines and pyrimidines under acid stress, while nucleotide metabolism and transport increased (64), suggesting a similar phenomenon in this species. Other enriched GO terms under mild acid stress include “choline transport,” “siderophore transmembrane transport,” “phosphate ion transmembrane transport,” “ribosomal small subunit assembly,” “tRNA aminoacylation for protein translation,” and “bacterial-type flagellum-dependent swarming motility” (Fig. 3). pH-dependent motility has previously been observed in *E. coli*, *Salmonella*, and *Helicobacter* (1). These observations suggest that bacterial cells use an escape strategy to migrate to more favorable pH environments when challenged with acidic conditions.

On the contrary, our findings reveal that many membrane and periplasmic proteins (18 of the 20 genes with the most diminished RPF counts, Table 2) were among the top candidates with decreased mRNA and RPF levels under mild acid stress. This affected, for example, genes encoding ABC transporters (*mal* regulon, *dpp* operon) and symporters (*actP*, *melB*, *gabP*), highlighting the superiority of Ribo-Seq over mass spectrometry-based approaches, namely, its independence of protein biochemistry and higher sensitivity (29). Furthermore, GSEA identified membrane transport and metabolic activities as the most downregulated biological processes in response to mild acid stress. For example, “maltose transport,” “isoleucine transport,” “heme transport,” “putrescine catabolic process,” “glycolate catabolic process,” and “aromatic amino acid family catabolic process” were among the most downregulated GO terms at pH 5.8 (Fig. 3). Downregulation of H⁺-coupled transport processes represents a key mechanism by which *E. coli* restricts proton influx into cells. In addition, the downregulated metabolic processes are in many cases associated with the synthesis and conversion of amino acids and carbon sources. For example, the catabolism of aromatic amino acids and arginine was also reduced at pH 5.8 (Fig. 3). Particularly noteworthy is the downregulation of the arginine catabolic pathway, which involves the protein products of the *astEBDAC* operon. At pH 5.8, hardly any reads were mapped in the *astEBDAC* region, despite detectable expression at pH 7.6 and pH 4.4 (Table S5). Presumably, *E. coli* preserves the intracellular arginine pool at pH 5.8, as this amino acid serves as a substrate for the Adi system during severe acid stress (15, 65).

In summary, the response of *E. coli* to mild acid stress is characterized by the activation of the motility machinery to escape to less acidic habitats, by induction of the *cad* operon, and by genes involved in polyamine transport and glycerol-3-phosphate conversion (Tables 1 and 2; Fig. 3). In addition, *E. coli* restricts the influx of protons and conserves energy by reducing its metabolic activities.

Functional implications of genes with differential mRNA and RPF levels under severe acid stress

Next, we analyzed genes with differential mRNA and ribosome coverage levels in response to severe acid stress (pH 4.4) compared with non-stress (pH 7.6). Genes with the highest number of increased read counts, which were not already upregulated at pH 5.8, were *asr*, encoding an acid shock protein, followed by *bdm*, encoding a biofilm-modulation protein, and *bhsA*, encoding a multiple stress resistance outer membrane protein (Table 3). Originally, *Asr* was classified as a periplasmic acid shock protein, although its role in acid adaptation remained unclear (66). Recently, *Asr* was shown to be an intrinsically disordered chaperone that contributes to outer membrane integrity and to

TABLE 2 Top 20 genes with decreased RPF levels at pH 5.8 compared to pH 7.6, sorted in ascending order by Ribo-Seq log₂ FC values^a

Gene name	Log ₂ FC (Ribo)	P-adjust (Ribo)	Log ₂ FC (RNA)	P-adjust (RNA)	Cellular location	Annotation
<i>yjch</i>	-5.59	3 × 10 ⁻²⁷	-3.14	1 × 10 ⁻⁸	IM	Conserved inner membrane protein Yjch
<i>actP</i>	-4.63	2 × 10 ⁻⁴⁷	-3.58	1 × 10 ⁻¹¹	IM	Acetate/glycolate:cation symporter
<i>lamB</i>	-4.32	3 × 10 ⁻⁵	-2.27	6 × 10 ⁻⁶	OM	Maltose outer membrane channel/phage lambda receptor protein
<i>dppD</i>	-4.23	5 × 10 ⁻³³	-3.79	9 × 10 ⁻¹⁵	IM	Dipeptide ABC transporter ATP-binding subunit DppD
<i>acs</i>	-4.06	3 × 10 ⁻²⁰	-2.60	3 × 10 ⁻⁶	C	Acetyl-CoA synthetase (AMP-forming)
<i>malK</i>	-3.96	2 × 10 ⁻¹⁸	-2.64	2 × 10 ⁻¹⁰	IM	Maltose ABC transporter ATP-binding subunit
<i>dppC</i>	-3.83	1 × 10 ⁻²⁸	-3.78	5 × 10 ⁻¹³	IM	Dipeptide ABC transporter membrane subunit DppC
<i>malG</i>	-3.82	5 × 10 ⁻²⁰	-2.52	4 × 10 ⁻⁷	IM	Maltose ABC transporter membrane subunit MalG
<i>dppF</i>	-3.75	4 × 10 ⁻³⁴	-3.93	4 × 10 ⁻¹⁸	IM	Dipeptide ABC transporter ATP-binding subunit DppF
<i>dppB</i>	-3.74	1 × 10 ⁻³¹	-3.74	1 × 10 ⁻¹⁶	IM	Dipeptide ABC transporter membrane subunit DppB
<i>malM</i>	-3.69	7 × 10 ⁻⁵	-2.06	2 × 10 ⁻⁶	P	Maltose regulon periplasmic protein
<i>melB</i>	-3.60	6 × 10 ⁻²⁸	-1.24	0.03	IM	Melibiose:H ⁺ /Na ⁺ /Li ⁺ symporter
<i>ycdT</i>	-3.59	2 × 10 ⁻²⁷	-3.61	1 × 10 ⁻¹⁰	IM	Putative ABC transporter ATP-binding protein YcdT
<i>ycdS</i>	-3.57	1 × 10 ⁻³¹	-4.05	9 × 10 ⁻¹⁵	IM, P	Putative ABC transporter periplasmic-binding protein/polyhydroxybutyrate synthase
<i>gabP</i>	-3.56	5 × 10 ⁻¹⁹	-2.76	9 × 10 ⁻⁸	IM	4-Aminobutyrate:H ⁺ symporter
<i>ycdV</i>	-3.48	1 × 10 ⁻²³	-3.39	1 × 10 ⁻⁸	IM	Putative ABC transporter membrane subunit YcdV
<i>ydhY</i>	-3.44	5 × 10 ⁻¹⁶	-0.40	0.23	IM	Putative 4Fe-4S ferredoxin-type protein
<i>gudP</i>	-3.42	5 × 10 ⁻²¹	-3.50	4 × 10 ⁻⁷	IM	Galactarate/glucarate/glycerate transporter GudP
<i>astE</i>	-3.34	2 × 10 ⁻¹⁵	-3.47	1 × 10 ⁻⁵	C	Succinylglutamate desuccinylase
<i>malE</i>	-3.32	1 × 10 ⁻¹²	-2.52	1 × 10 ⁻⁹	IM, P	Maltose ABC transporter periplasmic-binding protein

^aC, cytosol; P, periplasm; IM, inner membrane; OM, outer membrane.

TABLE 3 Top 20 genes with increased RPF levels at pH 4.4 compared to pH 7.6, sorted in descending order by Ribo-Seq log₂ FC values^a

Gene name	Log ₂ FC (Ribo)	P-adjust (Ribo)	Log ₂ FC (RNA)	P-adjust (RNA)	Cellular location	Annotation
<i>asr</i>	9.68	1 × 10 ⁻²¹⁴	9.37	2 × 10 ⁻⁵²	P	Acid shock protein
<i>cadA</i>	9.40	8 × 10 ⁻¹⁸⁶	9.39	5 × 10 ⁻⁹²	C	Lysine decarboxylase 1
<i>ydgU</i>	9.22	5 × 10 ⁻³⁵	12.39	3 × 10 ⁻¹⁶	IM	Uncharacterized protein YdgU
<i>yhcN</i>	8.32	5 × 10 ⁻¹²⁵	9.08	3 × 10 ⁻⁹⁴	P	DUF1471 domain-containing stress-induced protein YhcN
<i>bdm</i>	7.85	4 × 10 ⁻⁷¹	7.62	1 × 10 ⁻⁴⁷	C	Biofilm-dependent modulation protein
<i>cadB</i>	7.78	2 × 10 ⁻¹⁰⁸	8.90	2 × 10 ⁻⁵¹	IM	Lysine:cadaverine antiporter
<i>yjcB</i>	7.73	4 × 10 ⁻⁴⁵	5.92	6 × 10 ⁻²³	IM	Uncharacterized protein YjcB
<i>mdtJ</i>	7.45	2 × 10 ⁻⁵⁸	4.62	1 × 10 ⁻²³	IM	Multidrug/spermidine efflux pump membrane subunit MdtJ
<i>bhsA</i>	7.12	3 × 10 ⁻¹¹⁰	7.96	2 × 10 ⁻⁵⁴	OM	DUF1471 domain-containing multiple stress resistance outer membrane protein BhsA
<i>glpD</i>	7.06	2 × 10 ⁻¹²²	6.48	8 × 10 ⁻⁴⁸	C, IM	Aerobic glycerol 3-phosphate dehydrogenase
<i>azuC</i>	6.83	5 × 10 ⁻²⁴	8.17	1 × 10 ⁻²⁶	IM	Uncharacterized protein AzuC
<i>nrdH</i>	6.60	2 × 10 ⁻³⁰	6.46	1 × 10 ⁻²⁹	C	Glutaredoxin-like protein
<i>yedR</i>	6.35	2 × 10 ⁻²¹	5.30	8 × 10 ⁻²⁰	IM	Putative inner membrane protein
<i>yhdV</i>	6.18	4 × 10 ⁻³⁵	6.43	3 × 10 ⁻¹⁸	IM	Lipoprotein YhdV
<i>nrdI</i>	6.12	3 × 10 ⁻⁴²	6.03	3 × 10 ⁻²⁸	C	Dimanganese-tyrosyl radical cofactor maintenance flavodoxin NrdI
<i>ybiJ</i>	5.94	6 × 10 ⁻⁵⁴	4.56	2 × 10 ⁻²¹	P	DUF1471 domain-containing protein YbiJ
<i>fhuF</i>	5.92	9 × 10 ⁻³⁸	4.55	8 × 10 ⁻²¹	C	Hydroxamate siderophore iron reductase
<i>ycgZ</i>	5.73	3 × 10 ⁻⁵⁰	5.04	6 × 10 ⁻¹⁹	C	Putative two-component system connector protein YcgZ
<i>mdtI</i>	5.72	7 × 10 ⁻³¹	4.25	7 × 10 ⁻¹⁸	IM	Multidrug/spermidine efflux pump membrane subunit MdtI
<i>ycfJ</i>	5.15	7 × 10 ⁻⁴⁸	5.03	1 × 10 ⁻¹⁷	IM	PF05433 family protein YcfJ

^aC, cytosol; P, periplasm; IM, inner membrane; OM, outer membrane.

act as an aggregase in order to prevent aggregation of proteins with positive charges (67). Our Ribo-seq data clearly illustrate the enormous importance of *Asr* under severe acid stress in *E. coli*, as it is one of the most abundant proteins in the cell, with approximately 2% of all reads mapping in the *asr* coding region at pH 4.4 (corresponding to an ~1,000-fold upregulation compared to pH 7.6). Strikingly, almost half of the top 20 genes with increased ribosome coverage of transcripts (*ydgU*, *yhcN*, *yjcB*, *yedR*, *yhdV*, *ybiJ*, *ycgZ*, and *ycfJ*) are poorly characterized (Table 3). So far, only *YhcN* from the above list has been shown to be involved in the response to acid stress (68).

GSEA for biological processes identified the GO terms “enterobactin biosynthetic process,” “ferric-enterobactin import into cell,” “siderophore-dependent iron import into cell,” and “siderophore transmembrane transport” as significantly enriched at pH 4.4 (Fig. 3). Specifically, the complete enterobactin biosynthesis pathway, comprising the *entCEBAH* operon, *entF*, *entH*, and *ybdZ*, revealed significant enrichment under severe acidic conditions (Table S5). Furthermore, all subunits of the Ton complex (*tonB*, *exbB*, *exbD*) and its putative outer membrane receptor encoded by *yncD* exhibited significantly higher RPF and mRNA levels at pH 5.8 and pH 4.4 (Table S5). The Ton complex functions as a proton motive force-dependent molecular motor that facilitates the import of iron-bound siderophores (69, 70). Several other iron uptake systems, including a ferric dicitrate ABC transport system (*fecABCDE*), an iron (III) hydroxamate ABC transport system (*fhuACDB*), a ferric enterobactin ABC transport system (*fepA*, *fepB*, *fepCGD*), and a TonB-dependent iron-catecholate outer membrane transporter (*cirA*), were also induced under acidic conditions (Table S5). Moreover, the GO terms “protein maturation by iron-sulfur cluster assembly” and “iron-sulfur cluster assembly” were enriched at pH 4.4

(Fig. 3). Specifically, we detected a fivefold upregulation of all genes of the *isc* and *suf* operons (Table S5), which encode components of the complex machinery responsible for iron-sulfur cluster assembly in *E. coli* (71). In contrast, heme transport was among the most downregulated biological processes at both pH 5.8 and 4.4 (Fig. 3), which could potentially be the cause of iron limitation. Moreover, at low pH, the solubility of iron ions increases, which can destabilize iron-sulfur clusters (72). The iron limitation would be consistent with our data that *E. coli* upregulates the synthesis of iron-chelating siderophores and their transporters, as well as the components of the iron-sulfur assembly machinery. Given the better solubility of iron in a low pH environment, the question arises whether *E. coli* synthesizes siderophores to respond to iron limitation, or rather, protects itself against an iron excess. The latter function has been demonstrated for *Pseudomonas aeruginosa*, where siderophores protected cells from the harmful effects of reactive oxygen species. In this case, *P. aeruginosa* no longer secreted siderophores into the extracellular environment but instead stored them intracellularly (73). In conclusion, these results prompt the question of whether the upregulation of the iron uptake machinery counteracts iron limitation or rather provides protection against iron excess under severe acid stress.

We also detected a significant enrichment for the GO terms “cellular response to acidic pH,” “stress response to copper ion,” and “copper ion transmembrane transport” at pH 4.4 (Fig. 3). These results are in line with previous studies that have suggested an interplay between resistance to copper and acid stress in *Escherichia coli* (74, 75). This overlap between the two stress responses is further emphasized by our findings because at pH 4.4, substantial upregulation of the Cu⁺-exporting ATPase CopA and CusA, a component of the copper efflux system, was detected (Table S5). These results are of important physiological relevance, given that copper is an important antibacterial component in the innate immune system (76, 77).

Among the downregulated genes at pH 4.4, the *tnaAB* operon and its leader peptide (*tnaC*) showed the most significant decrease in terms of RPF counts (Table 4). *tnaA* encodes a tryptophanase, which cleaves L-tryptophan into indole, pyruvate, and NH₄⁺, whereas *tnaB* encodes a tryptophan:H⁺ symporter (78). This finding is particularly intriguing because, in a previous study, persister cell formation in *E. coli* was related to a lower cytoplasmic pH associated with tryptophan metabolism (79). It is important to note that we also detected a substantial upregulation in RPFs for *hipA* (Table S5), which encodes a serine/threonine kinase that plays a role in persistence in *E. coli* (80). Therefore, our data provide further evidence for the link between internal pH and persistence.

The expression of several outer membrane proteins and porins (*ompW*, *ompF*, *nmpC*, *lamB*) was also downregulated at pH 4.4 (Table 4). This observation is consistent with the extensive restructuring of the *E. coli* lipid bilayers to reduce membrane permeability and limit proton entry. Similar to pH 5.8, the majority of the 20 proteins with the most reduced RPF levels compared with physiological pH are membrane proteins (Table 4). Moreover, the GO term “ATP synthesis coupled proton transport” was significantly reduced at pH 4.4 (Fig. 3). This is explained by the reduction in RPF levels of genes encoding subunits of the F₀F₁-ATPase (Table S5). F₀F₁-ATPase uses the electrochemical gradient of protons to synthesize adenosine 5'-triphosphate (ATP) from ADP and inorganic phosphate but can also hydrolyze ATP to pump protons out of the cytoplasm (81, 82). As at pH 5.8, the most downregulated biological processes at pH 4.4 were almost exclusively GO terms related to transport and cellular metabolism (Fig. 3).

In summary, the response of *E. coli* to severe acid stress is dominated by the activation of survival strategies that limit the entry of protons into the cell, prevent protein aggregation, and maintain iron homeostasis. Severe acid stress leads to a reduction in metabolic, transcriptional, and translational activity, thereby preparing *E. coli* for a dormant state. Eventually, these dormant cells may be able to withstand antibiotic attack (i.e., persister cells).

TABLE 4 Top 20 genes with decreased RPF levels at pH 4.4 compared to pH 7.6, sorted in ascending order by Ribo-Seq log₂ FC values^a

Gene name	Log ₂ FC (Ribo)	P-adjust (Ribo)	Log ₂ FC (RNA)	P-adjust (RNA)	Cellular location	Annotation
<i>tnaC</i>	-6.82	4 × 10 ⁻³⁹	-6.18	5 × 10 ⁻²⁷	C	<i>tnaAB</i> operon leader peptide
<i>tnaA</i>	-6.53	6 × 10 ⁻⁷	-6.15	1 × 10 ⁻³⁴	C	Tryptophanase
<i>tnaB</i>	-6.40	6 × 10 ⁻⁴⁷	-5.40	6 × 10 ⁻²⁶	IM	Tryptophan:H ⁺ symporter TnaB
<i>mgIB</i>	-6.31	7 × 10 ⁻⁵¹	-4.08	1 × 10 ⁻¹⁷	IM, P	D-galactose/methyl-galactoside ABC transporter periplasmic-binding protein
<i>ompW</i>	-6.21	1 × 10 ⁻³⁹	-4.83	2 × 10 ⁻¹³	OM	Outer membrane protein W
<i>nmpC</i>	-6.05	3 × 10 ⁻⁶²	-3.87	1 × 10 ⁻¹⁷	OM	DLP12 prophage; putative outer membrane porin NmpC
<i>treB</i>	-5.94	3 × 10 ⁻⁶²	-4.57	3 × 10 ⁻²⁶	IM	Trehalose-specific PTS enzyme IIBC component
<i>borD</i>	-5.92	1 × 10 ⁻²⁵	-3.36	5 × 10 ⁻⁹	IM	DLP12 prophage; prophage lipoprotein BorD
<i>garP</i>	-5.86	4 × 10 ⁻⁴⁷	-5.10	1 × 10 ⁻¹⁶	IM	Galactarate/glucarate/glycerate transporter GarP
<i>tdcA</i>	-5.84	9 × 10 ⁻³²	-1.27	4 × 10 ⁻³	C	DNA-binding transcriptional activator TdcA
<i>lamB</i>	-5.79	2 × 10 ⁻⁵⁴	-2.60	4 × 10 ⁻⁸	OM	Maltose outer membrane channel/phage lambda receptor protein
<i>malK</i>	-5.65	2 × 10 ⁻⁷⁰	-2.14	7 × 10 ⁻⁵	IM	Maltose ABC transporter ATP-binding subunit
<i>ompF</i>	-5.59	1 × 10 ⁻⁶³	-4.03	6 × 10 ⁻²⁰	OM	Outer membrane porin F
<i>garD</i>	-5.54	3 × 10 ⁻⁴²	-3.12	2 × 10 ⁻⁶	C	Galactarate dehydratase
<i>nrfB</i>	-5.47	4 × 10 ⁻²⁴	-2.36	1 × 10 ⁻³	P	Periplasmic nitrite reductase penta-heme c-type cytochrome
<i>xyfJ</i>	-5.46	3 × 10 ⁻²²	-4.54	3 × 10 ⁻¹⁶	IM, P	Xylose ABC transporter periplasmic-binding protein
<i>malM</i>	-5.38	3 × 10 ⁻⁶⁵	-1.93	7 × 10 ⁻⁵	P	Maltose regulon periplasmic protein
<i>treC</i>	-5.38	1 × 10 ⁻⁴⁴	-4.47	3 × 10 ⁻²³	C	Trehalose-6-phosphate hydrolase
<i>malE</i>	-5.31	8 × 10 ⁻³⁵	-2.53	2 × 10 ⁻⁸	IM, P	Maltose ABC transporter periplasmic-binding protein
<i>ydeN</i>	-5.31	2 × 10 ⁻⁴⁹	-5.05	5 × 10 ⁻³⁰	P	Putative sulfatase

^aC, cytosol; P, periplasm; IM, inner membrane; OM, outer membrane.

Expanding the regulatory network of enzyme-based H⁺-consuming acid resistance systems

Recently, we have shown that the Adi and Cad AR systems are mutually exclusively activated in individual *E. coli* cells, indicating functional diversification and division of labor under acid stress (15). To gain further insights into the fine-tuned regulation of the three major AR systems, we first studied the mRNA and RPF levels of known enzyme-based H⁺-consuming AR components. The core components of the Gad system (AR2) (*gadA*, *gadB*, and *gadC*) and several transcriptional components (*gadW*, *gadX*, *gadY*, *phoP*, *phoQ*) showed an increase in mRNA and RPF levels by approximately two- to sixfold at pH 4.4, but not at pH 5.8, whereas the expression of *ydeO* was massively induced at pH 5.8 (particularly at the mRNA level), and RPF levels were decreased at pH 4.4 (Fig. S7). Expression of the core components of the Adi system (AR3), *adiA* and *adiC*, was induced at severe acid stress but not at pH 5.8, consistent with our previous study (15). Upregulation was not detected for regulatory components of the Adi system. A novel finding was that the levels of *adiA* but not *adiC* were significantly higher in the Ribo-Seq data than in the RNA-Seq data (Fig. S7). In fact, *adiA* had the sixth highest increase in TE among all *E. coli* genes at pH 4.4 (Table S4), indicating translational regulation by a thus far unknown mechanism. The only other component of an AR system in *E. coli*, known to be subject to translational regulation, is the major regulator CadC of the Cad (AR4) system. CadC contains a polyproline motif, and its translation therefore depends on the elongation factor P, a process that keeps the copy number of CadC extremely low (83). As expected, expression of the core components of the Cad system (AR4), *cadA* and *cadB*, was tremendously increased at both pH 5.8 and 4.4. Genes of the Orn system (AR5) were not induced in our experimental setup (Fig. S7).

Next, we analyzed the mRNA and RPF levels of all annotated TFs to search for other potential TFs involved in the acid stress response of *E. coli* (Fig. 4A and B). At pH 5.8, YdeO showed by far the strongest induction at the transcriptional and translational levels, but for all other TFs, the expression levels hardly changed (Fig. 4A). At pH 4.4, the expression of numerous TFs was induced, including GadW, YdcI, and the antibiotic resistance-controlling regulator MarR. The strongest upregulation was found for the lclR-type regulator MhpR and the iron-sulfur cluster-containing regulator IscR (Fig. 4B). Notably, while most acid-induced TFs were differentially expressed and displayed constant TE, YdcI exhibited constant mRNA levels but was differentially translated in response to acid stress (Fig. 4B). The contribution of all TFs with high FC values to survival under acid stress (Table S6) was tested in an acid shock assay. Cells of the corresponding knockout mutants (84) and, for comparison, the *rcsB* and *gadE* mutants (each lacking a TF important for acid resistance) were exposed to pH 3 for 1 h. All mutants except *marR* and *ydeO* showed significantly reduced survival compared to the parental strain (Fig. 4C). For *ydeO*, this result was consistent with our finding that transcript abundance and occupancy with ribosomes were upregulated at mild but not severe acid stress (Fig. 4; Fig. S7). Thus, YdeO appears to be only crucial under mild acid stress (Fig. 4A). In contrast, the *mhpR* mutant had a low survival rate comparable to that of *rcsB* and *gadE*, and the survival rates of the *iscR*, *ydcl*, and *gadW* mutants were only slightly higher (Fig. 4C). These results confirm the physiological relevance of these TFs for acid resistance. As controls, we re-introduced the corresponding genes *in trans* using isopropyl- β -D-thiogalactopyranosid (IPTG)-inducible pCA24N plasmids from the ASKA collection (85). Complementation of the *mhpR*, *iscR*, *ydcl*, and *gadW* mutants, as well as *rcsB* and *gadE* controls, resulted in strains with survival rates comparable to the wild-type (WT) strain carrying the pCA24N control vector (Fig. S8).

Subsequently, we tested whether these TFs are involved in the regulation and interconnectivity of the Gad, Adi, and Cad systems. Therefore, we examined the promoter activities of *gadBC*, *adiA*, and *cadBA* in the corresponding knockout mutants (84) using transcriptional reporter plasmids (promoter-*lux* fusions). The cultivation conditions were the same as those used for Ribo-Seq and RNA-Seq (Fig. 1A), and luciferase activity was monitored during growth in microtiter plates. We found that YdcI significantly

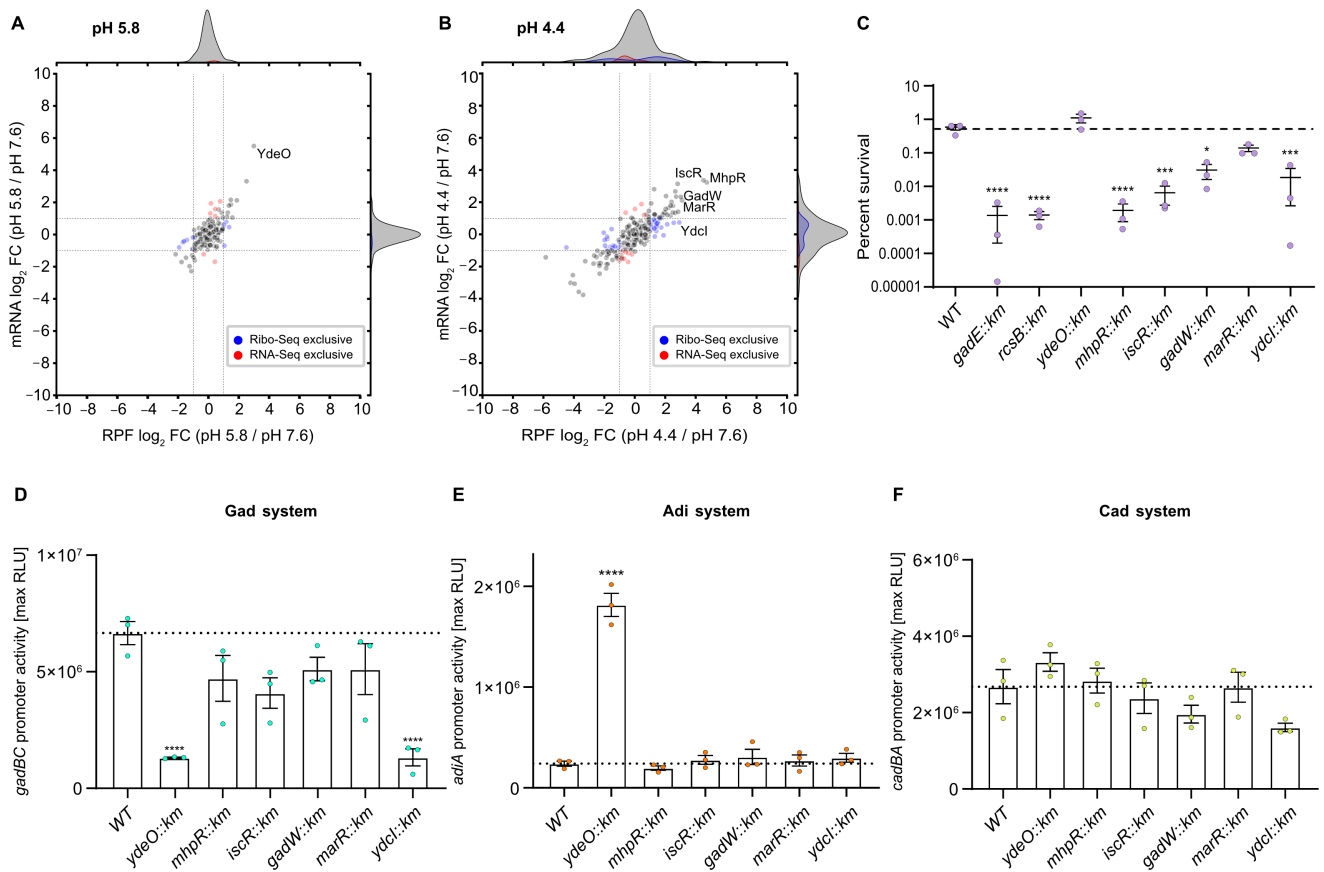


FIG 4 Contribution of TFs to survival and AR induction under acid stress. Comparison of global RPF and mRNA log₂ FC values of transcriptional regulators for (A) pH 5.8 vs pH 7.6 and (B) pH 4.4 vs pH 7.6. Dashed lines indicate log₂ fold changes of +1 or -1. Changes detected exclusively by either RNA-Seq (red dots) or Ribo-Seq (blue dots) are colored. TFs described in panels C-F are highlighted. (C) Acid shock assay to test the survival of *E. coli* BW25113 (WT) and the indicated mutants (84). Cells were grown in LB pH 7.6 to OD₆₀₀ = 0.5. The cultures were split and then either grown at pH 7.6 or stepwise stressed (15 min pH 5.8, 15 min pH 4.4) before being exposed to LB pH 3 for 1 h. Colony-forming units were counted, and the ratio of surviving cells was calculated. The dashed line indicates the average percentage of surviving WT cells. (D through F) Luciferase-based promoter assays. WT and the indicated mutants were transformed either with plasmid pBBR1-P*gadBC::lux* (D), pBBR1-P*adiA::lux* (E), or pBBR1-P*cadBA::lux* (F) and grown in LB medium (pH 7.6) until OD₆₀₀ = 0.5. The medium pH was then adjusted to 5.8 to induce the Cad system or to pH 4.4 to induce the Adi and Gad systems. Luminescence and growth were determined every 10 min in microtiter plates using a CLARIOstar plus plate reader (BMG Labtech). Data are reported as relative light units (RLUs) in counts per second per OD₆₀₀, with maximal RLU shown. Dashed lines indicate the average maximal RLU values of the WT. C-F, All experiments were performed in biological replicates (*n* = 3), and error bars represent standard deviations of the mean. Analysis of variance, followed by Bonferroni's multiple comparisons test, was used to compare log-transformed max. RLU values between mutant strains and the wild type (BW25113) (**P* ≤ 0.05, ****P* ≤ 0.001, *****P* ≤ 0.0001).

affected the promoter activity of *gadBC* (Fig. 4D). Although the LysR-type regulator YdcI has been shown to affect pH stress regulation in *Salmonella enterica* serovar Typhimurium and *E. coli*, its precise role is still unclear (86–88). Based on the data presented here, we hypothesize that the decreased survival of the *ydcI* mutant under severe acid stress is due to decreased expression of the Gad system. The absence of YdeO resulted in an eightfold stimulation of the *adiA* promoter activity (Fig. 4E). Thus, YdeO not only activates the Gad system (89) but also appears to be a repressor for the Adi system. This implies that the Adi system is regulated not only by the XylS/AraC-type regulator AdiY but also by YdeO. Thus, YdeO is the first example of a transcriptional activator shown to be involved in the regulation of more than one AR system in *E. coli* and might play a role in the heterogeneous activation of the Adi and Gad systems within a population. Although we observed a slight decrease in *cadBA* promoter activity in the *ydcI* mutant, the decrease was not statistically significant. Therefore, none of the tested TFs affected the Cad system (Fig. 4F).

In conclusion, based on the differential expression data and lower survival of mutants during acid shock, we identified two novel TFs, namely, MhpR and IscR, which are crucial under severe acid stress (Fig. 4C), but are not associated with the Gad, Adi, and Cad systems (Fig. 4D through F). This implies that these regulators ensure the survival of *E. coli* in acidic habitats by inducing other defense mechanisms. Of particular interest is MhpR, which had the highest increase in RPFs of all TFs at pH 4.4 (Fig. 4B), and the corresponding mutant had the lowest survival at pH 3 (Fig. 4C). Further studies are needed to determine whether MhpR, which is a specific regulator of the *mhpABCDE* operon-encoding enzymes for the degradation of phenylpropionate (90, 91), directly or indirectly contributes to acid resistance.

Differential expression of known and novel sORFs under mild and severe acid stress

In recent years, the annotation of many bacterial genomes has been extended by previously unknown small proteins (29), many of which are located in the membrane (92). This progress has been achieved primarily through the development of optimized detection strategies using adapted ribosome profiling and mass spectrometry protocols (28, 33, 93). Recently, additional sORFs were identified in *E. coli* using antibiotic-assisted Ribo-Seq, which captures initiating ribosomes at start codons (94, 95). Advanced detection strategies also revealed novel small proteins in other species, such as the archaeon *Haloferax volcanii*, the nitrogen-fixing plant symbiont *Sinorhizobium meliloti*, *Salmonella Typhimurium*, and *Staphylococcus aureus* (33–35, 96).

Among the previously known sORFs in *E. coli* K-12 and those discovered by Storz and colleagues (94), pH-dependent differential RPF levels were observed in our data sets for 12 and 29 small proteins at pH 5.8 and pH 4.4, respectively (Table S8). These findings validate the expression of these sORFs and highlight their physiological relevance in the acid stress response of *E. coli*. For example, induction of *mdtU*, an upstream ORF of *mdtJ*, was observed under mild acid stress (Fig. 5A) and corresponds to the observed upregulation of the multidrug/spermidine exporter MdtJI (Table 1). A previous study has shown that translation of MdtU is crucial for spermidine-mediated expression of the MdtJ subunit under spermidine supplementation at pH 9 (97). A similar mechanism could operate under acid stress conditions. The strongest induction of sORFs under severe acid stress was detected for *ydgU* (located in the same transcriptional unit as the acid shock protein-encoding gene *asr*) and *azuC* (Fig. 5B). AzuCR acts as a dual-function RNA and encodes a 28-amino acid protein, but it can also base pair as an sRNA (AzuR) with two target mRNAs, including *cadA* (98). AzuCR modulates carbon metabolism through interactions with the aerobic glycerol-3-phosphate dehydrogenase GlpD (98).

In addition to known sORFs, we aimed to uncover further hidden small proteins on the basis that our Ribo-Seq data were acquired under stress conditions to which *E. coli* is exposed in its natural habitat, the gastrointestinal tract. In particular, we searched for novel sORFs that remained undetected in previous Ribo-Seq approaches when *E. coli* was grown at a neutral pH.

Initial predictions for novel sORF candidates were acquired using the neural network-based prediction tool *DeepRibo* (99). All potential candidates were filtered based on coverage (rpkm >30 across all Ribo-Seq samples) and codon count [10–70 amino acids (aa)], with the exception of sORF15 (93 amino acids) (Table S7), which was manually discovered by inspecting the 3' UTR of *gadW*. To further refine our search, we focused on sORF candidates that were significantly induced at either pH 5.8 or pH 4.4 (RPF log₂ FC >2 and *P*-adjust <0.05) compared to pH 7.6. Predictions that overlapped with annotated genes on the same strand were excluded because Ribo-Seq signals were indistinguishable. This workflow yielded 152 candidates that were visually inspected using the web-based genome browser JBrowse2 (100). Candidates with continuous coverage across the predicted sORF, matching the ORF boundaries, and promising Shine-Dalgarno sequences were considered high-confidence candidates. In total, we identified 18 acid-induced sORF candidates (Table S7) that had not been previously detected. Of note, most of the

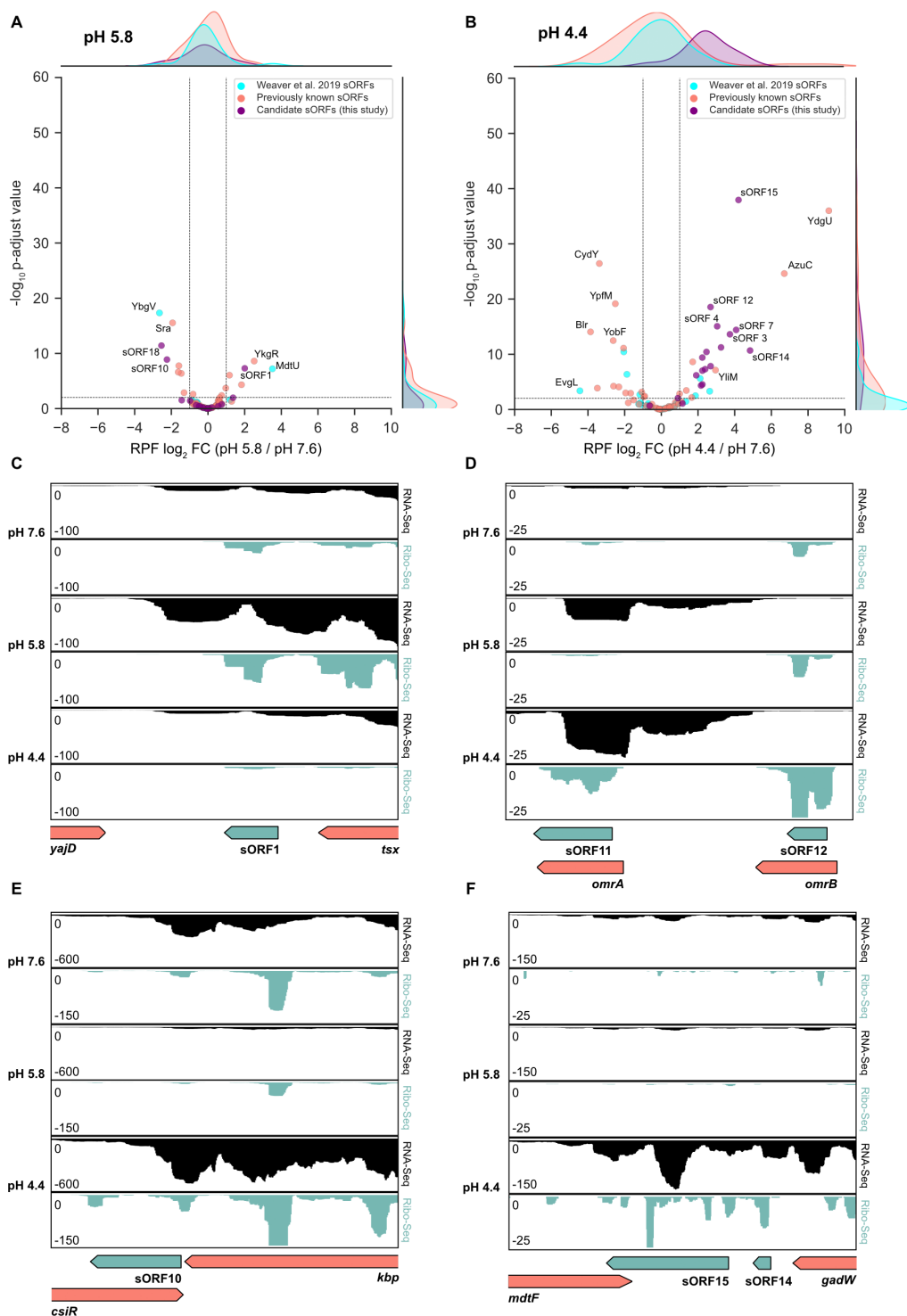


FIG 5 Differentially expressed sORF candidates upon exposure of *E. coli* to acid stress. Volcano plots illustrating differential RPF levels at (A) pH 5.8 vs 7.6 and (B) pH 4.4 vs 7.6 for sORF candidates identified in this study (Table S7), sORFs identified by Weaver *et al.* (94), and previously known sORFs. (C through F) JBrowse2 screenshots of read coverage from Ribo-Seq (green tracks) and RNA-Seq (black tracks) libraries at pH 7.6, pH 5.8, and pH 4.4. The schematic illustrations below indicate the genomic locations of enriched sORF candidates under acidic stress and adjacent annotated genes. Novel sORF candidates sORF1 (13 aa), sORF10 (38 aa), sORF11 (28 aa), sORF12 (11 aa), sORF14 (13 aa), and sORF15 (93 aa) are shown in green. aa, amino acids

candidates are encoded as part of operons or are located in the 3' UTR of annotated genes. In addition, we detected one independent antisense sORF (sORF2 encoded antisense to *tesA*) and two upstream ORFs (leader peptides): sORF18, located upstream of the translation start site of the periplasmic chaperone encoding *osmY*, and sORF8, located close to the glucokinase-encoding gene *glk* (Table S7).

Of these 18 acid-induced candidate small proteins (Table S7), 17 had higher RPF counts at pH 4.4 than at pH 5.8. This suggests that the contribution of sORFs to acid defense in *E. coli* is more relevant under severe acid stress. Only sORF1 showed a higher expression level in cells exposed to mild acid stress (Fig. 5C). sORF1 is located in the 3' UTR of *tsx*, which encodes a nucleoside-specific channel-forming protein. This finding is consistent with the observed increased requirement for nucleotides by *E. coli* at pH 5.8 (Fig. 3).

For the first time, we identified two sORF candidates located within genes encoding the redundant small regulatory RNAs OmrA and OmrB (Fig. 5D). *omrA* and *omrB* are highly identical at the 3' and 5' ends, differ mainly in their central parts, and regulate the expression of numerous outer membrane proteins (101). Our analysis suggests that both OmrA and OmrB act as dual-function RNAs under severe acid stress and encode small proteins: a 28-amino acid protein OmrA (sORF11) and an 11-amino acid protein OmrB (sORF12) (Fig. 5D). Due to the sequence variation in the central parts, the translation of OmrB ends at an earlier stop codon. Notably, both *omrA* and *omrB* displayed higher RPF levels at pH 4.4, whereas transcription of *omrA* but not *omrB* was induced at pH 4.4 (Fig. 5D). Thus, despite the high sequence similarity, *omrA* and *omrB* do not encode identical small proteins under severe acid stress and are differentially regulated at the transcriptional and translational levels. We also detected an acid-induced sORF candidate (sORF3) in *rybB* (Table S7), another sRNA involved in the regulation of outer membrane proteins (102). To our best knowledge, the presence of OmrA, OmrB, and RybB peptides has not yet been reported.

Three new candidate sORFs potentially involved in the regulation of AR systems were detected. sORF10 is located in the 3' UTR of a potassium-binding protein encoded by *kbp* and encoded antisense to the transcriptional regulator CsiR (Fig. 5E). The latter might be involved in the regulation of the Adi system (15, 103). Given the significant upregulation of sORF10 at pH 4.4 and its complete complementarity to the 3' end of the *csiR* mRNA, we hypothesize that sORF10 plays a role in fine-tuning the expression of the Adi system. Strikingly, we also discovered two high-confidence candidates for sORFs located in the relatively long 3' UTR of GadW, one of the major transcriptional regulators of the Gad system (Fig. 5F). sORF14 and sORF15 exhibit constant coverage across the predicted ORF and contain Shine-Dalgarno sequences (Table S7). These results suggest that the complex Gad system may consist of even more components.

To gain further insight into the subcellular location and features of the newly identified sORF candidates, we used PSORTb (104) and DeepTMHMM (105) for transmembrane topology prediction. Notably, sORF15 is predicted to be located in the inner membrane and has two transmembrane helices, which were predicted with a probability of >90% (Fig. S9A). Additionally, the sORF15 protein structure prediction using AlphaFold2 (106) in Google Colab (ColabFold) (107) revealed a potential third helix toward the C-terminal end (Fig. S9B). Using blastp and tblastn (108), we found homologs of sORF15 with >80% identity in *Vibrio*, *Shigella*, *Klebsiella*, *Salmonella*, *Enterococcus*, and *Escherichia* (Fig. S9C) and identified homologs with at least 60% identity for approximately half of the other candidate sORFs (sORF2, 4, 5, 6, 7, 9, 10, 11, 16, and 18). These results strengthen confidence in the correct prediction of these sORFs. However, homologs in other species often only displayed partial matches and were almost exclusively annotated as "hypothetical proteins," as illustrated for sORF15 (Figure S9C). Moreover, we evaluated whether sORF15 is translated in the absence of the upstream gene *gadW*. A pBAD24-sORF15:3xFLAG plasmid, which harbors the native Shine-Dalgarno sequence of sORF15 (Table S11), and a FLAG-tagged version of sORF15 were constructed. sORF15

translation was successfully verified by Western blotting (Fig. S9D), which exemplifies that sORFs detected in this study yield detectable protein products.

In conclusion, we identified 18 high-confidence candidates for novel sORFs that are significantly induced upon exposure of *E. coli* to mild or severe acid stress.

Differentiation of the acid stress and general stress responses using autoencoder-based machine learning

In general, stress response mechanisms can be broadly classified into two categories: global stress responses and adaptations to specific types of stress. Global stress responses can be triggered by various stimuli and provide protection against multiple other unrelated stress factors (109). The global response often involves the activation of alternative sigma factors that affect hundreds of genes. In contrast, adaptations to specific types of stress are tailored to the specific stressor and involve a regulator that senses an environmental cue and modulates the expression of a set of genes, which counteract the stress (109, 110).

Given the large number of differentially regulated genes and pathways in response to acid stress (Fig. 2 and 3), we asked which of these adaptive mechanisms are acid-specific and which are also triggered by other stressors. In order to distinguish acid-specific and general stress responses, we used denoising autoencoders (DAEs), deep learning models designed for meaningful dimensionality reduction (111, 112). DAEs accomplish this by passing data through an encoder that compresses it into activations of a bottleneck layer (Fig. 6A1), with each node in the bottleneck layer interpretable as a coordinated expression program (113). For our analysis, we employed an ensemble of deep DAEs (see Materials and Methods) (113), trained on the *E. coli* K-12 PRECISE 2.0 compendium (114), augmented with additional stress conditions (115), as well as the acid stress conditions of the current study (Fig. 6A1). Using this method and data set, we have conducted a comparative analysis of the transcriptional response of *E. coli* to pH 4.4 and pH 5.8, contrasted against an extensive range of other stress conditions, including heat stress (116), ethanol stress (117), osmotic stress (118), oxidative stress (119, 120), low oxygen (LOX) (115), and exposure to sublethal concentrations of chloramphenicol (CAM) (115) and trimethoprim (TMP) (115).

To identify biological processes associated with a particular stress condition, we passed the associated RNA-seq data set into the encoder of each network and identified bottleneck nodes that were uniquely turned on by that data set (Fig. 6A2). We then manually turned on these nodes to generate gene sets that are associated with that condition, which can be further analyzed through GO term enrichment (Fig. 6A3 and 4). Using this procedure, we identified groups of nodes that uniquely turn on for acid stress conditions and turn off for all other stress conditions, as well as groups that are simultaneously on for both acid and one additional stress condition. We observed that there are many nodes that turn on simultaneously upon both acid and ethanol exposure (Fig. 6B). The overlap between acid stress and ethanol stress responses has been noted previously and can be explained by the fact that ethanol fluidizes the cytosolic membrane and increases the permeability for protons (121). Furthermore, there are indications of an overlap between acid and antibiotic stress (122, 123), reflected in the high number of acid + CAM activating nodes (Fig. 6B).

To pinpoint which cellular adaptations cause acid-specificity for the 48 and 91 specific bottleneck nodes at pH 5.8 and 4.4 (Fig. 6B), respectively, we conducted GSEA for biological processes on each of the gene sets associated with acid-specific node groups (see Materials and Methods). The GO terms that were significantly enriched in the highest number of both pH 5.8- and pH 4.4-specific upregulating node gene sets were "siderophore transmembrane transport," "response to cold," "bacterial-type flagellum assembly," and "chemotaxis" (Fig. 6C), reflecting our previous differential RNA-seq analysis (Fig. 3). The appearance of the GO term "response to cold" might be a result of the lack of cold stress in our compendium of stressors. Additionally, it should be noted that genes associated with this GO term include cold shock proteins, which may have

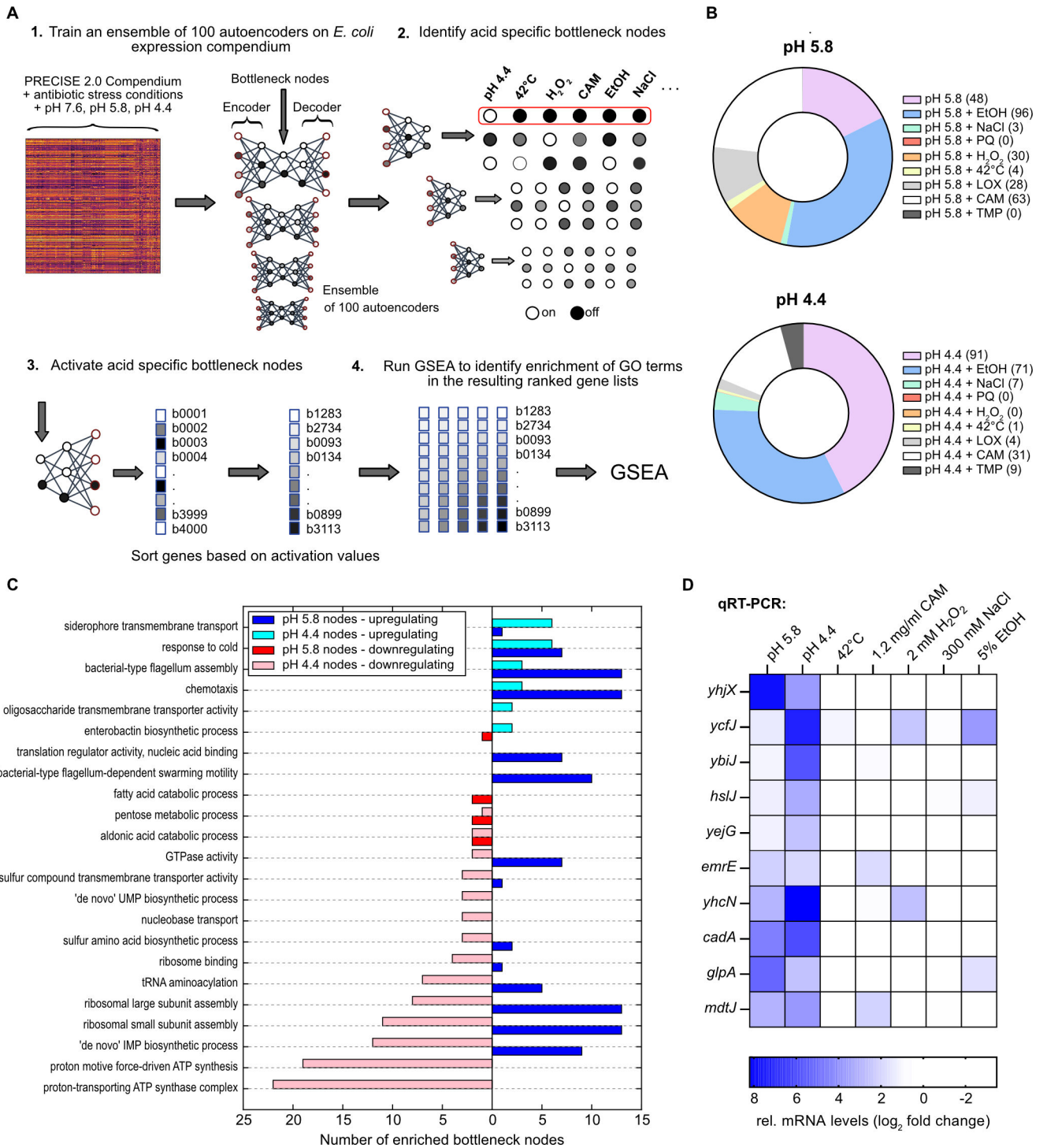


FIG 6 Differentiation between acid stress responses and general stress using autoencoders. (A) Schematic overview of the autoencoder ensemble training and subsequent bottleneck group identification pipeline. (B) Donut charts indicating the proportion of bottleneck nodes that turn on only under the specified conditions. Absolute numbers of specific bottleneck nodes are listed in brackets after each condition. (C) Significantly enriched GO terms associated with pH 4.4- and pH 5.8-specific nodes. Left-facing red bars indicate nodes that downregulate the corresponding GO term, while right-facing blue bars indicate upregulation. (D) Verification of acid stress-specific genes predicted by autoencoders. *E. coli* cells were either grown as indicated in Fig. 1A or exposed to heat (42°C), oxidative (H₂O₂), osmotic (NaCl), chloramphenicol (CAM), or ethanol (EtOH) stress. Total RNA was isolated, and relative mRNA levels were measured by RT-qPCR. Fold change values were determined relative to non-stress conditions and normalized using either *secA* or *recA* as reference genes. Standard deviations were calculated from three replicates (*n* = 3) and accounted for <10% of fold change values in all cases. PQ, paraquat; LOX, low oxygen; TMP, trimethoprim.

broader roles in the survival of stress conditions (124, 125), as well as several prophage genes and ribosome biogenesis factors. We found that mild acid stress turns on nodes, which correspond to gene sets associated with nucleotide and ribosome biosynthesis, including the GO terms “ribosome large subunit assembly,” “ribosome small subunit assembly,” and “*de novo* IMP biosynthetic process,” while severe acid stress turns them off (Fig. 6C). These findings are consistent with our previous observations, namely, that *E. coli* induces nucleotide and ribosome biosynthesis to cope with mild acid stress but enters a metabolically inactive state under severe acid stress. The GO terms significantly affected in the highest number of acid-specific pH 4.4 downregulated bottleneck nodes were “proton motive force-driven ATP synthesis” and “proton-transporting ATP synthase complex” (Fig. 6C). These two GO terms exclusively involve genes encoding subunits of the F₀F₁ ATP synthase and can be considered paradigms for acid-specific adaptations since the F₀F₁ ATP synthase can also pump protons (126).

Considering that we detected a high number of genes induced by severe acid stress with unknown functions (Table 3) and lacking GO associations, we expanded our search for acid-specific adaptations from GO terms to single genes. In order to select acid-specific candidate genes, we investigated all genes associated with acid-specific bottleneck nodes and calculated the log₂ FC between each acid stress and every other above-mentioned stress condition for these genes. Genes with the highest expression values under acidic conditions and log₂ FCs of at least 0.5 for at least 95% of comparisons were then selected. This procedure yielded 10 candidate genes (Fig. 6D). To experimentally validate that these genes are indeed specifically upregulated under acid stress, we exposed *E. coli* to a variety of common stressors and performed qRT-PCR. *E. coli* cells were either grown under acid stress (Fig. 1A) or exposed to heat (42°C), oxidative (H₂O₂), osmotic (NaCl), antibiotic (chloramphenicol), or ethanol (EtOH) stress. For all investigated genes, the strongest upregulation was observed at either pH 4.4 or pH 5.8 relative to non-stress conditions (Fig. 6D), except for *ycfJ*, which was activated at pH 4.4 and under oxidative and ethanol stress. The remaining investigated genes were only upregulated under one other stress condition at most (Fig. 6D). Given that *emrE* and *mdtJ* encode multidrug exporters, the induction upon supplementation with sublethal concentrations of chloramphenicol is not surprising and further underscores the interplay between acid and antibiotic stress. The observed upregulation of *yhcN* under oxidative stress (Fig. 6D) was also reported previously (127). Nevertheless, we uncovered four *bona fide* examples of genes (*ybiJ*, *hslJ*, *yejG*, and *yhjX*) that displayed exclusive pH-dependent expression (Fig. 6D). Induction of *yhjX*, encoding a putative pyruvate transporter, might be related to the deamination of serine, which yields ammonia and pyruvate in uropathogenic *E. coli* (128). The precise molecular functions of YbiJ, YejG, and HslJ in the context of acid stress are currently unclear. These results highlight that our autoencoder pipeline is complementary to differential gene expression analysis, yielding biologically consistent results while also identifying expression patterns that uniquely discriminate acid stress from other stress responses.

Conclusions

Here, we present the first comprehensive study on the global transcriptome- and translome-wide response of *E. coli* exposed to varying degrees of acid stress. Our investigation goes beyond previous research, which focused on comparing *E. coli* transcriptomes across different pH levels during growth (18, 21). Instead, we report on rapid changes occurring upon sudden pH shifts, which are relevant for bacteria such as *E. coli*, during passage of the gastrointestinal tract (129).

Using both Ribo- and RNA-Seq, we uncovered not only well-known acid defense mechanisms but also numerous previously undiscovered relevant genes and pathways to combat mild and severe acid stress (Fig. 7). The latter include siderophore production, glycerol-3-phosphate conversion, copper export, *de novo* nucleotide biosynthesis, and spermidine/multidrug export (Fig. 3 and 7). A striking number of membrane proteins and H⁺-coupled transporters were found to be downregulated under both mild and

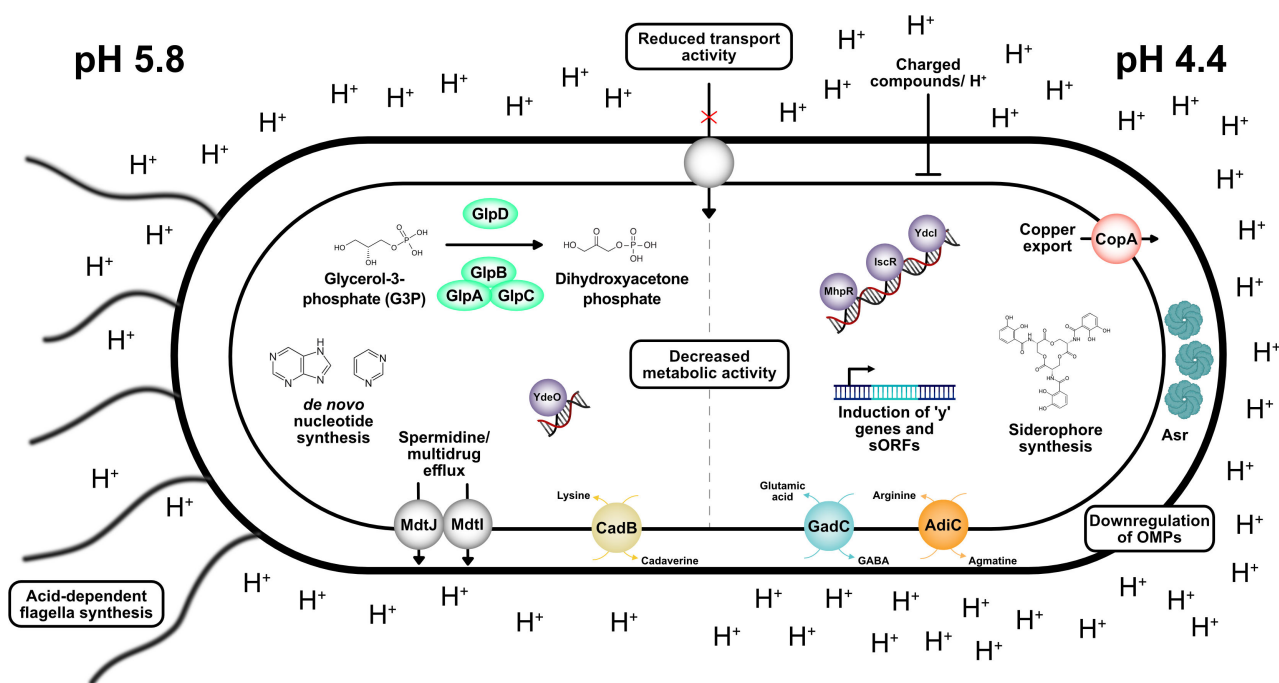


FIG 7 Overview of the fine-tuned response of *E. coli* to mild (pH 5.8) and severe (pH 4.4) acid stress. Acid stress counteracting mechanisms, including those revealed by Ribo-Seq and RNA-seq, are indicated.

severe acid stress (Fig. 7; Tables 2 and 4), underscoring the importance of the cytosolic membrane and its composition as a barrier for protons. Moreover, under severe stress, many outer membrane proteins were downregulated (Fig. 7; Table 4). Notably, a large proportion of genes with yet unknown functions were strongly induced, particularly under severe acid stress (Table 3). Our approach implies that exposing *E. coli* to culture conditions mimicking near-lethal habitats can offer valuable insights into the molecular functions of genes with low expression levels under standard growth conditions.

Our analysis revealed two new TFs, MhpR and IscR, involved in acid stress adaptation. Furthermore, we gained new insights into the role of the TFs YdeO and MarR. YdeO controls not only the transcription of genes in the Gad system but also *adiA* in the Adi system (Fig. 4), suggesting that YdeO connects the regulation of two AR systems in *E. coli*. The observed upregulation of MarR under acid stress, but the low contribution of this TF to acid resistance (Fig. 4B), may provide a link to antibiotic resistance and solvent stress tolerance in *E. coli* (130).

In addition to the pH-dependent differential expression levels of previously identified small proteins, such as YdgU, MdtU, and AzuC, we identified 18 high-confidence, not yet annotated, sORF candidates (Fig. 5). Of particular interest are sORF14 (13 amino acids) and sORF15 (93 amino acids), which are located in a transcriptional unit with *gadW* and *gadX*, suggesting their association with the Gad AR system and a potential involvement in glutamate transport and/or glutamate decarboxylation to gamma-aminobutyrate (GABA). Considering the predicted membrane location of sORF15 and its adjacent gene *mdtF*, an association with either the glutamate/GABA antiporter GadC and/or the multidrug efflux pump MdtF is conceivable.

The autoencoder-based comparison with other common stressors allowed us to distinguish acid stress-specific adaptations from general stress response programs (Fig. 6). Therefore, it was possible to differentiate between direct and indirect effects triggered by protonation and/or cellular damage. Considering the growing volume of next-generation sequence data, denoising autoencoders will be an increasingly important tool for interpreting future studies in the full context of accumulating RNA-seq data sets. Colonizing the intestinal tract is a complex process that includes not only rapid pH

changes but also alterations in oxygen and nutrient availability as well as competition with other bacteria. The ability of pathogenic *E. coli* strains to respond to such rapidly changing environments ensures their fitness advantage. We have shown here, for acid stress, the complexity of the regulatory network for ensuring survival and adaptation. The use of autoencoders, successfully tested here, could allow for the identification of physiological weak points associated with the survival of specific stresses. Targeting such weak points could lead to new classes of antibiotics or antivirulence treatments that take advantage of the unique expression patterns induced by natural stress conditions encountered in the host environment.

MATERIALS AND METHODS

Strains and growth conditions

Bacterial strains and plasmids used in this study are listed in Table S9. *E. coli* strains were cultivated in LB medium (10 g/L tryptone, 5 g/L yeast extract, 10 g/L NaCl) and incubated aerobically in a rotary shaker at 37°C. When appropriate, media were supplemented with 15 µg/mL gentamycin, 100 µg/mL carbenicillin, or 50 µg/mL chloramphenicol.

For ribosome profiling and RNA-Seq experiments, the pH of the medium was adjusted at the indicated time points by the direct addition of 5 M HCl to the growing cultures (Fig. 1A).

For comparison with other stress conditions (heat stress, osmotic stress, oxidative stress, antibiotic stress, and ethanol stress), *E. coli* was initially grown in LB medium to $OD_{600} = 0.5$. Stress conditions were initiated either by moving flasks to a pre-heated 42°C incubator or by the addition of either H₂O₂ (2 mM), NaCl (300 mM), chloramphenicol [1.2 µg/mL (wt/vol)], or ethanol [5% (vol/vol)]. In all cases, samples were collected after 15 min of stress treatment.

Plasmid construction

Molecular methods were performed according to standard protocols or according to the manufacturer's instructions. Kits for the isolation of plasmids and the purification of PCR products were purchased from Süd-Laborbedarf. Enzymes and HiFi DNA Assembly Master Mix were purchased from New England Biolabs. To construct the reporter plasmid pBBR1-MCS5-*P_{gadBC}:lux* (Table S11), 335 nt of the upstream region of *gadBC* were amplified by PCR using primers KSO-0131/KSO-0132 (Table S10) and MG1655 genomic DNA as a template. For the construction of the pBAD24-sORF15:3xFLAG plasmid (Table S11), the sORF15 coding region (excluding the stop codon) and an additional 15 nt upstream of the start codon (harboring the native Shine-Dalgarno sequence) were amplified using primers KSO-183/KSO-184 (Table S10) from MG1655 genomic DNA. After purification, promoter fragments were assembled into PCR-linearized pBBR1-MCS5 or pBAD24-3xFLAG vectors via Gibson assembly (131). The pCA24N-control plasmid was obtained by excising the *ycl* insert from a pCA24N-*ycl* vector using restriction enzymes XhoI and Sall (NEB) and subsequent ligation using T4 DNA Ligase (NEB). Correct insertions were verified by colony PCR and sequencing.

Sample collection for Ribo-Seq and RNA-Seq

Three sets of biological triplicates of MG1655 cells were inoculated to a starting OD_{600} of 0.05 from overnight cultures and grown to exponential phase ($OD_{600} = 0.5$) in 200 mL of unbuffered LB medium (pH 7.6). Two sets of cultures were adjusted to pH 5.8 by direct addition of 5 M HCl, while one set was further grown for 30 min at pH 7.6 (Fig. 1A). After 15 min, one set of biological triplicates was further adjusted from pH 5.8 to pH 4.4 by the addition of 5 M HCl, while the other cultures remained at pH 5.8 or pH 7.6, respectively (Fig. 1A). Cells were grown for another 15 min, samples were collected, and Ribo-Seq and RNA-Seq were performed as described below. pH values before and after pH shifts, as

well as final optical densities, were monitored throughout the experiment (Tables S1 and S2).

Ribosome profiling

Whole-culture flash freezing, cell lysis using a freezer mill, pelleting ribosomes over sucrose cushions, and ribosomal footprint isolation using a size selection gel were performed following the published protocol from Mohammad and Buskirk (40). MNase treatment, monosome recovery, RNA isolation, end-labelling by T4 polynucleotide kinase, and cDNA library construction were conducted by adapting the protocol from Latif and colleagues (39).

Briefly, 100 mL of liquid cultures and 10× lysis buffer [200 mM Tris pH 8, 1.5 M MgCl₂, 1 M NH₄Cl, 50 mM CaCl₂, 4% (vol/vol) Triton X-100, 1% (vol/vol) NP-40] were flash frozen in liquid nitrogen. For each sample, 90 g of frozen cells was mixed with 10 g of frozen 10× lysis buffer and lysed by cryogenic grinding in a SPEX SamplePrep 6875 Freezer/Mill (10 cycles, 10 Hz, 5 min precool, 1 min run, 1 min cool). The pulverized samples were thawed, and the lysate was pre-cleared by centrifugation (9,800 × *g*, 10 min, 4°C) in a Beckman Coulter Optima XE-90 Ultracentrifuge using a 50.2 Ti Rotor. The supernatant was used to pellet ribosomes over sucrose cushions by centrifugation in a Beckman Coulter Optima XE-90 Ultracentrifuge using a 70.1 Ti Rotor (330,000 × *g*, 1.5 h, 4°C). After resuspension of pellets in resuspension buffer (20 mM Tris pH 8, 15 mM MgCl₂, 100 mM NH₄Cl, 5 mM CaCl₂), nuclease digestion was performed using MNase (NEB) (2 h, 25°C). Monosomes were recovered using MicroSpin S-400 HR columns (GE Healthcare), and RNA was isolated using the miRNeasy Mini Kit (QIAGEN) in combination with the RNase-Free DNase Set (QIAGEN). The isolated RNA was loaded on a 15% TBE urea size selection gel, and after staining with SYBR Gold (Invitrogen), ribosomal footprints between 15 and 45 nt were excised from the gel. For elution of RNA, gel pieces were crushed by poking a hole with an 18 G needle in a 0.5-mL tube, placing it in a 1.5-mL tube, and subsequent centrifugation. RNA was recovered by precipitation after adding elution buffer (300 mM NaOAc pH 5.5, 1 mM EDTA pH 8) to the crushed gel, overnight incubation (4°C), and centrifugation in Corning-Costar Spin-X Centrifuge Tube Filters (20,000 × *g*, 3 min, room temperature). The isolation of RNA fragments corresponding to ribosomal footprints of 15–45 nt size was verified using the RNA 6000 Nano Kit (Agilent) and the Agilent 2100 Bioanalyzer. Then, 5′ phosphorylation of RNA fragments was achieved using T4 polynucleotide kinase (NEB) and ATP (NEB). After RNA recovery using an RNA MinElute Cleanup Kit (QIAGEN), footprint fragments were again evaluated using the Agilent 2100 Bioanalyzer as described above. cDNA libraries were constructed using the NEBNext Small RNA Library Prep Set for Illumina (NEB) with 14 PCR amplification cycles. cDNA library quality was assessed using a High Sensitivity DNA Kit (Agilent). cDNA libraries were purified using the QIAquick PCR Purification Kit (QIAGEN) and sequenced using a HiSeq 1500 machine (Illumina) in single-read mode with a 50-bp read length.

RNA-Seq analysis

After flash-freezing the cultures for Ribo-Seq, 6 mL of the remaining culture volume was mixed with 1.2 mL of Stop Mix solution [95% (vol/vol) ethanol, 5% (vol/vol) phenol] to terminate ongoing transcription and translation. Samples were frozen in liquid nitrogen and stored at –80°C until RNA isolation. Cells were pelleted (3,000 × *g*, 15 min, 4°C), and total RNA was isolated using the miRNeasy Mini Kit (QIAGEN) in combination with the RNase-Free DNase Set (QIAGEN). The integrity of RNA samples was evaluated using the RNA 6000 Nano Kit (Agilent) and the Agilent 2100 Bioanalyzer. RNA was quantified using the Qubit RNA HS Assay Kit (Invitrogen). Ribosomal RNA depletion was performed using the NEBNext rRNA Depletion Kit for bacteria (NEB), and directional cDNA libraries were prepared using the NEBNext Ultra II Directional RNA Library Prep Kit for Illumina (NEB). cDNA library quality was assessed using a High Sensitivity DNA Kit (Agilent). Finally,

cDNA libraries were sequenced using a NextSeq 1000 machine (Illumina) in single-read mode with a 60-bp read length.

Next-generation sequencing data analysis

E. coli Ribo-seq and RNA-seq raw sequencing libraries were processed and analyzed using the published HRIBO workflow (version 1.6.0) (37), which has previously been used for analysis of bacterial Ribo-seq data (35). HRIBO is a snakemake (132) workflow that downloads all required tools from Bioconda (133) and Singularity (134). All necessary processing steps are automatically determined by the workflow.

Adapter and quality trimming of the reads was performed using cutadapt (version 2.1) (135). The trimmed reads were then mapped against the *E. coli* K-12 MG1655 reference genome (ASM584v2) with segemehl (version 0.3.4) (136). Reads corresponding to ribosomal RNA (rRNA), transfer RNA (tRNA), and multi-mapping reads were removed with SAMtools (version 1.9) (137) using rRNA and tRNA annotations.

Quality control was performed by creating read count statistics for each processing step and RNA class with Subread featureCounts (1.6.3) (138). All processing steps were analyzed with FastQC (version 0.11.8) (139), and results were aggregated with MultiQC (version 1.7) (140). Additionally, a PCA was performed to determine whether the major source of variance in the data stems from the different experimental conditions. The PCA ensures the correctness of the downstream differential expression analysis. To generate the PCA plots, normalized read counts for all samples were generated using DESeq2 (141) normalization. To improve the clustering, a regularized log transform was applied to the normalized read counts. Standard deviations and variance were subsequently calculated using DESeq2, and the first three principle components were plotted using plotly (142).

Read coverage files were generated with HRIBO using different full read mapping approaches (global or centered) and single-nucleotide mapping strategies (5' or 3' end). Read coverage files were normalized using the counts per million (mil) normalization. For the mil normalization, read counts were normalized by the total number of mapped reads within the sample and scaled by a per-million factor.

Metagene analysis of ribosome density at start codons was performed as described previously (143). Here, annotated start codons of coding sequences are collected, and the density of the read coverage is determined for every position in a pre-determined window around the collected start codons.

A differential expression and translation analysis was performed using the tool deltaTE (43). The tool combines both Ribo-seq and RNA-seq data by calculating the TE of genes in order to capture changes in translational regulation when comparing different growth conditions.

Gene set enrichment analysis

GSEA was conducted using the tool *clusterProfiler* (52). To this end, the genome-wide annotation database for *E. coli* K-12 MG1655 (144) was used in combination with the results of the differential expression analysis. The analysis was focused on the biological process domain, omitting the cellular component and molecular function domains. Furthermore, the minimum gene set size was set to 5 and the maximum to 30. To avoid redundancy within the results, GO terms were filtered, and only terms at the bottom (lowest branch level) of the GO hierarchy were analyzed.

Detection and differential expression of novel acid-induced sORF candidates

sORF candidates were initially detected using the neural network *DeepRibo* (99). Summary statistics, including TE, rpkm, codon counts, and nucleotide and amino acid sequences, for annotated and potential novel sORFs were computed using HRIBO (version 1.6.0) (37). Moreover, GFF track files were created for detailed manual inspection using the web-based genome browser JBrowse2 (100).

DeepRibo was reported to produce high numbers of false positives (145). Therefore, the high number of initial predictions (>25,000) was reduced by introducing cut-off criteria based on sORF length and Ribo-Seq coverage. Predictions with average rpkm (reads per kilobase of transcript per million mapped reads) values <30 across all Ribo-Seq samples and outside of the codon count range of 10–70 amino acids were excluded from further analysis. To specifically detect sORFs, which are only detectable under acidic conditions and involved in the acid response of *E. coli*, the search was further restricted to predictions with deltaTE Ribo- and RNA log₂ FC values of ≥2, in combination with *P*-adjust values of ≤0.05, at either pH 5.8 or pH 4.4, compared to pH 7.6. Additionally, *DeepRibo* predictions of overlapping annotated genes on the same strand were excluded. The remaining 152 candidates were manually inspected in JBrowse2, and novel sORFs were included in our final candidate list (Table S7) if the coverage was even over the predicted ORF, restricted to the ORF boundaries, and potential Shine-Dalgarno sequences were detectable. The remaining candidates were manually curated, and, in a few cases, alternative sORFs in the genomic vicinity of *DeepRibo* predictions were selected, which matched better to the Ribo-Seq coverage signal. Differential expression values, comparing pH 7.6, pH 5.8, and pH 4.4, for novel sORF candidates, previously known sORFs, and sORFs detected by Storz and colleagues (94), were calculated using *deltaTE* (43).

Homologs for novel sORF candidates were identified using blastp and tblastn (108) within the “BLAST at NCBI” function in the CLC Main Workbench v. 20.0.4 (QIAGEN). For tblastn, the following parameters were used: an *E*-value (expected value) ≤0.05, a seed length that initiates an alignment (word size) of 6, and the filter for low-complexity regions off. Potential cellular localization was evaluated with PSORTb v3.0.3 (<https://www.psорт.org/psортb/>) (104), and transmembrane topology was assessed using DeepTMHMM v1.0.24 (105). The protein structure of sORF15 was predicted by running AlphaFold2 (106) via Google Colab (ColabFold v1.5.2) (107) with default settings.

RNA isolation and RT-qPCR analysis

RNA was isolated using the Quick-RNA Miniprep Kit (Zymo Research) or miRNeasy Mini Kit (QIAGEN) in combination with the RNase-Free DNase Set (QIAGEN) according to the manufacturer's instructions. Total RNA was DNase digested for 30 min at 37°C using 1 μL TURBO DNase (2 U/μL) (Invitrogen). A 500-ng aliquot of the isolated RNA was converted to cDNA with the iScript Advanced Kit (Bio-Rad) according to the manufacturer's instructions. Then, 1 μL of a 1:10 dilution in nuclease-free water of the cDNA samples was mixed with 5 μL of SsoAdvanced Univ SYBR Green Supermix (Bio-Rad) and 0.8 μL of 5 μM forward and reverse primers (Table S10). The total reaction volume was adjusted to 10 μL with nuclease-free water, dispensed in triplicates in a 96-well PCR plate (Bio-Rad), and subjected to qPCR in a Bio-Rad CFX real-time cycler. Evaluation of the obtained data were performed according to the ΔΔCt method (146), using *recA* or *secA* genes as internal references.

Acid shock assay

Acid resistance was determined based on previously described protocols (16, 147) with the following modifications: *E. coli* BW25113 cells were grown at 37°C in LB pH 7.6 to OD₆₀₀ = 0.5, adjusted to OD₆₀₀ = 1, and then shifted for 15 min each, first to LB pH 5.8 and then to LB pH 4.4. Then, cells were shifted to LB pH = 3 for 1 h at 37°C. As a control, cells were cultivated at pH 7.6 throughout the experiment. After 1 h at pH 7.6, or pH 3, samples were serially diluted in 1× phosphate-buffered saline (PBS) and plated on LB agar plates to count the number of colonies. Percent survival was calculated as the ratio of colony-forming units at pH 3 and pH 7.6. For complementation of mutants from the Keio collection (84), BW25113 strains were transformed with IPTG-inducible pCA24N plasmids from the ASKA collection (Table S11) (85). Acid shock survival rates were determined as described above, with the exception that media were supplemented with 50 μg/mL chloramphenicol and different concentrations of IPTG to mimic native

expression levels. pCA24N-control, *gadE*, and *gadW* vectors were induced with 100 μ M IPTG, pCA24N-*rcsB*, and *iscR* with 10 μ M IPTG, and pCA24N-*iscR*, *ydjI*, and *mhpR* with 1 μ M IPTG.

Promoter activity assay

In vivo promoter activities of *gadBC*, *adiA*, and *cadBA* were determined using luminescence-based reporter plasmids harboring fusions of the respective promoter regions to the *luxCDABE* genes from *Photobacterium luminescens*. BW25113 wild-type cells or corresponding mutants from the Keio collection (84) were transformed with plasmids pBBR1-P*gadBC*:*lux*, pBBR1-P*adiA*:*lux*, or pBBR1-P*cadBA*:*lux*. All strains were cultivated in LB medium supplemented with gentamycin overnight. The overnight cultures were inoculated to an OD₆₀₀ of 0.05 in fresh LB medium (pH 7.6), aerobically cultivated until exponential phase (OD₆₀₀ = 0.5), and shifted to LB pH 5.8. To assess the promoter activity of *adiA* and *gadBC*, the cultures were shifted again to LB pH 4.4 after 15 min of growth in LB pH 5.8. In the next step, the cells were transferred to a 96-well plate and aerobically cultivated at 37°C in LB medium at different pH values supplemented with gentamycin. Growth and bioluminescence were measured every 10 min in the microtiter plates using a CLARIOstar Plus plate reader (BMG Labtech). Data are reported as relative light units in counts per second of OD₆₀₀.

Autoencoder-based identification of acid-specific genes and biological processes

The denoising autoencoders in this study were implemented using the Python package Keras (148). Details of the various hyperparameter and network architecture choices were taken from reference (113). In brief, an ensemble of 100 DAEs with two hidden layers of 2,000 and 1,000 nodes between the input layer and the bottleneck was used. The bottleneck layer of each network consists of 50 nodes, as this was found to be within an optimal range for DAEs trained on the PRECISE 2.0 expression compendium (114) by Kion-Crosby and Barquist (113). All layers have sigmoid activation functions; the weights of each layer were randomly initialized based on the Glorot distribution, and the bias vectors were zeros. The weight matrices that make up the decoder of each network are tied together such that they consist of the transpose of the corresponding weight matrices of each encoder.

All networks were trained in each ensemble using the Adam optimization algorithm. Data corruption during training was employed to improve generalizability, such that 10% of the entries of each input data point were randomly set to zero during each training step. Additionally, early stopping was employed during training; the data were randomly partitioned into an 80% training set and a 10% validation set, and training was stopped once the validation score began to worsen. A 10% test set was also partitioned to determine the optimal training parameters. A local search over all training parameters, including the learning rate and batch size, was performed using the test score as a metric, and training was done with batch shuffling enabled.

For the training of the autoencoder ensemble, the PRECISE 2.0 compendium (114) was used, as well as six additional data points (115) representing *E. coli* K-12 MG1655 strains grown in M9 medium and treated with various antibiotics, in addition to the nine data points from the current study. All data were converted to log transcripts per million, and features were normalized after the train/validation/test split such that the expression of each gene was scaled between 0 and 1.

Following the procedure described by Kion-Crosby and Barquist (113), the encoder of each of the 100 trained networks was used to determine which nodes turn on for the specific stress conditions of interest (e.g., pH 4.4) and simultaneously turn off for alternative stress conditions (e.g., oxidative stress, heat stress, and ethanol). This was done by passing each data point into each encoder while observing the activations of nodes at the bottleneck layer. After identifying which nodes are specific to the stress condition of interest, each corresponding decoder was utilized to generate gene

expression predictions for all *E. coli* genes by activating each of these bottleneck nodes individually and propagating this signal through the decoder. After sorting all genes based on the average decoder output from all identified nodes, the top of this sorted vector was used to define a gene set associated with the condition of interest.

Additionally, GSEA was run on the outputs of each decoder for each node to determine which biological processes were associated with the condition of interest. Since these groups often consist of ~100 nodes and thousands of GO terms are evaluated, a conservative threshold for the adj. *P*-value of 0.0005 was set. The adj. *P*-value was found using the BH method, and each *P*-value was computed based on 1,000,000 permutations. Finally, for the selection of the high-confidence acid-specific gene candidates, first the log₂ FC between each acidic condition and every other stress condition was taken for all genes in the acid-specific gene sets. Genes corresponding to a log₂ FC of at least 0.5 for at least 95% of comparisons were then selected.

Propidium iodide viability staining

Cells were grown either at pH 7.6, 5.8, or 4.4 in the same manner as described for Ribo-Seq and RNA-Seq (Fig. 1A). As a positive control, cells were grown to an OD₆₀₀ of 1 and subsequently heat-shocked for 5 min at 80°C. After cultivation, 1 mL of each culture was centrifuged (15,000 × *g*, room temperature) and washed with PBS. Propidium iodide (Invitrogen) was added with a final concentration of 2 µg/mL, followed by a 5-min incubation at room temperature in the dark to label dead cells. After another wash step using PBS, 2 µL of the culture was spotted on 1% (wt/vol) agarose pads, placed onto microscope slides, and covered with a coverslip. Microscopic images were taken using a Leica DMI8 inverted microscope equipped with a Leica DFC365 FX camera. An excitation wavelength of 546 nm and a 605-nm emission filter with a 75-nm bandwidth were used to detect fluorescence with an exposure of 500 ms, a gain of 5, and 100% intensity in the Leica LAS X 3.7.4 software.

To quantify the relative fluorescent intensities (RF) of single cells, phase contrast and fluorescent images were analyzed using the ImageJ (149) plugin for MicrobeJ (150). Default settings of MicrobeJ were used for cell segmentation (Fit shape, rod-shaped bacteria) apart from the following settings: area, 0.1-max µm²; length, 1.2–5 µm; width, 0.1–1 µm; curvature, 0.–0.15; and angularity, 0.–0.25 for *E. coli* cells. In total, ≥1,000 cells were quantified per strain and condition, and the background of the agarose pad was subtracted from each cell per field of view. Cells with RF values ≥300 after subtraction of the background were considered dead.

Western blot analysis

To verify the translation of sORF15, *E. coli* MG1655 cells harboring a pBAD24-sORF15:3xFLAG plasmid were cultivated in LB medium. Once an OD₆₀₀ of 0.5 was reached, expression of sORF15 was induced for 1 h by supplementation of a final concentration of 0.2% (vol/vol) L-arabinose. Next, culture aliquots normalized to an OD₆₀₀ of 1 were collected by centrifugation (1 min, 13,000 × *g*, 4°C). Supernatants were removed, and pellets were resuspended in 100 µL of protein loading buffer [12% SDS (wt/vol), 30% glycerol (wt/vol), 0.05% Coomassie blue (wt/vol), 150 mM Tris-HCl pH 7]. Prior to loading, protein samples were denatured at 95°C for 5 min and then chilled on ice. Protein fractions were separated by Tricine-SDS-PAGE on a 16% gel containing 6 M urea (151). After separation, proteins were transferred onto a nitrocellulose membrane in a semidry blot chamber. The membrane was blocked for 1 h in 5% (wt/vol) skim milk in 1× TBS. After short washing with Tris-buffered saline with Tween (TBS-T), blots were hybridized with the primary antibody (α-FLAG, Invitrogen) for 1 h at room temperature. After three washing steps in TBS-T for 10 min each, membranes were incubated with an alkaline phosphatase-conjugated secondary antibody (α-rabbit, Rockland Immunochemicals) for 1 h at room temperature. After three washing steps conducted as described above, proteins were visualized using colorimetric detection of alkaline phosphatase activity with 5-bromo-4-chloro-3-indolyl phosphate and nitro blue tetrazolium chloride.

As a ladder, the PageRuler Prestained Protein Ladder (10–180 kDa, Thermo Fisher) was used.

ACKNOWLEDGMENTS

We thank Stefan Krebs and Helmut Blum for conducting Illumina sequencing and acknowledge Christoph Kurat for providing the freezer mill machine. We thank Sophie Brameyer for scientific discussions; Pol Bannasch, Annika Krimmel, and Djanna Braun for experimental assistance; and Lydia Hadjeras for help with sORF detection. In addition, K.S. acknowledges the support of the Graduate School Life Science Munich (LSM).

This work was financially supported by the Deutsche Forschungsgemeinschaft (DFG, German Research Foundation): project number 471254198-JU270/22-1, project number 395357507-SFB 1371 to K.J., and grant BA 2168/21-2 to R.B. and by the Bavarian State Ministry for Science and the Arts through the research network bayresq.net to L.B. Computational resources were provided by the BMBF-funded de.NBI Cloud within the German Network for Bioinformatics Infrastructure (de.NBI) (031A532B, 031A533A, 031A533B, 031A534A, 031A535A, 031A537A, 031A537B, 031A537C, 031A537D, 031A538A).

AUTHOR AFFILIATIONS

¹Faculty of Biology, Microbiology, Ludwig-Maximilians-Universität München, Martinsried, Germany

²Bioinformatics Group, Department of Computer Science, Albert-Ludwigs-Universität Freiburg, Freiburg, Germany

³Helmholtz Institute for RNA-based Infection Research (HIRI)/Helmholtz Centre for Infection Research (HZI), Würzburg, Germany

⁴University of Würzburg, Faculty of Medicine, Würzburg, Germany

⁵Signalling Research Centres BIOS and CIBSS, University of Freiburg, Freiburg, Germany

AUTHOR ORCID*s*

Kilian Schumacher  <http://orcid.org/0000-0002-4751-301X>

Rick Gelhausen  <http://orcid.org/0000-0003-4161-4394>

Willow Kion-Crosby  <http://orcid.org/0000-0001-9401-9340>

Kirsten Jung  <http://orcid.org/0000-0003-0779-6841>

FUNDING

Funder	Grant(s)	Author(s)
Deutsche Forschungsgemeinschaft (DFG)	471254198-JU270/22-1	Kirsten Jung
Deutsche Forschungsgemeinschaft (DFG)	395357507-SFB 1371	Kirsten Jung
Deutsche Forschungsgemeinschaft (DFG)	BA 2168/21-2	Rolf Backofen
Bayerisches Staatsministerium für Bildung und Kultus, Wissenschaft und Kunst (Bavarian State Ministry of Education, Science and the Arts)		Lars Barquist

AUTHOR CONTRIBUTIONS

Kilian Schumacher, Conceptualization, Investigation, Methodology, Writing – original draft, Writing – review and editing | Rick Gelhausen, Investigation, Methodology, Software, Writing – review and editing | Willow Kion-Crosby, Investigation, Methodology, Software, Writing – review and editing | Lars Barquist, Funding acquisition, Methodology, Software, Writing – review and editing | Rolf Backofen, Funding acquisition, Methodology, Software, Writing – review and editing | Kirsten Jung, Conceptualization, Funding

acquisition, Methodology, Supervision, Writing – original draft, Writing – review and editing

DATA AVAILABILITY

The raw sequencing data for both the Ribo-seq and RNA-seq were deposited at Gene Expression Omnibus (GEO) under the accession number [GSE219022](https://www.ncbi.nlm.nih.gov/geo/query/acc.cgi?acc=GSE219022). A JBrowse2 (100) online genome browser instance containing annotation files and read coverage files of the processed data is available via the RIBOBASE (<http://www.bioinf.uni-freiburg.de/ribo-base>). Additional information required to reanalyze the data reported in this paper is available from the lead contact upon request.

ADDITIONAL FILES

The following material is available [online](#).

Supplemental Material

Supplemental material (mSystems01037-23-S0001.docx). Fig. S1 to S9; Tables S1, S2, and S6.

Supplemental resource table (mSystems01037-23-S0002.docx). Table of key resources.

Table S3 (mSystems01037-23-S0003.xlsx). Ribo-Seq and RNA-Seq exclusive genes.

Table S4 (mSystems01037-23-S0004.xlsx). Genes with differential translation efficiency under acid stress.

Table S5 (mSystems01037-23-S0005.xlsx). Complete HRIBO results.

Table S7 (mSystems01037-23-S0006.xlsx). Acid-induced novel candidate sORFs.

Table S8 (mSystems01037-23-S0007.xlsx). Differential expression of sORFs under acid stress.

Table S9 (mSystems01037-23-S0008.xlsx). *Escherichia coli* strains used in this study.

Table S10 (mSystems01037-23-S0009.xlsx). Oligonucleotides used in this study.

Table S11 (mSystems01037-23-S0010.xlsx). Plasmids used in this study.

REFERENCES

- Schwarz J, Schumacher K, Brameyer S, Jung K. 2022. Bacterial battle against acidity. *FEMS Microbiol Rev* 46:fuac037. <https://doi.org/10.1093/femsre/fuac037>
- Tilden J, Young W, McNamara AM, Custer C, Boesel B, Lambert-Fair MA, Majkowski J, Vugia D, Werner SB, Hollingsworth J, Morris JG. 1996. A new route of transmission for *Escherichia coli*: infection from dry fermented salami. *Am J Public Health* 86:1142–1145. https://doi.org/10.2105/ajph.86.8_pt_1.1142
- Hirshfield IN, Terzulli S, O'Byrne C. 2003. Weak organic acids: a panoply of effects on bacteria. *Sci Prog* 86:245–269. <https://doi.org/10.3184/003685003783238626>
- Deamer DW. 1987. Proton permeation of lipid bilayers. *J Bioenerg Biomembr* 19:457–479. <https://doi.org/10.1007/BF00770030>
- Wilks JC, Slonczewski JL. 2007. pH of the cytoplasm and periplasm of *Escherichia coli*: rapid measurement by green fluorescent protein fluorimetry. *J Bacteriol* 189:5601–5607. <https://doi.org/10.1128/JB.00615-07>
- Goto Y, Takahashi N, Fink AL. 1990. Mechanism of acid-induced folding of proteins. *Biochemistry* 29:3480–3488. <https://doi.org/10.1021/bi00466a009>
- Lund P, Tramonti A, De Biase D. 2014. Coping with low pH: molecular strategies in neutralophilic bacteria. *FEMS Microbiol Rev* 38:1091–1125. <https://doi.org/10.1111/1574-6976.12076>
- Jeong KC, Hung KF, Baumler DJ, Byrd JJ, Kaspar CW. 2008. Acid stress damage of DNA is prevented by Dps binding in *Escherichia coli* O157:H7. *BMC Microbiol* 8:1–13. <https://doi.org/10.1186/1471-2180-8-181>
- Slonczewski JL, Fujisawa M, Dopson M, Krulwich TA. 2009. Cytoplasmic pH measurement and homeostasis in bacteria and archaea. *Adv Microb Physiol* 55:1–79. [https://doi.org/10.1016/S0065-2911\(09\)05501-5](https://doi.org/10.1016/S0065-2911(09)05501-5)
- Arcari T, Feger M-L, Guerreiro DN, Wu J, O'Byrne CP. 2020. Comparative review of the responses of *Listeria monocytogenes* and *Escherichia coli* to low pH stress. *Genes* 11:1330. <https://doi.org/10.3390/genes11111330>
- Foster JW. 2004. *Escherichia coli* acid resistance: tales of an amateur acidophile. *Nat Rev Microbiol* 2:898–907. <https://doi.org/10.1038/nrmicro1021>
- Castanie-Cornet MP, Foster JW. 2001. *Escherichia coli* acid resistance: cAMP receptor protein and a 20 bp *cis*-acting sequence control pH and stationary phase expression of the *gadA* and *gadBC* glutamate decarboxylase genes. *Microbiology* 147:709–715. <https://doi.org/10.1099/00221287-147-3-709>
- Kanjee U, Houry WA. 2013. Mechanisms of acid resistance in *Escherichia coli*. *Annu Rev Microbiol* 67:65–81. <https://doi.org/10.1146/annurev-micro-092412-155708>
- De Biase D, Lund PA. 2015. The *Escherichia coli* acid stress response and its significance for pathogenesis. *Adv Appl Microbiol* 92:49–88. <https://doi.org/10.1016/bs.aambs.2015.03.002>
- Brameyer S, Schumacher K, Kuppermann S, Jung K. 2022. Division of labor and collective functionality in *Escherichia coli* under acid stress. *Commun Biol* 5:327. <https://doi.org/10.1038/s42003-022-03281-4>
- Brameyer S, Hoyer E, Bibinger S, Burdack K, Lassak J, Jung K. 2020. Molecular design of a signaling system influences noise in protein abundance under acid stress in different gammaproteobacteria. *J Bacteriol* 202:e00121–20. <https://doi.org/10.1128/JB.00121-20>
- De Biase D, Pennacchiotti E. 2012. Glutamate decarboxylase-dependent acid resistance in orally acquired bacteria: function, distribution and biomedical implications of the *gadBC* operon. *Mol Microbiol* 86:770–786. <https://doi.org/10.1111/mmi.12020>

18. Maurer LM, Yohannes E, Bondurant SS, Radmacher M, Slonczewski JL. 2005. pH regulates genes for flagellar motility, catabolism, and oxidative stress in *Escherichia coli* K-12. *J Bacteriol* 187:304–319. <https://doi.org/10.1128/JB.187.1.304-319.2005>
19. Blankenhorn D, Phillips J, Slonczewski JL. 1999. Acid- and base-induced proteins during aerobic and anaerobic growth of *Escherichia coli* revealed by two-dimensional gel electrophoresis. *J Bacteriol* 181:2209–2216. <https://doi.org/10.1128/JB.181.7.2209-2216.1999>
20. Stancik LM, Stancik DM, Schmidt B, Barnhart DM, Yoncheva YN, Slonczewski JL. 2002. pH-dependent expression of periplasmic proteins and amino acid catabolism in *Escherichia coli*. *J Bacteriol* 184:4246–4258. <https://doi.org/10.1128/JB.184.15.4246-4258.2002>
21. Du B, Yang L, Lloyd CJ, Fang X, Palsson BO. 2019. Genome-scale model of metabolism and gene expression provides a multi-scale description of acid stress responses in *Escherichia coli*. *PLoS Comput Biol* 15:e1007525. <https://doi.org/10.1371/journal.pcbi.1007525>
22. Seo SW, Kim D, O'Brien EJ, Szubin R, Palsson BO. 2015. Decoding genome-wide GadEWX-transcriptional regulatory networks reveals multifaceted cellular responses to acid stress in *Escherichia coli*. *Nat Commun* 6:7970. <https://doi.org/10.1038/ncomms8970>
23. Schmidt A, Kochanowski K, Vedelaar S, Ahrné E, Volkmer B, Callipo L, Knoops K, Bauer M, Aebersold R, Heinemann M. 2016. The quantitative and condition-dependent *Escherichia coli* proteome. *Nat Biotechnol* 34:104–110. <https://doi.org/10.1038/nbt.3418>
24. Ingolia NT, Ghaemmaghami S, Newman JRS, Weissman JS. 2009. Genome-wide analysis in vivo of translation with nucleotide resolution using ribosome profiling. *Science* 324:218–223. <https://doi.org/10.1126/science.1168978>
25. Ingolia NT, Brar GA, Rouskin S, McGeachy AM, Weissman JS. 2012. The Ribosome profiling strategy for monitoring translation *in vivo* by deep sequencing of ribosome-protected mRNA fragments. *Nat Protoc* 7:1534–1550. <https://doi.org/10.1038/nprot.2012.086>
26. Ingolia NT, Hussmann JA, Weissman JS. 2019. Ribosome profiling: global views of translation. *Cold Spring Harb Perspect Biol* 11:1–20. <https://doi.org/10.1101/cshperspect.a032698>
27. Li GW, Burkhardt D, Gross C, Weissman JS. 2014. Quantifying absolute protein synthesis rates reveals principles underlying allocation of cellular resources. *Cell* 157:624–635. <https://doi.org/10.1016/j.cell.2014.02.033>
28. Vazquez-Laslop N, Sharma CM, Mankin A, Buskirk AR. 2022. Identifying small open reading frames in prokaryotes with ribosome profiling. *J Bacteriol* 204:e0029421. <https://doi.org/10.1128/JB.00294-21>
29. Gray T, Storz G, Papenfert K. 2022. Small proteins; big questions. *J Bacteriol* 204:e0034121. <https://doi.org/10.1128/JB.00341-21>
30. Liu X, Jiang H, Gu Z, Roberts JW. 2013. High-resolution view of bacteriophage lambda gene expression by ribosome profiling. *Proc Natl Acad Sci USA* 110:11928–11933. <https://doi.org/10.1073/pnas.1309739110>
31. Gelsinger DR, Dallon E, Reddy R, Mohammad F, Buskirk AR, DiRuggiero J. 2021. Ribosome profiling in archaea reveals leaderless translation, novel translational initiation sites, and ribosome pausing at single codon resolution. *Nucleic Acids Res* 48:5201–5216. <https://doi.org/10.1093/nar/gkaa304>
32. Fremin BJ, Sberro H, Bhatt AS. 2020. MetaRibo-seq measures translation in microbiomes. *Nat Commun* 11:3268. <https://doi.org/10.1038/s41467-020-17081-z>
33. Hadjeras L, Bartel J, Maier L-K, Maaß S, Vogel V, Svensson SL, Eggenhofer F, Gelhausen R, Müller T, Alkhnbashi OS, Backofen R, Becher D, Sharma CM, Marchfelder A. 2023. Revealing the small proteome of *Haloflex volcanii* by combining ribosome profiling and small-protein optimised mass spectrometry. *Microlife* 4:uqad001. <https://doi.org/10.1093/femsml/uqad001>
34. Fuchs S, Kucklick M, Lehmann E, Beckmann A, Wilkens M, Kolte B, Mustafayeva A, Ludwig T, Diwo M, Wissing J, Jänsch L, Ahrens CH, Ignatova Z, Engelmann S. 2021. Towards the characterization of the hidden world of small proteins in *Staphylococcus aureus*, a proteogenomics approach. *PLoS Genet* 17:e1009585. <https://doi.org/10.1371/journal.pgen.1009585>
35. Venturini E, Svensson SL, Maaß S, Gelhausen R, Eggenhofer F, Li L, Cain AK, Parkhill J, Becher D, Backofen R, Barquist L, Sharma CM, Westermann AJ, Vogel J. 2020. A global data-driven census of *Salmonella* small proteins and their potential functions in bacterial virulence. *Microlife* 1:uqaa002. <https://doi.org/10.1093/femsml/uqaa002>
36. Boulos L, Prévost M, Barbeau B, Coallier J, Desjardins R. 1999. LIVE/DEAD baclight: application of a new rapid staining method for direct enumeration of viable and total bacteria in drinking water. *J Microbiol Methods* 37:77–86. [https://doi.org/10.1016/S0167-7012\(99\)00048-2](https://doi.org/10.1016/S0167-7012(99)00048-2)
37. Gelhausen R, Svensson SL, Froschauer K, Heyl F, Hadjeras L, Sharma CM, Eggenhofer F, Backofen R. 2021. HRIBO: high-throughput analysis of bacterial ribosome profiling data. *Bioinformatics* 37:2061–2063. <https://doi.org/10.1093/bioinformatics/btaa959>
38. Mohammad F, Green R, Buskirk AR. 2019. A systematically-revised ribosome profiling method for bacteria reveals pauses at single-codon resolution. *Elife* 8:1–25. <https://doi.org/10.7554/eLife.42591>
39. Latif H, Szubin R, Tan J, Brunk E, Lechner A, Zengler K, Palsson BO. 2015. A streamlined ribosome profiling protocol for the characterization of microorganisms. *Biotechniques* 58:329–332. <https://doi.org/10.2144/000114302>
40. Mohammad F, Buskirk AR. 2019. Protocol for ribosome profiling in bacteria. *Bio Protoc* 9:e3468. <https://doi.org/10.21769/BioProtoc.3468>
41. Zhang Y, Xiao Z, Zou Q, Fang J, Wang Q, Yang X, Gao N. 2017. Ribosome profiling reveals genome-wide cellular translational regulation upon heat stress in *Escherichia coli*. *Genomics*, Proteomics & Bioinformatics 15:324–330. <https://doi.org/10.1016/j.gpb.2017.04.005>
42. Gerashchenko MV, Lobanov AV, Gladyshev VN. 2012. Genome-wide ribosome profiling reveals complex translational regulation in response to oxidative stress. *Proc Natl Acad Sci U S A* 109:17394–17399. <https://doi.org/10.1073/pnas.1120799109>
43. Chothani S, Adami E, Quyang JF, Viswanathan S, Hubner N, Cook SA, Schafer S, Rackham OJL. 2019. deltaTE: detection of translationally regulated genes by integrative analysis of Ribo-Seq and RNA-Seq data. *Curr Protoc Mol Biol* 129:e108. <https://doi.org/10.1002/cpmb.108>
44. Prior TI, Kornberg HL. 1988. Nucleotide sequence of *fruA*, the gene specifying enzyme I^{fru} of the phosphoenolpyruvate-dependent sugar phosphotransferase system in *Escherichia coli* K12. *Microbiology* 134:2757–2768. <https://doi.org/10.1099/00221287-134-10-2757>
45. Dai X, Zhu M, Warren M, Balakrishnan R, Okano H, Williamson JR, Fredrick K, Hwa T, Lee SY, Pedersen S, Record M. 2018. Slowdown of translational elongation in *Escherichia coli* under hyperosmotic stress. *mBio* 9:1. <https://doi.org/10.1128/mBio.02375-17>
46. Sin C, Chiarugi D, Valleriani A. 2016. Quantitative assessment of ribosome drop-off in *E. coli*. *Nucleic Acids Res* 44:2528–2537. <https://doi.org/10.1093/nar/gkw137>
47. Sharma IM, Woodson SA. 2020. RbfA and IF3 couple ribosome biogenesis and translation initiation to increase stress tolerance. *Nucleic Acids Res* 48:359–372. <https://doi.org/10.1093/nar/gkz1065>
48. Vesper O, Amitai S, Belitsky M, Byrgazov K, Kaberdina AC, Engelberg-Kulka H, Moll I. 2011. Selective translation of leaderless mRNAs by specialized ribosomes generated by MazF in *Escherichia coli*. *Cell* 147:147–157. <https://doi.org/10.1016/j.cell.2011.07.047>
49. Moll I, Engelberg-Kulka H. 2012. Selective translation during stress in *Escherichia coli*. *Trends Biochem Sci* 37:493–498. <https://doi.org/10.1016/j.tibs.2012.07.007>
50. Freedberg WB, Lin ECC. 1973. Three kinds of controls affecting the expression of the *glp* regulon in *Escherichia coli*. *J Bacteriol* 115:816–823. <https://doi.org/10.1128/jb.115.3.816-823.1973>
51. Higashi K, Ishigure H, Demizu R, Uemura T, Nishino K, Yamaguchi A, Kashiwagi K, Igarashi K. 2008. Identification of a spermidine excretion protein complex (MdtJ) in *Escherichia coli*. *J Bacteriol* 190:872–878. <https://doi.org/10.1128/JB.01505-07>
52. Wu T, Hu E, Xu S, Chen M, Guo P, Dai Z, Feng T, Zhou L, Tang W, Zhan L, Fu X, Liu S, Bo X, Yu G. 2021. clusterProfiler 4.0: a universal enrichment tool for interpreting omics data. *The Innovation* 2:100141. <https://doi.org/10.1016/j.xinn.2021.100141>
53. Yohannes E, Thurber AE, Wilks JC, Tate DP, Slonczewski JL. 2005. Polyamine stress at high pH in *Escherichia coli* K-12. *BMC Microbiol* 5:1–8. <https://doi.org/10.1186/1471-2180-5-59>
54. Iyer R, Delcour AH. 1997. Complex inhibition of OmpF and OmpC bacterial porins by polyamines. *J Biol Chem* 272:18595–18601. <https://doi.org/10.1074/jbc.272.30.18595>

55. Samartzidou H, Mehrazin M, Xu Z, Benedik MJ, Delcour AH. 2003. Cadaverine inhibition of porin plays a role in cell survival at acidic pH. *J Bacteriol* 185:13–19. <https://doi.org/10.1128/JB.185.1.13-19.2003>
56. Banerji R, Iyer P, Bhagwat A, Saroj SD. 2022. Spermidine promotes lysozyme tolerance and acid stress resistance in *Streptococcus pyogenes* M3. *Microbiology* 168. <https://doi.org/10.1099/mic.0.001228>
57. Fukuchi J, Kashiwagi K, Yamagishi M, Ishihama A, Igarashi K. 1995. Decrease in cell viability due to the accumulation of spermidine in spermidine acetyltransferase-deficient mutant of *Escherichia coli*. *J Biol Chem* 270:18831–18835. <https://doi.org/10.1074/jbc.270.32.18831>
58. Schryvers A, Weiner JH. 1981. The anaerobic *sn*-glycerol-3-phosphate dehydrogenase of *Escherichia coli*: purification and characterization. *J Biol Chem* 256:9959–9965. [https://doi.org/10.1016/S0021-9258\(19\)68723-5](https://doi.org/10.1016/S0021-9258(19)68723-5)
59. Schweizer H, Larson TJ. 1987. Cloning and characterization of the aerobic *sn*-glycerol-3-phosphate dehydrogenase structural gene *glpD* of *Escherichia coli* K-12. *J Bacteriol* 169:507–513. <https://doi.org/10.1128/jb.169.2.507-513.1987>
60. Paulsen IT, Reizer J, Jin RZ, Lin ECC, Saier MH Jr. 2000. Functional genomic studies of dihydroxyacetone utilization in *Escherichia coli*. *Microbiology* 146 (Pt 10):2343–2344. <https://doi.org/10.1099/00221287-146-10-2343>
61. Larson TJ, Ye SZ, Weissenborn DL, Hoffmann HJ, Schweizer H. 1987. Purification and characterization of the repressor for the *sn*-glycerol 3-phosphate regulon of *Escherichia coli* K12. *J Biol Chem* 262:15869–15874.
62. Sohlenkamp C. 2017. Membrane homeostasis in bacteria upon pH challenge, p 1–13. In Geiger O (ed), *Biogenesis of fatty acids, lipids and membranes*. Springer International Publishing, Cham. <https://doi.org/10.1007/978-3-319-43676-0>
63. Lindahl T, Nyberg B. 1972. Rate of depurination of native deoxyribonucleic acid. *Biochemistry* 11:3610–3618. <https://doi.org/10.1021/bi00769a018>
64. Qi Y, Wang H, Chen X, Wei G, Tao S, Fan M. 2021. Altered metabolic strategies: elaborate mechanisms adopted by *Oenococcus oeni* in response to acid stress. *J Agric Food Chem* 69:2906–2918. <https://doi.org/10.1021/acs.jafc.0c07599>
65. Blethen SL, Boeker EA, Snell EE. 1968. Arginine decarboxylase from *Escherichia coli*. *J Biol Chem* 243:1671–1677. [https://doi.org/10.1016/S0021-9258\(18\)93498-8](https://doi.org/10.1016/S0021-9258(18)93498-8)
66. Seputiene V, Motiejūnas D, Suziedelis K, Tomenius H, Normark S, Melefors O, Suziedeliene E. 2003. Molecular characterization of the acid-inducible *asr* gene of *Escherichia coli* and its role in acid stress response. *J Bacteriol* 185:2475–2484. <https://doi.org/10.1128/JB.185.8.2475-2484.2003>
67. Ren C, Zheng Y, Liu C, Mencius J, Wu Z, Quan S. 2022. Molecular characterization of an intrinsically disordered chaperone reveals net-charge regulation in chaperone action. *J Mol Biol* 434:167405. <https://doi.org/10.1016/j.jmb.2021.167405>
68. Kannan G, Wilks JC, Fitzgerald DM, Jones BD, Bondurant SS, Slonczewski JL. 2008. Rapid acid treatment of *Escherichia coli*: transcriptomic response and recovery. *BMC Microbiol* 8:1–13. <https://doi.org/10.1186/1471-2180-8-37>
69. Celia H, Noinaj N, Buchanan SK. 2020. Structure and stoichiometry of the Ton molecular motor. *Int J Mol Sci* 21:1–15. <https://doi.org/10.3390/ijms21020375>
70. Ratliff AC, Buchanan SK, Celia H. 2022. The Ton motor. *Front Microbiol* 13:852955. <https://doi.org/10.3389/fmicb.2022.852955>
71. Vinella D, Brochier-Armanet C, Loiseau L, Talla E, Barras F. 2009. Iron-sulfur (Fe/S) protein biogenesis: phylogenomic and genetic studies of A-type carriers. *PLoS Genet* 5:e1000497. <https://doi.org/10.1371/journal.pgen.1000497>
72. Oakley K, Sterling K, Shearer J, Kim E. 2021. Controlled protonation of [2Fe-2S] leading to MitoNEET analogues and concurrent cluster modification. *Inorg Chem* 60:16074–16078. <https://doi.org/10.1021/acs.inorgchem.1c02622>
73. Jin Z, Li J, Ni L, Zhang R, Xia A, Jin F. 2018. Conditional privatization of a public siderophore enables *Pseudomonas aeruginosa* to resist cheater invasion. *Nat Commun* 9:1383. <https://doi.org/10.1038/s41467-018-03791-y>
74. Djoko KY, Phan M-D, Peters KM, Walker MJ, Schembri MA, McEwan AG. 2017. Interplay between tolerance mechanisms to copper and acid stress in *Escherichia coli*. *Proc Natl Acad Sci USA* 114:6818–6823. <https://doi.org/10.1073/pnas.1620232114>
75. Kim Y, Lee S, Park K, Yoon H. 2022. Cooperative interaction between acid and copper resistance in *Escherichia coli*. *J Microbiol Biotechnol* 32:602–611. <https://doi.org/10.4014/jmb.2201.01034>
76. Hyre A, Casanova-Hampton K, Subashchandrabose S. 2021. Copper homeostatic mechanisms and their role in the virulence of *Escherichia coli* and *Salmonella enterica*. *EcoSal Plus* 9:eESP00142020. <https://doi.org/10.1128/ecosalplus.ESP-0014-2020>
77. Djoko KY, Ong CY, Walker MJ, McEwan AG. 2015. The role of copper and zinc toxicity in innate immune defense against bacterial pathogens. *J Biol Chem* 290:18954–18961. <https://doi.org/10.1074/jbc.R115.647099>
78. Yanofsky C, Horn V, Gollnick P. 1991. Physiological studies of tryptophan transport and tryptophanase operon induction in *Escherichia coli*. *J Bacteriol* 173:6009–6017. <https://doi.org/10.1128/jb.173.19.6009-6017.1991>
79. Goode O, Smith A, Zarkan A, Cama J, Invergo BM, Belgami D, Caño-Muñiz S, Metz J, O'Neill P, Jeffries A, Norville IH, David J, Summers D, Pagliara S. 2021. Persister *Escherichia coli* cells have a lower intracellular pH than susceptible cells but maintain their pH in response to antibiotic treatment. *mBio* 12:e0090921. <https://doi.org/10.1128/mBio.00909-21>
80. Balaban NQ, Merrin J, Chait R, Kowalik L, Leibler S. 2004. Bacterial persistence as a phenotypic switch. *Science* 305:1622–1625. <https://doi.org/10.1126/science.1099390>
81. Mitchell P. 1973. Performance and conservation of osmotic work by proton-coupled solute porter systems. *J Bioenerg* 4:63–91. <https://doi.org/10.1007/BF01516051>
82. Richard H, Foster JW. 2004. *Escherichia coli* glutamate- and arginine-dependent acid resistance systems increase internal pH and reverse transmembrane potential. *J Bacteriol* 186:6032–6041. <https://doi.org/10.1128/JB.186.18.6032-6041.2004>
83. Ude S, Lassak J, Starosta AL, Kraxenberger T, Wilson DN, Jung K. 2013. Translation elongation factor EF-P alleviates ribosome stalling at polyproline stretches. *Science* 339:82–85. <https://doi.org/10.1126/science.1228985>
84. Baba T, Ara T, Hasegawa M, Takai Y, Okumura Y, Baba M, Datsenko KA, Tomita M, Wanner BL, Mori H. 2006. Construction of *Escherichia coli* K-12 in-frame, single-gene knockout mutants: the Keio collection. *Mol Syst Biol* 2:2006.0008. <https://doi.org/10.1038/msb4100050>
85. Kitagawa M, Ara T, Arifuzzaman M, Ioka-Nakamichi T, Inamoto E, Toyonaga H, Mori H. 2005. Complete set of ORF clones of *Escherichia coli* ASKA library (a complete set of *E. coli* K-12 ORF archive): unique resources for biological research. *DNA Res* 12:291–299. <https://doi.org/10.1093/dnares/dsi012>
86. Romiyo V, Wilson JW. 2020. Phenotypes, transcriptome, and novel biofilm formation associated with the *ydjI* gene. *Antonie van Leeuwenhoek* 113:1109–1122. <https://doi.org/10.1007/s10482-020-01412-7>
87. Gao Y, Yurkovich JT, Seo SW, Kabimoldayev I, Dräger A, Chen K, Sastry AV, Fang X, Mih N, Yang L, Eichner J, Cho B-K, Kim D, Palsson BO. 2018. Systematic discovery of uncharacterized transcription factors in *Escherichia coli* K-12 MG1655. *Nucleic Acids Res* 46:10682–10696. <https://doi.org/10.1093/nar/gky752>
88. Jennings ME, Quick LN, Soni A, Davis RR, Crosby K, Ott CM, Nickerson CA, Wilson JW. 2011. Characterization of the *Salmonella enterica* serovar Typhimurium *ydjI* gene, which encodes a conserved DNA binding protein required for full acid stress resistance. *J Bacteriol* 193:2208–2217. <https://doi.org/10.1128/JB.01335-10>
89. Ma Z, Masuda N, Foster JW. 2004. Characterization of EvgAS-YdeO-GadE branched regulatory circuit governing glutamate-dependent acid resistance in *Escherichia coli*. *J Bacteriol* 186:7378–7389. <https://doi.org/10.1128/JB.186.21.7378-7389.2004>
90. Torres B, Porras G, Garcia JL, Diaz E. 2003. Regulation of the *mhp* cluster responsible for 3-(3-hydroxyphenyl)propionic acid degradation in *Escherichia coli*. *J Biol Chem* 278:27575–27585. <https://doi.org/10.1074/jbc.M303245200>
91. Ferrández A, García JL, Díaz E. 1997. Genetic characterization and expression in heterologous hosts of the 3-(3-hydroxyphenyl)propionate

- catabolic pathway of *Escherichia coli* K-12. *J Bacteriol* 179:2573–2581. <https://doi.org/10.1128/jb.179.8.2573-2581.1997>
92. Yadavalli SS, Yuan J. 2022. Bacterial small membrane proteins: the swiss army knife of regulators at the lipid bilayer. *J Bacteriol* 204:e0034421. <https://doi.org/10.1128/JB.00344-21>
 93. Petruschke H, Anders J, Stadler PF, Jehmlich N, von Bergen M. 2020. Enrichment and identification of small proteins in a simplified human gut microbiome. *J Proteomics* 213:103604. <https://doi.org/10.1016/j.jprot.2019.103604>
 94. Weaver J, Mohammad F, Buskirk AR, Storz G. 2019. Identifying small proteins by ribosome profiling with stalled initiation complexes. *mBio* 10:1–21. <https://doi.org/10.1128/mBio.02819-18>
 95. Meydan S, Marks J, Klepacki D, Sharma V, Baranov PV, Firth AE, Margus T, Kefi A, Vázquez-Laslop N, Mankin AS. 2019. Retapamulin-assisted ribosome profiling reveals the alternative bacterial proteome. *Mol Cell* 74:481–493. <https://doi.org/10.1016/j.molcel.2019.02.017>
 96. Hadjeras L, Heiniger B, Maaß S, Scheuer R, Gelhausen R, Azarderakhsh S, Barth-Weber S, Backofen R, Becher D, Ahrens CH, Sharma CM, Evguenieva-Hackenberg E. 2023. Unraveling the small proteome of the plant symbiont *Sinorhizobium meliloti* by ribosome profiling and proteogenomics. *Microlife* 4:uqad012. <https://doi.org/10.1093/femsml/uqad012>
 97. Adams PP, Baniulyte G, Esnault C, Chegireddy K, Singh N, Monge M, Dale RK, Storz G, Wade JT. 2021. Regulatory roles of *Escherichia coli* 5' UTR and ORF-internal RNAs detected by 3' end mapping. *Elife* 10:1–33. <https://doi.org/10.7554/eLife.62438>
 98. Raina M, Aoyama JJ, Bhatt S, Paul BJ, Zhang A, Updegrove TB, Miranda-Ríos J, Storz G. 2022. Dual-function AzuCR RNA modulates carbon metabolism. *Proc Natl Acad Sci U S A* 119:e2117930119. <https://doi.org/10.1073/pnas.21117930119>
 99. Clauwaert J, Menschaert G, Waegeman W. 2019. DeepRibo: a neural network for precise gene annotation of prokaryotes by combining ribosome profiling signal and binding site patterns. *Nucleic Acids Res* 47:e36. <https://doi.org/10.1093/nar/gkz061>
 100. Diesh C, Stevens GJ, Xie P, De Jesus Martinez T, Hershberg EA, Leung A, Guo E, Dider S, Zhang J, Bridge C, Hogue G, Duncan A, Morgan M, Flores T, Bimber BN, Haw R, Cain S, Buels RM, Stein LD, Holmes IH. 2022. JBrowse 2: a modular genome browser with views of synteny and structural variation. *bioRxiv*. <https://doi.org/10.1101/2022.07.28.501447>
 101. Guillier M, Gottesman S. 2008. The 5' end of two redundant sRNAs is involved in the regulation of multiple targets, including their own regulator. *Nucleic Acids Res* 36:6781–6794. <https://doi.org/10.1093/nar/gkn742>
 102. Johansen J, Rasmussen AA, Overgaard M, Valentin-Hansen P. 2006. Conserved small non-coding RNAs that belong to the σ^E regulon: role in down-regulation of outer membrane proteins. *J Mol Biol* 364:1–8. <https://doi.org/10.1016/j.jmb.2006.09.004>
 103. Aquino P, Honda B, Jaini S, Lyubetskaya A, Hosur K, Chiu JG, Ekladios I, Hu D, Jin L, Sayeg MK, et al. 2017. Coordinated regulation of acid resistance in *Escherichia coli*. *BMC Syst Biol* 11:1. <https://doi.org/10.1186/s12918-016-0376-y>
 104. Yu NY, Wagner JR, Laird MR, Melli G, Rey S, Lo R, Dao P, Sahinalp SC, Ester M, Foster LJ, Brinkman FSL. 2010. PSORTb 3.0: improved protein subcellular localization prediction with refined localization subcategories and predictive capabilities for all prokaryotes. *Bioinformatics* 26:1608–1615. <https://doi.org/10.1093/bioinformatics/btq249>
 105. Hallgren J, Tsigros KD, Pedersen MD, Almagro Armenteros JJ, Marcattili P, Nielsen H, Krogh A, Winther O. 2022. DeepTMHMM predicts alpha and beta transmembrane proteins using deep neural networks. *Bioinformatics*. <https://doi.org/10.1101/2022.04.08.487609>
 106. Jumper J, Evans R, Pritzel A, Green T, Figurnov M, Ronneberger O, Tunyasuvunakool K, Bates R, Židek A, Potapenko A, et al. 2021. Highly accurate protein structure prediction with AlphaFold. *Nature* 596:583–589. <https://doi.org/10.1038/s41586-021-03819-2>
 107. Mirdita M, Schütze K, Moriwaki Y, Heo L, Ovchinnikov S, Steinegger M. 2022. ColabFold: making protein folding accessible to all. *Nat Methods* 19:679–682. <https://doi.org/10.1038/s41592-022-01488-1>
 108. Altschul SF, Madden TL, Schäffer AA, Zhang J, Zhang Z, Miller W, Lipman DJ. 1997. Gapped BLAST and PSI-BLAST: a new generation of protein database search programs. *Nucleic Acids Res* 25:3389–3402. <https://doi.org/10.1093/nar/25.17.3389>
 109. Gottesman S. 2019. Trouble is coming: signaling pathways that regulate general stress responses in bacteria. *J Biol Chem* 294:11685–11700. <https://doi.org/10.1074/jbc.REV119.005593>
 110. Battesti A, Majdalani N, Gottesman S. 2011. The RpoS-mediated general stress response in *Escherichia coli*. *Annu Rev Microbiol* 65:189–213. <https://doi.org/10.1146/annurev-micro-090110-102946>
 111. Vincent P, Larochelle H, Bengio Y, Manzagol P-A. 2008. Extracting and composing robust features with denoising autoencoders. *Proceedings of the 25th International Conference on Machine Learning*:1096–1103. <https://doi.org/10.1145/1390156.1390294>
 112. Vincent P, Larochelle H, Lajoie I, Bengio Y, Manzagol P-A. 2010. Stacked denoising autoencoders: learning useful representations in a deep network with a local denoising criterion. *J Mach Learn Res* 11:3371–3408.
 113. Kion-Crosby W, Barquist L. 2023. Network depth affects inference of gene sets from bacterial transcriptomes using denoising autoencoders. *bioRxiv*. <https://doi.org/10.1101/2023.05.30.542622>
 114. Lamoureux CR, Decker KT, Sastry AV, Rychel K, Gao Y, McConn JL, Zielinski DC, Palsson BO. 2021. A multi-scale transcriptional regulatory network knowledge base for *Escherichia coli*. *bioRxiv*. <https://doi.org/10.1101/2021.04.08.439047>
 115. Bhatia RP, Kirit HA, Predeus AV, Bollback JP. 2022. Transcriptomic profiling of *Escherichia coli* K-12 in response to a compendium of stressors. *Sci Rep* 12:16865. <https://doi.org/10.1038/s41598-022-21625-2>
 116. Sandberg TE, Pedersen M, LaCroix RA, Ebrahim A, Bonde M, Herrgard MJ, Palsson BO, Sommer M, Feist AM. 2014. Evolution of *Escherichia coli* to 42°C and subsequent genetic engineering reveals adaptive mechanisms and novel mutations. *Mol Biol Evol* 31:2647–2662. <https://doi.org/10.1093/molbev/msu209>
 117. Choudhary KS, Kleinmanns JA, Decker K, Sastry AV, Gao Y, Szubin R, Seif Y, Palsson BO. 2020. Elucidation of regulatory modes for five two-component systems in *Escherichia coli* reveals novel relationships. *mSystems* 5:1–20. <https://doi.org/10.1128/mSystems.00980-20>
 118. Seo SW, Gao Y, Kim D, Szubin R, Yang J, Cho BK, Palsson BO. 2017. Revealing genome-scale transcriptional regulatory landscape of OmpR highlights its expanded regulatory roles under osmotic stress in *Escherichia coli* K-12 MG1655. *Sci Rep* 7:2181. <https://doi.org/10.1038/s41598-017-02110-7>
 119. Anand A, Chen K, Catoi E, Sastry AV, Olson CA, Sandberg TE, Seif Y, Xu S, Szubin R, Yang L, Feist AM, Palsson BO. 2020. OxyR is a convergent target for mutations acquired during adaptation to oxidative stress-prone metabolic states. *Mol Biol Evol* 37:660–667. <https://doi.org/10.1093/molbev/msz251>
 120. Seo SW, Kim D, Szubin R, Palsson BO. 2015. Genome-wide reconstruction of OxyR and SoxRS transcriptional regulatory networks under oxidative stress in *Escherichia coli* K-12 MG1655. *Cell Rep* 12:1289–1299. <https://doi.org/10.1016/j.celrep.2015.07.043>
 121. Cao H, Wei D, Yang Y, Shang Y, Li G, Zhou Y, Ma Q, Xu Y. 2017. Systems-level understanding of ethanol-induced stresses and adaptation in *E. coli*. *Sci Rep* 7:1–15. <https://doi.org/10.1038/srep44150>
 122. Reyes-Fernández EZ, Schuldiner S. 2020. Acidification of cytoplasm in *Escherichia coli* provides a strategy to cope with stress and facilitates development of antibiotic resistance. *Sci Rep* 10:9954. <https://doi.org/10.1038/s41598-020-66890-1>
 123. Mitosch K, Rieckh G, Bollenbach T. 2017. Noisy response to antibiotic stress predicts subsequent single-cell survival in an acidic environment. *Cell Systems* 4:393–403. <https://doi.org/10.1016/j.cels.2017.03.001>
 124. Yair Y, Michaux C, Biran D, Bernhard J, Vogel J, Barquist L, Ron EZ, Van Laar TA. 2022. Cellular RNA targets of cold shock proteins CspC and CspE and their importance for serum resistance in septicemic *Escherichia coli*. *mSystems* 7:e00086-22. <https://doi.org/10.1128/mSystems.00086-22>
 125. Michaux C, Holmqvist E, Vasicek E, Sharan M, Barquist L, Westermann AJ, Gunn JS, Vogel J. 2017. RNA target profiles direct the discovery of virulence functions for the cold-shock proteins CspC and CspE. *Proc Natl Acad Sci USA* 114:6824–6829. <https://doi.org/10.1073/pnas.1620772114>
 126. Sun Y, Fukamachi T, Saito H, Kobayashi H. 2012. Respiration and the F₁F₀-ATPase enhance survival under acidic conditions in *Escherichia coli*. *PLoS One* 7:e52577. <https://doi.org/10.1371/journal.pone.0052577>

127. Lee J, Hiibel SR, Reardon KF, Wood TK. 2010. Identification of stress-related proteins in *Escherichia coli* using the pollutant *cis*-dichloroethylene. *J Appl Microbiol* 108:2088–2102. <https://doi.org/10.1111/j.1365-2672.2009.04611.x>
128. Wiebe MA, Brannon JR, Steiner BD, Bamidele A, Schrimpe-Rutledge AC, Codreanu SG, Sherrod SD, McLean JA, Hadjifrangiskou M. 2022. Serine deamination is a new acid tolerance mechanism observed in uropathogenic *Escherichia coli*. *mBio* 13:e0296322. <https://doi.org/10.1128/mbio.02963-22>
129. Fallingborg J. 1999. Intraluminal pH of the human gastrointestinal tract. *Dan Med Bull* 46:183–196.
130. Martin RG, Rosner JL. 1995. Binding of purified multiple antibiotic-resistance repressor protein (MarR) to *mar* operator sequences. *Proc Natl Acad Sci USA* 92:5456–5460. <https://doi.org/10.1073/pnas.92.12.5456>
131. Gibson DG, Young L, Chuang R-Y, Venter JC, Hutchison CA III, Smith HO. 2009. Enzymatic assembly of DNA molecules up to several hundred kilobases. *Nat Methods* 6:343–345. <https://doi.org/10.1038/nmeth.1318>
132. Köster J, Rahmann S. 2012. Snakemake—a scalable bioinformatics workflow engine. *Bioinformatics* 28:2520–2522. <https://doi.org/10.1093/bioinformatics/bts480>
133. Grüning B, Dale R, Sjödin A, Chapman BA, Rowe J, Tomkins-Tinch CH, Valieris R, Köster J, Bioconda Team. 2018. Bioconda: sustainable and comprehensive software distribution for the life sciences. *Nat Methods* 15:475–476. <https://doi.org/10.1038/s41592-018-0046-7>
134. Kurtzer GM, Sochat V, Bauer MW. 2017. Singularity: scientific containers for mobility of compute. *PLoS One* 12:e0177459. <https://doi.org/10.1371/journal.pone.0177459>
135. Martin M. 2011. Cutadapt removes adapter sequences from high-throughput sequencing reads. *EMBnet j* 17:10. <https://doi.org/10.14806/ej.17.1.200>
136. Otto C, Stadler PF, Hoffmann S. 2014. Lacking alignments? The next-generation sequencing mapper segemehl revisited. *Bioinformatics* 30:1837–1843. <https://doi.org/10.1093/bioinformatics/btu146>
137. Li H, Handsaker B, Wysoker A, Fennell T, Ruan J, Homer N, Marth G, Abecasis G, Durbin R, 1000 Genome Project Data Processing Subgroup. 2009. The sequence alignment/map format and SAMtools. *Bioinformatics* 25:2078–2079. <https://doi.org/10.1093/bioinformatics/btp352>
138. Liao Y, Smyth GK, Shi W. 2014. Featurecounts: an efficient general purpose program for assigning sequence reads to genomic features. *Bioinformatics* 30:923–930. <https://doi.org/10.1093/bioinformatics/btt656>
139. Wingett SW, Andrews S. 2018. FastQ screen: a tool for multi-genome mapping and quality control. *F1000Res* 7:1338. <https://doi.org/10.12688/f1000research.15931.1>
140. Ewels P, Magnusson M, Lundin S, Käller M. 2016. MultiQC: summarize analysis results for multiple tools and samples in a single report. *Bioinformatics* 32:3047–3048. <https://doi.org/10.1093/bioinformatics/btw354>
141. Love MI, Huber W, Anders S. 2014. Moderated estimation of fold change and dispersion for RNA-Seq data with DESeq2. *Genome Biol* 15:1–21. <https://doi.org/10.1186/s13059-014-0550-8>
142. Inc. P.T. 2015. Collaborative data science. Montreal, QC. Plotly Technologies Inc. <https://plot.ly>
143. Becker AH, Oh E, Weissman JS, Kramer G, Bukau B. 2013. Selective ribosome profiling as a tool for studying the interaction of chaperones and targeting factors with nascent polypeptide chains and ribosomes. *Nat Protoc* 8:2212–2239. <https://doi.org/10.1038/nprot.2013.133>
144. Carlson M. 2019. Org.Eck12.Eg.db: genome wide annotation for *E coli* strain K12. <https://doi.org/https://doi.org/doi:10.18129/B9.bioc.org.Eck12.eg.db>
145. Gelhausen R, Müller T, Svensson SL, Alkhnbashi OS, Sharma CM, Eggenhofer F, Backofen R. 2022. RiboReport - benchmarking tools for ribosome profiling-based identification of open reading frames in bacteria. *Briefings in Bioinformatics* 23:1–22. <https://doi.org/10.1093/bib/bbab549>
146. Schmittgen TD, Livak KJ. 2008. Analyzing real-time PCR data by the comparative CT method. *Nat Protoc* 3:1101–1108. <https://doi.org/10.1038/nprot.2008.73>
147. Castanie-Cornet MP, Penfound TA, Smith D, Elliott JF, Foster JW. 1999. Control of acid resistance in *Escherichia coli*. *J Bacteriol* 181:3525–3535. <https://doi.org/10.1128/JB.181.11.3525-3535.1999>
148. Cholet F. 2015. Keras. Github. Available from: <https://keras.io>
149. Schneider CA, Rasband WS, Eliceiri KW. 2012. NIH image to ImageJ: 25 years of image analysis. *Nat Methods* 9:671–675. <https://doi.org/10.1038/nmeth.2089>
150. Ducret A, Quardokus EM, Brun YV. 2016. MicrobeJ, a tool for high throughput bacterial cell detection and quantitative analysis. *Nat Microbiol* 1:1–7. <https://doi.org/10.1038/nmicrobiol.2016.77>
151. Schägger H. 2006. Tricine-SDS-PAGE. *Nat Protoc* 1:16–22. <https://doi.org/10.1038/nprot.2006.4>

2.2 Motility-activating mutations upstream of *flhDC* reduce acid shock survival of *Escherichia coli*

Schumacher, K., Braun, D., Kleigrew, K. and Jung, K. (2024). Motility-activating mutations upstream of *flhDC* reduce acid shock survival of *Escherichia coli*. *Microbiol Spectr.* 12:e0054424.

Available online at:

<https://pubmed.ncbi.nlm.nih.gov/38651876/>

Motility-activating mutations upstream of *flhDC* reduce acid shock survival of *Escherichia coli*

Kilian Schumacher,¹ Djanna Braun,¹ Karin Kleigrew, ² Kirsten Jung¹

AUTHOR AFFILIATIONS See affiliation list on p. 15.

ABSTRACT Many neutralophilic bacterial species try to evade acid stress with an escape strategy, which is reflected in the increased expression of genes coding for flagellar components. Extremely acid-tolerant bacteria, such as *Escherichia coli*, survive the strong acid stress, e.g., in the stomach of vertebrates. Recently, we were able to show that the induction of motility genes in *E. coli* is strictly dependent on the degree of acid stress, i.e., they are induced under mild acid stress but not under severe acid stress. However, it was not known to what extent fine-tuned expression of motility genes is related to fitness and the ability to survive periods of acid shock. In this study, we demonstrate that the expression of FlhDC, the master regulator of flagellation, is inversely correlated with the acid shock survival of *E. coli*. We encountered this phenomenon when analyzing mutants from the Keio collection, in which the expression of *flhDC* was altered by an insertion sequence element. These results suggest a fitness trade-off between acid tolerance and motility.

IMPORTANCE *Escherichia coli* is extremely acid-resistant, which is crucial for survival in the gastrointestinal tract of vertebrates. Recently, we systematically studied the response of *E. coli* to mild and severe acidic conditions using Ribo-Seq and RNA-Seq. We found that motility genes are induced at pH 5.8 but not at pH 4.4, indicating stress-dependent synthesis of flagellar components. In this study, we demonstrate that motility-activating mutations upstream of *flhDC*, encoding the master regulator of flagella genes, reduce the ability of *E. coli* to survive periods of acid shock. Furthermore, we show an inverse correlation between motility and acid survival using a chromosomal isopropyl β -D-thiogalactopyranoside (IPTG)-inducible *flhDC* promoter and by sampling differentially motile subpopulations from swim agar plates. These results reveal a previously undiscovered trade-off between motility and acid tolerance and suggest a differentiation of *E. coli* into motile and acid-tolerant subpopulations, driven by the integration of insertion sequence elements.

KEYWORDS motility, flagella, acid resistance, acid shock survival, insertion sequences

Bacteria colonize habitats such as the human stomach and acidic soils, which have a low pH (1, 2). In these environments, protective mechanisms against acidity are crucial to ensure the growth and/or survival of neutralophilic bacteria. Particularly, *Escherichia coli* exhibits substantial tolerance to acidity and has a corresponding infective dose, which is several orders of magnitude lower in comparison to other enteropathogens (3). Pathogenic *E. coli* strains, as well as non-pathogenic K-12 lab strains, survive at extremely low pH (<2.5) (4). This is crucial for pathogenic strains in order to endure the low pH of the stomach, which constitutes the major bactericidal barrier of the human gastrointestinal tract (5, 6). As a consequence, a multitude of defensive strategies have evolved in *E. coli* in order to adapt to such extreme conditions, including H⁺-consum-

Editor Jan Claesen, Lerner Research Institute, Cleveland, Ohio, USA

Address correspondence to Kirsten Jung, kirsten.jung@lrz.uni-muenchen.de.

The authors declare no conflict of interest.

See the funding table on p. 15.

Received 28 February 2024

Accepted 3 April 2024

Published 23 April 2024

Copyright © 2024 Schumacher et al. This is an open-access article distributed under the terms of the [Creative Commons Attribution 4.0 International license](https://creativecommons.org/licenses/by/4.0/).

ing acid resistance systems, acid shock proteins, restrained membrane permeability by altered fatty acid compositions, proton pumps, and many others (3, 7–9).

At moderate acid stress, many neutrophilic bacterial species use an escape strategy to avoid acidity, which is reflected by the increased expression of flagellar genes (10, 11). Accordingly, our RNA-Seq and Ribo-Seq data indicated that chemotaxis and motility genes were induced only under mildly acidic (pH 5.8) but not under severely acidic conditions (pH 4.4) (12). Most of the pH-affected motility genes belonged to the FlhDC regulon (13, 14). FlhD and FlhC form heterohexamers, and the complex acts as the master regulator of flagella synthesis and motility in *E. coli* (15–17). Genes regulated by FlhDC involve class II flagellar operons encoding basal body components, flagella export systems, the alternative sigma factor FliA, and non-flagellar operons (14, 18, 19). The *flhDC* operon is under the transcriptional control of a large number of transcription factors and small RNAs, which implement environmental cues such as osmolarity, synthesis of fimbriae, catabolite repression, and quorum sensing (20–23).

Notably, several motility-activating mutations in the promoter region of *flhDC* have been described. These include insertion sequence (IS) elements and point mutations, which disrupt the binding sites of transcriptional repressors like OmpR or LrhA (24–27). The presence of such mutations varies among various *E. coli* K-12 strains and affects motility rates due to consequently enhanced *flhDC* expression levels (24–27). Strikingly, motility-activating mutations in the *flhDC* regulatory region have also been detected in several single-gene knockout mutants of the Keio collection (28).

In our previous study, we noted significantly increased transcript and ribosome footprint levels for FliA and FlhDC at pH 5.8 (12). However, the highest increase among all annotated transcription factors in *E. coli* was found for the lclR-type regulator MhpR at pH 4.4 (12). Moreover, an *mhpR* mutant obtained from the Keio collection (29) showed the lowest survival rate among all tested knockout mutants of crucial acid resistance regulators under acid shock (12). MhpR regulates the expression of an operon involved in the degradation of cinnamic acid derivatives such as phenylpropionate (PP), 3-(2,3-dihydroxyphenyl)propionate (DHPP), and 3-hydroxyphenylpropionate (3HPP) (30, 31). These aromatic compounds can bind individually or synergistically to MhpR and stimulate the interaction of MhpR with its operator sequence in the *mhpABCDFE* promoter region (32). Upon induction of the *mhpABCDFE* genes, 3-HPP and PP can be converted first to DHPP, which is ultimately degraded to intermediates of the citric acid cycle (30, 33). 3HPP and PP are commonly ingested through the uptake of plant material. For instance, several hydroxycinnamic acid derivatives are found to large extents in blueberries and huckleberries (34) and occur as secondary metabolites in other plants (35). However, the contribution of MhpR to acid resistance in *E. coli* is unclear.

In this study, we show that the reduced survival rate of an *mhpR* mutant from the Keio collection is caused by the integration of an IS5 element in the promoter region of *flhDC* and not by *mhpR* itself. RNA-Seq and soft agar swim assays confirmed that this mutant is hypermotile. The presence or absence of IS elements in *flhDC* promoter regions of different *E. coli* strains affected not only motility but also survival under acid shock. Using a strain with a chromosomal isopropyl β -D-thio-galactopyranoside (IPTG)-inducible *flhDC* promoter, we found an inverse correlation between motility and the ability to survive acid shock periods. These results indicate that induced expression of flagellar components, which is beneficial in mildly acidic environments, is detrimental for *E. coli* under severe acid stress and requires tight regulation of FlhDC target genes.

RESULTS

Examination of a putative role of MhpR under severe acid stress

We have previously detected enriched transcript and ribosome occupancy levels of *mhpR* in *E. coli* K-12 MG1655 at pH 4.4 (Fig. 1A) (12). To verify whether *mhpR* is upregulated under severe acid stress and to distinguish whether the regulation occurs at the transcriptional or post-transcriptional level, we examined *mhpR* mRNA levels and promoter activity under acid stress and non-stress conditions in *E. coli* MG1655. qRT-PCR

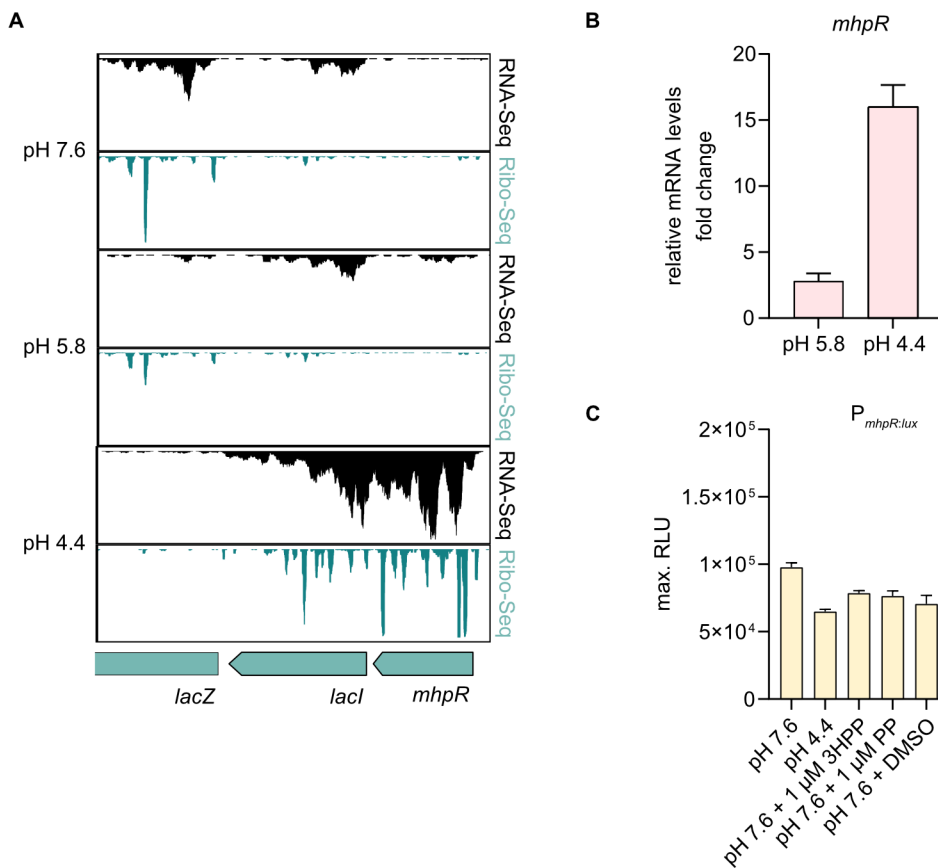


FIG 1 *mhpR* is post-transcriptionally upregulated under severe acid stress. (A) JBrowse2 (36) screenshots of read coverage from Ribo-Seq (green tracks) and RNA-Seq (black tracks) libraries at pH 7.6, 5.8, and 4.4. Schematic illustrations below indicate the genomic locations of *mhpR* and adjacent genes. Ribo- and RNA-Seq data were obtained from Schumacher et al. (12). (B) Verification of increased *mhpR* mRNA levels under acid stress using RT-qPCR. Cells were cultivated as described by Schumacher et al. (12). Fold change values were calculated relative to pH 7.6 and normalized using *secA* as a reference gene. Error bars indicate the standard deviation of three independent biological replicates ($n = 3$). (C) Luciferase-based promoter assay. *E. coli* MG1655 wild-type cells were transformed with the plasmid pBBR1-MCS5- $P_{mhpR:luc}$ and grown in LB medium (pH 7.6) until $OD_{600} = 0.5$. The pH of the medium was then either adjusted stepwise to 5.8 and to pH 4.4, or 1 mM 3HPP, 1 mM PP, or dimethyl sulfoxide (DMSO) was added. Luminescence and growth were determined every 10 min in microtiter plates using a CLARIOstar plus plate reader (BMG Labtech). Data are reported as relative light units (RLUs) in counts per second per OD_{600} , with maximal RLU shown. All experiments were performed in biological replicates ($n = 3$), and error bars represent standard deviations of the mean.

analysis revealed that *mhpR* transcript levels increased only slightly at pH 5.8, but 15-fold at pH 4.4 compared to pH 7.6 (Fig. 1B).

Next, we constructed a luciferase-based promoter-activity reporter plasmid (pBBR1-MCS5- $P_{mhpR:luc}$). The *mhpR* promoter was constitutively active regardless of the extracellular pH and the presence of PP or 3HPP (Fig. 1C). This implies that the *mhpR* promoter is not affected by acidification, which is in line with previous findings (31). These results suggest that the upregulation of *mhpR* under severe acid stress is mediated by a post-transcriptional mechanism.

We then tested whether the described activation of a catabolic pathway for cinnamic acid derivatives (30–32) is related to MhpR under acid stress. However, this hypothesis could be neglected as we did not detect any activation of the *mhpABCDE* promoter at pH 4.4 (Fig. S1). We also investigated whether cinnamic acid derivatives (3HPP, PP, and DHPP) are present in the LB medium and whether their abundance increases in a pH-dependent manner. For this purpose, we analyzed the LB medium and sterile-filtered

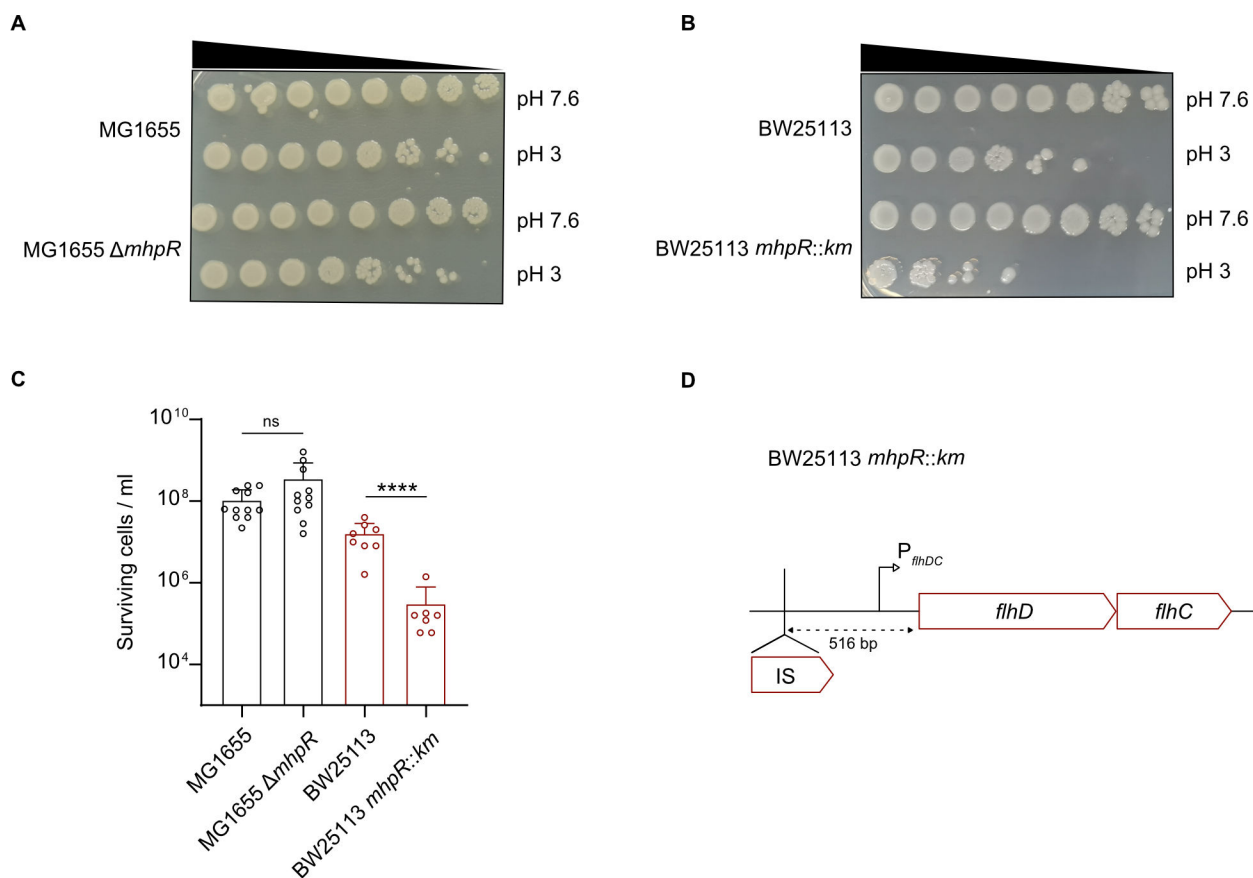


FIG 2 Survival under acid shock is exclusively affected in an *mhpR* mutant from the Keio collection. (A and B) Acid shock assays to evaluate the survival of *E. coli* MG1655 and MG1655 Δ *mhpR* (A) and BW25113 and BW25113 *mhpR::km* (B) at pH 3. Cells were grown in LB pH 7.6 to OD₆₀₀ = 0.5 and cell numbers were adjusted to 10⁹/mL. Cultures were split and then either grown at pH 7.6 or stepwise stressed (15 min pH 5.8 and 15 min pH 4.4) before being exposed to LB pH 3 for 1 h. Cultures were serially diluted by a factor of 10 in 1× PBS and plated on LB agar plates. Images were taken after overnight incubation. (C) Quantitative assessment of acid shock survival of *E. coli* MG1655 and MG1655 Δ *mhpR* as well as BW25113 and BW25113 *mhpR::km* strains. Cells were cultivated as described above, and the total number of colony-forming units at pH 3 was counted after overnight incubation. All experiments were performed in biological replicates ($n \geq 6$), and the error bars represent standard deviations of the mean. Significance was evaluated by performing a one-way ANOVA test followed by Bonferroni's multiple comparisons test to compare log-transformed numbers of surviving cells (ns, not significant and **** $P < 0.0001$). (D) Schematic representation of the genomic *flhDC* locus and the distance between the *flhD* start codon and the inserted IS5 element. The presence of the IS5 sequence was determined by colony PCR and sequencing.

supernatants of cultures grown at pH 7.6, 5.8, or 4.4 by LC-MS (see Materials and Methods for details). Neither PP, DHPP, nor 3HPP were detectable in any of the analyzed samples (data not shown). Thus, we conclude that both the enzymes responsible for 3HPP, PP degradation (MhpA-F) and the corresponding substrates for the pathway are not present in pH-neutral and acidified LB media. In summary, MhpR-induced catabolism of 3HPP and PP does not play a role under acid stress adaptation.

Phenotypic characterization of *E. coli mhpR* mutants with different genetic backgrounds

Nevertheless, as previously shown (12) and reconfirmed here again, we observed a strong phenotype of *E. coli* BW25113 *mhpR::km*, a knockout mutant from the Keio collection in an acid shock experiment (Fig. 2B and C). Based on this result, which somewhat contradicted all the results obtained with *E. coli* MG1655 described above, we decided to construct an MG1655 Δ *mhpR* mutant. We performed the acid shock assay (survival of cells at pH 3 for 1 h) and did not detect any significant difference between the MG1655 wild type and the Δ *mhpR* mutant (Fig. 2A and C).

To determine why an acid shock phenotype associated with the knockout of *mhpR* is exclusively detectable in *E. coli* BW25113 but not in MG1655, we searched for strain-specific differences between the two strains. It is important to note that some BW25113 mutants from the Keio collection have IS elements or point mutations in the regulatory region upstream of *flhDC*, which cause upregulation of motility genes (28). Therefore, we sequenced the corresponding region of the BW25113 *mhpR::km* mutant and found an IS5 element in the *flhDC* promoter (Fig. S2). The IS5 element was integrated 516 bp upstream of the *flhDC* start codon (Fig. 2D).

Upregulation of motility and chemotaxis genes is not associated with MhpR

We then conducted an RNA-Seq experiment to elucidate whether differentially expressed genes (DEGs) are detectable in *mhpR* mutants or whether the IS5 insertion 516 bp upstream of the *flhDC* start codon (Fig. 2D) leads exclusively to the induction of chemotaxis and motility genes. To this end, we compared the transcriptomes of *E. coli* MG1655 $\Delta mhpR$ and BW25113 *mhpR::km* under severe acid stress conditions (pH 4.4) with the respective parental strains. We did not detect differentially expressed genes (fold change > 2, FDR-adjusted *P*-value < 0.01) between MG1655 and MG1655 $\Delta mhpR$, with the exception of the deleted *mhpR* gene (Fig. 3A).

In contrast, 62 genes were differentially expressed in the *mhpR* mutant from the Keio collection (Fig. 3B). Almost all upregulated DEGs in BW25113 *mhpR::km* were related to motility and chemotaxis (Table 1) and are part of the FlhDC regulon (13, 14). This result indicates that the IS5 insertion upstream of *flhDC* leads to the induction of motility genes. The only DEGs in BW25113 *mhpR::km* that were not related to flagellar biosynthesis and chemotaxis were *mhpA* and *mhpB* (Table 1). However, it has already been described (37) that the *mhpC* gene in strain BW25113 contains an IS30 element, which leads to a strong expression of *mhpCDEF* and probably to the deregulation of the expression of *mhpAB* in the absence of *mhpR*.

To confirm the RNA-Seq results, we tested a representative selection of DEGs (Table 1) by RT-qPCR. As expected, genes encoding flagella components (*fliA*, *fliC*, *flgA*, *flhB*, and *motA*) and chemotaxis proteins (*cheA* and *tar*) showed enriched mRNA levels in BW25113 *mhpR::km* but not in MG1655 $\Delta mhpR$ (Fig. 3C). In parallel, we tested the motility of the two strains on soft agar [0.3% (wt/vol)] plates. In agreement with the RNA-Seq data (Fig. 3B), BW25113 *mhpR::km* showed significantly increased spreading (*P* < 0.001) compared to MG1655 $\Delta mhpR$ (Fig. 3D).

The presence or absence of an IS element upstream of *flhDC*, but not MhpR, determines survival under severe acid stress

To evaluate whether the presence of the motility-activating IS5 element is indeed the cause of reduced survival under severe acid stress, we removed the IS5 element from the *flhDC* promoter of BW25113 *mhpR::km*. We found that the strain obtained from the Keio collection (29) contained a mixture of cells with and without IS5 insertion in the *flhDC* regulatory region (Fig. S3). By re-streaking this strain several times on LB agar plates and screening individual colonies, we obtained a BW25113 *mhpR* mutant without IS5 insertion in the *flhDC* promoter (Fig. S3) and designated this strain as BW25113 *mhpR::km**. As expected, removal of the IS element from the *flhDC* regulatory region restored the motility of BW25113 back to wild-type levels (Fig. S4). Similar to MG1655 $\Delta mhpR$, BW25113 *mhpR::km**, with the restored *flhDC* regulatory region, showed no differential acid shock survival compared to the wild type (Fig. 4A and B). Furthermore, we constructed another *mhpR* knockout in BW25113 via double homologous recombination, which also contains the native *flhDC* promoter locus (BW25113 $\Delta mhpR$). This strain also showed no reduced survival in the acid shock assay (Fig. 4A and B). These findings indicate that survival under acid shock is not affected by MhpR but depends directly on the presence or absence of an IS element in the intergenic region between *flhDC* and *uspC*.

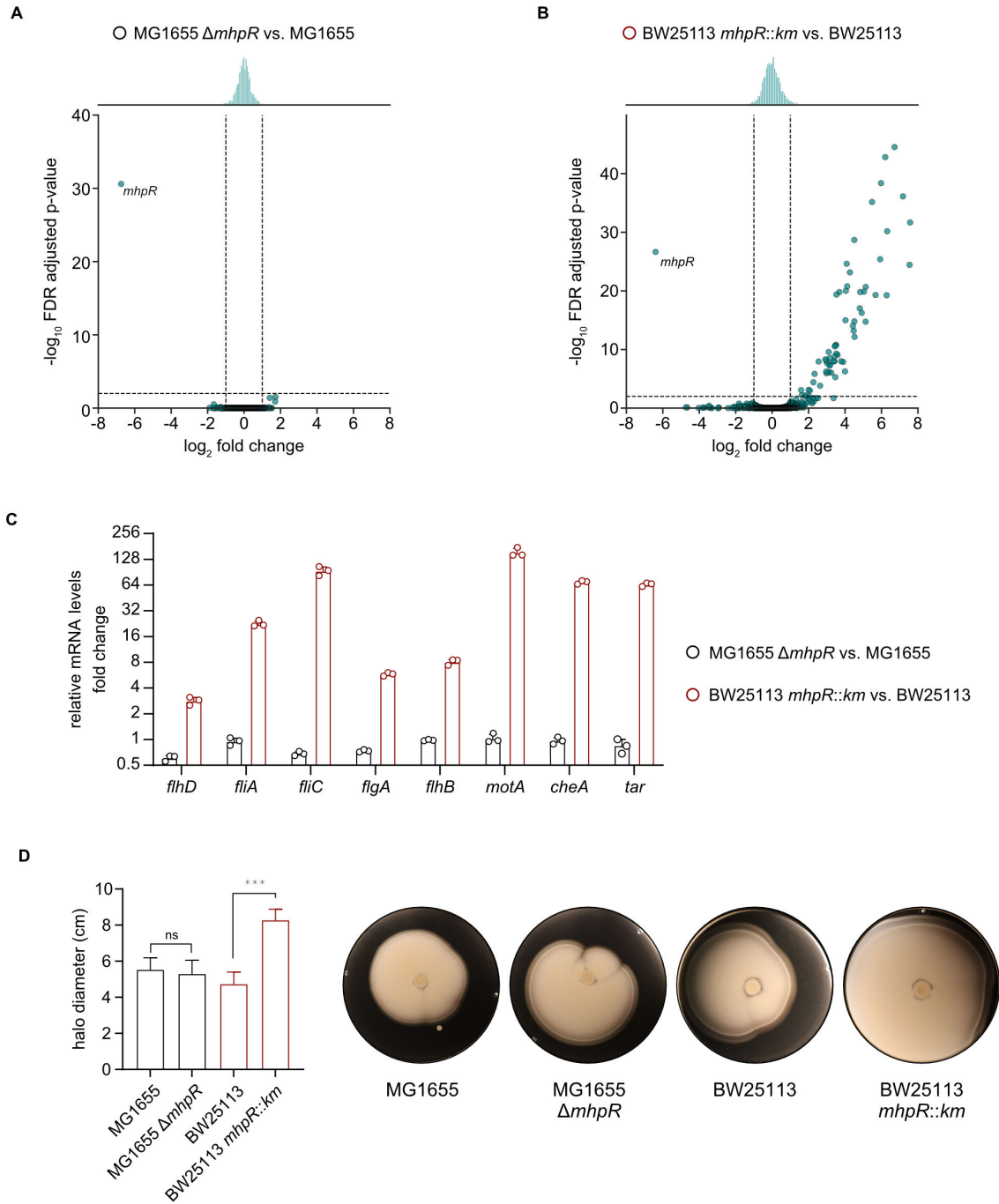


FIG 3 Motility and chemotaxis genes are upregulated in *E. coli* BW25113 $mhpR::km$ but not in MG1655 $\Delta mhpR$. (A and B) Volcano plots illustrating differential mRNA levels determined by RNA-Seq for MG1655 $\Delta mhpR$ compared to MG1655 (A) and BW25113 $mhpR::km$ compared to BW25113 (B). Cells were grown to an OD_{600} of 0.5 in LB pH 7.6 before being shifted to LB pH 5.8 for 15 min and LB pH 4.4 for another 15 min. Dashed lines indicate \log_2 fold change values of +1 or -1 and P -adjusted values of 0.01. (C) Verification of a selection of differentially expressed genes in BW25113 $mhpR::km$ compared to BW25113 at pH 4.4 by RT-qPCR. Cells were cultivated as described above. Fold change values were calculated relative to MG1655 or BW25113 and normalized using *secA* as a reference gene. Error bars indicate the standard deviation of independent biological replicates ($n = 3$). (D) Soft agar swim assay to evaluate the strains described in panels A–C. Overnight cultures normalized to an OD_{600} of 1 were spotted on LB soft agar [0.3% (wt/vol)] plates and incubated for 16 h. Halo diameters were measured, and all experiments were performed in biological replicates ($n \geq 4$). Error bars represent standard deviations of the mean, and significance was evaluated by performing a one-way ANOVA test followed by Bonferroni’s multiple comparisons test (ns, not significant and $***P < 0.001$). Representative images are shown.

TABLE 1 Top 20 genes with increased mRNA levels in BW25113 *mhpR::km* compared to BW25113, sorted in descending order by RNA-Seq fold change values

Gene name	Fold change	P-adjust	Annotation
<i>motA</i>	190.27	2.12×10^{-32}	Motility protein A
<i>tar</i>	186.37	3.58×10^{-25}	Methyl-accepting chemotaxis protein
<i>tap</i>	144.98	7.40×10^{-37}	Methyl-accepting chemotaxis protein— dipeptide-sensing
<i>motB</i>	105.21	2.90×10^{-45}	Motility protein B
<i>yhjH</i>	79.58	6.55×10^{-31}	Cyclic di-GMP phosphodiesterase
<i>fliC</i>	77.91	5.53×10^{-20}	Flagellar filament structural protein
<i>cheA</i>	73.86	1.49×10^{-43}	Chemotaxis protein
<i>mhpB</i>	62.98	4.13×10^{-39}	3-Carboxyethylcatechol 2,3-dioxygenase
<i>cheW</i>	60.85	4.06×10^{-26}	Chemotaxis protein
<i>cheB</i>	51.00	5.08×10^{-20}	Protein-glutamate methyltransferase/protein glutamine deamidase
<i>mhpA</i>	44.64	6.71×10^{-36}	3-(3-hydroxyphenyl)propanoate hydroxylase
<i>flxA</i>	35.15	2.11×10^{-21}	Qin prophage, PF14282 family protein
<i>tsr</i>	35.05	1.80×10^{-15}	Methyl-accepting chemotaxis protein— serine-sensing
<i>fliS</i>	32.82	1.38×10^{-20}	Flagellar biosynthesis protein
<i>fliT</i>	30.18	5.67×10^{-17}	Flagellar biosynthesis protein
<i>cheY</i>	28.51	1.58×10^{-20}	Chemotaxis protein
<i>ycgR</i>	28.03	9.35×10^{-18}	Flagellar brake protein
<i>fliE</i>	22.97	7.04×10^{-13}	Flagellar protein
<i>yjcZ</i>	22.81	1.59×10^{-15}	Regulator of diguanylate cyclase
<i>fliD</i>	22.77	2.06×10^{-29}	Flagellar filament capping protein

Considering that the removal of motility-activating insertions improved the survival of *E. coli* under severe acid stress, we wondered whether we could provoke the reverse phenomenon by introducing an IS element into a strain with a native *flhDC* promoter. Notably, variations in terms of the presence of IS elements upstream of *flhDC* have been observed in different *E. coli* K-12 MG1655 wild-type strains (25). As shown in Fig. S2, the MG1655 wild-type strain used in our laboratory does not harbor IS elements in the *flhDC* promoter and is correspondingly less motile (Fig. 3D). In contrast, another sequenced MG1655 wild-type version (CGSC 7740) contains an IS element in the *flhDC* promoter and is highly motile (25). We thus ordered this strain, detected the presence of the IS element (Fig. S5), and confirmed that motility is indeed significantly increased (Fig. S6). As expected, acid shock survival rates of MG1655 CGSC 7740 were significantly lower (Fig. 4C and D), suggesting that the IS insertion increased motility at the cost of acid tolerance.

Survival under severe acid stress and *flhDC* expression levels are inversely correlated

Due to the inherent capacity of IS elements for genomic transpositions, we cannot exclude the possibility of loss or gain of IS elements upstream of *flhDC* during our experimental procedures. To circumvent the issue of IS transposition and gain the ability to fine-tune *flhDC* expression levels over a wide range, we next used an MG1655 strain in which the regulatory *flhDC* region was chromosomally replaced by a synthetic IPTG-inducible P_{tac} promoter (Fig. 5A) (38). This strain contains a *flu* deletion to minimize cell aggregation (38). Intriguingly, we observed an inverse correlation between the supplemented IPTG concentrations, i.e., FlhDC levels, and the number of cells that survived the acid shock (Fig. 5B). The addition of 10 μ M IPTG corresponds to the native *flhDC* expression level (V. Sourjik, personal communication), and no decrease in survival after acid shock was observed under this condition (Fig. 5B and C). On the other hand, overexpression of *flhDC* as a result of the addition of 50 or 100 μ M IPTG led to a

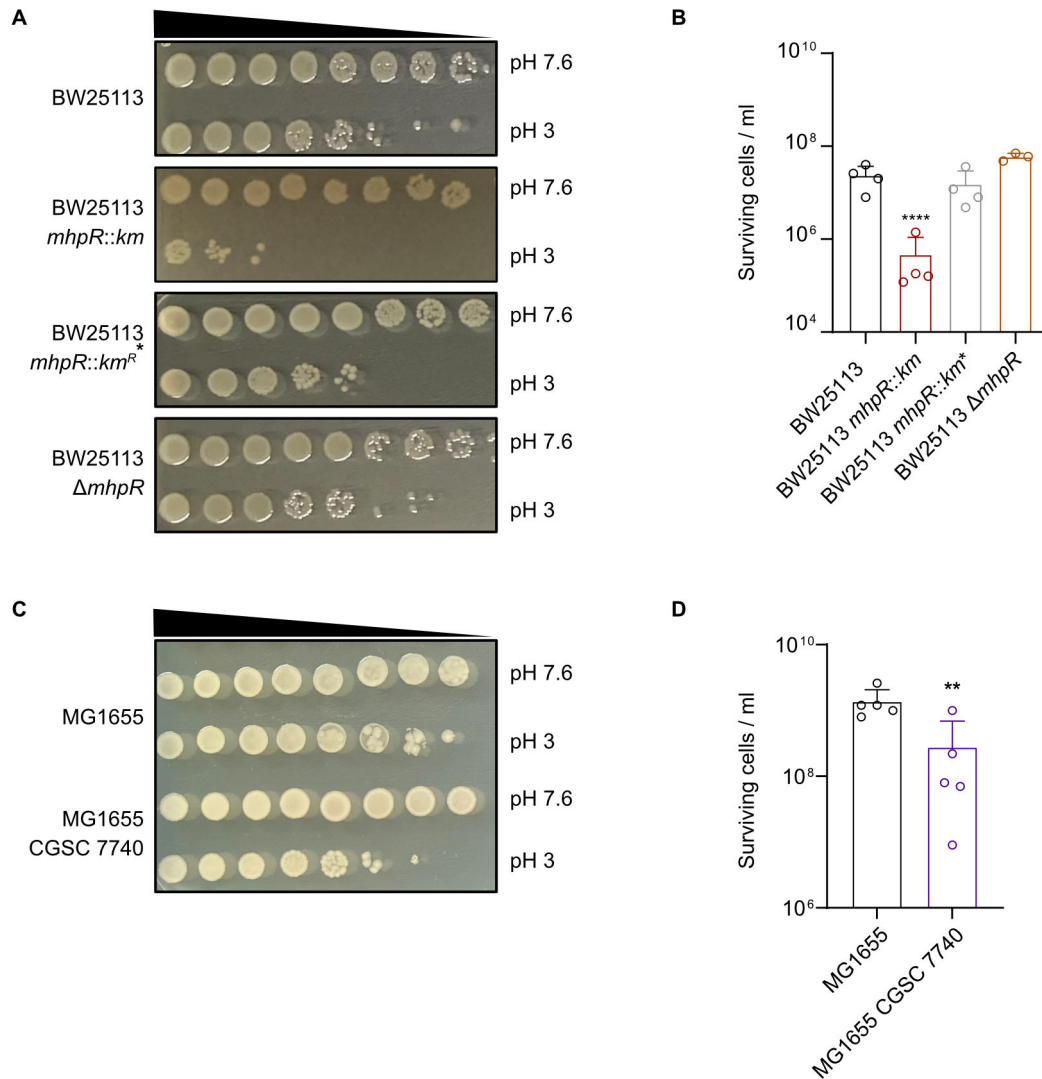


FIG 4 The presence or absence of insertion elements upstream of *flhDC* determines survival under severe acid stress. (A and C) Acid shock assays to evaluate the survival of *E. coli* BW25113, BW25113 *mhpR::km*, BW25113 *mhpR::km**, BW25113 $\Delta mhpR$, MG1655, and MG1655 CGSC 7740 at pH 3. Cells were grown in LB pH 7.6 to $OD_{600} = 0.5$ and cell numbers were adjusted to 10^9 /mL. Cultures were split and then either grown at pH 7.6 or stepwise stressed (15 min pH 5.8 and 15 min pH 4.4) before being exposed to LB pH 3 for 1 h. Cultures were serially diluted by a factor of 10 in 1× PBS and plated on LB agar plates. Images were taken after overnight incubation. (B and D) Quantitative assessment of acid shock survival of *E. coli* BW25113, BW25113 *mhpR::km*, BW25113 *mhpR::km**, BW25113 $\Delta mhpR$, MG1655, and MG1655 CGSC 7740. Cells were cultivated as described in panel A, and the total number of colony-forming units at pH 3 was counted after overnight incubation. All experiments were performed in biological replicates ($n \geq 3$), and error bars represent standard deviations of the mean. Significance was evaluated by performing a one-way ANOVA test followed by Bonferroni's multiple comparisons test (B) or an unpaired *t*-test (D) to compare log-transformed numbers of surviving cells (** $P < 0.01$ and **** $P < 0.0001$).

significant reduction in survival (Fig. 5C). Of note, neither the deletion of *flhC* nor the absence of an inducer for the P_{tac} promoter (0 μ M IPTG) had any effect on acid tolerance compared to the Δflh reference strain (Fig. 5B and C).

To further explore the inverse correlation between acid tolerance and the degree of motility/flagellation, we isolated subpopulations from soft-agar plates and subjected them to severe acid stress. As described previously (39), we sampled MG1655 wild type grown on soft agar [0.3% (wt/vol)] from three different halo positions with increasing distance to the center (1, center; 2, intermediate; and 3, edge) (Fig. 6A). After exposure to

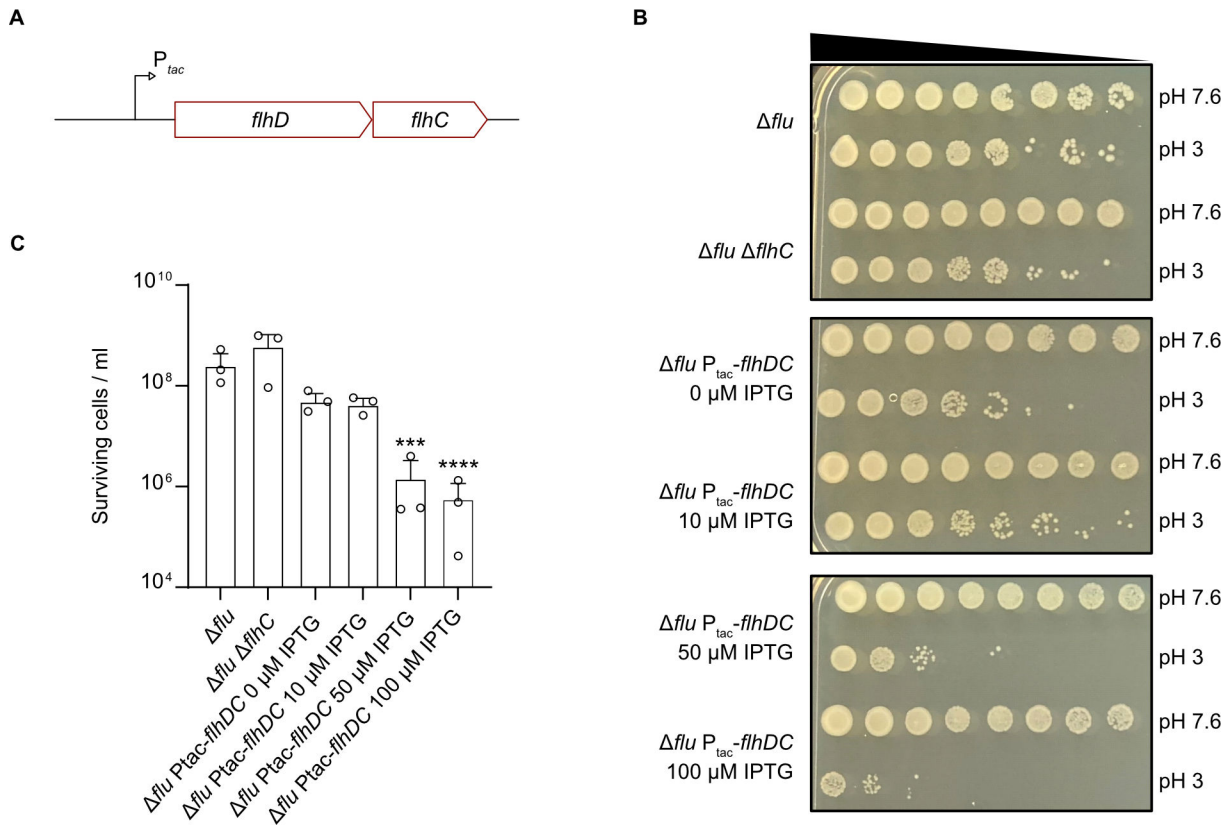


FIG 5 Survival under acid shock and the level of *flhDC* induction are inversely related. (A) Schematic representation of the *flhDC* locus with a replacement of the canonical *flhDC* promoter by an IPTG-inducible P_{tac} promoter. (B) Acid shock assays to evaluate the survival of *E. coli* Δflu , $\Delta flu \Delta flhC$, and $\Delta flu P_{tac}\text{-flhDC}$ strains supplemented with different concentrations of IPTG. Cells were grown in LB pH 7.6 containing the indicated IPTG concentrations to $OD_{600} = 0.5$ and cell numbers were adjusted to 10^9 /mL. Cultures were split and then either grown at pH 7.6 or stepwise stressed (15 min pH 5.8 and 15 min pH 4.4) before being exposed to LB pH 3 for 1 h. Cultures were serially diluted by a factor of 10 in 1× PBS and plated on LB agar plates. Images were taken after overnight incubation. (C) Quantitative assessment of acid shock survival of *E. coli* Δflu , $\Delta flu \Delta flhC$, and $\Delta flu P_{tac}\text{-flhDC}$ strains supplemented with different concentrations of IPTG. Cells were cultivated as described in panel B, and the total number of colony-forming units at pH 3 was counted after overnight incubation. All experiments were performed in biological replicates ($n = 3$), and error bars represent standard deviations of the mean. Significance was evaluated by performing a one-way ANOVA test followed by Bonferroni’s multiple comparisons test to compare log-transformed numbers of surviving cells (*** $P < 0.001$ and **** $P < 0.0001$).

acid shock, the cells collected from the center showed very high acid survival rates (Fig. 6B), even exceeding the values usually observed for *E. coli* MG1655 in liquid culture. Strikingly, cells from the intermediate position and especially those from the edge of the halo were characterized by a significantly lower survival rate (Fig. 6C). It should be noted that the tested subpopulations are in different growth stages and that the extreme resistance of the subpopulation from the center overlaps with the adaptation to the stationary phase (40). In conclusion, (hyper)flagellation mediates a survival deficit in very low pH habitats.

DISCUSSION

The RNA-Seq and Ribo-Seq data from our previous study revealed that the MhpR synthesis levels increased by about one order of magnitude at pH 4.4 and that survival of an *mhpR* mutant from the Keio collection was impaired under severe acid stress (12). Here, we confirmed a higher transcript level of *mhpR* under severe acid stress but found no effects of the transcription factor itself, the regulated 3HPP/PP-dependent catabolic operon, or the cinnamic acid derivatives on acid tolerance.

Thus, despite the upregulation of MhpR at pH 4.4, MhpR does not confer a survival benefit for *E. coli* when challenged with acid at pH 3, at least not in our experimental setup. It is important to note that we could not detect MhpR-inducers such as 3HPP or PP

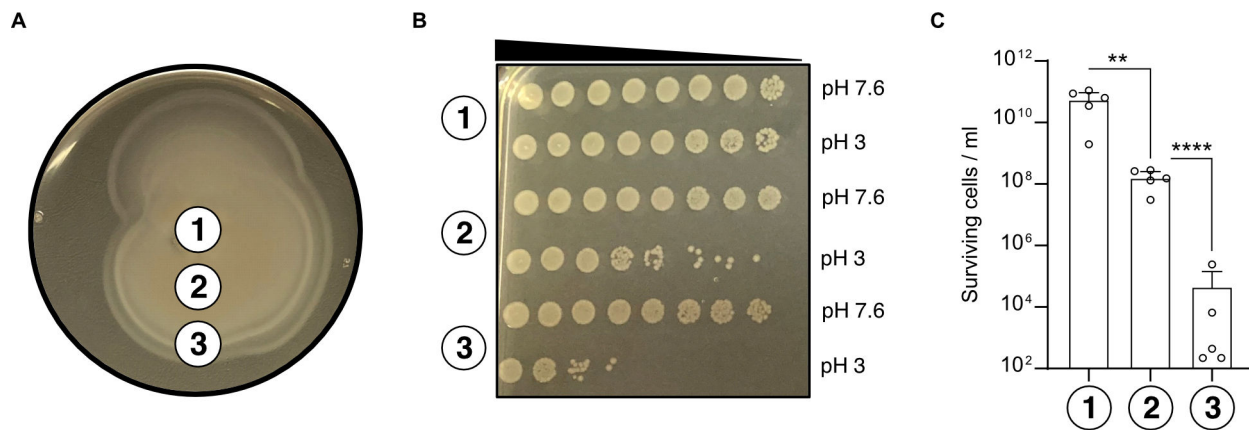


FIG 6 Subpopulations from swim agar plates have different abilities to survive acid shock. (A) Illustration of the MG1655 radial expansion on a soft agar [0.3% (wt/vol)] plate. Three microliters of exponentially grown MG1655 cultures were spotted on soft agar plates and incubated for 16 h. The labeled circles indicate the positions where the cells were collected (1, center; 2, intermediate; and 3, edge) and subsequently exposed to acid shock. (B) Acid shock survival assays of samples taken as described in panel A. Cells were punched out from soft agar plates using P1000 pipette tips and exposed to either LB pH 7.6 or 3 for 1 h. Cultures were serially diluted by a factor of 10 in 1× PBS and plated on LB agar plates. Images were taken after overnight incubation. (C) Quantitative assessment of acid shock survival of cells collected from sampling positions described in panel A. Cells were cultivated as in panels A and B, and the total number of colony-forming units at pH 3 was counted after overnight incubation. All experiments were performed in biological replicates ($n = 5$), and error bars represent standard deviations of the mean. Significance was evaluated by performing a one-way ANOVA test followed by Bonferroni's multiple comparisons test to compare log-transformed numbers of surviving cells (** $P < 0.01$ and **** $P < 0.0001$).

in pH-neutral or acidified LB media via LC-MS. Therefore, we cannot neglect that MhpR and the degradation of cinnamic acid derivatives are useful in nature. PP and 3HPP are present in the human gastrointestinal tract due to the metabolism of aromatic amino acids and plant-derived flavonoids (35), so *E. coli* is exposed to these molecules under natural conditions. Indeed, the expression of *mhp* catabolic genes in enterohemorrhagic *E. coli* (EHEC) increases during growth in the cecal contents of human gut microbiota-associated rats (41). Under these conditions, the cinnamic acid derivatives 3HPP and PP are utilized as carbon sources (30). *mhpR* expression was also significantly increased in EHEC upon infection of mice, and an *mhpR* mutant was outcompeted by a wild type during colonization of the mouse intestine (42). However, our RNA-Seq analysis of *E. coli* K12 provided no evidence that MhpR regulates a gene important for acid tolerance.

BW25113 mutants harboring both, an IS5 insertion in the *flhDC* promoter and an *mhpR* deletion, showed an acid shock phenotype, whereas the BW25113 $\Delta mhpR$ and *mhpR::km** strains with the native *flhDC* upstream region did not (Fig. 4). This indicated that the motility-inducing IS5 insertion is the cause of the observed phenotype in the BW25113 *mhpR::km* strain (Fig. 2). Similar IS insertions and point mutations were described in other mutants of the Keio collection. In fact, 49 of 71 tested strains had mutations in the upstream region of *flhDC*, and as a result, showed increased expression of genes involved in flagellar biosynthesis (28). It is known that the integration of IS elements in the *flhDC* promoter is favored under resting (nonshaking) conditions (28), and mutants from the Keio collection were constructed by culturing bacteria overnight without shaking (29). Moreover, it is hypothesized that IS insertion in this genomic locus is triggered by the cellular environment and depends on whether the encountered conditions permit motility (26).

Our results clearly indicate that IS5 integration upstream of *flhDC* reduces population survival under acid shock in a manner that is inversely correlated with *flhDC* expression levels (Fig. 5). Likewise, acid shock tolerance was dependent on the location of swimming cells on the soft-agar surface, and cells at the edge of the halo could barely survive at pH 3 (Fig. 6). As indicated by RNA-Seq and RT-qPCR, the reason for the reduced acid shock survival was increased flagellar and motility gene expression (Fig. 3). However, it remains to be clarified why increased flagellation and/or motility reduces survival under

severe acid stress. It appears plausible that hypermotile cells have increased energy demand resulting from flagellar synthesis, including the motor and filaments (43); the cost of synthesizing and operating the flagella accounts for up to 3.5% of the total cell energy (44–46). Therefore, cells with IS insertions upstream of *flhDC* are characterized by a reduced growth rate (26). Furthermore, a high number of rotating flagella affects not only the integrity of the membrane but also causes a high flux of protons back into the cytoplasm, which might be disadvantageous at low pH.

Under severe acid stress (pH 4.0–4.5), flagella are rapidly shed (47, 48), chemotaxis to attractants ceases, and the bacteria are no longer motile (49). On the other hand, several studies reported an increased expression of motility genes under mild acid stress (10–12). We propose that under mildly acidic conditions, *E. coli* uses an escape strategy to migrate to environments with optimal pH. Under severe acidic conditions, *E. coli* abandons the escape strategy, switches to an energy-saving mode, and also prevents the flux of protons into the cytoplasm. Considering that motility genes are still induced at pH 5.0 (10), we hypothesize that the inversion point at which motility stops to be beneficial is between pH 5.0 and 4.4.

Motility-activating mutations in the regulatory region of *flhDC* have already been shown to represent a trade-off between growth and biofilm formation (26). Strains containing IS5 upstream of *flhDC* produced more biofilms at the expense of overall growth (26). In this study, we present another trade-off associated with the presence of IS elements, namely the relationship between acid tolerance and the expression of motility genes. It is important to note that the transposition of IS elements can lead to phenotypic heterogeneity within bacterial populations. For example, the phenotypic variability of cells in a biofilm increased as a function of the frequency of IS5 insertions upstream of *flhDC* (26). Moreover, IS-mediated motility heterogeneity within a biofilm was beneficial for bacteria to increase biofilm mass (50). Also, in this study, we found a heterogeneous population of strain CGSC 7740 MG1655 with respect to cells carrying an IS element upstream of *flhDC* (Fig. S5). We have already shown the advantage of phenotypic heterogeneity under acid stress for the three major AR systems using a triple fluorescent reporter strain that enables bet-hedging and division of labor in *E. coli* (51). It is possible that the cytoplasmic membrane protein HdeD represents a link between the acid resistance Gad system and flagellar synthesis in *E. coli*. The expression of *hdeD* is controlled by GadE and HdeD represses the flagella biosynthesis via LrhA (52). Heterogeneous distribution of HdeD in the *E. coli* population (53) and heterogeneous expression of flagella in *Salmonella* are known (54, 55). Using single-cell RNA-Seq (M3-Seq), an acid-resistant subpopulation was found in stationary phase *E. coli* cells (56). According to the results of this study, the transposition of IS elements could be another important factor leading to heterogeneity under acid stress, and it is tempting to speculate that there might also be a motile subpopulation in stationary phase *E. coli* cells (56). This assumption is supported by the data collected here, which suggest an anti-correlation between motility and acid tolerance mediated by IS integrations upstream of *flhDC*. Of note, motility was also found to be correlated with oxygen availability (57). Given the different levels of acidity in the gastrointestinal tract, with a pH of <2 in the stomach (5, 58) and ~pH 6 in the duodenum (59, 60), it would certainly be advantageous for an *E. coli* population to diversify into a motile and an acid-tolerant subpopulation. Indeed, colonization of the mouse intestine was affected by the presence of IS upstream of *flhDC* in *E. coli* MG1655, indicating niches where motility is advantageous (61). In light of the presence of different intestinal niches where either acid tolerance or motility is beneficial, IS transposition upstream of *flhDC* could be crucial to ensure that *E. coli* is able to colonize both niches by dividing into a motile and an acid-tolerant subpopulation.

Taken together, this study demonstrates that the presence or absence of motility-activating mutations upstream of the master regulatory genes *flhDC* is important for *E. coli* to survive severe acid stress. The *FlhDC* levels are found to be anticorrelated with survival at pH 3, and motile subpopulations exhibit extremely low acid tolerance. These

findings highlight a fitness trade-off between acid tolerance and motility and suggest an IS-mediated differentiation of *E. coli* into motile and acid-tolerant subpopulations.

MATERIALS AND METHODS

Bacterial strains and growth conditions

E. coli MG1655 (62) and BW25113 strains (63) and plasmids used in this study are listed in Tables S2 and S3. Cells were grown in LB medium (10 g/L tryptone, 5 g/L yeast extract, and 10 g/L NaCl) and incubated aerobically in a rotary shaker at 37°C. When appropriate, media were supplemented with 15 µg/mL gentamicin or 50 µg/mL kanamycin. For RNA-Seq experiments, the pH of the medium was adjusted by the direct addition of 5 M HCl to growing cultures, as described in Schumacher et al. (12).

Plasmid construction

Molecular methods were performed according to standard protocols or according to the manufacturer's instructions. Kits for the isolation of plasmids and the purification of PCR products were purchased from Süd-Laborbedarf. Enzymes and HiFi DNA Assembly Master Mix were purchased from New England Biolabs. To construct the reporter plasmids pBBR1-MCS5-*P_{mhpR}:lux* and *P_{mhpABCDE}:lux*, 200 nt of the upstream regions of the respective genes were amplified by PCR using primers KSO-0169–KSO-0172 and MG1655 genomic DNA as a template. For the construction of the pNPTS-R6KT- Δ *mhpR* plasmid, 1,000 nt upstream and downstream of the *mhpR* coding region were amplified. After purification, fragments were assembled into PCR-linearized pBBR1-MCS5 or pNPTS-R6KT vectors via Gibson assembly (64). Correct insertions were verified by colony PCR and sequencing.

Construction of chromosomal *mhpR* deletions

Construction of the marker-less in-frame deletion strains of *mhpR* in *E. coli* MG1655 and BW25113 was achieved using the suicide plasmid pNPTS138-R6KT Δ *mhpR*. The plasmid pNPTS138-R6KT Δ *mhpR* was introduced into *E. coli* MG1655 and BW25113 by conjugative mating using *E. coli* ST18 (65) as a donor in LB medium containing 50 µg/mL 5-amino-levalulinic acid (Ala). Single-crossover integration mutants were selected on LB plates containing kanamycin but lacking Ala. Single colonies were grown over a day without antibiotics and plated onto LB plates containing 10% (wt/vol) sucrose and lacking NaCl to select for plasmid excision. Kanamycin-sensitive colonies were investigated in terms of *mhpR* deletion by colony PCR using primers up- and downstream of the site of the insertion. Deletion of *mhpR* was verified by sequencing.

Acid shock assay

Acid shock assays were conducted as described (12). Briefly, cells were incubated at 37°C in LB medium (pH 7.6) until an OD₆₀₀ of 0.5 was reached. Upon adjustment to an OD₆₀₀ of 1, cells were either grown at pH 7.6 throughout the experiment or stepwise pH adjusted (15 min pH 5.8 and 15 min pH 4.4) before being shifted to pH 3 for 1 h. Next, samples were serially diluted by a factor of 10 in 1× PBS and plated on LB agar plates. Colony-forming units were counted the next day, and significance was evaluated by performing a one-way ANOVA test followed by Bonferroni's multiple comparisons test.

To evaluate acid shock survival of MG1655 Δ *flu* *P_{tac}-flhDC*, cells were grown as described above. All media were supplemented with either 0, 10, 50, or 100 µM IPTG, throughout the experiment.

Acid shock survival of MG1655 subpopulations obtained from different sampling areas of soft agar plates was evaluated using 3 µL of cells grown to OD₆₀₀ of 0.4. Cells were spotted on soft agar plates [0.3% (wt/vol)] and incubated for 16 h at 37°C as described by Bubendorfer and colleagues (39). Subsequently, cells from three different

sampling areas (1, center; 2, intermediate; and 3, edge) (Fig. 6A) were punched out using a P1000 pipette tip and immediately resuspended in either 1 mL LB pH 7.6 or pH 3. Serial dilution and data analysis were conducted as described above.

RNA-Seq analysis

Biological triplicates of *E. coli* MG1655 wild type or $\Delta mhpR$, as well as BW25113 wild-type or *mhpR::km* cells, were inoculated to a starting OD₆₀₀ of 0.05 from overnight cultures and grown in 200 mL of unbuffered LB medium (pH 7.6) until an OD₆₀₀ of 0.5 was reached. Cultures were shifted first for 15 min to LB pH 5.8 and subsequently for 15 min to LB pH 4.4. pH shifts were achieved by adding 5 M HCl directly to growing cultures. pH values before and after pH shifts, as well as final optical densities, were monitored (Table S1). Upon exposure to pH 4.4, 1.6 mL of stop mix [95% (vol/vol) ethanol and 5% (vol/vol) phenol] was added to 8 mL aliquots of the respective cultures to terminate ongoing transcription and translation. Samples were flash frozen in liquid nitrogen and stored at -80°C until RNA isolation. Cells were pelleted ($3,000 \times g$, 15 min, 4°C), and total RNA was isolated using the miRNeasy Mini Kit (Qiagen) in combination with the RNase-Free DNase Set (Qiagen). RNA samples were evaluated in terms of integrity using an RNA 6000 Nano Kit (Agilent) and quantified using a Qubit RNA HS Assay Kit (Invitrogen). Ribosomal RNA depletion was performed using the NEBNext rRNA Depletion Kit for bacteria (NEB), and directional cDNA libraries were prepared using the NEBNext Ultra II Directional RNA Library Prep Kit for Illumina (NEB). cDNA library quality was evaluated using a High Sensitivity DNA Kit (Agilent). Finally, cDNA libraries were sequenced using a NextSeq 1000 machine (Illumina) in single-read mode with a 60 bp read length.

The demultiplexed read files in fastq format were imported into the CLC Genomics Workbench v20.0.4 (Qiagen) and trimmed for quality and adaptors. Reads were mapped to the *E. coli* MG1655 and BW25113 reference genomes (NCBI accession numbers: [NC_000913.3](#) and [CP009273.1](#)) using the “RNA-Seq Analysis” tool with default parameters. Reads that mapped to annotated genes were normalized (reads per kilobase per million reads mapped rpkm) and transformed (\log_2). Low-expression transcripts were filtered out, and we focused our analysis on genes with rpkm values ≥ 5 in at least one replicate. Differential expression was evaluated using the “Empirical Analysis of DGE” tool. Genes with a fold change ≥ 2 and an FDR-adjusted *P*-value ≤ 0.01 were considered as differentially expressed. Volcano plots were created using the `seaborn.jointplot` function in Python 3.8.8. A comprehensive overview of all expression values is available in Tables S5 and S6.

RNA isolation and RT-qPCR analysis

RNA isolation and RT-qPCR analysis were conducted as described (12). In brief, RNA was isolated using the miRNeasy Mini Kit (Qiagen) in combination with the RNase-Free DNase Set (Qiagen) according to the manufacturer’s instructions. A 500 ng aliquot of isolated RNA was converted to cDNA with the iScript Advanced Kit (Bio-Rad) according to the manufacturer’s instructions. Next, 1 μL of a 1:10 dilution of the cDNA samples in nuclease-free water was mixed with 5 μL of SsoAdvanced Univ SYBR Green Supermix (Bio-Rad) and 0.8 μL of 5 μM forward and reverse primers (Table S4), and the total reaction volume was adjusted to 10 μL with nuclease-free water. The mixture was dispensed in triplicates in a 96-well PCR plate (Bio-Rad) and subjected to qPCR in a Bio-Rad CFX real-time cycler. Data were analyzed according to the $\Delta\Delta\text{Ct}$ method (66), using the *secA* gene as a reference.

Promoter activity assay

Promoter activities of *mhpR* and *mhpABCDE* were determined using luminescence-based reporter plasmids harboring fusions of the respective promoter regions to the *luxCDABE* genes from *Photobacterium luminescens* encoded on a pBBR-MCS5 vector. MG1655 cells were transformed with plasmids pBBR1-P_{*mhpR*}:*lux* or pBBR1-P_{*mhpABCDE*}:*lux*.

All strains were cultivated in LB medium supplemented with gentamicin overnight, and day cultures were inoculated to an OD_{600} of 0.05 in fresh LB medium (pH 7.6) and aerobically cultivated until the exponential phase ($OD_{600} = 0.5$). Cultures were then either shifted to LB pH 5.8 for 15 min and LB pH 4.4 for 15 min or further cultivated at pH 7.6 and supplemented with 1 mM PP (Sigma-Aldrich), 1 mM 3HPP (Fisher Scientific), or DMSO. PP and 3HPP were solved in DMSO. In the next step, cells were transferred to a 96-well plate and cultivated at 37°C in the above-mentioned media supplemented with gentamicin. Growth and bioluminescence were measured every 10 min in microtiter plates using a CLARIOstar Plus plate reader (BMG Labtech). Data are reported as relative light units in counts per second of OD_{600} .

Swim agar assay

To determine colony expansion, overnight cultures grown in LB medium were diluted in fresh LB medium and normalized to an OD_{600} of 1 before being dropped in the center of an LB soft agar plate [0.3% (wt/vol)]. After incubation at 37°C for 16 h, the diameter of the halo was measured. Significance was evaluated by performing a one-way ANOVA test followed by Bonferroni's multiple comparisons test.

Analysis of cinnamic acid derivatives via LC-MS

For sample preparation, 100 μ L culture media was diluted with 100 μ L of acetonitrile. After vigorously shaking the samples for 1 min, the samples were centrifuged at 10,000 rpm for 10 min at 10°C. The supernatants were analyzed by means of LC-MS/MS with a 5500 QTrap (AB Sciex) coupled to an ExionLC AD UPLC (AB Sciex). For chromatographic separation, a Kinetex 1.7 μ m C18 100 \times 2.1 mm (Phenomenex) was used with 0.1% formic acid as solvent A and acetonitrile with 0.1% formic acid as solvent B. First, 5% B was held for 0.5 min and then a linear gradient was used from 5% B to 100% B in 5 min. Afterward, the column was flushed and equilibrated to starting conditions. The separation was performed using a 400 μ L/min flow rate at 40°C column oven temperature. Ions were analyzed by MS in the negative ionization mode. The spray voltage was set to $-4,500$ V at a source temperature of 400°C using nitrogen as collision gas. The parameters for the collision-activated dissociation were medium, curtain gas: 35 psi, ion source gas 1: 55 psi, ion source gas 2: 65 psi, entrance potential: -10 V, and the dwell time: 100 ms. The MRM (multiple reaction monitoring) transition for each compound was optimized by direct infusion of the reference standards. The MRM settings were as follows: 3-(4-hydroxyphenyl)propionic acid: 162.931 \geq 90.9 (quantifier), declustering potential (DP) -35 V, collision energy (CE) -36 V, cell exit potential (CXP) -1 V; 162.931 \geq 64.8 (qualifier), DP -35 V, CE -44 V, and CXP -9 V; trans-3-hydroxycinnamic acid: 164.917 \geq 120.8 (quantifier), DP -40 V, CE -16 V, CXP -19 V; 164.917 \geq 80.0 (qualifier), DP -40 V, CE -40 V, CXP -3 V; and hydrocinnamic acid: 148.949 \geq 149.0 (quantifier), DP -65 V, CE -10 V, CXP -7 V; 148.949 \geq 105.0 (qualifier), DP -65 V, CE -14 V, and CXP -5 V. Analyst 1.7. was used to acquire the data, and Multiquant 3.0.3 was used to analyze the data (both AB Sciex).

ACKNOWLEDGMENTS

We thank Stefan Krebs and Helmut Blum for conducting Illumina sequencing, Jürgen Lassak for scientific discussions, and Sabine Peschek for technical support. We thank Viktor Sourjik and Irina Lisevich for providing the Δ flu, Δ flu Δ flhC, and Δ flu P_{tac} -flhDC strains. K.S. acknowledges the support of the Graduate School Life Science Munich (LSM).

This work was financially supported by the Deutsche Forschungsgemeinschaft (DFG, German Research Foundation): Project numbers 471254198 (JU270/22-1) and 395357507 (SFB 1371).

K.S. and K.J. conceptualized the study. K.S., D.B., K.G., and K.J. designed the methodology. K.S. and D.B. performed the investigation. K.S. and K.J. wrote the original draft. K.S.,

D.B., K.G., and K.J. reviewed and edited the manuscript. K.J. acquired funding, provided resources, and supervised the study.

AUTHOR AFFILIATIONS

¹Faculty of Biology, Microbiology, Ludwig-Maximilians-Universität München, Martinsried, Germany

²Bavarian Center for Biomolecular Mass Spectrometry (BayBioMS), Technical University of Munich, Freising, Germany

AUTHOR ORCID*s*

Kilian Schumacher  <http://orcid.org/0000-0002-4751-301X>

Djanna Braun  <http://orcid.org/0009-0009-7565-6841>

Karin Kleigrewe  <http://orcid.org/0000-0002-7718-0252>

Kirsten Jung  <http://orcid.org/0000-0003-0779-6841>

FUNDING

Funder	Grant(s)	Author(s)
Deutsche Forschungsgemeinschaft (DFG)	471254198, 395357507	Kirsten Jung

DATA AVAILABILITY

The RNA-Seq raw data were deposited at Gene Expression Omnibus (GEO) under the accession number [GSE260455](https://www.ncbi.nlm.nih.gov/geo/query/acc.cgi?acc=GSE260455). Additional information required to reanalyze the data reported in this paper is available from the lead contact upon request.

ADDITIONAL FILES

The following material is available [online](#).

Supplemental Material

Supplemental material (Spectrum00544-24-S0001.pdf). Fig. S1 to S6; Table S1 to S4.

Table S5 (Spectrum00544-24-S0002.xlsx). RNA-Seq results MG1655 dmhR vs MG1655 - pH 4.4.

Table S6 (Spectrum00544-24-S0003.xlsx). RNA-Seq results BW25113 mhpR-km vs BW25113 - pH 4.4.

REFERENCES

- Fierer N, Jackson RB. 2006. The diversity and biogeography of soil bacterial communities. *Proc Natl Acad Sci U S A* 103:626–631. <https://doi.org/10.1073/pnas.0507535103>
- Matthies C, Erhard HP, Drake HL. 1997. Effects of pH on the comparative culturability of fungi and bacteria from acidic and less acidic forest soils. *J. Basic Microbiol* 37:335–343. <https://doi.org/10.1002/jobm.3620370506>
- Schwarz J, Schumacher K, Brameyer S, Jung K. 2022. Bacterial battle against acidity. *FEMS Microbiol Rev* 46:fuac037. <https://doi.org/10.1093/femsre/fuac037>
- Freter R, Brickner H, Fekete J, Vickerman MM, Carey KE. 1983. Survival and implantation of *Escherichia coli* in the intestinal tract. *Infect Immun* 39:686–703. <https://doi.org/10.1128/iai.39.2.686-703.1983>
- Fallingborg J. 1999. Intraluminal pH of the human gastrointestinal tract. *Dan Med Bull* 46:183–196.
- Beasley DE, Koltz AM, Lambert JE, Fierer N, Dunn RR. 2015. The evolution of stomach acidity and its relevance to the human microbiome. *PLoS One* 10:e0134116. <https://doi.org/10.1371/journal.pone.0134116>
- Lund P, Tramonti A, De Biase D. 2014. Coping with low pH: molecular strategies in neutralophilic bacteria. *FEMS Microbiol Rev* 38:1091–1125. <https://doi.org/10.1111/1574-6976.12076>
- Arcari T, Feger ML, Guerreiro DN, Wu J, O'Byrne CP. 2020. Comparative review of the responses of *Listeria monocytogenes* and *Escherichia coli* to low pH stress. *Genes* 11:1330. <https://doi.org/10.3390/genes11111330>
- Foster JW. 2004. *Escherichia coli* acid resistance: tales of an amateur acidophile. *Nat Rev Microbiol* 2:898–907. <https://doi.org/10.1038/nrmicro1021>
- Maurer LM, Yohannes E, Bondurant SS, Radmacher M, Slonczewski JL. 2005. pH regulates genes for flagellar motility, catabolism, and oxidative stress in *Escherichia coli* K-12. *J Bacteriol* 187:304–319. <https://doi.org/10.1128/JB.187.1.304-319.2005>
- Schumacher K, Brameyer S, Jung K. 2023. Bacterial acid stress response: from cellular changes to antibiotic tolerance and phenotypic heterogeneity. *Curr Opin Microbiol* 75:102367. <https://doi.org/10.1016/j.mib.2023.102367>
- Schumacher K, Gelhausen R, Kion-Crosby W, Barquist L, Backofen R, Jung K. 2023. Ribosome profiling reveals the fine-tuned response of *Escherichia coli* to mild and severe acid stress. *mSystems* 8:e0103723. <https://doi.org/10.1128/msystems.01037-23>
- Fitzgerald DM, Bonocora RP, Wade JT. 2014. Comprehensive mapping of the *Escherichia coli* flagellar regulatory network. *PLoS Genet* 10:e1004649. <https://doi.org/10.1371/journal.pgen.1004649>

14. Takada H, Kijima K, Ishiguro A, Ishihama A, Shimada T. 2023. Genomic SELEX reveals pervasive role of the flagella master regulator FlhDC in carbon metabolism. *Int J Mol Sci* 24:3696. <https://doi.org/10.3390/jjms24043696>
15. Wang S, Fleming RT, Westbrook EM, Matsumura P, McKay DB. 2006. Structure of the *Escherichia coli* FlhDC complex, a prokaryotic heteromeric regulator of transcription. *J Mol Biol* 355:798–808. <https://doi.org/10.1016/j.jmb.2005.11.020>
16. Claret L, Hughes C. 2002. Interaction of the atypical prokaryotic transcription activator FlhD2C2 with early promoters of the flagellar gene hierarchy. *J Mol Biol* 321:185–199. [https://doi.org/10.1016/S0022-2836\(02\)00600-9](https://doi.org/10.1016/S0022-2836(02)00600-9)
17. Stafford GP, Ogi T, Hughes C. 2005. Binding and transcriptional activation of non-flagellar genes by the *Escherichia coli* flagellar master regulator FlhD2C2. *Microbiology (Reading)* 151:1779–1788. <https://doi.org/10.1099/mic.0.27879-0>
18. Prüss B.M, Matsumura P. 1996. A regulator of the flagellar regulon of *Escherichia coli*, *flhD*, also affects cell division. *J Bacteriol* 178:668–674. <https://doi.org/10.1128/jb.178.3.668-674.1996>
19. Prüss B M, Campbell JW, Van Dyk TK, Zhu C, Kogan Y, Matsumura P. 2003. FlhD/FlhC is a regulator of anaerobic respiration and the Entner-Doudoroff pathway through induction of the methyl-accepting chemotaxis protein Aer. *J Bacteriol* 185:534–543. <https://doi.org/10.1128/JB.185.2.534-543.2003>
20. Shin S, Park C. 1995. Modulation of flagellar expression in *Escherichia coli* by acetyl phosphate and the osmoregulator OmpR. *J Bacteriol* 177:4696–4702. <https://doi.org/10.1128/jb.177.16.4696-4702.1995>
21. Soutourina O, Kolb A, Krin E, Laurent-Winter C, Rimsky S, Danchin A, Bertin P. 1999. Multiple control of flagellum biosynthesis in *Escherichia coli*: role of H-NS protein and the cyclic AMP-catabolite activator protein complex in transcription of the *flhDC* master operon. *J Bacteriol* 181:7500–7508. <https://doi.org/10.1128/JB.181.24.7500-7508.1999>
22. Sperandio V, Torres AG, Kaper JB. 2002. Quorum sensing *Escherichia coli* regulators B and C (QseBC): a novel two-component regulatory system involved in the regulation of flagella and motility by quorum sensing in *E. coli*. *Mol Microbiol* 43:809–821. <https://doi.org/10.1046/j.1365-2958.2002.02803.x>
23. Lehner D, Blumer C, Polen T, Wackwitz B, Wendisch VF, Unden G. 2002. LrhA as a new transcriptional key regulator of flagella, motility and chemotaxis genes in *Escherichia coli*. *Mol Microbiol* 45:521–532. <https://doi.org/10.1046/j.1365-2958.2002.03032.x>
24. Fahrner KA, Berg HC. 2015. Mutations that stimulate *flhDC* expression in *Escherichia coli* K-12. *J Bacteriol* 197:3087–3096. <https://doi.org/10.1128/JB.00455-15>
25. Barker CS, Prüss BM, Matsumura P. 2004. Increased motility of *Escherichia coli* by insertion sequence element integration into the regulatory region of the *flhD* operon. *J Bacteriol* 186:7529–7537. <https://doi.org/10.1128/JB.186.22.7529-7537.2004>
26. Wang X, Wood TK. 2011. IS5 inserts upstream of the master motility operon *flhDC* in a quasi-Lamarckian way. *ISME J* 5:1517–1525. <https://doi.org/10.1038/ismej.2011.27>
27. Lee C, Park C. 2013. Mutations upregulating the *flhDC* operon of *Escherichia coli* K-12. *J Microbiol* 51:140–144. <https://doi.org/10.1007/s12275-013-2212-z>
28. Parker DJ, Demetci P, Li G-W. 2019. Rapid accumulation of motility-activating mutations in resting liquid culture of *Escherichia coli*. *J Bacteriol* 201:3–6. <https://doi.org/10.1128/JB.00259-19>
29. Baba T, Ara T, Hasegawa M, Takai Y, Okumura Y, Baba M, Datsenko KA, Tomita M, Wanner BL, Mori H. 2006. Construction of *Escherichia coli* K-12 in-frame, single-gene knockout mutants: the Keio collection. *Mol Syst Biol* 2:2006.0008. <https://doi.org/10.1038/msb4100050>
30. Ferrández A, García JL, Díaz E. 1997. Genetic characterization and expression in heterologous hosts of the 3-(3-hydroxyphenyl) propionate catabolic pathway of *Escherichia coli* K-12. *J Bacteriol* 179:2573–2581. <https://doi.org/10.1128/jb.179.8.2573-2581.1997>
31. Torres B, Porras G, García JL, Díaz E. 2003. Regulation of the *Mhp* cluster responsible for 3-(3-hydroxyphenyl) propionic acid degradation in *Escherichia coli*. *J Biol Chem* 278:27575–27585. <https://doi.org/10.1074/jbc.M303245200>
32. Manso I, Torres B, Andreu JM, Menéndez M, Rivas G, Alfonso C, Díaz E, García JL, Galán B. 2009. 3-hydroxyphenylpropionate and phenylpropionate are synergistic activators of the MhpR transcriptional regulator from *Escherichia coli*. *J Biol Chem* 284:21218–21228. <https://doi.org/10.1074/jbc.M109.008243>
33. Díaz E, Ferrández A, Prieto MA, García JL. 2001. Biodegradation of aromatic compounds by *Escherichia coli*. *Microbiol Mol Biol Rev* 65:523–569. <https://doi.org/10.1128/MMBR.65.4.523-569.2001>
34. Padmanabhan P, Correa-Betanzo J, Paliyath G. 2016. Berries and related fruits, p 364–371. In Caballero B, Finglas PM, Toldrá F (ed), *Encyclopedia of food and health*. Academic Press, Oxford.
35. Guzman JD. 2014. Natural cinnamic acids, synthetic derivatives and hybrids with antimicrobial activity. *Molecules* 19:19292–19349. <https://doi.org/10.3390/molecules191219292>
36. Diesh C, Stevens GJ, Xie P, De Jesus Martinez T, Hershberg EA, Leung A, Guo E, Dider S, Zhang J, Bridge C, Hogue G, Hogue A, Morgan M, Flores T, Bimber BN, Haw R, Cain S, Buels RM, Stein LD, Holmes IH. 2023. JBrowse 2: a modular genome browser with views of synteny and structural variation. *Genome Biol* 24:74. <https://doi.org/10.1186/s13059-023-02914-z>
37. Sastry AV, Gao Y, Szubin R, Hefner Y, Xu S, Kim D, Choudhary KS, Yang L, King ZA, Palsson BO. 2019. The *Escherichia coli* transcriptome mostly consists of independently regulated modules. *Nat Commun* 10:1–14. <https://doi.org/10.1038/s41467-019-13483-w>
38. Ni B, Colin R, Link H, Endres RG, Sourjik V. 2020. Growth-rate dependent resource investment in bacterial motile behavior quantitatively follows potential benefit of chemotaxis. *Proc Natl Acad Sci U S A* 117:595–601. <https://doi.org/10.1073/pnas.1910849117>
39. Bubendorfer S, Koltai M, Rossmann F, Sourjik V, Thormann KM. 2014. Secondary bacterial flagellar system improves bacterial spreading by increasing the directional persistence of swimming. *Proc Natl Acad Sci U S A* 111:11485–11490. <https://doi.org/10.1073/pnas.1405820111>
40. Battesti A, Majdalani N, Gottesman S. 2011. The RpoS-mediated general stress response in *Escherichia coli*. *Annu Rev Microbiol* 65:189–213. <https://doi.org/10.1146/annurev-micro-090110-102946>
41. Le Bihan G, Jubelin G, Garneau P, Bernalier-Donadille A, Martin C, Beaudry F, Harel J. 2015. Transcriptome analysis of *Escherichia coli* O157: H7 grown *in vitro* in the sterile-filtrated cecal content of human gut microbiota associated rats reveals an adaptive expression of metabolic and virulence genes. *Microbes Infect* 17:23–33. <https://doi.org/10.1016/j.micinf.2014.09.008>
42. Gardette M, Le Hello S, Mariani-Kurkdjian P, Fabre L, Gravey F, Garrivier A, Loukiadis E, Jubelin G. 2019. Identification and prevalence of *in vivo*-induced genes in enterohaemorrhagic *Escherichia coli*. *Virulence* 10:180–193. <https://doi.org/10.1080/21505594.2019.1582976>
43. Li H, Sourjik V. 2011. Assembly and stability of flagellar motor in *Escherichia coli*. *Mol Microbiol* 80:886–899. <https://doi.org/10.1111/j.1365-2958.2011.07557.x>
44. Macnab RM. 1996. Flagella and motility. In Neidhardt FC (ed), *Escherichia coli and Salmonella: cellular and molecular biology*, 2nd ed. ASM Press.
45. Ziegler M, Takors R. 2020. Reduced and minimal cell factories in bioprocesses: towards a streamlined chassis, p 1–44. In Lara AR, Gosset G (ed), *Minimal cells: design, construction, biotechnological applications*. Springer International Publishing, Cham.
46. Schavemaker PE, Lynch M. 2022. Flagellar energy costs across the tree of life. *Elife* 11:e77266. <https://doi.org/10.7554/eLife.77266>
47. Yueh YG, Crain RC. 1993. Deflagellation of *Chlamydomonas reinhardtii* follows a rapid transitory accumulation of Inositol 1,4,5-trisphosphate and requires Ca²⁺ entry. *J Cell Biol* 123:869–875. <https://doi.org/10.1083/jcb.123.4.869>
48. Hartzell LB, Hartzell HC, Quarmby LM. 1993. Mechanisms of flagellar excision: I. the role of intracellular acidification. *Exp Cell Res* 208:148–153. <https://doi.org/10.1006/excr.1993.1232>
49. Adler J. 1973. A method for measuring chemotaxis and use of the method to determine optimum conditions for chemotaxis by *Escherichia coli*. *J Gen Microbiol* 74:77–91. <https://doi.org/10.1099/00221287-74-1-77>
50. Horne SM, Saylor J, Scarberry N, Schroeder M, Lynnes T, Prüb BM. 2016. Spontaneous mutations in the *flhD* operon generate motility heterogeneity in *Escherichia coli* biofilm. *BMC Microbiol* 16:262. <https://doi.org/10.1186/s12866-016-0878-1>

51. Brameyer S, Schumacher K, Kuppermann S, Jung K. 2022. Division of labor and collective functionality in *Escherichia coli* under acid stress. *Commun Biol* 5:327. <https://doi.org/10.1038/s42003-022-03281-4>
52. Yamanaka Y, Aizawa S-I, Yamamoto K. 2022. The *hdeD* gene represses the expression of flagellum biosynthesis via LrhA in *Escherichia Coli* K-12. *J Bacteriol* 204:e00420–21. <https://doi.org/10.1128/JB.00420-21>
53. Van Riet S, Tadesse W, Mortier J, Schlegel S, Simoens K, Bernaerts K, Dal Co A, Aertsen A. 2022. Heterogeneity and evolutionary tunability of *Escherichia coli* resistance against extreme acid stress. *Microbiol Spectr* 10:e0375722. <https://doi.org/10.1128/spectrum.03757-22>
54. Lyu Z, Yang A, Villanueva P, Singh A, Ling J. 2021. Heterogeneous flagellar expression in single *Salmonella* cells promotes diversity in antibiotic tolerance. *mBio* 12:e0237421. <https://doi.org/10.1128/mBio.02374-21>
55. Cummings LA, Wilkerson WD, Bergsbaken T, Cookson BT. 2006. *In vivo*, *fliC* expression by *Salmonella enterica* serovar Typhimurium is heterogeneous, regulated by ClpX, and anatomically restricted. *Mol Microbiol* 61:795–809. <https://doi.org/10.1111/j.1365-2958.2006.05271.x>
56. Wang B, Lin AE, Yuan J, Novak KE, Koch MD, Wingreen NS, Adamson B, Gitai Z. 2023. Single-cell massively-parallel multiplexed microbial sequencing (M3-seq) identifies rare bacterial populations and profiles phage infection. *Nat Microbiol* 8:1846–1862. <https://doi.org/10.1038/s41564-023-01462-3>
57. Douarhe C, Buguin A, Salman H, Libchaber A. 2009. *E. coli* and oxygen: a motility transition. *Phys Rev Lett* 102:198101. <https://doi.org/10.1103/PhysRevLett.102.198101>
58. Quigley EMM, Turnberg LA. 1987. pH of the microclimate lining human gastric and duodenal mucosa *in vivo*: studies in control subjects and in duodenal ulcer patients. *Gastroenterology* 92:1876–1884. [https://doi.org/10.1016/0016-5085\(87\)90619-6](https://doi.org/10.1016/0016-5085(87)90619-6)
59. Pye G, Evans DF, Ledingham S, Hardcastle JD. 1990. Gastrointestinal intraluminal pH in normal subjects and those with colorectal adenoma or carcinoma. *Gut* 31:1355–1357. <https://doi.org/10.1136/gut.31.12.1355>
60. Yamamura R, Inoue KY, Nishino K, Yamasaki S. 2023. Intestinal and fecal pH in human health. *Front Microbiomes* 2:1–12. <https://doi.org/10.3389/frmbi.2023.1192316>
61. Gauger EJ, Leatham MP, Mercado-Lubo R, Laux DC, Conway T, Cohen PS. 2007. Role of motility and the *flhDC* operon in *Escherichia coli* MG1655 colonization of the mouse intestine. *Infect Immun* 75:3315–3324. <https://doi.org/10.1128/IAI.00052-07>
62. Blattner FR, Plunkett G, Bloch CA, Perna NT, Burland V, Riley M, Collado-Vides J, Glasner JD, Rode CK, Mayhew GF, Gregor J, Davis NW, Kirkpatrick HA, Goeden MA, Rose DJ, Mau B, Shao Y. 1997. The complete genome sequence of *Escherichia coli* K-12. *Science* 277:1453–1462. <https://doi.org/10.1126/science.277.5331.1453>
63. Datsenko KA, Wanner BL. 2000. One-step inactivation of chromosomal genes in *Escherichia coli* K-12 using PCR products. *Proc Natl Acad Sci U S A* 97:6640–6645. <https://doi.org/10.1073/pnas.120163297>
64. Gibson DG, Young L, Chuang R-Y, Venter JC, Hutchison CA III, Smith HO. 2009. Enzymatic assembly of DNA molecules up to several hundred kilobases. *Nat Methods* 6:343–345. <https://doi.org/10.1038/nmeth.1318>
65. Thoma S, Schobert M. 2009. An improved *Escherichia coli* donor strain for diparental mating. *FEMS Microbiol Lett* 294:127–132. <https://doi.org/10.1111/j.1574-6968.2009.01556.x>
66. Schmittgen TD, Livak KJ. 2008. Analyzing real-time PCR data by the comparative CT method. *Nat Protoc* 3:1101–1108. <https://doi.org/10.1038/nprot.2008.73>

2.3 Eukaryotic catecholamine hormones influence the chemotactic control of *Vibrio campbellii* by binding to the coupling protein CheW

Muñoz, A.W., Hoyer, E., Schumacher, K., Grognot, M., Taute, K.M., Hacker, S.M., Sieber, S.A., and Jung, K. (2022). Eukaryotic catecholamine hormones influence the chemotactic control of *Vibrio campbellii* by binding to the coupling protein CheW. Proc. Natl. Acad. Sci. U. S. A. 119. 10.1073/pnas.2118227119.

Available online at:

<https://pubmed.ncbi.nlm.nih.gov/35238645/>



Eukaryotic catecholamine hormones influence the chemotactic control of *Vibrio campbellii* by binding to the coupling protein CheW

Angela Weigert Muñoz^a, Elisabeth Hoyer^b, Kilian Schumacher^b, Marianne Grognot^c, Katja M. Taute^{c,1}, Stephan M. Hacker^{d,e}, Stephan A. Sieber^{a,f,2}, and Kirsten Jung^{b,2}

^aCenter for Functional Protein Assemblies, Technical University of Munich, 85748 Garching, Germany; ^bDepartment of Biology I, Microbiology, Ludwig-Maximilians-University München, 82152 Martinsried, Germany; ^cRowland Institute, Harvard University, Cambridge, MA 02142; ^dLeiden Institute of Chemistry, Leiden University, 2333 CC Leiden, Netherlands; ^eDepartment of Chemistry, Technical University of Munich, 85748 Garching, Germany; and ^fHelmholtz Institute for Pharmaceutical Research Saarland, Helmholtz Center for Infection Research, 66123 Saarbrücken, Germany

Edited by Caroline Harwood, University of Washington, Seattle, WA; received October 18, 2021; accepted January 31, 2022

In addition to their well-known role as stress-associated catecholamine hormones in animals and humans, epinephrine (EPI) and norepinephrine (NE) act as interkingdom signals between eukaryotic hosts and bacteria. However, the molecular basis of their effects on bacteria is not well understood. In initial phenotypic studies utilizing *Vibrio campbellii* as a model organism, we characterized the bipartite mode of action of catecholamines, which consists of promotion of growth under iron limitation and enhanced colony expansion on soft agar. In order to identify the molecular targets of the hormones, we designed and synthesized tailored probes for chemical proteomic studies. As the catechol group in EPI and NE acts as an iron chelator and is prone to form a reactive quinone moiety, we devised a photoprobe based on the adrenergic agonist phenylephrine (PE), which solely influenced colony expansion. Using this probe, we identified CheW, located at the core of the chemotaxis signaling network, as a major target. In vitro studies confirmed that EPI, NE, PE, and labetalol, a clinically applied antagonist, bind to purified CheW with affinity constants in the submicromolar range. In line with these findings, exposure of *V. campbellii* to these adrenergic agonists affects the chemotactic control of the bacterium. This study highlights an effect of eukaryotic signaling molecules on bacterial motility.

interkingdom signaling | bacterial chemotaxis | chemical proteomics | bacterial pathogenicity | epinephrine

Catecholamine hormones are widespread signaling molecules present in animals and humans, where they act as neurotransmitters and stress hormones. They include epinephrine (EPI), norepinephrine (NE), and dopamine, which all bear a characteristic catechol motif and a side-chain amine. It is well known that stress of the mammalian host increases its susceptibility to bacterial infections, and EPI and NE, for example, stimulate growth of the enterobacteria *Salmonella enterica* serovar Typhimurium, *Escherichia coli*, and *Vibrio cholerae* in serum-based media (1–4). In addition, EPI and NE affect biofilm formation, siderophore production, invasion of epithelial cells, and the expression of virulence factors (5–8). It is thus assumed that some bacteria use these hormones as cues to recognize the eukaryotic host environment and to occupy a niche in it (9).

In eukaryotes, catecholamines bind to G protein-coupled receptors. The observation that certain antagonists of the human receptors also antagonize adrenergic effects in bacteria corroborates the hypothesis that receptors with a similar specificity may have evolved in prokaryotes. Indeed, binding of NE and EPI to the two-component system histidine kinases QseC and QseE was reported in enterohemorrhagic *E. coli* O157:H7 (10, 11). However, not all adrenergic responses depend on QseC and/or QseE, as mutants lacking the corresponding homologous genes in *Salmonella* and *V. cholerae* were still

responsive to catecholamines (4, 7, 12). Thus, other, as yet unexplored bacterial pathways may contribute to the catecholamine signaling and virulence.

Furthermore, catecholamines act as chemical signals in bacterial chemotaxis, a process in which bacteria navigate along chemical gradients toward attractants and away from repellents (13–15). While the individual components in the chemotaxis signaling cascades vary across different species, the core of the signaling complex typically consists of a transmembrane chemoreceptor (methyl-accepting chemotaxis protein, MCP) and a histidine kinase CheA, the two of which are bridged by the coupling protein CheW (16). In response to chemical stimuli, this complex controls the autophosphorylation of CheA, which consequently transfers its phosphoryl group to the response regulator CheY. Phosphorylated CheY induces clockwise rotation of the flagellar motor and thereby increases the frequency of tumbling in *E. coli*. Notably, NE behaved as a weak attractant at low concentrations, and as a repellent at higher concentrations (1 mM) and this response appeared not to be mediated by specific binding to an MCP in *E. coli* (17).

Significance

Host-emitted stress hormones significantly influence the growth and behavior of various bacterial species; however, their cellular targets have so far remained elusive. Here, we used customized probes and quantitative proteomics to identify the target of epinephrine and the α -adrenoceptor agonist phenylephrine in live cells of the aquatic pathogen *Vibrio campbellii*. Consequently, we have discovered the coupling protein CheW, which is in the center of the chemotaxis signaling network, as a target of both molecules. We not only demonstrate direct ligand binding to CheW but also elucidate how this affects chemotactic control. These findings are pivotal for further research on hormone-specific effects on bacterial behavior.

Author contributions: K.M.T., S.A.S., and K.J. designed research; A.W.M., E.H., K.S., M.G., and K.M.T. performed research; A.W.M., E.H., K.S., M.G., and S.M.H. analyzed data; and A.W.M., S.A.S., and K.J. wrote the paper.

The authors declare no competing interest.

This article is a PNAS Direct Submission.

This article is distributed under [Creative Commons Attribution-NonCommercial-NoDerivatives License 4.0 \(CC BY-NC-ND\)](https://creativecommons.org/licenses/by-nc-nd/4.0/).

¹Present address: Department of Biology I, Microbiology, Ludwig-Maximilians-University München, 82152 Martinsried, Germany.

²To whom correspondence may be addressed. Email: jung@lmu.de or stephan.sieber@tum.de.

This article contains supporting information online at <http://www.pnas.org/lookup/suppl/doi:10.1073/pnas.2118227119/-DCSupplemental>.

Published March 1, 2022.

Vibrio campbellii (previously *V. harveyi*) ATCC BAA-1116 (18) is an important model organism for quorum sensing (19–21). It is a marine, motile, bioluminescent γ -proteobacterium and an opportunistic pathogen for fish, shrimp, squid, and other marine invertebrates (22). The presence of NE and dopamine increased not only its growth in serum-supplemented medium but also siderophore production, swimming motility, and expression of genes involved in biofilm formation and virulence (5). Interestingly, antagonists of the mammalian α -adrenoreceptors such as labetalol (LAB), inhibited the effect of NE on motility, whereas β -adrenoreceptor antagonists such as propranolol (PRO) had no effect, suggesting that catecholamines act via a specific receptor in *V. campbellii* (5). Motility has long been recognized to be important for both commensals and pathogens to colonize their host. In particular, nonmotile mutants of different pathogenic *Vibrio* species showed reduced virulence (23). While the effect of catecholamines on growth most likely stems from the iron-sequestering properties of the catechol siderophore (24), diverging reports exist about the mechanism underlying the altered virulence (4, 5, 25).

In this study, we applied chemical proteomics to identify protein targets of catecholamine hormones in the model organism *V. campbellii*. First, we studied the effects of NE, EPI, and a set of chemically related structures as well as the adrenergic antagonists LAB and PRO on growth and motility. The α -adrenoreceptor agonist phenylephrine (PE) promoted colony expansion without facilitating iron uptake. Therefore, a corresponding chemical probe was used for subsequent photoaffinity labeling, which revealed the chemotaxis coupling protein CheW as a major target. Binding of catecholamines to purified CheW was confirmed by microscale thermophoresis (MST). The adrenergic agonists EPI, NE, and PE also influenced the chemotactic control of *V. campbellii*, suggesting a role of eukaryotic host signals on the physiology of bacteria.

Results

Effects of Catecholamines and Related Compounds on Colony Expansion of *V. campbellii* on Semisolid (Soft) Agar. We first tested the effect of the hormones EPI and NE and structurally related compounds on a readily detectable phenotype of *V. campbellii*. As previously shown for NE (5), NE, but even more strongly EPI, stimulated colony expansion of *V. campbellii* on semisolid (soft) agar. This assay reports swimming motility but also growth and chemotaxis. PE, a synthetic agonist of human α -adrenoreceptors, elicited a similar increase of colony expansion as the natural hormones, whereas its para-substituted analog, octopamine (OA), a neurotransmitter of invertebrates, had no significant effect (Fig. 1A and B). In addition, we included the adrenergic antagonists LAB (mammalian α - and β -adrenoreceptor specificity) and PRO (β -adrenoreceptor specificity). LAB has been reported to antagonize adrenergic effects in *V. campbellii*, while PRO showed no effect (5). Consistent with this literature report, the stimulation of colony expansion by EPI, NE, and PE was blocked by LAB but not by PRO (Fig. 1C). These results indicate the presence of a specific adrenergic sensor that, analogously to the mammalian receptor, can be activated by NE, EPI, and PE and blocked by LAB.

Design and Synthesis of Tailored Probes for Chemical Proteomic Studies. To decipher the cellular targets of catecholamine hormones, we designed and synthesized chemical probes containing an alkyne handle suitable for target protein enrichment via affinity-based protein profiling (26–28). As we could not exclude that the probe scaffold binds reversibly, we appended an alkyne-containing minimalist photocrosslinker to the EPI-based probe EPI-P1 via alkylation of NE at the amine (Fig. 1D; *SI Appendix, Fig. S1A*) (29). Here, the synthesis was challenged

by the instability of catecholamines. At neutral to basic pH, the catechol group is easily oxidized to an ortho-quinone, which can be attacked by the amine (30). This required purification under acidic conditions, resulting in a residual amount of acetic acid in the product needed for stability. Thus, in a second generation of probes, we used direct acylation of catecholamines, which yielded more stable products. Moreover, as we observed an inherent photoreactivity of the adrenergic compounds, we omitted the diazirine and appended an alkyne handle to the terminal amine of NE, norphenylephrine, and OA by standard amide coupling, yielding probes EPI-P2, PE-P, and OA-P, respectively (Fig. 1D; *SI Appendix, Fig. S1B*). Next, the derivatives were tested in soft agar motility assays in which enhanced colony expansion was confirmed for probes EPI-P1 (6 to 60 μ M), EPI-P2 (10 to 25 μ M), and PE-P (10 to 50 μ M), suggesting that these probes retain suitable biological activity to unravel their cellular targets (Fig. 1D; *SI Appendix, Fig. S2*). For EPI-P2 and PE-P, a drop in activity was observed at concentrations above 25 and 50 μ M, respectively (*SI Appendix, Fig. S2 B and C*). In contrast to its parent compound OA, OA-P proved slightly active (25 to 100 μ M), although still to a lesser extent than the other probes (*SI Appendix, Fig. S2D*).

Catechol-bearing Probes Enhance Growth Under Iron-limited Conditions. In the body fluids of eukaryotic hosts, bacterial growth is limited by extremely low levels of available iron, a phenomenon known as nutritional immunity (31). Iron limitation is achieved by high-affinity iron-binding proteins such as transferrin and lactoferrin. Nevertheless, bacteria are able to acquire iron via iron-binding molecules, so-called siderophores, either synthesized by the bacteria or scavenged from the environment. Among the most common classes of siderophores are catecholates, which include the bacterial enterobactin, but also catecholamine hormones (24, 32–34). We, therefore, tested the siderophore effects of our probes and their parent compounds on the growth of *V. campbellii*. These assays were performed in mineral salt medium supplemented with apo-transferrin, a setup typically used to mimic the iron-limited conditions encountered by the bacteria in eukaryotic hosts (35). As expected, catechol-containing compounds EPI-P1, EPI-P2, and EPI enhanced growth, while all other compounds, including PE-P, did not have an effect. The determined doubling times are summarized in *SI Appendix Table S1*. A comparable growth stimulation was not observed when the bacteria were grown in the absence of apo-transferrin, indicating that the growth-stimulating effect of catecholamines is due to their ability to sequester iron (Fig. 1E). The catechol-bearing compounds also stimulated growth of *V. campbellii* in LB35 medium containing 30% (vol/vol) adult calf serum (*SI Appendix, Fig. S3*).

Photolabeling Reveals the Chemotaxis Protein CheW as a Potential Adrenergic Target. Prior to mass spectrometry (MS)-based proteome profiling, we investigated general protein labeling of intact *V. campbellii* cells with EPI-P1, EPI-P2, PE-P, and OA-P, respectively, via gel-based fluorescence analysis of the proteomes. Live cells were incubated with 50 μ M of probes and irradiated with ultraviolet (UV) light to enable covalent bond formation of the probe to the target proteins. Following cell lysis, the proteome was separated into a phosphate-buffered saline (PBS)-soluble fraction, containing primarily cytosolic proteins, and a PBS-insoluble fraction, containing cytosolic and membrane proteins, and both fractions were subjected to copper-catalyzed azide-alkyne cycloaddition (CuAAC) to append a fluorescent tag to the labeled proteins (36, 37). Labeled proteins were separated by sodium dodecyl sulphate-polyacrylamide gel electrophoresis (SDS-PAGE) and visualized by in-gel fluorescence scanning. Interestingly, labeling was observed in both fractions, indicating cell permeability of the

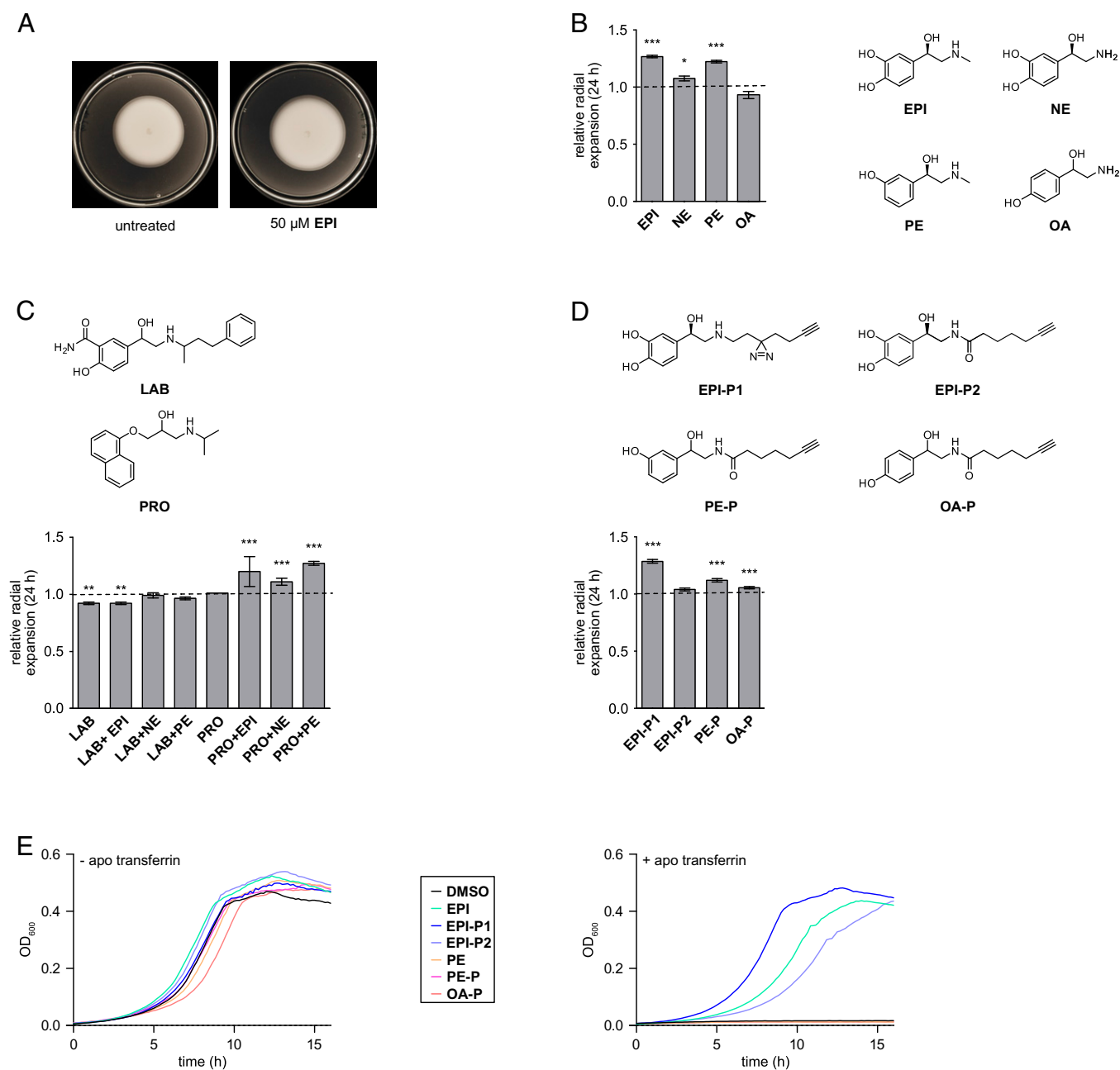


Fig. 1. Biological activity of catecholamines and related compounds on soft agar colony expansion and growth under iron limitation. (A) Example soft agar plates of *V. campbellii* treated with 50 μ M EPI compared to an untreated control. (B) Structure and activity in soft agar expansion assay of parent compounds EPI, NE, PE, and OA. (C) Structure and activity in soft agar expansion assay of adrenergic antagonists LAB and PRO added alone or in combination with EPI, NE, or PE. (D) Structure and activity in soft agar expansion assay of chemical probes EPI-P1, EPI-P2, PE-P, and OA-P. All compounds were added at 50 μ M except EPI-P1 at 60 μ M. Radial expansions were normalized to an untreated control. Error bars represent SD, $n = 6$ independent experiments. Significance was determined performing a one-way ANOVA with Tukey's post hoc test (* $P < 0.05$, ** $P < 0.01$, *** $P < 0.001$). (E) Bacterial growth in KE medium (Left plot) or in KE medium supplemented with 100 μ g/mL human apo-transferrin to generate iron limitation (Right plot) in a 96-well microtiter plate with continuous shaking at 30 $^{\circ}$ C. Compounds were added at 50 μ M. Data show the mean of triplicates; SDs between replicates account for less than 10% in all growth experiments. For doubling times, see *SI Appendix, Table S1*.

probes (*SI Appendix, Fig. S4*). Fluorescent SDS-PAGE analysis of EPI-P1- and EPI-P2-treated cells showed labeling both in the presence and absence of UV, albeit to a lesser extent in the latter case. The general reactivity of EPI-P1 and EPI-P2 toward proteins is likely attributed to the catechol moiety, which is known to form an electrophilic ortho-quinone upon oxidation even in the absence of UV light (30). Consistent with its lack of a catechol moiety, PE-P strongly labeled proteins solely upon UV irradiation, suggesting photoreactivity of the molecule.

Almost no protein reactivity was observed for OA-P, which is in line with its weak bioactivity, and it was therefore excluded from further analysis. We selected EPI-P1 and PE-P for further studies, as both exhibited a distinct labeling profile and activity in the motility assays. With two adrenergic probes at hand, we studied their cellular target proteins via quantitative liquid chromatography coupled to tandem mass spectrometry (LC-MS/MS) analysis (Fig. 2A). Treatment of live *V. campbellii* with EPI-P1 or PE-P was followed by UV irradiation, cell lysis,

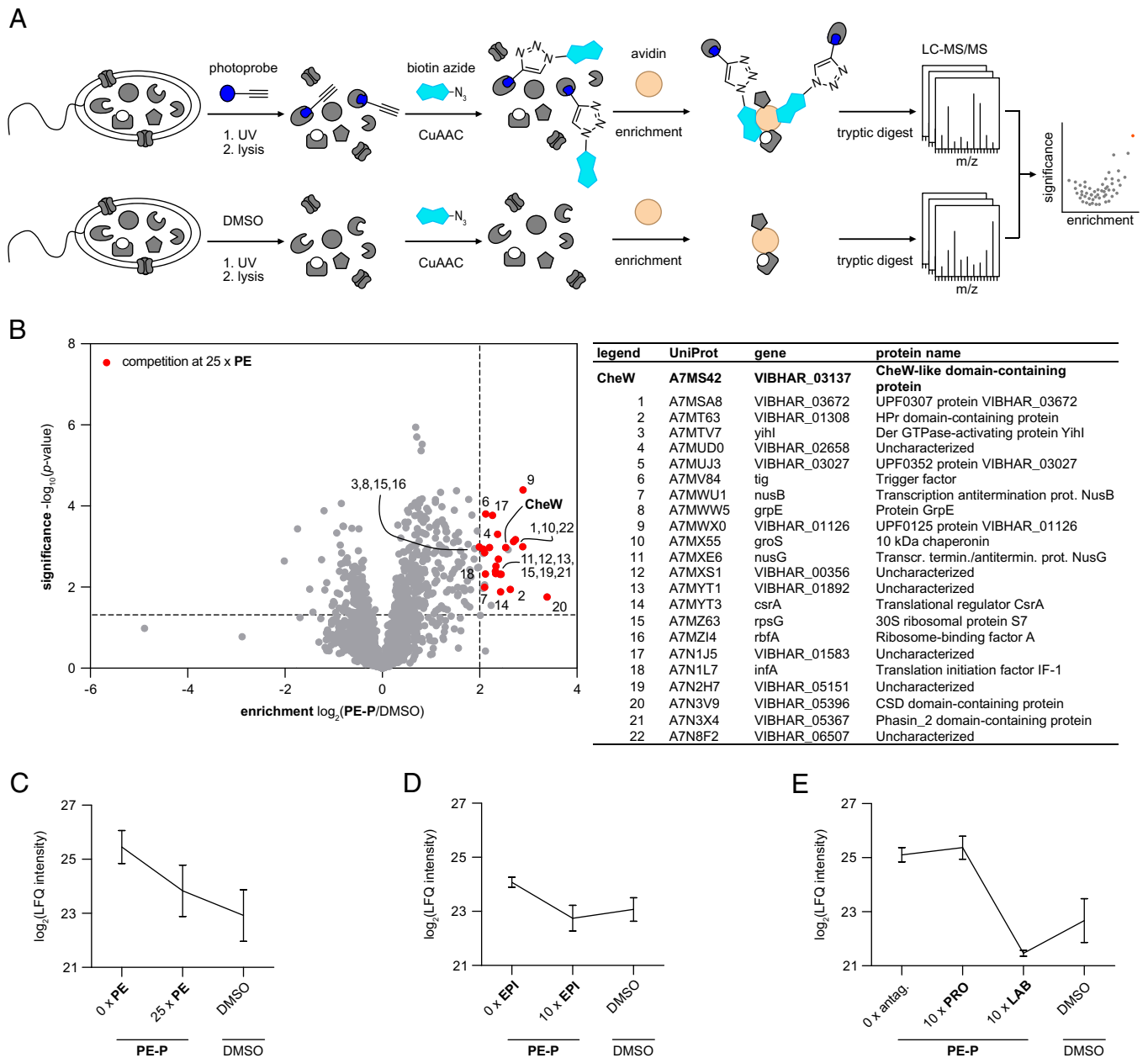


Fig. 2. CheW is identified as a potential adrenergic target by photoaffinity labeling with PE-P. (A) Chemical proteomics workflow applied for target identification. Live bacteria were treated with 10 μ M PE-P or DMSO as control or PE-P plus increasing concentrations of competitors (PE, EPI, LAB, PRO), irradiated, lysed, separated into soluble (PBS) and insoluble proteins, ligated by CuAAC to biotin azide, enriched on avidin beads, and digested, and peptides were analyzed by LC-MS/MS. (B) Volcano plot showing proteins enriched in samples treated with 10 μ M PE-P over DMSO controls. Proteins outcompeted by a 25-fold excess of PE are highlighted in red; the experiment was done in five biological replicates. MS data were analyzed by MaxLFQ (38) and filtered for proteins identified in four replicates, and missing values were imputed. Samples were compared using a two-sample permutation-corrected *t* test. (C) Profile plot of CheW LfQ intensities from competition with a 25-fold excess of PE. Error bars denote SD, *n* = 5 biological replicates. (D) Profile plot of CheW LfQ intensities from competition with a 10-fold excess of EPI, *n* = 4 biological replicates. (E) Profile plot from competition with a 10-fold excess of PRO or LAB, *n* = 4 biological replicates. All data shown here are from the insoluble fraction. See *SI Appendix, Figs. S6–S8* for more detailed competition data and soluble fractions.

CuAAC to biotin azide, enrichment on avidin beads, and tryptic digest, resulting in peptides, which were measured by LC-MS/MS with label-free quantification (LFQ) (38). All proteins that were significantly [$-\log_{10}(P \text{ value}) \geq 1.3$] enriched by at least twofold in the probe-treated samples compared to the dimethyl sulfoxide (DMSO) controls are visualized in the upper right quadrant of the corresponding volcano plot. EPI-P1 enriched, among others, an outer membrane receptor protein for ferrienterochelin and colicins (A7MZS4) and an iron-

hydroxamate ABC transporter substrate binding protein (A7MSY4), indicating that this probe indeed functions as a xenosiderophore (*SI Appendix, Fig. S5*). In fact, CheW was also enriched 3.9-fold in this dataset, although it was not among the most prominent hits. We hypothesized that the abundance of iron-uptake proteins interfered with the identification of further adrenergic targets. We therefore switched to labeling studies with PE-P, devoid of the catechol moiety (Fig. 2B). Here, proteins associated with iron uptake were no longer

significantly enriched. Importantly, the chemotaxis coupling protein CheW turned out to be one of the most prominent hits. Based on its role in chemotaxis, CheW is an intriguing candidate for catecholamine binding, and it was thus further investigated for displacement of probe binding in the presence of excess concentrations of the unmodified catecholamines. Cells were preincubated with different concentrations (100 to 250 μM) of PE, EPI, LAB, or PRO before adding PE-P (10 μM). EPI, PE, and LAB reduced enrichment of CheW by probe PE-P, indicating competitive binding and corroborating CheW as a specific target of these compounds (Fig. 2 C–E; *SI Appendix*, Figs. S6–S8). PRO, however, did not compete for binding, consistent with its lack of antagonism in the motility assays (Fig. 2E; *SI Appendix*, Fig. S8C). We identified additional proteins for which, as with CheW, the binding of PE-P was out-competed by EPI, PE, and LAB, but not by PRO (*SI Appendix*, Table S2). In the soluble fraction, we found three uncharacterized proteins (A7MXS1, A7N2H7, A7N8F2). In the insoluble fraction, we found the Der GTPase-activating protein YihI (A7MTV7), the 30S ribosomal protein S7 (A7MZ63), the translation initiation factor IF-1 (A7N1L7), and four other uncharacterized proteins (A7MYT1, A7MXS1, A7N8F2, A7MUD0). Notably, of all differentially outcompeted proteins, only CheW was also significantly enriched by EPI-P1.

Insights Into the Mechanism of PE-P Binding. To elucidate the UV-dependent binding mode of PE-P, we performed labeling experiments in the presence of radical scavengers. UV-dependent labeling by PE-P could be fully quenched by the addition of thiourea and tiron, suggesting a light-induced fragmentation of the molecule to form reactive radical intermediates (*SI Appendix*, Fig. S9). To further assess the nature of radical binding to proteins, we applied a mass-spectrometry method, which unravels the modified residues within proteins as well as the type of modification. This technology is based on isotopically labeled desthiobiotin azide (isoDTB) tags, which are clicked to probe-labeled proteins after lysis (39). Proteins are subsequently digested, followed by peptide enrichment on avidin beads and detection of modified peptides via LC-MS/MS analysis (Fig. 3A) (40). In an unbiased analysis (41), we detected modified peptides with the added mass of the adduct with PE-P plus a light or heavy isoDTB tag, respectively (Fig. 3B). Interestingly, we observed a high selectivity for tyrosine, which constituted 90% of all detected modified residues, corroborating a radical mechanism of binding (Fig. 3 C and D). Furthermore, MS-based site identification revealed two tyrosine residues, Y₄₄ and Y₁₁₂, within CheW, which were modified by the probe (Fig. 3E; *SI Appendix* Fig. S10 A and B). As there is no crystal structure of *V. campbellii* CheW available, we used AlphaFold for prediction (42). We found that the two tyrosine residues frame the conserved arginine at position 64, which is assumed to be necessary for modulating CheA activity (*SI Appendix*, Fig. S10C) (43).

Validation of Catecholamine Binding to CheW and Analysis of the CheW Interaction Network. To validate catecholamine binding to CheW, we measured the affinity of the ligands for CheW using MST (44). For this purpose, CheW was recombinantly expressed in *E. coli*, purified, and fluorescently labeled. Temperature-induced changes in fluorescence (temperature-related intensity changes and/or temperature dependent movements) were determined as a function of ligand concentration in glass capillaries. The parent compounds EPI, NE, and PE, the adrenergic antagonist LAB, and OA as negative control were tested as putative ligands. PRO could not be tested because of interference from its intrinsic fluorescence. Interestingly, EPI, NE, PE, and LAB caused concentration-dependent effects on the fluorescently labeled CheW with dissociation

constants K_d ranging from 300 to 740 nM (Fig. 4A), indicating strong affinity binding. These observations are consistent with the results from the colony expansion and competitive labeling experiments (Figs. 1 B and C and 2 C–E). In line with its lack of activity in the motility assays (Fig. 1B), OA showed no binding affinity for CheW.

Next, protein interaction partners of CheW were studied by coimmunoprecipitation (Co-IP) in cells treated first with 100 μM EPI or DMSO as control and then with disuccinimidyl sulfoxide to stabilize interaction partners by covalent cross-links (45). Numerous proteins annotated to be involved in chemotaxis (Gene Ontology [GO] or Kyoto Encyclopedia of Genes and Genomes [KEGG] database) were enriched compared to an isotype control, including CheA, CheZ, MCPs, and a CheW-like domain-containing protein, confirming the validity of the antibody and the methodology (*SI Appendix*, Fig. S11 A and B). The presence of EPI, however, did not result in any obvious catecholamine-dependent changes of interaction partners (*SI Appendix*, Fig. S11C). These results suggest that under the conditions tested, binding of catecholamines to CheW does not alter the associated protein networks. This is in line with the observation that transmembrane chemoreceptor arrays remain intact upon activation (46).

Adrenergic Compounds Affect the Chemotactic Control of *V. campbellii*. Colony expansion in soft agar is a complex phenotype that is driven by a combination of motility behavior, chemosensing, chemoattractant consumption, and growth (47). The increased colony expansion on soft agar plates with EPI and PE (Fig. 1B) could, in principle, result from growth benefits (*SI Appendix*, Fig. S3), chemoattraction, or changes in individual motility behavior such as the turning frequency. To gain deeper insights into the effect of EPI and PE on motility and chemotaxis, we first used 3D tracking to examine the motility of untreated *V. campbellii* cells of the midexponential growth phase. Similar to *Vibrio alginolyticus* (48), the cells exhibited a run-reverse-flick pattern at typical swimming speeds of $54 \pm 2 \mu\text{m/s}$ and a steady-state turning frequency of $0.52 \pm 0.03 \text{ s}^{-1}$ (Fig. 4B). We did not detect any significant effects of EPI on the average speed or steady-state turning frequency (*SI Appendix*, Fig. S12). Since EPI and PE bind to CheW, we next examined the motility of a $\Delta cheW$ mutant. The $\Delta cheW$ mutant had a similar average swimming speed as the wild-type ($48 \pm 4 \mu\text{m/s}$) but proved to be a smooth swimmer with a very low turning frequency (Fig. 4C). This mutant was unable to spread on soft agar (*SI Appendix*, Fig. S13), a phenomenon previously observed in other *Vibrio* species (49). Next, we used a multi-scale 3D chemotaxis assay (50) that combines high-throughput 3D bacterial tracking with a microfluidically created linear chemical gradient. A 100 $\mu\text{M/mm}$ EPI gradient elicited a weak chemoattractant response (positive chemotactic drift). Serine (50 $\mu\text{M/mm}$) and glucose (1 mM/mm), respectively, were recognized as stronger chemoattractants, and the presence of EPI or PE had no effect on the chemotactic drift (Fig. 4D).

Finally, we used a capillary chemotaxis assay originally developed for *E. coli* (51). Briefly, in this assay, a glass capillary filled with an attractant is inserted into a cell suspension, and the number of cells in the capillary is counted after 60 min of incubation (Fig. 4E). Using this assay, we detected a chemotactic response of *V. campbellii* to chitin, glucose, serine, and also EPI (*SI Appendix*, Fig. S14). Although this assay is not as sensitive as the 3D microfluidic chemotaxis assay (thus requiring higher concentrations of the chemoattractant), we found a significant reduction in cell numbers in the glucose-filled capillary in the presence of EPI and PE, whereas NE, LAB, PRO, and OA did not show an effect (Fig. 4E). Furthermore, the effect of EPI was suppressed in the presence of LAB. These results are consistent with the specific effect of EPI,

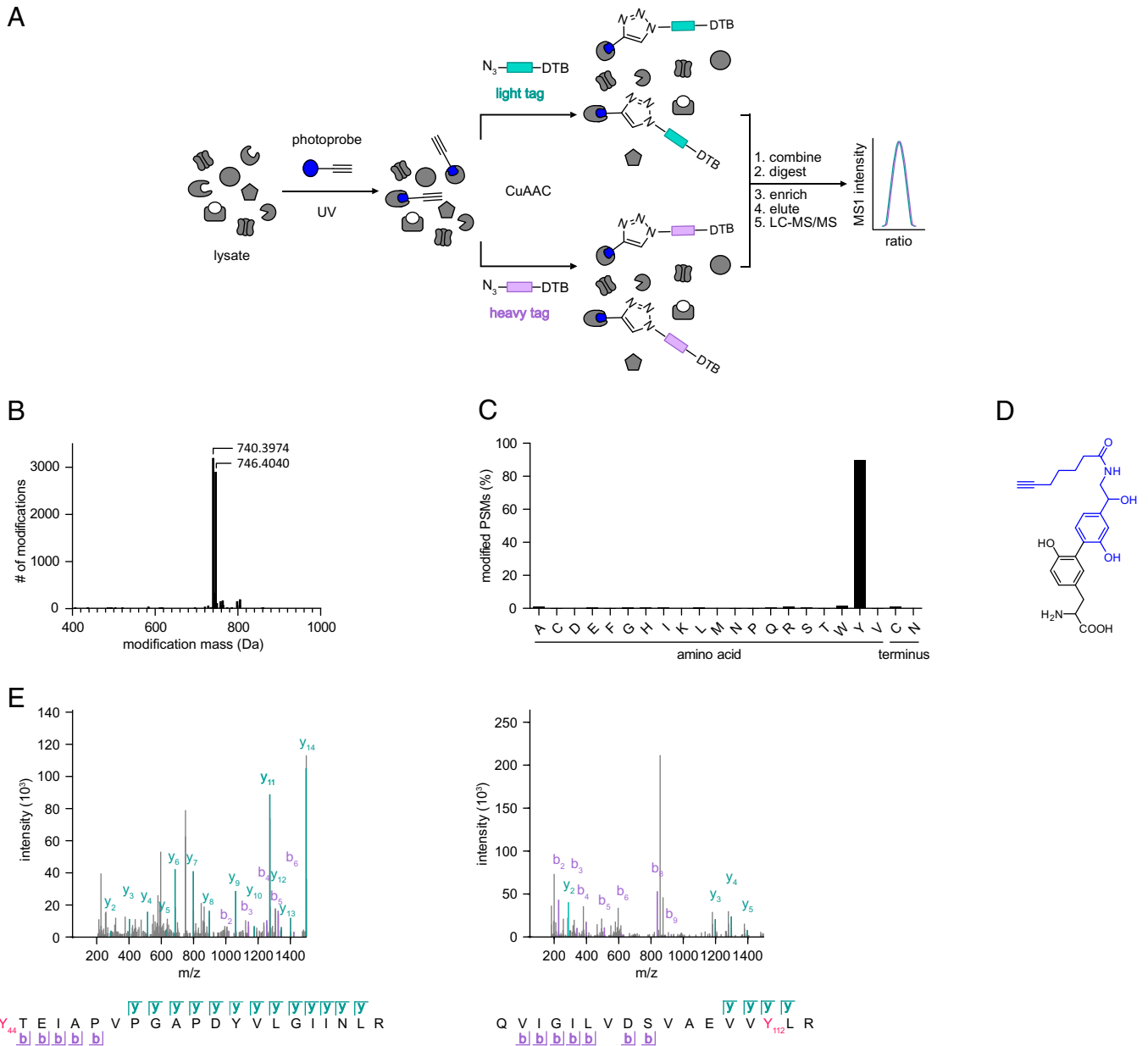


Fig. 3. Analysis of the modifications introduced by PE-P proteome-wide. (A) Workflow applied to study binding mode and sites of PE-P using isoDTB tags (39, 41). *V. campbellii* lysate was treated with 10 μ M PE-P (blue circle), irradiated, split, and subjected to CuAAC with either light- (turquoise rectangle) or heavy-labeled (purple rectangle) isoDTB azide. Differentially labeled lysates were combined in a ratio of 1:1, and proteins were precipitated and digested. Modified peptides were enriched on avidin, eluted, and analyzed by LC-MS/MS. Peptides detected with a ratio of close to 1:1 heavy/light tag were considered true hits. (B) Unbiased, proteome-wide analysis of the masses of modification introduced by PE-P and the light or heavy isoDTB tag, respectively. (C) Analysis of the amino acid selectivity of the detected modification with PE-P. PSM, peptide spectrum matches. (D) Potential structure of the modified tyrosine regioisomer corresponding to the observed modification mass. (E) MS2 spectra of CheW peptides modified by PE-P. Identified b- and y-ions are labeled with purple and turquoise, respectively. The PE-P binding sites and their position in the sequence are indicated in red. All data are based on technical duplicates.

PE, and EPI + LAB on colony expansion (Fig. 1 B and C) and suggest that binding of EPI or PE to CheW affects the swimming behavior of *V. campbellii* in chemical gradients over long distances.

Discussion

In this study, we report the direct binding of the eukaryotic stress hormone EPI to CheW, the coupling protein between MCPs and CheA, located in the core of the chemotaxis signaling network in *V. campbellii*. It is known that mammalian host

stress associated with the release of catecholamine hormones not only increases susceptibility to bacterial infection but that EPI and NE also stimulate the growth and motility of enterobacteria such as *Salmonella* Typhimurium, *E. coli*, and *V. cholerae* (1–4). We used an untargeted chemical proteomics approach to identify the cellular targets of EPI. We chose PE, which is a structural homolog of EPI, for probe design as it still promotes colony expansion but cannot bind iron. In these studies, the chemotaxis coupling protein CheW proved to be one of the most prominent hits. This finding was confirmed by competitive labeling in the presence of EPI, PE, and LAB, the

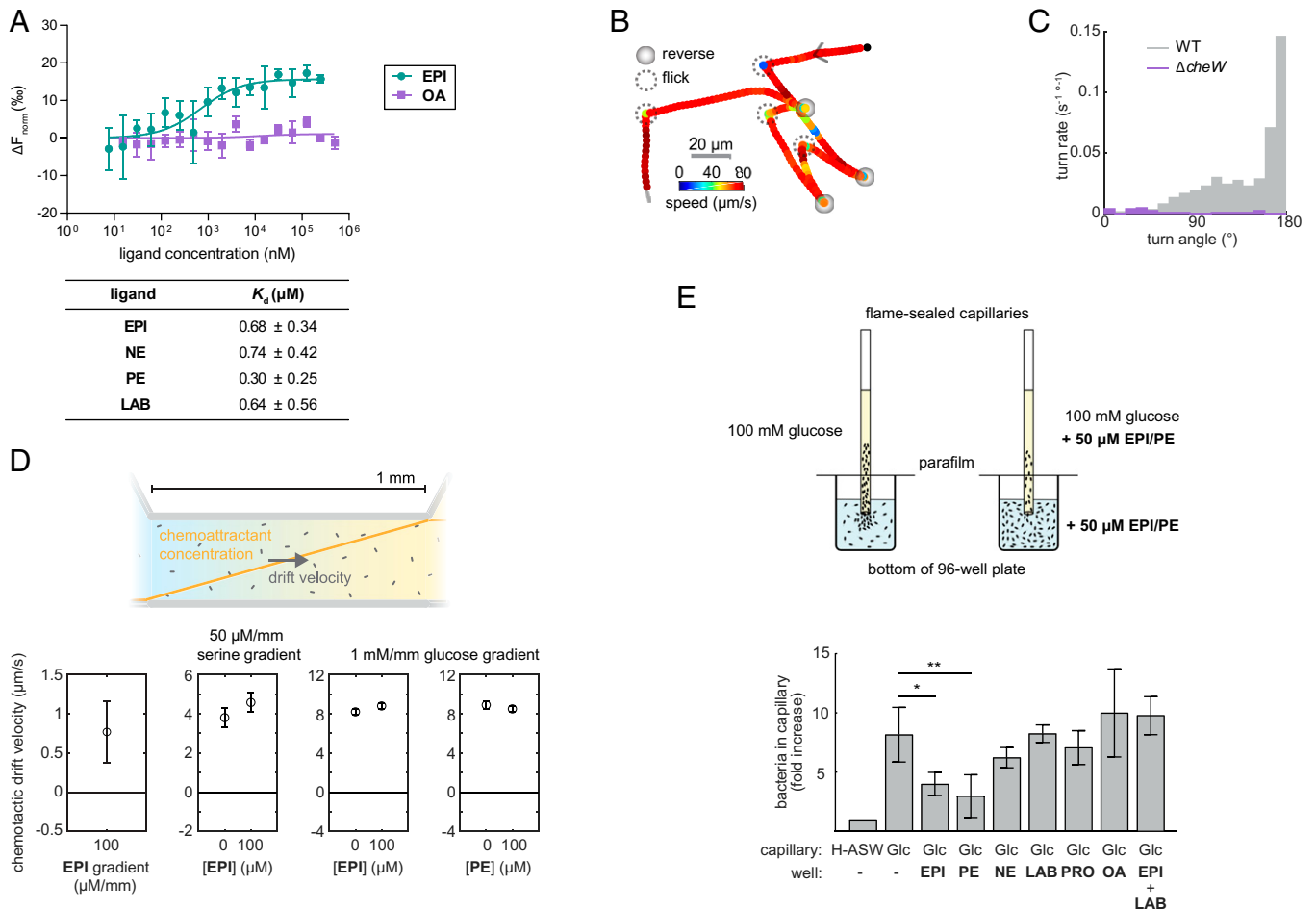


Fig. 4. Binding of adrenergic compounds to CheW *in vitro* and their effect on motility and chemotaxis of *V. campbellii* *in vivo*. (A) Binding of adrenergic compounds to purified CheW was determined using MST. Increasing concentrations of the test compounds ($c = 7.63$ nM to 500 μM) were titrated to a constant concentration of fluorescently labeled CheW ($c = 50$ nM), and temperature-induced changes in fluorescence were monitored in glass capillaries using the Monolith NT.115 (NanoTemper Technologies). K_d values were determined using the Thermophoresis + T-Jump signal for data analysis (NT Analysis software version 1.5.41, NanoTemper Technologies, $n = 3$ independent measurements, error bars represent SD). (B) Example 3D trajectory of *V. campbellii* showing run-reverse-flick motility with turns alternating between reversals and flicks. (C) Rate of turn events as a function of turn angle for wild-type (WT) and the ΔcheW mutant, based on 1,447 turn events detected in 1,295 s of trajectory time for WT and 29 events in 3,250 s of trajectory time for ΔcheW . (D) The 3D chemotaxis assay was performed by 3D tracking of cells in linear chemical gradients established in a 1-mm-long channel between two reservoirs of different chemical but matched bacterial concentration (concept is schematically shown in the *Upper* part). The drift velocity was determined as the average speed of motile cells along the gradient direction. Error bars represent SEM. The drift measured in a 100 $\mu\text{M/mm}$ EPI gradient (left panel) is statistically significant at a P value of 0.029 in a one-tailed Student's t test against the null hypothesis of no drift. Differences in the drift to other compounds in the presence and absence of EPI or PE (other panels) are not significant. (E) In the capillary chemotaxis assay, bacteria swim from a reservoir in a microtiter plate into a glass capillary filled with an attractant (100 mM glucose) (concept is schematically shown in the *Upper* part). After 60 min, the number of bacteria in the capillary is determined by plating the cells on agar plates. The concentration of EPI and structurally related compounds was constant (50 μM) in the capillary and reservoir. Values were normalized to their respective control (H-ASW). Error bars represent SD, $n = 4$ biological replicates. Statistical significance was determined using an unpaired two-tailed t test (* $P < 0.05$, ** $P < 0.01$).

latter being a clinically applied antagonist of α -adrenergic receptors in eukaryotes. We also demonstrated direct binding of EPI, NE, PE, and LAB to purified CheW. The binding of EPI to CheW is an unexpected discovery but nevertheless consolidates previous reports seeking to find a specific chemoreceptor for catecholamines. For example, a *V. cholerae* mutant lacking the *qseC*-like gene still responded to catecholamines (4). Based on studies on the influence of catecholamines on chemotaxis, Sourjik and coworkers proposed that in *E. coli*, these hormones are sensed by a mechanism other than specific binding to an MCP (17).

The ΔcheW mutant of *V. campbellii* is motile but has an extremely low turning frequency, and it is nonchemotactic (Fig. 4C; *SI Appendix*, Fig. S14C). This finding is consistent with results for many other bacterial species that lack *cheW*

(summarized in Alexander et al.; ref. 43). Our 3D tracking assays revealed that EPI does not affect the turning rate or swimming speed of wild-type *V. campbellii* but acts as a weak attractant. These results indicate that binding of EPI to CheW does not phenocopy the behavior of the ΔcheW mutant (Fig. 4). However, in the capillary assay, which depends on the motility and chemotactic behavior of a population over large distances that span a wide range of gradient conditions, the presence of EPI and PE led to a significant decrease in the accumulation of cells in the glucose-filled capillary. While the 3D tracking experiments in linear gradients did not identify an effect of EPI or PE on chemotaxis to other compounds under the conditions tested, the very steep concentration gradients likely present in the immediate vicinity of the capillary are not accessible in the linear-gradient device. The effect of

EPI might thus be restricted to steep gradients or other specific conditions that are not recapitulated in the linear-gradient assay. Another open question is whether the interaction between EPI and CheW is causal either for the chemoattraction to EPI or for the reduced chemoattractive effect of glucose in the capillary assay. The latter effect, however, is specific for EPI and PE because the presence of NE, LAB, PRO, and OA did not affect the movement of the cells along the glucose gradient. Interestingly, LAB, which binds to CheW, prevents the effect of EPI and PE both in the capillary-based chemotaxis and in the soft agar assays. The lack of activity of LAB itself is reminiscent of the behavior of classical pharmacological antagonists, which typically block agonist activity by binding to their target proteins but without exerting any effects themselves. Similar to its weak effect on colony expansion, NE was barely active in the capillary-based chemotaxis assay. As determined by MST, NE had a lower affinity for CheW compared to all tested compounds, which could explain these observations. Overall, our results suggest that binding of EPI and PE to CheW influences the chemotactic control of the bacterium.

Both chemotaxis and net motility are known to affect the infectivity of *V. cholerae* (52). The results described here could potentially provide an explanation for the hyperinfective transient phenotype of stool-derived *V. cholerae* (53–55). Although the stool-derived *V. cholerae* are highly motile, many chemotaxis genes, including *cheW* and *cheR*, are repressed compared to in vitro grown cells, resulting in a smooth-swimming state. Our finding that EPI targets CheW suggests a previously unknown mechanism for such host-triggered phenotypes. This work reveals a previously unknown role of CheW as adrenergic receptor that, given its conserved position in the core of chemotaxis complexes, could have broad implications for many other bacterial species.

Materials and Methods

Chemical Synthesis. For synthetic procedures and compound characterization data, see *SI Appendix, Supplementary Methods and Figs. S1, S15–S19*.

General Information. Detailed information on compounds, bacterial strains, culture conditions, preparation of overnight cultures, and media composition are provided in the *SI Appendix, Supplementary Methods and Tables S3–S6*.

Growth Assays. A *V. campbellii* overnight culture was diluted 1:100 into Kim-Epstein (KE) medium (10 mL) (56) or lysogeny broth containing 3.5% (wt/vol) NaCl (LB35) medium (60 mL) and grown until early exponential growth phase (optical density at 600 nm [OD₆₀₀] 0.5, KE medium) or early stationary phase (OD₆₀₀ 5.0, LB35). The KE medium was modified as follows: The pH was adjusted to 7.6 with the corresponding phosphate buffer, the salt concentration was increased to 2% (wt/vol) NaCl, and FeSO₄ was omitted. Compounds were added from DMSO stocks to 50 μM into a clear flat-bottom 96-well plate. Next, 200 μL bacterial culture previously diluted to OD₆₀₀ 0.01 in KE medium + 20 mM NaHCO₃ or in KE medium + 20 mM NaHCO₃ supplemented with 100 μg/mL human apo-transferrin (Sigma-Aldrich) or to OD₆₀₀ 0.005 in LB35 or in LB35 supplemented with 30% (vol/vol) of adult bovine serum (Sigma-Aldrich) was added. The plates were incubated in an Infinite M200 Pro plate reader (Tecan) at 30 °C with continuous shaking (KE medium) or with 20 s shaking every 5 min (LB35 medium). The optical density at 600 nm was measured every 10 to 30 min. Blank values (only medium) were subtracted from data values, and data were plotted using GraphPad Prism.

Soft Agar Colony Expansion Assay. Soft agar colony expansion assays were performed as described previously on LB35 plates containing 0.3% (wt/vol) agar (5). Catecholamines and antagonists were dissolved in water and added as supplements directly to the autoclaved medium before pouring plates. As control, the appropriate volume of water was added to the plates. *V. campbellii* overnight culture was diluted in fresh LB35 (OD₆₀₀ 1), and 5 μL was dropped in the center of the plate with six independent replicates for each condition. After an incubation of 24 h at 30 °C, the expansion of the colony (diameter) was measured. Radial expansions were normalized to an untreated control, and significance was determined performing a one-way ANOVA with Tukey's post hoc test.

Preparative Photolabeling with PE-P. Overnight cultures of *V. campbellii* were diluted 1:100 into 60 mL fresh medium and grown until early stationary phase (30 °C, 200 rpm, 7 h, OD₆₀₀ ~5.0 to 5.2). Bacteria were harvested by centrifugation (6,000 × g, 10 min, 4 °C), washed with PBS (10 mL), and adjusted to OD₆₀₀ 4.0 in 10 mL PBS. Competitors PE, EPI, LAB, PRO, or DMSO were added from 1,000-fold concentrated DMSO stocks to the final concentrations as indicated, and the suspensions were incubated 15 min, 30 °C, 200 rpm in 50-mL falcons with the lids fixed loosely. Next, DMSO or the photoprobe PE-P was added from a 1,000-fold concentrated stock (10 mM) to a final concentration of 10 μM and incubated 1 h, 30 °C, 200 rpm. Samples were transferred to 10-cm dishes and irradiated for 10 min with UV light (UV low-pressure mercury-vapor fluorescent lamp, Philips TL-D 18W BLB, 360 nm maximum) on a cooling pack. Labeled bacteria were centrifuged (6,000 × g, 10 min, 4 °C), and the pellet was washed twice with cold PBS (1 mL). Pellets were flash frozen and stored at –80 °C. Pellets were resuspended in 1 mL PBS + ethylenediaminetetraacetic acid-free protease inhibitor (Roche) and sonicated 2 × 15 s, 60% intensity, on ice. Following centrifugation (16,060 × g, 30 min, 4 °C), the supernatant was removed (“soluble”), and the pellet was resuspended in 1% (wt/vol) SDS/PBS with sonication for 2 × 15 s, 40% intensity. Cell debris was pelleted (16,060 × g, 10 min, room temperature [RT]), and the supernatant was transferred into a new tube (“insoluble”). For analytical scale photolabeling and preparative photolabeling with EPI-P1, see *SI Appendix*.

CuAAC, Preparative Scale Photolabeling. Protein concentration was determined using the Roti-Quant kit (Carl Roth) and adjusted to ~1 μg/μL in 500 μL. SDS was added to 0.8% (wt/vol) in the “soluble” samples. Click reagents were added to the lysate from a premix to the following concentrations: 100 μM rhodamine-biotin-azide tag (10 mM stock in DMSO) (57), 1 mM CuSO₄ (50 mM stock in water), 1 mM Tris(2-carboxyethyl)phosphine hydrochloride (52 mM stock in water), and 100 μM Tris((1-benzyl-4-triazolyl)methyl)amine [1.667 mM stock in 20% (vol/vol) DMSO/*t*-BuOH] and incubated 1 h, 25 °C, 400 rpm. Proteins were precipitated in 2 mL acetone at –20 °C overnight, pelleted (20,450 × g, 15 min, 4 °C), and washed twice with 1 mL ice-cold methanol with sonication (1 × 10 s, 10% intensity). Pellets were air-dried, and proteins were resolubilized in 1 mM dithiothreitol (DTT), 0.2% (wt/vol) SDS/PBS with sonication (1 × 10 s, 10% intensity) and transferred to LoBind microcentrifuge tubes.

General MS Sample Preparation. Protein LoBind microcentrifuge tubes and MS-grade reagents were used throughout MS sample preparation.

Enrichment, Alkylation, and Digest for Photoaffinity Labeling Experiments. Per sample, 50 μL avidin slurry (Sigma) was dispensed into a microcentrifuge tube and washed 3× with 0.2% (wt/vol) SDS/PBS (3 min, 400 × g). Protein samples were centrifuged (21,000 × g, 10 min, RT) to remove particulates, then added to the beads and incubated at RT under constant rotation for 1 to 2 h. Beads were pelleted, the supernatant was discarded, and beads were washed with 0.5 to 1 mL of the following solutions: 2 × 1% (wt/vol) SDS/PBS, then 3 × 4 M urea/PBS, and 3 × 50 mM triethylammonium bicarbonate buffer (TEAB). The beads were resuspended in 100 μL 50 mM TEAB and reduced with 10 mM DTT (from 250 mM stock in water) at 55 °C for 30 min with shaking. Next, beads were washed with 0.5 mL TEAB and resuspended in 100 μL TEAB, and thiols were alkylated with 20 mM iodoacetamide (from 500 mM stock in TEAB) at 25 °C from 30 min with shaking. Beads were washed twice with 100 μL TEAB and resuspended in 100 μL TEAB, and 1 μg trypsin was added (from 0.5 μg/μL in 50 mM acetic acid, Promega). Proteins were digested at 37 °C for 14 h under vigorous shaking. The digest was quenched with formic acid [1% (vol/vol) final concentration (pH 2 to 3)], beads were washed twice with 100 μL 0.1% (vol/vol) formic acid, and the washes were combined with the supernatant.

Desalting on Stage Tip for Photoaffinity Labeling Experiments. Stage tips consisted of three layers of C-18 material (Empore C18 disk-C18, 47 mm, Agilent Technologies) plunged into p200 tips and were inserted into holes in the lids of microcentrifuge tubes. The following solutions were added and the stage tips centrifuged (≤1 to 2 min, 500 × g) after every addition: Stage tips were washed with 1 × 80 μL methanol and then equilibrated with 1 × 80 μL 80% (vol/vol) acetonitrile, 0.5% (vol/vol) formic acid and with 2 × 100 μL 0.5% (vol/vol) formic acid. Next, peptides were loaded and desalted with 1 × 150 μL 0.1% (vol/vol) formic acid. Stage tips were transferred to fresh LoBind microcentrifuge tubes, and the peptides were eluted with 100 μL 80% (vol/vol) acetonitrile, 0.5% (vol/vol) formic acid. Solvents were removed in a speed vac, and dry peptides were stored at –80 °C until analysis.

Chemoproteomic Experiments with isoDTB Tags. A pellet of *V. campbellii* grown to stationary phase (OD₆₀₀ ~5.0, ~24 mL) was washed 3× with PBS and stored at –80 °C before lysis in 1.5 mL PBS with sonication (5 × 15 s, 60%

intensity, on ice), and insoluble proteins were removed by centrifugation ($16,060 \times g$, 30 min, 4°C). Protein concentration was adjusted to 1 mg/mL, and 2 mL lysate was labeled with 10 μM PE-P (2 μL of a 10 mM stock in DMSO) at 30°C for 1 h, 200 rpm. Following 10 min UV irradiation (UV low-pressure mercury-vapor fluorescent lamp, Philips TL-D 18W BLB, 360 nm maximum) in a 6-well plate (Thermo Fisher Scientific), the lysate was split into $2 \times 800 \mu\text{L}$ and adjusted to 1% (wt/vol) SDS [from a 10% (wt/vol) stock in PBS] before adding the Click reagents as for the photoaffinity labeling experiments, except using either heavy- or light-labeled isoDTB azide (100 μM final from a 5 mM DMSO stock, isoDTB azide synthesized as reported previously; ref. 39). After the Click reaction, heavy- and light-labeled lysates (800 μL each) were combined in 8 mL cold acetone and precipitated overnight at -20°C . Precipitated proteins were centrifuged ($10,178 \times g$, 10 min, 4°C), the supernatant decanted, and the pellet resuspended in 1 mL cold methanol with sonication (10% intensity) and pelleted again ($13,000 \times g$, 10 min, 4°C). The methanol wash was repeated, and protein pellets were air-dried and resuspended in 300 μL 8 M urea in 0.1 M TEAB with sonication (10% intensity). Samples were centrifuged ($16,249 \times g$, 3 min) and reduced with 10 mM DTT (15 μL of 201 mM stock in water) for 45 min at 37°C , 850 rpm. Next, thiols were alkylated with 20 mM iodoacetamide (15 μL from a 400 mM stock in water) for 30 min at 25°C , 850 rpm (protected from light), and the remaining iodoacetamide was quenched with 10 mM DTT for 30 min at 25°C , 850 rpm. Then, 900 μL 0.1 M TEAB was added (to achieve pH ~ 8 and 2 M urea), and proteins were digested with 20 μg trypsin (40 μL from 0.5 $\mu\text{g}/\mu\text{L}$ in 50 mM acetic acid, Promega) overnight at 37°C with intense shaking. Per sample, $2 \times 25 \mu\text{L}$ avidin slurry (Sigma-Aldrich) in Protein LoBind tubes was washed with $3 \times 1 \text{ mL}$ 1% (vol/vol) Nonidet P-40 in PBS with centrifugation ($400 \times g$, 2 min). The tryptic digest was split into two portions, added to 600 μL 0.2% (vol/vol) Nonidet P-40 and then to the avidin beads, and incubated for 2.5 h with constant rotation. Beads were then centrifuged ($1,000 \times g$, 2 min), the supernatant was discarded, and the beads were resuspended in 600 μL 0.1% (vol/vol) Nonidet P-40 and transferred to a centrifuge column (Thermo Fisher Scientific) recombining the two portions of one sample. Beads were washed with $2 \times 600 \mu\text{L}$ 0.1% (vol/vol) Nonidet P-40, then with $3 \times 600 \mu\text{L}$ PBS and with $3 \times 600 \mu\text{L}$ water; after every washing step, the solutions were removed by suction. The columns were transferred into LoBind tubes, and peptides were eluted with 400 μL (in three batches) 50% (vol/vol) acetonitrile, 0.1% (vol/vol) formic acid in water with centrifugation ($5,000 \times g$, 3 min). Solvents were removed in a speed vac, and dry peptides were stored at -80°C until analysis.

Co-IP. For details on Co-IP experimental procedures and antibody generation, see *SI Appendix, Supplementary Methods*.

Peptide Reconstitution (All Proteomics Experiments). Dry peptides were reconstituted in 30 μL 1% (vol/vol) formic acid with vortexing and in a sonication bath (10 min) and filtered through centrifugal filters (0.22 μm , Durapore, polyvinylidene fluoride, Merck KGaA) pre-equilibrated with 300 μL 1% (vol/vol) formic acid ($16,249 \times g$, 2 min, RT). For details on MS instrument settings and MS data analysis, see *SI Appendix*.

Plasmid Construction and Protein Purification. For a detailed description of the construction of the *V. campbellii* ΔcheW knockout strain, the plasmid coding for N-terminally His6-tagged CheW, and CheW purification, see *SI Appendix, Supplementary Methods and Tables S6 and S7*.

Microscale Thermophoresis. PD-10 desalting columns packed with Sephadex G-25 resin (GE Healthcare) were used to exchange 6His-CheW protein buffer to MST buffer [PBS with 0.05% (vol/vol) Tween 20]. Purified CheW was labeled using the RED-Tris-NTA Labeling kit (NanoTemper Technologies) according to the manufacturer's instructions. Ligands were dissolved in MST buffer and serially diluted. For thermophoresis, a constant concentration of fluorescently labeled 6His-CheW (100 nM) was mixed with increasing ligand concentrations, resulting in a final concentration of 50 nM labeled 6His-CheW and final ligand concentrations in a range of 7.63 nM to 500 μM . After 10 min incubation at RT, followed by centrifugation ($10,000 \times g$, 10 min) to remove aggregates, the solution was soaked into Monolith NT.115 Series Standard Treated Capillaries. MST measurements were carried out using a Monolith NT.115 instrument (NanoTemper Technologies) with 60% light-emitting diode/excitation power and medium MST power (40%). Three independent measurements were analyzed (NT Analysis software version 1.5.41, NanoTemper Technologies) using the signal from Thermophoresis + T-Jump.

3D Motility Assay. First, 20 μL bacterial culture was added to 1 mL Tris/Mg/NaCl buffer (TMN) (50 mM Tris/HCl, pH 7.4, 5 mM glucose, 100 mM NaCl, 5 mM MgCl₂) containing EPI at the specified concentration, mixed gently, and

left on the bench for 30 min. The solutions were then flowed into sample chambers, consisting of three layers of parafilm as spacers between a microscopy slide and a #1 coverslip that had been heated and pressed to seal. After filling, the ends of the filled chamber were sealed with molten valap (a mixture of vaseline, lanolin, and paraffin) and immediately brought to the microscope for recording, all within 60 min of dilution from the day culture. EPI was diluted into TMN from a 50 mM stock solution in DMSO stored at -20°C within 3 h before the experiment.

3D Chemotaxis Assays. Cells were prepared as for 3D motility assays. For glucose chemotaxis experiments, glucose was omitted in the motility medium TMN. Then, 3D chemotaxis experiments were performed using a high-throughput chemotaxis assay (50) using a commercially available microfluidic device (Ibidi) consisting of two 65- μL reservoirs connected by a 1-mm-long channel with a height of 70 μm and a width of 1 mm. *V. campbellii* cultures were diluted into chemotaxis buffer without (creating solution A) or with the putative chemoattractant (creating solution B) to a target OD₆₀₀ of 0.008 for EPI gradients or OD₆₀₀ 0.005 for serine and glucose gradients. Chemotaxis buffer consisted of TMN, with an added background of EPI or PE for some experiments as specified, and without glucose for glucose gradients. Chemoattractants included EPI, L-serine, and D-glucose at the specified concentrations. First, the entire microfluidic device was overfilled with solution A. Then, the content of one reservoir was exchanged by solution B. A linear chemical gradient was established in the narrow channel between reservoirs within ~ 30 min and stable for several hours. About 40 to 60 min after closing the device, 3D bacterial trajectories were acquired in the middle of this gradient. For experiments with EPI gradients, EPI was prepared as a 40 mM stock in TMN within 3 h before the experiment. For serine chemotaxis experiments, EPI was prepared as 20 mM stock in TMN within 3 h before the experiments. For glucose chemotaxis experiments, EPI and PE were prepared as 60 mM stock in water within 3 h before the experiment. For data acquisition and analysis of 3D trajectories, see *SI Appendix*.

Chemotaxis Capillary Assay. The capillary assay was performed following a published protocol (51) adapted for *Vibrio* species (58, 59). Briefly, *V. campbellii* overnight cultures were diluted into LB35 medium (1:100) and grown to OD₆₀₀ 0.5. The cells were gently washed three times (10 min, $2,000 \times g$) and resuspended in Hepes-buffered artificial seawater [H-ASW: 100 mM MgSO₄, 20 mM CaCl₂, 20 mM KCl, 400 mM NaCl, and 50 mM Hepes (pH 7.5)] (60). The OD₆₀₀ was adjusted to 0.1, and 200 μL culture was transferred into a 96-well plate. The plate was covered with three layers of parafilm, and the open end of a flame-sealed 1- μL capillary (64 mm, Drummond Scientific) was inserted into the bacterial suspension. The capillaries were filled with either H-ASW alone or with attractants dissolved in H-ASW. Solutions containing attractants and cell suspensions were supplemented with catecholamines and antagonists as indicated. The hormones were either dissolved in H-ASW or diluted from a 100-fold concentrated stock solution in 0.1 M HCl prepared immediately before the experiment (EPI and NE) and added directly after the wash steps. After 60 min incubation at room temperature, the contents of the capillaries were expelled and plated in appropriate dilutions on LB agar plates containing carbenicillin. The plates were incubated at 30°C overnight, and colony-forming units were enumerated. Each experiment was conducted at least three times with four technical replicates per condition. Statistical significance was determined using an unpaired two-tailed t test ($*P < 0.05$, $**P < 0.01$).

Data Availability. The mass-spectrometry proteomics data have been deposited to the ProteomeXchange Consortium via the PRIDE partner repository (61) with the dataset identifier PXD029119 (62). All 3D trajectory data are available on the Harvard Dataverse at <https://doi.org/10.7910/DVNV/SJQDEG> (63).

ACKNOWLEDGMENTS. A.W.M. was supported by the Studienstiftung des Deutschen Volkes. S.M.H. acknowledges funding by the Fonds der Chemischen Industrie through a Liebig Fellowship and by the Technical University of Munich Junior Fellow Fund. S.A.S. acknowledges funding from the European Research Council (ERC) and the European Union's Horizon 2020 research and innovation program (grant agreement no. 725085, CHEMMINE, ERC consolidator grant) as well as from the Helmholtz Institute for Pharmaceutical Research Saarland. M.G. and K.M.T. were supported by the Rowland Institute at Harvard. K.J. acknowledges funding from the Deutsche Forschungsgemeinschaft, project no. 395357507-SFB1371. We acknowledge Dr. Anthe Janssen and Prof. Gerard van Westen (Leiden University) and Dr. Nathalie Sisattana for predicting the structure of CheW using AlphaFold. We thank Professor Simon Ringgaard for help with the capillary assay, Mona Wolff and Katja Bäuml for technical support, Juanita Ferreira Olmos for synthetic assistance, Professor Heinrich Jung for his support in the development of the iron-limited medium, and Dr. Isabel Wilkinson for critical reading of this manuscript.

1. P. P. Freestone *et al.*, Growth stimulation of intestinal commensal *Escherichia coli* by catecholamines: A possible contributory factor in trauma-induced sepsis. *Shock* **18**, 465–470 (2002).
2. P. P. Freestone *et al.*, The mammalian neuroendocrine hormone norepinephrine supplies iron for bacterial growth in the presence of transferrin or lactoferrin. *J. Bacteriol.* **182**, 6091–6098 (2000).
3. B. L. Bearson, S. M. Bearson, The role of the QseC quorum-sensing sensor kinase in colonization and norepinephrine-enhanced motility of *Salmonella enterica* serovar Typhimurium. *Microb. Pathog.* **44**, 271–278 (2008).
4. P. Halang *et al.*, Response of *Vibrio cholerae* to the catecholamine hormones epinephrine and norepinephrine. *J. Bacteriol.* **197**, 3769–3778 (2015).
5. Q. Yang, N. D. Q. Anh, P. Bossier, T. Defoirdt, Norepinephrine and dopamine increase motility, biofilm formation, and virulence of *Vibrio harveyi*. *Front. Microbiol.* **5**, 584 (2014).
6. V. Sperandio, A. G. Torres, B. Jarvis, J. P. Nataro, J. B. Kaper, Bacteria–host communication: The language of hormones. *Proc. Natl. Acad. Sci. U.S.A.* **100**, 8951–8956 (2003).
7. M. Merighi *et al.*, Genome-wide analysis of the PreA/PreB (QseB/QseC) regulon of *Salmonella enterica* serovar Typhimurium. *BMC Microbiol.* **9**, 42 (2009).
8. C. G. Moreira, D. Weinschenker, V. Sperandio, QseC mediates *Salmonella enterica* serovar typhimurium virulence *in vitro* and *in vivo*. *Infect. Immun.* **78**, 914–926 (2010).
9. P. Freestone, Communication between bacteria and their hosts. *Scientifica (Cairo)* **2013**, 361073–361087 (2013).
10. N. C. Reading, D. A. Rasko, A. G. Torres, V. Sperandio, The two-component system QseF and the membrane protein QseG link adrenergic and stress sensing to bacterial pathogenesis. *Proc. Natl. Acad. Sci. U.S.A.* **106**, 5889–5894 (2009).
11. M. B. Clarke, D. T. Hughes, C. Zhu, E. C. Boedeker, V. Sperandio, The QseC sensor kinase: A bacterial adrenergic receptor. *Proc. Natl. Acad. Sci. U.S.A.* **103**, 10420–10425 (2006).
12. G. D. Pullinger *et al.*, Norepinephrine augments *Salmonella enterica*-induced enteritis in a manner associated with increased net replication but independent of the putative adrenergic sensor kinases QseC and QseE. *Infect. Immun.* **78**, 372–380 (2010).
13. T. Bansal *et al.*, Differential effects of epinephrine, norepinephrine, and indole on *Escherichia coli* O157:H7 chemotaxis, colonization, and gene expression. *Infect. Immun.* **75**, 4597–4607 (2007).
14. N. Sule *et al.*, The norepinephrine metabolite 3,4-dihydroxymandelic acid is produced by the commensal microbiota and promotes chemotaxis and virulence gene expression in enterohemorrhagic *Escherichia coli*. *Infect. Immun.* **85**, e00431–e00448 (2017).
15. S. Pasupuleti *et al.*, Chemotaxis of *Escherichia coli* to norepinephrine (NE) requires conversion of NE to 3,4-dihydroxymandelic acid. *J. Bacteriol.* **196**, 3992–4000 (2014).
16. S. Bi, V. Sourjik, Stimulus sensing and signal processing in bacterial chemotaxis. *Curr. Opin. Microbiol.* **45**, 22–29 (2018).
17. J. G. Lopes, V. Sourjik, Chemotaxis of *Escherichia coli* to major hormones and polyamines present in human gut. *ISME J.* **12**, 2736–2747 (2018).
18. B. Lin *et al.*, Comparative genomic analyses identify the *Vibrio harveyi* genome sequenced strains BAA-1116 and HY01 as *Vibrio campbellii*. *Environ. Microbiol. Rep.* **2**, 81–89 (2010).
19. B. L. Bassler, M. Wright, R. E. Showalter, M. R. Silverman, Intercellular signalling in *Vibrio harveyi*: Sequence and function of genes regulating expression of luminescence. *Mol. Microbiol.* **9**, 773–786 (1993).
20. K. Papenfort, B. L. Bassler, Quorum sensing signal-response systems in Gram-negative bacteria. *Nat. Rev. Microbiol.* **14**, 576–588 (2016).
21. C. Anetzberger *et al.*, Autoinducers act as biological timers in *Vibrio harveyi*. *PLoS One* **7**, e48310 (2012).
22. B. Austin, X.-H. Zhang, *Vibrio harveyi*: A significant pathogen of marine vertebrates and invertebrates. *Lett. Appl. Microbiol.* **43**, 119–124 (2006).
23. K. M. Ottemann, J. F. Miller, Roles for motility in bacterial–host interactions. *Mol. Microbiol.* **24**, 1109–1117 (1997).
24. S. M. Sandrini *et al.*, Elucidation of the mechanism by which catecholamine stress hormones liberate iron from the innate immune defense proteins transferrin and lactoferrin. *J. Bacteriol.* **192**, 587–594 (2010).
25. C. Toulouse *et al.*, Mechanism and impact of catecholamine conversion by *Vibrio cholerae*. *Biochim. Biophys. Acta Bioenerg.* **1860**, 478–487 (2019).
26. M. Fonović, M. Bogyo, Activity-based probes as a tool for functional proteomic analysis of proteases. *Expert Rev. Proteomics* **5**, 721–730 (2008).
27. M. J. Evans, B. F. Cravatt, Mechanism-based profiling of enzyme families. *Chem. Rev.* **106**, 3279–3301 (2006).
28. M. H. Wright, S. A. Sieber, Chemical proteomics approaches for identifying the cellular targets of natural products. *Nat. Prod. Rep.* **33**, 681–708 (2016).
29. Z. Li *et al.*, Design and synthesis of minimalist terminal alkyne-containing diazirine photo-crosslinkers and their incorporation into kinase inhibitors for cell- and tissue-based proteome profiling. *Angew. Chem. Int. Ed. Engl.* **52**, 8551–8556 (2013).
30. E. Monzani *et al.*, Dopamine, oxidative stress and protein–quinone modifications in Parkinson’s and other neurodegenerative diseases. *Angew. Chem. Int. Ed. Engl.* **58**, 6512–6527 (2019).
31. M. Marchetti *et al.*, Iron metabolism at the interface between host and pathogen: From nutritional immunity to antibacterial development. *Int. J. Mol. Sci.* **21**, 2145–2188 (2020).
32. K. S. Kinney, C. E. Austin, D. S. Morton, G. Sonnenfeld, Norepinephrine as a growth stimulating factor in bacteria–mechanistic studies. *Life Sci.* **67**, 3075–3085 (2000).
33. A. Khan, P. Singh, A. Srivastava, Synthesis, nature and utility of universal iron chelator—Siderophore: A review. *Microbiol. Res.* **212–213**, 103–111 (2018).
34. S. Sandrini, M. Aldriwesh, M. Alruwas, P. Freestone, Microbial endocrinology: Host–bacteria communication within the gut microbiome. *J. Endocrinol.* **225**, R21–R34 (2015).
35. H. Takase, H. Nitanai, K. Hoshino, T. Otani, Requirement of the *Pseudomonas aeruginosa tonB* gene for high-affinity iron acquisition and infection. *Infect. Immun.* **68**, 4498–4504 (2000).
36. V. V. Rostovtsev, L. G. Green, V. V. Fokin, K. B. Sharpless, A stepwise huisgen cycloaddition process: Copper(I)-catalyzed regioselective “ligation” of azides and terminal alkynes. *Angew. Chem. Int. Ed. Engl.* **41**, 2596–2599 (2002).
37. H. C. Kolb, M. G. Finn, K. B. Sharpless, Click chemistry: Diverse chemical function from a few good reactions. *Angew. Chem. Int. Ed. Engl.* **40**, 2004–2021 (2001).
38. J. Cox *et al.*, Accurate proteome-wide label-free quantification by delayed normalization and maximal peptide ratio extraction, termed MaxLFQ. *Mol. Cell. Proteomics* **13**, 2513–2526 (2014).
39. P. R. A. Zanon, L. Lewald, S. M. Hacker, Isotopically labeled desthiobiotin azide (isoDTB) tags enable global profiling of the bacterial cysteinome. *Angew. Chem. Int. Ed. Engl.* **59**, 2829–2836 (2020).
40. P. W. A. Allihn, M. W. Hackl, C. Ludwig, S. M. Hacker, S. A. Sieber, A tailored phosphopartate probe unravels CprR as a response regulator in *Pseudomonas aeruginosa* interkingdom signaling. *Chem. Sci. (Camb.)* **12**, 4763–4770 (2021).
41. P. R. A. Zanon *et al.*, Profiling the proteome-wide selectivity of diverse electrophiles. ChemRxiv [Preprint] (2021) <https://doi.org/10.26434/chemrxiv.14186561.v1> (accessed 10 September 2021).
42. J. Jumper *et al.*, Highly accurate protein structure prediction with AlphaFold. *Nature* **596**, 583–589 (2021).
43. R. P. Alexander, A. C. Lowenthal, R. M. Harshey, K. M. Ottemann, CheV: CheW-like coupling proteins at the core of the chemotaxis signaling network. *Trends Microbiol.* **18**, 494–503 (2010).
44. C. J. Wienken, P. Baaske, U. Rothbauer, D. Braun, S. Duhr, Protein-binding assays in biological liquids using microscale thermophoresis. *Nat. Commun.* **1**, 100–106 (2010).
45. A. Fux, V. S. Korotkov, M. Schneider, I. Antes, S. A. Sieber, Chemical cross-linking enables drafting ClpXP proximity maps and taking snapshots of *in situ* interaction networks. *Cell Chem. Biol.* **26**, 48–59.e7 (2019).
46. A. Briegel, M. Beeby, M. Thanbichler, G. J. Jensen, Activated chemoreceptor arrays remain intact and hexagonally packed. *Mol. Microbiol.* **82**, 748–757 (2011).
47. A. V. Narla, J. Cremer, T. Hwa, A traveling-wave solution for bacterial chemotaxis with growth. *Proc. Natl. Acad. Sci. U.S.A.* **118**, e2105138118 (2021).
48. L. Xie, T. Altindal, S. Chattopadhyay, X.-L. Wu, From the Cover: Bacterial flagellum as a propeller and as a rudder for efficient chemotaxis. *Proc. Natl. Acad. Sci. U.S.A.* **108**, 2246–2251 (2011).
49. S. Ringgaard *et al.*, ParP prevents dissociation of CheA from chemotactic signaling arrays and tethers them to a polar anchor. *Proc. Natl. Acad. Sci. U.S.A.* **111**, E255–E264 (2014).
50. M. Grognot, K. M. Taute, A multiscale 3D chemotaxis assay reveals bacterial navigation mechanisms. *Commun. Biol.* **4**, 669–676 (2021).
51. J. Adler, A method for measuring chemotaxis and use of the method to determine optimum conditions for chemotaxis by *Escherichia coli*. *J. Gen. Microbiol.* **74**, 77–91 (1973).
52. S. M. Butler, A. Camilli, Both chemotaxis and net motility greatly influence the infectivity of *Vibrio cholerae*. *Proc. Natl. Acad. Sci. U.S.A.* **101**, 5018–5023 (2004).
53. S. M. Butler *et al.*, Cholera stool bacteria repress chemotaxis to increase infectivity. *Mol. Microbiol.* **60**, 417–426 (2006).
54. S. H. Lee, S. M. Butler, A. Camilli, Selection for *in vivo* regulators of bacterial virulence. *Proc. Natl. Acad. Sci. U.S.A.* **98**, 6889–6894 (2001).
55. D. S. Merrell *et al.*, Host-induced epidemic spread of the cholera bacterium. *Nature* **417**, 642–645 (2002).
56. W. Epstein, B. S. Kim, Potassium transport loci in *Escherichia coli* K-12. *J. Bacteriol.* **108**, 639–644 (1971).
57. J. Eirich *et al.*, Pretubulysin derived probes as novel tools for monitoring the microtubule network via activity-based protein profiling and fluorescence microscopy. *Mol. Biosyst.* **8**, 2067–2075 (2012).
58. N. Sar, L. McCarter, M. Simon, M. Silverman, Chemotactic control of the two flagellar systems of *Vibrio parahaemolyticus*. *J. Bacteriol.* **172**, 334–341 (1990).
59. C. A. Brennan, M. J. Mandel, M. C. Gyllborg, K. A. Thomasgard, E. G. Ruby, Genetic determinants of swimming motility in the squid light-organ symbiont *Vibrio fischeri*. *MicrobiologyOpen* **2**, 576–594 (2013).
60. E. G. Ruby, K. H. Nealson, Symbiotic association of *Photobacterium fischeri* with the marine luminous fish *Monocentris japonica*: A model of symbiosis based on bacterial studies. *Biol. Bull.* **151**, 574–586 (1976).
61. Y. Perez-Riverol *et al.*, The PRIDE database and related tools and resources in 2019: Improving support for quantification data. *Nucleic Acids Res.* **47**, D442–D450 (2019).
62. A. Weigert Muñoz, S. M. Hacker, S. A. Sieber, Eukaryotic catecholamine hormones influence the chemotactic control of *Vibrio campbellii* by binding to the coupling protein CheW. PRIDE database. <http://www.ebi.ac.uk/pride/archive/projects/PXD029119>. Deposited 14 October 2021.
63. M. Grognot, K. M. Taute, 3D trajectory data for “Eukaryotic catecholamine hormones influence the chemotactic control of *Vibrio campbellii* by binding to the coupling protein CheW”. Harvard Dataverse. <https://doi.org/10.7910/DVN/5JQDEG>. Deposited 15 February 2022.

2.4 Division of labor and collective functionality in *Escherichia coli* under acid stress

Brameyer, S., Schumacher, K., Kuppermann, S., and Jung, K. (2022). Division of labor and collective functionality in *Escherichia coli* under acid stress. *Commun. Biol.* 5, 1–14. 10.1038/s42003-022-03281-4.

Available online at:

<https://pubmed.ncbi.nlm.nih.gov/35393532/>

Division of labor and collective functionality in *Escherichia coli* under acid stress

Sophie Brameyer ¹, Kilian Schumacher ¹, Sonja Kuppermann¹ & Kirsten Jung ¹✉

The acid stress response is an important factor influencing the transmission of intestinal microbes such as the enterobacterium *Escherichia coli*. *E. coli* activates three inducible acid resistance systems - the glutamate decarboxylase, arginine decarboxylase, and lysine decarboxylase systems to counteract acid stress. Each system relies on the activity of a proton-consuming reaction catalyzed by a specific amino acid decarboxylase and a corresponding antiporter. Activation of these three systems is tightly regulated by a sophisticated interplay of membrane-integrated and soluble regulators. Using a fluorescent triple reporter strain, we quantitatively illuminated the cellular individuality during activation of each of the three acid resistance (AR) systems under consecutively increasing acid stress. Our studies highlight the advantages of *E. coli* in possessing three AR systems that enable division of labor in the population, which ensures survival over a wide range of low pH values.

¹Department of Biology, Microbiology, Ludwig-Maximilians-Universität München, Martinsried, Germany. ✉email: jung@lmu.de

The acquisition of acid resistance (AR) is an important property of *Escherichia coli* and many other neutralophilic bacteria that enables survival in acidic environments, such as the human gastrointestinal tract or acidic soils^{1,2}. Although the cytoplasmic membrane is impermeable for protons, some protons enter the cytoplasm through protein channels, transient water chains, or damaged membranes^{3,4}. Bacteria are generally able to maintain a fairly constant internal pH when grown in a wide range of media at different external pH values^{5,6}. Despite this, pH homeostasis varies among individual bacterial cells as reported amongst others for *E. coli* and *Bacillus subtilis*⁷. Interestingly, persister cells of *E. coli* display a lower intracellular pH allowing survival after antibiotic treatment⁸. Nevertheless, after exposure of *E. coli* to an external pH of 5.8, the pH of its cytoplasm drops transiently; however, the pH rapidly returns to a neutral level due to the intrinsic buffering capacity of the cytoplasm or alterations in the flux of ions⁹. A lower external pH such as 4.4 causing a lower intracellular pH of around 6.0 has adverse effects on all macromolecules of a cell, which might result in lowered enzyme activity, acid-induced protein unfolding, membrane damage, and DNA damage.

Besides its passive mechanisms, *E. coli* possesses several inducible AR systems to counteract acidic environments^{1,3}. The major systems are the glutamate decarboxylase (Gad) system, arginine decarboxylase (Adi) system, and lysine decarboxylase (Cad) system (AR2, AR3, and AR4, respectively)^{10–12}. AR1 does not require an amino acid and is regulated by the alternative σ -factor (RpoS) and the cAMP receptor protein^{10,13}. The ornithine decarboxylase system (AR5) plays only a minor role in *E. coli* MG1655, yet has a more important role in avian pathogenic *E. coli*¹⁴. The core components of each of the three major AR systems are a proton-consuming amino acid decarboxylase and a cognate antiporter to excrete the decarboxylated (more alkaline) compounds in exchange with the corresponding extracellular amino acid. In this way, both the intracellular and extracellular pH values can be increased^{3,11,15,16}. Each system is active at different external pH values and growth phases, and induction is regulated by a sophisticated interplay of membrane-integrated and soluble regulators.

Activation of the Gad System occurs during the transition of an *E. coli* culture to stationary phase and during exponential growth in acidified media. Furthermore, this system is essential for cell survival at an extremely low pH of 2.5^{10,17–19}. The Gad system employs GadA and GadB, two pyridoxal phosphate-dependent decarboxylases that catalyze the proton-consuming decarboxylation of L-glutamate to generate γ -aminobutyrate (GABA), and GadC, the cognate antiporter that performs the import of L-glutamate and the export of GABA^{17,20}. It is important to note that the activity of GadC is pH-dependent, and the antiporter preferentially exchanges protonated glutamate (Glu⁰) in exchange for protonated GABA (GABA⁺) at an external pH of 3.0 and lower^{21–23}. The induction of the *gad* genes is rather complex. The main transcriptional regulator is GadE, whose expression is regulated by the transcription factors EvgA, GadW, GadX, and YdeO as well as σ -factor RpoS. RpoS is activated and stabilized in response to different conditions, including the stationary phase, various stress treatments, and for example by the signal transduction cascade proceeding from PhoQ/PhoP to RssB and IraM^{24,25}. Furthermore, the EvgS/EvgA histidine kinase/response regulator system is a primary detector of mild acidic environments (pH 5) and additionally regulates the activation of the Gad system through a cascade of EvgA-YdeO-GadE regulators^{26,27} (Fig. 1). In addition, RcsB is a critical partner of GadE and the binding of both regulators as a heterodimer to the GAD box activates *gadA* transcription^{28–30}.

The Adi system is responsible for the conversion of arginine to agmatine under the consumption of one proton (Fig. 1). The main components are the transcriptional activator AdiY, a member of the AraC-family; the arginine decarboxylase AdiA; and the arginine/agmatine antiporter AdiC. The genes encoding the Adi system have an unusual genomic arrangement in *E. coli*, as the gene of *adiY* is located downstream of *adiA* and upstream of *adiC*. The Adi system is maximally induced under the conditions of acidic pH (pH 4.4), anaerobiosis, and a rich medium³¹. The activity of AdiC is regulated in response to acidic pH and remains fully active at a pH of ≤ 6.0 ³². The expression of *adiY* seems to be indirectly influenced by the transcriptional repressor CsiR, as its overexpression results in the repression of *adiY* and *adiA*¹⁶. Under anaerobic conditions, the *adiY* mRNA can be base-paired by the small RNA SgrS resulting in post-transcriptional downregulation³³.

The Cad system, which is activated when *E. coli* is exposed to pH 5.8 in the presence of lysine, uses external lysine, which is converted to cadaverine by the lysine decarboxylase CadA under the consumption of one proton. The lysine/cadaverine antiporter CadB imports lysine and excretes the more alkaline cadaverine, thereby elevating the external pH³⁴. Expression of the *cadBA* operon is activated by the membrane-integrated one-component regulator CadC, which is a representative of the ToxR-family³⁵ (Fig. 1). The pH-sensory function and the feedback inhibition by cadaverine could be assigned to distinct amino acids within the periplasmic sensory domain of CadC^{36,37}. The availability of external lysine is transduced to CadC via the co-sensor and inhibitor LysP, which is a lysine-specific transporter^{38,39}. Recently, we demonstrated that not only the copy number of CadC affects the dual-stress response⁴⁰, but also the noise of the target protein abundance. Using fluorophore-tagged CadB, a heterogeneous output in the single cells of *E. coli* occurred under mild acidic stress. Moreover, an increase in the CadC copy number was correlated with decreased heterogeneous behavior⁴¹.

The ON/OFF behavior of the *E. coli* population in activating the Cad system prompted us to ask whether the “Cad-OFF” cells activate the Gad and/or Adi systems. Here, we used a fluorescent triple reporter to study the induction of the three inducible AR systems, Gad, Adi, and Cad, in individual *E. coli* cells under consecutively increasing acid stress. We herein report extensive heterogeneity and division of labor in the acid stress response of individual *E. coli* cells. For the first time, we present a model that explains the cellular individuality that occurs during activation of each of the three AR systems in the context of ensuring AR for the whole population over a wide range of acidic pH values.

Results

Heterogenous activation of the three inducible AR systems by acid stress in *E. coli*. In our previous studies, we demonstrated that heterogenous activation of the Cad system results in ~70% ON and ~30% OFF cells⁴¹. Here, we constructed a three-color reporter strain *E. coli* (*gadC::eGFP-adiC::mCerulean-cadB::mCherry*) to study whether the “Cad-OFF” cells activate the Gad and/or the Adi systems and whether these two systems are activated heterogeneously. In this strain, each of the antiporter genes (*gadC*, *adiC*, and *cadB*) is fused with a different fluorophore gene coding for eGFP, mCerulean, or mCherry, respectively (Fig. 1). These fusions were chromosomally integrated to avoid a copy number effect, and the functionality of the hybrid proteins was confirmed (Supplementary Fig. 1).

First, the three-color reporter strain was exposed to consecutively increasing acidic conditions (pH 7.6, pH 5.8, and pH 4.4) in a well-mixed environment (Fig. 2a). Then, at the indicated time

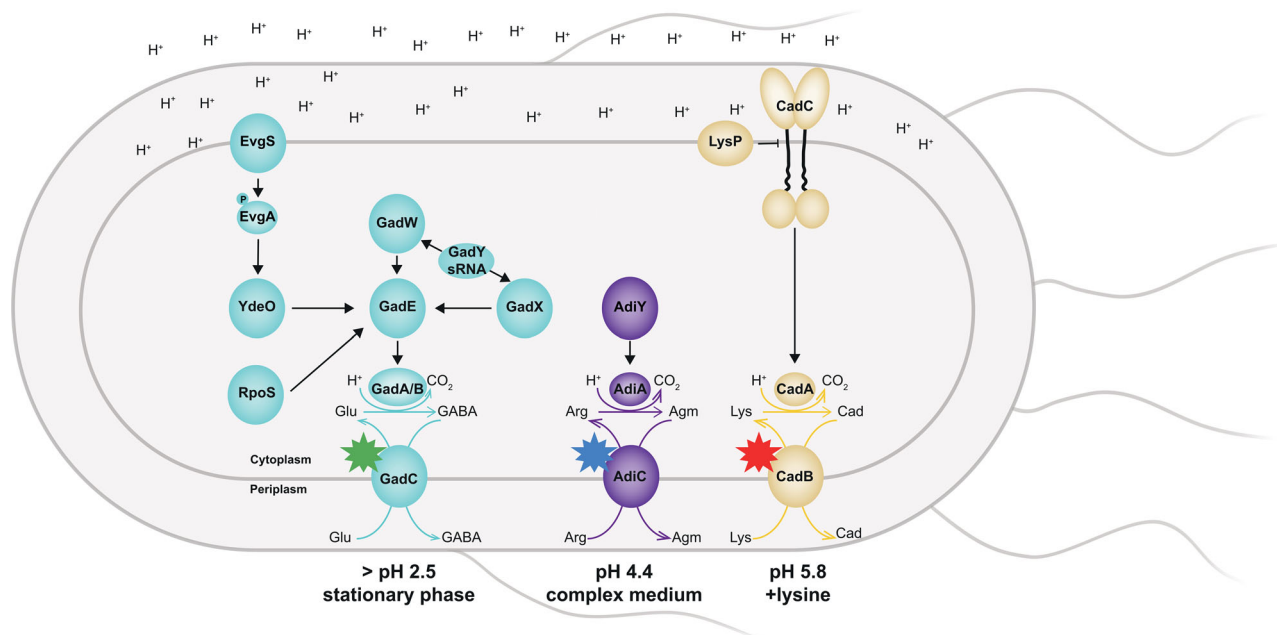


Fig. 1 The regulatory network of inducible amino acid decarboxylase-antiporter systems in *E. coli* three-color strain. Regulated induction of the Gad (blue symbols), Adi (purple symbols), and Cad (yellow symbols) systems requires a network of membrane-integrated pH-sensors, namely EvgS and CadC; interconnected transcription factors; and the sRNA GadY. The glutamate decarboxylases GadA and GadB convert glutamate (Glu) into γ -aminobutyrate (GABA), which is excreted by GadC. The arginine decarboxylase AdiA converts arginine (Arg) into agmatine (Agm), which is excreted by AdiC. The lysine decarboxylase CadA converts lysine (Lys) into cadaverine (Cad), which is excreted by CadB. Adapted from^{3, 15, 24, 25, 47, 74}. The stimuli leading to an induction of each of the three AR systems is indicated below each system. Each fluorescent hybrid of the three antiporter is indicated with a star symbol: GadC:eGFP (green star), AdiC:mCerulean (blue star), and CadB:mCherry (red star) according to the hybrid with the fluorophore eGFP, mCerulean, and mCherry, respectively.

points, cells were imaged, and the fluorescence intensities were quantified (Fig. 2b).

GadC:eGFP showed the highest production during the stationary phase and under the acidic conditions of pH 5.8 and pH 4.4 (Fig. 2b–d, t_{300}). In the stationary phase at physiological pH, GadC:eGFP was produced two times less than under acidic conditions; however, its heterogeneous distribution increased, as indicated by noise values of 0.11 (defined as the standard deviation divided by the mean of log-transformed intensity values⁴²) (t_{300}) (Fig. 2c; left panel). When cells were exposed to mild acid stress (pH 5.8), GadC:eGFP was homogeneously distributed among individual cells in the *E. coli* population and exhibited low noise values of 0.04–0.08 (Fig. 2b, c; left panel).

The Cad system is activated by mild acidic stress in the presence of lysine; therefore, CadB:mCherry became visible after 2.5 h of growth in a minimal medium supplemented with lysine at pH 5.8. At this time point, CadB:mCherry was heterogeneously distributed, as reflected by a high noise value of 0.37 (Fig. 2b–d), which is in perfect agreement with previous experiments of CadB tagged with eGFP⁴¹. The distribution of CadB:mCherry remained heterogeneous at pH 4.4 in complex medium, but the mean value increased 1.5-fold (Fig. 2c; right panel, t_{300}).

The Adi system is only activated under stronger acidic conditions, such as pH 4.4 in a complex medium with a noise value of 0.12 (Fig. 2b, c; middle panel).

Overall, the distribution of CadB:mCherry among single *E. coli* cells under acid stress was not a symmetric Gaussian-like distribution but rather an asymmetric right-skewed distribution (Fig. 2d), as up to 83% of the population produced CadB:mCherry at varying high levels, and the remaining cells were in the OFF state, which was in agreement with previous findings using CadB:eGFP⁴¹. The distribution of GadC:eGFP and AdiC:mCerulean follows a symmetric Gaussian-like distribution (Fig. 2d),

which indicated that individual cells produce different amounts of GadC:eGFP and AdiC:mCerulean. However, almost all cells produced varying amounts of GadC:eGFP (99%), whereas only half of the population (47.7%) produced AdiC:mCerulean at pH 4.4 (Fig. 2d; right panel). As a control, non-tagged *E. coli* MG1655 cells were examined under the same conditions; these cells exhibited low background fluorescence and extremely low noise values (Supplementary Table 1).

To exclude pH-effects on the fluorophores, each of the three fluorophores (eGFP, mCherry, and mCerulean) was fused to the antiporter gene *gadC*, because GadC is produced under all tested external pH values. Neither the different fluorophores nor the external pH affected the output or noise of the fluorescent hybrids (Supplementary Fig. 2; Supplementary Table 1).

Overall, the three inducible AR systems were heterogeneously activated with a different degree of noise. The Cad system showed the highest heterogeneous distribution (pH 5.8 t_{150}) of all three systems, whereas the Gad and Adi systems showed comparable noise values (0.11 and 0.12, respectively), but under different conditions. The Gad system was the most heterogeneous during the stationary phase, whereas the Adi system was activated heterogeneously by stronger acid stress (pH 4.4).

Simultaneous activation of the AR systems in single *E. coli* cells. Since the three AR systems showed a heterogeneous output, although each had a different strength of heterogeneity, we examined their simultaneous activation within individual *E. coli* cells under exposure to consecutively increasing acid stress (Fig. 2a).

The correlation between GadC:eGFP and CadB:mCherry was analyzed at the time point of the highest degree of heterogeneity of the Cad system (pH 5.8 t_{150} ; Fig. 3a); however, no correlation occurred, thus indicating that there was a lack of dependency

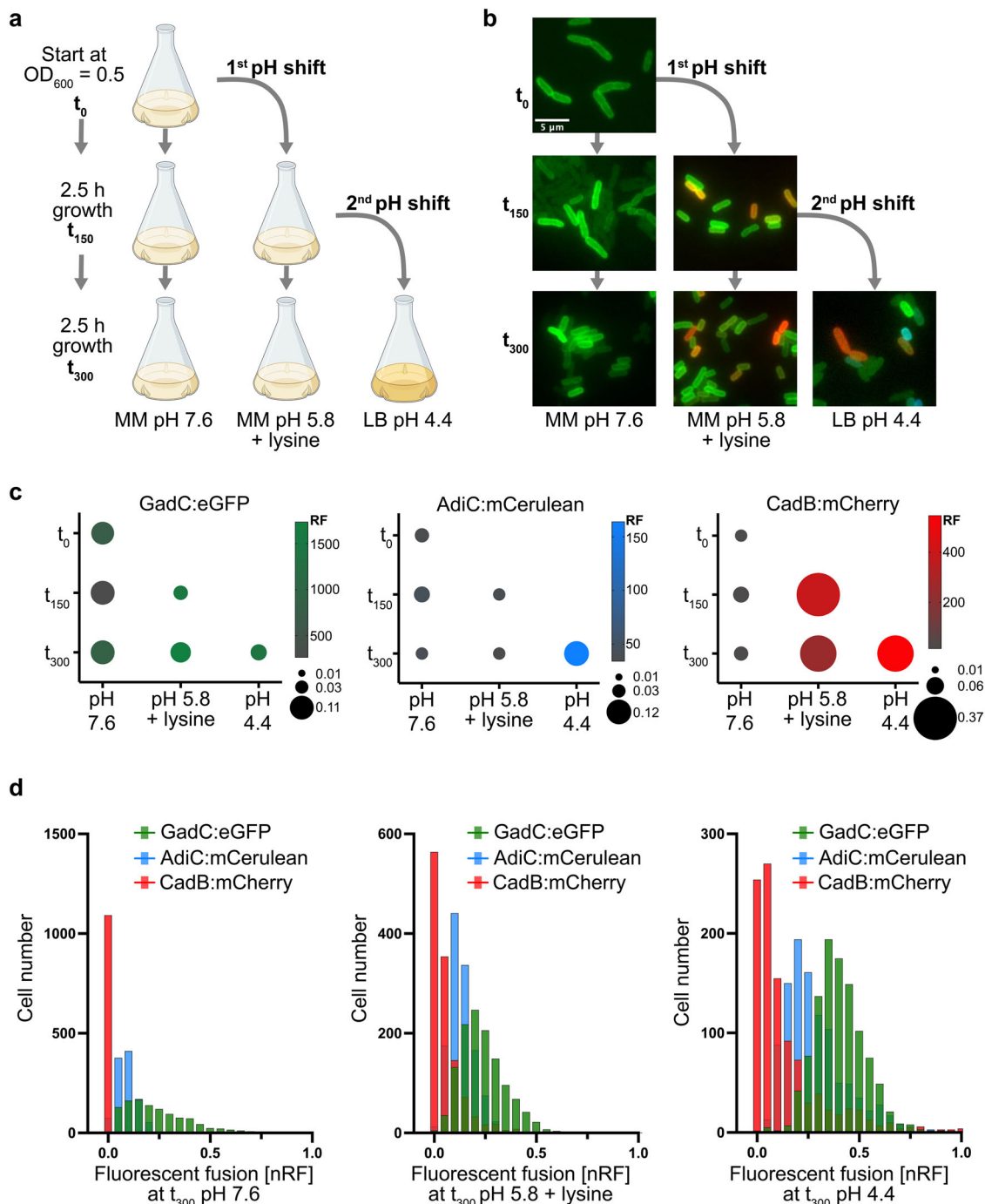


Fig. 2 Heterogenous activation of the three inducible AR systems in *E. coli* in response to acid stress. **a** Schematic representation of the experimental setup: at the exponential phase (t_0), the three-color reporter strain *E. coli gadC:eGFP-adiC:mCerulean-cadB:mCherry* was shifted from the MM at pH 7.6 to MM at pH 5.8 supplemented with 10 mM lysine, followed by a second shift to the LB medium at pH 4.4. In parallel, half of the culture was incubated under the original pH condition. **b** Fluorescent microscopic images of the three-color reporter strain *E. coli gadC:eGFP-adiC:mCerulean-cadB:mCherry*, cultivated as presented in **(a)**, were taken at the indicated time points. Representative fluorescence overlay images are shown. Scale bar, 5 μm . **c** Quantified noise and mean RF were calculated for 1000 cells per condition and time point of the cultivated three-color reporter strain *E. coli gadC:eGFP-adiC:mCerulean-cadB:mCherry*, as presented in **(a)**. Noise (standard deviation/mean of log-transformed values) is presented by the size of the dots (the higher the noise, the larger the size of the dot), and the average of the RF is presented with a color code for each fluorescent hybrid, GadC:eGFP (left panel), AdiC:mCerulean (middle panel), and CadB:mCherry (right panel). RF was quantified by using the MicrobeJ plugin of the ImageJ software of the fluorescent microscopic images. **d** Histogram presentation of the nRF quantified for 1000 cells per fluorescent hybrid, GadC:eGFP, AdiC:mCerulean, and CadB:mCherry, grown at t_{300} in MM pH 7.6 (left panel), MM at pH 5.8 supplemented with 10 mM lysine (middle panel), and LB medium at pH 4.4 (right panel), respectively. A comparison of the frequencies of CadB:mCherry with AdiC:mCerulean and with GadC:eGFP using the Chi-square test showed a p -value < 0.0001 for each time point. LB lysogeny broth, MM minimal medium, nRF normalized relative fluorescence intensity, RF relative fluorescence intensity.

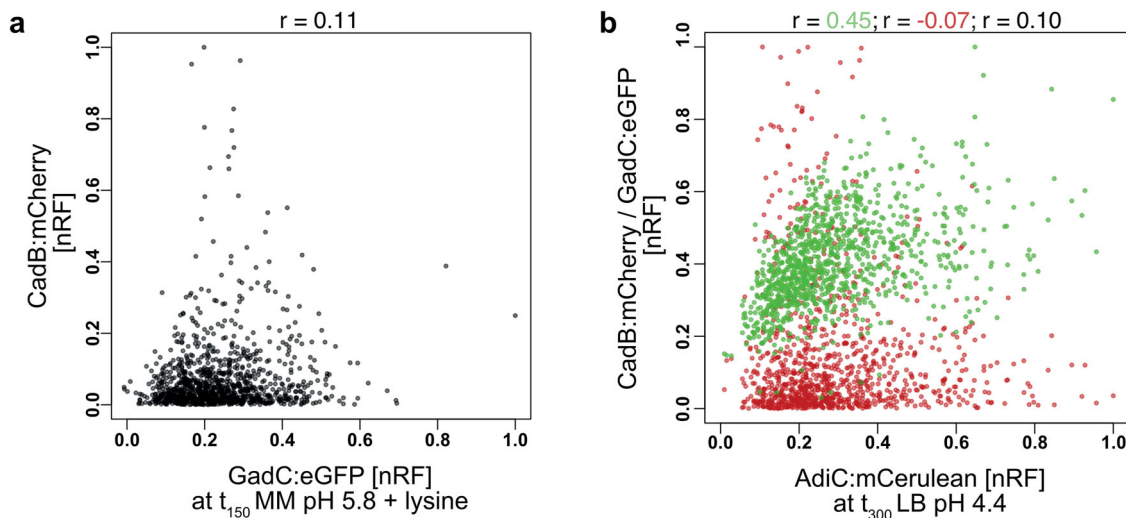


Fig. 3 Simultaneous activation of the AR systems in single *E. coli*. **a** Normalized fluorescence intensity (nRF) presented in a correlation plot of CadC:eGFP versus CadB:mCherry of the strain *E. coli* *gadC:eGFP-adiC:mCerulean-cadB:mCherry* in MM at pH 5.8 supplemented with lysine at t_{150} . Pearson's correlation coefficient (r) is shown on top of the graph: $r = 0.11$ for GadC:eGFP and CadB:mCherry with a p -value of $3.28e^{-4}$. **b** nRF presented in a correlation plot of AdiC:mCerulean versus GadC:eGFP (green dots) and versus CadB:mCherry (red dots) of *E. coli* *gadC:eGFP-adiC:mCerulean-cadB:mCherry* in LB medium at pH 4.4 at t_{300} . Pearson's correlation coefficient is shown on top of the graph: $r = 0.45$ for GadC:eGFP and AdiC:mCerulean (green) with a p -value of 4.4^{-56} ; $r = -0.07$ for AdiC:mCerulean and CadB:mCherry (red) with a p -value of <0.05 ; $r = 0.10$ for GadC:eGFP and CadB:mCherry (black) with a p -value of <0.05 . Pearson's correlation coefficient was calculated using GraphPad Prism 9.1.0. Correlation plots were created using R 4.0.3. LB lysogeny broth, MM minimal medium, RF relative fluorescence intensity, nRF normalized RF values, noise standard deviation/mean of log-transformed values.

between these two systems (Pearson's correlation coefficient, $r = 0.11$). During the stationary phase under strong acid stress (pH 4.4 t_{300}), when all three systems were activated, GadC:eGFP and AdiC:mCerulean showed a positive correlation ($r = 0.45$; green dots); however, no correlation occurred between CadB:mCherry and GadC:eGFP or AdiC:mCerulean ($r = 0.10$ and $r = -0.07$, respectively) (Fig. 3b). In summary, in stationary phase under strong acid stress, almost all cells activated the Gad system; however, simultaneous activation of the Cad and Adi systems did not occur.

Phylogenetic distribution of the components of the three AR systems within the bacterial kingdom. To identify connecting regulators between the three AR systems and to understand the segregation of the Adi and the Cad systems in *E. coli*, we used a bioinformatic approach to investigate the presence and distribution of regulatory components of the three AR systems within the bacterial kingdom. We used the antiporters GadC, AdiC, and CadB as the basis for the construction of phylogenetic trees and focused on discovering a potential co-occurrence of their specific regulators (Fig. 1; Supplementary Table 2).

According to our study, there are 1112 homologs of *E. coli* GadC that mainly occur in the phylum Proteobacteria (42.4%), such as *Enterobacteriaceae* (31.1%, with 27.8% belonging to *Escherichia*); *Morganellaceae* (4.5%); and *Yersiniaceae* (3.0%). Moreover, 51.3% of the GadC homologs belong to the bacteria of Firmicutes (56.0%), such as *Listeriaceae* (14.8%), *Enterococcaceae* (14.1%), *Clostridaceae* (9.8%), *Lactobacillaceae* (7.3%) and *Streptococcaceae* (5.2%) (Fig. 4a). Although GadC and GadB homologs are widely occurring, the regulators responsible for the sophisticated regulation of the Gad system of *E. coli* are mainly present in *Enterobacteriaceae* (Fig. 4a). GadW, GadX, GadY, GadE, and YdeO are predominantly conserved in *Escherichia* (89.3%) and, to some extent, in *Shigella* (0.04%) species. GadE is found in *Escherichia* and *Shigella* but also in other *Enterobacteriaceae* species, such as *Citrobacter freundii* and *Kluyvera ascorbate*. (Fig. 4a; Supplementary Table 2). The carbon induced

starvation transcriptional regulator CsiR, a member of the GntR-family, mainly occurs within γ -proteobacteria in 30.3% of species containing a GadC homolog, especially in *Enterobacteriaceae* (94.9%), such as *E. coli* (Fig. 4a). In *E. coli*, CsiR presumably affects all three AR systems: overexpression of CsiR stimulates binding to promoters of the Gad system, *gadX* and *gadW*; of the Cad system, *cadC*; and leads to lower expression of the *adiY* and *adiA* genes¹⁶. The sensor kinase EvgS is mainly found in *Enterobacteriaceae* (85.6%) but also in members of *Hafniaceae*, like *Hafnia alvei*, and *Yersiniaceae*, such as *Yersinia fredericksonii* and *Serratia fonticola*, all of which belong to γ -proteobacteria (Fig. 4a).

The components of the Adi and Cad systems are mainly conserved within γ -proteobacteria. In total, 756 AdiC homologs were identified within *Enterobacteriaceae* (70.8%), *Lysobacteriaceae* (11.6%), *Yersiniaceae* (7.5%), and *Morganellaceae* (4.4%) (Fig. 4b). Of species containing an AdiC homolog, the Adi system-specific transcriptional activator AdiY is present in 69.0%, all of which, like *Escherichia* (68.9%), *Salmonella* (20.1%), and *Shigella* (4.9%), belong to the *Enterobacteriaceae* family. CsiR is distributed in a similar manner and is present in 70.4% of species containing an AdiC homolog. The 533 CsiR homologs that were identified mainly belonged to *Enterobacteriaceae* and *Hafniaceae* species, such as *Escherichia* (67.7%), *Salmonella* (19.7%), *Shigella* (4.9%), and *Hafnia* (2.8%) species. Moreover, CsiR homologs co-occur to a high degree with AdiY homologs, as 96.4% of species containing AdiY also have a CsiR homolog, except for *Hafnia* species, which lack AdiY homologs (Fig. 4b; Supplementary Table 2).

The antiporter CadB of the Cad system was found mainly in γ -proteobacteria. 857 homologs were identified belonging to *Enterobacteriaceae* (55.8%), *Vibrionaceae* (20.0%), *Aeromonadaceae* (7.0%), *Hafniaceae* (5.6%), and *Yersiniaceae* (4.7%). CadB mainly co-occurs with CadA and CadC homologs. Of the species that have a CadB homolog, 94.3% also possess a CadA homolog of the cognate lysine decarboxylase of the Cad system, and 95.5% also have a homolog of the cognate pH-sensor CadC (Fig. 4c). In total, 573 homologs of the lysine-permease LysP were identified,

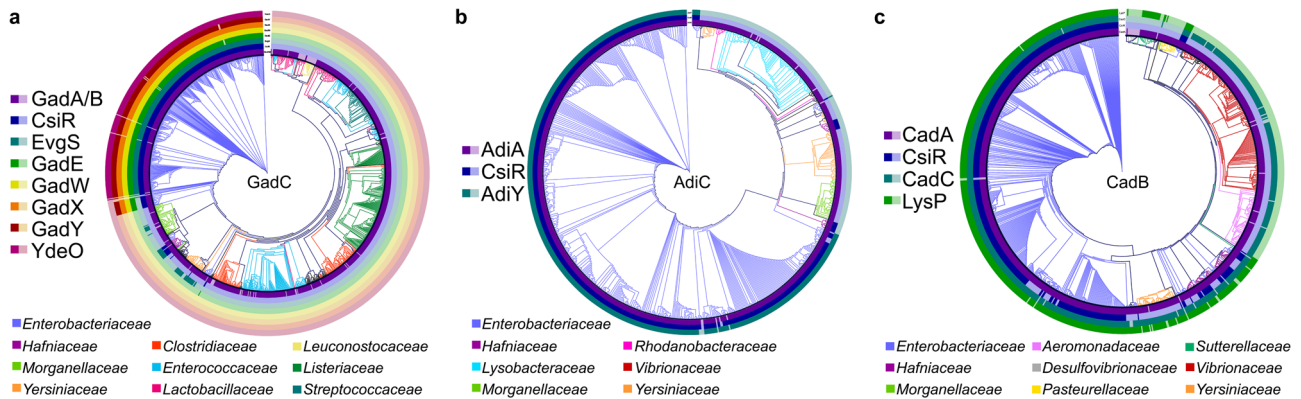


Fig. 4 Phylogenetic trees of the *E. coli* antiporters GadC, AdiC, and CadB and co-occurring regulators of the three AR systems within the bacterial kingdom. **a** The protein sequences of 1112 of *E. coli* GadC homologs were aligned, and a phylogenetic tree was generated, which is shown as a circular cladogram. The branches of the tree were colored according to the family of the organisms containing a GadC homolog. The presence of different regulatory components CsiR, EvgS, GadE, GadW, GadX, GadY, and YdeO and the decarboxylases GadA and GadB (GadA/B) is indicated by solid colors in the respective ring layer. Translucent colors represent components that were not detected. **b** The protein sequences of 756 *E. coli* AdiC homologs were aligned, and a phylogenetic tree was generated, which is shown as a circular cladogram. The branches of the tree are colored according to the family of organisms containing an AdiC homolog. The presence of the different regulatory components CsiR and AdiY as well as the decarboxylase AdiA is indicated by solid colors in the respective ring layer. If these components were not found, the colors are translucent. **c** The protein sequences of 857 *E. coli* CadB homologs were aligned, and a phylogenetic tree was generated, which is shown as a circular cladogram. The branches of the tree are colored according to the family of organisms containing a CadB homolog. The presence of the different regulatory components CsiR, CadC, and LysP as well as the decarboxylase CadA are indicated by solid colors in the respective ring layer. Translucent colors represent components that were not detected. Identifiers of all GadC, AdiC, and CadB homologs with an indication of the presence or absence of their main regulators are summarized in Supplementary Data 1.

66.9% of which were found in species containing a CadB homolog. As previously reported, LysP predominantly co-occurs with the Cad system within the *Enterobacteriaceae* family (82.3%) and is mostly absent in *Vibrionaceae* (Fig. 4c; Supplementary Table 2)⁴¹. CsiR homologs are less coupled with CadB compared to other components of the Cad system. However, similar to LysP, CsiR is mainly found in *Enterobacteriaceae* and *Hafniaceae*, such as *Escherichia* (49.1%), *Klebsiella* (23.4%), *Salmonella* (14.6%), and *Hafnia* (4.1%) species. In summary, the regulatory components specific to *E. coli* of the three AR systems that were studied were predominantly conserved in *Enterobacteriaceae*. The Gad system was the most widespread AR system, whereas the Adi and Cad systems were restricted to γ -proteobacteria. Interestingly, the decarboxylases, together with their cognate antiporters, were more widely distributed than other regulatory components. The central regulators of the Cad system and the Adi system were more specific to the *Enterobacteriaceae* family.

Mechanisms of heterogeneous activation of the three AR systems. To gain insight into the molecular mechanisms of heterogeneous activation of the AR systems in *E. coli*, we analyzed the importance of different transcriptional regulators. We focused mainly on the Adi and Cad systems, as these systems exhibited a higher degree of heterogeneity. First, we assessed the role of the regulator CsiR, which co-occurs with the components of the Gad, Adi, and Cad systems, mainly in *Enterobacteriaceae* (Fig. 4), and is supposed to modulate AR in *E. coli*¹⁶. However, artificially increased CsiR levels affected only the Adi system and not the Gad or Cad systems (Supplementary Table 1). Higher intracellular CsiR levels caused a 2.4-fold decrease in the amount of AdiC:mCerulean but did not affect the heterogeneous distribution. The measured noise value was 0.10 under these conditions and is consistent with the wild type (Supplementary Table 1). These results are in good agreement with the suggested repressing impact of CsiR on the Adi system according to ChIP-Seq analysis¹⁶.

Second, we already know that the native low CadC copy number generates heterogeneous activation of the Cad system, as

an increase in the CadC copy number correlates with a decrease in heterogeneous distribution of the Cad system⁴¹. In addition, CadC itself is distributed heterogeneously⁴³. Because of the mutually exclusive activation of the Cad and Adi systems (Fig. 3b), we tested whether CadC also has an influence on the Adi system. When we artificially elevated the copy number of CadC, we found four-times lower mean fluorescence of AdiC:mCherry (Fig. 5a). Moreover, the heterogeneous distribution of AdiC:mCherry was much lower under this condition (Fig. 5a). It should be noted that the higher level of CadC decreased the amount of GadC:mCerulean by only two-fold in cells exposed to pH 5.8, and the already less heterogeneous distribution of the Gad system was not affected (noise value of 0.05, which is comparable to that of the wild type) (Supplementary Table 1). In agreement with previous observations, the higher level of CadC increased the production of CadB:eGFP while reducing its heterogeneous distribution (Supplementary Table 1).

Third, AdiY also belongs to low copy number regulators with approximately 11–37 copies per cell⁴⁴. Based on our previous experience with CadC⁴¹, we analyzed the influence of the copy number of AdiY on heterogeneous activation of the Adi system in pH 4.4-stressed cells. We increased the copy number by placing *adiY* under the control of the P_{BAD} promoter on a plasmid. The artificially increased copy number of AdiY resulted in a two-fold increase in the mean fluorescence and thus a higher amount of AdiC:mCerulean, which is not surprising, since AdiY is the main transcriptional activator of *adiC*. Furthermore, the heterogeneous distribution of AdiC:mCerulean was strongly reduced (Fig. 5b). However, *E. coli* cells producing a higher copy number of AdiY had a growth disadvantage under acid stress compared with wild-type cells (Fig. 5c). A similar effect on growth was previously demonstrated for *E. coli* cells producing a higher CadC copy number⁴¹ (Supplementary Fig. 3).

The effect of CadC on the Adi system could be direct or indirect. A direct effect, i.e., that CadC binds upstream of *adiC* as a transcriptional regulator, can be excluded, as we did not find a second binding site for CadC in *E. coli*^{43,45,46}. Therefore, we hypothesized that an indirect effect was caused by a CadC-

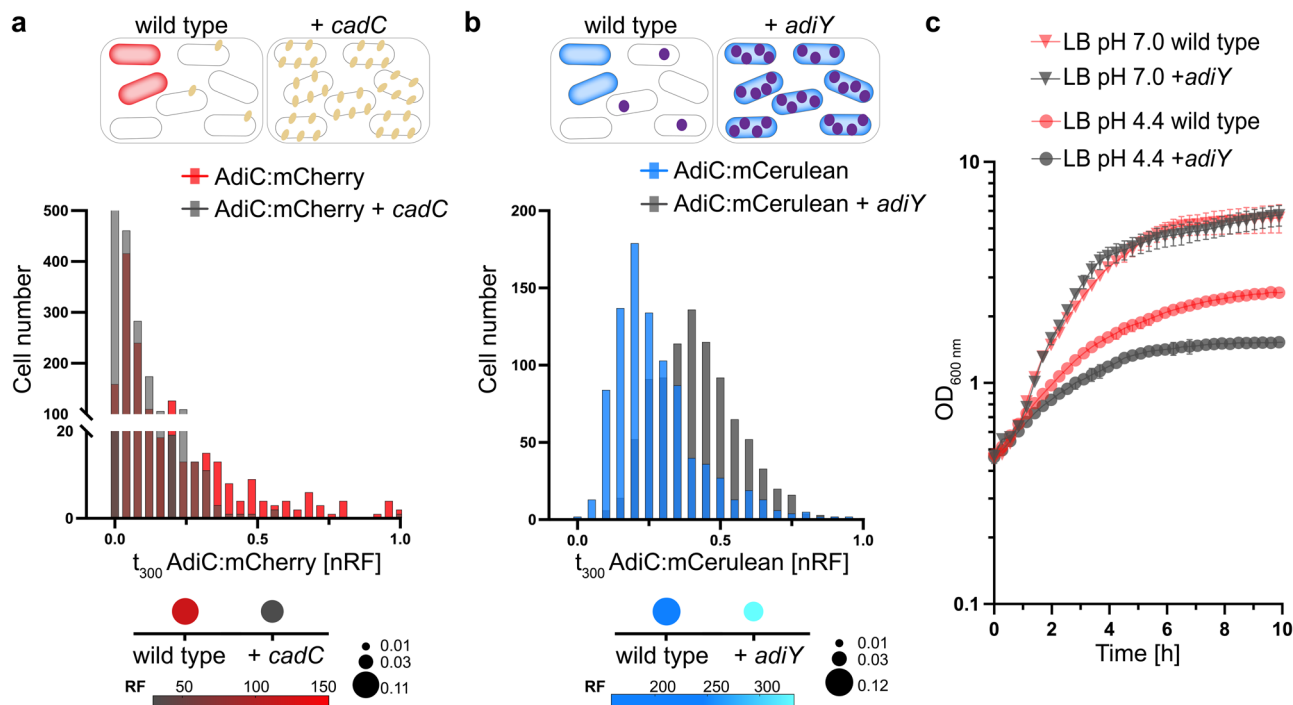


Fig. 5 An increase of the copy number of *AdiY* or *CadC* affects the degree of heterogeneity of the *Adi* system. **a** nRF values of cells expressing *AdiC:mCherry* in the wild type background (red) or with an elevated *CadC* copy number (gray) at pH 4.4 in LB medium at t_{300} . +*cadC*, the expression of *cadC* under the control of the arabinose (0.1%)-inducible promoter in plasmid pBAD24. The comparison of frequencies of *AdiC:mCherry* in wild type or +*cadC* cells using the Chi-square test showed a p -value < 0.001. On top of the histogram: red cells represent the *AdiC:mCherry* ON state; +*cadC* is represented by yellow dots. Below the histogram: noise is presented by the size of the dots; average RF is represented by color intensity (Supplementary Table 1). RF was quantified using the MicrobeJ plugin of the ImageJ software of the fluorescent microscopic images for 1000 cells per condition. nRF normalized RF values. **b** nRF values of cells expressing *AdiC:mCerulean* in the wild type background (blue) or with an elevated *AdiY* copy number (gray) and cultivated as in (a). +*adiY*, expression of *adiY* under the control of the arabinose (0.1%)-inducible promoter in plasmid pBAD24. Comparison of the frequencies of *AdiC:mCerulean* in wild type or +*adiY* cells using the Chi-square test showed a p -value < 0.0001. On top of the histogram: blue cells represent the *AdiC:mCerulean* ON state; +*adiY* is represented by purple dots. Below the histogram: noise level is represented by the size of the dots; average RF is represented by color intensity (Supplementary Table 1). RF was quantified using the MicrobeJ plugin of the ImageJ software of the fluorescent microscopic images for 1000 cells per condition. nRF normalized RF values. **c** *E. coli* MG1655 wild type transformed with the plasmid pBAD24-*adiY* or with empty pBAD24 were grown in minimal medium at pH 5.8 supplemented with lysine and then shifted to LB medium of the indicated pH values. Growth (OD_{600}) was determined every 10 min in microtiter plates with continuous shaking. All experiments were performed three times ($n = 3$), and error bars represent standard deviation of the means. LB lysogeny broth.

induced increase in H^+ -consuming lysine decarboxylase *CadA*, thus conferring moderate AR to all cells (homogeneous response; Fig. 6a). To test this hypothesis, we deleted *cadA* from our reporter strain ($\Delta cadA$ *gadC:eGFP-adiC:mCerulean-cadB:mCherry*). Deletion of *cadA* reduced the heterogenous distribution of *AdiC:mCerulean* and strongly increased the mean fluorescence of *AdiC:mCerulean* (by 11-fold), thus suggesting that many more cells produced *AdiC:mCerulean* compared with the wild type (Fig. 6a). Deletion of *cadA* did not affect the heterogenous distribution of either *GadC:eGFP* or *CadB:mCherry* in pH-4.4-stressed cells. Only the overall mean level of *CadB:mCherry* was increased under this condition, which was due to the lack of negative feedback inhibition of cadaverine on *CadC* (Supplementary Table 1)^{34,36}.

To further support these results, we analyzed *AdiY*-driven pH-dependent activation of the *adiA* promoter at the population level. In wild-type cells, *adiA* expression began when cells were exposed to an acidic environment of pH < 4.8 (Fig. 6b). The increased number of *CadC* molecules did not change the pH-dependent induction profile but caused downregulation of the *adiA* promoter activity. In contrast, in the *cadA* mutant, the promoter activity of *adiA* not only increased, but the onset of induction shifted to a higher external pH such as 5.8 (Fig. 6b). These data suggest that activation of the *Adi* system is influenced

by the intracellular pH, as a manipulation of the cytosolic proton concentration by either deletion of *cadA* or overproduction of *cadA* (triggered by increased *CadC* copy numbers) leads to increased activation or downregulation, respectively, of the *Adi* system in *E. coli*.

Discussion

To counteract acidic environments, many bacteria possess inducible AR systems that rely on H^+ -consuming amino acid decarboxylases and their corresponding antiporters. The latter function as importers for corresponding amino acids and exporters for decarboxylated products. The number and complexity of the three inducible *Gad*, *Adi*, and *Cad* AR systems vary among bacteria and reflect an adaptation to the needs of their individual natural habitat⁴⁷. Our phylogenetic analysis of the distribution of antiporters *GadC*, *AdiC*, and *CadB* revealed that the *Gad* system is the most widely distributed AR system, whereas the *Adi* system and *Cad* system are restricted to γ -proteobacteria (Fig. 4). Consistent with previous reports, *Salmonella* has *Adi* and *Cad* systems, whereas *Shigella* has the *Gad* system⁴⁷. In *Shigella*, we also identified the *Adi* system, and in some species, the *Cad* system, i.e., in *S. boydii* and *S. flexneri* (Supplementary Table 2, Supplementary Data 1). However, not only does the number of

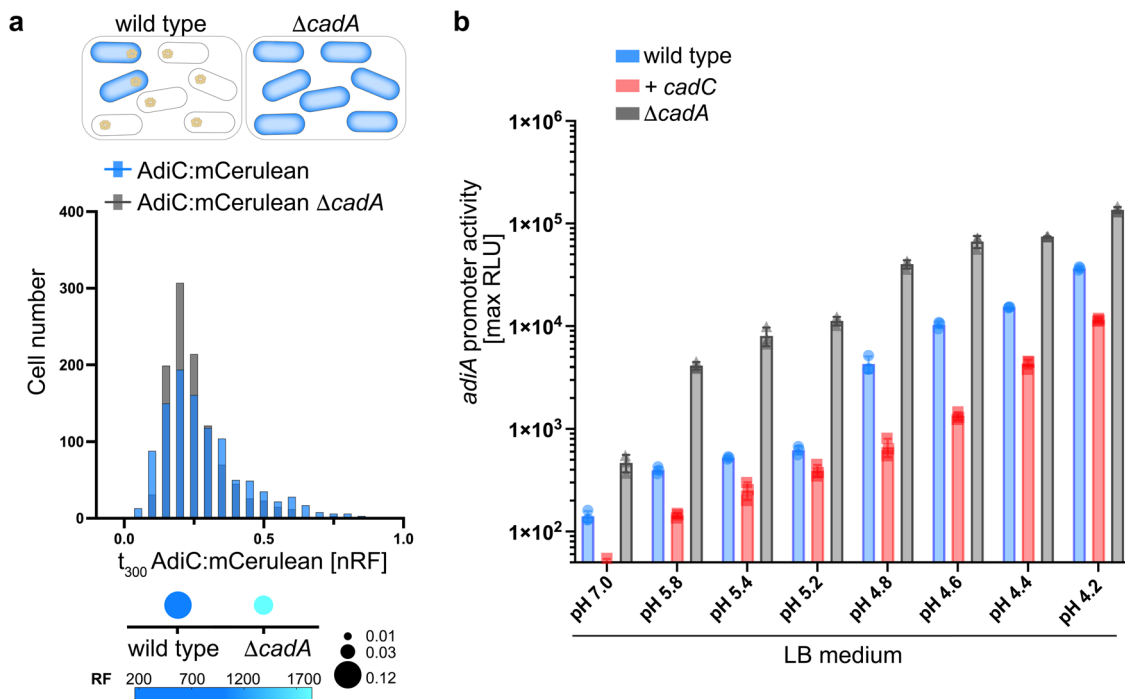


Fig. 6 Manipulation of intracellular stress resistance by either eliminating ($\Delta cadA$) or increasing (+*cadC*) the activity of the Cad system affects the degree of heterogeneity and pH-dependent induction of the Adi system. **a** Normalized RF values of cells expressing AdiC:mCerulean in the *E. coli* wild type background (blue) or the *cadA* mutant (gray). Cells were monitored after growth at pH 4.4 in LB medium at t_{300} . On top of the histogram, the cells are shown in a schematic overview, with blue cells representing the AdiC:mCerulean ON state and yellow dots representing CadA. Below the histogram, the noise (standard deviation/mean of log-transformed values) is presented by the size of the dots (the higher the noise, the larger the size of the dot), and the average RF is represented by a blue color (the more intense the blue, the higher the average relative fluorescence intensity). RF was quantified using the MicrobeJ plugin of the ImageJ software of the fluorescent microscopic images for 1000 cells per condition. The calculated mean RF and noise values are summarized in Supplementary Table 1. nRF normalized RF values. **b** *E. coli* MG1655 wild type and the *cadA* mutant (each transformed with the plasmid pBBR1-MCS5-*P_{adiA}-lux*) were grown in MM at pH 5.8 supplemented with 10 mM lysine and then shifted to LB medium of the indicated pH values. Luminescence and growth were determined every 10 min in microtiter plates with a Tecan Infinite F500 system (Tecan, Crailsheim, Germany). Data are reported as relative light units (RLUs) in counts per second per milliliter per OD₆₀₀, and maximal RLU at 1.9 h is shown. All experiments were performed three times ($n = 3$), and error bars represent standard deviation of the means. Growth over 10 h is presented in Supplementary Fig. 3 at selected pH values. LB lysogeny broth, MM minimal medium, RF relative fluorescence intensity.

AR systems possessed by bacteria differ, but the complexity of their regulation varies (Fig. 4). The most sophisticated regulatory network of AR systems is found in *E. coli*. Its close relatives *E. albertii* have almost all components as well but lack the EvgSA two-component system and YdeO.

For the first time, we investigated the activation of the three major AR systems in *E. coli* simultaneously at the single-cell level under consecutive increasing acid stress. By using the three-color reporter strain *E. coli gadC:eGFP-adiC:mCerulean-cadB:mCherry*, we confirmed that each of the three AR systems is specialized for a certain strength of acid stress under certain environmental conditions. The Gad system was activated under mild acid strength and during the stationary phase. The Cad system was induced at pH 5.8 and required the presence of lysine. The Adi system was induced at pH 4.4 and required the lysogeny broth medium, which contains tryptone and yeast extract. However, activation of the three systems differs greatly from cell to cell (Figs. 2 and 7). The Cad system showed the highest heterogeneous distribution of all three systems, when activated at pH 5.8 in the presence of lysine. Under almost all conditions, all cells of the population activate the Gad system but to varying degrees. The Adi system is activated heterogeneously under strong acid stress (pH 4.4) (Fig. 2).

Phenotypic variations can be beneficial for the *E. coli* population under acid stress. Our results provide a model of how the three inducible AR systems overlap and generate a division of

labor and functional cooperation in the population (Fig. 7). All cells of the *E. coli* population individually adapt to mild acid stress by activating the Gad system to varying degrees, and the glutamate decarboxylases GadA and GadB might initially utilize intracellularly available glutamate under the consumption of protons. As described below, the antiporter GadC becomes more important under extreme acid stress. It should also be noted here that the decarboxylase GadB also undergoes a pH-dependent conformational change and exhibits an activity optimum at low pH⁴⁸. Furthermore, glutamate is the most abundant intracellular metabolite, with a concentration of 100 mM, and its concentration is much higher compared to that of lysine (0.41 mM) and arginine (0.57 mM)⁴⁹. Under stronger acid stress (pH 5.8 to pH 4.4), some cells in the population activate the Cad system, whereas others activate the Adi system. These two subpopulations each contribute to acid stress relief by secreting the more alkaline cadaverine and agmatine, respectively (Fig. 7). These two polyamines are considered common goods and contribute to an increase of the extracellular pH, which benefits the whole population. This behavior can be considered as an example of true division of labor in bacteria, as the metabolic burden of the individual cells to produce both the Adi and Cad systems is prevented, but nevertheless, the whole population benefits from the elevation of external pH by secretion of cadaverine and agmatine (Fig. 7). The fact that homogenous production of the components of the Adi system in all cells would be a burden for

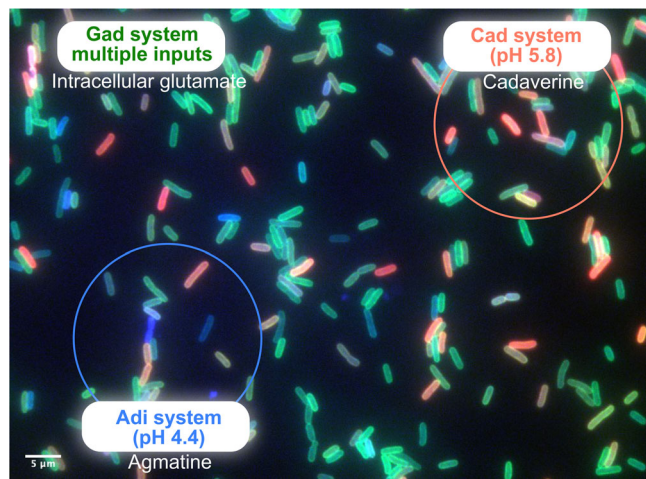


Fig. 7 Model of the heterogenous activation of three inducible acid resistance systems and division of labor in the *E. coli* population.

Fluorescent microscopic images of the three-color reporter strain *E. coli* *gadC::eGFP-adiC::mCherry-cadB::mCherry* at pH 4.4 in a complex medium at t_{300} . All cells of the *E. coli* population individually adapt to acid stress by activating the Gad system to varying degrees (green fluorescent cells) due to multiple extracellular and intracellular inputs. These cells utilize primarily intracellularly available glutamate under consumption of protons to increase their internal pH. Under stronger acid stress (pH 5.8 to pH 4.4), some cells in the population activate the Cad system (red fluorescent cells), while others activate the Adi system (blue fluorescent cells). These cells secrete (as indicated by the rings) the more alkaline products cadaverine and agmatine, respectively, thereby contributing to acid-stress relief with an increase of the extracellular pH, which benefits the whole population. In addition, their internal pH is elevated by consuming protons due to the conversion of lysine to cadaverine and arginine to agmatine, respectively.

the population is clearly shown by the reduced growth rate under this condition (Fig. 6c), which was similar for a homogenous production of the Cad system⁴¹ (Supplementary Fig. 3).

We were then interested in the molecular mechanisms that not only lead to this phenotypic heterogeneity but that are also heritable. CadC and AdiY are low copy number proteins; therefore, they are stochastically distributed among the cells of the population⁴⁴. Here and in our previous studies⁴¹, we showed that an increase of their copy number was sufficient to shift the population into homogeneous behavior. Cells that activated the Cad system are protected against acid stress due to the H⁺-consuming activity of the CadA decarboxylase. It should be noted that CadA is produced on average with 60,000 copies per cell, which accounts for at least 2% of all cytoplasmic proteins in CadA-producing cells⁵⁰. In cells lacking the Cad system, the intracellular pH decreases under strong external acid stress, such as pH 4.4. Our results have shown that any manipulation of the activity of the Cad system, such as its elimination ($\Delta cadA$) or increase ($+cadC$), affected the degree of heterogeneity and pH-dependent induction of the Adi system, which suggests that the regulator of the Adi system is an intracellular pH sensor that senses a decrease of cytoplasmic pH.

Induction of the Gad system of *E. coli* is controlled by an unusually high number of transcription factors, the stationary sigma factor, and a small RNA GadY (Figs. 1 and 4a). Moreover, its activation is strongly influenced by the medium composition and growth phase^{10,17}. The transcription factors GadX and GadW were already associated with higher noise levels of their target genes of unstressed cells⁴² and potentially contribute to the heterogenous distribution of GadC::eGFP (Fig. 2b). In addition, the stationary sigma factor RpoS is known generate extensive

transcriptional heterogeneity^{51–53}. Thus, the Gad system integrates multiple extracellular and intracellular inputs, which results in quantitative differences and continuous variation of phenotypic traits in the individual cells of the population. The noisy activation of the *gadBC* promoter enables prediction of the survival of single cells⁵⁴. Usually, high levels of noise are found for genes that are involved in either the energy metabolism of carbon sources or adaptation to stress, like osmotic pressure, temperature extremes, starvation response, pH response, and mechanical, nutritional, or oxidative stress. Indeed, the Gad system is a major system under extreme acid stress (pH \leq 2.5)¹⁰. The antiporter GadC preferentially transports protonated glutamate (Glu⁺) in exchange for protonated GABA (GABA⁺) at an external pH of 3.0 and lower^{21–23}. This transport activity is crucial for protecting cells against incoming protons. It should be noted that at extremely low pH values, such as pH 2.5, only <0.01% of a non-preadapted population survives²⁷, and therefore, for maintenance of the population, it is extremely important that all *E. coli* cells produce the Gad system, albeit with different levels.

We can only speculate to what extent this model might hold up in a natural epitope of *E. coli*, such as digestive system of humans or animals. Before *E. coli* arrives in the intestine, it is exposed to an extreme acid stress with HCl in the stomach that this bacterium can only survive with the help of the Gad system. The mean pH in the proximal small intestine is 6.6 and increases in the terminal ileum to 7.5. Then, there is a sharp fall in pH to 6.4 in the caecum, and an increase in colon with a final value of 7.0⁵⁵. Depending on the availability of the amino acids lysine and arginine, the Cad and Adi systems might be switched on under these conditions. The latter system is increasingly activated due to the anaerobic conditions³¹. Both systems will still be heterogeneously distributed due to the low copy number of the main regulators CadC and AdiY. Fermentation products, such as acetate, also activate the Gad system⁵⁶. The extent to which microcolonies of *E. coli* exist in the colon, in which common goods such as cadaverine and agmatine can change the micro-milieu, is also unclear, as is the extent to which the host plays a role in acid stress. In fact, the levels of putrescine, a conversion product of agmatine, and cadaverine were found to be 15- and 3-fold, increased, respectively, in the inflamed mouse intestine mono-colonized with *E. coli* compared to an equally colonized healthy mouse cohort⁵⁷.

Considered together, our results provide a model for the advantage of *E. coli* to have three AR systems that allow for division of labor in the population and ensure its survival over a wide range of low pH values, thus making this bacterium highly acid-stress resistant.

Methods

Bacteria and growth conditions. Bacterial strains and plasmids used in this study are listed in Table 1. *E. coli* strains were cultivated in LB medium (10 g/liter NaCl, 10 g/l tryptone, 5 g/l yeast extract) or in Kim-Epstein (KE) minimal medium⁵⁸ adjusted to pH 5.8 (MM pH 5.8) or pH 7.6 (MM pH 7.6), using the corresponding phosphate buffer. *E. coli* strains were incubated aerobically in a rotary shaker at 37 °C. KE medium was always supplemented with 0.2% (w/v) glucose. When indicated lysine was added to a final concentration of 10 mM.

If necessary, media were supplemented with 100 μ g/ml ampicillin, or 50 μ g/ml kanamycin sulfate. To allow the growth of the conjugation strain *E. coli* WM3064, *meso*-diamino-pimelic acid (DAP) was added to a final concentration of 300 μ M.

Construction of plasmids. Molecular methods were carried out according to standard protocols or according to the manufacturer's instructions. Kits for the isolation of plasmids and the purification of PCR products were purchased from Süd-Laborbedarf (SLG; Gauting, Germany). Enzymes and HiFi DNA Assembly Master Mix were purchased from New England BioLabs (Frankfurt, Germany).

To construct different fluorescent fusions with *gadC*, *adiC* and *cadB*, to be inserted in-frame chromosomally, the corresponding flanking regions (600 bp upstream and downstream) of *gadC*, *adiC* or *cadB* were amplified by PCR using MG1655 genomic DNA as template. Plasmid pET-*mCherry-cadC*⁴³ was used as

Table 1 Strains and plasmids used in this study.

Strains	Relevant genotype or description	Reference
<i>E. coli</i> MG1655	K-12 F ⁻ λ ⁻ <i>ilvG</i> ⁻ <i>rfb</i> -50 <i>rph</i> -1	68
<i>E. coli</i> DH5αpir	<i>endA1 hsdR17 glnV44</i> (= <i>supE44</i>) <i>thi</i> -1 <i>recA1 gyrA96 relA1</i> φ80' <i>lacΔ(lacZ)</i>	69
<i>E. coli</i> WM3064	M15 Δ(<i>lacZYA-argF</i>)U169 <i>zdg</i> -232::Tn10 <i>uidA</i> :: <i>pir</i> + <i>thrB1004 pro thi rpsL hsdS lacZΔM15</i> RP4-1360 Δ(<i>araBAD</i>)567 Δ <i>dapA1341</i> ::[<i>erm pir</i>]	W. Metcalf, Univ. of Illinois, Urbana
<i>E. coli</i> MG1655 <i>cadB::egfp</i>	Chromosomally integrated C-terminal <i>cadB::egfp</i> fusion in <i>E. coli</i> MG1655	41
<i>E. coli</i> MG1655 <i>adiC::mCherry-cadB::egfp</i>	Chromosomally integrated C-terminal <i>adiC::mCherry</i> and <i>cadB::egfp</i> fusion in <i>E. coli</i> MG1655	This work
<i>E. coli</i> MG1655 <i>gadC::mCerulean-adiC::mCherry-cadB::egfp</i>	Chromosomally integrated C-terminal <i>gadC::mCerulean</i> ^a , <i>adiC::mCherry</i> and <i>cadB::egfp</i> fusion in <i>E. coli</i> MG1655	This work
<i>E. coli</i> MG1655 <i>adiC::mCerulean-cadB::egfp</i>	Chromosomally integrated C-terminal <i>adiC::mCerulean</i> and <i>cadB::egfp</i> fusion in <i>E. coli</i> MG1655	This work
<i>E. coli</i> MG1655 <i>gadC::mCherry-adiC::mCerulean-cadB::egfp</i>	Chromosomally integrated C-terminal <i>gadC::mCherry</i> ^a , <i>adiC::mCerulean</i> and <i>cadB::egfp</i> fusion in <i>E. coli</i> MG1655	This work
<i>E. coli</i> MG1655 <i>cadB::mCherry</i>	Chromosomally integrated C-terminal <i>cadB::mCherry</i> fusion in <i>E. coli</i> MG1655	This work
<i>E. coli</i> MG1655 <i>adiC::mCerulean-cadB::mCherry</i>	Chromosomally integrated C-terminal <i>adiC::mCerulean</i> and <i>cadB::mCherry</i> fusion in <i>E. coli</i> MG1655	This work
<i>E. coli</i> MG1655 <i>gadC::egfp-adiC::mCerulean-cadB::mCherry</i>	Chromosomally integrated C-terminal <i>gadC::egfp</i> ^a , <i>adiC::mCerulean</i> and <i>cadB::mCherry</i> fusion in <i>E. coli</i> MG1655	This work
<i>E. coli</i> MG1655 Δ <i>cadA gadC::eGFP-adiC::mCerulean-cadB::mCherry</i>	In-frame deletion of <i>cadA</i> in <i>E. coli</i> MG1655 <i>gadC::egfp</i> ^a - <i>adiC::mCerulean-cadB::mCherry</i>	This work
<i>E. coli</i> Δ <i>gadC</i>	Deletion of <i>gadC</i> (JW1487), <i>gadC</i> ::Km	70
<i>E. coli</i> Δ <i>adiC</i>	Deletion of <i>adiC</i> (JW4076), <i>adiC</i> ::Km	70
<i>E. coli</i> Δ <i>cadA</i>	Deletion of <i>cadA</i> (JW4092), <i>cadA</i> ::Km	70
Plasmids		
pBAD24	Arabinose-inducible P _{BAD} promoter, pBR322 ori, Amp ^R	71
pBAD- <i>cadC</i>	<i>cadC</i> under control of arabinose inducible promoter in pBAD24, Amp ^R	40
pNPTS138-R6KT	<i>mobRP4</i> + <i>ori</i> -R6K <i>sacB</i> ; suicide plasmid for in-frame deletions, Km ^R	72
pNPTS138-R6KT- <i>cadB::egfp-EC</i>	pNPTS-138-R6KT-derived suicide plasmid for in-frame insertion of <i>cadB::egfp</i> in <i>E. coli</i> MG1655, Km ^R	41
pNPTS138-R6KT- <i>gadC::egfp</i>	pNPTS-138-R6KT-derived suicide plasmid for in-frame insertion of <i>gadC::egfp</i> ^a in <i>E. coli</i> MG1655, Km ^R	This work
pNPTS138-R6KT- <i>cadB::mCherry</i>	pNPTS-138-R6KT-derived suicide plasmid for in-frame insertion of <i>cadB::mCherry</i> in <i>E. coli</i> MG1655, Km ^R	This work
pNPTS138-R6KT- <i>adiC::mCerulean</i>	pNPTS-138-R6KT-derived suicide plasmid for in-frame insertion of <i>adiC::mCerulean</i> in <i>E. coli</i> MG1655 strains, Km ^R	This work
pNPTS138-R6KT- <i>gadC::mCherry</i>	pNPTS-138-R6KT-derived suicide plasmid for in-frame insertion of <i>gadC::mCherry</i> ^a in <i>E. coli</i> MG1655, Km ^R	This work
pNPTS138-R6KT- <i>gadC::mCerulean</i>	pNPTS-138-R6KT-derived suicide plasmid for in-frame insertion of <i>gadC::mCerulean</i> ^a in <i>E. coli</i> MG1655, Km ^R	This work
pNPTS138-R6KT- <i>adiC::mCherry</i>	pNPTS-138-R6KT-derived suicide plasmid for in-frame insertion of <i>adiC::mCherry</i> in <i>E. coli</i> MG1655, Km ^R	This work
pBAD-His ₆ - <i>csiR</i>	N-terminal His ₆ -tagged <i>csiR</i> in pBAD24, Amp ^R	This work
pBAD-His ₆ - <i>adiY</i>	N-terminal His ₆ -tagged <i>adiY</i> in pBAD24, Amp ^R	This work
pBBR1-MCS5-TT-RBS- <i>lux</i>	<i>luxCDABE</i> and terminators lambda <i>T0 rrmB1 T1</i> cloned into pBBR1-MCS5 for plasmid-based transcriptional fusions, Gm ^R	73
pBBR1-MCS5-P _{adiA} - <i>lux</i>	<i>adiA</i> promoter controlling expression of <i>luxCDABE</i> , in pBBR1-MCS5-TT-RBS- <i>lux</i> , Gm ^R	This work
pNPTS138-R6KT-Δ <i>cadA</i>	pNPTS-138-R6KT-derived suicide plasmid for in-frame deletion of <i>cadA</i> in MG1655 <i>gadC::eGFP</i> ^a - <i>adiC::mCerulean-cadB::mCherry</i> , Km ^R	This work
pET- <i>mCherry-cadC</i>	N-terminal fusion of <i>CadC</i> with <i>mCherry</i> in pET16b, Amp ^R	43
pK18mob2-TriFluoR	pK18mob2 Km carrying triple reporter construct with MCS I- <i>cerulean</i> , PT5- <i>mCherry</i> , MCS II- <i>mVenus</i>	59

EC *E. coli* MG1655.^aAll *gadC* genes encode a truncated protein (amino acids 1–470) that lacks the C-plug²¹.

template (720 bp) to amplify *mCherry*. Plasmid pK18mob2-TriFluoR⁵⁹ was used as template (720 bp) to amplify *mCerulean*. Plasmid pNPTS138-R6KT-*cadB::egfp-EC* was used as template (720 bp) to amplify *egfp*. After purification of the different fragments, the respective combinations were assembled via Gibson assembly⁶⁰ into EcoRV-digested pNPTS138-R6KT plasmid, resulting in the plasmids pNPTS138-R6KT-*gadC::egfp*, pNPTS138-R6KT-*gadC::mCherry*, pNPTS138-R6KT-*gadC::mCerulean*, pNPTS138-R6KT-*cadB::mCherry*, pNPTS138-R6KT-*adiC::mCerulean* and pNPTS138-R6KT-*adiC::mCherry*. Each plasmid was verified by colony PCR and sequencing.

Functional hybrid proteins of *GadC* with each of the three different fluorophores was only achieved by using a shorter version of *GadC* (amino acids 1–470), in which the C-terminal C-plug is removed. Truncation of this C-plug does not affect the transport activity, but shifts the pH-optimum to a higher pH²¹.

To construct a marker-less in-frame deletion of *cadA* in *E. coli* MG1655 *gadC::eGFP-adiC::mCerulean-cadB::mCherry*, the suicide plasmid pNPTS138-R6KT-Δ*cadA* was generated. Briefly, flanking regions (1000 bp upstream and downstream) of *cadA* were amplified by PCR using MG1655 *gadC::eGFP-adiC::mCerulean-cadB::mCherry* genomic DNA as template. After purification of the different fragments, the DNA fragments were assembled via Gibson assembly⁶⁰ into by PCR

linearized pNPTS138-R6KT plasmid, resulting in the plasmid pNPTS138-R6KT- Δ cadA. Correct insertion was verified by sequence analysis using primer pNTPS_Seq_fwd.

For construction of the reporter plasmid pBBR1-MCS5-P_{adiY}-lux, 200 bp of the region upstream of *adiA* was amplified by PCR using primers (PadiA_XbaI_fwd and PadiA_XmaI_rev) and MG1655 genomic DNA as template, and cloned into plasmid pBBR1-MCS5-TT-RBS-lux using restriction sites XbaI and XmaI. Correct insertion was verified by colony PCR and sequencing.

For construction of N-terminal His₆-tagged AdiY and His₆-tagged CsiR, *adiY* and *csiR* were amplified by PCR using MG1655 genomic DNA as template. The codons for the His₆-tag were introduced by using a respective forward primer. After purification of the different fragments, the DNA fragments were assembled via Gibson assembly⁶⁰ into SmaI-digested pBAD24 plasmid, resulting in the plasmids pBAD24-His₆-*adiY* and pBAD24-His₆-*csiR*. Correct insertion was verified by colony PCR and sequencing.

Construction of chromosomally integrated fluorescent fusions and deletion strains.

The genes encoding the three different fluorophores, *egfp*, *mCherry* and *mCerulean*, are separately C-terminally fused to the genes *gadC*, *adiC* and *cadB* encoding the antiporter of the three AR systems. Expression of each fusion is under the control of the respective native promoter.

To generate the three-color *E. coli* MG1655 *gadC:mCerulean-adiC:mCherry-cadB:egfp* strain, at first the suicide plasmid pNPTS138-R6KT-*adiC:mCherry* was introduced into *E. coli* MG1655 *cadB:egfp* by conjugative mating using *E. coli* WM3064 as a donor in LB medium containing DAP. Single-crossover integration mutants were selected on LB plates containing kanamycin but lacking DAP. Single colonies were grown over a day without antibiotics and plated onto LB plates containing 10% (w/v) sucrose but lacking NaCl to select for plasmid excision. Kanamycin-sensitive colonies were checked for targeted deletion by colony PCR using primers bracketing the site of the insertion. Insertion of *mCherry* was verified by colony PCR and sequencing resulting in the strain *E. coli* MG1655 *adiC:mCherry-cadB:egfp*. In the next step tagging of *gadC* with *mCerulean* was achieved using the suicide plasmid pNPTS138-R6KT-*gadC:mCerulean*. The plasmid pNPTS138-R6KT-*gadC:mCerulean* was introduced into *E. coli* MG1655 *adiC:mCherry-cadB:egfp* by conjugative mating using *E. coli* WM3064 as a donor in LB medium containing DAP as described above. Insertion of *mCerulean* was verified by colony PCR and sequencing, resulting in the strain *E. coli* MG1655 *gadC:mCerulean-adiC:mCherry-cadB:egfp*.

To generate the three-color *E. coli* MG1655 *gadC:mCherry-adiC:mCerulean-cadB:egfp* strain, at first the suicide plasmid pNPTS138-R6KT-*adiC:mCerulean* was introduced into *E. coli* MG1655 *cadB:egfp* by conjugative mating using *E. coli* WM3064 as a donor in LB medium containing DAP as described above. Insertion of *mCerulean* was verified by colony PCR and sequencing, resulting in the strain *E. coli* MG1655 *adiC:mCerulean-cadB:egfp*. In the next step tagging of *gadC* with *mCherry* was achieved using the suicide plasmid pNPTS138-R6KT-*gadC:mCherry*. The plasmid pNPTS138-R6KT-*gadC:mCherry* was introduced into *E. coli* MG1655 *adiC:mCerulean-cadB:egfp* by conjugative mating using *E. coli* WM3064 as a donor in LB medium containing DAP as described above. Insertion of *mCherry* was verified by colony PCR and sequencing resulting in the strain *E. coli* MG1655 *gadC:mCherry-adiC:mCerulean-cadB:egfp*.

To generate the two-color *E. coli* MG1655 *gadC:mCerulean-cadB:mCherry* strain, at first the suicide plasmid pNPTS138-R6KT-*cadB:mCherry* was introduced into *E. coli* MG1655 by conjugative mating using *E. coli* WM3064 as a donor in LB medium containing DAP as described above. Insertion of *mCherry* was verified by colony PCR and sequencing, resulting in the strain *E. coli* MG1655 *cadB:mCherry*. In the next step tagging of *gadC* with *mCerulean* in this strain was achieved using the suicide plasmid pNPTS138-R6KT-*gadC:mCerulean*. The plasmid pNPTS138-R6KT-*gadC:mCerulean* was introduced into *E. coli* MG1655 *cadB:mCherry* by conjugative mating using *E. coli* WM3064 as a donor in LB medium containing DAP as described above. Insertion of *mCerulean* was verified by colony PCR and sequencing resulting in the strain *E. coli* MG1655 *gadC:mCerulean-cadB:mCherry*.

To generate the three-color *E. coli* MG1655 *gadC:egfp-adiC:mCerulean-cadB:mCherry* strain, at first the suicide plasmid pNPTS138-R6KT-*adiC:mCerulean* was introduced into *E. coli* MG1655 *cadB:mCherry* by conjugative mating using *E. coli* WM3064 as a donor in LB medium containing DAP as described above. Insertion of *mCerulean* was verified by colony PCR and sequencing, resulting in the strain *E. coli* MG1655 *adiC:mCerulean-cadB:mCherry*. In the next step tagging of *gadC* with *egfp* was achieved using the suicide plasmid pNPTS138-R6KT-*gadC:egfp*. The plasmid pNPTS138-R6KT-*gadC:egfp* was introduced into *E. coli* MG1655 *adiC:mCerulean-cadB:mCherry* by conjugative mating using *E. coli* WM3064 as a donor in LB medium containing DAP as described above. Insertion of *egfp* was verified by colony PCR and sequencing, resulting in the strain *E. coli* MG1655 *gadC:egfp-adiC:mCerulean-cadB:mCherry*.

Construction of the marker-less in-frame deletion strain of *cadA* in *E. coli* MG1655 *gadC:eGFP-adiC:mCerulean-cadB:mCherry* was achieved using the suicide plasmid pNPTS138-R6KT- Δ cadA. The plasmid pNPTS138-R6KT- Δ cadA was introduced into *E. coli* MG1655 *gadC:eGFP-adiC:mCerulean-cadB:mCherry* by conjugative mating using *E. coli* WM3064 as a donor in LB medium containing DAP as described above. Deletion of *cadA* was verified by colony PCR and sequencing, resulting in the strain *E. coli* MG1655 Δ cadA *gadC:eGFP-adiC:mCerulean-cadB:mCherry*.

In vivo fluorescence microscopy and data analysis. To analyze the spatial temporal localization of the different fluorescent hybrids in *E. coli*, overnight cultures were prepared in KE medium pH 7.6 and aerobically cultivated at 37 °C. The overnight cultures were used to inoculate day cultures (OD₆₀₀ of 0.1) in fresh medium at pH 7.6. At an OD₆₀₀ of 0.5 (t₀), half of the culture was gently centrifuged and resuspended in KE medium pH 5.8 + lysine as the first pH shift. The rest of the culture continued growing in KE medium pH 7.6 at 37 °C. Then the cultures were cultivated aerobically at 37 °C for 2.5 h (t₁₅₀), and half of the culture was gently centrifuged and resuspended in LB medium pH 4.4 as the second pH shift. The rest of the culture continued growing in KE medium pH 5.8 + lysine at 37 °C (t₃₀₀). At the beginning of the experiment (t₀) and at every pH shift (t₁₅₀ and t₃₀₀), 2 μ l of the culture was spotted on 1% (w/v) agarose pads (prepared with the respective media), placed onto microscope slides and covered with a coverslip. Subsequently, images were taken on a Leica DMI8 inverted microscope equipped with a Leica DFC365 FX camera (Wetzlar, Germany). An excitation wavelength of 546 nm and a 605-nm emission filter with a 75-nm bandwidth was used for *mCherry* fluorescence with an exposure of 500 ms, gain 5, and 100% intensity for *mCherry*-tagged strains. An excitation wavelength of 485 nm and a 510-nm emission filter with a 75-nm bandwidth was used for eGFP fluorescence with an exposure of 500 ms, gain 5, and 100% intensity for eGFP-tagged strains. An excitation wavelength of 436 nm and 480-nm emission filter with a 40-nm bandwidth was used for *mCerulean* fluorescence with an exposure of 500 ms, gain 5, and 100% intensity for *mCerulean*-tagged strains.

To analyze the influence of an increased copy number of CsiR, the *E. coli* strains *gadC:mCerulean-cadB:mCherry* and *adiC:mCerulean-cadB:mCherry* were transformed with plasmid pBAD-His₆-*csiR* by electroporation. 0.1% (w/v) L-arabinose was added throughout the experiment and cells were cultivated as described above.

To analyze the influence of an increased copy number of AdiY, the *E. coli* strain *adiC:mCerulean-cadB:mCherry* was transformed with plasmid pBAD-His₆-*adiY* by electroporation. 0.1% (w/v) L-arabinose was added throughout the experiment and cells were cultivated as described above.

To analyze the influence of an increased copy number of CadC, the *E. coli* strains *gadC:mCerulean-cadB:mCherry* and *adiC:mCherry-cadB:eGFP* were transformed with plasmid pBAD-His₆-*adiY* by electroporation. 0.1% (w/v) L-arabinose was added throughout the experiment and cells were cultivated as described above.

To quantify relative fluorescent intensities (RF) representing fluorescent hybrids of single cells, phase contrast and fluorescent images were analyzed using the ImageJ⁶¹ plugin MicrobeJ⁶². Default settings of MicrobeJ was used for cell segmentation (Fit shape, rod-shaped bacteria) apart from the following settings: area: 0.1-max μ m²; length: 1.2–5 μ m; width: 0.1–1 μ m; curvature 0.–0.15 and angularity 0.–0.25 for *E. coli* cells. In total >1000 cells were quantified per strain and condition and time point. The background of the agarose pad was subtracted from each cell per field of view.

Mean and standard deviation (std) of the relative fluorescence (RF) were quantified using MicrobeJ and background was subtracted. Moreover, the RF of the GFP channel was corrected for the overlapping signal of the CFP channel via linear regression with the experimentally determined proportionality factor of 0.456. The noise was defined as std/mean of log-transformed values per sample. Log-transformed values were used because the coefficient of variation, as a measure of noise, is based on the assumption that the underlying data are normally distributed. However, not all data were normally distributed under all conditions, therefore the log-transformed values were used (log(x + 1)) as previously published for CadB:eGFP⁴¹. In addition, this helped to overcome the problem that the noise becomes higher with lower gene expression, which is often observed⁴².

In order to compare fluorescence intensity values of the different fluorophores, the RF values were normalized (nRF) according to the highest values, as each of the three fluorophores has a different brightness (eGFP: 33; *mCerulean*: 16; *mCherry*: 15)⁶³.

Statistical analysis and presentation were performed using GraphPad Prism 9.1.0 and R 4.0.3⁶⁴.

Localization of fluorescently tagged GadC, AdiC, and CadB hybrids.

To verify the localization of fluorescently tagged GadC, AdiC and CadB in the membrane, the three-color *E. coli* strains *gadC:egfp-adiC:mCerulean-cadB:mCherry*, *gadC:mCherry-adiC:mCerulean-cadB:eGFP* and *gadC:mCerulean-adiC:mCherry-cadB:eGFP* were cultivated as described above for fluorescence microscopy. After the second pH shift to pH 4.4 (t₃₀₀) cells were harvested and then adjusted to OD₆₀₀ = 30. Cells were disrupted by passage through a high-pressure cell disrupter (Constant Systems, Northants, United Kingdom) in ice-cold disruption buffer (50 mM Tris-HCl pH 7.5, 10% (v/v) glycerol, 10 mM MgCl₂, 100 mM NaCl, 1 mM dithiothreitol, 0.5 mM PMSF and 0.03 mg ml⁻¹ DNase). After removal of intact cells and cell debris via centrifugation (5000 \times g, 30 min, 4 °C), membrane vesicles were collected by ultracentrifugation (45,000 \times g, 60 min, 4 °C), whereas the pellet contained the membrane fraction and the supernatant the cytoplasm. The membrane fractions were separated by SDS-PAGE⁶⁵ on 12.5% acrylamide gels and transferred to a nitrocellulose membrane. Fluorophore-tagged proteins were labeled either with the primary polyclonal α -*mCherry* antibody (Invitrogen), α -eGFP antibody (Roche) or the α -*mCerulean* antibody PABG1 (Chromotek). The α -

rabbit or α -mouse alkaline phosphatase-conjugated antibody (Rockland Immunochemicals) was used as secondary antibody according to the manufacturer's recommendations. Localization of the secondary antibody was visualized using colorimetric detection of alkaline phosphatase activity with 5-bromo-4-chloro-3-indolyl phosphate and nitro blue tetrazolium chloride. As ladder the PageRuler Prestained Protein Ladder (10–180 kDa, Thermo Fisher) was used.

Functionality of fluorescent antiporter hybrids. The functionality of the CadB:eGFP hybrid was previously confirmed using a liquid-based colorimetric assay with a pH indicator⁴¹. To test the functionality of the fluorescent hybrid proteins GadC:eGFP and AdiC:mCherry, an acid survival assay was performed as described previously^{10,41} with the following modifications. *E. coli* strains were cultivated in LB medium (pH 7.6) to an OD₆₀₀ of 0.6–0.8, then the cultures were adjusted to an OD₆₀₀ of 0.5 and resuspended in LB medium with a pH of 3.0 or 4.4. The low pH challenge was conducted at 37 °C and samples were collected immediately after resuspension ($t = 0$) and then hourly for 3 h. Samples were serially diluted and plated onto LB agar plates to assess the number of colonies surviving the acid challenge. As controls, the parental *E. coli* MG1655 and the *gadC* and *adiC* deletion mutants were used.

Measurement of *adiA* promoter activity in vivo. In vivo promoter activity of *adiA* was probed with a luminescence-based reporter (*P_{adiA}-luxCDABE*). The influence of the Cad system and the AdiY copy number was tested in cells exposed to different external pH values in LB medium using luminescence as readout. The strains *E. coli* MG1655 carrying pBBR1-MCS5-*P_{adiA}-lux*, *E. coli* MG1655 Δ *cadA* carrying pBBR1-MCS5-*P_{adiA}-lux*, *E. coli* MG1655 carrying pBBR1-MCS5-*P_{adiA}-lux* co-transformed with pBAD-*cadC* were incubated in KE medium pH 7.6 supplemented with the respective antibiotics overnight. The overnight cultures were inoculated to an OD₆₀₀ of 0.1 in fresh KE medium pH 7.6, aerobically cultivated until exponential phase and then shifted to KE medium pH 5.8 + 10 mM lysine and cultivated for another 2.5 h at 37 °C (comparable to the experimental setup described in Fig. 2a). In the next step, the cultures were shifted into a 96-well plate and aerobically cultivated at 37 °C in LB medium at different pH values supplemented with the respective antibiotics. Bioluminescence and growth were determined every 10 min in the microtiter plates with a Tecan Infinite F500 system (Tecan, Crailsheim, Germany). Data are reported as relative light units (RLU) in counts per second per milliliter per OD₆₀₀.

To analyze the effect of an increased copy number of CadC or AdiY, 0.1% (w/v) L-arabinose was added during the growth at pH 5.8 + 10 mM lysine and at pH 4.4. Thereby the CadC copy number is elevated to about 100 CadC molecules per cell, whereas the *E. coli* MG1655 wild type strain contains only ≤ 4 CadC molecules per cell⁴⁰.

Alignment and construction of phylogenetic trees. To identify non-redundant orthologues of the components of the three AR systems in relation to each antiporter GadC, AdiC and CadB, a Protein BLAST search of the NCBI RefSeq protein database⁶⁶ using the full-length sequence of either GadC (XasA), AdiC and CadB from *E. coli* MG1655 as the query sequence was carried out. Different expect thresholds were used for the Protein BLAST search ($e < 10^{-100}$ for GadC, $e < 10^{-120}$ for AdiC and CadB), in order to include all homologous yet functional similar proteins (June 2020). A tolerance of 10% of the amino acid length was set as default parameters.

Three alignments and phylogenetic trees were constructed, each based on the antiporter GadC, AdiC or CadB with the different components, and visualized as metadata. Therefore, a pairwise alignment of 1112 sequences for GadC, of 755 sequences for AdiC and of 857 sequences for CadB was done with a progressive algorithm from the software CLC Main Workbench 20.0.3 (CLC Bio Qiagen, Hilden, Germany) using the following parameters: gap open cost 10, gap extension cost 1, high accuracy⁶⁷. The results served as the basis for the construction of three phylogenetic trees by the software's high-accuracy, distance-based neighbor-joining algorithm (100 bootstrap replicates and the Jukes-Cantor distance correction as default parameters). The branch lengths, therefore, represent the degree of evolutionary divergence between any two nodes in the tree.

We screened the organisms containing a GadC orthologue for the presence of the GadB, GadE, GadX, GadW, GadY, CsiR, EvgS and YdeO by searching for orthologues of *E. coli* MG1655 with NCBI Protein BLAST ($e < 10^{-20}$ for GadE, $e < 10^{-50}$ for CsiR, $e < 10^{-60}$ for YdeO, $e < 10^{-80}$ for GadB, $e < 10^{-100}$ for GadW and GadX, $e < 10^{-170}$ for EvgS). Homologies of the sRNA GadY were determined by a NCBI Nucleotide BLAST⁶⁶ search using *gadY* from *E. coli* MG1655 as the query sequence with an expect threshold of $e < 10^{-20}$.

We screened the organisms containing a AdiC orthologue for the presence of the *AdiA*, *AdiY* and *CsiR* by searching for orthologues of *E. coli* MG1655 with NCBI Protein BLAST ($e < 10^{-170}$ for *AdiA*, $e < 10^{-100}$ for *AdiY*, $e < 10^{-50}$ for *CsiR*).

We screened the organisms containing a CadB orthologue for the presence of the *CadA*, *CadC*, *LysP* and *CsiR* by searching for orthologues of *E. coli* MG1655 with NCBI Protein BLAST ($e < 10^{-170}$ for *CadA*, $e < 10^{-120}$ for *LysP*, $e < 10^{-50}$ for *CsiR*). For the phylogenetic distribution of CadC, the data from our previous publication⁴¹ were used.

All data for the construction of these phylogenetic trees are available in Supplementary Data 1.

Statistics and reproducibility. All experiments were repeated multiple (three replicates unless stated) times to ensure reproducibility. Statistics were performed using either a two-tailed *t*-test, one-way ANOVA, or a two-tailed Pearson correlation coefficients comparison using GraphPad Prism 9.1.0. All graphs were plotted using the GraphPad Prism 9.1.0 and R 4.0.3⁶⁴. For multi-well plate assays, replicates were also contained within the plate to determine well to well variability.

Reporting summary. Further information on research design is available in the Nature Research Reporting Summary linked to this article.

Data availability

Supplementary Data 1 contains a list of all GadC, AdiC, and CadB homologs identified by a local alignment search based on the full-length sequence of *E. coli* GadC, AdiC, and CadB underlying Fig. 4. All source data underlying the graphs and charts presented in Figs. 2, 3, 5 and 6 are presented in Supplementary Data 2. Plasmids and primer sequences are available on request.

Received: 26 October 2021; Accepted: 3 March 2022;

Published online: 07 April 2022

References

- Bearson, S., Bearson, B. & Foster, J. W. Acid stress responses in enterobacteria. *FEMS Microbiol. Lett.* **147**, 173–180 (1997).
- Torres, A. G. The *cad* locus of *Enterobacteriaceae*: more than just lysine decarboxylation. *Anaerobe* **15**, 1–6 (2009).
- Foster, J. W. *Escherichia coli* acid resistance: tales of an amateur acidophile. *Nat. Rev. Microbiol.* **2**, 898–907 (2004).
- Deamer, D. W. Proton permeation of lipid bilayers. *J. Bioenerg. Biomembr.* **19**, 457–479 (1987).
- Krulwich, T. A., Sachs, G. & Padan, E. Molecular aspects of bacterial pH sensing and homeostasis. *Nat. Rev. Microbiol.* **9**, 330–343 (2011).
- Slonczewski, J. L., Fujisawa, M., Dopson, M. & Krulwich, T. A. Cytoplasmic pH measurement and homeostasis in Bacteria and Archaea. *Adv. Microb. Physiol.* **55**, 1–317 (2009).
- Martinez, K. A. et al. Cytoplasmic pH response to acid stress in individual cells of *Escherichia coli* and *Bacillus subtilis* observed by fluorescence ratio imaging microscopy. *Appl. Environ. Microbiol.* **78**, 3706–3714 (2012).
- Goode, O. et al. Persister *Escherichia coli* cells have a lower intracellular pH than susceptible cells but maintain their pH in response to antibiotic treatment. *mBio* **12**, e00909–e00921 (2021).
- Wilks, J. C. & Slonczewski, J. L. pH of the cytoplasm and periplasm of *Escherichia coli*: rapid measurement by green fluorescent protein fluorimetry. *J. Bacteriol.* **189**, 5601–5607 (2007).
- Castanié-Cornet, M. P., Penfound, T. A., Smith, D., Elliott, J. F. & Foster, J. W. Control of acid resistance in *Escherichia coli*. *J. Bacteriol.* **181**, 3525–3535 (1999).
- Kanjee, U. & Houry, W. A. Mechanisms of acid resistance in *Escherichia coli*. *Annu. Rev. Microbiol.* **67**, 65–81 (2013).
- Richard, H. T. & Foster, J. W. Acid resistance in *Escherichia coli*. *Adv. Appl. Microbiol.* **52**, 167–186 (2003).
- Small, P., Blankenhorn, D., Welty, D., Zinsler, E. & Slonczewski, J. L. Acid and base resistance in *Escherichia coli* and *Shigella flexneri*: role of *rpoS* and growth pH. *J. Bacteriol.* **176**, 1729–1737 (1994).
- Guerra, P. R. et al. Putrescine biosynthesis and export genes are essential for normal growth of avian pathogenic *Escherichia coli*. *BMC Microbiol.* **18**, 226 (2018).
- Richard, H. & Foster, J. W. *Escherichia coli* glutamate- and arginine-dependent acid resistance systems increase internal pH and reverse transmembrane potential. *J. Bacteriol.* **186**, 6032–6041 (2004).
- Aquino, P. et al. Coordinated regulation of acid resistance in *Escherichia coli*. *BMC Syst. Biol.* **11**, 1 (2017).
- Biase, D. D., Tramonti, A., Bossa, F. & Visca, P. The response to stationary-phase stress conditions in *Escherichia coli*: role and regulation of the glutamic acid decarboxylase system. *Mol. Microbiol.* **32**, 1198–1211 (1999).
- Weber, H., Polen, T., Heuveling, J., Wendisch, V. F. & Hengge, R. Genome-wide analysis of the general stress response network in *Escherichia coli*: σ S-dependent genes, promoters, and sigma factor selectivity. *J. Bacteriol.* **187**, 1591–1603 (2005).
- Bergholz, T. M. et al. Global transcriptional response of *Escherichia coli* O157:H7 to growth transitions in glucose minimal medium. *BMC Microbiol.* **7**, 97–97 (2007).

20. Biase, D. D. & Pennacchietti, E. Glutamate decarboxylase-dependent acid resistance in orally acquired bacteria: function, distribution and biomedical implications of the *gadBC* operon. *Mol. Microbiol.* **86**, 770–786 (2012).
21. Ma, D. et al. Structure and mechanism of a glutamate-GABA antiporter. *Nature* **483**, 632–636 (2012).
22. Tsai, M.-F., McCarthy, P. & Miller, C. Substrate selectivity in glutamate-dependent acid resistance in enteric bacteria. *Proc. Natl. Acad. Sci. USA* **110**, 5898–5902 (2013).
23. Ma, D., Lu, P. & Shi, Y. Substrate selectivity of the acid-activated glutamate/ γ -aminobutyric acid (GABA) antiporter GadC from *Escherichia coli*. *J. Biol. Chem.* **288**, 15148–15153 (2013).
24. Eguchi, Y., Ishii, E., Hata, K. & Utsumi, R. Regulation of acid resistance by connectors of two-component signal transduction systems in *Escherichia coli*. *J. Bacteriol.* **193**, 1222–1228 (2011).
25. Boudgour, A., Cunning, C., Baptiste, P. J., Elliott, T. & Gottesman, S. Multiple pathways for regulation of σ S (RpoS) stability in *Escherichia coli* via the action of multiple anti-adaptors. *Mol. Microbiol.* **68**, 298–313 (2008).
26. Itou, J., Eguchi, Y. & Utsumi, R. Molecular mechanism of transcriptional cascade initiated by the EvgS/EvgA System in *Escherichia coli* K-12. *Biosci. Biotechnol. Biochem.* **73**, 870–878 (2014).
27. Masuda, N. & Church, G. M. Regulatory network of acid resistance genes in *Escherichia coli*. *Mol. Microbiol.* **48**, 699–712 (2003).
28. Krin, E., Danchin, A. & Soutourina, O. RcsB plays a central role in H-NS-dependent regulation of motility and acid stress resistance in *Escherichia coli*. *Res. Microbiol.* **161**, 363–371 (2010).
29. Castanié-Cornet, M.-P. et al. Acid stress response in *Escherichia coli*: mechanism of regulation of *gadA* transcription by RcsB and GadE. *Nucleic Acids Res.* **38**, 3546–3554 (2010).
30. Johnson, M. D., Burton, N. A., Gutiérrez, B., Painter, K. & Lund, P. A. RcsB is required for inducible acid resistance in *Escherichia coli* and acts at *gadE*-dependent and -independent promoters. *J. Bacteriol.* **193**, 3653–3656 (2011).
31. Stim-Herndon, K. P., Flores, T. M. & Bennett, G. N. Molecular characterization of *adiY*, a regulatory gene which affects expression of the biodegradable acid-induced arginine decarboxylase gene (*adiA*) of *Escherichia coli*. *Microbiology* **142**, 1311–1320 (1996).
32. Wang, S., Yan, R., Zhang, X., Chu, Q. & Shi, Y. Molecular mechanism of pH-dependent substrate transport by an arginine- α -glutamate antiporter. *Proc. Natl. Acad. Sci. USA* **111**, 12734–12739 (2014).
33. Bobrovskyy, M. Diverse mechanisms of post-transcriptional repression by the small RNA regulator of glucose-phosphate stress. *Mol. Microbiol.* **99**, 254–273 (2016).
34. Fritz, G. et al. Induction kinetics of a conditional pH stress response system in *Escherichia coli*. *J. Mol. Biol.* **393**, 272–286 (2009).
35. Jung, K., Fabiani, F., Hoyer, E. & Lassak, J. Bacterial transmembrane signalling systems and their engineering for biosensing. *Open Biol.* **8**, 180023 (2018).
36. Haneburger, I. et al. Deactivation of the *E. coli* pH stress sensor CadC by cadaverine. *J. Mol. Biol.* **424**, 15–27 (2012).
37. Haneburger, I., Eichinger, A., Skerra, A. & Jung, K. New insights into the signaling mechanism of the pH-responsive, membrane-integrated transcriptional activator CadC of *Escherichia coli*. *J. Biol. Chem.* **286**, 10681–10689 (2011).
38. Rauschmeier, M., Schüppel, V., Tetsch, L. & Jung, K. New insights into the interplay between the lysine transporter LysP and the pH sensor CadC in *Escherichia coli*. *J. Mol. Biol.* **426**, 215–229 (2014).
39. Tetsch, L., Koller, C., Haneburger, I. & Jung, K. The membrane-integrated transcriptional activator CadC of *Escherichia coli* senses lysine indirectly via the interaction with the lysine permease LysP. *Mol. Microbiol.* **67**, 570–583 (2008).
40. Ude, S. et al. Translation elongation factor EF-P alleviates ribosome stalling at polyproline stretches. *Science* **339**, 82–85 (2013).
41. Brameyer, S. et al. Molecular design of a signaling system influences noise in protein abundance under acid stress in different gammaproteobacteria. *J. Bacteriol.* **202**, 95–15 (2020).
42. Silander, O. K. et al. A genome-wide analysis of promoter-mediated phenotypic noise in *Escherichia coli*. *PLoS Genet.* **8**, e1002443–13 (2012).
43. Brameyer, S. et al. DNA-binding directs the localization of a membrane-integrated receptor of the ToxR family. *Commun. Biol.* **2**, 1–10 (2019).
44. Li, G.-W., Burkhardt, D., Gross, C. & Weissmann, J. S. Quantifying absolute protein synthesis rates reveals principles underlying allocation of cellular resources. *Cell* **24**, 624–635 (2014).
45. Schlundt, A. et al. Structure-function analysis of the DNA-binding domain of a transmembrane transcriptional activator. *Sci. Rep.* **7**, 1–16 (2017).
46. Martini, L., Brameyer, S., Hoyer, E., Jung, K. & Gerland, U. Dynamics of chromosomal target search by a membrane-integrated one-component receptor. *PLoS Comput. Biol.* **17**, e1008680 (2021).
47. Zhao, B. & Houry, W. A. Acid stress response in enteropathogenic gammaproteobacteria: an aptitude for survival. *Biochem. Cell Biol.* **88**, 301–314 (2010).
48. Capitani, G. et al. Crystal structure and functional analysis of *Escherichia coli* glutamate decarboxylase. *EMBO J.* **22**, 4027–4037 (2003).
49. Bennett, B. D. et al. Absolute metabolite concentrations and implied enzyme active site occupancy in *Escherichia coli*. *Nat. Chem. Biol.* **5**, 593–599 (2009).
50. Gale, E. F. & Epps, H. M. R. *l*-Lysine decarboxylase: preparation of specific enzyme and coenzyme. *Nature* **152**, 327–328 (1943).
51. Heins, A.-L., Reyelt, J., Schmidt, M., Kranz, H. & Weuster-Botz, D. Development and characterization of *Escherichia coli* triple reporter strains for investigation of population heterogeneity in bioprocesses. *Microb. Cell Fact.* **19**, 14 (2020).
52. Battesti, A., Majdalani, N. & Gottesman, S. The RpoS-mediated general stress response in *Escherichia coli*. *Microbiol.* **65**, 189–213 (2011).
53. Hengge, R. Stationary-phase gene regulation in *Escherichia coli*. *EcoSal Plus.* **4**, <https://doi.org/10.1128/ecosalplus.5.6.3> (2011).
54. Mitosch, K., Rieckh, G. & Bollenbach, T. Noisy response to antibiotic stress predicts subsequent single-cell survival in an acidic environment. *Cell Syst.* **4**, 393–403.e5 (2017).
55. Evans, D. F. et al. Measurement of gastrointestinal pH profiles in normal ambulant human subjects. *Gut* **29**, 1035 (1988).
56. Zhao, H. et al. The soluble transhydrogenase UdhA affecting the glutamate-dependent acid resistance system of *Escherichia coli* under acetate stress. *Biol. Open.* **7**, bio031856 (2018).
57. Kitamoto, S. et al. Dietary *L*-serine confers a competitive fitness advantage to *Enterobacteriaceae* in the inflamed gut. *Nat. Microbiol.* **5**, 116–125 (2020).
58. Epstein, W. & Kim, B. S. Potassium transport loci in *Escherichia coli* K-12. *J. Bacteriol.* **108**, 639–644 (1971).
59. Schlüter, J.-P. et al. Classification of phenotypic subpopulations in isogenic bacterial cultures by triple promoter probing at single cell level. *J. Biotechnol.* **198**, 3–14 (2015).
60. Gibson, D. G. et al. Enzymatic assembly of DNA molecules up to several hundred kilobases. *Nat. Methods* **6**, 343–345 (2009).
61. Schneider, C. A., Rasband, W. S. & Eliceiri, K. W. NIH Image to ImageJ: 25 years of image analysis. *Nat. Methods* **9**, 671–675 (2012).
62. Ducret, A., Quardokus, E. M. & Brun, Y. V. MicrobeJ, a tool for high throughput bacterial cell detection and quantitative analysis. *Nat. Microbiol.* **1**, 16077–14 (2016).
63. Lambert, T. J. FPbase: a community-editable fluorescent protein database. *Nat. Methods* **16**, 277–278 (2019).
64. Team, R. C. R: A language and environment for statistical computing. *R Foundation for Statistical Computing, Vienna, Austria.* (2018).
65. Laemmli, U. K. Cleavage of structural proteins during the assembly of the head of bacteriophage T4. *Nature* **227**, 680–685 (1970).
66. Altschul, S. F. et al. Gapped BLAST and PSI-BLAST: a new generation of protein database search programs. *Nucleic Acids Res.* **25**, 3389–3402 (1997).
67. Hogeweg, P. & Hesper, B. The alignment of sets of sequences and the construction of phyletic trees: An integrated method. *J. Mol. Evol.* **20**, 175–186 (1984).
68. Blattner, F. R. et al. The complete genome sequence of *Escherichia coli* K-12. *Science* **277**, 1453–1462 (1997).
69. Macinga, D. R., Parojcic, M. M. & Rather, P. N. Identification and analysis of *aarP*, a transcriptional activator of the 2'-N-acetyltransferase in *Providencia stuartii*. *J. Bacteriol.* **177**, 3407–3413 (1995).
70. Baba, T. et al. Construction of *Escherichia coli* K-12 in-frame, single-gene knockout mutants: the Keio collection. *Mol. Syst. Biol.* **2**, 1–11 (2006).
71. Guzman, L. M., Belin, D., Carson, M. J. & Beckwith, J. Tight regulation, modulation, and high-level expression by vectors containing the arabinose P_{BAD} promoter. *J. Bacteriol.* **177**, 4121–4130 (1995).
72. Lassak, J., Henche, A.-L., Binnenkade, L. & Thormann, K. M. ArcS, the cognate sensor kinase in an atypical Arc system of *Shewanella oneidensis* MR-1. *Appl. Environ. Microbiol.* **76**, 3263–3274 (2010).
73. Gödeke, J., Heun, M., Bubendorfer, S., Paul, K. & Thormann, K. M. Roles of two *Shewanella oneidensis* MR-1 extracellular endonucleases. *Appl. Environ. Microbiol.* **77**, 5342–5351 (2011).
74. Lund, P., Tramonti, A. & Biase, D. D. Coping with low pH: molecular strategies in neutralophilic bacteria. *FEMS Microbiol. Rev.* **38**, 1091–1125 (2014).

Acknowledgements

We thank Jürgen Lassak for stimulating scientific discussions. We thank Sabine Peschek for excellent technical assistance and Anke Becker for providing the plasmid pK18mob2-TriFluoR. This work was financially supported by the Deutsche Forschungsgemeinschaft [Projects 26942323 (TRR174), 395357507 (SFB 1371) and 471254198 (JU270/21-1) to K.J.].

Author contributions

K.J. and S.B. designed the study. S.B. and K.S. performed the experiments and analyzed the data. S.K. performed the phylogenetic analysis. S.B. and K.J. wrote the manuscript with input from all authors.

Funding

Open Access funding enabled and organized by Projekt DEAL.

Competing interests

The authors declare no competing interests.

Additional information

Supplementary information The online version contains supplementary material available at <https://doi.org/10.1038/s42003-022-03281-4>.

Correspondence and requests for materials should be addressed to Kirsten Jung.

Peer review information *Communications Biology* thanks Peter Lund, Stefano Pagliara and the other, anonymous, reviewer(s) for their contribution to the peer review of this work. Primary Handling Editors: Calvin Henard and Luke R. Grinham. Peer reviewer reports are available.

Reprints and permission information is available at <http://www.nature.com/reprints>

Publisher's note Springer Nature remains neutral with regard to jurisdictional claims in published maps and institutional affiliations.



Open Access This article is licensed under a Creative Commons Attribution 4.0 International License, which permits use, sharing, adaptation, distribution and reproduction in any medium or format, as long as you give appropriate credit to the original author(s) and the source, provide a link to the Creative Commons license, and indicate if changes were made. The images or other third party material in this article are included in the article's Creative Commons license, unless indicated otherwise in a credit line to the material. If material is not included in the article's Creative Commons license and your intended use is not permitted by statutory regulation or exceeds the permitted use, you will need to obtain permission directly from the copyright holder. To view a copy of this license, visit <http://creativecommons.org/licenses/by/4.0/>.

© The Author(s) 2022

2.5 Bacterial battle against acidity

Schwarz, J.*, Schumacher, K.*, Brameyer, S., and Jung K. (2022). Bacterial battle against acidity. *FEMS Microbiol. Rev.* 46. 10.1093/femsre/fuac037.

* These authors contributed equally

Available online at:

<https://pubmed.ncbi.nlm.nih.gov/35906711/>

Bacterial battle against acidity

Julia Schwarz[‡], Kilian Schumacher[‡], Sophie Brameyer^{*}, Kirsten Jung[‡] 

Faculty of Biology, Microbiology, Ludwig-Maximilians-University München, Großhaderner Str. 2-4, 82152 Martinsried, Germany

***Corresponding author:** Faculty of Biology, Microbiology, Ludwig-Maximilians-University München, Großhaderner Str. 2-4, 82152 Martinsried, Germany.

Tel: + 4989/2180-74500, E-mail: jung@lmu.de; s.brameyer@bio.lmu.de

[‡]These authors contributed equally to this work.

Editor: Franz Narberhaus

Abstract

The Earth is home to environments characterized by low pH, including the gastrointestinal tract of vertebrates and large areas of acidic soil. Most bacteria are neutralophiles, but can survive fluctuations in pH. Herein, we review how *Escherichia*, *Salmonella*, *Helicobacter*, *Brucella*, and other acid-resistant Gram-negative bacteria adapt to acidic environments. We discuss the constitutive and inducible defense mechanisms that promote survival, including proton-consuming or ammonia-producing processes, cellular remodeling affecting membranes and chaperones, and chemotaxis. We provide insights into how Gram-negative bacteria sense environmental acidity using membrane-integrated and cytosolic pH sensors. Finally, we address in more detail the powerful proton-consuming decarboxylase systems by examining the phylogeny of their regulatory components and their collective functionality in a population.

Keywords: Gram-negative bacteria, protons, glutamate acid-dependent acid resistance, lysine-dependent acid resistance, pH-sensor

Introduction

Compared to acidophilic organisms, which grow optimally at a pH near 3.0, and alkaliphiles, which prefer a pH between 8 and 10.5, most bacteria are neutralophilic and grow best at pH values between 7.0 and 7.8 (Slonczewski et al. 2009). However, neutralophilic bacteria are able to adapt and grow in environments with pH values ranging from 5.5 to 9.0, and thereby occupy a wide range of environmental niches including acidic environments such as human and animal digestive systems, acidic soils, and fermented foods (Fig. 1), which has important effects on the environment and public health. The evolution of molecular systems conferring acid tolerance and/or acid resistance (AR) is an important survival strategy for these bacteria, including the pathogenic ones (Castanié-Cornet et al. 1999).

The pH of the human stomach ranges between 1 and 3 under fasting conditions and increases during digestion. The stomach, thus is a major bactericidal barrier against enterobacteria (Martinsen et al. 2005, Kalantzi et al. 2006). Its low pH causes growth arrest and even death of bacteria (e.g. only 10% of the highly resistant *E. coli* population survives in the stomach). Under this condition, an acidification of the bacterial cytoplasm occurs as protons (H^+) use water bridges or weak organic acids to traverse the cytoplasmic membranes (Brahmachari et al. 2019). This acidification has two important effects: slowing biological activity of macromolecules and decreasing or abolishing the pH difference at the cytoplasmic membrane. The latter is an important component of the proton motive force and crucial for bioenergetics (Foster 2004, Lund et al. 2014).

Neutralophilic enterobacteria that survive the stomach also confront mild acid stress (pH 6.4 or lower) in the colon due to the presence of short-chain fatty acids (Hirshfield et al. 2003), such as butyric, propionic, lactic, acetic, and formic acids, which are produced by anaerobic fermenting bacteria (Evans et al. 1988, Boets

et al. 2015). Intracellular pathogens, such as *Salmonella*, also encounter low-pH (pH 4–5) environments in the macrophage phagosome (Rathman et al. 1996, Steinberg et al. 2007) (Fig. 1).

On Earth there are large areas of soil with an acidic pH-value (pH 6.5–3.5; Wieder et al. 2014; Fig. 1). Many processes contribute to soil acidification. For example, carbon dioxide (CO_2) emissions combine with water in the atmosphere to form carbonic acid (H_2CO_3), and the burning of fossil fuels releases oxides of sulfur and nitrogen into the atmosphere that react with water to form sulfuric and nitric acids. This acidic rain then accumulates in the soil. Root respiration and decomposition of organic matter by microorganisms also release CO_2 , which increases the level of H_2CO_3 in the soil. Simultaneously, cations are exchanged resulting in leaching of base cations, such as Ca^{2+} , Mg^{2+} , from the soil and an increase of the percentage of Al^{3+} and H^+ (vanLoon 1984). Severely acidic conditions also can form in soils located near acid mine drainage sites (Johnson and Hallberg 2005).

In food industry, acidity plays an important role for bacteria (Fig. 1). Homofermentative and heterofermentative lactic acid bacteria and propionic bacteria, which are predominant in dairy products, trigger the production of lactic acid, propionic acid, ethanol, and CO_2 , all of which enhance flavor, digestibility, nutritional properties, and preservation (Fröhlich-Wyder et al. 2017, Siedler et al. 2019). As a consequence, these bacteria are exposed to acidity of their own fermentation activities. On the other hand, weak acid preservatives such as potassium sorbate, calcium propionate, and sodium benzoate are often added to foods to inhibit the growth of bacteria and to extend the shelf life of products (Guynot et al. 2005).

In this review, we focus on the manifold adaptive responses of neutralophilic Gram-negative proteobacteria and the molecular mechanisms of sensing acid stress. For detailed information on

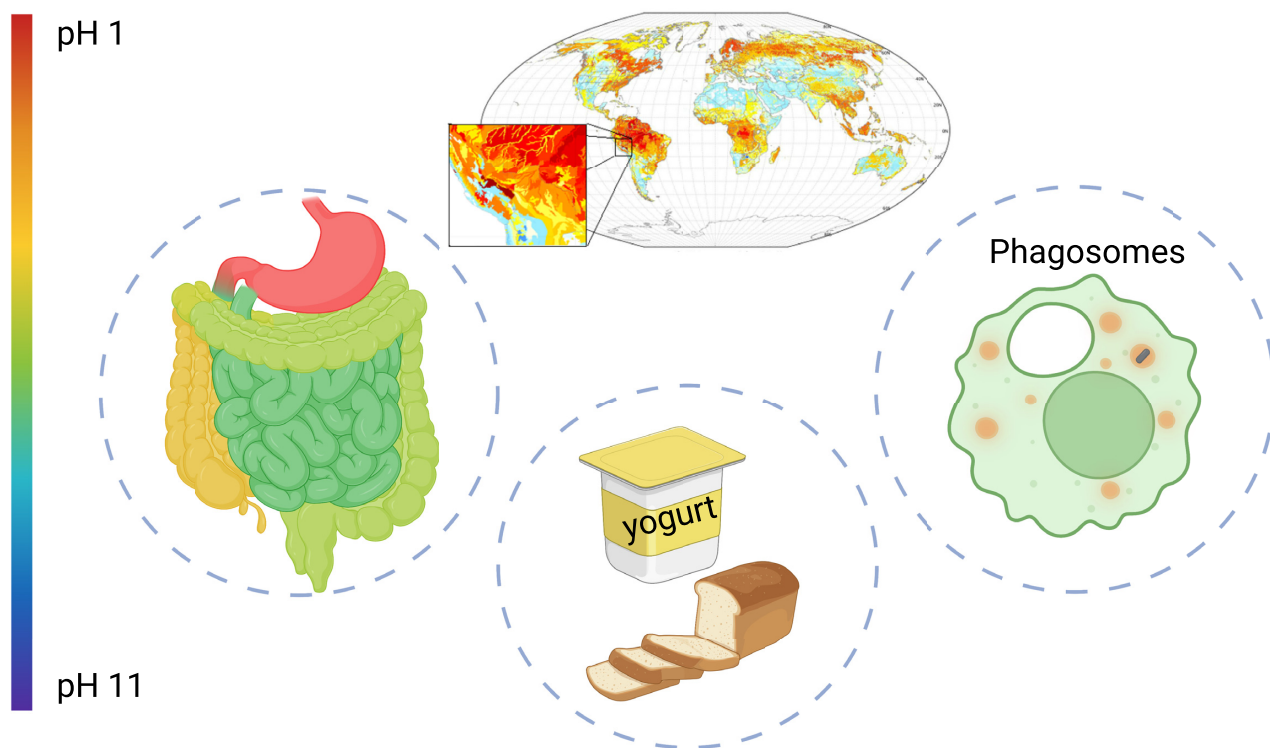


Figure 1. Schematic overview of acidic environments encountered by bacteria.

the acid-stress response of neutralophilic Gram-positive bacteria, see reviews by Guan and Li (2020) and Arcadi et al. (2020).

Acid stress adaptation of Gram-negative γ -proteobacteria

pH homeostasis and ion transport

In response to rapid drops in external pH, prokaryotic cells can retain a fairly constant internal pH from 7.5 to 8.0 for neutralophiles, 6.5 to 7.0 for acidophiles, and 8.4 to 9.0 for alkaliphiles (Booth 1985). In contrast to the periplasm, the cytoplasm transiently acidifies and restores neutral pH within short time intervals due to numerous cellular acid stress adaptations (Wilks and Slonczewski 2007, Krulwich et al. 2011). An important factor for preserving a constant internal pH is the intrinsic buffering capacity of the cytoplasm (Fig. 2). Excess intracellular protons can be sequestered by pH-titratable cellular components, such as amino acid side-chains, polyamines, polyphosphates, or inorganic phosphates, as summarized in Slonczewski et al. (2009).

The cytoplasmic membrane constitutes a major barrier to protons due to the intrinsic impermeability of the lipid bilayer and specifically controlled ion influx (Booth 1985). However, protons can pass this natural barrier using transient water chains, channels, or damaged membranes (Deamer 1987, Lund et al. 2014). Different types of acid stress counteracting membrane-integrated transporters exist, such as monovalent cation-proton antiporters, or proton pumps associated to the respiratory chain (Fig. 2).

The active transport of H^+ is a constitutive mechanism that maintains a constant internal pH, but the activity of H^+ pumps is constrained by the generation of the proton motive force (Mitchell 1973). In low-pH conditions, *E. coli* downregulates synthesis of the F_0F_1 -ATP synthase to limit proton re-entry (Maurer et al. 2005, Sun et al. 2012). In various other organisms, the F_0F_1 -ATP synthase re-

lieves acid stress via ATP-dependent extrusion of protons from the cytoplasm (Kobayashi et al. 1986, Foster and Hall 1991, Cotter et al. 2000, Sun et al. 2012). Net potassium uptake is the dominant means of maintaining ion homeostasis (Booth 1985).

Acidophilic bacteria also can relieve acid stress by reversing the usually negative transmembrane potential ($\Delta\psi$) (Matin 1999). An inside-positive membrane potential helps prevent further proton uptake due to charge repulsion (Matin et al. 1982). A similar mechanism has been suggested for neutralophilic bacteria (Foster 2004, Richard and Foster 2004). In addition, in *E. coli*, two genes (*eriC* and *mriT*) coding for two chloride channels are induced at extremely low pH levels. Export of Cl^- prevents H^+ uptake and restores an inside-negative $\Delta\psi$ once the external pH is recovered (Iyer et al. 2002, Accardi and Miller 2004).

Enzyme-based H^+ -consuming acid stress resistance systems

A total of four different H^+ -consuming AR systems have been identified in *E. coli* (Figs. 2 and 3). These are the glutamate-dependent AR2 (Gad) system (also known as GDAR), the arginine-dependent AR3 (Adi) system (also known as ADAR), the lysine-dependent AR4 (Cad) system (also known as LDAR) and the ornithine-dependent AR5 (Orn) system (also known as ODAR). Each of these four systems relies on a cytoplasmic amino acid decarboxylase and a corresponding antiporter. In an H^+ -consuming reaction, the pyridoxal-5'-phosphate (PLP)-dependent decarboxylase converts a specific amino acid (e.g. glutamate, arginine, lysine, and ornithine) into a more alkaline product, which is then exported by a specific antiporter in exchange for the amino acid. Through these biochemical reactions, the internal and external pH levels rise. The AR2–AR5 systems are activated at different pH ranges (< 6) (Fig. 3) with varying strengths in individual cells, and each decarboxylase has its own optimum pH (Gale 1940, 1946, Lin

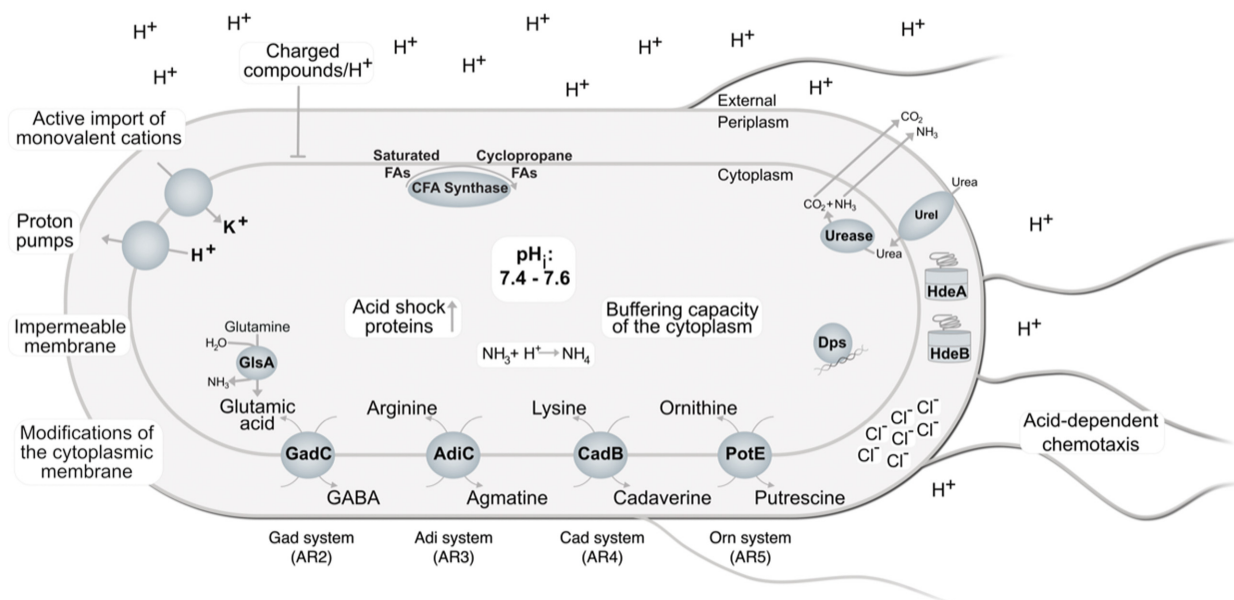


Figure 2. Overview of mechanisms in Gram-negative proteobacteria to cope with acidic environments. The various mechanisms to counteract acidic stress are discussed in detail in the text.

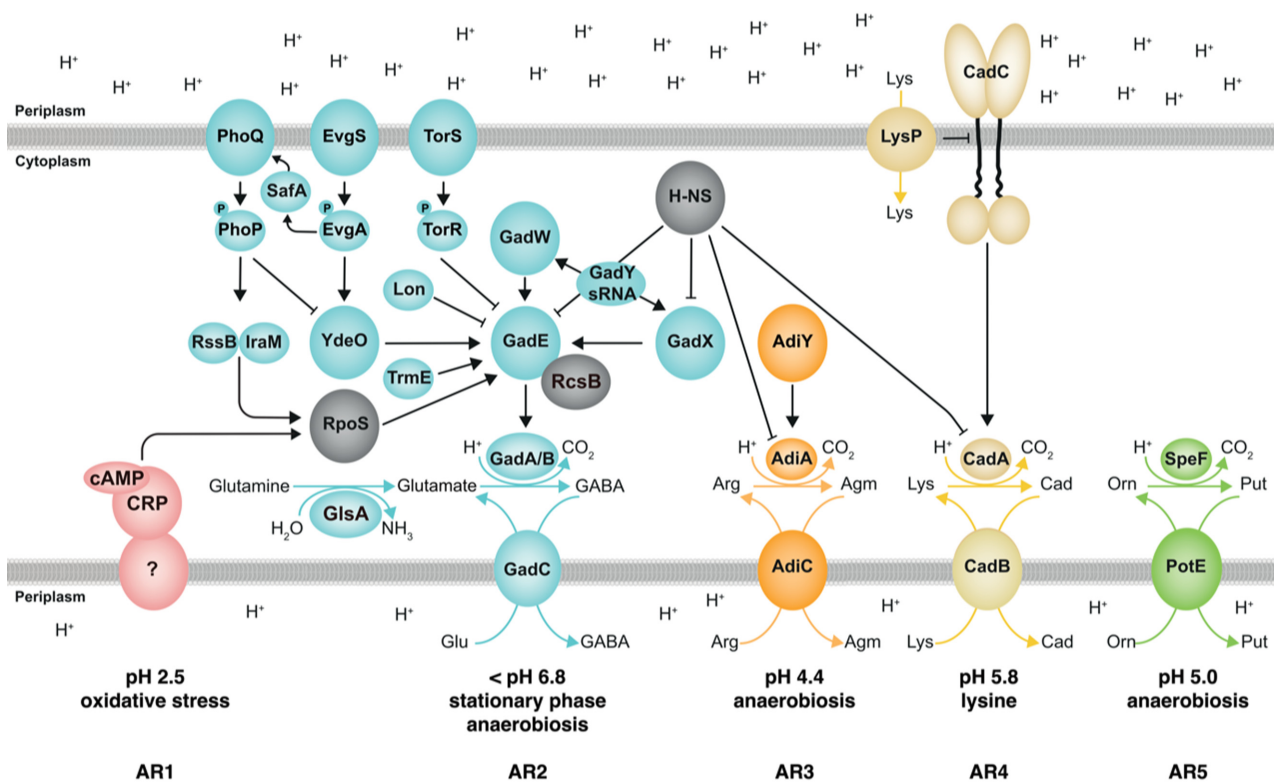


Figure 3. The regulatory network of the enzyme-based acid stress resistance systems in *E. coli*. Regulated induction of AR1 (in red), the Gad (AR2; in light blue), Adi (AR3; in orange), Cad (AR4; in pale yellow), and Orn (AR5; in green) systems requires a network of membrane-integrated pH-sensors, namely EvgS, PhoQ, and CadC; interconnected transcription factors; and the sRNA GadY. The glutamate decarboxylases GadA and GadB convert glutamate (Glu) into γ -aminobutyrate (GABA), which is excreted by GadC. The glutaminase GluA (formerly YbaS) converts glutamine in glutamate and NH_3 . The arginine decarboxylase AdiA converts arginine (Arg) into agmatine (Agm), which is excreted by AdiC. The lysine decarboxylase CadA converts lysine (Lys) into cadaverine (Cad), which is excreted by CadB. The ornithine decarboxylase SpeF converts ornithine (Orn) into putrescine (Put), which is excreted by PotE. RpoS, RcsB, and H-NS (gray symbols) are involved in the regulation of several enzyme-based acid stress resistance systems. Adapted from Lin et al. (1996), Castanié-Cornet et al. (1999), Foster (2004), Richard and Foster (2004), Bougdour et al. (2008), Zhao and Houry (2010), Eguchi et al. (2011), and Lund et al. (2014). The stimuli leading to an induction of each of the five AR systems are indicated below each system.

et al. 1995, Bearson et al. 1997, Castanié-Cornet et al. 1999, Foster 2004, Kanjee et al. 2011b, Kanjee and Houry 2013, Aquino et al. 2017). Little is known about AR1, an oxidative or glucose repressed system, which is independent of an external amino acid.

Acid-resistance system 1 (AR1)

The AR1 system is induced in stationary phase cells in complex media, or in minimal medium under extremely acidic stress conditions (pH 2.5) (Lin et al. 1996, Castanié-Cornet et al. 1999, Foster 2004). Its expression is regulated by alternative sigma factor σ^S (RpoS) and the cyclic adenosine monophosphate (cAMP) receptor protein (CRP). Part of the protective function of the AR1 system is the F_0F_1 -ATP-synthase, which hydrolyzes ATP to pump protons out of the cell and lower internal pH (Richard and Foster 2004). Aquino et al. (2017) predicted a model according to which the AR1 system uses the enzymes of the Gad system, which are described in the next chapter, to decarboxylate intracellular glutamate.

Glutamate-dependent AR (Gad) system (AR2)

The core components of the Gad system are the decarboxylase isoenzymes GadA and GadB and the glutamate/ γ -amino butyrate antiporter GadC in *E. coli*. Both GadA and GadB convert L-glutamate into γ -amino butyrate (GABA), consuming a proton in this process. The *gadBC* genes form one operon, while *gadA* is located inside the acid fitness island in *E. coli* (Biase and Pennacchiotti 2012). The Gad system is induced during transition to the stationary phase and during exponential growth in acidified media (Biase et al. 1999, Castanié-Cornet et al. 1999, Castanié-Cornet and Foster 2001, Weber et al. 2005). In addition, the Gad system is essential for survival at pH levels below 3, but is also induced during anaerobiosis and salt stress (Biase et al. 1999, Hayes et al. 2006).

GadA and GadB form hexamers, have maximal activities at pH 3.7–3.8 (Shukuya and Schwert 1960, Lawson and Quinn 1967) and are 98% identical at the nucleotide level (Smith et al. 1992). More functional and structural details of GadB are summarized in excellent reviews of Biase and Pennacchiotti (2012) and Zhao and Houry (2010).

The high-resolution X-ray crystal structure of GadC, determined by Ma et al. (2012), reveals detailed insights into substrate binding and pH-dependent transport activity. GadC antiport activity has been observed at pH ≤ 6 *in vitro*, and *in vivo* measurements of GABA export suggest maximum activity at pH ≤ 3 (Richard and Foster 2004, Ma et al. 2012). Notably, GadC recognizes substrates by their net electric charge and exclusively transports $\text{Glu}^{0/-1}$ or Gln^0 in exchange for GABA^{+1} (Ma et al. 2013, Tsai et al. 2013). Under nonactivating conditions, a C-terminal plug in GadC prevents substrate-binding. Correspondingly, mutants lacking the C-plug display a shift in pH-dependent transport activity towards higher pH-units (Ma et al. 2012).

In addition to glutamate, GadC also transports the amino acid glutamine (Ma et al. 2012, 2013), which is subsequently converted to glutamate by the glutaminase GlsA (formerly YbaS; Figs. 2 and 3). During this reaction, NH_3 is released, which itself sequesters protons while the produced glutamate serves as further substrate for GadA and GadB (Lu et al. 2013). Correspondingly, *glsA* is upregulated under the same conditions as *gadBC* (Biase and Pennacchiotti 2012). In contrast to substrates and reaction products from other AR systems, glutamate and GABA both contribute to cytoplasmic buffering due to carboxyl groups with suitable pK_a values (Richard and Foster 2004, Lund et al. 2014).

The transcriptional regulation of *gadA*, *gadB*, and *gadC* represents one of the most complex examples thereof within bacteria. More than 20 regulatory elements with partially interconnected circuits and several small noncoding RNAs are involved in controlling their expression (Foster 2004, Zhao and Houry 2010).

The central activator of the Gad system is the transcriptional regulator GadE, which belongs to the LuxR-family (Ma et al. 2003; Fig. 3). GadE binds to the so-called *gad* box, a 20-nt region 63 bp upstream of the *gadA* and *gadBC* transcriptional start site (Castanié-Cornet and Foster 2001, Ma et al. 2002). In stationary phase *E. coli* cells, the 3' end of the GadE mRNA is processed and a 91-nt small regulatory RNA, GadF, is generated, which is involved in regulation of acid resistant genes (Melamed et al. 2016). To initiate expression of *gadA*, GadE forms a heterodimer with RcsB (Castanié-Cornet et al. 2007, 2010). RcsB is the response regulator (RR) of the Rcs phosphorelay system, which is responsible for adapting to cell envelope stress in *Enterobacteriaceae* (Meng et al. 2021). Beyond RcsB, the Rcs system consists of the transmembrane hybrid histidine kinase (HK) RcsC, another transmembrane protein RcsD and the outer membrane protein RcsF. RcsC and RcsD dephosphorylate RcsB in the absence of envelope stress. RcsB is not only able to form heterodimers with GadE, but also with RcsA, MatA, DctR, BglJ, and presumably EvgA, to control numerous target genes (Castanié-Cornet et al. 2010, Venkatesh et al. 2010, Johnson et al. 2011, Pannen et al. 2015).

gadE transcription is regulated by the AraC/XylS-like regulator YdeO of the EvgS/EvgA-PhoQ/PhoP-YdeO circuit (Fig. 3). YdeO and EvgA have additive effects on *gadE* transcription (Ma et al. 2004). EvgA also contributes indirectly to *gadE* transcription, on the one hand through activation of YdeO by phosphorylation and on the other hand by induction of the PhoQ/PhoP HK/RR system via the small connector protein SafA (Ma et al. 2004, Eguchi et al. 2012, Ishii et al. 2013). The PhoQ/PhoP system in turn activates the anti-adaptor protein IraM, which inhibits activity of the protease adaptor RssB. RssB is responsible for degradation of RpoS by ClpXP, which implies that an active PhoP leads to increased RpoS levels (Eguchi et al. 2011).

The GadX-GadY-GadW regulatory circuit is required for induction of the Gad system in stationary phase cells, independently of the culture conditions (Ma et al. 2002), as shown in Fig. 3. GadW and GadX both belong to the AraC/XylS family and activate *gadA* and *gadBC* directly and indirectly through transcriptional activation of *gadE* (Ma et al. 2002, Tramonti et al. 2006, Sayed et al. 2007). Both regulators exert a dual role and can also repress the above-mentioned genes when bound to the *gad* box (Tramonti et al. 2002). Another element adding even more complexity to this circuit is the small RNA GadY. GadY directly base pairs and thereby stabilizes the 3' untranslated region of the *gadX* mRNA (Opdyke et al. 2004). Another factor linked to AR via GadW is the LuxR-like protein SdiA, which presumably regulates *gadW* and *gadY* at the transcriptional level (Ma et al. 2020). This effect is further influenced by N-acyl homoserine lactones, which stabilize the SdiA protein and increase its binding affinity to DNA (Nguyen et al. 2015, Ma et al. 2020).

Other elements, including CRP and several sRNAs, influence induction of the Gad system through RpoS. Increased amounts of RpoS promotes *gadE*, *gadX*, and *gadY* expression (Castanié-Cornet and Foster 2001, Ma et al. 2002). For example, cAMP-CRP negatively controls *rpoS* transcription during exponential growth (Lange and Hengge-Aronis 1994). The DsrA small noncoding RNA stabilizes the *rpoS* mRNA and simultaneously inhibits *hns* mRNA translation via RNA–RNA interactions, which is expected to reduce gene silencing caused by the histone-like nucleoid-structuring protein

(H-NS) (Lease et al. 2004). This contributes to AR as H-NS represses *gadA*, *gadE*, and *gadX* (Giangrossi et al. 2005). The expression of *rpoS* is also positively regulated by the GcvB, RprA, and ArcZ small RNAs (Jin et al. 2009, Bak et al. 2014).

The expression of *gadE* is also induced during anaerobic growth of *E. coli* via the MnmE (TrmE) circuit. The Era-like GTPase MnmE can indirectly activate *gadE* in stationary-phase cells in rich medium supplemented with glucose (Gong et al. 2004). This activation also appears to be associated with anaerobic conditions and the ArcA/ArcB HK/RR system (Deng et al. 2013).

A combined ChIP-Seq RNA-Seq approach by Aquino et al. (2017) reports binding of the carbon starvation-induced regulator CsiR to *gadX*, *ydeO*, and *gadW* promoter regions, as well as effects of CsiR on gene expression of multiple *gad* genes. In addition to vast amounts of direct and indirect activators, examples of negative regulation of the Gad system also have been reported. In addition to H-NS, the RR TorR also negatively regulates *gad* genes, and the Lon protease is involved in GadE proteolysis (Bordi et al. 2003, Heuveling et al. 2008).

In summary, the Gad system is the most important AR system under extremely acidic conditions. In *E. coli* and other bacteria (see below), this system includes several decarboxylase isoenzymes. Up to now, no differences have been demonstrated in the induction of *gadA* and *gadB* and protein function.

It would be interesting to find out why two nearly identical decarboxylase genes have evolved or to find a condition in which only one of the two enzymes is produced. It also remains puzzling why the network of transcriptional regulators and small RNAs controlling the Gad system reaches such enormous complexity in *E. coli*. In contrast, the molecular design of the Cad, Adi, and Orn systems is simpler.

Arginine-dependent AR (Adi) system (AR3)

The arginine-dependent AR (Adi) system, shown in Fig. 3, consists of the arginine decarboxylase AdiA, the arginine/agmatine transporter AdiC, and the AraC/XylS-like regulator AdiY. The *adiA*, *adiY*, and *adiC* genes are clustered but not arranged in an operon, as *adiY* separates *adiA* and *adiC* on the chromosome. This system is maximally activated in *E. coli* grown in rich medium with an external pH of 4.4 under anaerobic conditions (Melnykovich and Snell 1958, Blethen et al. 1968, Kanjee and Houry 2013). AdiA decarboxylates arginine to produce agmatine, which is then secreted by AdiC via an exchange with extracellular arginine.

AdiA activity is pH-dependent and regulated via changes in oligomerization. At pH 5.2, AdiA mainly forms decamers. Oligomers dissociate into inactive dimers at higher pH values, and this transition is enhanced through electrostatic repulsion because AdiA has many negatively charged surface residues (Nowak and Boeker 1981).

Like AdiA, the activity of AdiC is pH-dependent, increasing at extremely acidic pH levels (< ~4) compared to physiological pH (Fang et al. 2007). The outward- and inside-facing domains of the antiporter also are sensitive to pH. AdiC functions as a homodimer, but each monomer can exchange one arginine to one agmatine (Fang et al. 2007, Gao et al. 2009, 2010, Kowalczyk et al. 2011, Krammer et al. 2016, 2018, Ilgü et al. 2018). The maximum uptake for arginine from the periplasm is reached at pH < 4, and the optimal pH for the cytoplasm is 5.5, showing that AdiC is a pH sensor of the periplasm and the cytoplasm (Gao et al. 2009, Zomot and Bahar 2011, Tsai and Miller 2013, Wang et al. 2014, Krammer et al. 2018).

Transcription of the *adi* genes is influenced by the growth phase, the switch to anaerobic conditions and several transcriptional regulators. Nevertheless, the main transcriptional regulator of the Adi system is AdiY, a member of the AraC/XylS-family, which activates the transcription of its target genes *adiA* and *adiC* (Stim-Herndon et al. 1996). *adiY* transcription itself is downregulated upon entry into the stationary phase of *E. coli* (Smith et al. 2018) and *adiY* mRNA can be base-paired by the small RNA SgrS, resulting in post-transcriptional downregulation under anaerobic conditions (Bobrovskyy and Vanderpool 2015). In addition to the main activator AdiY, CysB, CsiR, and H-NS have modulating effects on the expression of the Adi system (Shi and Bennett 1994, Aquino et al. 2017).

Recently, it was shown that pH-dependent activation of the *adiA* promoter can be manipulated by changes in intracellular pH, as activation of the Adi system can be influenced by manipulation of the cytosolic proton concentration either by deletion of *cadA* or by overproduction of *cadA* (triggered by increased CadC copy numbers) (Brameyer et al. 2022). These data suggest that AdiY acts as an intracellular pH sensor that detects a decrease in cytoplasmic pH (Brameyer et al. 2022). The molecular mechanism of how AdiY responds to low pH is still unclear. But it is an interesting hypothesis that low cytosolic pH, which normally has deleterious effects, is sensed by one sensor to activate another AR system.

Lysine-dependent AR (Cad) system (AR4)

The Cad system consists of the lysine decarboxylase CadA, the lysine/cadaverine antiporter CadB and the regulatory protein CadC, a member of the ToxR-family (Fig. 3). This system only moderately protects the cells from extreme acid shock, but it is important for growth in mildly acidic environments (Watson et al. 1992, Dell et al. 1994). Together with the Gad system, the Cad system contributes to cell survival in anaerobic environments with fermentation acids and phosphate starvation, such as the small intestine (Moreau 2007).

CadC functions as a periplasmic pH sensor and regulates the expression of *cadA* and *cadB*. Like all members of the ToxR-family, CadC is a membrane-integrated sensor with DNA-binding capacity. The *cadA* and *cadB* genes are organized in one operon, which is activated by CadC in *E. coli* cells exposed in mildly acidic conditions (pH 5.8) and in the presence of lysine (> 1 mM) (Watson et al. 1992, Neely et al. 1994, Neely and Olson 1996, Soksawatmaekhin et al. 2004, Tetsch et al. 2008, Fritz et al. 2009). Detection of low pH leads to dimerization of the periplasmic sensory domain of CadC. A disordered CadC linker on the cytoplasmic side is required to transduce the pH-dependent response into a structural rearrangement that facilitates dimerization of the cytoplasmic DNA-binding domain (Haneburger et al. 2011, Buchner et al. 2015, Schlundt et al. 2017). By recruiting the RNA polymerase, CadC binds to the *cadBA* promoter at two specific binding sites, with each binding site occupied by a CadC homodimer (Neely et al. 1994, Kuper and Jung 2005, Eichinger et al. 2011, Haneburger et al. 2011, Lindner and White 2014, Schlundt et al. 2017).

The availability of external lysine is transduced to CadC by the cosensor and inhibitor LysP, a lysine-specific permease in *E. coli*. CadC is inactivated by an interaction with LysP in low-lysine conditions. This interaction is released when lysine is abundant (Tetsch et al. 2008, Rauschmeier et al. 2014). Additionally, CadC activity is negatively feedback-inhibited by cadaverine (Fritz et al. 2009, Haneburger et al. 2011, 2012). LysP and H-NS act as negative regulators of the Cad system in *E. coli*. H-NS binds under noninducing conditions to four potential binding sites within the *cadBA*

promoter region and forms a repressor complex. This complex dissolves when CadC binds to the Cad1 site. Binding of CadC to Cad2 initiates transcription of *cadBA* (Shi et al. 1993, Neely et al. 1994, Kuper and Jung 2005, Buchner et al. 2015, Schlundt et al. 2017).

In *E. coli*, *cadC* transcription is constitutive (Watson et al. 1992, Dell et al. 1994), but *cadC* translation depends on the elongation factor P (EF-P) due to the presence of a polyproline motif. EF-P is an elongation factor that enhances translation of polyproline-containing proteins through alleviating of the ribosome stalling. This translational regulation keeps the copy number of CadC low at only 1–3 copies per cell, on average (Ude et al. 2013). Brameyer et al. (2019) showed that a fluorophore-tagged CadC appears uniformly in the membrane of cells exposed to physiological pH. Under CadC-activating conditions, a distinct cluster appears at the lateral cellular position, which immediately disappears under nonstress conditions. The results suggest that binding of CadC to DNA determines its localization in the cell. This finding is confirmed using various CadC variants that mimic the active state of CadC, independent of environmental stimuli, or in mutants in which the DNA-binding site is relocated (Brameyer et al. 2019, Martini et al. 2021). Due to the low copy number and consequent stochastic distribution of CadC in single *E. coli* cells, the Cad system is heterogeneously activated, resulting in about two thirds of cells in an ON state and the rest in an OFF state (Brameyer et al. 2020). For more details on the molecular mechanism of pH-sensing by CadC, see below.

CadA catalyzes the decarboxylation of L-lysine into the more alkaline polyamine cadaverine and into CO₂ by consuming a proton. The enzymatic activity is regulated by oligomerization and the alarmone guanosine 3',5'-bis(diphosphate) (ppGpp). Active CadA comprises five dimers that form a decamer in a double-ringed structure with a distinct 5-fold symmetry homologous to AdiA (Snider et al. 2006). A total of 10 molecules of the stringent response molecule ppGpp can bind to a CadA decamer to inhibit activity (Kanjee et al. 2011a), enabling cells to react quickly to changing environmental conditions. The maximum activity for CadA occurs at pH 5.7 (Gale and Epps 1944, Sabo et al. 1974, Kanjee and Houry 2013).

The structure of the lysine/cadaverine antiporter CadB is presently unknown. CadB performs an electrogenic exchange of lysine with cadaverine. At physiological pH, CadB mediates uptake of cadaverine, i.e. driven by proton-motive force (Soksawatmaekhin et al. 2004, 2006).

The Cad system is also important for survival and growth of other pathogenic bacteria in acidic conditions, such as *S. Typhimurium* (Park et al. 1996) and *V. cholerae* (Merrell and Camilli 1999). However, regulation of the Cad system varies among species. For example, in *Vibrio campbellii*, the Cad system is the major pH stress response system, but its Cad module is missing the cosensor LysP. In *Vibrio* spp., *cadC* expression is activated by the LysR-type transcriptional activator AphB (Rhee et al. 2006, Kovackova et al. 2010). Another difference compared to *E. coli* is that the translation of CadC does not depend on EF-P. Consequently, CadC has higher copy numbers of about 41–69 copies per cell under activating conditions. The Cad system, thus is homogeneously activated in all cells of the *V. campbellii* population (Brameyer et al. 2020).

Ornithine-dependent AR (Orn) system (AR5)

The Orn system is an exceptional AR system because it converts a nonproteinogenic amino acid. The system consists

of the inducible ornithine decarboxylase SpeF and the ornithine/putrescine antiporter PotE (Fig. 3). The main activity of this system occurs during anaerobic growth of *E. coli* at low pH and high ornithine levels (Gale 1946, Applebaum et al. 1977, Kashiwagi et al. 1991, 1992). The genes *speF* and *potE* are arranged in one operon and induced at pH ~5.0. Dimerization and GTP regulate the decarboxylase activity, and the alarmone ppGpp binds weakly to SpeF (Applebaum et al. 1977, Kanjee et al. 2011b). The optimal enzymatic activity for SpeF occurs at pH 7.0. This relatively high optimal pH, in comparison to other amino acid decarboxylases, highlights the efficiency of these four systems to deal with extremely acidic conditions (Gad > Adi > Cad >> Orn) (Foster 2004, Kanjee and Houry 2013). Under mildly acidic conditions, PotE exchanges ornithine or lysine with putrescine. At neutral pH, PotE catalyzes the proton motive force-dependent uptake of putrescine (Kashiwagi et al. 1992, 1997). Regulation of the *speF-potB* operon is unusual and involves ribosome stalling and antitermination (Ben-Zvi et al. 2019, Herrero Del Valle et al. 2020). Upstream of *speF* is a short open reading frame (ORF) that encodes the 34-amino acid peptide SpeFL (also known as *orf34*). This ORF is conserved in many γ -proteobacteria. In the absence of ornithine, translation of *speFL* causes ribosome stalling and transcription of *speF* pauses. In the presence of ornithine, translation of SpeFL activates *speF* expression by preventing Rho-dependent transcription termination (Herrero Del Valle et al. 2020).

Enzyme-based ammonia-producing AR systems

Deiminase and deaminase systems

Different bacterial species, such as *Helicobacter pylori*, *Pseudomonas aeruginosa*, and many Gram-positive bacteria like *Streptococcus mutans*, use deiminase and deaminase systems to withstand acidic environments. These enzymes produce ammonia (NH₃) to neutralize internal protons, which are used to create ammonium ions (NH₄⁺) and in turn increase the internal pH. Different deiminase and deaminase systems are present in different groups of bacteria in varying combinations.

The agmatine deiminase (AgD) belongs to the family of guanidino-group modifying enzymes (GMEs) (Linsky and Fast 2010). It catalyzes the conversion of agmatine to N-carbamoyl putrescine and NH₃. AgD mediates acid resistance in *Streptococcus mutans*, *P. aeruginosa* and *H. pylori* (Jones et al. 2010).

Another GME is the L-arginine deiminase, it belongs to the arginine deiminase system (Linsky and Fast 2010), which protects cells against acid damage (Cunin et al. 1986, Marquis et al. 1987, Liu et al. 1995, D'Hooghe et al. 1997, Angelis et al. 2002). This system is present in a variety of bacteria, including *Mycoplasma*, *Pseudomonas*, *Bacillus*, *Rhizobium*, and lactic acid bacteria. A total of three enzymes are responsible for its acid tolerance: (i) arginine deiminase, which degrades arginine into citrulline and NH₃, (ii) ornithine carbamoyl transferase (OTC), which cleaves citrulline into carbamoyl phosphate and ornithine, and (iii) carbamate kinase, which produces ATP, NH₃, and CO₂ through dephosphorylation of carbamoyl phosphate. These enzymes show maximal activity at a pH of 3.1 or lower (Cunin et al. 1986, Marquis et al. 1987, Casiano-Colón and Marquis 1988). The generation of NH₃ and of one ATP per arginine contributes to the internal pH homeostasis through the F₀F₁-ATPase, which extrudes cytoplasmic protons.

In *E. coli*, the glutaminase GlsA (formerly YbaS) is part of the Gad system, i.e. activated under acidic conditions (Figs 2 and 3). L-glutamine is imported by GadC and then converted by GlsA to

L-glutamate and NH_3 (Ma et al. 2012, 2013, Sun et al. 2012, Lu et al. 2013). Another deaminase system in *E. coli* is based on adenosine. Internal pH can increase when adenosine is converted into inosine and NH_3 , a reaction catalyzed by the adenosine deaminase Add (Maurer et al. 2005, Sun et al. 2012).

Urease

Another enzyme frequently used to combat acidification is urease, which is present in a wide variety of bacterial genera (e.g. *Helicobacter*, *Brucella*, *Klebsiella*, *Pseudomonas*, *Yersinia*, *Proteus*, *Staphylococcus*, and *Streptococcus*) (Lund et al. 2014), as well as members of the human gut microbiota (Mora and Arioli 2014). Urease catalyzes the hydrolysis of its substrate urea to NH_3 and carbamate, which subsequently decomposes into another molecule of NH_3 and CO_2 (Mobley et al. 1995). NH_3 contributes to cytoplasmic and periplasmic buffering by neutralizing protons and yielding NH_4^+ (Scott et al. 2010), and CO_2 is converted to bicarbonate by alpha-carbonic anhydrase (Marcus et al. 2005). The *ureAB* genes encode the urease subunits, whereas the protein products of *ureDEFG* are involved in urea metabolism, urease biogenesis and incorporation of nickel (Lund et al. 2014). Nickel ions are essential cofactors of urease activity and are inserted into the active site of the enzyme. Additionally, the NikR transcription factor of *H. pylori* regulates nickel uptake and induces expression from the *ureA* promoter in low-pH conditions (van Vliet et al. 2002, Li and Zamble 2009).

The importance of urease activity is best studied in *H. pylori*, in which the proton-gated urea channel UreI mediates urea uptake into the cytoplasm. Urea is present in 1–3 mM concentrations in gastric juice. UreI activity is strictly pH dependent, which prevents urea import and alkalization of the cytoplasm during physiological pH conditions (Weeks et al. 2000). Correspondingly, the previously mentioned genes encoding urease subunits are regulated in a pH-responsive manner, mediated by the ArsS/ArsR HK/RR system (see below) and the cytoplasmic HK FlgS (Wen et al. 2009). *Helicobacter pylori* produces urease up to 10% of its total protein content (Sachs et al. 2005). In animal models, urease-negative mutants are unable to colonize, further confirming the essential role of urease in gastric habitation (Eaton et al. 1991, Skouloubris et al. 1998, Mollenhauer-Rektorschek et al. 2002).

In several *Brucella* spp., urease activity is crucial to increase infectivity (Bandara et al. 2007, Sangari et al. 2007). Urea is also present at 3–10 mM concentrations in saliva and constitutes a nitrogen source for oral plaque microbiota (Mora and Arioli 2014). *Streptococcus salivarius* and *Actinomyces naeslundii* have been demonstrated to be urease positive (Morou-Bermudez and Burne 1999, Chen and Burne 2003), and viability of *S. salivarius* at extremely low pH increases in a urea concentration dependent manner (Chen et al. 2000).

Cellular remodeling to withstand acid stress

Synthesis of chaperones

Acidification leads to protein unfolding, denaturation, or damage as more amino acid residues become fully protonated (Goto et al. 1990). *Escherichia coli* has efficient chaperone-based mechanisms to protect proteins from acid-dependent denaturation and damage, especially in the periplasm (Fig. 2). HdeA and HdeB are two structurally related periplasmic chaperones that function in an ATP-independent manner and minimize protein aggregation due to high proton and chloride concentrations in the periplasm during acid stress (Fig. 2). They also assist in refolding the substrate after acid stress relief in *E. coli*, *Shigella flexneri*, *Brucella abortus*,

and other species (Waterman and Small 1996, Gajiwala and Burley 2000, Valderas et al. 2005, Kern et al. 2007, Malki et al. 2008, Stull et al. 2018). The corresponding genes are usually part of the acid fitness island, where genes are induced in cells exposed to acid stress (Tucker et al. 2002).

In vitro, both chaperones are inactive dimers at neutral pH. At pH 2, the HdeA dimer rapidly converts into partially disordered, chaperone-active monomers. In its monomeric form, HdeA binds to proteins that were unfolded at low pH, effectively preventing them from aggregating (Tapley et al. 2009b). Upon return to neutral pH, HdeA slowly releases the bound proteins, allowing them to refold while minimizing the concentration of aggregation-prone intermediates (Tapley et al. 2009a). HdeA then converts back to its chaperone-inactive dimer.

In vivo, HdeA functions optimally in cells exposed to extreme acid stress of pH 2–3, and HdeB functions optimally at a moderately acidic pH of 4 (Dahl et al. 2015). The cytoplasmic chaperone Hsp31 (*hchA*) also contributes to acid stress resistance of stationary-phase *E. coli* cells (Mujacic and Baneyx 2006). Its transcription is controlled by sigma factor σ^S , but its exact function remains unclear. Some evidence indicates that cytoplasmic chaperones such as GroE, DnaK, and IbpB are upregulated in some Gram-negative bacteria under acid stress (Lund et al. 2014). Further experimental evidence is needed to determine the extent to which strong acidification of the cytoplasm leads to significant protein unfolding in the cytoplasm of these organisms.

Modifications of the cytoplasmic membrane

The cytoplasmic membrane is a major barrier to proton influx in acid exposed cells. To protect this membrane against acid damage, bacteria modulate its integrity, fluidity, and lipid composition. Under acid stress, the ratio of saturated to unsaturated fatty acids in the membrane increases (Yang et al. 2014). Furthermore, cyclopropane fatty acids (CFAs) are synthesized and incorporated into the membrane (Brown et al. 1997) (Fig. 2). In this process, unsaturated fatty acids are converted to CFAs by the postsynthetic addition of a methyl group from S-adenosyl-methionine to a double bond (Chang and Cronan 1999). An *E. coli* mutant lacking *cfa*, the gene encoding CFA synthase, is highly sensitive to acid stress, but this sensitivity can be partially overcome by an exogenous supply of CFAs (Chang and Cronan 1999). In addition, *E. coli* membranes lacking CFAs are more permeable to protons, suggesting that the presence of CFAs is important to maintain membrane integrity under acid stress (Shabala and Ross 2008). The transcription of the *cfa* gene is upregulated at low external pH, indicating that alteration of the cytoplasmic membrane fatty acid composition is an adaptive response mechanism (Chang and Cronan 1999). Changes in the cytoplasmic membrane composition in response to acid stress have also been observed in *Salmonella* and *Helicobacter* (Haque et al. 1996, Kim et al. 2005, Alvarez-Ordóñez et al. 2009).

In addition to modifications of fatty acids, the modification of lipid types has been described in acid-stressed bacteria. Common responses involve hopanoid formation and the introduction of hydroxyl groups into existing membrane lipids such as ornithine lipids, lipid A, or sphingolipids (Sohlenkamp 2019).

Synthesis of acid-shock proteins

Of the previously mentioned amino-acid decarboxylase systems, the Gad system contributes most to the survival of an *E. coli* population in extremely acidic conditions at or below a pH of 2.5 (Biase et al. 1999, Biase and Pennacchietti 2012). Such conditions however, as they are encountered in the human gastrointestinal tract,

generally require adaptations on a global scale beyond amino-acid dependent AR systems (Kalantzi et al. 2006). Proteomic and microarray analyses have identified several candidates as acid shock proteins in cells exposed to acidified media (Blankenhorn et al. 1999, Audia et al. 2001, Stancik et al. 2002, Maurer et al. 2005) (Fig. 2). One prominent example is the periplasmic Asr protein, which is crucial for survival in extreme acidity (Šeputienė et al. 2003). Expression of the *asr* gene can be induced by at least three transcriptional regulators, RstA, RcdA, and PhoB (Sužiedėlienė et al. 1999, Ogasawara et al. 2007, Shimada et al. 2012). Upon expression, Asr is post-translationally cleaved into an 8- and a 5-kDa protein, however, the biological significance of this processing is still unclear. Maximum induction occurs at pH 4.0–4.5, and *asr* null mutants display an acid-sensitive phenotype (Šeputienė et al. 2003). Other strongly induced potential acid shock proteins in *E. coli* have been identified in moderate acidity of pH 4.3–5.0 (Foster and Hall 1991), including several poorly characterized proteins and known heat shock proteins (Heyde 1990, Blankenhorn et al. 1999, Stancik et al. 2002, Maurer et al. 2005). Several acid shock proteins have also been identified in *S. Typhimurium*. For most acid shock proteins, the exact mechanisms of protection during acid shock remain elusive and require further characterization.

Another important cellular component that protects DNA from damage is the Dps protein. In *dps* mutants, acid-induced DNA damage is significantly increased (Choi et al. 2000, Jeong et al. 2008). In stationary-phase cells, Dps becomes the most abundant nucleoid component (180 000 molecules per cell) and causes compaction of DNA characteristics of this growth phase (Ali Azam et al. 1999). Dps also protects DNA from oxidative cleavage (Martinez and Kolter 1997). Both oxidative and acid stress are associated with the production of hydroxyl radicals (OH^\bullet) via Fenton-type reactions, which mainly lead to DNA single and double strand breaks by oxidizing the sugar and base moieties. Dps proteins inhibit formation of these toxic hydroxyl radicals via a multistep process of removing Fe(II) (Ceci et al. 2003, 2004). In conclusion, further proteome and transcriptome wide studies and an in-depth characterization of the most promising candidate proteins at various pH levels are needed to unravel the full spectrum of acid shock proteins in bacteria.

Acid-dependent chemotaxis

Beyond the above-mentioned AR mechanisms, chemotactic movements have been described in several bacterial species as a direct adaptation to physically avoid low pH environments (Fig. 2) (Kihara and Macnab 1981, Repaske and Adler 1981, Tohidifar et al. 2020). When bacteria sense acidic pH or weak organic acids such as acetate, they migrate to more desirable environments (Tsang et al. 1973, Tso and Adler 1974). For instance, weak acids induce prolonged tumbling in *E. coli* and *Salmonella* cells at pH 5.5 (Kihara and Macnab 1981). Moreover, a microarray study conducted at various pH levels revealed that flagellar and chemotaxis genes in *E. coli* are regulated in response to the pH (Maurer et al. 2005). Correspondingly, genes encoding the flagellar motility apparatus are upregulated in *H. pylori* at low pH (Merrell et al. 2003, Wen et al. 2003). The swimming behavior of bacterial cells is controlled by the direction of the flagellar motor, which alternates between clockwise and counterclockwise rotations (Berg 1974). If repellents such as acids are perceived, tumbling is enhanced by prolonged clockwise flagella rotation (Berg and Brown 1972, Silverman and Simon 1974).

In *E. coli*, alkaline and acidic environments are sensed by two methyl-accepting chemotaxis proteins (MCPs), the aspartate

binding receptor, Tar, and the serine binding receptor, Tsr (Repaske and Adler 1981, Krikos et al. 1985, Khan et al. 1995). Using a fluorescence resonance energy transfer-based reporter, Yang and Sourjik (2012) reported a “push–pull” mode of action in which Tar initiates an attractant response to low pH and a repellent response to high pH, whereas Tsr exerts the opposing mode of action. This bidirectional response helps *E. coli* avoid extremely low or high pH by transitioning from acid-seeking to base-seeking and *vice versa* at specific pH inversion points. Another example for an MCP involved in pH taxis has been found in *H. pylori* (Croxen et al. 2006, Sweeney et al. 2012). Besides perception of the quorum-sensing molecule AI-2 (Rader et al. 2011), the chemotaxis receptor TlpB is indispensable for pH taxis and colonization of the gastric mucosa (Croxen et al. 2006). See below for further discussion of Tar, Tsr, and TlpB. To date, the strategy of avoiding acidic environments by chemotaxis has only been observed in *E. coli* and *H. pylori*. It remains unclear whether this strategy is specific to these species or whether it represents a universal stress response within bacteria. Further research is needed to clarify whether the number of flagella per cell is increased under low pH conditions, as upregulation of genes encoding the flagellar motility apparatus was observed.

Molecular mechanisms of pH-sensing

In the next chapters, we will discuss the molecular processes of pH-responsive receptors that are able to sense changes in pH outside and inside bacteria. In most cases, stimulus perception is coupled to transmembrane signaling.

Hybrid HK EvgS

The hybrid HK EvgS senses low external pH and transmits this signal to its cognate RR EvgA in *E. coli* (Utsumi et al. 1994, Eguchi and Utsumi 2014) (Figs. 3 and 4). The multidomain cytoplasmic part of EvgS comprises three signal transduction modules, including a transmitter domain (composed of an H-box containing dimerization and histidine phosphotransfer domain and a catalytic domain), a receiver domain, and a histidine-containing phosphotransfer (HPr) domain. The periplasmic part is connected via a cytoplasmic linker and includes two Venus flytrap (VFT) domains (Perraud et al. 1998, Sen et al. 2017). Upon signal perception, the phosphoryl group at the first histidine residue (His721) in EvgS is transferred to an aspartate residue (Asp1009) in the receiver domain and then transmitted to another histidine residue (His1137) in the HPr domain. To complete the four-step His-Asp-His-Asp phosphorelay, the phosphoryl group is transferred to the aspartate residue (Asp52) in EvgA (Utsumi et al. 1996, Perraud et al. 1998, Tanabe et al. 1998, Kinoshita-Kikuta et al. 2015).

EvgS displays maximum activity at pH 5.0–5.5, and a leucine residue at position 152 in the first VFT domain is crucial for activation (Fig. 4) (Eguchi and Utsumi 2014). Sen et al. (2017) also elucidated the structure of the periplasmic domain of EvgS. Additionally, the residues His226 and Pro522 are presumably involved in sensing acidity and signal transduction (Fig. 4).

In a proposed model, the stimulus is transduced from the VFT domains to the cytoplasmic Per-Arnt-Sim (PAS) domain via structural rearrangements mediated by the region comprising Leu152, His226, and Pro522. In combination with further stimuli sensed in the cytoplasm, the structural change putatively triggers a weakening of subunit interactions in an inactive tight EvgS dimer. Subsequently, the loose dimer, which constitutes the active EvgS conformation, induces autokinase activity and initiates the described phosphorelay (Johnson et al. 2014, Sen et al. 2017). This model is further supported by the fact that several amino

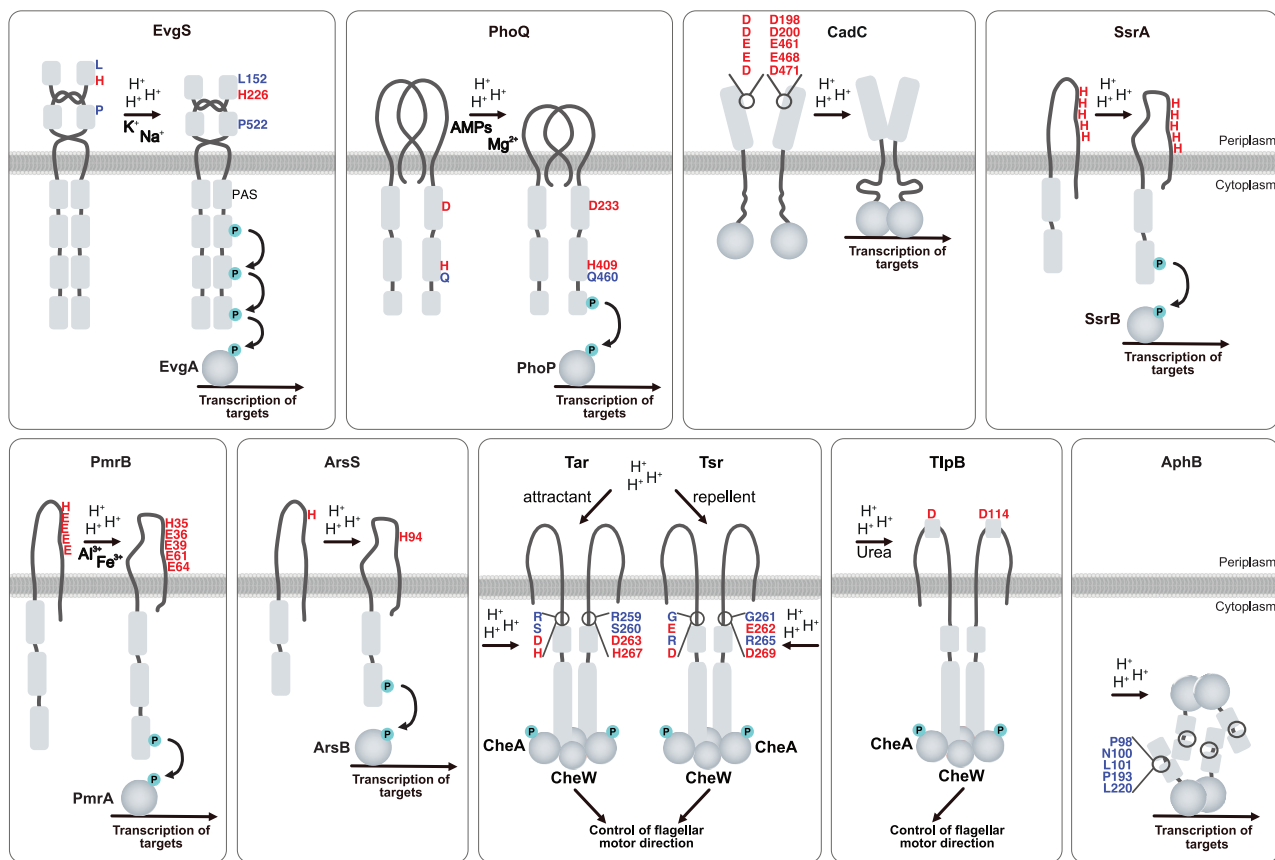


Figure 4. Schematic overview of the mechanisms of acid sensing of membrane-integrated and soluble pH sensors. The overall structure and mode of activation by low pH and various cations are indicated for the membrane-integrated sensors EvgS (Eguchi and Utsumi 2014, Hicks et al. 2015, Choi and Groisman 2016, Sen et al. 2017), PhoQ (Choi and Groisman 2016), CadC (Haneburger et al. 2011), SsrA (Mulder et al. 2015), PmrB (Perez and Groisman 2007), ArsS (Müller et al. 2009), Tar and Tsr (Umemura et al. 2002), as well as TlpB (Sweeney et al. 2012) and for the soluble regulator AphB (Taylor et al. 2012). Amino acid residues of the regulators are marked in red when described to be important for the recognition of low pH. For SsrA, only five histidine residues in the C-terminal end are described to be important for the recognition of low pH. Amino acid residues marked in blue are connected with the adaptation to low pH. Low pH is indicated via “H+.” AMPs, antimicrobial peptides. PAS, Per-Arnt-Sim domain.

acid replacements, which constitutively activate EvgS, have been identified in the PAS domain. These amino acid replacements might mimic the rearrangement from an inactive tight dimer to a more dissociated conformation, which constitutes the active state (Johnson et al. 2014).

In addition to the required mild acidity, alkali metals with a concentration of at least 150 mM are necessary to activate the EvgS/EvgA system (Eguchi and Utsumi 2014). To sense acidic pH, both the periplasmic region and the PAS domain are required, while alkali metals (e.g. K⁺) can be sensed by either domain individually (Eguchi and Utsumi 2014, Johnson et al. 2014). Beyond these findings, EvgS is active in mildly acidic environments under aerobic but not in anaerobic growth conditions. The EvgS PAS domain is hypothesized to act as an intermediate redox switch that transmits information from the periplasm to the cytoplasmic catalytic core, depending on the oxidation state of ubiquinone in the electron transport chain (Inada et al. 2021).

Due to substantial amino acid polymorphisms across different *E. coli* isolates, EvgS displays large variability in its pH-sensing capacity, including pH nonresponsive variants (Roggiani et al. 2017). The kinase forms clusters in *E. coli* (Sommer et al. 2013). Once EvgA is phosphorylated, it activates expression of two genes coding for regulators of the Gad system, *ydeO* and *gadE* (Ma et al. 2004, Itou et al. 2009). EvgA acts as a homodimer; however, it may also form heterodimers with RcsB (Johnson et al. 2011, Pannen et al.

2015). Moreover, the EvgS/EvgA system regulates the expression of multiple multidrug efflux pumps, including EmrYK and MdtEF (formerly YhiUV) (Kato et al. 2000, Nishino and Yamaguchi 2001, Eguchi et al. 2003).

HK PhoQ

Together with EvgS, PhoQ is responsible to transmit the activating signal of the Gad system in *E. coli*. In addition, the kinase has also been extensively studied in *S. Typhimurium*. The amino acid sequences of PhoQ in both bacterial species are 86% identical (Kasahara et al. 1992). As shown in Fig. 4, the bifunctional PhoQ is membrane-integrated and comprises a periplasmic sensor domain, a transmembrane TM 4-helix bundle, cytoplasmic HAMP domain, DHp domain, and a kinase domain (Goldberg et al. 2010). Under physiological conditions, PhoQ acts as a homodimer (Goldberg et al. 2008). Activation by various stimuli leads to autophosphorylation of PhoQ at a conserved histidine residue and subsequent phosphotransfer to the RR PhoP (Groisman et al. 1989, Miller et al. 1989). Under noninducing conditions, PhoQ displays phosphatase activity and dephosphorylates PhoP (Gunn and Miller 1996, Shin and Groisman 2005).

In *E. coli*, the phosphorelay between PhoQ and PhoP is fine-tuned by the small membrane protein SafA, which accelerates PhoQ autophosphorylation and accumulation of phosphorylated PhoP by direct interaction between its C-terminal domain and

the periplasmic sensor domain of PhoQ (Ishii et al. 2013). Transcription of *safA* itself is under the control of EvgA and thus connects the PhoQ/PhoP to the EvgS/EvgA system (Masuda and Church 2003, Eguchi et al. 2007, Itou et al. 2009). This connection to the EvgS acid-sensor is crucial, as direct pH-sensing has not been demonstrated for PhoQ in *E. coli*. Similar to *E. coli*, an additional horizontally acquired gene (*ugtL*) is needed to enhance autophosphorylation of PhoQ in *S. Typhimurium* (Choi and Groisman 2017). Both *UgtL* and *SafA* are required for the response of the PhoQ/PhoP system in mildly acidic conditions but not for sensing low Mg^{2+} levels and also do not affect phosphotransfer from PhoQ to PhoP (Groisman et al. 2021). *SsrB* (see below) is another factor involved in *S. Typhimurium*'s response to acid stress mediated by PhoQ/PhoP, as it binds to the *ugtL* promoter region and counteracts the repressing effects of H-NS (Choi and Groisman 2020).

In *E. coli*, the PhoQ/PhoP system is regulated at the post-transcriptional level by two Hfq-dependent small RNAs, *MicA* and *GcvB*. Both independently base-pair with the translation initiation region of the *phoPQ* mRNA, which impairs ribosomal binding and promotes transcript degradation (Coornaert et al. 2010, 2013). In addition, the PhoQ/PhoP system also involves a negative feedback inhibition loop via the small-membrane protein *MgrB* (formerly *YobG*). PhoP initiates expression of *mgrB*, and *MgrB* in turn inhibits the kinase activity of PhoQ (Lippa and Goulian 2009, Salazar et al. 2016). Once the PhoP RR is phosphorylated, it transcriptionally controls hundreds of target genes (5% of all genes) in *S. Typhimurium* (Belden and Miller 1994, Soncini et al. 1996, Zwir et al. 2005, Harari et al. 2010, Zwir et al. 2012). The PhoQ/PhoP system reaches maximum activity around pH 5.0, which corresponds to the pH of the macrophage phagosomes (Alpuche Aranda et al. 1992, Rathman et al. 1996, Bearson et al. 1998). PhoP-dependent gene regulation itself depends on phosphorylated PhoP amounts, which are affected by numerous factors including PhoP acetylation, feedback loops, proteolysis by ClpSAP, the Mg^{2+} transporter *MgtA*, *EIIA^{Ntr}*, and others, as reviewed in Groisman et al. (2021). In *E. coli*, the PhoP regulon includes several AR genes, including *hdeD*, *hdeAB*, and the central Gad system regulators *gadW* and *gadE* (Belden and Miller 1994, Zwir et al. 2005, Eguchi et al. 2011).

Only in *S. Typhimurium*, protons have been shown to be directly sensed by PhoQ (Prost et al. 2007, Hicks et al. 2015, Choi and Groisman 2016). Nuclear magnetic resonance studies show that the PhoQ periplasmic sensor domain undergoes a conformational change at mildly acidic pH levels and involves a network of residues surrounding His157 (Prost et al. 2007). Moreover, α -helices 4 and 5 in this domain may act as potential pH-responsive structural elements altering the dynamic behavior of PhoQ in an acid-dependent manner. Introducing a nonphysiological disulfide bond between the substitutions Trp104Cys and Ala128Cys restrains flexibility in α -helices 4 and 5 of the periplasmic domain and subsequently impairs PhoP-mediated gene expression during acid stress (Hicks et al. 2015). However, those results have been challenged by the findings of Choi and Groisman (2016), who discovered three residues in the cytoplasmic PhoQ domain (Asp233, His409, and Gln460) that are indispensable for pH sensing (Fig. 4). Their results also indicate that PhoQ senses acidic pH exclusively in the cytoplasm, as *in vivo* experiments demonstrate that mutants lacking the PhoQ transmembrane and periplasmic regions, as well as chimeras with the EnvZ periplasmic domain, still respond to acidity. Nevertheless, it remains elusive whether protons itself are sensed by the critical amino acids in the cytoplasm or rather a different stimulus which is triggered by intracellular acidification (Choi and Groisman 2016, Groisman et al. 2021).

In addition to sensing low pH, PhoQ in *S. Typhimurium* and *E. coli* can sense a wide variety of other signals, including divalent cations (Mg^{2+} , Mn^{2+} , and Ca^{2+}), hyperosmotic stress, the periplasmic redox state, and acetate (Groisman et al. 2021). Antimicrobial peptides (AMPs) and long-chain unsaturated fatty acids can be bound by the periplasmic PhoQ domain in *Salmonella* (Bader et al. 2003, Shprung et al. 2012, Viarengo et al. 2013, Carabajal et al. 2020). Protons and AMPs are presumably sensed via distinct signaling mechanism as they have additive effects on PhoQ activation, whereas divalent cations and AMPs compete for binding in the periplasmic domain (Bader et al. 2005, Prost et al. 2007, Hicks et al. 2015). Remarkably, in the nonpathogenic strain *Salmonella bongori*, Mg^{2+} and AMPs can be sensed, but mildly acidic pH levels do not trigger PhoP-dependent gene expression, presumably because the crucial residues involved in cytoplasmic pH sensing (Fig. 4) are not conserved in *S. bongori* (Choi and Groisman 2016). In *E. coli*, only His409 but not Asp233 and Glu460 are conserved, which supports the idea that protons are not directly, but rather indirectly sensed via EvgS and *SafA*. A further critical residue for signaling in *E. coli* PhoQ is Asn202 in the second transmembrane helix. A substitution with other hydrophobic residues after exposure to Mg^{2+} results in disrupted signal propagation and failed expression of PhoP-activated genes (Goldberg et al. 2010).

ToxR-like receptor CadC

Unlike EvgS and PhoQ, CadC belongs to the one-component signal transduction systems (ToxR-like family) of transcriptional regulators. These low-copy membrane-integrated receptors combine sensory and transcriptional regulatory functions in one polypeptide (Miller et al. 1987). ToxR controls virulence in *V. cholerae*. Nevertheless, other members of this family contribute to virulence, acidic stress response and biofilm and type VI pilus formation (DiRita and Mekalanos 1991, Merrell and Camilli 2000, Stelzer et al. 2006). These receptors have a conserved modular composition: a C-terminal periplasmic sensor domain that senses external stimuli and a single transmembrane helix to transduce the signal to the N-terminal cytoplasmic winged helix-turn-helix DNA-binding domain, which then regulates gene expression. This signal transduction is independent from chemical modifications (Miller et al. 1987).

In 2011, the crystal structure of the periplasmic domain of *E. coli* CadC was solved (Eichinger et al. 2011). This sensory domain consists of two subdomains: the N-terminal subdomain comprises a mixture of parallel and antiparallel β -sheets and a three-helix-bundle, and the C-terminal subdomain is a pure bundle of 11 α -helices. Distinct amino acids within the periplasmic sensory domain of CadC are responsible for dimerization, pH sensory function, and feedback inhibition by cadaverine. To detect alterations in external pH, a cluster of negatively charged amino acids, namely Asp198, Asp200, Glu461, Glu468, and Asp471, are essential (Fig. 4). This negatively charged patch extends across the N- and the C-terminal subdomains. It is proposed that protonation of this cluster at the dimer interface within the periplasmic domain of CadC enables conformational changes resulting in dimerization and signal transduction (Eichinger et al. 2011, Haneburger et al. 2011, 2012, Buchner et al. 2015, Schlundt et al. 2017).

HK SsrA

The HK/RR system *SsrA/SsrB* of *S. Typhimurium* controls, amongst others, the virulence genes encoded in the *Salmonella pathogenicity island 2* (SPI-2), which are required for intracellular survival in host cells. *SsrA* signaling requires acidification of

the cytoplasm of *S. Typhimurium* due to the acidic environment of the macrophage vacuole of the host in which the bacteria reside. Response to external acidification is integrated through SsrA, whereas acidification of the cytoplasm affects the RR SsrB. As shown in Fig. 4, five histidine residues in the C-terminal end of the periplasmic sensor domain are important for the full acid-responsiveness of SsrA (Mulder et al. 2015). Yet, an SsrA variant lacking the important histidine residues of the periplasmic domain shows basal activity at neutral pH, similar to the activity of wild type. As no single histidine is responsible for the full acid activation of SsrA, Mulder et al. (2015) concluded that the concerted action of multiple histidine residues is needed, as with the diphtheria toxin T domain (Perier et al. 2007).

Acidification of the cytosol induces conformational changes in SsrB, increasing its affinity to bind to DNA (Liew et al. 2019). This pH-dependent DNA-binding of SsrB has been shown by atomic force microscopy and single-particle tracking assays. Binding of PhoP or OmpR is not pH-sensitive; thus, acid-dependent DNA binding of SsrB is not an intrinsic property of transcriptional regulators (Liew et al. 2019). Nevertheless, *S. Typhimurium* acidifies its cytoplasm in an OmpR-dependent manner by repressing the CadC-regulated *cadBA* operon (Chakraborty et al. 2015). Moreover, the HK/RR system EnvZ/OmpR upregulates the SsrA/SsrB system upon stimulation by acid stress by directly activating the *ssrAB* promoter (Lee et al. 2000, Garmendia et al. 2003, Fass and Groisman 2009, Chakraborty et al. 2015, Liew et al. 2019). The EnvZ/OmpR system integrates acidic pH, absence of Ca²⁺ and low osmolarity (Garmendia et al. 2003) and is required for the replication and survival (Lee et al. 2000) of *Salmonellae* in macrophages. It also is necessary for full virulence in mice (Dorman et al. 1989, Chatfield et al. 1991). Overall, instead of recovering from acid stress, *S. Typhimurium* use the acidification of its cytoplasm as a signal to activate on the one hand PhoQ (Choi and Groisman 2016) and on the other hand its pathogenesis via SsrB that upregulates the expression and secretion of SPI-2 effector proteins (Kenney 2019).

HK PmrB

In addition to the SsrA/SsrB and PhoQ/PhoP systems, *S. Typhimurium* also possess the PmrB/PmrA HK/RR system, which is involved in perceiving extracellular acidic conditions. The HK PmrB is activated in mildly acidic conditions (pH 5.8), and the RR PmrA promotes transcription of several genes (Perez and Groisman 2007). PmrB and PmrA are required for various pathways, such as virulence in mice (Gunn et al. 2000), infection of chicken macrophages (Zhao et al. 2002), growth in soil (Chamnongpol et al. 2002), resistance to the cationic peptide antibiotic polymyxin B (Roland et al. 1993), and resistance to Fe³⁺ (Wösten et al. 2000) and Al³⁺ (Nishino et al. 2006). For full acid-responsiveness of PmrB, a histidine and four glutamic acid residues in the periplasmic domain of PmrB are required (Fig. 4) (Perez and Groisman 2007). Sub-millimolar levels of extracellular Fe³⁺ or Al³⁺ are perceived directly by PmrB (Wösten et al. 2000), and low concentrations of extracellular Mg²⁺ (Soncini and Groisman 1996) trigger transcription of PmrA-activated genes. The activation of PmrA by low extracellular Mg²⁺ levels occurs via activated PhoQ, which directly senses the extracellular Mg²⁺, followed by phosphorylation of its cognate RR PhoP, which then activates transcription of *pmrD*. PmrD then promotes phosphorylation of PmrA and inhibits PmrB-promoted dephosphorylation of phosphorylated PmrA (Kox et al. 2000, Kato and Groisman 2004). Multiple signals are integrated into two-

component systems similar to the signal transduction cascades in eukaryotes.

HK ArsS

The human gastric pathogen *H. pylori* is extremely well-adapted to the fluctuating low-pH conditions in the human stomach. This adaptation is mainly mediated via the NH₃-producing enzyme urease, which is essential for maintaining neutral pH in both the cytoplasm and periplasm. Urease-independent mechanisms are likely to contribute to acid adaptation. In response to low pH, hundreds of genes are regulated, including the urease gene cluster, as identified by four independent studies performing genome-wide transcriptional profiling (Merrell et al. 2003, Wen et al. 2003, Bury-Moné et al. 2004, Pflock et al. 2006).

The ArsS/ArsR HK/RR system is the main regulator for the acid response. An acidic pH of 5.0 triggers autophosphorylation of ArsS, followed by the subsequent phosphorylation of its cognate RR, ArsR. Phosphorylated ArsR then acts both as an activator and repressor of pH-responsive genes (Pflock et al. 2006). To perceive low pH, the histidine residue at position 94 of ArsS is crucial (Fig. 4). Moreover, depending on the degree of protonation of several acidic amino acids in the periplasmic domain, ArsS can adopt different conformations resulting in different activation states to allow a gradual transcriptional response to moderate low pH conditions (pH 5.0). Müller et al. (2009) concluded that pH sensing by ArsS does not rely exclusively on protonation of histidine residues but rather on protonatable amino acids other than histidine that contribute substantially to acidity. The acid-induced upregulation of the urease gene cluster requires the sensor kinase ArsS but not phosphorylation of the RR ArsR. Although ArsR phosphorylation increases expression of the urease gene cluster, it is not required for acid survival.

Chemoreceptors Tar and Tsr

Tar and Tsr are required to navigate *E. coli* to a desired intermediate pH level and to physically avoid habitats with extreme pH levels. Both receptors form clusters that associate with the adaptor protein CheW and the HK CheA, resulting in initiation of a signal transduction cascade and ultimately in regulation of the flagellar motor to navigate the cell to desired environments (Maddock and Shapiro 1993, Kentner et al. 2006, Hazelbauer et al. 2008). Both MCPs can sense internal as well as external pH. Ambient pH is sensed by the periplasmic domains, and residues for sensing the internal pH have been identified in cytoplasmic regions (Krikos et al. 1985). By characterizing chimeras, residues in Tsr (Gly261, Glu262, Arg265, and Asp269) and Tar (Arg259, Ser261, Asp263, and His267) have been identified as crucial in the chemotactic response to alterations of the internal pH (Fig. 4). Interchanging these residues located in the linker region, which connects the second transmembrane helix to the first methylation helix, affects the pH response of Tar and Tsr. While a replacement of Arg259 by the corresponding residue of Tsr reversed the swimming behavior, a substitution of Asp263 or His267 only altered the time course of pH response (Umemura et al. 2002).

Especially for Tsr but also for Tar, adaptive receptor methylation was indicated to fine-tune the strength of the pH response due to a weakened response upon methylation of either receptor. At low pH levels, Tsr is the dominant receptor as it has fewer methylated glutamyl residues and guides the cells toward higher pH values, whereas at alkaline pH levels, Tar is less methylated and dominates the pH response. Moreover, the pH inversion point is affected by culture density-dependent alterations in Tar and Tsr

expression levels (Yang and Sourjik 2012). At high cell densities, the preferential pH point is shifted toward lower pH units as the ratio of Tar/Tsr increases, presumably to avoid nutrient-depleted regions of high cell numbers, which were demonstrated to display more alkaline pH values (Salman and Libchaber 2007, Kalinin et al. 2010, Yang and Sourjik 2012).

Chemoreceptor TlpB

Similar to Tar and Tsr in *E. coli*, TlpB is the crucial receptor for pH taxis in *H. pylori*. In a mouse infection model, *tlpB* mutants were shown to be pH nonresponsive and defective for colonization (Croxen et al. 2006). An atomic resolution structure of the periplasmic domain has been solved by Sweeney et al. (2012), showing that TlpB forms dimers via extracellular urea-binding PAS-domains and contains two transmembrane regions per subunit and a cytoplasmic HAMP domain.

Asp114 in the extracellular PAS-domain of the TlpB dimer is proposed to be the key titratable residue for signaling, while urea acts as a cofactor for acid sensing. In a proposed model, urea binding is weakened via protonation of Asp114 at low pH levels and a structural rearrangement within the PAS-domain is induced. Moreover, urea protects the TlpB periplasmic domain against thermal denaturation in a pH-dependent manner. Thereby, Asp114 accepts two hydrogen bonds from the amide nitrogen atoms of urea at neutral pH and stabilizes the PAS domain. This interaction, however, is disrupted or weakened in acidic environments due to protonation of Asp114. This in turn may cause a loosening of urea binding and partial unfolding of the PAS-domain. Subsequent movement of TM2 relative to TM1 could affect the phosphorylation state of CheA (Sweeney et al. 2012). Little is known about the transcriptional regulation of *tlpB*. The only thus far identified protein to bind the promoter region of *tlpB* is the orphan RR HP1043 (Delany et al. 2002).

Transcriptional regulator AphB

In addition to membrane integrated proteins, also cytosolic regulators like AphB have been described to harbor pH-sensing residues. AphB is an important regulator in several *Vibrio* spp. for adapting to environmental conditions and pathogenicity. AphB belongs to the family of LysR-type transcriptional regulators (LTTR), one of the largest families of regulators in prokaryotes (Maddocks and Oyston 2008). Together with the quorum sensing-regulated activator AphA, AphB_{Vc} activates the virulence cascade via *tcpPH* expression of the human pathogen *V. cholerae* (Kovacikova and Skorupski 1999). AphB_{Vc} also regulates several genes involved in pH regulation like CadC (Kovacikova et al. 2010). In *V. cholerae*, low pH and anaerobiosis are the two environmental signals leading to activation of AphB (Kovacikova et al. 2010).

Taylor et al. (2012) solved the crystal structure of full-length AphB_{Vc}, showing that AphB forms a tetramer by dimerization of dimers like other members of the LTTR family. AphB consists of an N-terminal winged helix DNA-binding domain and a C-terminal regulatory domain. The DNA-binding domain is formed by three α -helices ($\alpha 1$ – $\alpha 3$) followed by two β -strands that form the wing. The C-terminal regulator domain has two subdomains, RD-I and RD-II, connected by two extended antiparallel β -strands. Their interface harbors a putative ligand-binding pocket formed by hydrophobic and polar amino acids. A total of five residues in the ligand-binding pocket of AphB can render the activity of the protein to nearly constitutive activity, with respect to pH and oxygen, when they are replaced by negatively charged amino acids. These residues are Pro98, Asn100, and Leu101, which are located in the

loop between $\beta 3$ and $\alpha 5$; residue Pro193, located in the loop between $\beta 7$ and $\beta 8$, and residue Leu220 (Fig. 4).

AphB_{Vc} was crystallized alone (wild type) and bound to the DNA (Asn100Glu variant). A comparison of these two structures shows that AphB_{Vc} undergoes a major conformational change to alter the position of the DNA-binding domain (Taylor et al. 2012). These findings also have been observed for AphB in *Vibrio vulnificus*, where AphB_{Vv} affects the expression of more than 10% of the genome, including *cadC* (Jeong and Choi 2008). The crystal structure of the regulatory domain of AphB_{Vv} has been solved and shows high similarity to AphB_{Vc}. The putative ligand binding pocket consists of 12 amino acids (Pro98, Asp100, Leu101, Ser128, Val144, Asp162, His192, Pro193, Leu220, Pro237, Met240, and Arg262). An additional small cavity on the backside of the regulatory domain also has been identified (Lys103, Arg104, Asn221, Asn224, Met240, and Tyr244). Further study is needed to determine if it also contributes to ligand binding (Park et al. 2017).

Phylogenetic occurrence of the Gad, Adi, Cad, and Orn systems in the bacterial kingdom

Enteropathogenic bacteria (e.g. *Escherichia*, *Salmonella*, and *Yersinia*) generally possess several enzyme-based AR systems to survive in highly acidic environments, such as the stomach, and mild acidic ones, such as the caecum and ascending colon, however, this is not the usual case. Overall, the number, architecture and the complexity of regulation of the four main systems, Gad, Adi, Cad, and Orn, vary amongst bacterial species and often reflect an adaptation to their (acidic) habitat (Zhao and Houry 2010). The most widespread systems are the Gad and Orn systems, which co-occur in many Proteobacteria and Firmicutes. Bacterial species such as *Escherichia*, *Shigella*, *Citrobacter*, *Hafnia*, and *Serratia* have all four enzyme-based AR systems; *Salmonellae* have the Adi, Cad, and Orn systems; whereas the Gram-positive *Lactococcus* (Amachi et al. 1998, Sanders et al. 1998, O'Sullivan and Condon 1999) and *Listeria* (Davis et al. 1996, Cotter et al. 2001a, Arcari et al. 2020) possess the Gad system only (Zhao and Houry 2010). Species, like *Vibrio* spp. that generally are more sensitive to acid (Brenneman et al. 2014, Brameyer et al. 2020), contain only the Cad and Orn systems.

The different number of enzyme-based AR systems in the various bacteria is also reflected by the number of bacteria required to cause infection in humans. For example, *Shigella* spp. have a uniquely low infective dose of only 10–100 *Shigella* cells, whereas *Vibrio cholerae* infection requires about 10⁸ organisms and *Salmonella* infection requires 10⁵ to 10⁷ (Table 1). *Escherichia* and *Shigella* spp. are the most acid-resistant neutralophilic bacteria. The *E. coli* K12 lab strains DH5 α and MC4100 are as acid resistant as naturally occurring *E. coli* isolates (Gorden and Small 1993).

Pseudomonas spp. contain only the Orn system (Brameyer et al. 2022), which generally plays a minor role in AR, but are additionally equipped with deiminase and urease systems to withstand acidic environments.

The Gad system plays an important role for commensal and pathogenic bacteria, such as *E. coli* and *S. flexneri* (Waterman and Small 2003, Bhagwat and Bhagwat 2004), and it was recently identified in *Yersinia* (Foster 2004, Biase and Pennacchietti 2012, Pennacchietti et al. 2018, Brameyer et al. 2022), *Clostridium* (Villarreal et al. 2000, Tennant et al. 2007, Biase and Pennacchietti 2012), *Listeria monocytogenes* (Cotter et al. 2001a, 2001b), *Lactobacillus brevis* (Gong et al. 2019) and *Lactococcus lactis* (Sanders et al. 1998, O'Sullivan and Condon 1999). See Table 2 and Fig. 5 for details

Table 1. Infective doses of food-borne pathogens.

Pathogen	Infective dose	Reference
Enterohemorrhagic <i>E. coli</i> (EHEC)	< 50	Tilden et al. (1996)
<i>Brucella</i> spp.	< 10	Román et al. (2013)
<i>Shigella</i> spp.	10–100	Sansonetti (2001)
<i>Salmonella</i> spp.	10 ⁵ –10 ⁷	D'Aoust et al. (2001)
<i>Vibrio cholerae</i>	10 ⁴ –10 ⁸	Cash et al. (1974)
<i>Yersinia enterocolitica</i>	10 ⁴ –10 ⁹	Bottone (1997)
<i>Campylobacter jejuni</i>	500–800	Robinson (1981)
<i>Clostridium perfringens</i>	10 ⁷	Brynstad and Granum (2002)
<i>Listeria monocytogenes</i>	> 100 bacteria/g*	Swaminathan (2001)

*Number in contaminated food responsible for foodborne human cases.

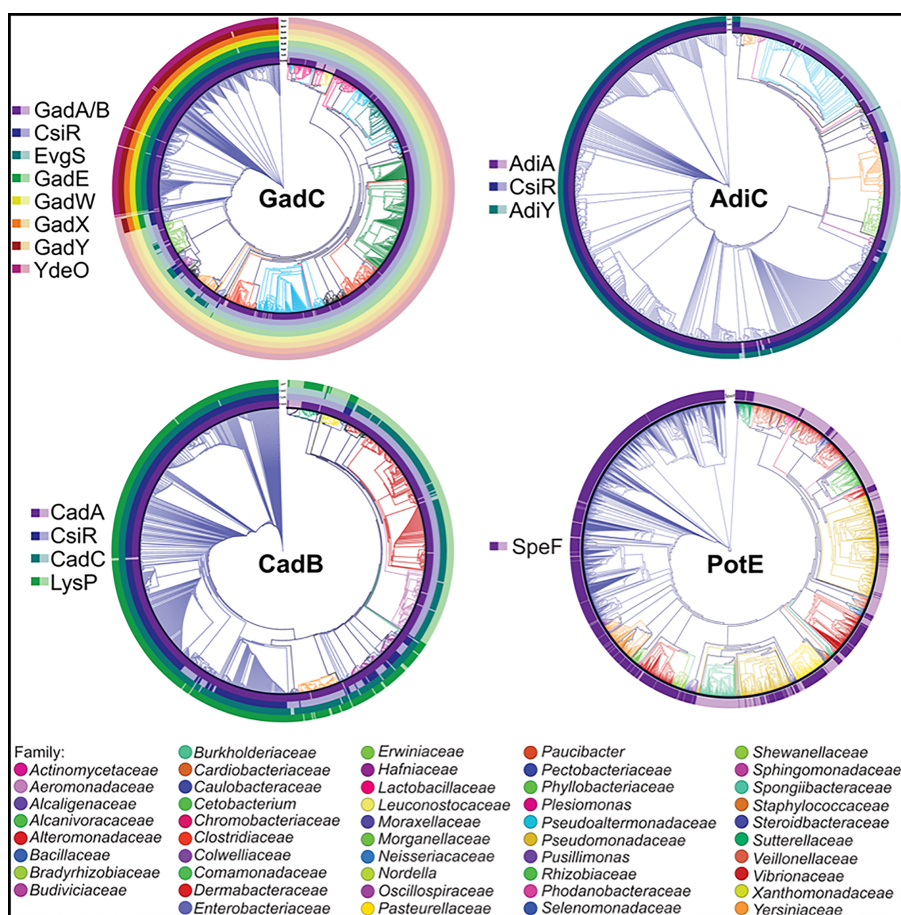


Figure 5. Phylogenetic trees of the *E. coli* antiporters GadC, AdiC, CadB, and PotE and co-occurring regulators within the bacterial kingdom. The protein sequences of 1112 of *E. coli* GadC homologs (upper left) were aligned, and a phylogenetic tree was generated. The presence of different regulatory components CsiR, EvgS, GadE, GadW, GadX, GadY, and YdeO and the decarboxylases GadA and GadB (GadA/B) is indicated by solid colors in the respective ring layer. Translucent colors represent components that were not detected. The protein sequences of 756 *E. coli* AdiC homologs (upper right) were aligned, and a phylogenetic tree was generated. The presence of the different regulatory components CsiR and AdiY as well as the decarboxylase AdiA is indicated by solid colors in the respective ring layer. If these components were not found, the colors are translucent. The protein sequences of 857 *E. coli* CadB homologs (lower left) were aligned, and a phylogenetic tree was generated. The presence of the different regulatory components CsiR, CadC, and LysP as well as the decarboxylase CadA are indicated by solid colors in the respective ring layer. Translucent colors represent components that were not detected. The protein sequences of 2577 *E. coli* PotE homologs (lower right) were aligned, and a phylogenetic tree was generated. The presence of the decarboxylase SpeF is indicated by solid colors in the respective ring layer. See legend of Table 2 for more details. Each phylogenetic tree is shown as a circular cladogram. For each phylogenetic tree the branches of the tree were colored according to the family of the organisms containing a GadC, AdiC, CadB, or PotE homolog, respectively.

on these and other bacteria discussed in this section.

Regulation of the Gad system has been studied in great detail in *E. coli* (see above). The regulators responsible for the sophisticated regulation of the Gad, Adi, and Cad systems of *E. coli* (Fig. 3) are

present mainly in the *Enterobacteriaceae* family. The central regulator of the Gad system, GadE, is found in *Escherichia* and *Shigella*, as well as other *Enterobacteriaceae* species, such as *Citrobacter freundii* and *Kluyvera ascorbate* (Fig. 5) (Brameyer et al. 2022). The carbon-

induced starvation transcriptional regulator CsiR is a member of the GntR-family and mainly occurs in γ -proteobacteria. A total of 30.3% of species containing a GadC homolog possess an CsiR homolog (Fig. 5). Comparison of GadB homologs from Gram-positive and Gram-negative enteric bacteria shows that 84 residues (18% of the *E. coli* GadB sequence) are strictly conserved, including residues at critical positions in or near the active site of *E. coli* GadB or at sites of conformational change. Moreover, eight residues that are shared with group II decarboxylases may serve as signatures for bacterial glutamate-dependent AR (Biase and Pennacchietti 2012).

Besides using ureases to encounter acidic threats, *Brucella microti* also uses the Gad system to increase AR and oral infection in mice (Occhialini et al. 2012). An intact *gadBC* operon helps *B. microti* to survive in acidic soils and supports intracellular survival, such as within host macrophages (Audic et al. 2009). In 2015, Damiano et al. (2015) investigated the functionality of the Gad system among a collection of strains belonging to the *Brucella* genus and showed that not all species could export GABA and survive at extremely low pH levels; the authors thus concluded that the Gad system may reflect the adaptive evolution of *Brucella* spp.

In addition to the variations in bacterial AR systems, the architecture of individual AR systems also can vary. For example, the number of glutamate decarboxylases (up to three) and number of antiporters (up to two) varies in some bacteria, such as *Edwardsiella tarda*, *L. brevis*, and *L. monocytogenes* (Cotter et al. 2001a, 2001b, Cotter et al. 2005, Karatzas et al. 2010, Feehily and Karatzas 2013). Moreover, *E. coli* (Smith et al. 1992) and *S. flexneri* (Waterman and Small 2003) each contain two glutamate decarboxylases, GadA and GadB (Feehily and Karatzas 2013).

The Adi and Cad systems are not as widely distributed as the Gad system and occur mainly within γ -proteobacteria in the *Enterobacteriaceae*, *Lysobacteraceae*, *Yersiniaceae*, and *Hafniaceae* families (Brameyer et al. 2022) (see Table 2 and Fig. 5 for details).

However, *S. Typhimurium* is one well-studied example that harbors the Adi (Kieboom and Abee 2006), Cad (Lee et al. 2007), and Orn systems (Viala et al. 2011) (Table 2 and Fig. 5), and its virulent strains are more acid tolerant than its nonvirulent strains (Wilmes-Riesenberg et al. 1996, 1997, Berk et al. 2005). These three systems confer AR in different ways in this serovar. Specifically, the Adi system is effective at extremely acidic pH levels but ineffective during growth at moderately acidic pH levels. The Orn system improves growth at moderately acidic pH levels in the absence of oxygen, but it plays a minor role in survival. The Cad system has a broad range of actions and confers both to significant survival at pH 2.3 and to growth improvement at pH 4.5 in an oxygen-independent manner (Viala et al. 2011). Unlike *E. coli*, in which transcription of *cadC* is constitutive, in *S. Typhimurium*, *cadC* expression is induced by mildly acidic pH levels and by lysine (Lee et al. 2007). Instead of recovering from acid stress, *S. Typhimurium* uses acidity as a signal to control pathogenesis via the action of OmpR, which represses the *cadC/cadBA* module, thereby preventing neutralization of the bacterial cytoplasm (Chakraborty et al. 2015, Kenney 2019). Both the Cad and Orn systems enhance *S. Typhimurium*'s acid tolerance. The *spe* genes (*speB*, *speC*, *speE*, and *speF*) have been shown to contribute to intracellular survival and bacterial replication for 18 h in human epithelial cells and for 21 h in macrophages (Espinel et al. 2016).

Functionality and pH-dependent regulation of the Orn system are less studied, however, the presence of a system does not necessarily indicate its contribution to AR in these species. For example, putrescine is linked to the formation of biofilm (Patel et al. 2006), expression of virulence genes in *S. flexneri* (Durand and

Björk 2003) and the counteraction of toxic effects caused by reactive oxygen species in *E. coli* (Jung and Kim 2003). Nevertheless, the cognate ornithine decarboxylase SpeF of the Orn system has been identified in about two-thirds (63.6%) of species harboring the ornithine/putrescine antiporter PotE, such as *E. coli*, *Shigella boydii*, *S. enterica*, *C. freundii*, and *Serratia fonticola*. Homologs of the ornithine/putrescine antiporter PotE, which belongs to the Orn system, are widely distributed and occur in species belonging to 48 different families of Proteobacteria (e.g. *Enterobacteriaceae*, *Pseudomonaceae*, *Vibrionaceae*, and *Burkholderiaceae*) and several from the phylum Firmicutes (e.g. *Streptococcaceae*, *Yersiniaceae*, *Lactobacillaceae*, and *Clostridaceae*) (see Table 2 and Fig. 5 for details). The Orn system often occurs in conjunction with the other three inducible AR systems, however, it seems to play a minor role in acid adaptation. For example, it plays only a minor role in *E. coli* MG1655 but has a more important function in avian pathogenic *E. coli*, in which growth attenuation occurs after the addition of membrane stress by sodium dodecyl sulfate. This finding suggests that PotE is more involved in membrane stress tolerance than acidic tolerance (Guerra et al. 2018). As previously mentioned, the Orn systems plays only a minor role compared to the Cad system during acid adaptation of *V. cholerae* (Merrell and Camilli 1999) (Table 2 and Fig. 5). Mutation analyses have revealed a significant role of the lysine decarboxylase *cadA*, but not the ornithine decarboxylase *speF* in both inorganic and organic acid adaptation of *V. cholerae* (Merrell and Camilli 1999). In summary, the *E. coli*-specific regulation of the Gad, Adi, Cad, and Orn systems are predominantly conserved in the *Enterobacteriaceae* family. The Gad and Orn systems occur in many bacteria, whereas the Adi and Cad systems are restricted to γ -proteobacteria. Interestingly, the decarboxylases together with their respective cognate antiporters in each system are more widely distributed than known regulatory components. The central regulators of the Cad and Adi systems identified in *E. coli* are more specific to the *Enterobacteriaceae* family.

Functional diversification of bacterial populations under acid stress

Escherichia coli possesses all four enzyme-based H⁺-consuming AR systems (Gad, Adi, Cad, and Orn) and is one of the best studied organisms with respect to acid tolerance (Table 1). Individual cells do not always respond uniformly to different external pH values. The responses can be highly variable depending on the AR system, and each system is activated at different external pH values and growth phases (Fig. 3). This phenotypic heterogeneity can be beneficial for populations under acid stress. Between individual *E. coli* cells pH homeostasis varies (Martinez et al. 2012). Furthermore, persister cells of *E. coli* have a lower intracellular pH that allows survival after antibiotic treatment (Goode et al. 2021). Moreover, the induction of enzyme-based AR systems is regulated by a sophisticated interplay of membrane-integrated and soluble regulators. For example, the noisy activation of the *gadBC* promoter is highly variable under acid stress and supports the survival of single *E. coli* cells by maintaining a sufficient high intracellular pH (Mitosch et al. 2017).

Activation of the Gad, Adi, and Cad systems has been quantitatively analyzed using a fluorescent triple reporter strain under consecutively increasing acid stress conditions in *E. coli* (Brameyer et al. 2022). As shown in Fig. 6, the Cad system shows the highest heterogeneous distribution of the three systems when activated at pH 5.8 in the presence of lysine. The Adi system is activated heterogeneously under moderate acid stress (pH 4.4), though simultaneous activation of the Cad and Adi systems does not occur.

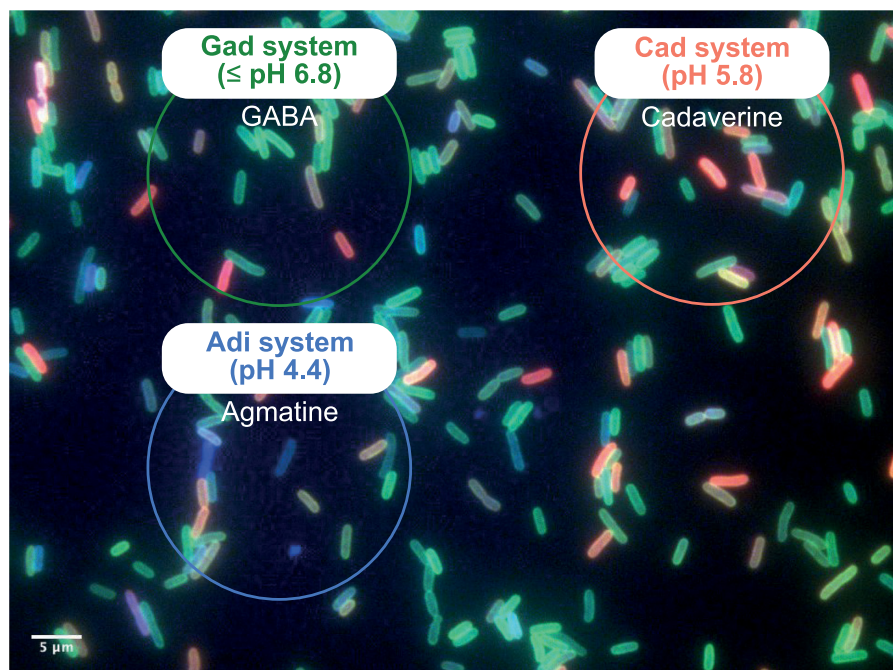


Figure 6. Model of the heterogeneous activation of enzyme-based AR systems and division of labor in the *E. coli* population. Fluorescent microscopic image of the three-color reporter strain *E. coli gadC:eGFP-adiC:mCerulean-cadB:mCherry* at pH 4.4 in a complex medium. All cells of the *E. coli* population individually adapt to acid stress by activating the Gad system to varying degrees (green fluorescent cells), due to multiple extracellular and intracellular inputs, and secrete GABA. Under mild to moderate acid stress (pH 5.8–4.4), some cells in the population activate the Cad system (red fluorescent cells), while others activate the Adi system (blue fluorescent cells). These cells secrete (as indicated by the rings) the more alkaline products cadaverine and agmatine, respectively, thereby contributing to acid-stress relief with an increase of the extracellular pH, which benefits the whole population (Brameyer et al. 2022).

Under almost all conditions, bacterial cells activate the Gad system to varying degrees, primarily using intracellularly available glutamate by consuming protons to raise their internal pH. In response to high acid stress, glutamic acid is imported and GABA excreted. Heterogeneous activation of the Cad and Adi systems is driven by the low copy numbers of their main regulators CadC and AdiY (Brameyer et al. 2020, 2022). Furthermore, CadC itself is distributed heterogeneously (Brameyer et al. 2019). An artificial increase in the copy number of these regulators leads to reduced heterogeneity and a growth disadvantage under acid stress, representing a metabolic burden for individual cells (Brameyer et al. 2020, 2022).

Although Adi and Cad system activation occurs only in a sub-population of cells, the whole population benefits from the elevated external pH via secretion of the polyamine compounds cadaverine and agmatine, which are considered common goods (Fig. 6). The extent to which microcolonies of *E. coli* exist in the colon, where cadaverine and agmatine can change the microclimate, remains unclear. Additionally, the internal pH of these cells is elevated by consuming protons during the conversion of lysine to cadaverine and arginine to agmatine, respectively (Brameyer et al. 2022). Overall, the heterogeneous activation of these three enzyme-based AR systems enables division of labor in the bacterial population, which ensures its survival over a wide range of low pH values (Fig. 6).

In contrast to *E. coli*, *V. campbellii* is more acid sensitive and uses mainly the Cad system to counteract acidic conditions. Additionally, its CadC signaling system is simpler, as CadC lacks the regulatory inputs by LysP and the polyproline motif known from *E. coli* CadC (see above). Without this tight regulation, all the cells of the *V. campbellii* population activate the Cad system, which is important, as the Cad system is the main AR system in this bac-

terium (Brameyer et al. 2020). Although the presence and function of the variety of AR systems are well-described in several bacterial species, their behavior at single cell level and specific niches is highly unexplored yet.

Concluding remarks

Bacteria have sophisticated and varying mechanisms for sensing and adapting to acidity. Depending on the bacterial genus, the number and complexity of AR mechanisms vary greatly, which is best reflected in the number of bacteria that survive challenging environments, such as the human stomach, and thus contribute to bacterial pathogenesis (Table 1). For example, *Escherichia* and *Shigella* spp. have the most complex regulatory network and are extremely acid-resistant, followed by *Salmonella* and *Brucella* spp., whereas *Yersinia* and *Vibrio* spp. are less acid-resistant.

At the population level, there is strong evidence for the heterogeneous behavior of individual cells in response to acid stress (Mitosch et al. 2017, Smith et al. 2018, Brameyer et al. 2020, 2022). In *E. coli*, functional diversification of several AR mechanisms in single cells allows division of labor and energy conservation to ensure that at least a small percentage of the population survives even the most acidic conditions (e.g. pH 1–3). The cells' regulatory networks also affect their behavior. For example, implementing additional components or reducing the network to basic components allows heterogeneous activation of the Cad system in *Escherichia* spp., whereas it is homogeneous in *Vibrio* spp. (Brameyer et al. 2020). Further studies are required to analyze the single-cell acid stress response in more species, preferably in mixed bacterial communities and in natural environments. This analysis also could identify differences in responses to inorganic and organic acids (Wilks and Slonczewski 2007).

pH is one of the most important parameters for bacterial interactions (Ratzke and Gore 2018). The human and animal caecum and colon are characterized by dense communities of numerous obligate anaerobic fermenting bacteria that produce a variety of short-chain fatty acids resulting in a low pH environment. Depending on the acidity and availability of amino acids (e.g. glutamic acid, lysine, arginine, and ornithine), decarboxylase-dependent systems are activated in Proteobacteria phylum members. These systems produce GABA (an important neurotransmitter); cadaverine, agmatine, and putrescine (polyamines used by prokaryotes and eukaryotes) and histamine (an allergen). However, it is unclear how these molecules change the microenvironment and to what extent they affect the host. In fact, the levels of putrescine and cadaverine are found to increase 15-fold and 3-fold, respectively, in inflamed mouse intestine monocolonized with *E. coli*, compared to an equally colonized healthy mouse cohort (Kitamoto et al. 2020). Further studies are needed to better understand the adaptation of complex communities to partially self-caused acid stress and the effects of the involved metabolites on the host.

Neutralophilic bacteria can maintain a constant intracellular pH under most conditions. However, under strong acid stress (pH < 4.4) or amplification of stress by weak organic acids, such as acetate, the cytoplasmic pH decreases (e.g. by about one pH unit in *E. coli*) (Wilks and Slonczewski 2007). A lower intracellular pH affects all macromolecules in cells and can reduce enzyme activity, acid-induced protein unfolding, membrane damage, and DNA damage. Some bacteria use low intracellular pH as a stimulus to induce other mechanisms. For example, in the acidic environment of the macrophage vacuole, *S. Typhimurium* induces virulence genes encoded in its pathogenicity island SPI-2. This induction depends on the SsrA/SsrB system, which requires acidification of the cytoplasm for activation (Liew et al. 2019). Once in the vacuole, *S. Typhimurium* acidifies its cytoplasm in an OmpR-dependent manner by repressing the CadC-regulated *cadBA* operon (Chakraborty et al. 2015). Thus, intracellular acidification of *Salmonella* spp. provides an important signal for expression of the SPI-2 type III secretion system. Recent evidence also shows that acidification of the cytoplasm in *E. coli* is linked to antibiotic resistance (Reyes-Fernández and Schuldiner 2020). The authors analyzed two mutants, derived by laboratory evolution, that are resistant to norfloxacin and chloramphenicol. They found that intracellular pH was significantly lower in the mutants than of the parental strain. The mediators of this relationship between cytoplasmic acidification and antibiotic resistance are not yet known. Interestingly, persister cells of *E. coli* display a lower intracellular pH, allowing survival after antibiotic treatment (Goode et al. 2021). Further work is needed to elucidate the mechanism by which acidification is related to virulence and antibiotic resistance.

Finally, we would like to highlight an important applied aspect for future research on acid stress resistance in bacteria. Probiotic bacteria are becoming increasingly important for their pharmaceutical value in maintaining and improving gut microbiota. So-called superfoods are marketed as products that provide nutritional value and health benefits. However, the incorporation of probiotics into food remains a challenge as the number of live bacteria declines during manufacturing and storage and especially during gastrointestinal transit (Palanivelu et al. 2022).

In summary, a better understanding of the mechanisms of AR of bacteria that have evolved during evolution has great potential for infection biology, microbiome research, and ecology.

Authors' contributions

All authors wrote the manuscript and gave final approval for publication.

Acknowledgments

We thank all current and former members of the research group for their important contributions to this work. Figure 1 and the graphical abstract were created with BioRender.com.

Conflict of interest. The authors declare no conflict of interest.

Funding

Research of K.J. was funded by the Deutsche Forschungsgemeinschaft (DFG, German Research Foundation)—Project numbers 269423233 (TRR 174), 395357507 (SFB1371) and 471254198 (JU270/22–1).

References

- Accardi A, Miller C. Secondary active transport mediated by a prokaryotic homologue of ClC Cl⁻ channels. *Nature* 2004;**427**:803–7. DOI : 10.1038/nature02314.
- Ali Azam T, Iwata A, Nishimura A et al. Growth phase-dependent variation in protein composition of the *Escherichia coli* nucleoid. *J Bacteriol* 1999;**181**:6361–70.
- Alpuche Aranda CM, Swanson JA, Loomis WP et al. *Salmonella typhimurium* activates virulence gene transcription within acidified macrophage phagosomes. *Proc Natl Acad Sci* 1992;**89**:10079–83. DOI: 10.1073/pnas.89.21.10079.
- Alvarez-Ordóñez A, Fernández A, López M et al. Relationship between membrane fatty acid composition and heat resistance of acid and cold stressed *Salmonella senftenberg* CECT 4384. *Food Microbiol* 2009;**26**:347–53. DOI: 10.1016/j.fm.2008.11.002.
- Amachi S, Ishikawa K, Toyoda S et al. Characterization of a mutant of *Lactococcus lactis* with reduced membrane-bound ATPase activity under acidic conditions. *Biosci Biotechnol Biochem* 1998;**62**:1574–80. DOI: 10.1271/bbb.62.1574.
- Angelis M de, Mariotti L, Rossi J et al. Arginine catabolism by sourdough lactic acid bacteria: purification and characterization of the arginine deiminase pathway enzymes from *Lactobacillus sanfranciscensis* CB1. *Appl Environ Microbiol* 2002; **68**:6193–201. DOI: 10.1128/AEM.68.12.6193-6201.2002.
- Applebaum DM, Dunlap JC, Morris DR. Comparison of the biosynthetic and biodegradative ornithine decarboxylases of *Escherichia coli*. *Biochemistry* 1977;**16**:1580–4. DOI: 10.1021/bi00627a008.
- Aquino P, Honda B, Jaini S et al. Coordinated regulation of acid resistance in *Escherichia coli*. *BMC Syst Biol* 2017;**11**. DOI: 10.1186/s12918-016-0376-y.
- Arcari T, Feger M-L, Guerreiro DN et al. Comparative review of the responses of *Listeria monocytogenes* and *Escherichia coli* to low pH stress. *Genes* 2020;**11**:1330. DOI: 10.3390/genes11111330.
- Audia JP, Webb CC, Foster JW. Breaking through the acid barrier: an orchestrated response to proton stress by enteric bacteria. *Int J Med Microbiol* 2001;**291**:97–106. DOI: 10.1078/1438-4221-00106.
- Audic S, Lescot M, Claverie J-M et al. *Brucella microti*: the genome sequence of an emerging pathogen. *BMC Genomics* 2009;**10**:352. DOI: 10.1186/1471-2164-10-352.
- Bader MW, Navarre WW, Shiao W et al. Regulation of *Salmonella typhimurium* virulence gene expression by cationic antimicrobial peptides. *Mol Microbiol* 2003;**50**:219–30. DOI: 10.1046/j.1365-2958.2003.03675.x.

- Bader MW, Sanowar S, Daley ME et al. Recognition of antimicrobial peptides by a bacterial sensor kinase. *Cell* 2005;**122**:461–72. DOI: 10.1016/j.cell.2005.05.030.
- Bak G, Han K, Kim D et al. Roles of *rpoS*-activating small RNAs in pathways leading to acid resistance of *Escherichia coli*. *Microbiologyopen* 2014;**3**:15–28. DOI: 10.1002/mbo3.143.
- Bandara AB, Contreras A, Contreras-Rodriguez A et al. *Brucella suis* urease encoded by *ure1* but not *ure2* is necessary for intestinal infection of BALB/c mice. *BMC Microbiol* 2007;**7**. DOI: 10.1186/1471-2180-7-57.
- Bearson BL, Wilson L, Foster JW. A low pH-inducible, PhoPQ-dependent acid tolerance response protects *Salmonella typhimurium* against inorganic acid stress. *J Bacteriol* 1998;**180**:3734. DOI: 10.1128/JB.180.9.2409-2417.1998.
- Bearson S, Bearson B, Foster JW. Acid stress responses in enterobacteria. *FEMS Microbiol Lett* 1997;**147**:173–80. DOI: 10.1111/j.1574-6968.1997.tb10238.x.
- Belden WJ, Miller SI. Further characterization of the PhoP regulon: identification of new PhoP-activated virulence loci. *Infect Immun* 1994;**62**:5095–101.
- Ben-Zvi T, Pushkarev A, Seri H et al. mRNA dynamics and alternative conformations adopted under low and high arginine concentrations control polyamine biosynthesis in *Salmonella*. *PLoS Genet* 2019;**15**:e1007646. DOI: 10.1371/journal.pgen.1007646.
- Berg HC, Brown DA. Chemotaxis in *Escherichia coli* analysed by three-dimensional tracking. *Nature* 1972;**239**:500–4. DOI: 10.1038/239500a0.
- Berg HC. Dynamic properties of bacterial flagellar motors. *Nature* 1974;**249**:77–9. DOI: 10.1038/249077a0.
- Berk PA, Jonge R, Zwietering MH et al. Acid resistance variability among isolates of *Salmonella enterica* serovar typhimurium DT104. *J Appl Microbiol* 2005;**99**:859–66. DOI: 10.1111/j.1365-2672.2005.02658.x.
- Bhagwat AA, Bhagwat M. Comparative analysis of transcriptional regulatory elements of glutamate-dependent acid-resistance systems of *Shigella flexneri* and *Escherichia coli* O157:H7. *FEMS Microbiol Lett* 2004;**234**:139–47. DOI: 10.1111/j.1574-6968.2004.tb09525.x.
- Biase D de, Pennacchietti E. Glutamate decarboxylase-dependent acid resistance in orally acquired bacteria: function, distribution and biomedical implications of the *gadBC* operon. *Mol Microbiol* 2012; **86**:770–86. DOI: 10.1111/mmi.12020.
- Biase D de, Tramonti A, Bossa F et al. The response to stationary-phase stress conditions in *Escherichia coli*: role and regulation of the glutamic acid decarboxylase system. *Mol Microbiol* 1999;**32**:1198–211. DOI: 10.1046/j.1365-2958.1999.01430.x.
- Blankenhorn D, Phillips J, Slonczewski JL. Acid- and base-induced proteins during aerobic and anaerobic growth of *Escherichia coli* revealed by two-dimensional gel electrophoresis. *J Bacteriol* 1999;**181**:2209–16.
- Blethen SL, Boeker EA, Snell EE. Arginine decarboxylase from *Escherichia coli*. I. Purification and specificity for substrates and coenzyme. *J Biol Chem* 1968;**243**:1671–7.
- Bobrovskyy M, Vanderpool CK. Diverse mechanisms of post-transcriptional repression by the small RNA regulator of glucose-phosphate stress. *Mol Microbiol* 2015;**99**:254–73. DOI: 10.1111/mmi.13230.
- Boets E, Deroover L, Houben E et al. Quantification of in vivo colonic short chain fatty acid production from inulin. *Nutrients* 2015;**7**:8916–29. DOI: 10.3390/nu7115440.
- Booth IR. Regulation of cytoplasmic pH in bacteria. *Microbiol Rev* 1985;**49**:359–78.
- Bordi C, Thérault L, Méjean V et al. Anticipating an alkaline stress through the Tor phosphorelay system in *Escherichia coli*. *Mol Microbiol* 2003;**48**:211–23. DOI: 10.1046/j.1365-2958.2003.03428.x.
- Bottone EJ. *Yersinia enterocolitica*: the charisma continues. *Clin Microbiol Rev* 1997;**10**:257–76. DOI: 10.1128/CMR.10.2.257.
- Bougdour A, Cuning C, Baptiste PJ et al. Multiple pathways for regulation of σ^S (RpoS) stability in *Escherichia coli* via the action of multiple anti-adaptors. *Mol Microbiol* 2008;**68**:298–313. DOI: 10.1111/j.1365-2958.2008.06146.x.
- Brahmachari U, Gonthier JF, Sherrill CD et al. Water bridges conduct sequential proton transfer in photosynthetic oxygen evolution. *J Phys Chem B* 2019;**123**:4487–96. DOI: 10.1021/acs.jpcc.9b01523.
- Brameyer S, Hoyer E, Bibinger S et al. Molecular design of a signaling system influences noise in protein abundance under acid stress in different γ -Proteobacteria. *J Bacteriol* 2020;**202**. DOI: 10.1128/JB.00121-20.
- Brameyer S, Rösch TC, El Andari J et al. DNA-binding directs the localization of a membrane-integrated receptor of the ToxR family. *Commun Biol* 2019;**2**. DOI: 10.1038/s42003-018-0248-7.
- Brameyer S, Schumacher K, Kuppermann S et al. Division of labor and collective functionality in *Escherichia coli* under acid stress. *Commun Biol* 2022;**5**. DOI: 10.1038/s42003-022-03281-4.
- Brenneman KE, Willingham C, Kilbourne JA et al. A low gastric pH mouse model to evaluate live attenuated bacterial vaccines. *PLoS ONE* 2014;**9**:e87411. DOI: 10.1371/journal.pone.0087411.
- Brown JL, Ross T, McMeekin TA et al. Acid habituation of *Escherichia coli* and the potential role of cyclopropane fatty acids in low pH tolerance. *Int J Food Microbiol* 1997;**37**:163–73. DOI: 10.1016/S0168-1605(97)00068-8.
- Brynstad S, Granum PE. *Clostridium perfringens* and foodborne infections. *Int J Food Microbiol* 2002;**74**:195–202. DOI: 10.1016/S0168-1605(01)00680-8.
- Buchner S, Schlundt A, Lassak J et al. Structural and functional analysis of the signal-transducing linker in the pH-responsive one-component system CadC of *Escherichia coli*. *J Mol Biol* 2015;**427**:2548–61. DOI: 10.1016/j.jmb.2015.05.001.
- Bury-Moné S, Thiberge J-M, Contreras M et al. *Mol Microbiol* 2004;**53**:623–38. DOI: 10.1111/j.1365-2958.2004.04137.x.
- Carabajal MA, Viarengo G, Yim L et al. PhoQ is an unsaturated fatty acid receptor that fine-tunes *Salmonella pathogenic* traits. *Sci Signal* 2020;**13**. DOI: 10.1126/scisignal.aaz3334.
- Cash RA, Music SI, Libonati JP et al. Response of man to infection with *Vibrio cholerae*. I. Clinical, serologic, and bacteriologic responses to a known inoculum. *J Infect Dis* 1974; **129**:45–52. DOI: 10.1093/infdis/129.1.45.
- Casiano-Colón A, Marquis RE. Role of the arginine deiminase system in protecting oral bacteria and an enzymatic basis for acid tolerance. *Appl Environ Microbiol* 1988;**54**:1318–24. DOI: 10.1128/aem.54.6.1318-1324.1988.
- Castanié-Cornet M-P, Cam K, Bastiat B et al. Acid stress response in *Escherichia coli*: mechanism of regulation of *gadA* transcription by RcsB and GadE. *Nucleic Acids Res* 2010;**38**:3546–54. DOI: 10.1093/nar/gkq097.
- Castanié-Cornet M-P, Foster JW. *Escherichia coli* acid resistance: cAMP receptor protein and a 20 bp cis-acting sequence control pH and stationary phase expression of the *gadA* and *gadBC* glutamate decarboxylase genes. *Microbiology* 2001;**147**:709–15. DOI: 10.1099/00221287-147-3-709.
- Castanié-Cornet M-P, Penfound TA, Smith D et al. Control of acid resistance in *Escherichia coli*. *J Bacteriol* 1999;**181**:3525–35.
- Castanié-Cornet M-P, Treffandier H, Francez-Charlot A et al. The glutamate-dependent acid resistance system in *Escherichia coli*:

- essential and dual role of the his-asp phosphorelay RcsCDB/AF. *Microbiology* 2007;**153**:238–46. DOI: 10.1099/mic.0.29278-0.
- Ceci P, Cellai S, Falvo E et al. DNA condensation and self-aggregation of *Escherichia coli* Dps are coupled phenomena related to the properties of the N-terminus. *Nucleic Acids Res* 2004;**32**:5935–44. DOI: 10.1093/nar/gkh915.
- Ceci P, Ilari A, Falvo E et al. *J Biol Chem* 2003;**278**:20319–26. DOI: 10.1074/jbc.M302114200.
- Chakraborty S, Mizusaki H, Kenney LJ. A FRET-based DNA biosensor tracks OmpR-dependent acidification of *Salmonella* during macrophage infection. *PLoS Biol* 2015;**13**:e1002116. DOI: 10.1371/journal.pbio.1002116.
- Chamnongpol S, Dodson W, Cromie MJ et al. Fe(III)-mediated cellular toxicity. *Mol Microbiol* 2002;**45**:711–9. DOI: 10.1046/j.1365-2958.2002.03041.x.
- Chang YY, Cronan JE. Membrane cyclopropane fatty acid content is a major factor in acid resistance of *Escherichia coli*. *Mol Microbiol* 1999;**33**:249–59. DOI: 10.1046/j.1365-2958.1999.01456.x.
- Chatfield SN, Dorman CJ, Hayward C et al. Role of *ompR*-dependent genes in *Salmonella typhimurium* virulence: mutants deficient in both *ompC* and *ompF* are attenuated in vivo. *Infect Immun* 1991;**59**:449–52.
- Chen Y-YM, Burne RA. Identification and characterization of the nickel uptake system for urease biogenesis in *Streptococcus salivarius* 57.1. *J Bacteriol* 2003;**185**:6773–9. DOI: 10.1128/JB.185.23.6773-6779.2003.
- Chen YY, Weaver CA, Burne RA. Dual functions of *Streptococcus salivarius* urease. *J Bacteriol* 2000;**182**:4667–9. DOI: 10.1128/JB.182.16.4667-4669.2000.
- Choi J, Groisman EA. Acidic pH sensing in the bacterial cytoplasm is required for *Salmonella* virulence. *Mol Microbiol* 2016;**101**:1024–38. DOI: 10.1111/mmi.13439.
- Choi J, Groisman EA. Activation of master virulence regulator PhoP in acidic pH requires the *Salmonella*-specific protein UgtL. *Sci Signal* 2017;**10**. DOI: 10.1126/scisignal.aan6284.
- Choi J, Groisman EA. Horizontally acquired regulatory gene activates ancestral regulatory system to promote *Salmonella* virulence. *Nucleic Acids Res* 2020;**48**:10832–47. DOI: 10.1093/nar/gkaa813.
- Choi SH, Baumler DJ, Kaspar CW. Contribution of Dps to acid stress tolerance and oxidative stress tolerance in *Escherichia coli* O157:H7. *Appl Environ Microbiol* 2000;**66**:3911–6.
- Coornaert A, Chiaruttini C, Springer M et al. Post-transcriptional control of the *Escherichia coli* PhoQ-PhoP two-component system by multiple sRNAs involves a novel pairing region of GcvB. *PLoS Genet* 2013;**9**:e1003156. DOI: 10.1371/journal.pgen.1003156.
- Coornaert A, Lu A, Mandin P et al. MicA sRNA links the PhoP regulon to cell envelope stress. *Mol Microbiol* 2010;**76**:467–79. DOI: 10.1111/j.1365-2958.2010.07115.x.
- Cotter PD, Gahan CG, Hill C. *J Biol Chem* 2001a;**276**:465–75. DOI: 10.1046/j.1365-2958.2001.02398.x.
- Cotter PD, Gahan CGM, Hill C. Analysis of the role of the *Listeria monocytogenes* FOF1-ATPase operon in the acid tolerance response. *Int J Food Microbiol* 2000;**60**:137–46. DOI: 10.1016/S0168-1605(00)00305-6.
- Cotter PD, O'Reilly K, Hill C. Role of the glutamate decarboxylase acid resistance system in the survival of *Listeria monocytogenes* LO28 in low pH foods. *J Food Prot* 2001b;**64**:1362–8. DOI: 10.4315/0362-028x-64.9.1362.
- Cotter PD, Ryan S, Gahan CGM et al. Presence of Gadd1 glutamate decarboxylase in selected *Listeria monocytogenes* strains is associated with an ability to grow at low pH. *Appl Environ Microbiol* 2005;**71**:2832–9. DOI: 10.1128/AEM.71.6.2832-2839.2005.
- Croxen MA, Sisson G, Melano R et al. The *Helicobacter pylori* chemotaxis receptor TlpB (HP0103) is required for pH taxis and for colonization of the gastric mucosa. *J Bacteriol* 2006;**188**:2656–65. DOI: 10.1128/JB.188.7.2656-2665.2006.
- Cunin R, Glansdorff N, Piérard A et al. Biosynthesis and metabolism of arginine in bacteria. *Microbiol Rev* 1986;**50**:314–52.
- D'Aoust J-Y, Maurer J, Bailey JS. *Salmonella* species. In: Doyle MP (ed.). *Food Microbiology: Fundamentals and Frontiers*. Washington: ASM Press, 2001, 141–78.
- D'Hooghe I, Vander Wauven C, Michiels J et al. The arginine deiminase pathway in *Rhizobium etli*: DNA sequence analysis and functional study of the *arcABC* genes. *J Bacteriol* 1997;**179**:7403–9. DOI: 10.1128/jb.179.23.7403-7409.1997.
- Dahl J-U, Koldewey P, Salmon L et al. HdeB functions as an acid-protective chaperone in bacteria. *J Biol Chem* 2015;**290**:65–75. DOI: 10.1074/jbc.M114.612986.
- Damiano MA, Bastianelli D, Al Dahouk S et al. Glutamate decarboxylase-dependent acid resistance in *Brucella* spp.: distribution and contribution to fitness under extremely acidic conditions. *Appl Environ Microbiol* 2015;**81**:578–86. DOI: 10.1128/AEM.02928-14.
- Davis MJ, Coote PJ, O'Byrne CP. Acid tolerance in *Listeria monocytogenes*: the adaptive acid tolerance response (ATR) and growth-phase-dependent acid resistance. *Microbiology* 1996;**142**:2975–82. DOI: 10.1099/13500872-142-10-2975.
- Deamer DW. Proton permeation of lipid bilayers. *J Bioenerg Biomembr* 1987;**19**:457–79. DOI: 10.1007/BF00770030.
- Delany I, Spohn G, Rappuoli R et al. Growth phase-dependent regulation of target gene promoters for binding of the essential orphan response regulator HP1043 of *Helicobacter pylori*. *J Bacteriol* 2002;**184**:4800–10. DOI: 10.1128/JB.184.17.4800-4810.2002.
- Dell CL, Neely MN, Olson ER. Altered pH and lysine signalling mutants of *cadC*, a gene encoding a membrane-bound transcriptional activator of the *Escherichia coli* *cadBA* operon. *Mol Microbiol* 1994;**14**:7–16. DOI: 10.1111/j.1365-2958.1994.tb01262.x.
- Deng Z, Shan Y, Pan Q et al. Anaerobic expression of the *gadE-mdtEF* multidrug efflux operon is primarily regulated by the two-component system ArcBA through antagonizing the H-NS mediated repression. *Front Microbiol* 2013;**4**. DOI: 10.3389/fmicb.2013.00194.
- DiRita VJ, Mekalanos JJ. Periplasmic interaction between two membrane regulatory proteins, ToxR and ToxS, results in signal transduction and transcriptional activation. *Cell* 1991;**64**:29–37. DOI: 10.1016/0092-8674(91)90206-E.
- Dorman CJ, Chatfield S, Higgins CF et al. Characterization of porin and *ompR* mutants of a virulent strain of *Salmonella typhimurium*: *ompR* mutants are attenuated in vivo. *Infect Immun* 1989;**57**:2136–40.
- Durand JMB, Björk GR. Putrescine or a combination of methionine and arginine restores virulence gene expression in a tRNA modification-deficient mutant of *Shigella flexneri*: a possible role in adaptation of virulence. *Mol Microbiol* 2003;**47**:519–27. DOI: 10.1046/j.1365-2958.2003.03314.x.
- Eaton KA, Brooks CL, Morgan M et al. Essential role of urease in pathogenesis of gastritis induced by *Helicobacter pylori* in gnotobiotic piglets. *Infect Immun* 1991;**59**:2470–5. DOI: 10.1128/iai.59.7.2470-2475.1991.
- Eguchi Y, Ishii E, Hata K et al. Regulation of acid resistance by connectors of two-component signal transduction systems in *Escherichia coli*. *J Bacteriol* 2011;**193**:1222–8. DOI: 10.1128/JB.01124-10.
- Eguchi Y, Ishii E, Yamane M et al. The connector SafA interacts with the multi-sensing domain of PhoQ in *Escherichia coli*. *Mol Microbiol* 2012;**85**:299–313. DOI: 10.1111/j.1365-2958.2012.08114.x.

- Eguchi Y, Itou J, Yamane M et al. B1500, a small membrane protein, connects the two-component systems EvgS/EvgA and PhoQ/PhoP in *Escherichia coli*. *Proc Natl Acad Sci* 2007;**104**:18712–7. DOI: 10.1073/pnas.0705768104.
- Eguchi Y, Oshima T, Mori H et al. Transcriptional regulation of drug efflux genes by EvgAS, a two-component system in *Escherichia coli*. *Microbiology* 2003;**149**:2819–28. DOI: 10.1099/mic.0.26460-0.
- Eguchi Y, Utsumi R. Alkali metals in addition to acidic pH activate the EvgS histidine kinase sensor in *Escherichia coli*. *J Bacteriol* 2014;**196**:3140–9. DOI: 10.1128/JB.01742-14.
- Eichinger A, Haneburger I, Koller C et al. Crystal structure of the sensory domain of *Escherichia coli* CadC, a member of the toxr-like protein family. *Protein Sci* 2011;**20**:656–69. DOI: 10.1002/pro.594.
- Epinel IC, Guerra PR, Jelsbak L. Multiple roles of putrescine and spermidine in stress resistance and virulence of *Salmonella enterica* serovar typhimurium. *Microb Pathog* 2016;**95**:117–23. DOI: 10.1016/j.micpath.2016.03.008.
- Evans DF, Pye G, Bramley R et al. Measurement of gastrointestinal pH profiles in normal ambulant human subjects. *Gut* 1988;**29**:1035–41. DOI: 10.1136/gut.29.8.1035.
- Fang Y, Kolmakova-Partensky L, Miller C. A bacterial arginine-arginine exchange transporter involved in extreme acid resistance. *J Biol Chem* 2007;**282**:176–82. DOI: 10.1074/jbc.M610075200.
- Fass E, Groisman EA. Control of *Salmonella pathogenicity island-2* gene expression. *Curr Opin Microbiol* 2009;**12**:199–204. DOI: 10.1016/j.mib.2009.01.004.
- Feehily C, Karatzas KAG. Role of glutamate metabolism in bacterial responses towards acid and other stresses. *J Appl Microbiol* 2013;**114**:11–24. DOI: 10.1111/j.1365-2672.2012.05434.x.
- Foster JW, Hall HK. Inducible pH homeostasis and the acid tolerance response of *Salmonella typhimurium*. *J Bacteriol* 1991;**173**:5129–35. DOI: 10.1128/jb.173.16.5129-5135.1991.
- Foster JW. *Escherichia coli* acid resistance: tales of an amateur acidophile. *Nat Rev Microbiol* 2004;**2**:898–907. DOI: 10.1038/nrmi-cro1021.
- Fritz G, Koller C, Burdack K et al. Induction kinetics of a conditional pH stress response system in *Escherichia coli*. *J Mol Biol* 2009;**393**:272–86. DOI: 10.1016/j.jmb.2009.08.037.
- Fröhlich-Wyder M-T, Bisig W, Guggisberg D et al. Cheeses with propionic acid fermentation. In: Everet DW, McSweeney PLH, Fox PF et al. (eds.). *Cheese: Chemistry, Physics & Microbiology*. Saint Louis: Elsevier Science, 2017, 889–910.
- Gajiwala KS, Burley SK. HDEA, a periplasmic protein that supports acid resistance in pathogenic enteric bacteria. *J Mol Biol* 2000;**295**:605–12. DOI: 10.1006/jmbi.1999.3347.
- Gale EF, Epps HM. Studies on bacterial amino-acid decarboxylases: 1. l(+)-lysine decarboxylase. *Biochem J* 1944;**38**:232–42. DOI: 10.1042/bj0380232.
- Gale EF. The bacterial amino acid decarboxylases. In: Nord FF (ed.). *Advances in Enzymology and Related Subjects of Biochemistry: Volume VI*. New York: Wiley, 1946;1–32.
- Gale EF. The production of amines by bacteria: the decarboxylation of amino-acids by strains of *Bacterium coli*. *Biochem J* 1940;**34**:846–52. DOI: 10.1042/bj0340392.
- Gao X, Lu F, Zhou L et al. Structure and mechanism of an amino acid antiporter. *Science* 2009;**324**:1565–8. DOI: 10.1126/science.1173654.
- Gao X, Zhou L, Jiao X et al. Mechanism of substrate recognition and transport by an amino acid antiporter. *Nature* 2010;**463**:828–32. DOI: 10.1038/nature08741.
- Garmendia J, Beuzón CR, Ruiz-Albert J et al. The roles of SsrA-SsrB and OmpR-EnvZ in the regulation of genes encoding the *Salmonella typhimurium* SPI-2 type III secretion system. *Microbiology* 2003;**149**:2385–96. DOI: 10.1099/mic.0.26397-0.
- Giangrossi M, Zattoni S, Tramonti A et al. Antagonistic role of HNS and GadX in the regulation of the glutamate decarboxylase-dependent acid resistance system in *Escherichia coli*. *J Biol Chem* 2005;**280**:21498–505. DOI: 10.1074/jbc.M413255200.
- Goldberg SD, Clinthorne GD, Goulian M et al. Transmembrane polar interactions are required for signaling in the *Escherichia coli* sensor kinase PhoQ. *Proc Natl Acad Sci* 2010;**107**:8141–6. DOI: 10.1073/pnas.1003166107.
- Goldberg SD, Soto CS, Waldburger CD et al. Determination of the physiological dimer interface of the PhoQ sensor domain. *J Mol Biol* 2008;**379**:656–65. DOI: 10.1016/j.jmb.2008.04.023.
- Gong L, Ren C, Xu Y. Deciphering the crucial roles of transcriptional regulator GadR on gamma-aminobutyric acid production and acid resistance in *Lactobacillus brevis*. *Microb Cell Fact* 2019;**18**. DOI: 10.1186/s12934-019-1157-2.
- Gong S, Ma Z, Foster JW. The Era-like GTPase TrmE conditionally activates *gadE* and glutamate-dependent acid resistance in *Escherichia coli*. *Mol Microbiol* 2004;**54**:948–61. DOI: 10.1111/j.1365-2958.2004.04312.x.
- Goode O, Smith A, Zarkan A et al. Persister *Escherichia coli* cells have a lower intracellular pH than susceptible cells but maintain their pH in response to antibiotic treatment. *Mbio* 2021;**12**. DOI: 10.1128/mBio.00909-21.
- Gorden J, Small PL. Acid resistance in enteric bacteria. *Infect Immun* 1993;**61**:364–7. DOI: 10.1128/iai.61.1.364-367.1993.
- Goto Y, Calciano LJ, Fink AL. Acid-induced folding of proteins. *Proc Natl Acad Sci* 1990;**87**:573–7. DOI: 10.1073/pnas.87.2.573.
- Groisman EA, Chiao E, Lipps CJ et al. *Salmonella typhimurium* *phoP* virulence gene is a transcriptional regulator. *Proc Natl Acad Sci* 1989;**86**:7077–81.
- Groisman EA, Duprey A, Choi J. How the PhoP/PhoQ system controls virulence and Mg²⁺ homeostasis: lessons in signal transduction, pathogenesis, physiology, and evolution. *Microbiol Mol Biol Rev* 2021;**85**. DOI: 10.1128/MMBR.00176-20.
- Guan N, Liu L. Microbial response to acid stress: mechanisms and applications. *Appl Microbiol Biotechnol* 2020;**104**:51–65. DOI: 10.1007/s00253-019-10226-1.
- Guerra PR, Herrero-Fresno A, Ladero V et al. Putrescine biosynthesis and export genes are essential for normal growth of avian pathogenic *Escherichia coli*. *BMC Microbiol* 2018;**18**. DOI: 10.1186/s12866-018-1355-9.
- Gunn JS, Miller SI. PhoP-PhoQ activates transcription of *pmrAB*, encoding a two-component regulatory system involved in *Salmonella typhimurium* antimicrobial peptide resistance. *J Bacteriol* 1996;**178**:6857–64.
- Gunn JS, Ryan SS, van Velkinburgh JC et al. Genetic and functional analysis of a PmrA-PmrB-regulated locus necessary for lipopolysaccharide modification, antimicrobial peptide resistance, and oral virulence of *Salmonella enterica* serovar typhimurium. *Infect Immun* 2000;**68**:6139–46.
- Guynot ME, Ramos AJ, Sanchis V et al. Study of benzoate, propionate, and sorbate salts as mould spoilage inhibitors on intermediate moisture bakery products of low pH (4.5–5.5). *Int J Food Microbiol* 2005;**101**:161–8. DOI: 10.1016/j.ijfoodmicro.2004.11.003.
- Haneburger I, Eichinger A, Skerra A et al. New insights into the signaling mechanism of the pH-responsive, membrane-integrated transcriptional activator CadC of *Escherichia coli*. *J Biol Chem* 2011;**286**:10681–9. DOI: 10.1074/jbc.M110.196923.
- Haneburger I, Fritz G, Jurkschat N et al. Deactivation of the *E. coli* pH stress sensor CadC by cadaverine. *J Mol Biol* 2012;**424**:15–27. DOI: 10.1016/j.jmb.2012.08.023.

- Haque M, Hirai Y, Yokota K et al. Lipid profile of *Helicobacter* spp.: presence of cholesteryl glucoside as a characteristic feature. *J Bacteriol* 1996;**178**:2065–70.
- Harari O, Park S-Y, Huang H et al. Defining the plasticity of transcription factor binding sites by deconstructing DNA consensus sequences: the PhoP-binding sites among gamma/enterobacteria. *PLoS Comput Biol* 2010;**6**:e1000862. DOI: 10.1371/journal.pcbi.1000862.
- Hayes ET, Wilks JC, Sanfilippo P et al. Oxygen limitation modulates pH regulation of catabolism and hydrogenases, multidrug transporters, and envelope composition in *Escherichia coli* K-12. *BMC Microbiol* 2006;**6**. DOI: 10.1186/1471-2180-6-89.
- Hazelbauer GL, Falke JJ, Parkinson JS. Bacterial chemoreceptors: high-performance signaling in networked arrays. *Trends Biochem Sci* 2008;**33**:9–19. DOI: 10.1016/j.tibs.2007.09.014.
- Herrero Del Valle A, Seip B, Cervera-Marzal I et al. Ornithine capture by a translating ribosome controls bacterial polyamine synthesis. *Nat Microbiol* 2020;**5**:554–61. DOI: 10.1038/s41564-020-0669-1.
- Heuveling J, Possling A, Hengge R. A role for Lon protease in the control of the acid resistance genes of *Escherichia coli*. *Mol Microbiol* 2008;**69**:534–47. DOI: 10.1111/j.1365-2958.2008.06306.x.
- Heyde M. Acid shock proteins of *Escherichia coli*. *FEMS Microbiol Lett* 1990;**69**:19–26. DOI: 10.1016/0378-1097(90)90406-G.
- Hicks KG, Delbecq SP, Sancho-Vaello E et al. Acidic pH and divalent cation sensing by PhoQ are dispensable for systemic *Salmonella* virulence. *Elife* 2015. DOI: 10.7554/eLife.06792.
- Hirshfield IN, Terzulli S, O'Byrne C. Weak organic acids: a panoply of effects on bacteria. *Sci Prog* 2003;**86**:245–70. DOI: 10.3184/003685003783238626.
- Ilgü H, Jeckelmann J-M, Colas C et al. Effects of mutations and ligands on the thermostability of the L-arginine/arginine antiporter AdiC and deduced insights into ligand-binding of human L-type amino acid transporters. *Int J Mol Sci* 2018;**19**:918. DOI: 10.3390/ijms19030918.
- Inada S, Okajima T, Utsumi R et al. Acid-sensing histidine kinase with a redox switch. *Front Microbiol* 2021;**12**. DOI: 10.3389/fmicb.2021.652546.
- Ishii E, Eguchi Y, Utsumi R. *Biosci Biotechnol Biochem* 2013;**77**:814–9. DOI: 10.1271/bbb.120970.
- Itou J, Eguchi Y, Utsumi R. Molecular mechanism of transcriptional cascade initiated by the EvgS/EvgA system in *Escherichia coli* K-12. *Biosci Biotechnol Biochem* 2009;**73**:870–8. DOI: 10.1271/bbb.80795.
- Iyer R, Iverson TM, Accardi A et al. A biological role for prokaryotic ClC chloride channels. *Nature* 2002;**419**:715–8. DOI: 10.1038/nature01000.
- Jeong HG, Choi SH. Evidence that AphB, essential for the virulence of *Vibrio vulnificus*, is a global regulator. *J Bacteriol* 2008;**190**:3768–73. DOI: 10.1128/JB.00058-08.
- Jeong KC, Hung KF, Baumler DJ et al. Acid stress damage of DNA is prevented by Dps binding in *Escherichia coli* O157:H7. *BMC Microbiol* 2008;**8**. DOI: 10.1186/1471-2180-8-181.
- Jin Y, Watt RM, Danchin A et al. *BMC Genomics* 2009;**10**. DOI: 10.1186/1471-2164-10-165.
- Johnson DB, Hallberg KB. Acid mine drainage remediation options: a review. *Sci Total Environ* 2005;**338**:3–14. DOI: 10.1016/j.scitotenv.2004.09.002.
- Johnson MD, Bell J, Clarke K et al. *Mol Microbiol* 2014;**93**:911–27. DOI: 10.1111/mmi.12704.
- Johnson MD, Burton NA, Gutiérrez B et al. RcsB is required for inducible acid resistance in *Escherichia coli* and acts at *gadE*-dependent and -independent promoters. *J Bacteriol* 2011;**193**:3653–6. DOI: 10.1128/JB.05040-11.
- Jones JE, Dreyton CJ, Flick H et al. Mechanistic studies of agmatine deiminase from multiple bacterial species. *Biochemistry* 2010;**49**:9413–23. DOI: 10.1021/bi101405y.
- Jung IL, Kim IG. Polyamines reduce paraquat-induced soxS and its regulon expression in *Escherichia coli*. *Cell Biol Toxicol* 2003;**19**:29–41. DOI: 10.1023/a:1022065614490.
- Kalantzi L, Goumas K, Kalioras V et al. Characterization of the human upper gastrointestinal contents under conditions simulating bioavailability/bioequivalence studies. *Pharm Res* 2006;**23**:165–76. DOI: 10.1007/s11095-005-8476-1.
- Kalinin Y, Neumann S, Sourjik V et al. Responses of *Escherichia coli* bacteria to two opposing chemoattractant gradients depend on the chemoreceptor ratio. *J Bacteriol* 2010;**192**:1796–800. DOI: 10.1128/JB.01507-09.
- Kanjee U, Gutsche I, Alexopoulos E et al. Linkage between the bacterial acid stress and stringent responses: the structure of the inducible lysine decarboxylase. *EMBO J* 2011a;**30**:931–44. DOI: 10.1038/emboj.2011.5.
- Kanjee U, Gutsche I, Ramachandran S et al. The enzymatic activities of the *Escherichia coli* basic aliphatic amino acid decarboxylases exhibit a pH zone of inhibition. *Biochemistry* 2011b;**50**:9388–98. DOI: 10.1021/bi201161k.
- Kanjee U, Houry WA. Mechanisms of acid resistance in *Escherichia coli*. *Annu Rev Microbiol* 2013;**67**:65–81. DOI: 10.1146/annurev-micro-092412-155708.
- Karatzas K-AG, Brennan O, Heavin S et al. Intracellular accumulation of high levels of γ -aminobutyrate by *Listeria monocytogenes* 10403S in response to low pH: uncoupling of γ -aminobutyrate synthesis from efflux in a chemically defined medium. *Appl Environ Microbiol* 2010;**76**:3529–37. DOI: 10.1128/AEM.03063-09.
- Kasahara M, Nakata A, Shinagawa H. Molecular analysis of the *Escherichia coli* *phoP-phoQ* operon. *J Bacteriol* 1992;**174**:492–8.
- Kashiwagi K, Miyamoto S, Suzuki F et al. Excretion of putrescine by the putrescine-ornithine antiporter encoded by the *potE* gene of *Escherichia coli*. *Proc Natl Acad Sci* 1992;**89**:4529–33. DOI: 10.1073/pnas.89.10.4529.
- Kashiwagi K, Shibuya S, Tomitori H et al. Excretion and uptake of putrescine by the PotE protein in *Escherichia coli*. *J Biol Chem* 1997;**272**:6318–23. DOI: 10.1074/jbc.272.10.6318.
- Kashiwagi K, Suzuki T, Suzuki F et al. Coexistence of the genes for putrescine transport protein and ornithine decarboxylase at 16 min on *Escherichia coli* chromosome. *J Biol Chem* 1991;**266**:20922–7.
- Kato A, Groisman EA. Connecting two-component regulatory systems by a protein that protects a response regulator from dephosphorylation by its cognate sensor. *Genes Dev* 2004;**18**:2302–13. DOI: 10.1101/gad.1230804.
- Kato A, Ohnishi H, Yamamoto K et al. *Biosci Biotechnol Biochem* 2000;**64**:1203–9. DOI: 10.1271/bbb.64.1203.
- Kenney LJ. The role of acid stress in *Salmonella* pathogenesis. *Curr Opin Microbiol* 2019;**47**:45–51. DOI: 10.1016/j.mib.2018.11.006.
- Kentner D, Thiem S, Hildenbeutel M et al. Determinants of chemoreceptor cluster formation in *Escherichia coli*. *Mol Microbiol* 2006;**61**:407–17. DOI: 10.1111/j.1365-2958.2006.05250.x.
- Kern R, Malki A, Abdallah J et al. *Escherichia coli* HdeB is an acid stress chaperone. *J Bacteriol* 2007;**189**:603–10. DOI: 10.1128/JB.01522-06.
- Khan S, Spudich JL, McCray JA et al. Chemotactic signal integration in bacteria. *Proc Natl Acad Sci* 1995;**92**:9757–61. DOI: 10.1073/pnas.92.21.9757.
- Kieboom J, Abee T. Arginine-dependent acid resistance in *Salmonella enterica* serovar typhimurium. *J Bacteriol* 2006;**188**:5650–3. DOI: 10.1128/JB.00323-06.

- Kihara M, Macnab RM. Cytoplasmic pH mediates pH taxis and weak-acid repellent taxis of bacteria. *J Bacteriol* 1981;**145**:1209–21. DOI: 10.1128/jb.145.3.1209-1221.1981.
- Kim BH, Kim S, Kim HG et al. The formation of cyclopropane fatty acids in *Salmonella enterica* serovar typhimurium. *Microbiology* 2005;**151**:209–18. DOI: 10.1099/mic.0.27265-0.
- Kinoshita-Kikuta E, Kinoshita E, Eguchi Y et al. Functional characterization of the receiver domain for phosphorelay control in hybrid sensor kinases. *PLoS ONE* 2015;**10**:e0132598. DOI: 10.1371/journal.pone.0132598.
- Kitamoto S, Alteri CJ, Rodrigues M et al. Dietary L-serine confers a competitive fitness advantage to enterobacteriaceae in the inflamed gut. *Nat Microbiol* 2020;**5**:116–25. DOI: 10.1038/s41564-019-0591-6.
- Kobayashi H, Suzuki T, Unemoto T. Streptococcal cytoplasmic pH is regulated by changes in amount and activity of a proton-translocating ATPase. *J Biol Chem* 1986;**261**:627–30.
- Kovacikova G, Lin W, Skorupski K. The LysR-type virulence activator AphB regulates the expression of genes in *Vibrio cholerae* in response to low pH and anaerobiosis. *J Bacteriol* 2010;**192**:4181–91. DOI: 10.1128/JB.00193-10.
- Kovacikova G, Skorupski K. A *Vibrio cholerae* LysR homolog, AphB, cooperates with AphA at the *tcpPH* promoter to activate expression of the ToxR virulence cascade. *J Bacteriol* 1999;**181**:4250–6. DOI: 10.1128/JB.181.14.4250-4256.1999.
- Kowalczyk L, Ratera M, Paladino A et al. Molecular basis of substrate-induced permeation by an amino acid antiporter. *Proc Natl Acad Sci* 2011;**108**:3935–40. DOI: 10.1073/pnas.1018081108.
- Kox LFF, Wösten MMSM, Groisman EA. A small protein that mediates the activation of a two-component system by another two-component system. *EMBO J* 2000;**19**:1861–72. DOI: 10.1093/emboj/19.8.1861.
- Krammer E-M, Ghaddar K, André B et al. Unveiling the mechanism of arginine transport through AdiC with molecular dynamics simulations: the guiding role of aromatic residues. *PLoS ONE* 2016;**11**:e0160219. DOI: 10.1371/journal.pone.0160219.
- Krammer E-M, Gibbons A, Roos G et al. Molecular mechanism of substrate selectivity of the arginine-arginine Antiporter AdiC. *Sci Rep* 2018;**8**. DOI: 10.1038/s41598-018-33963-1.
- Krikos A, Conley MP, Boyd A et al. Chimeric chemosensory transducers of *Escherichia coli*. *Proc Natl Acad Sci* 1985;**82**:1326–30. DOI: 10.1073/pnas.82.5.1326.
- Krulwich TA, Sachs G, Padan E. Molecular aspects of bacterial pH sensing and homeostasis. *Nat Rev Microbiol* 2011;**9**:330–43. DOI: 10.1038/nrmicro2549.
- Kuper C, Jung K. CadC-mediated activation of the *cadBA* promoter in *Escherichia coli*. *J Mol Microbiol Biotechnol* 2005. DOI: 10.1159/000090346.
- Lange R, Hengge-Aronis R. The cellular concentration of the σ^S subunit of RNA polymerase in *Escherichia coli* is controlled at the levels of transcription, translation, and protein stability. *Genes Dev* 1994;**8**:1600–12. DOI: 10.1101/gad.8.13.1600.
- Lawson A, Quinn AG. Studies on amino acid decarboxylases in *Escherichia coli*. *Biochem J* 1967;**105**:483–90. DOI: 10.1042/bj1050483.
- Lease RA, Smith D, McDonough K et al. The small noncoding DsrA RNA is an acid resistance regulator in *Escherichia coli*. *J Bacteriol* 2004;**186**:6179–85. DOI: 10.1128/JB.186.18.6179-6185.2004.
- Lee AK, Detweiler CS, Falkow S. OmpR regulates the two-component system SsrA-SsrB in *Salmonella pathogenicity island 2*. *J Bacteriol* 2000;**182**:771–81.
- Lee YH, Kim BH, Kim JH et al. CadC has a global translational effect during acid adaptation in *Salmonella enterica* serovar typhimurium. *J Bacteriol* 2007;**189**:2417–25. DOI: 10.1128/JB.01277-06.
- Li Y, Zamble DB. pH-responsive DNA-binding activity of *Helicobacter pylori* NikR. *Biochemistry* 2009;**48**:2486–96. DOI: 10.1021/bi801742r.
- Liew ATF, Foo YH, Gao Y et al. Single cell, super-resolution imaging reveals an acid pH-dependent conformational switch in SsrB regulates SPI-2. *Elife* 2019. DOI: 10.7554/eLife.45311.
- Lin J, Lee IS, Frey J et al. Comparative analysis of extreme acid survival in *Salmonella typhimurium*, *Shigella flexneri*, and *Escherichia coli*. *J Bacteriol* 1995;**177**:4097–104.
- Lin J, Smith MP, Chapin KC et al. Mechanisms of acid resistance in enterohemorrhagic *Escherichia coli*. *Appl Environ Microbiol* 1996;**62**:3094–100.
- Lindner E, White SH. Topology, dimerization, and stability of the single-span membrane protein CadC. *J Mol Biol* 2014;**426**:2942–57. DOI: 10.1016/j.jmb.2014.06.006.
- Linsky T, Fast W. Mechanistic similarity and diversity among the guanidine-modifying members of the pentain superfamily. *Biochim Biophys Acta Proteins Proteomics* 2010;**1804**:1943–53. DOI: 10.1016/j.bbapap.2010.07.016.
- Lippa AM, Goulian M. Feedback inhibition in the PhoQ/PhoP signaling system by a membrane peptide. *PLoS Genet* 2009;**5**:e1000788. DOI: 10.1371/journal.pgen.1000788.
- Liu S, Pritchard GG, Hardman MJ et al. Occurrence of arginine deiminase pathway enzymes in arginine catabolism by wine lactic acid bacteria. *Appl Environ Microbiol* 1995;**61**:310–6. DOI: 10.1128/aem.61.1.310-316.1995.
- Lu P, Ma D, Chen Y et al. L-glutamine provides acid resistance for *Escherichia coli* through enzymatic release of ammonia. *Cell Res* 2013;**23**:635–44. DOI: 10.1038/cr.2013.13.
- Lund P, Tramonti A, Biase D de. Coping with low pH: molecular strategies in neutralophilic bacteria. *FEMS Microbiol Rev* 2014;**38**:1091–125. DOI: 10.1111/1574-6976.12076.
- Ma D, Lu P, Shi Y. Substrate selectivity of the acid-activated glutamate/ γ -aminobutyric acid (GABA) antiporter GadC from *Escherichia coli*. *J Biol Chem* 2013;**288**:15148–53. DOI: 10.1074/jbc.M113.474502.
- Ma D, Lu P, Yan C et al. Structure and mechanism of a glutamate-GABA antiporter. *Nature* 2012;**483**:632–6. DOI: 10.1038/nature10917.
- Ma X, Zhang S, Xu Z et al. SdiA improves the acid tolerance of *E. coli* by regulating GadW and GadY expression. *Front Microbiol* 2020;**11**. DOI: 10.3389/fmicb.2020.01078.
- Ma Z, Gong S, Richard H et al. GadE (YhiE) activates glutamate decarboxylase-dependent acid resistance in *Escherichia coli* K-12. *Mol Microbiol* 2003;**49**:1309–20. DOI: 10.1046/j.1365-2958.2003.03633.x.
- Ma Z, Masuda N, Foster JW. Characterization of EvgAS-YdeO-GadE branched regulatory circuit governing glutamate-dependent acid resistance in *Escherichia coli*. *J Bacteriol* 2004;**186**:7378–89. DOI: 10.1128/JB.186.21.7378-7389.2004.
- Ma Z, Richard H, Tucker DL et al. Collaborative regulation of *Escherichia coli* glutamate-dependent acid resistance by two AraC-like regulators, GadX and GadW (YhiW). *J Bacteriol* 2002;**184**:7001–12. DOI: 10.1128/JB.184.24.7001-7012.2002.
- Maddock JR, Shapiro L. Polar location of the chemoreceptor complex in the *Escherichia coli* cell. *Science* 1993;**259**:1717–23. DOI: 10.1126/science.8456299.
- Maddocks SE, Oyston PCF. Structure and function of the LysR-type transcriptional regulator (LTTR) family proteins. *Microbiology* 2008;**154**:3609–23. DOI: 10.1099/mic.0.2008/022772-0.

- Malki A, Le H-T, Milles S et al. Solubilization of protein aggregates by the acid stress chaperones HdeA and HdeB. *J Biol Chem* 2008;**283**:13679–87. DOI: 10.1074/jbc.M800869200.
- Marcus EA, Moshfegh AP, Sachs G et al. The periplasmic α -carbonic anhydrase activity of *Helicobacter pylori* is essential for acid acclimation. *J Bacteriol* 2005;**187**:729–38. DOI: 10.1128/JB.187.2.729-738.2005.
- Marquis RE, Bender GR, Murray DR et al. Arginine deiminase system and bacterial adaptation to acid environments. *Appl Environ Microbiol* 1987;**53**:198–200. DOI: 10.1128/aem.53.1.198-200.1987.
- Martinez A, Kolter R. Protection of DNA during oxidative stress by the nonspecific DNA-binding protein Dps. *J Bacteriol* 1997;**179**:5188–94.
- Martinez KA, Kitko RD, Mershon JP et al. Cytoplasmic pH response to acid stress in individual cells of *Escherichia coli* and *Bacillus subtilis* observed by fluorescence ratio imaging microscopy. *Appl Environ Microbiol* 2012;**78**:3706–14. DOI: 10.1128/AEM.00354-12.
- Martini L, Brameyer S, Hoyer E et al. Dynamics of chromosomal target search by a membrane-integrated one-component receptor. *PLoS Comput Biol* 2021;**17**:e1008680. DOI: 10.1371/journal.pcbi.1008680.
- Martinsen TC, Bergh K, Waldum HL. Gastric juice: a barrier against infectious diseases. *Basic Clin Pharmacol Toxicol* 2005;**96**:94–102. DOI: 10.1111/j.1742-7843.2005.pto960202.x.
- Masuda N, Church GM. Regulatory network of acid resistance genes in *Escherichia coli*. *Mol Microbiol* 2003;**48**:699–712. DOI: 10.1046/j.1365-2958.2003.03477.x.
- Matin A, Wilson B, Zychlinsky E et al. Proton motive force and the physiological basis of delta pH maintenance in *Thiobacillus acidophilus*. *J Bacteriol* 1982;**150**:582–91. DOI: 10.1128/jb.150.2.582-591.1982.
- Matin A. pH homeostasis in acidophiles. *Novartis Found Symp* 1999;**221**:152–63. DOI: 10.1002/9780470515631.ch10.
- Maurer LM, Yohannes E, BonDurant SS et al. pH regulates genes for flagellar motility, catabolism, and oxidative stress in *Escherichia coli* K-12. *J Bacteriol* 2005;**187**:304–19. DOI: 10.1128/JB.187.1.304-319.2005.
- Melamed S, Peer A, Faigenbaum-Romm R et al. Global mapping of small RNA-target interactions in bacteria. *Mol Cell* 2016;**63**:884–97. DOI: 10.1016/j.molcel.2016.07.026.
- Melnikovych G, Snell EE. Nutritional requirements for the formation of arginine decarboxylase in *Escherichia coli*. *J Bacteriol* 1958;**76**:518–23.
- Meng J, Young G, Chen J. The Rcs system in *Enterobacteriaceae*: envelope stress responses and virulence regulation. *Front Microbiol* 2021;**12**. DOI: 10.3389/fmicb.2021.627104.
- Merrell DS, Camilli A. Regulation of *Vibrio cholerae* genes required for acid tolerance by a member of the “ToxR-like” family of transcriptional regulators. *J Bacteriol* 2000;**182**:5342–50. DOI: 10.1128/JB.182.19.5342-5350.2000.
- Merrell DS, Camilli A. The *cadA* gene of *Vibrio cholerae* is induced during infection and plays a role in acid tolerance. *Mol Microbiol* 1999;**34**:836–49. DOI: 10.1046/j.1365-2958.1999.01650.x.
- Merrell DS, Goodrich ML, Otto G et al. pH-regulated gene expression of the gastric pathogen *Helicobacter pylori*. *Infect Immun* 2003;**71**:3529–39. DOI: 10.1128/IAI.71.6.3529-3539.2003.
- Miller SI, Kukral AM, Mekalanos JJ. A two-component regulatory system (*phoP phoQ*) controls *Salmonella typhimurium* virulence. *Proc Natl Acad Sci* 1989;**86**:5054–8.
- Miller VL, Taylor RK, Mekalanos JJ. Cholera toxin transcriptional activator ToxR is a transmembrane DNA binding protein. *Cell* 1987;**48**:271–9. DOI: 10.1016/0092-8674(87)90430-2.
- Mitchell P. Performance and conservation of osmotic work by proton-coupled solute porter systems. *J Bioenerg* 1973;**4**:63–91. DOI: 10.1007/BF01516051.
- Mitosch K, Rieckh G, Bollenbach T. Noisy response to antibiotic stress predicts subsequent single-cell survival in an acidic environment. *Cell Syst* 2017;**4**:393–403.e5. DOI: 10.1016/j.cels.2017.03.001.
- Mobley HL, Island MD, Hausinger RP. Molecular biology of microbial ureases. *Microbiol Rev* 1995;**59**:451–80. DOI: 10.1128/mr.59.3.451-480.1995.
- Mollenhauer-Rektorschek M, Hanauer G, Sachs G et al. Expression of UreI is required for intragastric transit and colonization of gerbil gastric mucosa by *Helicobacter pylori*. *Res Microbiol* 2002;**153**:659–66. DOI: 10.1016/s0923-2508(02)01380-3.
- Mora D, Arioli S. Microbial urease in health and disease. *PLoS Pathog* 2014;**10**:e1004472. DOI: 10.1371/journal.ppat.1004472.
- Moreau PL. The lysine decarboxylase CadA protects *Escherichia coli* starved of phosphate against fermentation acids. *J Bacteriol* 2007;**189**:2249–61. DOI: 10.1128/JB.01306-06.
- Morou-Bermudez E, Burne RA. Genetic and physiologic characterization of urease of *Actinomyces naeslundii*. *Infect Immun* 1999;**67**:504–12. DOI: 10.1128/IAI.67.2.504-512.1999.
- Mujacic M, Baneyx F. Chaperone hsp31 contributes to acid resistance in stationary-phase *Escherichia coli*. *Appl Environ Microbiol* 2006;**73**:1014–8. DOI: 10.1128/AEM.02429-06.
- Mulder DT, McPhee JB, Reid-Yu SA et al. Multiple histidines in the periplasmic domain of the *Salmonella enterica* sensor kinase SsrA enhance signaling in response to extracellular acidification. *Mol Microbiol* 2015;**95**:678–91. DOI: 10.1111/mmi.12895.
- Müller S, Götz M, Beier D. Histidine residue 94 is involved in pH sensing by histidine kinase ArsS of *Helicobacter pylori*. *PLoS ONE* 2009. DOI: 10.1371/journal.pone.0006930.
- Neely MN, Dell CL, Olson ER. Roles of LysP and CadC in mediating the lysine requirement for acid induction of the *Escherichia coli* *cad* operon. *J Bacteriol* 1994;**176**:3278–85. DOI: 10.1128/jb.176.11.3278-3285.1994.
- Neely MN, Olson ER. Kinetics of expression of the *Escherichia coli* *cad* operon as a function of pH and lysine. *J Bacteriol* 1996;**178**:5522–8. DOI: 10.1128/jb.178.18.5522-5528.1996.
- Nguyen Y, Nguyen NX, Rogers JL et al. Structural and mechanistic roles of novel chemical ligands on the SdiA quorum-sensing transcription regulator. *Mbio* 2015;**6**. DOI: 10.1128/mBio.02429-14.
- Nishino K, Hsu F-F, Turk J et al. Identification of the lipopolysaccharide modifications controlled by the *Salmonella* PmrA/PmrB system mediating resistance to Fe(III) and Al(III). *Mol Microbiol* 2006;**61**:645–54. DOI: 10.1111/j.1365-2958.2006.05273.x.
- Nishino K, Yamaguchi A. Overexpression of the response regulator EvgA of the two-component signal transduction system modulates multidrug resistance conferred by multidrug resistance transporters. *J Bacteriol* 2001;**183**:1455–8. DOI: 10.1128/JB.183.4.1455-1458.2001.
- Nowak S, Boeker EA. The inducible arginine decarboxylase of *Escherichia coli* B: activity of the dimer and the decamer. *Arch Biochem Biophys* 1981;**207**:110–6. DOI: 10.1016/0003-9861(81)90015-1.
- O’Sullivan E, Condon S. Relationship between acid tolerance, cytoplasmic pH, and ATP and H⁺-ATPase levels in chemostat cultures of *Lactococcus lactis*. *Appl Environ Microbiol* 1999;**65**:2287–93.
- Occhialini A, Jiménez de Bagüés MP, Saadeh B et al. The glutamic acid decarboxylase system of the new species *Brucella microti* contributes to its acid resistance and to oral infection of mice. *J Infect Dis* 2012;**206**:1424–32. DOI: 10.1093/infdis/jis522.
- Ogasawara H, Hasegawa A, Kanda E et al. Genomic SELEX search for target promoters under the control of the PhoQP-RstBA signal relay cascade. *J Bacteriol* 2007;**189**:4791–9. DOI: 10.1128/JB.00319-07.

- Opdyke JA, Kang J-G, Storz G. GadY, a small-RNA regulator of acid response genes in *Escherichia coli*. *J Bacteriol* 2004;**186**:6698–705. DOI: 10.1128/JB.186.20.6698-6705.2004.
- Palanivelu J, Thanigaivel S, Vickram S et al. Probiotics in functional foods: survival assessment and approaches for improved viability. *Appl Sci* 2022;**12**:455. DOI: 10.3390/app12010455.
- Pannen D, Fabisch M, Gausling L et al. Interaction of the RcsB response regulator with auxiliary transcription regulators in *Escherichia coli*. *J Biol Chem* 2015. DOI: 10.1074/jbc.M115.696815.
- Park N, Song S, Choi G et al. Crystal structure of the regulatory domain of AphB from *Vibrio vulnificus*, a virulence gene regulator. *Mol Cells* 2017;**40**:299–306. DOI: 10.14348/molcells.2017.0015.
- Park YK, Bearson B, Bang SH et al. Internal pH crisis, lysine decarboxylase and the acid tolerance response of *Salmonella typhimurium*. *Mol Microbiol* 1996;**20**:605–11. DOI: 10.1046/j.1365-2958.1996.5441070.x.
- Patel CN, Wortham BW, Lines JL et al. Polyamines are essential for the formation of plague biofilm. *J Bacteriol* 2006;**188**:2355–63. DOI: 10.1128/JB.188.7.2355-2363.2006.
- Pennacchietti E, D'Alonzo C, Freddi L et al. The glutaminase-dependent acid resistance system: qualitative and quantitative assays and analysis of its distribution in enteric bacteria. *Front Microbiol* 2018;**9**. DOI: 10.3389/fmicb.2018.02869.
- Perez JC, Groisman EA. Acid pH activation of the PmrA/PmrB two-component regulatory system of *Salmonella enterica*. *Mol Microbiol* 2007;**63**:283–93. DOI: 10.1111/j.1365-2958.2006.05512.x.
- Perier A, Chassaing A, Raffestin S et al. Concerted protonation of key histidines triggers membrane interaction of the diphtheria toxin T domain. *J Biol Chem* 2007;**282**:24239–45. DOI: 10.1074/jbc.M703392200.
- Perraud AL, Kimmel B, Weiss V et al. Specificity of the BvgAS and EvgAS phosphorelay is mediated by the C-terminal HPt domains of the sensor proteins. *Mol Microbiol* 1998;**27**:875–87. DOI: 10.1046/j.1365-2958.1998.00716.x.
- Pflock M, Finsterer N, Joseph B et al. Characterization of the ArsRS regulon of *Helicobacter pylori*, involved in acid adaptation. *J Bacteriol* 2006;**188**:3449–62. DOI: 10.1128/JB.188.10.3449-3462.2006.
- Prost LR, Daley ME, Le Sage V et al. Activation of the bacterial sensor kinase PhoQ by acidic pH. *Mol Cell* 2007;**26**:165–74. DOI: 10.1016/j.molcel.2007.03.008.
- Rader BA, Wreden C, Hicks KG et al. *Helicobacter pylori* perceives the quorum-sensing molecule AI-2 as a chemorepellent via the chemoreceptor TlpB. *Microbiology* 2011;**157**:2445–55. DOI: 10.1099/mic.0.049353-0.
- Rathman M, Sjaastad MD, Falkow S. Acidification of phagosomes containing *Salmonella typhimurium* in murine macrophages. *Infect Immun* 1996;**64**:2765–73.
- Ratzke C, Gore J. Modifying and reacting to the environmental pH can drive bacterial interactions. *PLoS Biol* 2018;**16**:e2004248. DOI: 10.1371/journal.pbio.2004248.
- Rauschmeier M, Schüppel V, Tetsch L et al. New insights into the interplay between the lysine transporter LysP and the pH sensor CadC in *Escherichia coli*. *J Mol Biol* 2014;**426**:215–29. DOI: 10.1016/j.jmb.2013.09.017.
- Repaske DR, Adler J. Change in intracellular pH of *Escherichia coli* mediates the chemotactic response to certain attractants and repellents. *J Bacteriol* 1981;**145**:1196–208.
- Reyes-Fernández EZ, Schuldiner S. Acidification of cytoplasm in *Escherichia coli* provides a strategy to cope with stress and facilitates development of antibiotic resistance. *Sci Rep* 2020;**10**. DOI: 10.1038/s41598-020-66890-1.
- Rhee JE, Jeong HG, Lee JH et al. AphB influences acid tolerance of *Vibrio vulnificus* by activating expression of the positive regulator CadC. *J Bacteriol* 2006;**188**:6490–7. DOI: 10.1128/JB.00533-06.
- Richard H, Foster JW. *Escherichia coli* glutamate- and arginine-dependent acid resistance systems increase internal pH and reverse transmembrane potential. *J Bacteriol* 2004;**186**:6032–41. DOI: 10.1128/JB.186.18.6032-6041.2004.
- Robinson DA. Infective dose of *Campylobacter jejuni* in milk. *BMJ* 1981;**282**:1584.
- Roggiani M, Yadavalli SS, Goulian M. Natural variation of a sensor kinase controlling a conserved stress response pathway in *Escherichia coli*. *PLoS Genet* 2017;**13**:e1007101. DOI: 10.1371/journal.pgen.1007101.
- Roland KL, Martin LE, Esther CR et al. Spontaneous *pmrA* mutants of *Salmonella typhimurium* LT2 define a new two-component regulatory system with a possible role in virulence. *J Bacteriol* 1993;**175**:4154–64.
- Román K, Castillo R, Gilman RH et al. A foodborne outbreak of brucellosis at a police station cafeteria, Lima, Peru. *Am J Trop Med Hyg* 2013;**88**:552–8. DOI: 10.4269/ajtmh.12-0606.
- Sabo DL, Boeker EA, Byers B et al. Purification and physical properties of inducible *Escherichia coli* lysine decarboxylase. *Biochemistry* 1974;**13**:662–70. DOI: 10.1021/bi00701a005.
- Sachs G, Weeks DL, Wen Y et al. Acid acclimation by *Helicobacter pylori*. *Physiology* 2005;**20**:429–38. DOI: 10.1152/physiol.00032.2005.
- Salazar ME, Podgornaia AI, Laub MT. The small membrane protein MgrB regulates PhoQ bifunctionality to control PhoP target gene expression dynamics. *Mol Microbiol* 2016;**102**:430–45. DOI: 10.1111/mmi.13471.
- Salman H, Libchaber A. A concentration-dependent switch in the bacterial response to temperature. *Nat Cell Biol* 2007;**9**:1098–100. DOI: 10.1038/ncb1632.
- Sanders JW, Leenhouts K, Burghoorn J et al. A chloride-inducible acid resistance mechanism in *Lactococcus lactis* and its regulation. *Mol Microbiol* 1998;**27**:299–310. DOI: 10.1046/j.1365-2958.1998.00676.x.
- Sangari FJ, Seoane A, Rodríguez MC et al. Characterization of the urease operon of *Brucella abortus* and assessment of its role in virulence of the bacterium. *Infect Immun* 2007;**75**:774–80. DOI: 10.1128/IAI.01244-06.
- Sansonetti PJ. Rupture, invasion and inflammatory destruction of the intestinal barrier by *Shigella*, making sense of prokaryote-eukaryote cross-talks. *FEMS Microbiol Rev* 2001;**25**:3–14. DOI: 10.1111/j.1574-6976.2001.tb00569.x.
- Sayed AK, Odom C, Foster JW. The *Escherichia coli* AraC-family regulators GadX and GadW activate *gadE*, the central activator of glutamate-dependent acid resistance. *Microbiology* 2007;**153**:2584–92. DOI: 10.1099/mic.0.2007/007005-0.
- Schlundt A, Buchner S, Janowski R et al. Structure-function analysis of the DNA-binding domain of a transmembrane transcriptional activator. *Sci Rep* 2017;**7**. DOI: 10.1038/s41598-017-01031-9.
- Scott DR, Marcus EA, Wen Y et al. Cytoplasmic histidine kinase (HP0244)-regulated assembly of urease with UreI, a channel for urea and its metabolites, CO₂, NH₃, and NH₄⁺, is necessary for acid survival of *Helicobacter pylori*. *J Bacteriol* 2010;**192**:94–103. DOI: 10.1128/JB.00848-09.
- Sen H, Aggarwal N, Ishionwu C et al. Structural and functional analysis of the *Escherichia coli* acid-sensing histidine kinase EvgS. *J Bacteriol* 2017;**199**. DOI: 10.1128/JB.00310-17.
- Šepūtienė V, Motiejūnas D, Sužiedėlis K et al. Molecular characterization of the acid-inducible *asr* gene of *Escherichia coli* and its role in acid stress response. *J Bacteriol* 2003;**185**:2475–84. DOI: 10.1128/JB.185.8.2475-2484.2003.

- Shabala L, Ross T. Cyclopropane fatty acids improve *Escherichia coli* survival in acidified minimal media by reducing membrane permeability to H⁺ and enhanced ability to extrude H⁺. *Res Microbiol* 2008;**159**:458–61. DOI: 10.1016/j.resmic.2008.04.011.
- Shi X, Bennett GN. Effects of *rpoA* and *cysB* mutations on acid induction of biodegradative arginine decarboxylase in *Escherichia coli*. *J Bacteriol* 1994;**176**:7017–23. DOI: 10.1128/jb.176.22.7017-7023.1994.
- Shi X, Waasdorp BC, Bennett GN. Modulation of acid-induced amino acid decarboxylase gene expression by *hns* in *Escherichia coli*. *J Bacteriol* 1993;**175**:1182–6.
- Shimada T, Katayama Y, Kawakita S et al. A novel regulator RcdA of the *csgD* gene encoding the master regulator of biofilm formation in *Escherichia coli*. *Microbiologyopen* 2012;**1**:381–94. DOI: 10.1002/mbo3.42.
- Shin D, Groisman EA. Signal-dependent binding of the response regulators PhoP and PmrA to their target promoters in vivo. *J Biol Chem* 2005;**280**:4089–94. DOI: 10.1074/jbc.M412741200.
- Shprung T, Peleg A, Rosenfeld Y et al. Effect of PhoP-PhoQ activation by broad repertoire of antimicrobial peptides on bacterial resistance. *J Biol Chem* 2012;**287**:4544–51. DOI: 10.1074/jbc.M111.278523.
- Shukuya R, Schwert GW. Glutamic acid decarboxylase. *J Biol Chem* 1960;**235**:1649–52. DOI: 10.1016/S0021-9258(19)76858-6.
- Siedler S, Balti R, Neves AR. Bioprotective mechanisms of lactic acid bacteria against fungal spoilage of food. *Curr Opin Biotechnol* 2019;**56**:138–46. DOI: 10.1016/j.copbio.2018.11.015.
- Silverman M, Simon M. Flagellar rotation and the mechanism of bacterial motility. *Nature* 1974;**249**:73–4. DOI: 10.1038/249073a0.
- Skouloubris S, Thiberge JM, Labigne A et al. The *Helicobacter pylori* UreI protein is not involved in urease activity but is essential for bacterial survival in vivo. *Infect Immun* 1998;**66**:4517–21. DOI: 10.1128/IAI.66.9.4517-4521.1998.
- Slonczewski JL, Fujisawa M, Dopson M et al. Cytoplasmic pH measurement and homeostasis in bacteria and archaea. In: Poole RK (ed.). *Advances in Microbial Physiology*: Vol. **55**. London, New York: Academic Press, 2009, 1–317.
- Smith A, Kaczmar A, Bamford RA et al. The culture environment influences both gene regulation and phenotypic heterogeneity in *Escherichia coli*. *Front Microbiol* 2018;**9**. DOI: 10.3389/fmicb.2018.01739.
- Smith DK, Kassam T, Singh B et al. *Escherichia coli* has two homologous glutamate decarboxylase genes that map to distinct loci. *J Bacteriol* 1992;**174**:5820–6. DOI: 10.1128/jb.174.18.5820-5826.1992.
- Snider J, Gutsche I, Lin M et al. Formation of a distinctive complex between the inducible bacterial lysine decarboxylase and a novel AAA+ ATPase. *J Biol Chem* 2006;**281**:1532–46. DOI: 10.1074/jbc.M511172200.
- Sohlenkamp C. Membrane homeostasis in bacteria upon pH challenge. In: Geiger O (ed.). *Biogenesis of Fatty Acids, Lipids and Membranes*. Cham: Springer, 2019;1–13.
- Soksawatmaekhin W, Kuraishi A, Sakata K et al. Excretion and uptake of cadaverine by CadB and its physiological functions in *Escherichia coli*. *Mol Microbiol* 2004;**51**:1401–12. DOI: 10.1046/j.1365-2958.2003.03913.x.
- Soksawatmaekhin W, Uemura T, Fukiwake N et al. Identification of the cadaverine recognition site on the cadaverine-lysine antiporter CadB. *J Biol Chem* 2006;**281**:29213–20. DOI: 10.1074/jbc.M600754200.
- Sommer E, Koler M, Frank V et al. The sensory histidine kinases TorS and EvgS tend to form clusters in *Escherichia coli* cells. *PLoS ONE* 2013;**8**:e77708. DOI: 10.1371/journal.pone.0077708.
- Soncini FC, García Véscovi E, Solomon F et al. Molecular basis of the magnesium deprivation response in *Salmonella typhimurium*: identification of PhoP-regulated genes. *J Bacteriol* 1996;**178**:5092–9.
- Soncini FC, Groisman EA. Two-component regulatory systems can interact to process multiple environmental signals. *J Bacteriol* 1996;**178**:6796–801.
- Stancik LM, Stancik DM, Schmidt B et al. pH-dependent expression of periplasmic proteins and amino acid catabolism in *Escherichia coli*. *J Bacteriol* 2002;**184**:4246–58. DOI: 10.1128/JB.184.15.4246-4258.2002.
- Steinberg BE, Huynh KK, Grinstein S. Phagosomal acidification: measurement, manipulation and functional consequences. *Biochem Soc Trans* 2007;**35**:1083–7. DOI: 10.1042/BST0351083.
- Stelzer S, Egan S, Larsen MR et al. Unravelling the role of the ToxR-like transcriptional regulator WmpR in the marine antifouling bacterium *Pseudoalteromonas tunicata*. *Microbiology* 2006;**152**:1385–94. DOI: 10.1099/mic.0.28740-0.
- Stim-Herndon KP, Flores TM, Bennett GN. Molecular characterization of *adiY*, a regulatory gene which affects expression of the biodegradative acid-induced arginine decarboxylase gene (*adiA*) of *Escherichia coli*. *Microbiology* 1996;**142**:1311–20. DOI: 10.1099/13500872-142-5-1311.
- Stull F, Hipp H, Stockbridge RB et al. In vivo chloride concentrations surge to proteotoxic levels during acid stress. *Nat Chem Biol* 2018;**14**:1051–8. DOI: 10.1038/s41589-018-0143-z.
- Sun Y, Fukamachi T, Saito H et al. Respiration and the F₁F_o-ATPase enhance survival under acidic conditions in *Escherichia coli*. *PLoS ONE* 2012;**7**:e52577. DOI: 10.1371/journal.pone.0052577.
- Sužiedėlienė E, Sužiedėlis K, Garbenčiūtė V et al. The acid-inducible *asr* gene in *Escherichia coli*: transcriptional control by the *phoBR* operon. *J Bacteriol* 1999;**181**:2084–93.
- Swaminathan B. *Listeria monocytogenes*. In: Doyle MP (ed.). *Food Microbiology: Fundamentals and Frontiers*. Washington: ASM Press, 2001;383–409.
- Sweeney EG, Henderson JN, Goers J et al. Structure and proposed mechanism for the pH sensing *Helicobacter pylori* chemoreceptor TlpB. *Structure* 2012. DOI: 10.1016/j.str.2012.04.021.
- Tanabe H, Masuda T, Yamasaki K et al. Molecular interaction between proteins involved in EvgAS signal transduction of *Escherichia coli*. *Biosci Biotechnol Biochem* 1998;**62**:78–82. DOI: 10.1271/bbb.62.78.
- Tapley TL, Franzmann TM, Chakraborty S et al. Protein refolding by pH-triggered chaperone binding and release. *Proc Natl Acad Sci USA* 2009a;**107**:1071–6. DOI: 10.1073/pnas.0911610107.
- Tapley TL, Körner JL, Barge MT et al. Structural plasticity of an acid-activated chaperone allows promiscuous substrate binding. *Proc Natl Acad Sci USA* 2009b;**106**:5557–62. DOI: 10.1073/pnas.0811811106.
- Taylor JL, Silva RS de, Kovacicova G et al. The crystal structure of AphB, a virulence gene activator from *Vibrio cholerae*, reveals residues that influence its response to oxygen and pH. *Mol Microbiol* 2012;**83**:457–70. DOI: 10.1111/j.1365-2958.2011.07919.x.
- Tennant SM, Hartland EL, Phumoonna T et al. Influence of gastric acid on susceptibility to infection with ingested bacterial pathogens. *Infect Immun* 2007;**76**:639–45. DOI: 10.1128/IAI.01138-07.
- Tetsch L, Koller C, Haneburger I et al. The membrane-integrated transcriptional activator CadC of *Escherichia coli* senses lysine indirectly via the interaction with the lysine permease LysP. *Mol Microbiol* 2008;**67**:570–83. DOI: 10.1111/j.1365-2958.2007.06070.x.
- Tilden J, Young W, McNamara AM et al. A new route of transmission for *Escherichia coli*: infection from dry fermented salami. *Am J Pub Health* 1996;**86**:1142–5. DOI: 10.2105/ajph.86.8_pt_1.1142.

- Tohidifar P, Plutz MJ, Ordal GW et al. The mechanism of bidirectional pH taxis in *Bacillus subtilis*. *J Bacteriol* 2020;**202**. DOI: 10.1128/JB.00491-19.
- Tramonti A, Canio M de, Delany I et al. Mechanisms of transcription activation exerted by GadX and GadW at the *gadA* and *gadBC* gene promoters of the glutamate-based acid resistance system in *Escherichia coli*. *J Bacteriol* 2006;**188**:8118–27. DOI: 10.1128/JB.01044-06.
- Tramonti A, Visca P, Canio M de et al. Functional characterization and regulation of *gadX*, a gene encoding an AraC/XylS-like transcriptional activator of the *Escherichia coli* glutamic acid decarboxylase system. *J Bacteriol* 2002;**184**:2603–13. DOI: 10.1128/JB.184.10.2603-2613.2002.
- Tsai M-F, McCarthy P, Miller C. Substrate selectivity in glutamate-dependent acid resistance in enteric bacteria. *Proc Natl Acad Sci USA* 2013;**110**:5898–902. DOI: 10.1073/pnas.1301444110.
- Tsai M-F, Miller C. Substrate selectivity in arginine-dependent acid resistance in enteric bacteria. *Proc Natl Acad Sci USA* 2013;**110**:5893–7. DOI: 10.1073/pnas.1301442110.
- Tsang N, Macnab R, Koshland DE. Common mechanism for repellents and attractants in bacterial chemotaxis. *Science* 1973;**181**:60–3. DOI: 10.1126/science.181.4094.60.
- Tso WW, Adler J. Negative chemotaxis in *Escherichia coli*. *J Bacteriol* 1974;**118**:560–76. DOI: 10.1128/jb.118.2.560-576.1974.
- Tucker DL, Tucker N, Conway T. Gene expression profiling of the pH response in *Escherichia coli*. *J Bacteriol* 2002;**184**:6551–8. DOI: 10.1128/JB.184.23.6551-6558.2002.
- Ude S, Lassak J, Starosta AL et al. Translation elongation factor EF-P alleviates ribosome stalling at polyproline stretches. *Science* 2013;**339**:82–5. DOI: 10.1126/science.1228985.
- Umemura T, Matsumoto Y, Ohnishi K et al. Sensing of cytoplasmic pH by bacterial chemoreceptors involves the linker region that connects the membrane-spanning and the signal-modulating helices. *J Biol Chem* 2002;**277**:1593–8. DOI: 10.1074/jbc.M109930200.
- Utsumi R, Katayama S, Taniguchi M et al. Newly identified genes involved in the signal transduction of *Escherichia coli* K-12. *Gene* 1994;**140**:73–7. DOI: 10.1016/0378-1119(94)90733-1.
- Utsumi R, Kawamoto K, Yamazaki K et al. Characterization of the signal transduction via EvgS and EvgA in *Escherichia coli*. *J Gen Appl Microbiol* 1996;**42**:155–62. DOI: 10.2323/jgam.42.155.
- Valderas MW, Alcantara RB, Baumgartner JE et al. Role of HdeA in acid resistance and virulence in *Brucella abortus* 2308. *Vet Microbiol* 2005;**107**:307–12. DOI: 10.1016/j.vetmic.2005.01.018.
- van Vliet AHM, Poppelaars SW, Davies BJ et al. NikR mediates nickel-responsive transcriptional induction of urease expression in *Helicobacter pylori*. *Infect Immun* 2002;**70**:2846–52. DOI: 10.1128/IAI.70.6.2846-2852.2002.
- vanLoon GW. Acid rain and soil. *Can J Physiol Pharmacol* 1984;**62**:991–7. DOI: 10.1139/y84-168.
- Venkatesh GR, Kembou Koungni FC, Paukner A et al. BglJ-RcsB heterodimers relieve repression of the *Escherichia coli* *bgl* operon by H-NS. *J Bacteriol* 2010;**192**:6456–64. DOI: 10.1128/JB.00807-10.
- Viala JPM, Méresse S, Pocachard B et al. Sensing and adaptation to low pH mediated by inducible amino acid decarboxylases in *Salmonella*. *PLoS ONE* 2011;**6**:e22397. DOI: 10.1371/journal.pone.0022397.
- Viarengo G, Sciarra MI, Salazar MO et al. Unsaturated long chain free fatty acids are input signals of the *Salmonella enterica* PhoP/PhoQ regulatory system. *J Biol Chem* 2013;**288**:22346–58. DOI: 10.1074/jbc.M113.472829.
- Villarreal L, Heredia NL, García S. Changes in protein synthesis and acid tolerance in *Clostridium perfringens* type a in response to acid shock. *Int Microbiol* 2000;**3**:113–6.
- Wang S, Yan R, Zhang X et al. Molecular mechanism of pH-dependent substrate transport by an arginine-agmatine antiporter. *Proc Natl Acad Sci USA* 2014;**111**:12734–9. DOI: 10.1073/pnas.1414093111.
- Waterman SR, Small PL. Identification of σ^S -dependent genes associated with the stationary-phase acid-resistance phenotype of *Shigella flexneri*. *Mol Microbiol* 1996;**21**:925–40. DOI: 10.1046/j.1365-2958.1996.00058.x.
- Waterman SR, Small PLC. The glutamate-dependent acid resistance system of *Escherichia coli* and *Shigella flexneri* is inhibited in vitro by L-trans-pyrrolidine-2,4-dicarboxylic acid. *FEMS Microbiol Lett* 2003;**224**:119–25. DOI: 10.1016/S0378-1097(03)00427-0.
- Watson N, Duniak DS, Rosey EL et al. Identification of elements involved in transcriptional regulation of the *Escherichia coli* *cad* operon by external pH. *J Bacteriol* 1992;**174**:530–40.
- Weber H, Polen T, Heuveling J et al. Genome-wide analysis of the general stress response network in *Escherichia coli*: σ^S -dependent genes, promoters, and sigma factor selectivity. *J Bacteriol* 2005;**187**:1591–603. DOI: 10.1128/JB.187.5.1591-1603.2005.
- Weeks DL, Eskandari S, Scott DR et al. A H⁺-gated urea channel: the link between *Helicobacter pylori* urease and gastric colonization. *Science* 2000;**287**:482–5. DOI: 10.1126/science.287.5452.482.
- Wen Y, Feng J, Scott DR et al. The pH-responsive regulon of HP0244 (FlgS), the cytoplasmic histidine kinase of *Helicobacter pylori*. *J Bacteriol* 2009;**191**:449–60. DOI: 10.1128/JB.01219-08.
- Wen Y, Marcus EA, Matrubutham U et al. Acid-adaptive genes of *Helicobacter pylori*. *Infect Immun* 2003;**71**:5921–39. DOI: 10.1128/IAI.71.10.5921-5939.2003.
- Wieder W.R., Boehnert J, Bonan G.B. et al. ReGRIDDED harmonized world soil database v1.2. Oak Ridge: ORNL Distributed Active Archive Center. 2014.
- Wilks JC, Slonczewski JL. pH of the cytoplasm and periplasm of *Escherichia coli*: rapid measurement by green fluorescent protein fluorimetry. *J Bacteriol* 2007;**189**:5601–7. DOI: 10.1128/JB.00615-07.
- Wilmes-Riesenberg MR, Bearson B, Foster JW et al. Role of the acid tolerance response in virulence of *Salmonella typhimurium*. *Infect Immun* 1996;**64**:1085–92.
- Wilmes-Riesenberg MR, Foster JW, Curtiss R. An altered *rpoS* allele contributes to the avirulence of *Salmonella typhimurium* LT2. *Infect Immun* 1997;**65**:203–10.
- Wösten MMSM, Kox LFF, Chamnongpol S et al. A signal transduction system that responds to extracellular iron. *Cell* 2000;**103**:113–25. DOI: 10.1016/S0092-8674(00)00092-1.
- Yang Y, Kadim MI, Khoo WJ et al. Membrane lipid composition and stress/virulence related gene expression of *Salmonella enteritidis* cells adapted to lactic acid and trisodium phosphate and their resistance to lethal heat and acid stress. *Int J Food Microbiol* 2014;**191**:24–31. DOI: 10.1016/j.ijfoodmicro.2014.08.034.
- Yang Y, Sourjik V. Opposite responses by different chemoreceptors set a tunable preference point in *Escherichia coli* pH taxis. *Mol Microbiol* 2012;**86**:1482–9. DOI: 10.1111/mmi.12070.
- Zhao B, Houry WA. Acid stress response in enteropathogenic gamma proteobacteria: an aptitude for survival. *Biochem Cell Biol* 2010;**88**:301–14. DOI: 10.1139/o09-182.
- Zhao Y, Jansen R, Gastra W et al. Identification of genes affecting *Salmonella enterica* serovar enteritidis infection of chicken macrophages. *Infect Immun* 2002;**70**:5319–21. DOI: 10.1128/IAI.70.9.5319-5321.2002.
- Zomot E, Bahar I. Protonation of glutamate 208 induces the release of agmatine in an outward-facing conformation of an arginine/agmatine antiporter. *J Biol Chem* 2011;**286**:19693–701. DOI: 10.1074/jbc.M110.202085.

Zwir I, Latifi T, Perez JC et al. The promoter architectural landscape of the *Salmonella* PhoP regulon. *Mol Microbiol* 2012;**84**:463–85. DOI: 10.1111/j.1365-2958.2012.08036.x.

Zwir I, Shin D, Kato A et al. Dissecting the PhoP regulatory network of *Escherichia coli* and *Salmonella enterica*. *Proc Natl Acad Sci* 2005;**102**:2862–7. DOI: 10.1073/pnas.0408238102.

2.6 Bacterial acid stress response: from cellular changes to antibiotic tolerance and phenotypic heterogeneity

Schumacher, K., Brameyer, S., and Jung, K. (2023). Bacterial acid stress response: from cellular changes to antibiotic tolerance and phenotypic heterogeneity. *Curr. Opin. Microbiol.* 75:102367.10.1016/j.mib.2023.102367

Available online at:

<https://pubmed.ncbi.nlm.nih.gov/37633223/>



ELSEVIER



Bacterial acid stress response: from cellular changes to antibiotic tolerance and phenotypic heterogeneity

Kilian Schumacher, Sophie Brameyer and Kirsten Jung

Most bacteria are neutrophiles but can survive fluctuations in pH in their environment. Herein, we provide an overview of the adaptation of several human, soil, and food bacteria to acid stress, mainly based on next-generation sequencing studies, highlighting common and specific strategies. We also discuss the interplay between acid stress response and antibiotic tolerance, as well as the response of individual cells.

Address

Faculty of Biology, Microbiology, Ludwig-Maximilians-Universität München, 82152 Martinsried, Germany

Corresponding author: Jung, Kirsten (jung@lmu.de)

Current Opinion in Microbiology 2023, 75:102367

This review comes from a themed issue on **Microbial Systems and Synthetic Biology**

Edited by **Victor Sourjik** and **Kiran Patel**

For complete overview of the section, please refer to the article collection, "[Microbial Systems and Synthetic Biology 2023](#)"

Available online 24 August 2023

<https://doi.org/10.1016/j.mib.2023.102367>

1369–5274/© 2023 Elsevier Ltd. All rights reserved.

Introduction

Bacteria have evolved sophisticated acid resistance systems to survive and even multiply in acidic environments (Figure 1a). Acid stress sensing and adaptation enable neutrophilic bacteria to maintain constant intracellular pH under moderate acid stress [1]. As acidification of the cytoplasm has severe effects on all macromolecules of a cell that might lead to protein unfolding, decreased enzyme activity, membrane damage, and DNA damage [2–4], bacteria have evolved a variety of acid stress resistance systems to counteract and survive in mild and highly acidic environments [5]. Detailed information on the molecular mechanisms of acid resistance in bacteria can be found in reviews by Cotter & Hill 2003, Foster 2004, Kanjee & Houry 2013, Lund et al. 2014, Guan & Li 2020, Arcari et al. 2020, Schwarz et al. 2022, and Rai et al. 2022 [5–12].

Here, we focus on systemic studies of the acid response of various bacteria and describe common and species-

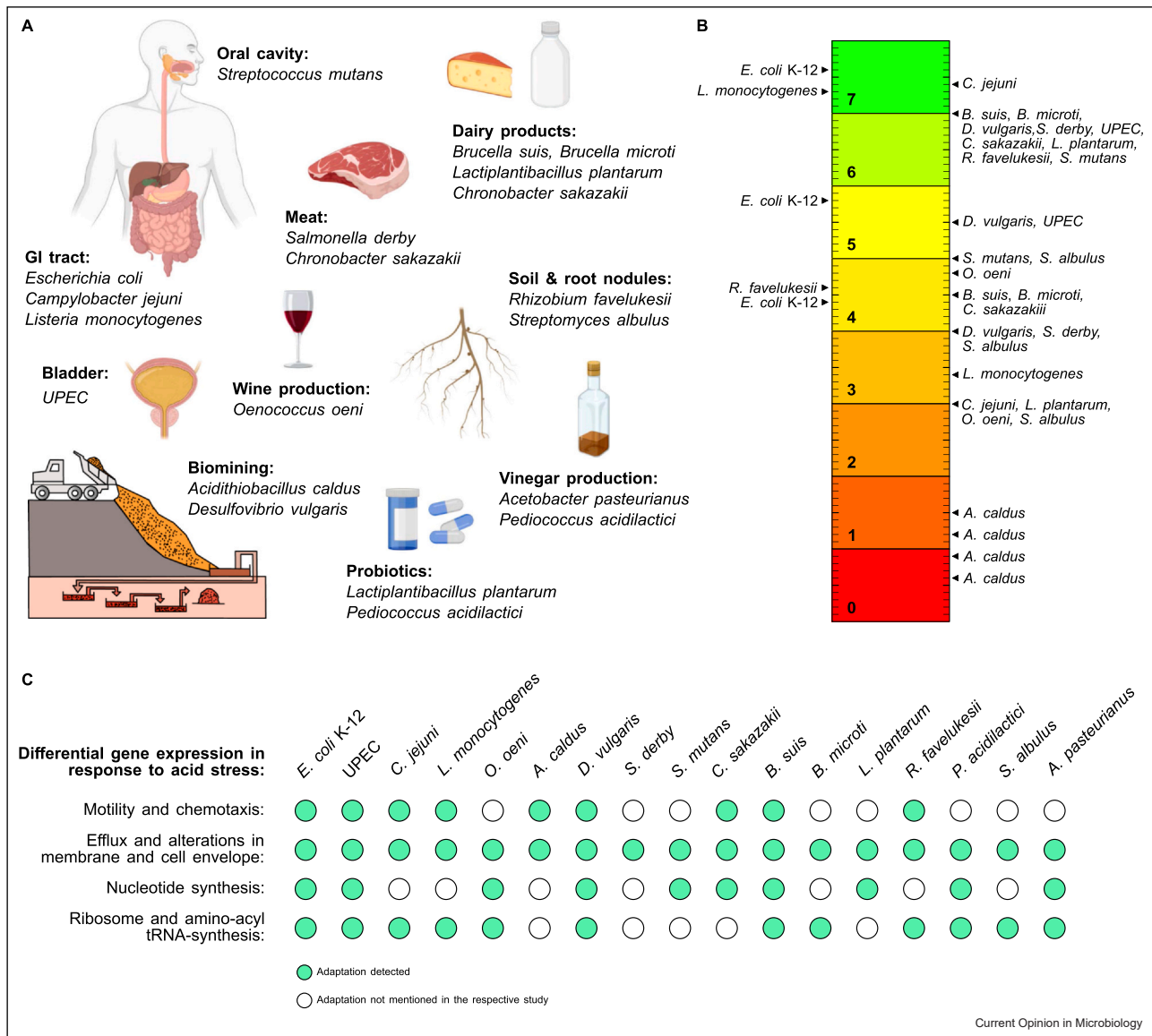
specific acid resistance mechanisms. We will also discuss how acid stress resistance facilitates development of antibiotic resistance [13]. Although most studies of stress response dynamics have focused on the population level and thus on the average response of millions of cells, recent work has also examined the acid stress response of individual cells, revealing phenotypic heterogeneity, which is also discussed.

Acid stress-dependent alterations of the transcriptome and proteome of various bacteria

Significant advances have been made in understanding how bacteria interact with their environment, particularly after the development of powerful next-generation sequencing techniques such as bacterial single-cell RNA-Seq, dual RNA-Seq, and triple RNA-Seq [14–17]. This trend of rapid large-scale data collection has now also impacted the field of acid stress research, as more and more next-generation sequencing techniques have become routine workflows in many laboratories. Since 2020, over a dozen studies, which are reviewed here, have been published with the aim of revealing genome-wide responses to acidity in a broad range of bacterial species (Figure 1), using a variety of techniques. These included mainly bulk RNA-Seq to analyze bacterial transcriptomes, with fewer studies using mass spectrometry to examine the translational level [18,19] (Table 1). Additionally, ribosome profiling (Ribo-Seq) has been employed to evaluate global protein synthesis rates under mild and severe acid stress in *E. coli* K-12 MG1655 (designated as *E. coli*) [20]. Ribo-Seq is a powerful tool that provides a global overview of protein synthesis rates and enables the detection of unidentified small open-reading frames [21,22]. Further insights into the microbial defense against low pH were provided by transposon-insertion-directed sequencing (TraDis), also called Tn-Seq. In the respective studies, transposon libraries were used for deep sequencing to provide information on the contribution of single genes to fitness in acidic habitats in uropathogenic *E. coli* (UPEC) and *Salmonella derby* [23,24].

Recent multi-omics studies focused on bacterial species from a broad range of phylogenetic classes, including *Acidithiobacillia*, *Actinomycetes*, *Alphaproteobacteria*, *Bacilli*, *Deltaproteobacteria*, *Epsilonproteobacteria*, and *Gammaproteobacteria* (Table 1). These organisms colonize a variety of environmental niches, including the

Figure 1



Overview of omics studies from 2020 to 2023, investigating global acid stress responses in various bacteria. (a) Habitats and industrial applications of bacterial species being studied using next-generation sequencing. (b) Visual representation of pH values selected as acid stress and controls for experiments listed in Table 1. (c) Schematic overview of acid stress responses. Common adaptations detected in several bacterial species are highlighted in green, adaptations that were not mentioned in the respective studies are marked in white. Figure (a) is created using BioRender.com and Affinity Designer 1.10.4.

gastrointestinal tract (GI tract), the human oral cavity and bladder, processed and unprocessed foods, acidic soils and root nodules, as well as biomining sites (Figure 1a). Among the strains listed in Table 1, *Escherichia coli*, *Campylobacter jejuni*, and *Listeria monocytogenes* colonize the human GI tract and can induce diseases. Further investigated bacteria include *Streptococcus mutans*, which is associated with dental caries and causes dysbiosis in the oral cavity [19], and UPEC, which is the primary cause of urinary tract infections. In

addition, genome-wide acid responses of other food-borne pathogens, including *Salmonella derby*, *Chronobacter sakazakii*, *Brucella suis*, and *Brucella microti* have been characterized [24–26]. Other bacteria that have been the subject of recent multi-omics studies were *Rhizobium favelukesii* [27], an alfalfa-nodulating rhizobia frequently found in low-pH soils, and *Streptomyces albus*, which is used for the industrial production of ε-poly-L-lysine [28]. Additionally, *Oenococcus oeni*, *Pediococcus acidilactici*, and *Acetobacter pasteurianus* are

Table 1

Bacterial species, methods, and growth media used to study genome-wide responses to acid stress.

Strain	Family	Class	Methods	Growth medium	Reference
<i>Acetobacter pasteurianus</i> Ab3	Acetobacteraceae	Alphaproteobacteria	RNA-Seq	Yeast extract-peptone-dextrose (YPD) medium + 20 g/l ethanol	[45]
<i>Acidithiobacillus calidus</i> CCTCC M 2018054	Acidithiobacillaceae	Acidithiobacillia	RNA-Seq	Modified Starkey medium	[37]
<i>Brucella suis</i> ATCC 23444, <i>Brucella microti</i> CCM4915	Brucellaceae	Alphaproteobacteria	RNA-Seq	Tryptic Soy broth (TSB) and Gerhardt's minimal medium (GMM)	[25]
<i>Campylobacter jejuni</i> NCTC11168	Campylobacteraceae	Epsilonproteobacteria	Microarray	Mueller Hinton (MH)	[38]
<i>Cronobacter sakazakii</i> CICC 21544	Enterobacteriaceae	Gammaproteobacteria	RNA-Seq	TSB	[26]
<i>Desulfovibrio vulgaris</i> ATCC 7757	Desulfovibrionaceae	Deltaproteobacteria	RNA-Seq	Self-created medium containing yeast extract	[36]
<i>Escherichia coli</i> K-12 MG1655	Enterobacteriaceae	Gammaproteobacteria	RNA-Seq, Ribo-Seq	Luria-Bertani (LB)	[20]
<i>Escherichia coli</i> serotype ST131 strain EO499 (UPEC)	Enterobacteriaceae	Gammaproteobacteria	RNA-Seq, TraDIS	M9 medium supplemented with glucose and cas-amino acids + 100 mM 3-(N-morpholino)propanesulfonic acid (MOPS) /100 mM 2-(N-morpholino)ethanesulfonic acid (MES)	[23]
<i>Lactiplantibacillus plantarum</i> ZDY2013	Lactobacillaceae	Bacilli	RNA-Seq	De Man, Rogosa, and Sharpe (MRS) broth	[39]
<i>Listeria monocytogenes</i> 6179 and R479a	Listeriaceae	Bacilli	RNA-Seq	TSB	[40]
<i>Oenococcus oeni</i> SD-2a	Leuconostocaceae	Bacilli	RNA-Seq, metabolomics	Fructose-malate-acid-tomato juice broth medium	[48]
<i>Pediococcus acidilactici</i> CGMCC 17856	Lactobacillaceae	Bacilli	Proteomics	MRS	[18]
<i>Rhizobium favelukesii</i> LPU83	Rhizobiaceae	Alphaproteobacteria	RNA-Seq	Sucrose-glutamate minimal medium + 10 mM 4-(2-hydroxyethyl)-1-piperazineethanesulfonic acid (HEPES) /MES	[27]
<i>Salmonella derby</i> 14T	Enterobacteriaceae	Gammaproteobacteria	Tn-Seq	LB	[24]
<i>Streptococcus mutans</i> UA159	Streptococcaceae	Bacilli	Proteomics	Tryptone yeast medium + 1% (w/v) glucose	[19]
<i>Streptomyces albulus</i> M-Z18	Streptomycetaceae	Actinomycetes	RNA-Seq	Agar slant medium	[28]

See text for details.

exposed to acidity during industrial applications (Figure 1a). *Oenococcus oeni* is commonly used in wine production for malolactic fermentation, during which L-malate is converted to L-lactate and carbon dioxide under low-pH conditions [29]. *Pediococcus acidilactici* is utilized in the production of vinegar and as a probiotic food supplement [18,30]. Acid tolerance is crucial for these applications because acetic and lactic acids accumulate during vinegar production [31], and probiotic supplements are supposed to exhibit robustness toward acidity encountered in the stomach [32]. While most transcriptome and proteome analyses were conducted with neutralophilic bacteria, *Acidithiobacillus caldus* is acidophilic and commonly used for bioleaching to recover valuable metals from reduced sulfides [33]. During this process, metal ions are oxidized, and sulfuric acid is produced, resulting in an ambient pH of < 1.5 [34]. Despite being exposed to extreme acid stress, acidophilic organisms are capable of maintaining an internal pH of approximately 6.0 [35]. In this regard, the transcriptome of *A. caldus* was studied within the pH range of 0.6–1.5, whereas other bacteria were typically subjected to experiments performed within the range of pH 3.0–4.5, or 5.0–5.8 (Figure 1b). In addition to *A. caldus*, *Desulfovibrio vulgaris*, a sulfate-reducing bacterium, can be applied during biomining to remediate acid mine wastewater [36].

A comparison of these global systemic studies (Table 1) reveals both common changes in the expression of specific genes and species-specific adaptation strategies. Remarkably, despite substantial differences in sampling time points, stress treatment, stress duration, growth medium, pH (Figure 1b), oxygen availability, strain physiology, and habitats (Figure 1a), a number of common acid stress adaptations are detectable, even among distantly related bacteria. These adaptations include differential expression of genes associated with motility and chemotaxis, efflux and alterations in membrane and cell envelope, nucleotide synthesis, and ribosome and amino-acyl tRNA synthesis (Figure 1c). For example, differential expression of motility and chemotaxis-associated genes is found in *E. coli*, UPEC, *A. caldus*, *B. suis*, *C. jejuni*, *D. vulgaris*, *C. sakazakii*, *L. monocytogenes*, and *R. favelukesii* [20,23,25–27,36–40]. pH-dependent expression of genes involved in flagellar assembly and locomotion, as well as pH taxis, has previously been observed in both *E. coli* and *B. subtilis* and represents a strategy to migrate to territories with desired proton concentrations [41–43]. In response to low pH, modifications in inner and outer membrane composition are noted, which include differential synthesis of transporters, efflux pumps, and fatty acids. These adaptations restrict proton uptake and accelerate proton extrusion, and are detectable in all studied species (Figure 1c). A common adaptation of this type is the upregulation of genes encoding the subunits of F₀F₁-

adenosine triphosphate (ATP) synthase, which exports protons in an ATP-dependent manner [44], in *E. coli*, *A. caldus*, *A. pasteurianus*, *B. microti*, and *S. mutans* [19,25,37,45]. Bacterial nucleotide metabolism is also undergoing significant changes (Figure 1c). Particularly in *B. suis*, *E. coli*, and *S. mutans*, genes involved in purine biosynthesis are upregulated under acid stress [19,20,25]. It is worth noting that DNA damage is accelerated by acid stress, and DNA depurination increases proportionally with lower pH [46]. Depurination refers to the loss of purine caused by hydrolysis of *N*-glycosyl bonds, which occurs more rapidly compared with depyrimidination [47]. Thus, the observed increase in purine biosynthesis in acid-stressed bacteria might provide additional purine nucleotides for DNA repair. This hypothesis is supported by metabolomics data from *O. oeni*, which suggest a decrease in the abundance of nucleotides upon acid treatment [48]. In the same study, increased expression of genes related to translation and post-translational modifications is suggested. Indeed, genes encoding ribosomal subunits are differentially expressed upon acid stress, for example, in *E. coli*, *C. jejuni*, *D. vulgaris*, *P. acidilactici*, *O. oeni*, *R. favelukesii*, and *S. albulus* (Figure 1c) [18,20,27,28,36,38,48]. Accordingly, amino-acyl tRNA synthesis in *E. coli*, UPEC, and *L. monocytogenes* is affected by low pH [20,23,40].

In addition to common adaptation strategies, there are also different species-specific mechanisms. The plasmid-encoded putative metal-ion sensing riboswitch is specific for the acid response of *L. monocytogenes* [40]. Acid stress in *B. microti* induces production of the cold-shock protein CspA. A deletion of the corresponding gene decreases the survival of these bacteria in acidified media [25]. Intriguingly, *cspA* is a pseudogene in *B. suis*, a feature that could explain the observed difference in acid tolerance between *B. suis* and *B. microti* [25]. Among other transcriptional changes in the acidophilic *A. caldus*, a decrease in external pH resulted in downregulation of several transcriptional regulators of the LysR family, which have been demonstrated to be essential for maintaining cytoplasmic pH [37]. In *E. coli* K-12, about 2% of all ribosome profiling reads at pH 4.4 mapped to the *asr* region, which encodes an acid-shock protein [20]. This highlights the crucial role of Asr, a periplasmic chaperone that contributes to membrane integrity by preventing aggregation of proteins with positive charges [49]. Moreover, altered pyruvate metabolism was observed in *P. acidilactici* and *O. oeni* [18,48]. UPEC in acidic habitats, is protected by serine deamination resulting in increased levels of pyruvate and ammonia. Presumably, the produced pyruvate is taken up by the putative pyruvate transporter YhjX [50].

In conclusion, while many mechanisms of acid resistance are conserved in a variety of bacterial genera, there are also species- and strain-specific adaptations, which is

ultimately reflected in the different degrees of acid tolerance among bacteria [5].

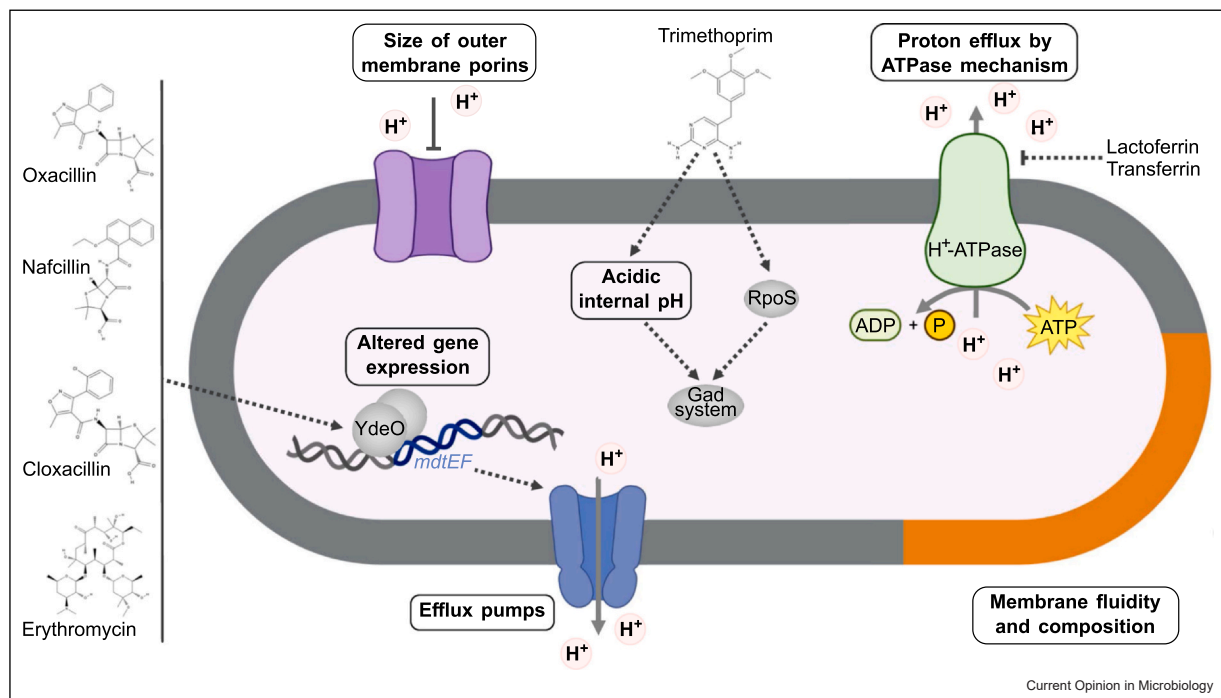
Acid stress and antibiotic tolerance

The activation of stress response programs often protects bacteria from subsequent higher levels of the same stress, or other environmental stresses. Acid-induced changes in the size of outer membrane porins, and membrane fluidity and lipid composition, as a mechanism against proton penetration, contribute to a cross-protection against antibiotics of bacterial cells [9,13] (Figure 2). Moreover, the proton-pumping ATPase (H^+ -ATPase) is necessary for pumping protons out of bacterial cells and even H^+ -ATPase inhibitors are known to enhance antibiotic activity against several Gram-negative bacteria [51–53] (Figure 2). Additionally, multidrug efflux pumps, which contribute to antibiotic tolerance, have been associated with acid stress response systems and are discussed for their role in pH homeostasis [54]. Under acidic conditions, the expression of numerous efflux-encoding and efflux-associated genes is altered. For example, in *E. coli*, the expression of the multidrug locus *mdtEF* is

upregulated by pH-induced transcription factors such as GadX–GadW [55] and EvgA–YdeO [56,57] (Figure 2). During the exposure to extreme acidic conditions (pH 2.0), the efflux pump MdtEF–TolC confers a fitness advantage for *E. coli* cells [58]. The expression of *emrKY*, coding for a drug efflux pump, in *Shigella flexneri* is enhanced under acidic pH and high K^+ concentrations to mediate survival during macrophage infection [59]. The expression of *norB*, coding for a drug efflux pump of *Staphylococcus aureus*, is derepressed under moderate acidic conditions via the transcriptional regulator MgrA, leading to a decrease in bacterial killing by the antibiotic moxifloxacin [60].

In recent years, more attention has been paid to the link between intracellular pH and its variability and the bacterial susceptibility to antibiotics. Adaptation to acidic conditions leads to a shift in pH homeostasis toward intracellular acidification that prevents antibiotic killing of bacteria, such as *S. aureus*, *E. coli*, *Pseudomonas aeruginosa*, and *Mycobacterium tuberculosis*, as well as *M. smegmatis* [61]. For example, when *E. coli*

Figure 2



The interplay between acid stress response and antibiotic tolerance. Examples of the interconnectivity between acid stress and antibiotic tolerance include changes in cell membrane fluidity and composition, altered gene expression, acidification of cytoplasmic pH, size of outer membrane porins, regulation of efflux pumps spanning the inner and outer membranes, and proton efflux by H^+ -ATPase (all circled in black boxes). Notably, the pH-responsive transcriptional regulator YdeO is also affected by several antibiotics such as oxacillin, nafcillin, cloxacillin, and erythromycin, leading to upregulation of the *mdtEF* operon (blue), which encodes an efflux pump [56]. TMP influences the intracellular pH and copy number of RpoS, leading to heterogeneous activation of the Gad system [65]. Lactoferrin and transferrin inhibit the H^+ -ATPase activity and impair proton efflux [53]. The cell envelope is shown as a gray, partially orange ring. Solid gray arrows indicate transport, dashed arrows indicate influences of compounds and their consequences. The figure is created with BioRender.com and Affinity Designer 1.10.4, and MolView v2.4 was used to draw the chemical structures.

is cultivated under conditions that cause intracellular acidification, its susceptibility to antibiotics, including kanamycin, norfloxacin, and carbenicillin, has been reduced [61]. Furthermore, a reduction in transcripts, all regulated by RpoS and involved in multiple stress response cascades, including acid resistance, multi-drug resistance, and osmotic resistance, led to an increase in persistence of *E. coli* [62]. Persister cells survive the antibiotic challenge and allow regrowth after antibiotic removal [63]. *E. coli* cells that become persisters have a more acidic intracellular pH than cells that are either susceptible or viable but non-culturable. The key to this differential pH regulation in persister cells seems to be the enzyme tryptophanase, encoded by *tnaA* [63]. In *Salmonella*, vacuolar acidification and nutritional deprivation induced persistence immediately after uptake by macrophages of the host [64]. Furthermore, acidification of the intracellular pH of *E. coli* cells contributes to the full implementation of resistance to antibiotics, such as mediated via the *marRAB* operon [2].

Mitosch and colleagues [65] analyzed quantitatively at the single-cell level, using fluorescence microscopy, the survival of *E. coli* cells under extreme acid stress (pH 3.0) when the cells were prestressed with antibiotics. Of the tested antibiotics, the folate biosynthesis inhibitor trimethoprim (TMP) activated an acid stress response and thus cross-protection of bacteria from subsequent extreme acid stress (Figure 2). This response to acidity is mediated via the Gad system by the expression of *gadBC*, which in turn is highly variable under acid stress. The highly variable *gadBC* expression correlated with single-cell survival by maintaining higher intracellular pH (see below). It has been hypothesized that the acid stress response to TMP is activated as a downstream effect of the depletion of purine bases [65]. In a subsequent study [66], they showed that the acid stress response caused by TMP in single cells does not have a strict temporal order with the DNA damage repair response, known as SOS response.

In conclusion, the correlation between the degree of intracellular acidification of individual cells and a resulting antibiotic tolerance/resistance of subpopulations needs to be further investigated.

The heterogeneous acid stress response

Under acid stress, bacteria often show heterogeneous behavior to increase the fitness of a population by enabling division of labor. Phenotypic heterogeneity arises from internal factors such as individual physiological state and stochastic gene expression and is strongly influenced by external factors such as physical and chemical stresses, availability of nutrients, and cell density [67,68].

E. coli, for example, possesses the four enzyme-based H⁺-consuming acid-resistant systems Gad, Adi, Cad, and Orn. Recently, activation of the Gad, Adi, and Cad systems was quantitatively analyzed using a fluorescent triple *E. coli* reporter strain under consecutively increasing acid stress conditions [69]. The Cad system (activated at pH 5.8 in the presence of lysine) and the Adi system (activated at pH 4.4) were found to be mutually exclusively activated, with a high level of ON-OFF cells. These phenotypic variations are not only due to differences in the pH homeostasis of individual *E. coli* cells [70], but also to the low copy number of the transcriptional regulators CadC and AdiY [69,71,72]. It should be noted that activation of the Cad or Adi system leads to an increase in internal pH based on the consumption of protons in the decarboxylation of lysine to cadaverine or arginine to agmatine, respectively, in individual cells, but the entire population also benefits due to the secretion of the more alkaline cadaverine and agmatine, which raise the external pH [69].

The Gad system (activated at moderate acid stress and essential under extreme acid stress) was activated in all *E. coli* cells, albeit to varying degrees [69]. Activation of two promoters of the Gad system, namely *gadBC* and *gadX*, is highly dynamic and variable, leading to cell-to-cell heterogeneity [65,73] that ensures the survival of at least a subpopulation of *E. coli* under extreme acid stress. A recent study revealed that *gadE*, encoding the master regulator of the Gad system, is heterogeneously expressed even in the absence of acid stress, thereby preemptively generating acid-resistant subpopulations within a clonal *E. coli* population [74]. The heterogeneous activation of these three enzyme-based acid resistance systems enables division of labor in the bacterial population and survival over a wide range of low-pH values.

Vibrio species have only the Cad and Orn systems to counteract acidic conditions. In contrast to *E. coli*, the Cad system was shown to be activated in all cells in *V. campbellii* [72]. Apparently, all cells in the *Vibrio* population need the Cad system to increase their intracellular pH by inducing the proton-consuming lysine decarboxylase.

In *Salmonella*, which resides in acidic vacuoles of macrophages, transcriptional heterogeneity can have functional consequences for host-pathogen interactions [75,76]. This phenotype involves regulation by the transcription factors SsrB and PhoP [77], but further studies are required to understand the exact mechanism.

Phenotypic heterogeneity is certainly inherent in many other neutralophilic bacteria that survive in acidic environments, but has been less documented. In addition, the underlying molecular mechanisms that give rise to it and maintain it evolutionarily need to be further investigated.

Conclusions and perspectives

In the past decades, great progress has been made in understanding the different molecular mechanisms of acid stress response in model bacteria, such as *E. coli*, *Salmonella*, and *Listeria*, which have diverse acid resistance systems. New opportunities are now emerging using next-generation sequencing methods that allow the systemic analysis of acid stress response of various bacteria originating from humans, soil, and food. As described above, many mechanisms of acid stress response, such as differential expression of genes involved in transport, H⁺-efflux, and membrane permeability, as well as motility and chemotaxis, but also nucleotide synthesis, and translation, are conserved in phylogenetically distantly related bacteria. Nevertheless, bacterial species differ in terms of additional components and degree of acid tolerance, which in turn reflect optimal adaptation to pH fluctuations in the habitats they colonize.

An exciting new aspect is that the acid stress response, in particular the reduction in membrane fluidity, the change in membrane channel size, proton flux through H⁺-ATPases, the activation of other proton pumps, and the differential gene induction due to decreased intracellular pH are associated with antibiotic tolerance/resistance (Figure 2). In the future, proteins involved in acid stress adaptation could be explored as targets to sensitize pathogenic bacteria to antibiotics.

pH plays a crucial role in bacterial interactions [78]. It is important to note that low pH in nature is often caused by weak organic acids such as acetic acid, lactic acid, and propionic acid, also known as short-chain fatty acids. These acids originate from fermentation processes under anaerobic growth conditions and accumulate in high concentrations, for example, in the human large intestine (100 mM) [79] or rumen. Even mild acid stress (pH 6–7) strongly enhances the uptake of acetic acid (pKa value = 4.75), since this acid is membrane-permeable in the protonated form. In the cytoplasm, acetic acid dissociates, leading to anion accumulation but also to dissipation of the electrochemical gradient. In the future, it will be important to focus on the stress response to organic acids in prominent intestinal bacteria belonging, for example, to the phyla Actinobacteria, Firmicutes, Bacteroidetes, and Verrucomicrobiota. These studies will help to better understand the complexity of the human gut microbiota.

Finally, there are already examples of transient acidification of an environment to coordinate effective symbiosis between bacteria and eukaryotes [80], a still underestimated phenomenon with major implications for host–bacterial interactions that needs to be further explored.

In conclusion, acidification and adaptation to acid stress are exciting areas of research with far-reaching implications for human health, food industry, and agriculture.

CRedit authorship contribution statement

Kilian Schumacher: Conceptualization, Writing – original draft, preparation of figures. **Sophie Brameyer:** Conceptualization, Writing – original draft, preparation of figures. **Kirsten Jung:** Conceptualization, Writing – original draft and editing.

Data Availability

No data were used for the research described in the article.

Declaration of Competing Interest

The authors declare that they have no known competing financial interests or personal relationships that could have appeared to influence the work reported in this paper.

Acknowledgements

We thank all current and former members of the group for their important contributions to this research. This work was funded by the Deutsche Forschungsgemeinschaft, Germany (DFG, German Research Foundation) — Projects 471254198 (JU270/22-1) and 395357507 (SFB 1371) to KJ.

References and recommended reading

Papers of particular interest, published within the period of review, have been highlighted as:

- of special interest
- of outstanding interest

1. Booth IR: **Regulation of cytoplasmic pH in bacteria.** *Microbiol Rev* 1985, **49**:359-378.
2. Reyes-Fernández EZ, Schuldiner S: **Acidification of cytoplasm in *Escherichia coli* provides a strategy to cope with stress and facilitates development of antibiotic resistance.** *Sci Rep* 2020, **10**:1-13.
3. Goto Y, Calciano LJ, Fink AL: **Acid-induced folding of proteins.** *Proc Natl Acad Sci USA* 1990, **87**:573-577.
4. Jeong KC, Hung KF, Baumberg DJ, Byrd JJ, Kaspar CW: **Acid stress damage of DNA is prevented by Dps binding in *Escherichia coli* O157:H7.** *BMC Microbiol* 2008, **8**:1-13.
5. Schwarz J, Schumacher K, Brameyer S, Jung K: **Bacterial battle against acidity.** *FEMS Microbiol Rev* 2022, **46**:fuac037.
6. Foster JW: ***Escherichia coli* acid resistance: tales of an amateur acidophile.** *Nat Rev Microbiol* 2004, **2**:898-907.
7. Lund P, Tramonti A, De Biase D: **Coping with low pH: molecular strategies in neutralophilic bacteria.** *FEMS Microbiol Rev* 2014, **38**:1091-1125.
8. Kanjee U, Houry WA: **Mechanisms of acid resistance in *Escherichia coli*.** *Annu Rev Microbiol* 2013, **67**:65-81.
9. Guan N, Liu L: **Microbial response to acid stress: mechanisms and applications.** *Appl Microbiol Biotechnol* 2020, **104**:51-65.
10. Arcari T, Feger M-L, Guerreiro DN, Wu J, O'Byrne CP: **Comparative review of the responses of *Listeria monocytogenes* and *Escherichia coli* to low pH stress.** *Genes* 2020, **11**:1330.

11. Rai R, Singh V, Mathew BJ, Singh AK, Chaurasiya SK: **Mycobacterial response to an acidic environment: protective mechanisms.** *Pathog Dis* 2022, **80**:ftac032.
12. Cotter PD, Hill C: **Surviving the acid test: responses of gram-positive bacteria to low pH.** *Microbiol Mol Biol Rev* 2003, **67**:429-453.
13. Dawan J, Ahn J: **Bacterial stress responses as potential targets in overcoming antibiotic resistance.** *Microorganisms* 2022, **10**:1385.
14. Westermann AJ, Gorski SA, Vogel J: **Dual RNA-seq of pathogen and host.** *Nat Rev Microbiol* 2012, **10**:618-630.
15. Seelbinder B, Wallstabe J, Marischen L, Weiss E, Wurster S, Page L, Löffler C, Bussemer L, Schmitt AL, Wolf T, et al.: **Triple RNA-seq reveals synergy in a human virus-fungus co-infection model.** *Cell Rep* 2020, **33**:108389.
16. Imdahl F, Vafadarnejad E, Homberger C, Saliba AE, Vogel J: **Single-cell RNA-sequencing reports growth-condition-specific global transcriptomes of individual bacteria.** *Nat Microbiol* 2020, **5**:1202-1206.
17. Ma P, Amemiya HM, He LL, Gandhi SJ, Nicol R, Bhattacharyya RP, Smillie CS, Hung DT: **Bacterial droplet-based single-cell RNA-seq reveals antibiotic-associated heterogeneous cellular states.** *Cell* 2023, **186**:877-891 e14.
- This work introduces BacDrop, a novel single-cell RNA-Seq technology. The authors successfully applied BacDrop in antibiotic-stressed populations and uncovered heterogeneous responses that would not have been captured by standard bulk RNA-Seq.
18. Zhang M, Wu N, Fan Y, Xu C, Luo JM, Wang Y, Yu K, Wang M: **Proteomic profiling and stress response in *Pediococcus acidilactici* under acetic acid.** *J Agric Food Chem* 2022, **70**:12708-12721.
19. Tinder EL, Faustoferri RC, Buckley AA, Quivey RG, Baker JL: **Analysis of the *Streptococcus mutans* proteome during acid and oxidative stress reveals modules of protein coexpression and an expanded role for the TreR transcriptional regulator.** *mSystems* 2022, **7**:1-6.
20. Schumacher K, Gelhausen R, Kion-Crosby W, Barquist L, Backofen R, Jung K: **Ribosome profiling reveals the fine-tuned response of *Escherichia coli* to mild and severe acid stress.** *bioRxiv* 2023, <https://doi.org/10.1101/2023.06.02.543275>
21. Ingolia NT, Hussmann JA, Weissman JS: **Ribosome profiling: global views of translation.** *Cold Spring Harb Perspect Biol* 2019, **11**:1-20.
22. Vazquez-Laslop N, Sharma CM, Mankin A, Buskirk AR: **Identifying small open reading frames in prokaryotes with ribosome profiling.** *J Bacteriol* 2022, **204**:1-12.
23. Bushell F, Herbert JMJ, Sannasiddappa TH, Warren D, Turner AK, Falciani F, Lund PA: **Mapping the transcriptional and fitness landscapes of a pathogenic *E. coli* strain: the effects of organic acid stress under aerobic and anaerobic conditions.** *Genes* 2020, **12**:53.
24. Gu D, Xue H, Yuan X, Yu J, Xu X, Huang Y, Li M, Zhai X, Pan Z, Zhang Y, et al.: **Genome-wide identification of genes involved in acid stress resistance of *Salmonella Derby*.** *Genes* 2021, **12**:476.
25. de la Garza-García JA, Ouahrani-Bettache S, Lyonais S, Ornelas-Eusebio E, Freddi L, Al Dahouk S, Occhialini A, Köhler S: **Comparative genome-wide transcriptome analysis of *Brucella suis* and *Brucella microti* under acid stress at pH 4.5: cold shock protein CspA and Dps are associated with acid resistance of *B. microti*.** *Front Microbiol* 2021, **12**:1-22.
- This publication distinguishes the genome-wide acid stress response of *Brucella suis* and *Brucella microti*, two intracellular bacteria responsible for brucellosis. The authors point to species-specific adaptations in *B. microti*, which exhibits greater acid tolerance compared to *B. suis*. Notably, many relevant genes for acid adaptation in *B. microti*, underwent pseudogenization in *B. suis*.
26. Zhou A, Cao Y, Zhou D, Hu S, Tan W, Xiao X, Yu Y, Li X: **Global transcriptomic analysis of *Cronobacter sakazakii* CICC 21544 by RNA-seq under inorganic acid and organic acid stresses.** *Food Res Int* 2020, **130**:108963.
27. Nilsson JF, Castellani LG, Draghi WO, Mogro EG, Wibberg D, Winkler A, Hansen LH, Schlüter A, Pühler A, Kalinowski J, et al.: **Global transcriptome analysis of *Rhizobium favelukesii* LPU83 in response to acid stress.** *FEMS Microbiol Ecol* 2021, **97**:1-16.
28. Wang C, Ren X, Yu C, Wang J, Wang L, Zhuge X, Liu X: **Physiological and transcriptional responses of *Streptomyces albulus* to acid stress in the biosynthesis of ϵ -poly-L-lysine.** *Front Microbiol* 2020, **11**:1-15.
29. Moreno-Arribas MV, Polo MC: **Winemaking biochemistry and microbiology: current knowledge and future trends.** *Crit Rev Food Sci Nutr* 2005, **45**:265-286.
30. Ferguson RMW, Merrifield DL, Harper GM, Rawling MD, Mustafa S, Picchietti S, Balcázar JL, Davies SJ: **The effect of *Pediococcus acidilactici* on the gut microbiota and immune status of on-growing red tilapia (*Oreochromis niloticus*).** *J Appl Microbiol* 2010, **109**:851-862.
31. Mas A, Torija MJ, García-Parrilla MDC, Troncoso AM: **Acetic acid bacteria and the production and quality of wine vinegar.** *Sci World J* 2014, **2014**:1-7.
32. Palanivelu J, Thanigaivel S, Vickram S, Dey N, Mihaylova D, Desseva I: **Probiotics in functional foods: survival assessment and approaches for improved viability.** *Appl Sci* 2022, **12**:455.
33. Jerez CA: **Biomining of metals: how to access and exploit natural resource sustainably.** *Micro Biotechnol* 2017, **10**:1191-1193.
34. Jones DS, Schaperdoth I, Macalady JL: **Biogeography of sulfur-oxidizing *Acidithiobacillus* populations in extremely acidic cave biofilms.** *ISME J* 2016, **10**:2879-2891.
35. Krulwich TA, Sachs G, Padan E: **Molecular aspects of bacterial pH sensing and homeostasis.** *Nat Rev Microbiol* 2011, **9**:330-343.
36. Yu H, Jiang Z, Lu Y, Yao X, Han C, Ouyang Y, Wang H, Guo C, Ling F, Dang Z: **Transcriptome analysis of the acid stress response of *Desulfovibrio vulgaris* ATCC 7757.** *Curr Microbiol* 2020, **77**:2702-2712.
37. Feng S, Qiu Y, Huang Z, Yin Y, Zhang H, Zhu D, Tong Y, Yang H: **The adaptation mechanisms of *Acidithiobacillus caldus* CCTCC M 2018054 to extreme acid stress: bioleaching performance, physiology, and transcriptomics.** *Environ Res* 2021, **199**:111341.
38. Askoura M, Youns M, Halim Hegazy WA: **Investigating the influence of iron on *Campylobacter jejuni* transcriptome in response to acid stress.** *Microb Pathog* 2020, **138**:103777.
39. Peng L, Zhao K, Chen S, Ren Z, Wei H, Wan C: **Whole genome and acid stress comparative transcriptome analysis of *Lactiplantibacillus plantarum* ZDY2013.** *Arch Microbiol* 2021, **203**:2795-2807.
40. Cortes BW, Naditz AL, Anast JM, Schmitz-Esser S: **Transcriptome sequencing of *Listeria monocytogenes* reveals major gene expression changes in response to lactic acid stress exposure but a less pronounced response to oxidative stress.** *Front Microbiol* 2020, **10**:1-14.
41. Maurer LM, Yohannes E, Bondurant SS, Radmacher M, Slonczewski JL: **pH regulates genes for flagellar motility, catabolism, and oxidative stress in *Escherichia coli* K-12.** *J Bacteriol* 2005, **187**:304-319.
42. Tohidifar P, Plutz MJ, Ordal GW, Rao CV: **The mechanism of bidirectional pH taxis in *Bacillus subtilis*.** *J Bacteriol* 2020, **202**:e00491-19.
43. Yang Y, Sourjik V: **Opposite responses by different chemoreceptors set a tunable preference point in *Escherichia coli* pH taxis.** *Mol Microbiol* 2012, **86**:1482-1489.

44. Sun Y, Fukamachi T, Saito H, Kobayashi H: **Respiration and the F₁F_o-ATPase enhance survival under acidic conditions in *Escherichia coli*.** *PLoS One* 2012, **7**:1-7.
45. Xia K, Han C, Xu J, Liang X: **Transcriptome response of *Acetobacter pasteurianus* Ab3 to high acetic acid stress during vinegar production.** *Appl Microbiol Biotechnol* 2020, **104**:10585-10599.
46. Lindahl T, Nyberg B: **Rate of depurination of native deoxyribonucleic acid.** *Biochemistry* 1972, **11**:3610-3618.
47. Nelson DL, Cox MM: *Lehninger Principles of Biochemistry*. 7th ed., W.H. Freeman; 2017.
48. Qi Y, Wang H, Chen X, Wei G, Tao S, Fan M: **Altered metabolic strategies: elaborate mechanisms adopted by *Oenococcus oeni* in response to acid stress.** *J Agric Food Chem* 2021, **69**:2906-2918.
- This work demonstrates the powerful approach of synergizing transcriptomics, metabolomics, and genome-wide metabolic modelling approaches. Using this experimental design, the authors uncover metabolic strategies of *Oenococcus oeni* to counteract acidity.
49. Ren C, Zheng Y, Liu C, Mencius J, Wu Z, Quan S: **Molecular characterization of an intrinsically disordered chaperone reveals net-charge regulation in chaperone action.** *J Mol Biol* 2022, **434**:167405.
50. Wiebe MA, Brannon JR, Steiner BD, Bamidele A, Schrimpe-Rutledge AC, Codreanu SG, Sherrod SD, McLean JA, Hadjiifrangiskou M: **Serine deamination is a new acid tolerance mechanism observed in uropathogenic *Escherichia coli*.** *MBio* 2022, **13**:1-12.
51. Jain P, Jain V, Singh A, Chauhan A, Sinha S: **Evaluation on the responses of succinate dehydrogenase, isocitrate dehydrogenase, malate dehydrogenase and glucose-6-phosphate dehydrogenase to acid shock generated acid tolerance in *Escherichia coli*.** *Adv Biomed Res* 2013, **2**:75.
52. Farha MA, French S, Stokes JM, Brown ED: **Bicarbonate alters bacterial susceptibility to antibiotics by targeting the proton motive force.** *ACS Infect Dis* 2018, **4**:382-390.
53. Andrés MT, Fierro JF: **Antimicrobial mechanism of action of transferrins: selective inhibition of H⁺-ATPase.** *Antimicrob Agents Chemother* 2010, **54**:4335-4342.
54. Teelucksingh T, Thompson LK, Cox G: **The evolutionary conservation of *Escherichia coli* drug efflux pumps supports physiological functions.** *J Bacteriol* 2020, **202**:1-17.
55. Tucker DL, Tucker N, Zhuo M, Foster JW, Miranda RL, Cohen PS, Conway T: **Genes of the GadX-GadW regulon in *Escherichia coli*.** *J Bacteriol* 2003, **185**:3190-3201.
56. Nishino K, Senda Y, Hayashi-Nishino M, Yamaguchi A: **Role of the AraC-XylS family regulator YdeO in multi-drug resistance of *Escherichia coli*.** *J Antibiot* 2009, **62**:251-257.
57. Yamanaka Y, Oshima T, Ishihama A, Yamamoto K: **Characterization of the YdeO regulon in *Escherichia coli*.** *PLoS One* 2014, **9**:e111962.
58. Schaffner SH, Lee AV, Pham MTN, Kassaye BB, Li H, Tallada S, Lis C, Lang M, Liu Y, Ahmed N, et al.: **Extreme acid modulates fitness trade-offs of multidrug efflux pumps MdtEF-TolC and AcrAB-TolC in *Escherichia coli* K-12.** *Appl Environ Microbiol* 2021, **87**:1-12.
- In this work, the authors developed a method to measure the contribution of multidrug-resistance pumps to the relative fitness of *E. coli*. They demonstrate that exposure of *E. coli* to pH 2 is required for the MdtEF-TolC pump to confer positive relative fitness.
59. Pasqua M, Grossi M, Scinicariello S, Aussel L, Barras F, Colonna B, Prosseda G: **The MFS efflux pump EmrKY contributes to the survival of *Shigella* within macrophages.** *Sci Rep* 2019, **9**:1-11.
60. Truong-Bolduc QC, Bolduc GR, Okumura R, Celino B, Bevis J, Liao CH, Hooper DC: **Implication of the NorB efflux pump in the adaptation of *Staphylococcus aureus* to growth at acid pH and in resistance to moxifloxacin.** *Antimicrob Agents Chemother* 2011, **55**:3214-3219.
61. Bartek IL, Reichlen MJ, Honaker RW, Leistikow RL, Clambey ET, Scobey MS, Hinds AB, Born SE, Covey CR, Schurr MJ, et al.: **Antibiotic bactericidal activity is countered by maintaining pH homeostasis in *Mycobacterium smegmatis*.** *mSphere* 2016, **1**:1-18.
62. Hong SH, Wang X, O'Connor HF, Benedik MJ, Wood TK: **Bacterial persistence increases as environmental fitness decreases.** *Micro Biotechnol* 2012, **5**:509-522.
63. Goode O, Smith A, Zarkan A, Cama J, Invergo BM, Belgami D, Caño-Muñiz S, Metz J, O'Neill P, Jeffries A, et al.: **Persister *Escherichia coli* cells have a lower intracellular pH than susceptible cells but maintain their pH in response to antibiotic treatment.** *MBio* 2021, **12**:1-18.
- Here, the authors monitored the dynamics of intracellular pH using a combination of microfluidics, time-lapse microscopy, and a plasmid-encoded fluorescent pH reporter in different *E. coli* subpopulations. This allowed them to show that regulation of intracellular pH is not homogeneous, leading to dedicated functions, including survival after antibiotic treatment.
64. Helaine S, Cheverton AM, Watson KG, Faure LM, Matthews SA, Holden DW: **Internalization of *Salmonella* by macrophages induces formation of nonreplicating persisters.** *Science* 2014, **343**:204-208.
65. Mitosch K, Rieckh G, Bollenbach T: **Noisy response to antibiotic stress predicts subsequent single-cell survival in an acidic environment.** *Cell Syst* 2017, **4**:393-403, e5.
66. Mitosch K, Rieckh G, Bollenbach T: **Temporal order and precision of complex stress responses in individual bacteria.** *Mol Syst Biol* 2019, **15**:1-15.
67. Silander OK, Nikolic N, Zaslaver A, Bren A, Kikoin I, Alon U, Ackermann M: **A genome-wide analysis of promoter-mediated phenotypic noise in *Escherichia coli*.** *PLoS Genet* 2012, **8**:e1002443.
68. Jung K, Brameyer S, Fabiani F, Gasperotti A, Hoyer E: **Phenotypic heterogeneity generated by histidine kinase-based signaling networks.** *J Mol Biol* 2019, **431**:4547-4558.
69. Brameyer S, Schumacher K, Kuppermann S, Jung K: **Division of labor and collective functionality in *Escherichia coli* under acid stress.** *Commun Biol* 2022, **5**:1-14.
- This publication provides new insights into the activation patterns of the Gad, Adi and Cad acid resistance systems in individual cells. By monitoring a triple fluorescent reporter strain under consecutively increasing acid stress conditions, the authors demonstrate that the three systems are heterogeneously distributed in single cells, suggesting a division of labor under acidic conditions.
70. Martinez KA, Kitko RD, Mershon JP, Adcox HE, Malek KA, Berkmen MB, Slonczewski JL: **Cytoplasmic pH response to acid stress in individual cells of *Escherichia coli* and *Bacillus subtilis* observed by fluorescence ratio imaging microscopy.** *Appl Environ Microbiol* 2012, **78**:3706-3714.
71. Brameyer S, Rösch TC, El Andari J, Hoyer E, Schwarz J, Graumann PL, Jung K: **DNA-binding directs the localization of a membrane-integrated receptor of the ToxR family.** *Commun Biol* 2019, **2**:4.
72. Brameyer S, Hoyer E, Bibinger S, Burdack K, Lassak J, Jung K: **Molecular design of a signaling system influences noise in protein abundance under acid stress in different gammaproteobacteria.** *J Bacteriol* 2020, **202**:e00121-20.
73. Sampaio NMV, Blassick CM, Andreani V, Lugagne JB, Dunlop MJ: **Dynamic gene expression and growth underlie cell-to-cell heterogeneity in *Escherichia coli* stress response.** *Proc Natl Acad Sci USA* 2022, **119**:1-12.
74. Van Riet S, Tadesse W, Mortier J, Schlegel S, Simoens K, Bernaerts K, Dal Co A, Aertsen A: **Heterogeneity and evolutionary tunability of *Escherichia coli* resistance against extreme acid stress.** *Microbiol Spectr* 2022, **10**:1-13.

10 Microbial Systems and Synthetic Biology

75. Avraham R, Haseley N, Brown D, Penaranda C, Jijon HB, Trombetta JJ, Satija R, Shalek AK, Xavier RJ, Regev A, *et al.*: **Pathogen cell-to-cell variability drives heterogeneity in host immune responses.** *Cell* 2015, **162**:1309-1321.
76. Chakraborty S, Mizusaki H, Kenney LJ: **A FRET-based DNA biosensor tracks OmpR-dependent acidification of *Salmonella* during macrophage Infection.** *PLoS Biol* 2015, **13**:1-32.
77. Liew ATF, Foo YH, Gao Y, Zangoui P, Singh MK, Gulvady R, Kenney LJ: **Single cell, super-resolution imaging reveals an acid pH-dependent conformational switch in SsrB regulates SPI-2.** *Elife* 2019, **8**:1-26.
78. Ratzke C, Gore J: **Modifying and reacting to the environmental pH can drive bacterial interactions.** *PLoS Biol* 2018, **16**:1-20.
79. Cummings JH, Pomare EW, Branch WJ, Naylor CPE, Macfarlane GT: **Short chain fatty acids in human large intestine, portal, hepatic and venous blood.** *Gut* 1987, **28**:1221-1227.
80. Pipes BL, Nishiguchi MK: **Nocturnal acidification: a coordinating cue in the *Euprymna scolopes-Vibrio fischeri* symbiosis.** *Int J Mol Sci* 2022, **23**:1-14.

This review highlights how chitin secreted by the eukaryotic host is fermented by the bacteria, lowering the pH in the light organ, which in turn is essential for their symbiosis.

3 Concluding discussion

Parts of this chapter were adapted from:

Schumacher, K., Gelhausen, R., Kion-Crosby, W., Barquist, L., Backofen, R., and Jung, K. (2023). Ribosome profiling reveals the fine-tuned response of *Escherichia coli* to mild and severe acid stress. *mSystems*.10.1128/msystems.01037-23.

Schumacher, K., Braun, D., Kleigrewe, K., and Jung, K. (2024). Motility-activating mutations upstream of *flhDC* reduce acid shock survival of *Escherichia coli*. *Microbiol Spectr.* 12:e0054424.

Muñoz, A.W., Hoyer, E., Schumacher, K., Grognot, M., Taute, K.M., Hacker, S.M., Sieber, S.A., and Jung, K. (2022). Eukaryotic catecholamine hormones influence the chemotactic control of *Vibrio campbellii* by binding to the coupling protein CheW. *Proc. Natl. Acad. Sci. U. S. A.* 119. 10.1073/pnas.2118227119.

Brameyer, S., Schumacher, K., Kuppermann, S., and Jung, K. (2022). Division of labor and collective functionality in *Escherichia coli* under acid stress. *Commun. Biol.* 5, 1–14. 10.1038/s42003-022-03281-4.

3.1 Novel adaptations of *Escherichia coli* to acid stress uncovered by Ribo-Seq

Acidic environments are frequently occurring on earth and involve acidic soils, macrophage phagosomes, and gastrointestinal tracts (Figure 1). In recent decades, a magnitude of studies both on the systematic and molecular levels have been conducted to understand which defense mechanisms against acidity evolved in bacteria. Thereby several strategies for restricting proton uptake, accelerating extrusion, and limiting damage to cellular components have been detected. Nevertheless, most studies were limited to microarrays, proteomics, or only mildly acidic conditions. Using a combined ribosome profiling and RNA-Seq approach, entirely new adaptations to mildly and severely acidic conditions were uncovered (Chapter 2.1). These previously overlooked adaptations were revealed by leveraging the advantages of the Ribo-Seq technique which include the distinction between coding and non-coding RNAs, the detection of novel sORFs, and its independence of protein biochemistry (139, 144, 146, 157). Moreover, Ribo-Seq is less sensitive to acid treatment compared to proteomics (133). Conclusively, Ribo-Seq allowed monitoring of protein synthesis rates also at pH 4.4 and revealed the induction of a large spectrum of so far uncharacterized genes (Chapter 2.1). Moreover, the differential synthesis of membrane proteins, restricted cellular metabolism, induction of siderophore and iron uptake, and the differential expression of sORFs were highlighted (Figure 7). These novel acid stress adaptations are further discussed below.

3.1.1. Differential synthesis of membrane proteins and putatively altered membrane fluidity

Ribo-Seq revealed restricted synthesis of a high proportion of membrane proteins under acidic conditions. In particular, 18 of the 20 genes with the most reduced ribosome footprint levels at pH 5.8 encoded inner- or outer membrane proteins. Correspondingly, 75% of the Top 20 genes with reduced RPFs under severe acid stress encoded non-cytosolic proteins (Chapter 2.1). It appears plausible, that synthesis of these membrane components is restricted to limit proton intake. Examples of integral membrane components with reduced RPF levels involved, amongst others, the DppABCDF dipeptide transport system, the MalEFGK maltose uptake system, the melibiose/H⁺ symporter MelB, and the 4-aminobutanote/H⁺ symporter GabP (pH 5.8). Along this line, examples of transporters that were synthesized in lower amounts at pH 4.4 included the tryptophan/H⁺ symporter TnaB, as well as several OMPs such as OmpW, OmpF, NmpC, and LamB (Chapter 2.1).

As indicated by the restricted synthesis of H⁺ symporters such as GabP and MelB, proton influx is restricted under acidity. GabP and MelB are driven by the membrane potential and transport protons as co-substrates (169, 170). While decreased production of H⁺ co-transporting symporters was detected regardless of the stress intensity, diminished synthesis of OMPs was exclusively noted at pH 4.4 (Chapter 2.1). OMPs consist of antiparallel beta-strands that form

a barrel-like pore in the outer membrane and facilitate the transport of nutrients, ions, and other molecules (171). The exclusive alteration of OMP synthesis at pH 4.4 (Figure 7) demonstrates that *E. coli* rather modifies the inner membrane under mild acid stress whereas both the inner- and outer membrane composition are adjusted under severe acid stress.

It is well known that *E. coli* incorporates CFAs into the membrane under acid stress (32, 33). Furthermore, the polar phospholipid content can be modified and derivatives of phosphatidylglycerol, hopanoids, and sphingolipids are formed in these conditions (35). Together with the downregulation of OMPs and other transporters (Figure 7), such adaptations likely also affect the fluidity of the membrane. Of note, Ribo-Seq also revealed a significant increase of CIsA, CIsB, and CIsC synthesis at pH 4.4 (Figure 7), with the most drastic induction being noted for CIsB (12-fold). These proteins are responsible for synthesizing cardiolipin, which is formed by the condensation of two phosphatidylglycerol molecules (172–174). Cardiolipin is a unique phospholipid with a dimeric structure containing four acyl chains and its presence in the membrane alters the packing arrangement of phospholipids due to its conical shape and increased molecular size compared to other phospholipids (175, 176). Elevated cardiolipin levels contributed to membrane stabilization under osmotic conditions in *E. coli*, indicating a reduction of membrane fluidity and permeability (177). For future studies, it will be important to directly measure and confirm changes in membrane fluidity under acid stress, for instance via excimer fluorescence of pyrene lipid probes (178).

The hypothesis of alterations in phospholipid content in *E. coli* under acid stress was further underlined as a significant induction of a catabolic pathway for glycerol and glycerol 3-phosphate (G3P), encoded by the *glp* regulon, was detected (Figure 7). Glycerol and G3P can be released during polar phospholipid breakdown, especially during turnover of phosphatidylglycerol (179), and act as inducers for the *glp* regulon (180, 181). Thus, it is tempting to speculate that in addition to elevated cardiolipin synthesis, *E. coli* can gain energy under acid stress via the catabolic breakdown of glycerol and G3P, which are putatively released from phospholipid turnover.

Collectively, these results highlight the superiority of Ribo-Seq over LC-MS in terms of membrane protein analysis. The underlying reason for this is that membrane proteins have a tendency to aggregate and precipitate in solution and are oftentimes lacking target residues (lysine and arginine) which are essential for tryptic cleavage, an essential step within bottom-up proteomic approaches (133). This difference between the methods mentioned above is an important consideration point for future studies since ~ 20–30% of genes in an organism encode integral membrane components (182).

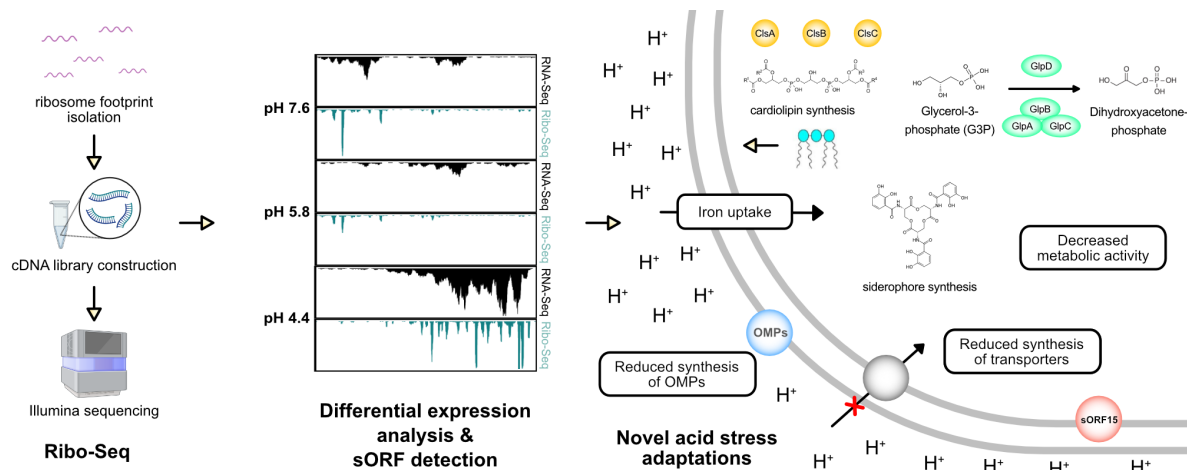


Figure 7: Overview of the final steps of the Ribo-Seq workflow which yielded the discovery of novel adaptations of *E. coli* to acid stress. These included the reduced synthesis of transport proteins, catabolism of glycerol-3-phosphate, decreased metabolic activities, iron uptake, siderophore synthesis, and the discovery of novel sORFs. Parts of this figure were created using Biorender.com.

3.1.2 Restriction of cellular metabolism

In addition to restricted membrane protein synthesis, reduced global metabolism was detected at both pH 5.8 and pH 4.4 (Chapter 2.1). This finding was mainly revealed by gene set enrichment analysis (GSEA). GSEA is a bioinformatic approach determining whether predefined gene sets show statistical differences in high-throughput sequencing data (183). Using the tool *clusterProfiler* (184) and the RNA-Seq and Ribo-Seq data as input, differences in gene ontology (GO) terms for biological processes were evaluated. Thereby a large spectrum of metabolic and catabolic processes was detected to be restricted under low pH (Figure 7). This included for instance putrescine catabolism, threonine catabolism, xylose metabolism, and glucan catabolism (Chapter 2.1).

Particularly interesting was the downregulation of arginine catabolism. This GO term is mainly associated with a pathway involving the protein products of the *astEBDAC* operon, responsible for the L-arginine degradation II (AST) pathway. The AST pathway is the main arginine-degrading pathway in *E. coli* and yields two molecules of glutamate and ammonia (185). Importantly, reduced catabolism of arginine was detected at pH 5.8, but not at pH 4.4. Thus, *E. coli* may preserve the intracellular arginine pool under mild acid stress to ensure enough substrate for the Adi system is available during severe acid stress (see Chapter 2.5). This is important as the conversion of arginine to agmatine via the Adi system is a crucial acid stress mechanism, which is maximally induced at pH 4.4 (186).

The strongest downregulation among all biosynthetic operons at pH 4.4 was observed for *tnaABC*. *tnaA* encodes a tryptophanase, which cleaves L-tryptophan into indole, pyruvate, and NH_4^+ , *tnaB* encodes a tryptophan/ H^+ symporter, and *TnaC* functions as a leader peptide (187,

188). Importantly, *E. coli* persister cells were previously indicated to display a lower intracellular pH. This effect was linked to the activity of TnaA, as the pH difference was abolished in a $\Delta tnaA$ mutant (189). Considering the detected pH-dependent regulation of *tnaABC* (Chapter 2.1), the link between pH and bacterial persistence is further emphasized.

3.1.3 Induction of siderophore and iron uptake

GSEA also identified GO terms related to iron- and siderophore uptake as statistically enriched at pH 4.4 (Figure 7). These included 'siderophore-dependent iron import into cell', 'siderophore transmembrane transport', 'enterobactin biosynthetic process', and 'ferric-enterobactin import' (Chapter 2.1). Specifically, the complete enterobactin biosynthesis pathway, comprising the *entCEBAH* operon, *entF*, *entH*, and *ybdZ*, was induced at pH 4.4. Enterobactin is a key component for *E. coli* to scavenge iron from the environment, mainly by binding Fe(III) ions and enhancing solubility (190).

Furthermore, all subunits of the Ton complex were enriched at pH 5.8 and pH 4.4. The Ton complex functions as a proton motive force-dependent molecular motor that facilitates the import of iron-bound siderophores (191, 192). Along this line, several other iron uptake systems were also induced under acidic conditions. These included a ferric dicitrate ABC transport system (*fecABCDE*), an iron (III) hydroxamate ABC transport system (*fhuACDB*), and a ferric enterobactin ABC transport system (*fepA*, *fepB*, *fepCGD*). Moreover, upregulation of genes of the *isc* and *suf* operons was detected, encoding components of the complex machinery responsible for iron-sulfur cluster assembly in *E. coli* (193).

These results are somewhat contradictory considering the increased solubility of iron under low pH which is expected to increase bioavailability (194). The above described induction of iron and siderophore uptake systems might also be caused by restricted heme transport under acidity. Indeed, GSEA revealed significant downregulation of the GO term 'heme transport' (Chapter 2.1). Heme is a molecule consisting of an iron atom contained in the center of a large organic ring and can serve as an iron source (195). Specifically, synthesis of the DppABCDF dipeptide transporter was detected. This protein complex is responsible for transporting heme from the periplasm into the cytoplasm in *E. coli* (196).

Considering the enhanced solubility of iron under low pH (194), it is worth discussing whether *E. coli* synthesizes siderophores to respond to iron limitation or rather protects itself against putative iron excess. The latter was demonstrated for *Pseudomonas aeruginosa*, where siderophores protected cells from the harmful effects of ROS. In this case, the cells no longer secreted siderophores but instead stored them intracellularly (197). Overall, the questions raised above are of high importance for future work since iron acquisition is a crucial factor for pathogenesis due to limited availability in host environments (198).

3.1.4 Discovery of sORFs that are exclusively detectable under acid stress conditions

A unique advantage of Ribo-Seq is the possibility to detect sORFs which were previously overlooked due to their small size (155–157). Upon conducting Ribo-Seq at pH 7.6, pH 5.8, and pH 4.4, 18 novel candidate sORFs were identified in *E. coli* (Chapter 2.1). Moreover, it was demonstrated that several previously known sORFs such as YdgU, AzuC, and MdtU, are differentially expressed under acidic conditions. These results indicate that small proteins play a significant role in stress adaptation. Considering that the majority of sORFs are located in the membrane (161), small proteins may affect the membrane permeability for protons.

Ribo-Seq yielded novel sORFs in the UTRs of annotated genes, antisense sORFs, and dual-function sRNAs (Chapter 2.1). For instance, the sRNAs OmrA and OmrB, which were previously thought to be non-coding, encoded small peptides under severe acid stress (Chapter 2.1). This finding may be of high relevance considering that the OmrA and OmrB sRNAs regulate the expression of numerous OMPs (199). Particularly striking however was the discovery of two novel candidate sORFs in the 3'UTR of the major acid resistance regulator GadW (sORF14 and sORF15). While the expression of sORF14 was not confirmed, sORF15 protein production could be successfully detected via western blotting (Chapter 2.1). This suggests that the complex Gad system (see Chapter 2.5) consists of even more components than thus far assumed. sORF15 is predicted to be membrane-bound (Figure 7), and considering that most sORFs interact with other cellular components rather than exerting *bona fide* enzymatic activities (155), sORF15 may associate with other crucial membrane proteins for acid resistance. Since sORF15 is located in a transcriptional unit with *gadW* and *gadX*, it could bind to GadC, the transporter of the Gad system. Alternatively, sORF15 may associate with MdtF, which is adjacently encoded and partially overlapping the *sORF15* gene. MdtF is the inner membrane subunit of the tripartite MdtEF-TolC efflux pump responsible for the extrusion of bile salts, dyes, and antibiotics such as novobiocin, ciprofloxacin, and erythromycin (200, 201). Notably, an overlap between antibiotic resistance mediated by efflux pumps and acid resistance in bacteria was previously demonstrated (see Chapter 2.6). Thus, it will be of great relevance for future investigations to determine binding partners of sORF15, for instance via Co-IP (202).

Examples of successful functional descriptions of sORFs have been provided in recent years. For instance, the VdcP small protein of *Vibrio cholerae* binds to the GlTA citrate synthase of the citric acid cycle and thereby reroutes carbon metabolism (203). In *Methanosarcina mazei*, the small protein sP36 regulates nitrogen metabolism as it inhibits the activity of the AmtB₁ ammonium transporter (204) and in *Haloferax volcanii*, HVO_2753 mediates biofilm formation and swarming behaviors (205).

Nevertheless, the lack of conserved domains due to restricted ORF lengths complicates the search for evolutionary relationships of small proteins. Theories for sORF evolution involve the degeneration of larger sORFs, partial ORF duplications, the evolution of a promoter upstream of a non-coding gene, and the evolution of a protease cleavage site towards the 5'- or 3' end of a canonical longer ORF (155). Moreover, a proto-gene model involving the *de novo* birth of sORFs from random non-coding genomic DNA sequences via pervasive transcription and subsequent ribosome association is discussed (206–208).

In sum, the discovery of sORF15 and other small proteins demonstrates that alterations in genomic coverage as a consequence of stress adaptations can guide the discovery of new small proteins, even in well-studied model organisms such as *Escherichia coli*. This exemplifies that certain sORFs previously not only remained hidden due to their small size but also because they are exclusively expressed under stress conditions.

3.2 Stress-dependent adaptations of chemotaxis and motility

Chemotaxis and the ability to regulate flagella biosynthesis are essential for *E. coli* to react to external stimuli and environmental alterations (209). Such adaptations have already been described under acidity but were expanded within this thesis. The following chapters will discuss modifications of the signal transduction cascade responsible for propagating the signals received via MCPs to the flagellar motor. In particular, the effects of insertion sequence (IS) element integration upstream of *flhDC*, encoding the master regulators for motility and chemotaxis (Chapter 2.2), as well as binding of eukaryotic catecholamine hormones to the chemotaxis coupling protein CheW (Chapter 2.3), will be discussed.

3.2.1 pH-dependent differential expression of motility genes

The Ribo- and RNA-Seq data gathered at varying pH levels revealed strong induction of motility genes under mild acidity (pH 5.8) but not under severe acidity (pH 4.4) (Chapter 2.1). Conclusively, the induction of the motility machinery in *E. coli* appears to be strictly dependent on the degree of acid stress. It is tempting to speculate that bacteria use an escape strategy to migrate to habitats with optimal pH under mild acid stress but abandon this strategy under severely acidic conditions and switch to an energy-saving mode (Figure 8). These assumptions are supported by independent findings suggesting that flagella are rapidly shed at pH 4.0 – 4.5 (77, 78) and reports noting diminished chemotaxis and overall motility in severely acidic conditions (210). The switch to an energy-saving mode at pH 4.4 is in alignment with the overall reduction of metabolic activity (see Chapter 3.1.3). Importantly, a microarray study conducted in *E. coli* reported that motility was still induced at pH 5.0 (37). Thus, the inversion point at which motility stops to be beneficial is likely situated between pH 5.0 and pH 4.4 (Figure 8), at least in *E. coli*.

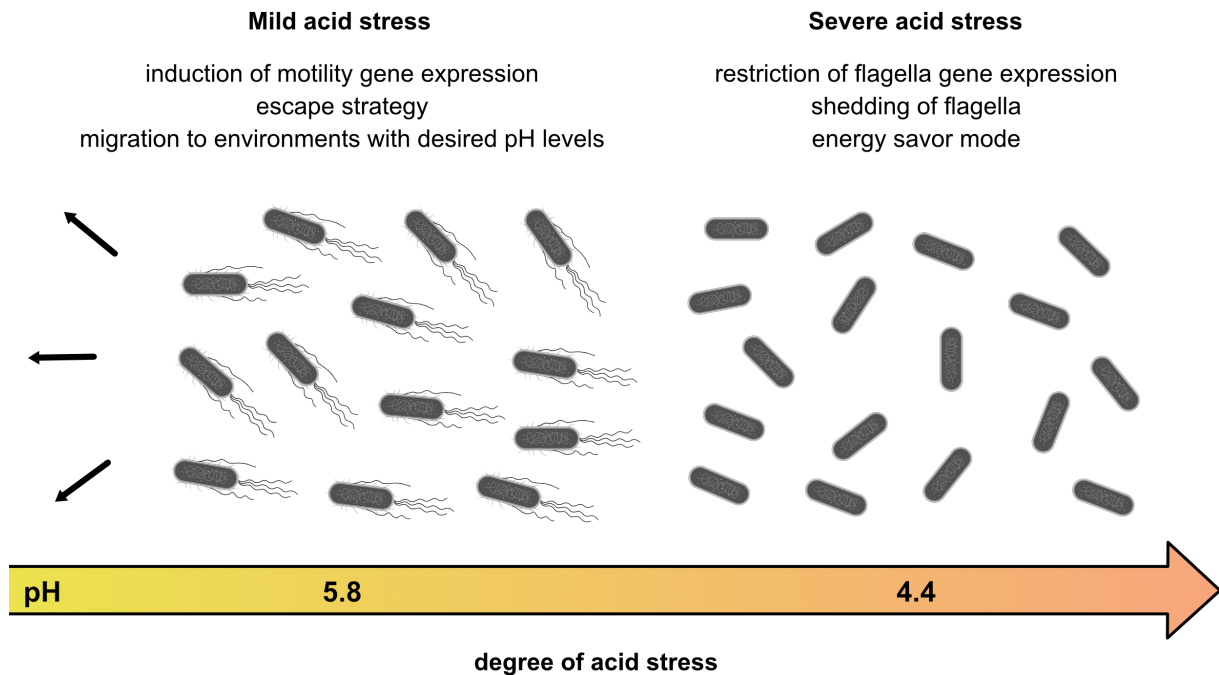


Figure 8: Adaptation of motility in *E. coli* depending on the degree of acid stress. Responses to mild and severe acid stress, as well as migration behaviors are indicated. Parts of this figure were created using Biorender.com.

Along this note, several NGS studies were recently performed in a broad spectrum of bacteria from distinct habitats (see Chapter 2.6). In nearly all investigated species, differential motility and chemotaxis gene expression were reported in response to acidity. Thus, the effect appears to be a universal phenomenon in motile bacteria. However, the respective RNA-Seq and proteomic studies detected in some cases upregulation and in others downregulation of motility genes (Chapter 2.6). For instance, motility was induced at pH 3 in *Campylobacter jejuni* (211) but restricted in *Listeria monocytogenes* at pH 3.4 (212). This suggests, that the inversion point at which motility stops to be beneficial is correlated to the overall acid tolerance of a species.

3.2.2 Insertion sequence element-controlled regulation of motility

Another link between motility and acid stress was discovered upon analysis of an *mhpR* mutant from the Keio collection (213). The acid shock phenotype observed in this strain was surprisingly not mediated by the MhpR knockout itself, but by the integration of an IS element in the promoter region of *flhDC* (Chapter 2.2). IS integration and point mutations in the upstream region of *flhDC* have previously been described to activate motility due to disruption of transcriptional repressor binding sites (214–217). Notably, motility-activating mutations in the *flhDC* regulatory region have been detected in the majority of strains from the Keio collection (218). IS elements are mobile genetic elements and consist of two inverted repeat sequences flanking a central region containing genes responsible for transposition (219, 220). Moreover, they are usually less than 2.5 kb in length, exclusively encode genes involved in translocation, and are major drivers for genomic plasticity in prokaryotes (221).

Motility-activating mutations in the regulatory region of *flhDC* have also been shown to introduce a trade-off between growth and biofilm formation (216). This indicates, that the consequences of IS integration upstream of *flhDC* are not restricted to acid survival but entail further consequences. This is in agreement with findings of FlhDC regulating also non-motility genes involved in processes including carbon source metabolism, anaerobic respiration, and cell division (230, 231). Moreover, transposition frequencies were previously indicated to be affected by different stressors such as UV light, oxidative stress, and DNA damage (232–234). Thus, it will be of interest for future studies to investigate whether the likelihood of IS integration also increases relative to the degree of acid stress.

It is worth noting that IS transposition can cause phenotypic heterogeneity within bacterial populations. For instance, phenotypic variability in a biofilm increased relative to the frequency of IS5 insertion upstream of *flhDC* (216) and IS-related heterogeneity was beneficial for bacteria as it increased biofilm mass (235). Importantly, a heterogeneous population of MG1655 CGSC 7740 carrying an IS element upstream of *flhDC* was detected (Chapter 2.2), suggesting the existence of subpopulations that are either acid-tolerant or motile (Chapter 3.3).

3.2.3 Binding of stress hormones to the motility machinery

In addition to alterations in gene expression levels, chemotactic behaviors can be affected by modifications of the signal transduction cascade connecting MCPs to the flagellar motor. The latter was demonstrated for eukaryotic catecholamine hormones which bound to the chemotaxis coupling protein CheW in *Vibrio campbellii* (Chapter 2.3). CheW is located at the core of the chemotaxis signaling network and was demonstrated to be targeted by stress-related catecholamine hormones of animals and humans, such as EPI and NE (Figure 10). This interaction, with affinity constants in the submicromolar range, was confirmed by an untargeted chemical proteomics approach and MST (Chapter 2.3).

The binding of the mammalian compounds also affected the chemotactic control of *V. campbellii* (Figure 10). In particular, supplementation of 50 μ M EPI or PE significantly reduced the chemotactic response to glucose in a capillary chemotaxis assay (Chapter 2.3). This assay measures the number of cells migrating into attractant-containing glass capillaries after fixed time intervals (210). The results demonstrated, that the capacity to sense attractants is disturbed when eukaryotic catechol hormones are bound to CheW in *V. campbellii* (Figure 10).

CheW is a crucial determinant of the chemotaxis signaling network and connects MCPs to the HK CheA (Figure 9) (236). However, the exact mechanism of catecholamine binding to CheW regarding signal transduction interference remained unclear. One possible explanation is that the binding of stress hormones interferes with the autophosphorylation of CheA, which transfers its phosphoryl group to the RR CheY (89). Thus, the interaction with catecholamine

hormones may mimic a $\Delta cheW$ phenotype, i.e. smooth swimming and non-chemotactic (237). This would explain why taxis towards glucose was abolished in the presence of eukaryotic catecholamine hormones. Nevertheless, 3D tracking experiments revealed that the turning rate and swimming speed of *V. campbellii* are unaffected by EPI (Chapter 2.3), contradicting the statement above and the capillary assay data. This discrepancy may be explained by the fact that 3D tracking experiments rely on linear gradients while the capillary assay operates with steep gradients in the capillary vicinity. Thus, the effects of catecholamines on chemotactic behaviors could be restricted to steep gradients or other conditions specifically encountered in the capillary assay. Another noteworthy difference between the capillary assay and the 3D chemotaxis assay conducted in microfluidic devices (Chapter 2.3) is the measured swimming distance covered by the bacteria, which is significantly higher in the capillary assay.

***Vibrio campbellii*:**

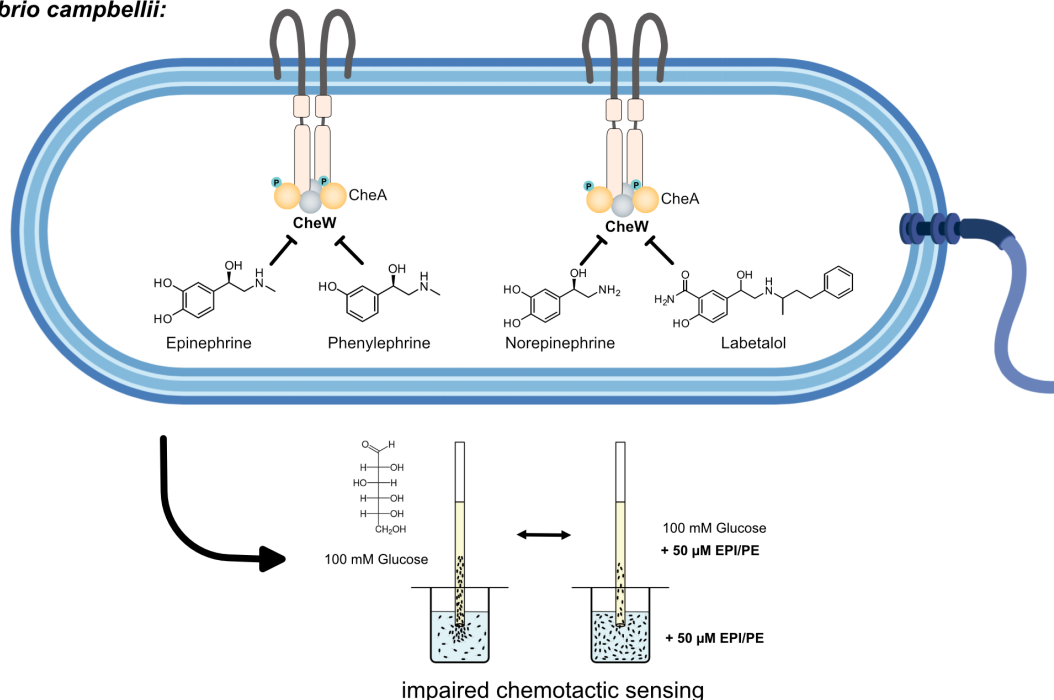


Figure 10: Impaired chemotactic sensing in *Vibrio campbellii* as a consequence of the binding of eukaryotic catecholamine hormones to the chemotaxis coupling protein CheW. Significantly lower numbers of bacteria were detected in glass capillaries filled with 100 mM glucose upon supplementation with 50 μM EPI or PE (Chapter 2.3). Parts of this figure were created using Biorender.com.

Even though the impact on chemotactic signaling should be elaborated, the results further emphasize that stress hormones such as EPI and NE act as interkingdom signals between eukaryotic hosts and bacteria. In eukaryotes, catecholamines bind to G protein-coupled receptors, and certain antagonists of human receptors can also antagonize adrenergic effects in bacteria (88). This suggests that similar receptors may have also evolved in prokaryotes, which indeed has been demonstrated in EHEC where EPI and NE bound to the two-component system HKs QseC and QseE (95, 96). Thus, binding of catecholamines in *V. campbellii* to the

coupling protein CheW, and not to a receptor, was a somewhat surprising finding. However, *Salmonella* and *V. cholerae* mutants lacking QseC and/or QseE still responded to catecholamines (87, 97, 98). It will be important for follow-up studies to pinpoint the exact residues in CheW where catecholamine hormones bind to elucidate the regulatory mechanism exerted on chemotactic control. Importantly, the findings (Chapter 2.3) also have notable physiological implications considering that chemotaxis and net motility affected the infectivity of *V. cholerae* (238). Stool-derived *V. cholerae* cells commonly display a smooth-swimming state and exhibit repression of chemotaxis genes such as *cheR* and *cheW* (239–241). Thus, chemotactic control mediated by binding to CheW may not only be important for the perception of interkingdom signals, but also affect the overall infectivity of bacterial cells.

3.3 Phenotypic heterogeneity under consecutively increasing acid stress

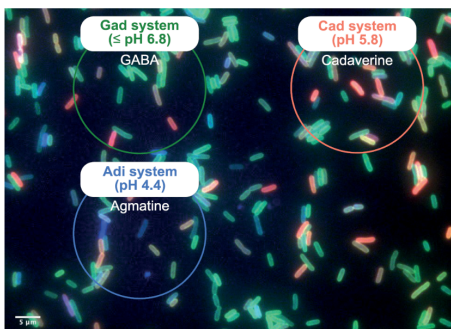
An example of heterogeneity under acid stress was presented using a chromosomal fluorescent triple reporter strain in Chapter 2.4. The antiporters of the three major ARs in *E. coli* (GadC, AdiC, CadB) were fused to fluorophores (eGFP, mCherry, mCerulean) and exposed to consecutively increasing acidity. This approach revealed a heterogeneous activation of the three systems with a different degree of noise and suggested a division of labor among the *E. coli* population (Chapter 2.4). The Adi system (induced at pH 4.4) and the Cad system (induced at pH 5.8 in the presence of lysine) were activated in a mutually exclusive manner, with a large proportion of ON-OFF cells (Figure 11). On the other hand, the Gad system was heterogeneously activated in exponential phase, but nearly all cells activated the system in stationary phase. The low copy numbers of the transcriptional activators CadC and AdiY (122, 242) and their stochastic distribution were suggested as the underlying cause for heterogeneous activation among single cells. Correspondingly, an artificial increase in CadC and AdiY copy numbers shifted the populations to homogeneity (Chapter 2.4).

It is also worth noting that the number of ARs in *E. coli* is higher than in other γ -proteobacteria, reflected in significantly increased acid tolerance (Chapter 2.5). The benefit of possessing several ARs but activating them heterogeneously among the population can be explained, for instance, by the efficient differential consumption of amino acids. Glutamate is the most abundant amino acid in the cell (100 mM), while arginine (0.57 mM) and lysine (0.41 mM) are less abundant (243). Since the Gad system is homogeneously distributed under mild acid stress (Chapter 2.4), all cells of the population can initially use the available glutamate in the cytoplasm. When the stress increases, only a limited percentage of cells activate either the Cad or Adi system (Figure 11). These resulting subpopulations however contribute to combat acidity by releasing the more alkaline cadaverine and agmatine, which serve as common goods for the entire population. This strategy can be considered as 'bet-hedging', as producing both the Cad and Adi system would represent a major metabolic burden for an individual cell.

This assumption is underlined by findings demonstrating reduced growth rates upon artificial overexpression of the Adi or Cad system respectively (Chapter 2.4). Moreover, preemptive expression of AR genes under mild acid stress in a limited cell percentage may also be important to prepare the population against future strong acid stresses. The latter was indicated for *gadA* and *gadB*, which are essential for acid shock survival but confer a growth deficit upon overexpression (244). Nevertheless, limited expression in a subpopulation will not affect the overall growth rate of the population drastically, but ensure the survival of a limited number of cells in case of sudden unexpected strong stress, such as encountered in the human stomach.

Importantly, the Ribo- and RNA-Seq approach (Chapter 2.1) revealed further crucial regulators for the adaptation of *E. coli* to acidity such as YdcI, which affected the transcription of the Gad and Cad systems. It will be of interest for future studies to investigate whether copy number manipulations of YdcI may also affect the heterogeneity of AR systems in a manner as described for AdiY and CadC (Chapter 2.4).

Phenotypic heterogeneity of the three major ARs in *E. coli*



Gad system:
homogeneously activated in stationary phase
heterogeneously activated in acidified media in exponential phase
complex transcriptional regulation

Adi system:
max. induction at pH 4.4
activated by AdiY
heterogeneously distributed

Cad system:
max. induction at pH 5.8 in the presence of lysine
activated by CadC
heterogeneously distributed

— mutually exclusive

Differential integration of IS elements in the *flhDC* regulatory region

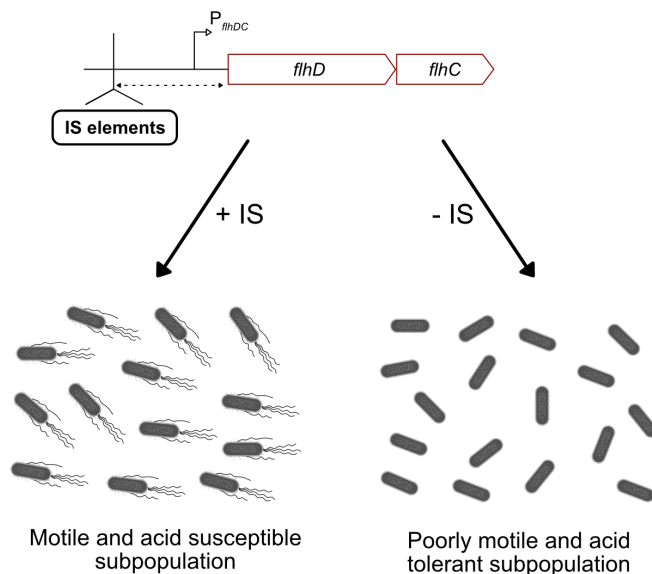


Figure 11: Examples of phenotypic heterogeneity detected in *E. coli* under acid stress. Division of labor among an *E. coli* population in terms of heterogeneous AR activation was determined by fluorescence microscopy using a triple-fluorescent reporter strain (Chapter 2.4). Differential integration of IS elements into the regulatory region of *flhDC* is responsible for the differentiation into subpopulations that are either motile and acid-susceptible, or poorly motile and acid-tolerant (Chapter 2.2).

As mentioned in Chapter 3.2.2, heterogeneity was also detected in terms of MG1655 cells harboring a motility-activating IS element upstream of *flhDC*. Considering that this insertion induces motility while reducing the capacity to survive acid shock (Chapter 2.2), it is tempting to speculate that *E. coli* diversifies into a motile and an acid tolerant subpopulation under acid stress in a manner dependent on IS elements (Figure 11). This hypothesis is supported as bacterial heterogeneity in flagella expression was previously demonstrated (245, 246). Furthermore, colonization efficiencies of mouse intestines were heavily affected by differential IS element integration upstream of *flhDC* in *E. coli*, indicating existing niches in the gut where motility is beneficial (247). Given distinct intestinal niches where either acid tolerance or motility is advantageous, IS transposition may be crucial to ensure that *E. coli* can colonize both niches by diversifying into motile and acid-tolerant subpopulations (Figure 11).

Importantly, the study of collective behaviors in *E. coli* was so far mainly restricted to AR components (121, 122). Thus, it will be crucial for future investigations to study the potential heterogeneity of other cellular defense proteins such as chaperones, enzymes responsible for membrane modifications, or efflux pumps. Moreover, the potential heterogeneity of the Orn system should be addressed. For instance, the triple-fluorescent reporter described in Chapter 2.4 could be utilized and PotE, the transporter of the Orn system, labeled with a fourth fluorophore. A potential approach to address all above raised suggestions on a systematic level is scRNA-Seq, which is further discussed in Chapter 3.4.

3.4 Conclusions and outlook

Reacting to pH fluctuations is essential for the survival of prokaryotes in various habitats on earth (Figure 1). Within this thesis, the spectrum of acid defense mechanisms in *E. coli* was extended by leveraging the advantages of the Ribo-Seq technique. This approach revealed novel adaptation strategies, detected previously overlooked sORFs, and provided a genome-wide overview of mRNA and RPF levels under mild and severe acid stress (Chapter 2.1). Furthermore, a novel fitness trade-off between motility and acid survival was demonstrated (Chapter 2.2). An alteration in chemotactic signaling was noted as mammalian stress hormones bound to the chemotaxis coupling protein CheW in *V. campbellii* (Chapter 2.3). Finally, division of labor and phenotypic heterogeneity were detected in *E. coli* upon conducting fluorescence microscopy with a triple-fluorescent reporter strain (Chapter 2.4).

Fluorescence microscopy is a valuable approach for gathering spatial information and assessing the distribution of a small number of proteins in single cells. Nevertheless, the method is limited in terms of information beyond the labeled proteins, introduces biases due to delayed fluorophore folding, and is restricted in terms of throughput due to limitations of cell numbers per experiment (114, 248). To overcome these limitations, scRNA-Seq could be conducted under consecutively increasing acid stress. Unlike bulk RNA-Seq, which provides

an average expression profile of cells in a sample, scRNA-Seq allows monitoring global gene expression patterns at the single-cell level (114, 249). The immense potential of scRNA-Seq was demonstrated in numerous recent studies (249–252), and a recent scRNA-Seq approach (M3-Seq) revealed an acid resistant subpopulation in stationary phase *E. coli* cells which was characterized by very high expression levels of *gadA* and *gadB* (244). Moreover, scRNA-Seq and/or Ribo-Seq could be applied upon bacterial exposure to mammalian stress hormones.

The continuously growing amount of sequencing data is an important consideration for future NGS studies. For instance, the storage capacity for human genomic data alone is estimated to account for up to 40 exabytes by 2025 (253). Thus, it is essential to implement workflows for automated prioritization of important findings from large-scale genomic datasets. The latter was successfully demonstrated within this thesis through machine learning via denoising autoencoders (Chapter 2.1). This self-supervised method can generate new hypotheses from expression data and identify genes uniquely expressed in a certain condition (254).

The significance of phenotypic heterogeneity in isogenic bacterial populations is another key finding of this work (Chapters 2.2 and 2.4) and underlines that addressing bacterial heterogeneity is crucial for the upcoming antibiotic crisis. Links and overlaps exist between the acid and antibiotic stress responses (63, 64), and severe near-lethal acid stress caused a drastic reduction in bacterial metabolism (Chapter 2.1). Thus, acid shock periods may prepare *E. coli* for a persistent state which in turn confers antibiotic resistance. Along this line, highly resistant strains towards chloramphenicol were recently characterized by a significantly decreased internal pH (65). The above-described overlap between acidity and antibiotic stress could be leveraged for drug design with the ultimate aim of modifying the cytoplasmic pH of bacteria. Such drugs would automatically also affect the antibiotic tolerance of pathogens and could be prescribed together with conventional antibiotics.

While the reduction of acid tolerance is desirable for pathogens, limited acid susceptibility is important for certain bacteria with industrial relevance. For example, probiotic bacteria have significant pharmaceutical value while their incorporation into food remains challenging (255). Conferring acid resistance to probiotics would enhance live cell numbers upon gastrointestinal transition and improve the value and shelf-life of these products.

It is worth noting, that the Ribo-Seq study (Chapter 2.1) was conducted by the addition of HCl to growing cultures. However, environments such as the human gastrointestinal tract usually comprise a mixture of different acids. For instance, bile acids are present in the small intestine (256), and SCFAs are produced by gut bacteria in the large intestine upon fermentation of dietary fibers (257, 258). Thus, it will be of interest to study the response to a cocktail of acids including organic acids, which rather resembles the naturally encountered conditions of bacteria when traversing the gastrointestinal tract.

In summary, pH is a crucial determinant for bacterial survival on earth and shapes the composition of environments such as gastrointestinal tracts, soils, or phagosomes (see Chapter 1). Thereby, the degree of acid tolerance dictates whether a strain can occupy a certain niche or not. The results obtained in this thesis suggest that bacterial responses to acidity are more intricate than thus far assumed and showcase the tremendous complexity of bacterial integration of information from distinct environments. Thinking one step ahead, this complexity will be even more pronounced when studying bacteria in mixed biofilms, or communities. Such experiments are needed to understand the effect of acidity on a community level encountered, for example, in the human microbiome, which is ultimately linked to the overall health of a person. Correspondingly, studying stress hormones within the scope of mixed bacterial populations will provide further insights into the interplay of eukaryotes and prokaryotes.

References for Chapters 1 and 3

1. Jensen WB. 2004. The symbol for pH. *J Chem Educ* 81:21.
2. Buck R, Rondinini S, Covington A, Baucke F, Brett C, Camões M, Milton M, Mussini T, Naumann R, Pratt K, et al. 2010. Measurement of pH definition, standards, and procedures. *Handb Biochem Mol Biol Fourth Ed* 74:675–692.
3. Akcil A, Koldas S. 2006. Acid mine drainage (AMD): causes, treatment and case studies. *J Clean Prod* 14:1139–1145.
4. Sorokin DY, Kuenen JG. 2005. Chemolithotrophic haloalkaliphiles from soda lakes. *FEMS Microbiol Ecol* 52:287–295.
5. Fallingborg J. 1999. Intraluminal pH of the human gastrointestinal tract. *Dan Med Bull* 46:183–196.
6. Quigley EMM, Turnberg LA. 1987. pH of the microclimate lining human gastric and duodenal mucosa *in vivo*: Studies in control subjects and in duodenal ulcer patients. *Gastroenterology* 92:1876–1884.
7. Beasley DE, Koltz AM, Lambert JE, Fierer N, Dunn RR. 2015. The evolution of stomach acidity and its relevance to the human microbiome. *PLoS One* 10:1–12.
8. Cash RA, Music SI, Joseph P, Snyder MJ, Wenzel RP, Hornick RB. 1974. Response of man to infection with *Vibrio cholerae*. *J Infect Dis* 129:45–52.
9. Sansonetti PJ. 2001. Rupture, invasion and inflammatory destruction of the intestinal barrier by *Shigella*, making sense of prokaryote-eukaryote cross-talks. *FEMS Microbiol Rev* 25:3–14.
10. Tilden J, Young W, McNamara AM, Custer C, Boesel B, Lambert-Fair MA, Majkowski J, Vugia D, Werner SB, Hollingsworth J, et al. 1996. A new route of transmission for *Escherichia coli*: Infection from dry fermented salami. *Am J Public Health* 86:1142–1145.
11. Pye G, Evans DF, Ledingham S, Hardcastle JD. 1990. Gastrointestinal intraluminal pH in normal subjects and those with colorectal adenoma or carcinoma. *Gut* 31:1355–1357.
12. Yamamura R, Inoue KY, Nishino K, Yamasaki S. 2023. Intestinal and fecal pH in human health. *Front Microbiomes* 2:1–12.
13. Crawford N, Brooke BN. 1955. The pH and buffering power of human bile. *Lancet* 265:1096–1097.

14. Hirshfield IN, Terzulli S, O'Byrne C. 2003. Weak organic acids: a panoply of effects on bacteria. *Sci Prog* 86:245–269.
15. Steinberg BE, Huynh KK, Grinstein S. 2007. Phagosomal acidification: measurement, manipulation and functional consequences. *Biochem Soc Trans* 35:1083–1087.
16. Hackam DJ, Rotstein OD, Grinstein S. 1999. Phagosomal acidification mechanisms and functional significance, p. 299–319. *In* Gordon, S (ed.), *Phagocytosis: The Host*. JAI.
17. Pierre WH. 1925. The H-ion concentration of soils as affected by carbonic acid and the soil-water ratio, and the nature of soil acidity as revealed by these studies. *Soil Sci* 20.
18. Singh A, Agrawal M. 2008. Acid rain and its ecological consequences. *J Environ Biol* 29:15–24.
19. Murphy D V, Stockdale EA, Brookes PC, Goulding KWT. 2007. Impact of microorganisms on chemical transformations in soil, p. 37–59. *In* Abbott, LK, Murphy, D V (eds.), *Soil Biological Fertility: A Key to Sustainable Land Use in Agriculture*. Springer Netherlands, Dordrecht.
20. van Loon GW. 1984. Acid rain and soil. *Can J Physiol Pharmacol* 62:991–997.
21. von Uexküll HR, Mutert E. 1995. Global extent, development and economic impact of acid soils. *Plant Soil* 171:1–15.
22. Dedysh SN. 2002. Methanotrophic bacteria of acidic *Sphagnum* peat bogs. *Microbiology* 71:638–650.
23. McDonald IR, Upton M, Hall G, Pickup RW, Edwards C, Saunders JR, Ritchie DA, Murrell JC. 1999. Molecular ecological analysis of methanogens and methanotrophs in blanket bog peat. *Microb Ecol* 38:225–233.
24. N. Basiliko J. B. Yavitt PMD, Merkel SM. 2003. Methane biogeochemistry and methanogen communities in two northern peatland ecosystems, New York State. *Geomicrobiol J* 20:563–577.
25. Fröhlich-Wyder M-T, Bisig W, Guggisberg D, Jakob E, Turgay M, Wechsler D. 2017. Cheeses with propionic acid fermentation, p. 889–910. *In* McSweeney, PLH, Fox, PF, Cotter, PD, Everett, DW (eds.), *Cheese (Fourth Edition) Fourth Edi*. Academic Press, San Diego.
26. Siedler S, Balti R, Neves AR. 2019. Bioprotective mechanisms of lactic acid bacteria against fungal spoilage of food. *Curr Opin Biotechnol* 56:138–146.
27. Erfle JD, Boila RJ, Teather RM, Mahadevan S, Sauer FD. 1982. Effect of pH on

- fermentation characteristics and protein degradation by rumen microorganisms *in vitro*. J Dairy Sci 65:1457–1464.
28. Jerez CA. 2017. Biomining of metals: how to access and exploit natural resource sustainably. Microb Biotechnol 10:1191–1193.
 29. Jones DS, Schaperdoth I, Macalady JL. 2016. Biogeography of sulfur-oxidizing *Acidithiobacillus* populations in extremely acidic cave biofilms. ISME J 10:2879–2891.
 30. Slonczewski JL, Fujisawa M, Dopson M, Krulwich TA. 2009. Cytoplasmic pH measurement and homeostasis in bacteria and archaea. Adv Microb Physiol 55:1-79,317.
 31. Deamer DW. 1987. Proton permeation of lipid bilayers. J Bioenerg Biomembr 19:161–177.
 32. Chang YY, Cronan JE. 1999. Membrane cyclopropane fatty acid content is a major factor in acid resistance of *Escherichia coli*. Mol Microbiol 33:249–259.
 33. Shabala L, Ross T. 2008. Cyclopropane fatty acids improve *Escherichia coli* survival in acidified minimal media by reducing membrane permeability to H⁺ and enhanced ability to extrude H⁺. Res Microbiol 159:458–461.
 34. Yang Y, Kadim MI, Khoo WJ, Zheng Q, Setyawati MI, Shin YJ, Lee SC, Yuk HG. 2014. Membrane lipid composition and stress/virulence related gene expression of *Salmonella* Enteritidis cells adapted to lactic acid and trisodium phosphate and their resistance to lethal heat and acid stress. Int J Food Microbiol 191:24–31.
 35. Sohlenkamp C. 2017. Membrane homeostasis in bacteria upon pH challenge, p. 1–13. In Geiger, O (ed.), Biogenesis of Fatty Acids, Lipids and Membranes. Springer International Publishing, Cham.
 36. Mitchell P. 1973. Performance and conservation of osmotic work by proton-coupled solute porter systems. J Bioenerg 4:63–91.
 37. Maurer LM, Yohannes E, Bondurant SS, Radmacher M, Slonczewski JL. 2005. pH regulates genes for flagellar motility, catabolism, and oxidative stress in *Escherichia coli* K-12. J Bacteriol 187:304–319.
 38. Sun Y, Fukamachi T, Saito H, Kobayashi H. 2012. Respiration and the F₁F_o-ATPase enhance survival under acidic conditions in *Escherichia coli*. PLoS One 7:1–7.
 39. Kobayashi H, Suzuki T, Unemoto T. 1986. Streptococcal cytoplasmic pH is regulated by changes in amount and activity of a proton-translocating ATPase. J Biol Chem

261:627–630.

40. Foster JW, Hall HK. 1991. Inducible pH homeostasis and the acid tolerance response of *Salmonella typhimurium*. *J Bacteriol* 173:5129–5135.
41. Cotter PD, Gahan CGM, Hill C. 2000. Analysis of the role of the *Listeria monocytogenes* F₀F₁-ATPase operon in the acid tolerance response. *Int J Food Microbiol* 60:137–146.
42. Arcari T, Feger M-L, Guerreiro DN, Wu J, O’Byrne CP. 2020. Comparative review of the responses of *Listeria monocytogenes* and *Escherichia coli* to low pH stress. *Genes (Basel)* 11.
43. Lund P, Tramonti A, De Biase D. 2014. Coping with low pH: Molecular strategies in neutrophilic bacteria. *FEMS Microbiol Rev* 38:1091–1125.
44. Foster JW. 2004. *Escherichia coli* acid resistance: Tales of an amateur acidophile. *Nat Rev Microbiol* 2:898–907.
45. Kanjee U, Houry WA. 2013. Mechanisms of acid resistance in *Escherichia coli*. *Annu Rev Microbiol* 67:65–81.
46. De Biase D, Pennacchietti E. 2012. Glutamate decarboxylase-dependent acid resistance in orally acquired bacteria: Function, distribution and biomedical implications of the *gadBC* operon. *Mol Microbiol* 86:770–786.
47. Guan N, Liu L. 2020. Microbial response to acid stress: mechanisms and applications. *Appl Microbiol Biotechnol* 104:51–65.
48. Herrero del Valle A, Seip B, Cervera-Marzal I, Sacheau G, Seefeldt AC, Innis CA. 2020. Ornithine capture by a translating ribosome controls bacterial polyamine synthesis. *Nat Microbiol* 5:554–561.
49. Neely MN, Dell CL, Olson ER. 1994. Roles of LysP and CadC in mediating the lysine requirement for acid induction of the *Escherichia coli cad* operon. *J Bacteriol* 176:3278–3285.
50. Stim-Herndon KP, Flores TM, Bennett GN. 1996. Molecular characterization of *adiY*, a regulatory gene which affects expression of the biodegradative acid-induced arginine decarboxylase gene (*adiA*) of *Escherichia coli*. *Microbiology* 142:1311–1320.
51. Castanie-Cornet MP, Foster JW. 2001. *Escherichia coli* acid resistance: CAMP receptor protein and a 20 bp *cis*-acting sequence control pH and stationary phase expression of the *gadA* and *gadBC* glutamate decarboxylase genes. *Microbiology* 147:709–715.
52. Castanié-Cornet MP, Cam K, Bastiat B, Cros A, Bordes P, Gutierrez C. 2010. Acid

- stress response in *Escherichia coli*: Mechanism of regulation of *gadA* transcription by RcsB and GadE. *Nucleic Acids Res* 38:3546–3554.
53. Küper C, Jung K. 2005. CadC-mediated activation of the *cadBA* promoter in *Escherichia coli*. *J Mol Microbiol Biotechnol* 10:26–39.
 54. Aquino P, Honda B, Jaini S, Lyubetskaya A, Hosur K, Chiu JG, Ekladios I, Hu D, Jin L, Sayeg MK, et al. 2017. Coordinated regulation of acid resistance in *Escherichia coli*. *BMC Syst Biol* 11:1–15.
 55. Goto Y, Takahashi N, Fink AL. 1990. Mechanism of acid-induced folding of proteins. *Biochemistry* 29:3480–3488.
 56. Dahl J-U, Koldewey P, Salmon L, Horowitz S, Bardwell JCA, Jakob U. 2015. HdeB functions as an acid-protective chaperone in bacteria. *J Biol Chem* 290:65–75.
 57. Tapley TL, Franzmann TM, Chakraborty S, Jakob U, Bardwell JCA. 2010. Protein refolding by pH-triggered chaperone binding and release. *Proc Natl Acad Sci U S A* 107:1071–1076.
 58. Šeputiene V, Motiejunas D, Sužiedelis K, Tomenius H, Normark S, Melefors Ö, Sužiedeliene E. 2003. Molecular characterization of the acid-inducible *asr* gene of *Escherichia coli* and its role in acid stress response. *J Bacteriol* 185:2475–2484.
 59. Ren C, Zheng Y, Liu C, Mencius J, Wu Z, Quan S. 2022. Molecular characterization of an intrinsically disordered chaperone reveals net-charge regulation in chaperone action. *J Mol Biol* 434:167405.
 60. Tucker DL, Tucker N, Zhuo M, Foster JW, Miranda RL, Cohen PS, Conway T. 2003. Genes of the GadX-GadW regulon in *Escherichia coli*. *J Bacteriol* 185:3190–3201.
 61. Yamanaka Y, Oshima T, Ishihama A, Yamamoto K. 2014. Characterization of the YdeO regulon in *Escherichia coli*. *PLoS One* 9.
 62. Teelucksingh, T., Thompson, L.K., Cox G. 2020. The evolutionary conservation of *Escherichia coli* drug efflux pumps supports physiological functions. *J Bacteriol* 202:1–17.
 63. Mitosch K, Rieckh G, Bollenbach T. 2017. Noisy response to antibiotic stress predicts subsequent single-cell survival in an acidic environment. *Cell Syst* 4:393-403.e5.
 64. Mitosch K, Rieckh G, Bollenbach T. 2019. Temporal order and precision of complex stress responses in individual bacteria. *Mol Syst Biol* 15:1–15.
 65. Reyes-Fernández EZ, Schuldiner S. 2020. Acidification of cytoplasm in *Escherichia coli*

- provides a strategy to cope with stress and facilitates development of antibiotic resistance. *Sci Rep* 10:1–13.
66. Wadhams GH, Armitage JP. 2004. Making sense of it all: bacterial chemotaxis. *Nat Rev Mol Cell Biol* 5:1024–1037.
 67. Sourjik V, Wingreen NS. 2012. Responding to chemical gradients: bacterial chemotaxis. *Curr Opin Cell Biol* 24:262–268.
 68. Kentner D, Thiem S, Hildenbeutel M, Sourjik V. 2006. Determinants of chemoreceptor cluster formation in *Escherichia coli*. *Mol Microbiol* 61:407–417.
 69. Hazelbauer GL, Falke JJ, Parkinson JS. 2008. Bacterial chemoreceptors: high-performance signaling in networked arrays. *Trends Biochem Sci* 33:9–19.
 70. Maddock JR, Shapiro L. 1993. Polar location of the chemoreceptor complex in the *Escherichia coli* cell. *Science* 259:1717–1723.
 71. Krikos A, Conley MP, Boydt A, Berg HC, Simon MI. 1985. Chimeric chemosensory transducers of *Escherichia coli*. *Proc Natl Acad Sci USA* 82:1326–1330.
 72. Umemura T, Matsumoto Y, Ohnishi K, Homma M, Kawagishi I. 2002. Sensing of cytoplasmic pH by bacterial chemoreceptors involves the linker region that connects the membrane-spanning and the signal-modulating helices. *J Biol Chem* 277:1593–1598.
 73. Yang Y, Sourjik V. 2012. Opposite responses by different chemoreceptors set a tunable preference point in *Escherichia coli* pH taxis. *Mol Microbiol* 86:1482–1489.
 74. Croxen MA, Sisson G, Melano R, Hoffman PS. 2006. The *Helicobacter pylori* chemotaxis receptor *tlpB* (HP0103) is required for pH taxis and for colonization of the gastric mucosa. *J Bacteriol* 188:2656–2665.
 75. Goers Sweeney E, Henderson JN, Goers J, Wreden C, Hicks KG, Foster JK, Parthasarathy R, Remington SJ, Guillemin K. 2012. Structure and proposed mechanism for the pH-sensing *Helicobacter pylori* chemoreceptor TlpB. *Structure* 20:1177–1188.
 76. Adler J. 1973. A method for measuring chemotaxis and use of the method to determine optimum conditions for chemotaxis by *Escherichia coli*. *J Gen Microbiol* 74:77–91.
 77. Yueh YG, Crain RC. 1993. Deflagellation of *Chlamydomonas reinhardtii* follows a rapid transitory accumulation of inositol 1,4,5-trisphosphate and requires Ca²⁺ entry. *J Cell Biol* 123:869–875.
 78. Hartzell LB, Hartzell HC, Quarmby LM. 1993. Mechanisms of flagellar excision: I. The role of intracellular acidification. *Exp Cell Res* 208:148–153.

79. Marles-Wright J, Lewis RJ. 2007. Stress responses of bacteria. *Curr Opin Struct Biol* 17:755–760.
80. Sarkodie EK, Zhou S, Baidoo SA, Chu W. 2019. Influences of stress hormones on microbial infections. *Microb Pathog* 131:270–276.
81. Freestone PP, Lyte M, Neal CP, Maggs AF, Haigh RD, Williams PH. 2000. The mammalian neuroendocrine hormone norepinephrine supplies iron for bacterial growth in the presence of transferrin or lactoferrin. *J Bacteriol* 182:6091–6098.
82. Freestone PP, Williams PH, Haigh RD, Maggs AF, Neal CP, Lyte M. 2002. Growth stimulation of intestinal commensal *Escherichia coli* by catecholamines: a possible contributory factor in trauma-induced sepsis. *Shock* 18:465–470.
83. Sandrini SM, Shergill R, Woodward J, Muralikuttan R, Haigh RD, Lyte M, Freestone PP. 2010. Elucidation of the mechanism by which catecholamine stress hormones liberate iron from the innate immune defense proteins transferrin and lactoferrin. *J Bacteriol* 192:587–594.
84. Sperandio V, Torres AG, Jarvis B, Nataro JP, Kaper JB. 2003. Bacteria-host communication: the language of hormones. *Proc Natl Acad Sci U S A* 100:8951–8956.
85. Moreira CG, Weinshenker D, Sperandio V. 2010. QseC mediates *Salmonella enterica* serovar typhimurium virulence *in vitro* and *in vivo*. *Infect Immun* 78:914–926.
86. Yang Q, Anh NDQ, Bossier P, Defoirdt T. 2014. Norepinephrine and dopamine increase motility, biofilm formation, and virulence of *Vibrio harveyi*. *Front Microbiol* 5:584.
87. Merighi M, Septer AN, Carroll-Portillo A, Bhatiya A, Porwollik S, McClelland M, Gunn JS. 2009. Genome-wide analysis of the PreA/PreB (QseB/QseC) regulon of *Salmonella enterica* serovar Typhimurium. *BMC Microbiol* 9:42.
88. Freestone P. 2013. Communication between bacteria and their hosts. *Scientifica (Cairo)* 2013:361073.
89. Lopes JG, Sourjik V. 2018. Chemotaxis of *Escherichia coli* to major hormones and polyamines present in human gut. *ISME J* 12:2736–2747.
90. Nakano M, Takahashi A, Sakai Y, Nakaya Y. 2007. Modulation of pathogenicity with norepinephrine related to the type III secretion system of *Vibrio parahaemolyticus*. *J Infect Dis* 195:1353–1360.
91. Lyte M, Vulchanova L, Brown DR. 2011. Stress at the intestinal surface: catecholamines and mucosa–bacteria interactions. *Cell Tissue Res* 343:23–32.

92. Peterson G, Kumar A, Gart E, Narayanan S. 2011. Catecholamines increase conjugative gene transfer between enteric bacteria. *Microb Pathog* 51:1–8.
93. Caron MG, Lefkowitz RJ. 1993. Catecholamine receptors: structure, function, and regulation, p. 277–290. *In* BARDIN, CW (ed.), *Recent Progress in Hormone Research*. Academic Press.
94. Deupi X, Kobilka B. 2007. Activation of G protein–coupled receptors, p. 137–166. *In* *Mechanisms and Pathways of Heterotrimeric G Protein Signaling*. Academic Press.
95. Reading NC, Rasko DA, Torres AG, Sperandio V. 2009. The two-component system QseEF and the membrane protein QseG link adrenergic and stress sensing to bacterial pathogenesis. *Proc Natl Acad Sci U S A* 106:5889–5894.
96. Clarke MB, Hughes DT, Zhu C, Boedeker EC, Sperandio V. 2006. The QseC sensor kinase: a bacterial adrenergic receptor. *Proc Natl Acad Sci U S A* 103:10420–10425.
97. Halang P, Toulouse C, Geißel B, Michel B, Flauger B, Müller M, Voegele RT, Stefanski V, Steuber J. 2015. Response of *Vibrio cholerae* to the catecholamine hormones epinephrine and norepinephrine. *J Bacteriol* 197:3769–3778.
98. Pullinger GD, Carnell SC, Sharaff FF, van Diemen PM, Dziva F, Morgan E, Lyte M, Freestone PPE, Stevens MP. 2010. Norepinephrine augments *Salmonella enterica*-induced enteritis in a manner associated with increased net replication but independent of the putative adrenergic sensor kinases QseC and QseE. *Infect Immun* 78:372–380.
99. Anetzberger C, Reiger M, Fekete A, Schell U, Stambrau N, Plener L, Kopka J, Schmitt-Kopplin P, Hilbi H, Jung K. 2012. Autoinducers act as biological timers in *Vibrio harveyi*. *PLoS One* 7:e48310.
100. Bassler BL, Wright M, Showalter RE, Silverman MR. 1993. Intercellular signalling in *Vibrio harveyi*: sequence and function of genes regulating expression of luminescence. *Mol Microbiol* 9:773–786.
101. Austin B, Zhang X-H. 2006. *Vibrio harveyi*: a significant pathogen of marine vertebrates and invertebrates. *Lett Appl Microbiol* 43:119–124.
102. Fonović M, Bogoy M. 2008. Activity-based probes as a tool for functional proteomic analysis of proteases. *Expert Rev Proteomics* 5:721–730.
103. Wright MH, Sieber SA. 2016. Chemical proteomics approaches for identifying the cellular targets of natural products. *Nat Prod Rep* 33:681–708.
104. Rayo J, Gregor R, Jacob NT, Dandela R, Dubinsky L, Yashkin A, Aranovich A,

- Thangaraj M, Ernst O, Barash E, et al. 2021. Immunoediting role for major vault protein in apoptotic signaling induced by bacterial N-acyl homoserine lactones. *Proc Natl Acad Sci U S A* 118.
105. Wright MH, Fetzer C, Sieber SA. 2017. Chemical probes unravel an antimicrobial defense response triggered by binding of the human opioid dynorphin to a bacterial sensor kinase. *J Am Chem Soc* 139:6152–6159.
 106. Wilkinson IVL, Bottlinger M, El Harraoui Y, Sieber SA. 2023. Profiling the heme-binding proteomes of bacteria using chemical proteomics. *Angew Chem Int Ed Engl* 62:e202212111.
 107. Ackermann M. 2015. A functional perspective on phenotypic heterogeneity in microorganisms. *Nat Rev Microbiol* 13:497–508.
 108. Gasperotti A, Brameyer S, Fabiani F, Jung K. 2020. Phenotypic heterogeneity of microbial populations under nutrient limitation. *Curr Opin Biotechnol* 62:160–167.
 109. Davis KM, Isberg RR. 2016. Defining heterogeneity within bacterial populations via single cell approaches. *BioEssays* 38:782–790.
 110. Silander OK, Nikolic N, Zaslaver A, Bren A, Kikoin I, Alon U, Ackermann M. 2012. A genome-wide analysis of promoter-mediated phenotypic noise in *Escherichia coli*. *PLoS Genet* 8.
 111. Jung K, Brameyer S, Fabiani F, Gasperotti A, Hoyer E. 2019. Phenotypic heterogeneity generated by histidine kinase-based signaling networks. *J Mol Biol* 431:4547–4558.
 112. Veening J-W, Smits WK, Kuipers OP. 2008. Bistability, epigenetics, and bet-hedging in bacteria. *Annu Rev Microbiol* 62:193–210.
 113. Grimbergen AJ, Siebring J, Solopova A, Kuipers OP. 2015. Microbial bet-hedging: the power of being different. *Curr Opin Microbiol* 25:67–72.
 114. Saliba AE, Westermann AJ, Gorski SA, Vogel J. 2014. Single-cell RNA-seq: advances and future challenges. *Nucleic Acids Res* 42:8845–8860.
 115. Choudhary D, Lagage V, Foster KR, Uphoff S. 2023. Phenotypic heterogeneity in the bacterial oxidative stress response is driven by cell-cell interactions. *Cell Rep* 42:112168.
 116. den Besten HMW, Ingham CJ, van Hylckama Vlieg JET, Beerthuyzen MM, Zwietering MH, Abee T. 2007. Quantitative analysis of population heterogeneity of the adaptive salt stress response and growth capacity of *Bacillus cereus* ATCC 14579. *Appl Environ*

Microbiol 73:4797–4804.

117. Dewachter L, Fauvart M, Michiels J. 2019. Bacterial heterogeneity and antibiotic survival: Understanding and combatting persistence and heteroresistance. *Mol Cell* 76:255–267.
118. Dhar N, McKinney JD. 2007. Microbial phenotypic heterogeneity and antibiotic tolerance. *Curr Opin Microbiol* 10:30–38.
119. Gefen O, Balaban NQ. 2009. The importance of being persistent: heterogeneity of bacterial populations under antibiotic stress. *FEMS Microbiol Rev* 33:704–717.
120. Liew ATF, Foo YH, Gao Y, Zangoui P, Singh MK, Gulvady R, Kenney LJ. 2019. Single cell, super-resolution imaging reveals an acid pH-dependent conformational switch in SsrB regulates SPI-2. *Elife* 8:1–26.
121. Van Riet S, Tadesse W, Mortier J, Schlegel S, Simoens K, Bernaerts K, Dal Co A, Aertsen A. 2022. Heterogeneity and evolutionary tunability of *Escherichia coli* resistance against extreme acid stress. *Microbiol Spectr* 10:1–13.
122. Brameyer S, Hoyer E, Bibinger S, Burdack K, Lassak J, Jung K. 2020. Molecular design of a signaling system influences noise in protein abundance under acid stress in different gammaproteobacteria. *J Bacteriol* 202.
123. Slatko BE, Gardner AF, Ausubel FM. 2018. Overview of next-generation sequencing technologies. *Curr Protoc Mol Biol* 122:e59.
124. van Dijk EL, Auger H, Jaszczyszyn Y, Thermes C. 2014. Ten years of next-generation sequencing technology. *Trends Genet* 30:418–426.
125. Conway T, K. G. 2003. Microarray expression profiling: capturing a genome-wide portrait of the transcriptome. *Mol Microbiol* 47:879–889.
126. Cheung VG, Morley M, Aguilar F, Massimi A, Kucherlapati R, Childs G. 1999. Making and reading microarrays. *Nat Genet* 21:15–19.
127. Lucchini S, Thompson A, Hinton JCD. 2001. Microarrays for microbiologists. *Microbiology* 147:1403–1414.
128. Jaksik R, Iwanaszko M, Rzeszowska-Wolny J, Kimmel M. 2015. Microarray experiments and factors which affect their reliability. *Biol Direct* 10:46.
129. Blankenhorn D, Phillips J, Slonczewski JL. 1999. Acid- and base-induced proteins during aerobic and anaerobic growth of *Escherichia coli* revealed by two-dimensional gel electrophoresis. *J Bacteriol* 181:2209–2216.

130. Stancik LM, Stancik DM, Schmidt B, Barnhart DM, Yoncheva YN, Slonczewski JL. 2002. pH-dependent expression of periplasmic proteins and amino acid catabolism in *Escherichia coli*. *J Bacteriol* 184:4246–4258.
131. Chen G, Pramanik BN. 2009. Application of LC/MS to proteomics studies: current status and future prospects. *Drug Discov Today* 14:465–471.
132. Patterson SD, Aebersold RH. 2003. Proteomics: the first decade and beyond. *Nat Genet* 33:311–323.
133. Chandramouli K, Qian PY. 2009. Proteomics: challenges, techniques and possibilities to overcome biological sample complexity. *Hum Genomics Proteomics* 2009.
134. O'Farrell PH. 1975. High resolution two-dimensional electrophoresis of proteins. *J Biol Chem* 250:4007–4021.
135. Shevchenko A, Wilm M, Vorm O, Mann M. 1996. Mass spectrometric sequencing of proteins silver-stained polyacrylamide gels. *Anal Chem* 68:850–858.
136. Wilkins MR, Pasquali C, Appel RD, Ou K, Golaz O, Sanchez JC, Yan JX, Gooley AA, Hughes G, Humphery-Smith I, et al. 1996. From proteins to proteomes: Large scale protein identification by two-dimensional electrophoresis and amino acid analysis. *Nat Biotechnol* 14:61–65.
137. DeRisi JL, Iyer VR, Brown PO. 1997. Exploring the metabolic and genetic control of gene expression on a genomic scale. *Science* (80-) 278:680–686.
138. Mortazavi A, Williams BA, McCue K, Schaeffer L, Wold B. 2008. Mapping and quantifying mammalian transcriptomes by RNA-Seq. *Nat Methods* 5:621–628.
139. Ingolia NT, Ghaemmaghami S, Newman JRS, Weissman JS. 2009. Genome-wide analysis *in vivo* of translation with nucleotide resolution using ribosome profiling. *Science* 324:218–223.
140. Croucher NJ, Thomson NR. 2010. Studying bacterial transcriptomes using RNA-seq. *Curr Opin Microbiol* 13:619–624.
141. Creecy JP, Conway T. 2015. Quantitative bacterial transcriptomics with RNA-seq. *Curr Opin Microbiol* 23:133–140.
142. Ares M. 2012. Bacterial RNA isolation. *Cold Spring Harb Protoc* 2012:pdb.prot071068.
143. Wahl A, Huptas C, Neuhaus K. 2022. Comparison of rRNA depletion methods for efficient bacterial mRNA sequencing. *Sci Rep* 12:5765.
144. Ingolia NT, Hussmann JA, Weissman JS. 2019. Ribosome profiling: Global views of

- translation. *Cold Spring Harb Perspect Biol* 11:1–20.
145. Ingolia NT, Brar GA, Rouskin S, McGeachy AM, Weissman JS. 2012. The ribosome profiling strategy for monitoring translation *in vivo* by deep sequencing of ribosome-protected mRNA fragments. *Nat Protoc* 7:1534–1550.
 146. Brar GA, Weissman JS. 2015. Ribosome profiling reveals the what, when, where and how of protein synthesis. *Nat Rev Mol Cell Biol* 16:651–664.
 147. Kitahara K, Miyazaki K. 2011. Specific inhibition of bacterial RNase T2 by helix 41 of 16S ribosomal RNA. *Nat Commun* 2:549.
 148. Oh E, Becker AH, Sandikci A, Huber D, Chaba R, Gloge F, Nichols RJ, Typas A, Gross CA, Kramer G, et al. 2011. Selective ribosome profiling reveals the cotranslational chaperone action of trigger factor *in vivo*. *Cell* 147:1295–1308.
 149. Li G-W, Oh E, Weissman JS. 2012. The anti-Shine–Dalgarno sequence drives translational pausing and codon choice in bacteria. *Nature* 484:538–541.
 150. Mohammad F, Green R, Buskirk AR. 2019. A systematically-revised ribosome profiling method for bacteria reveals pauses at single-codon resolution. *Elife* 8:1–25.
 151. Latif H, Szubin R, Tan J, Brunk E, Lechner A, Zengler K, Palsson BO. 2015. A streamlined ribosome profiling protocol for the characterization of microorganisms. *Biotechniques* 58:329–332.
 152. Li GW, Burkhardt D, Gross C, Weissman JS. 2014. Quantifying absolute protein synthesis rates reveals principles underlying allocation of cellular resources. *Cell* 157:624–635.
 153. Mohammad F, Buskirk A. 2019. Protocol for ribosome profiling in bacteria. *Bio-Protocol* 9.
 154. Zhang Y, Xiao Z, Zou Q, Fang J, Wang Q, Yang X, Gao N. 2017. Ribosome profiling reveals genome-wide cellular translational regulation upon heat stress in *Escherichia coli*. *Genomics, Proteomics Bioinforma* 15:324–330.
 155. Gray T, Storz G, Papenfort K. 2022. Small proteins; big questions. *J Bacteriol* 204:e0034121.
 156. Vazquez-Laslop N, Sharma CM, Mankin A, Buskirk AR. 2022. Identifying small open reading frames in prokaryotes with ribosome profiling. *J Bacteriol* 204:1–12.
 157. Jordan B, Weidenbach K, Schmitz RA. 2023. The power of the small: the underestimated role of small proteins in bacterial and archaeal physiology. *Curr Opin*

Microbiol 76:102384.

158. Kute PM, Soukarieh O, Tjeldnes H, Trégouët DA, Valen E. 2022. Small open reading frames, how to find them and determine their function. *Front Genet* 12.
159. Ahrens CH, Wade JT, Champion MM, Langer JD. 2022. A practical guide to small protein discovery and characterization using mass spectrometry. *J Bacteriol* 204:e00353-21.
160. Hemm MR, Weaver J, Storz G. 2020. *Escherichia coli* small proteome. *EcoSal Plus* 9:10.1128/ecosalplus.ESP-0031–2019.
161. Yadavalli SS, Yuan J. 2022. Bacterial small membrane proteins: The swiss army knife of regulators at the lipid bilayer. *J Bacteriol* 204.
162. Garai P, Blanc-Potard A. 2020. Uncovering small membrane proteins in pathogenic bacteria: Regulatory functions and therapeutic potential. *Mol Microbiol* 114:710–720.
163. Meydan S, Marks J, Klepacki D, Sharma V, Baranov P, Firth AE, Margus T, Kefi A, Vázquez-Laslop N, Mankin AS. 2019. Retapamulin-assisted ribosome profiling reveals the alternative bacterial proteome. *Mol Cell* 74:481-493.e6.
164. Weaver J, Mohammad F, Buskirk AR, Storz G. 2019. Identifying small proteins by ribosome profiling with stalled initiation complexes. *MBio* 10:1–21.
165. Stringer A, Smith C, Mangano K, Wade JT. 2022. Identification of novel translated small open reading frames in *Escherichia coli* using complementary ribosome profiling approaches. *J Bacteriol* 204:e00352-21.
166. Venturini E, Svensson SL, Maaß S, Gelhausen R, Eggenhofer F, Li L, Cain AK, Parkhill J, Becher D, Backofen R, et al. 2020. A global data-driven census of *Salmonella* small proteins and their potential functions in bacterial virulence. *microLife* 1:1–20.
167. Hadjeras L, Bartel J, Maier LK, Maaß S, Vogel V, Svensson SL, Eggenhofer F, Gelhausen R, Müller T, Alkhnabshi OS, et al. 2023. Revealing the small proteome of *Haloferax volcanii* by combining ribosome profiling and small-protein optimised mass spectrometry. *microLife* 1–17.
168. Hadjeras L, Heiniger B, Maaß S, Scheuer R, Gelhausen R, Barth-Weber S, Backofen R, Evguenieva-Hackenberg E, Becher D, Ahrens CH, et al. 2023. Unraveling the small proteome of the plant symbiont *Sinorhizobium meliloti* by ribosome profiling and proteogenomics. *microLife* 1–22.
169. Niegemann E, Schulz A, Bartsch K. 1993. Molecular organization of the *Escherichia coli*

- gab* cluster: nucleotide sequence of the structural genes *gabD* and *gabP* and expression of the GABA permease gene. Arch Microbiol 160:454–460.
170. Bassilana M, Pourcher T, Leblanc G. 1987. Facilitated diffusion properties of melibiose permease in *Escherichia coli* membrane vesicles. Release of co-substrates is rate limiting for permease cycling. J Biol Chem 262:16865–16870.
 171. Schulz GE. 2002. The structure of bacterial outer membrane proteins. Biochim Biophys Acta - Biomembr 1565:308–317.
 172. Guo D, Tropp BE. 2000. A second *Escherichia coli* protein with CL synthase activity. Biochim Biophys Acta 1483:263–274.
 173. Tan BK, Bogdanov M, Zhao J, Dowhan W, Raetz CRH, Guan Z. 2012. Discovery of a cardiolipin synthase utilizing phosphatidylethanolamine and phosphatidylglycerol as substrates. Proc Natl Acad Sci U S A 109:16504–16509.
 174. Nishijima S, Asami Y, Uetake N, Yamagoe S, Ohta A, Shibuya I. 1988. Disruption of the *Escherichia coli cls* gene responsible for cardiolipin synthesis. J Bacteriol 170:775–780.
 175. Carranza G, Angius F, Ilioaia O, Solgadi A, Miroux B, Arechaga I. 2017. Cardiolipin plays an essential role in the formation of intracellular membranes in *Escherichia coli*. Biochim Biophys Acta - Biomembr 1859:1124–1132.
 176. Yokota K, Kanamoto R, Kito M. 1980. Composition of cardiolipin molecular species in *Escherichia coli*. J Bacteriol 141:1047–1051.
 177. Romantsov T, Guan Z, Wood JM. 2009. Cardiolipin and the osmotic stress responses of bacteria. Biochim Biophys Acta 1788:2092–2100.
 178. Galla HJ, Hartmann W. 1980. Excimer-forming lipids in membrane research. Chem Phys Lipids 27:199–219.
 179. Parsons JB, Rock CO. 2013. Bacterial lipids: metabolism and membrane homeostasis. Prog Lipid Res 52:249–276.
 180. Larson TJ, Ehrmann M, Boos W. 1983. Periplasmic glycerophosphodiester phosphodiesterase of *Escherichia coli*, a new enzyme of the *glp* regulon. J Biol Chem 258:5428–5432.
 181. Larson TJ, Cantwell JS, Van Loo-Bhattacharya AT. 1992. Interaction at a distance between multiple operators controls the adjacent, divergently transcribed *glpTQ-glpACB* operons of *Escherichia coli* K-12. J Biol Chem 267:6114–6121.
 182. Strausberg RL, Feingold EA, Grouse LH, Derge JG, Klausner RD, Collins FS, Wagner

- L, Shenmen CM, Schuler GD, Altschul SF, et al. 2002. Generation and initial analysis of more than 15,000 full-length human and mouse cDNA sequences. *Proc Natl Acad Sci U S A* 99:16899–16903.
183. Subramanian A, Tamayo P, Mootha VK, Mukherjee S, Ebert BL, Gillette MA, Paulovich A, Pomeroy SL, Golub TR, Lander ES, et al. 2005. Gene set enrichment analysis: A knowledge-based approach for interpreting genome-wide expression profiles. *Proc Natl Acad Sci* 102:15545–15550.
184. Wu T, Hu E, Xu S, Chen M, Guo P, Dai Z, Feng T, Zhou L, Tang W, Zhan L, et al. 2021. clusterProfiler 4.0: A universal enrichment tool for interpreting omics data. *Innov* 2:100141.
185. Cunin R, Glansdorff N, Piérard A, Stalon V. 1986. Biosynthesis and metabolism of arginine in bacteria. *Microbiol Rev* 50:314–352.
186. Blethen SL, Boeker EA, Snell EE. 1968. Arginine decarboxylase from *Escherichia coli*. *J Biol Chem* 243:1671–1677.
187. Yanofsky C, Horn V, Gollnick P. 1991. Physiological studies of tryptophan transport and tryptophanase operon induction in *Escherichia coli*. *J Bacteriol* 173:6009–6017.
188. Cruz-Vera LR, Gong M, Yanofsky C. 2006. Changes produced by bound tryptophan in the ribosome peptidyl transferase center in response to TnaC, a nascent leader peptide. *Proc Natl Acad Sci* 103:3598–3603.
189. Goode O, Smith A, Zarkan A, Cama J, Invergo BM, Belgami D, Caño-Muñiz S, Metz J, O’neill P, Jeffries A, et al. 2021. Persister *Escherichia coli* cells have a lower intracellular pH than susceptible cells but maintain their pH in response to antibiotic treatment. *MBio* 12:1–18.
190. Sewell AK, Han M, Qi B. 2018. An unexpected benefit from *E. coli*: how enterobactin benefits host health. *Microb cell (Graz, Austria)* 5:469–471.
191. Celia H, Noinaj N, Buchanan SK. 2020. Structure and stoichiometry of the Ton molecular motor. *Int J Mol Sci* 21:1–15.
192. Ratliff AC, Buchanan SK, Celia H. 2022. The Ton motor. *Front Microbiol* 13.
193. Vinella D, Brochier-Armanet C, Loiseau L, Talla E, Barras F. 2009. Iron-sulfur (Fe/S) protein biogenesis: Phylogenomic and genetic studies of A-type carriers. *PLoS Genet* 5.
194. Oakley K, Sterling K, Shearer J, Kim E. 2021. Controlled protonation of [2Fe-2S] leading

- to MitoNEET analogues and concurrent cluster modification. *Inorg Chem* 60:16074–16078.
195. Woodard SI, Dailey HA. 1995. Regulation of heme biosynthesis in *Escherichia coli*. *Arch Biochem Biophys* 316:110–115.
 196. Létoffé S, Delepelaire P, Wandersman C. 2006. The housekeeping dipeptide permease is the *Escherichia coli* heme transporter and functions with two optional peptide binding proteins. *Proc Natl Acad Sci U S A* 103:12891–12896.
 197. Jin Z, Li J, Ni L, Zhang R, Xia A, Jin F. 2018. Conditional privatization of a public siderophore enables *Pseudomonas aeruginosa* to resist cheater invasion. *Nat Commun* 9:1–11.
 198. Zughaiier SM, Cornelis P. 2018. Editorial: Role of iron in bacterial pathogenesis. *Front Cell Infect Microbiol* 8.
 199. Guillier M, Gottesman S. 2008. The 5' end of two redundant sRNAs is involved in the regulation of multiple targets, including their own regulator. *Nucleic Acids Res* 36:6781–6794.
 200. Bohnert JA, Schuster S, Fähnrich E, Trittler R, Kern W. 2006. Altered spectrum of multidrug resistance associated with a single point mutation in the *Escherichia coli* RND-type MDR efflux pump YhiV (MdtF). *J Antimicrob Chemother* 59:1216–1222.
 201. Elkins CA, Nikaido H. 2003. Chimeric analysis of AcrA function reveals the importance of its C-terminal domain in its interaction with the AcrB multidrug efflux pump. *J Bacteriol* 185:5349–5356.
 202. Lin JS, Lai EM. 2017. Protein-protein interactions: co-immunoprecipitation, p. 211–219. *In* Journet, L, Cascales, E (eds.), *Bacterial Protein Secretion Systems: Methods and Protocols*. Springer New York, New York, NY.
 203. Venkat K, Hoyos M, Haycocks JRJ, Cassidy L, Engelmann B, Rolle-Kampczyk U, von Bergen M, Tholey A, Grainger DC, Papenfort K. 2021. A dual-function RNA balances carbon uptake and central metabolism in *Vibrio cholerae*. *EMBO J* 40:e108542.
 204. Habenicht T, Weidenbach K, Velazquez-Campoy A, Buey RM, Balsera M, Schmitz RA. 2023. Small protein mediates inhibition of ammonium transport in *Methanosarcina mazei* - an ancient mechanism? *Microbiol Spectr* 11:e02811-23.
 205. Zahn S, Kubatova N, Pyper DJ, Cassidy L, Saxena K, Tholey A, Schwalbe H, Soppa J. 2021. Biological functions, genetic and biochemical characterization, and NMR structure determination of the small zinc finger protein HVO_2753 from *Haloferax volcanii*. *FEBS*

J 288:2042–2062.

206. Carvunis AR, Rolland T, Wapinski I, Calderwood MA, Yildirim MA, Simonis N, Charlotheaux B, Hidalgo CA, Barbette J, Santhanam B, et al. 2012. Proto-genes and *de novo* gene birth. *Nature* 487:370–374.
207. Knopp M, Gudmundsdottir JS, Nilsson T, König F, Warsi O, Rajer F, Ädelroth P, Andersson DI. 2019. *de novo* emergence of peptides that confer antibiotic resistance. *MBio* 10:10.1128/mbio.00837-19.
208. Babina AM, Surkov S, Ye W, Jerlström-Hultqvist J, Larsson M, Holmqvist E, Jemth P, Andersson DI, Knopp M. 2023. Rescue of *Escherichia coli* auxotrophy by *de novo* small proteins. *Elife* 12:e78299.
209. Zhao K, Liu M, Burgess RR. 2007. Adaptation in bacterial flagellar and motility systems: from regulon members to ‘foraging’-like behavior in *E. coli*. *Nucleic Acids Res* 35:4441–4452.
210. Adler J. 1973. A method for measuring chemotaxis and use of the method to determine optimum conditions for chemotaxis by *Escherichia coli*. *Microbiology* 74:77–91.
211. Askoura M, Youns M, Halim Hegazy WA. 2020. Investigating the influence of iron on *Campylobacter jejuni* transcriptome in response to acid stress. *Microb Pathog* 138:103777.
212. Cortes BW, Naditz AL, Anast JM, Schmitz-Esser S. 2020. Transcriptome sequencing of *Listeria monocytogenes* reveals major gene expression changes in response to lactic acid stress exposure but a less pronounced response to oxidative stress. *Front Microbiol* 10:1–14.
213. Baba T, Ara T, Hasegawa M, Takai Y, Okumura Y, Baba M, Datsenko KA, Tomita M, Wanner BL, Mori H. 2006. Construction of *Escherichia coli* K-12 in-frame, single-gene knockout mutants: The Keio collection. *Mol Syst Biol* 2.
214. Fahrner KA, Berg HC. 2015. Mutations that stimulate *flhDC* expression in *Escherichia coli* K-12. *J Bacteriol* 197:3087–3096.
215. Barker CS, Prüß BM, Matsumura P. 2004. Increased motility of *Escherichia coli* by insertion sequence element integration into the regulatory region of the *flhD* operon. *J Bacteriol* 186:7529–7537.
216. Wang X, Wood TK. 2011. IS5 inserts upstream of the master motility operon *flhDC* in a quasi-Lamarckian way. *ISME J* 5:1517–1525.

217. Lee C, Park C. 2013. Mutations upregulating the *flhDC* operon of *Escherichia coli* K-12. *J Microbiol* 51:140–144.
218. Parker DJ, Demetci P, Li G-W. 2019. Rapid accumulation of motility-activating mutations in resting liquid culture of *Escherichia coli*. *J Bacteriol* 201:3–6.
219. Starlinger P. 1980. IS elements and transposons. *Plasmid* 3:241–259.
220. Starlinger P, Saedler H. 1976. IS-elements in microorganisms, p. 111–152. *In* Arber, W, Henle, W, Hofschneider, PH, Humphrey, JH, Jerne, NK, Koldovský, P, Koprowski, H, Maaløe, O, Rott, R, Schweiger, HG, et al. (eds.), *Current Topics in Microbiology and Immunology / Ergebnisse der Microbiologie und Immunitätsforschung*. Springer Berlin Heidelberg, Berlin, Heidelberg.
221. Mahillon J, Léonard C, Chandler M. 1999. IS elements as constituents of bacterial genomes. *Res Microbiol* 150:675–687.
222. Fitzgerald DM, Bonocora RP, Wade JT. 2014. Comprehensive mapping of the *Escherichia coli* flagellar regulatory network. *PLoS Genet* 10.
223. Takada H, Kijima K, Ishiguro A, Ishihama A, Shimada T. 2023. Genomic SELEX reveals pervasive role of the flagella master regulator FlhDC in carbon metabolism. *Int J Mol Sci* 24.
224. Fitzgerald DM, Smith C, Lapierre P, Wade JT. 2018. The evolutionary impact of intragenic FliA promoters in proteobacteria. *Mol Microbiol* 108:361–378.
225. Barembruch C, Hengge R. 2007. Cellular levels and activity of the flagellar sigma factor FliA of *Escherichia coli* are controlled by FlgM-modulated proteolysis. *Mol Microbiol* 65:76–89.
226. Ni B, Colin R, Link H, Endres RG, Sourjik V. 2020. Growth-rate dependent resource investment in bacterial motile behavior quantitatively follows potential benefit of chemotaxis. *Proc Natl Acad Sci* 117:595–601.
227. Macnab RM. 1996. Flagella and motility. Neidhardt FC, editors. *Escherichia coli* and *Salmonella: Cellular and Molecular Biology* (2nd ed). ASM Press.
228. Ziegler M, Takors R. 2020. Reduced and minimal cell factories in bioprocesses: Towards a streamlined chassis, p. 1–44. *In* Lara, AR, Gosset, G (eds.), *Minimal Cells: Design, Construction, Biotechnological Applications*. Springer International Publishing, Cham.
229. Schavemaker PE, Lynch M. 2022. Flagellar energy costs across the tree of life. *Elife*

11:e77266.

230. Prüss BM, Campbell JW, Van Dyk TK, Zhu C, Kogan Y, Matsumura P. 2003. FlhD/FlhC is a regulator of anaerobic respiration and the Entner-Doudoroff pathway through induction of the methyl-accepting chemotaxis protein Aer. *J Bacteriol* 185:534–543.
231. Prüss BM, Matsumura P. 1996. A regulator of the flagellar regulon of *Escherichia coli*, *flhD*, also affects cell division. *J Bacteriol* 178:668–674.
232. Pasternak C, Ton-Hoang B, Coste G, Bailone A, Chandler M, Sommer S. 2010. Irradiation-induced *Deinococcus radiodurans* genome fragmentation triggers transposition of a single resident insertion sequence. *PLoS Genet* 6:e1000799.
233. Drevinek P, Baldwin A, Lindenburg L, Joshi LT, Marchbank A, Vosahlikova S, Dowson CG, Mahenthiralingam E. 2010. Oxidative stress of *Burkholderia cenocepacia* induces insertion sequence-mediated genomic rearrangements that interfere with macrorestriction-based genotyping. *J Clin Microbiol* 48:34–40.
234. Eichenbaum Z, Livneh Z. 1998. UV light induces IS10 transposition in *Escherichia coli*. *Genetics* 149:1173–1181.
235. Horne SM, Saylor J, Scarberry N, Schroeder M, Lynnes T, Prüss BM. 2016. Spontaneous mutations in the *flhD* operon generate motility heterogeneity in *Escherichia coli* biofilm. *BMC Microbiol* 16:1–13.
236. Bi S, Sourjik V. 2018. Stimulus sensing and signal processing in bacterial chemotaxis. *Curr Opin Microbiol* 45:22–29.
237. Alexander RP, Lowenthal AC, Harshey RM, Ottemann KM. 2010. CheV: CheW-like coupling proteins at the core of the chemotaxis signaling network. *Trends Microbiol* 18:494–503.
238. Butler SM, Camilli A. 2004. Both chemotaxis and net motility greatly influence the infectivity of *Vibrio cholerae*. *Proc Natl Acad Sci U S A* 101:5018–5023.
239. Butler SM, Nelson EJ, Chowdhury N, Faruque SM, Calderwood SB, Camilli A. 2006. Cholera stool bacteria repress chemotaxis to increase infectivity. *Mol Microbiol* 60:417–426.
240. Lee SH, Butler SM, Camilli A. 2001. Selection for *in vivo* regulators of bacterial virulence. *Proc Natl Acad Sci U S A* 98:6889–6894.
241. Merrell DS, Butler SM, Qadri F, Dolganov NA, Alam A, Cohen MB, Calderwood SB, Schoolnik GK, Camilli A. 2002. Host-induced epidemic spread of the cholera bacterium.

- Nature 417:642–645.
242. Brameyer S, Rösch TC, El Andari J, Hoyer E, Schwarz J, Graumann PL, Jung K. 2019. DNA-binding directs the localization of a membrane-integrated receptor of the ToxR family. *Commun Biol* 2.
 243. Bennett BD, Kimball EH, Gao M, Osterhout R, Van Dien SJ, Rabinowitz JD. 2009. Absolute metabolite concentrations and implied enzyme active site occupancy in *Escherichia coli*. *Nat Chem Biol* 5:593–599.
 244. Wang B, Lin AE, Yuan J, Novak KE, Koch MD, Wingreen NS, Adamson B, Gitai Z. 2023. Single-cell massively-parallel multiplexed microbial sequencing (M3-seq) identifies rare bacterial populations and profiles phage infection. *Nat Microbiol* 8:1846–1862.
 245. Lyu Z, Yang A, Villanueva P, Singh A, Ling J. 2021. Heterogeneous flagellar expression in single *Salmonella* cells promotes diversity in antibiotic tolerance. *MBio* 12:e0237421.
 246. Cummings LA, Wilkerson WD, Bergsbaken T, Cookson BT. 2006. *In vivo*, *fliC* expression by *Salmonella enterica* serovar Typhimurium is heterogeneous, regulated by ClpX, and anatomically restricted. *Mol Microbiol* 61:795–809.
 247. Gauger EJ, Leatham MP, Mercado-Lubo R, Laux DC, Conway T, Cohen PS. 2007. Role of motility and the *flhDC* operon in *Escherichia coli* MG1655 colonization of the mouse intestine. *Infect Immun* 75:3315–3324.
 248. Levsky JM, Shenoy SM, Pezo RC, Singer RH. 2002. Single-cell gene expression profiling. *Science* 297:836–840.
 249. Imdahl F, Vafadarnejad E, Homberger C, Saliba AE, Vogel J. 2020. Single-cell RNA-sequencing reports growth-condition-specific global transcriptomes of individual bacteria. *Nat Microbiol* 5:1202–1206.
 250. Saliba AE, Li L, Westermann AJ, Appenzeller S, Stapels DAC, Schulte LN, Helaine S, Vogel J. 2016. Single-cell RNA-seq ties macrophage polarization to growth rate of intracellular *Salmonella*. *Nat Microbiol* 2:16206.
 251. Blattman SB, Jiang W, Oikonomou P, Tavazoie S. 2020. Prokaryotic single-cell RNA sequencing by *in situ* combinatorial indexing. *Nat Microbiol* 5:1192–1201.
 252. Kuchina A, Brettner LM, Paleologu L, Roco CM, Rosenberg AB, Carignano A, Kibler R, Hirano M, DePaolo RW, Seelig G. 2021. Microbial single-cell RNA sequencing by split-pool barcoding. *Science* 371.
 253. Stephens ZD, Lee SY, Faghri F, Campbell RH, Zhai C, Efron MJ, Iyer R, Schatz MC,

- Sinha S, Robinson GE. 2015. Big data: Astronomical or genomics? PLoS Biol 13:e1002195.
254. Kion-Crosby W, Barquist L. 2024. Network depth affects inference of gene sets from bacterial transcriptomes using denoising autoencoders. *Bioinforma Adv* 4:vbae066.
255. Palanivelu J, Thanigaivel S, Vickram S, Dey N, Mihaylova D, Desseva I. 2022. Probiotics in functional foods: Survival assessment and approaches for improved viability. *Appl Sci* 12.
256. Antal Bajor PGG, Abrahamsson H. 2010. Bile acids: short and long term effects in the intestine. *Scand J Gastroenterol* 45:645–664.
257. Cummings JH, Pomare EW, Branch WJ, Naylor CPE, G.T. M. 1987. Short chain fatty acids in human large intestine, portal, hepatic and venous blood. *Gut* 28:1221–1227.
258. McNeil NI, Cummings JH, James WP. 1978. Short chain fatty acid absorption by the human large intestine. *Gut* 19:819–822.

Supplemental information – Chapter 2.1

Available online at:

<https://journals.asm.org/doi/10.1128/msystems.01037-23>

Supplementary information

Ribosome profiling reveals the fine-tuned response of *Escherichia coli* to mild and severe acid stress

Kilian Schumacher, Rick Gelhausen, Willow Kion-Crosby, Lars Barquist, Rolf Backofen and Kirsten Jung

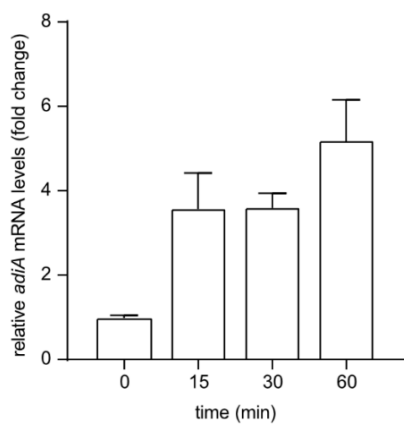


Figure S1: Temporal dynamics of *adiA* transcription under acid stress (pH 4.4). Cells were cultivated as described in Figure 1. After the shift to pH 4.4, cells were collected after 0, 15, 30 and 60 min and total RNA was prepared. Relative levels of *adiA* mRNA were quantified by RT-qPCR. Fold-change values were determined relative to the 0-min time point and normalized using *recA* as a reference gene. Error bars indicate the standard deviation of three independent biological replicates (n=3).

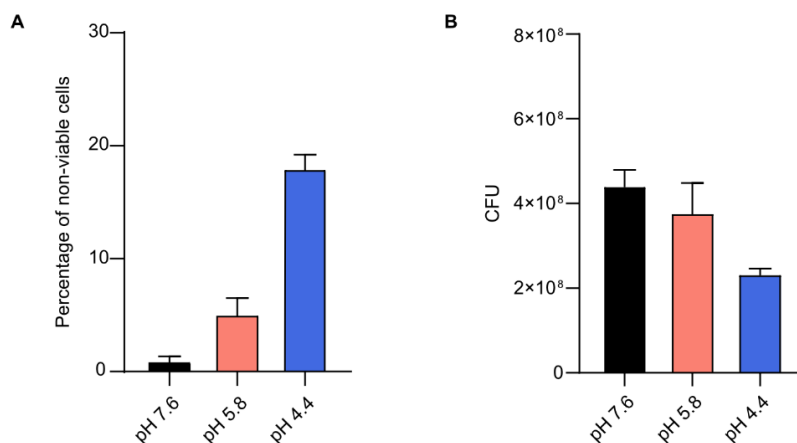


Figure S2: Quantification of viable and non-viable cells at varying pH conditions. (A) *E. coli* MG1655 cells were cultured as outlined in Figure 1A. Following sample collection, dead cells were distinguished by propidium iodide staining. Microscopy was performed using a Leica DMI8 inverted microscope equipped with a Leica DFC365 FX camera. A minimum of 1,000 cells were evaluated per condition, and relative fluorescence was measured using the MicrobeJ plugin for the ImageJ software. Cells exhibiting relative fluorescence values ≥ 300 after subtraction of the background were considered non-viable. **(B)** Quantification of colony forming units (CFU) at varying pH conditions. *E. coli* MG1655 cells were cultured as outlined in Figure 1A. Upon sample collection, samples were serially diluted in 1x PBS and plated on LB agar plates. Following overnight incubation, CFUs were enumerated. CFUs, colony forming units.

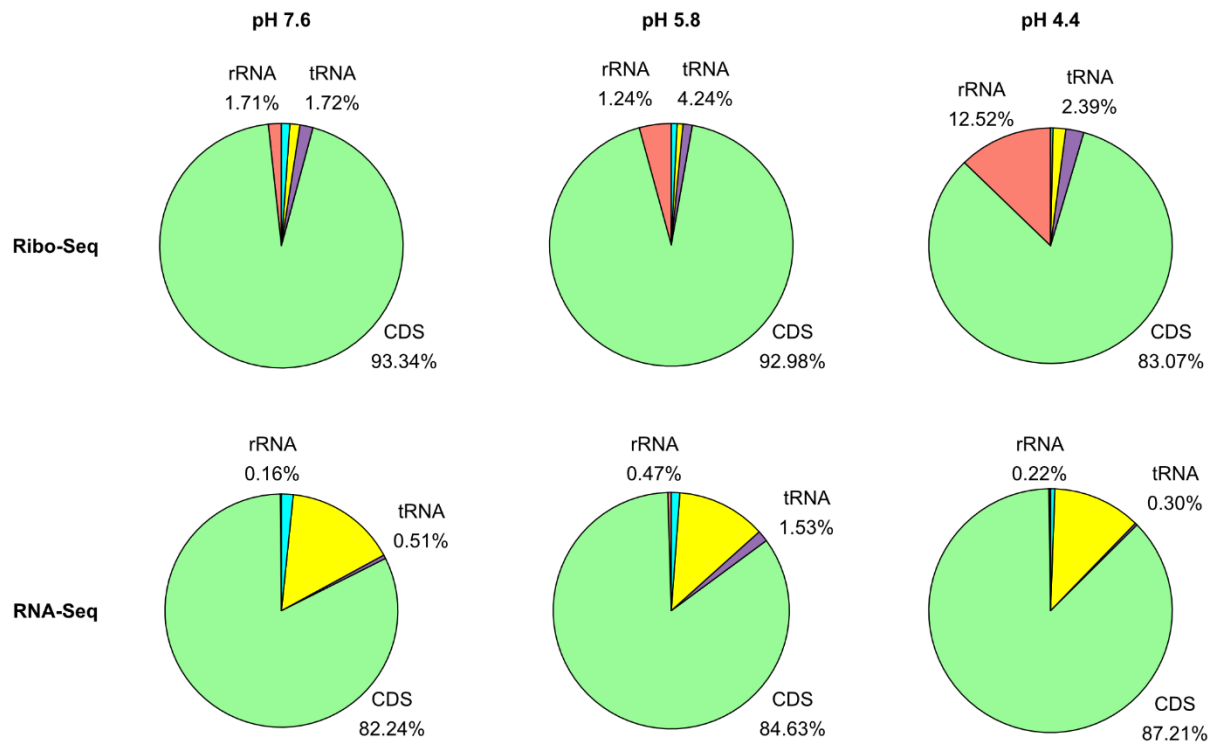


Figure S3: Read mapping statistics for Ribo-Seq and RNA-Seq data. Pie charts illustrate the percentage of uniquely mapped reads either to CDS (green), rRNA (salmon), tRNA (purple), ncRNA (yellow), or pseudogenes (lightblue). The percentages provided indicate the average ratios relative to the total number of uniquely mapped reads per condition, which were calculated from biological triplicates. CDS, coding sequence; rRNA, ribosomal RNA; tRNA, transfer RNA; nc RNA, non-coding RNA.

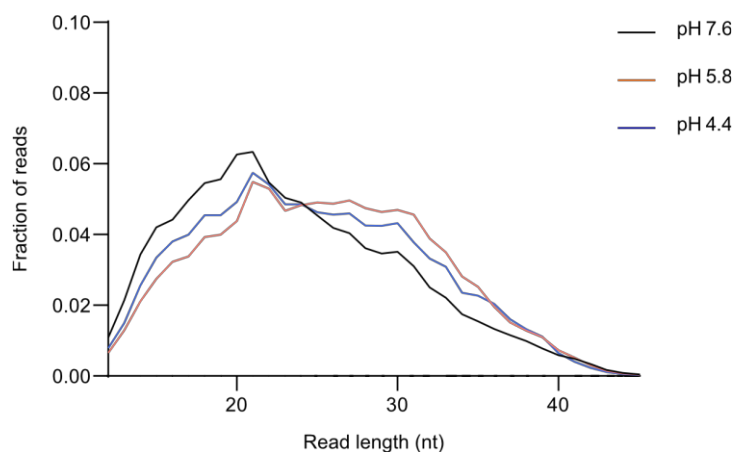


Figure S4: Read length distribution of ribosome-protected mRNA fragments (RPF) at different degrees of acidity.

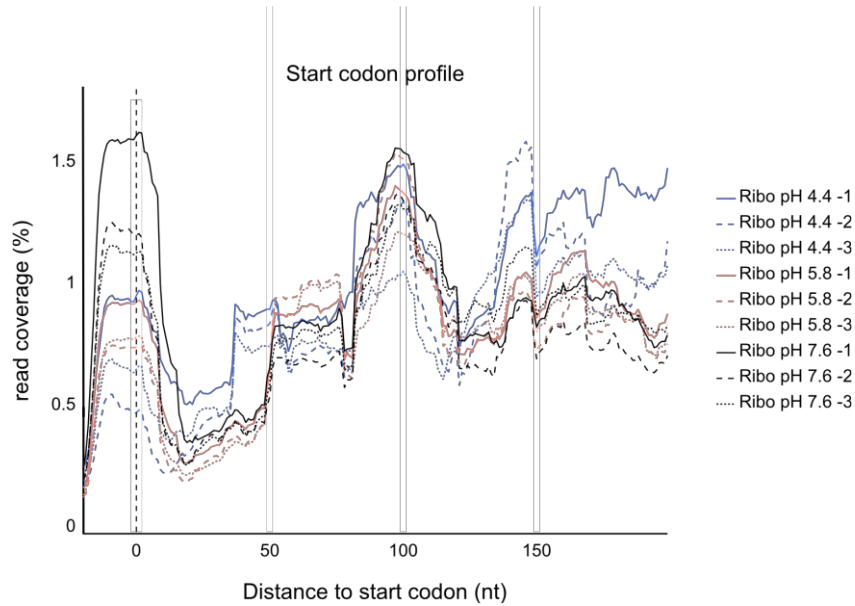


Figure S5: Reduction of ribosome occupancy in translation initiation regions at pH 5.8 and pH 4.4. Alignments of reads from ribosome-protected fragments in the 5'UTR and the first 200 nucleotides of the coding sequence from all *E. coli* genes. The percentage of read coverage is shown relative to the total number of mapped reads per condition for each specific nucleotide position. The position of the first nucleotide of the start codon is indicated by a vertical dashed line.

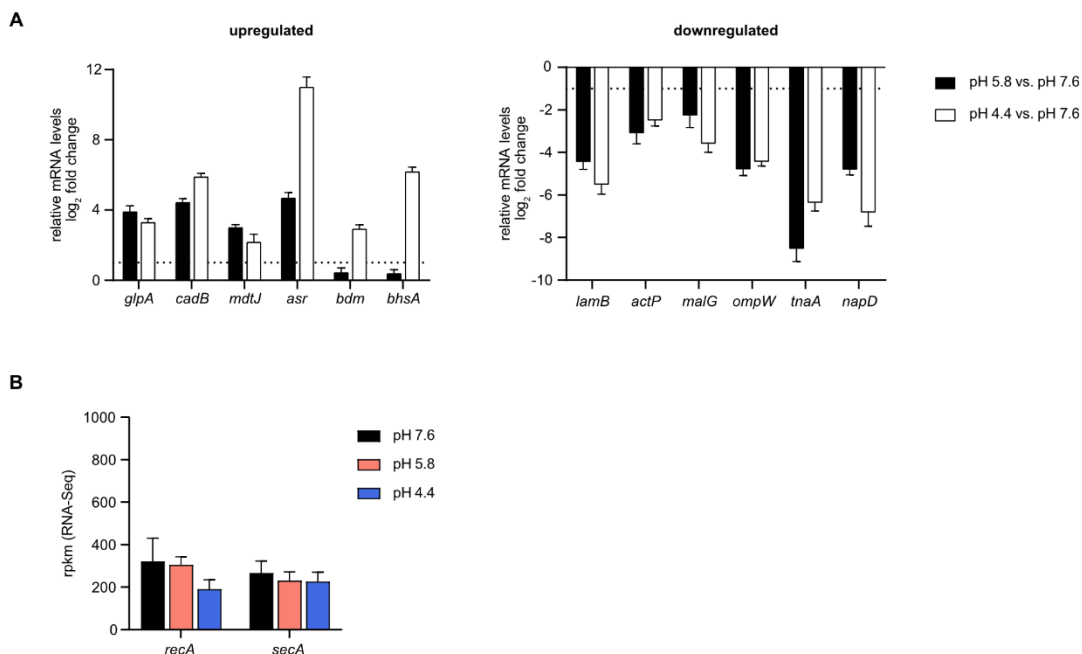


Figure S6: Verification of differentially expressed genes under acid stress using RT-qPCR. (A) Cells were cultivated as described in Figure 1. Relative mRNA levels were measured by RT-qPCR and fold change values were calculated relative to pH 7.6 and normalized using *recA*, or *secA* as reference genes. Error bars indicate the standard deviation of three independent biological replicates (n=3). **(B)** Eligibility of *recA* and *secA* as reference genes for RT-qPCR data under acid stress conditions. rpkM values determined by RNA-Seq are shown. Error bars indicate the standard deviation of three independent biological replicates (n=3). rpkM = reads per kilobase of transcript per million mapped reads.

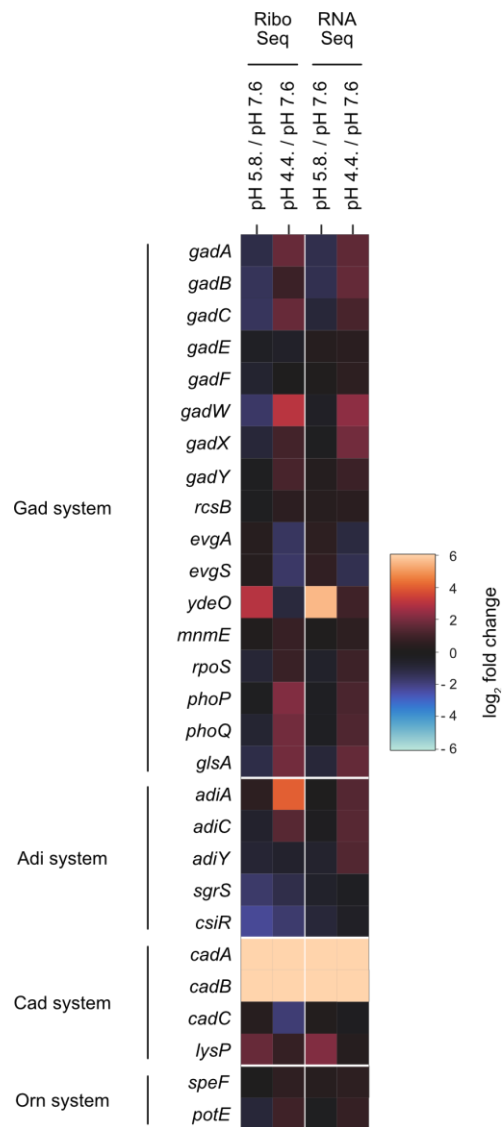


Figure S7: Transcriptional and translational expression profiles of genes associated with enzyme-based H⁺-consuming acid resistance (AR) systems in *E. coli*. Heatmap displaying RNA-Seq and Ribo-Seq log₂ fold change values of genes encoding amino acid decarboxylases, antiporters, or regulatory elements associated with either the Gad, Adi, Cad, or Orn system. Log₂ fold changes of normalized expression values at pH 4.4 and 5.8 were calculated relative to the normalized expression values at pH 7.6.

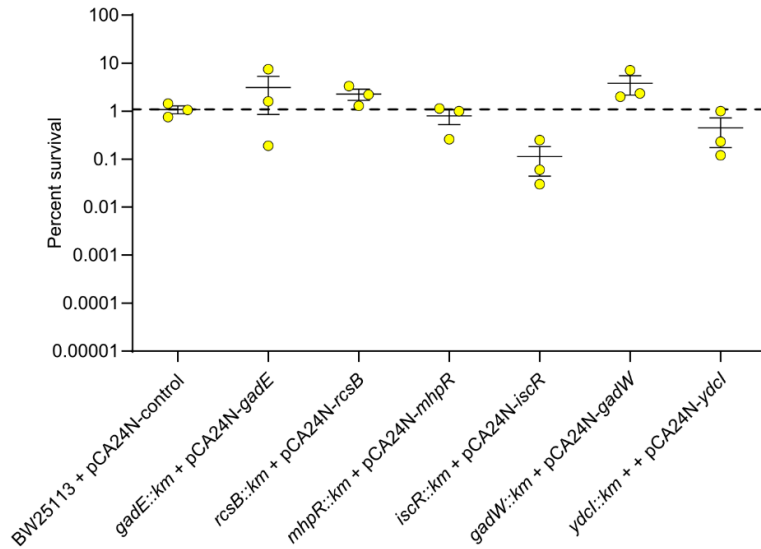


Figure S8: Survival of complemented mutants under acid shock. BW25113 wildtype, or indicated mutant strains from the Keio collection were complemented with pCA24N plasmids from the ASKA collection, or a pCA24N control vector. Cells were grown in LB pH 7.6 to $OD_{600} = 0.5$. The cultures were split and then either grown at pH 7.6, or stepwise stressed (15 min pH 5.8, 15 min pH 4.4) before being exposed to LB pH 3 for 1 h. Media were supplemented with 50 $\mu\text{g/ml}$ (w/v) chloramphenicol and IPTG. Upon overnight incubation, colony forming units were counted and the ratio of surviving cells was calculated. The dashed line indicates the average percentage of surviving WT cells.

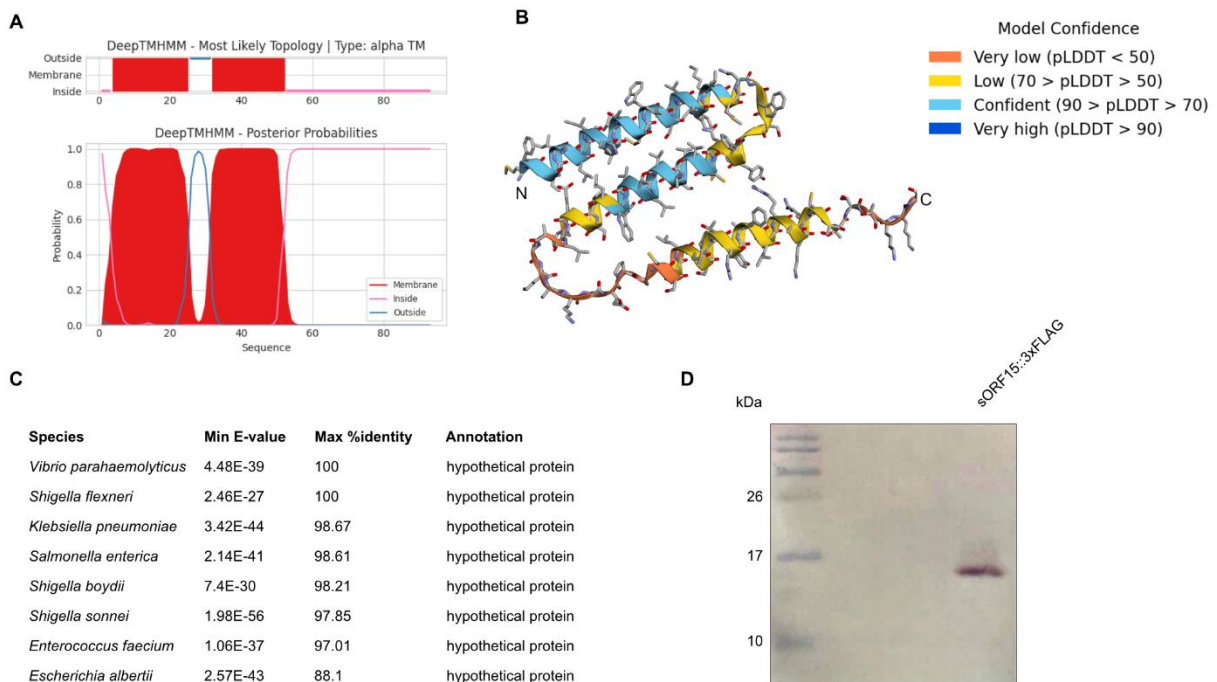


Figure S9: Subcellular location, homology, and verification of sORF15. (A) Transmembrane topology of sORF15 predicted by DeepTMHMM. (B) Predicted protein structure of sORF15 using ColabFold. N- and C-termini are indicated. (C) Homologs of sORF15 identified using blastp. The sORF15 amino acid sequence was used as the query sequence and homologs with an E-value < 0.05 and Max % identity of > 80% are listed. (D) Validation of sORF15 via Western Blot using a pBAD24-sORF15::3xFLAG construct. *E. coli* MG1655 cells harboring a pBAD24-sORF15:3xFLAG plasmid were cultivated to an OD_{600} of 0.5, before expression of sORF15 was induced for 1 h by addition of 0.2% (v/v) L-Arabinose. Protein levels of sORF15:3xFLAG were monitored via Tricine-SDS-PAGE followed by detection using primary α -FLAG and secondary alkaline phosphatase conjugated α -rabbit antibodies.

Table S1: OD₆₀₀ values determined at t₃₀ (Fig. 1A) prior to sample collection for Ribo-Seq and RNA-Seq experiments.

	Replicate I			Replicate II			Replicate III		
	pH 7.6	pH 5.8	pH 4.4	pH 7.6	pH 5.8	pH 4.4	pH 7.6	pH 5.8	pH 4.4
OD ₆₀₀ (t ₃₀)	1.05	0.93	0.69	1.18	1.08	0.66	1.13	1.04	0.72

Table S2: pH values monitored during cultivation of *E. coli* for Ribo-Seq and RNA-Seq experiments (Fig. 1A). pH-shifts were initiated by direct addition of 5 M HCl to the cultures and are indicated by (*).

	Replicate I			Replicate II			Replicate III		
	pH 7.6	pH 5.8	pH 4.4	pH 7.6	pH 5.8	pH 4.4	pH 7.6	pH 5.8	pH 4.4
pH 0 min (t ₀)	7.24	5.90*	5.84*	7.29	5.84*	5.82*	7.28	5.81*	5.87*
pH 15 min (t ₁₅)	7.17	5.95	4.41*	7.21	5.87	4.37*	7.24	5.83	4.33*
pH 30 min (t ₃₀)	7.15	6.01	4.43	7.17	5.93	4.39	7.16	5.88	4.39

Table S6: Candidate transcriptional regulators evaluated in Figure 4. Transcription factors were chosen based on Ribo-Seq log₂ fold change values at either pH 4.4 or pH 5.8 compared to pH 7.6.

Regulator	log ₂ fold change
YdeO	2.96 (pH 5.8)
MhpR	4.72 (pH 4.4)
IscR	4.52 (pH 4.4)
MarR	3.10 (pH 4.4)
GadW	3.03 (pH 4.4)
YdcI	2.92 (pH 4.4)

Supplemental information – Chapter 2.2

Available online at:

<https://journals.asm.org/doi/abs/10.1128/spectrum.00544-24>

Supplementary information

Motility-activating mutations upstream of *flhDC* reduce acid shock survival of *Escherichia coli*

Kilian Schumacher, Djanna Braun, Karin Kleigrewe, and Kirsten Jung

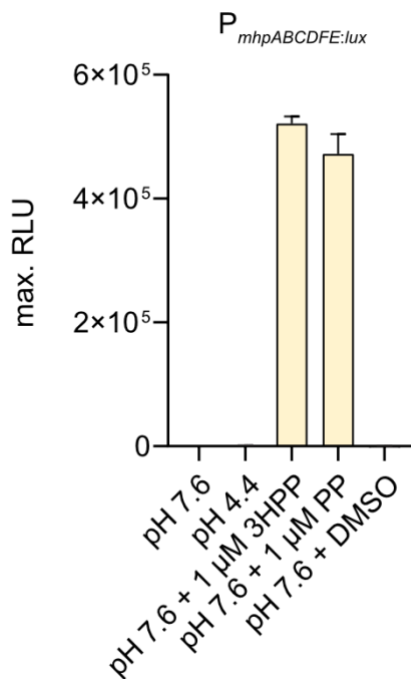


Figure S1: Promoter activity of the *mhpABCDE* operon. *E. coli* MG1655 wild type cells were transformed with plasmid pBBR1-MCS5- $P_{mhpABCDE:luc}$ and grown in LB medium (pH 7.6) until $OD_{600} = 0.5$. The medium pH was then either stepwise adjusted to 5.8 and pH 4.4, or 1 mM 3HPP, 1 mM PP, or DMSO were added. Luminescence and growth were determined every 10 min in microtiter plates using a CLARIOstar plus plate reader (BMG Labtech). Data are reported as relative light units (RLUs) in counts per second per OD_{600} , with maximal RLU shown. All experiments were performed in biological replicates ($n = 3$), and error bars represent standard deviations of the mean.

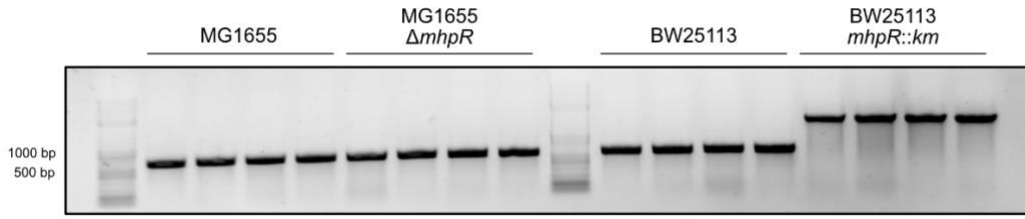


Figure S2: Transposon insertions in the promoter region of *flhDC*. The presence of IS elements in the intergenic region between *flhD* and *uspC* was verified by colony PCR using primers KSO-244 and KSO-245. The expected PCR product sizes were 767 bp in the absence of an IS element and ~2000 bp in the presence.

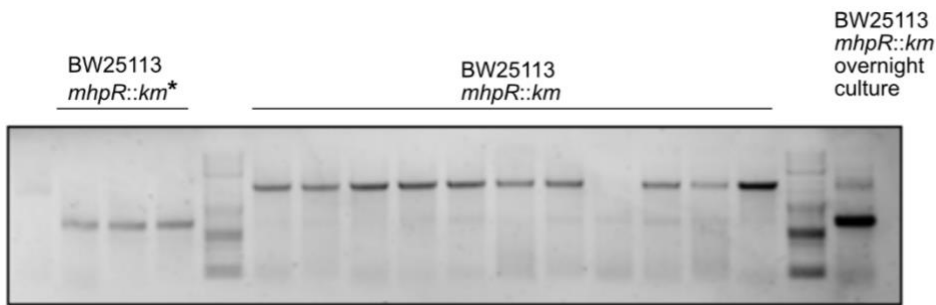


Figure S3: Verification of a BW25113 *mhpR::km strain without IS insertion in the promoter region of *flhDC*.** BW25113 *mhpR::km* was streaked on LB agar plates, and single colonies were screened by colony PCR using primers KSO-244 and KSO-245 for an intact *flhDC* promoter. The expected PCR product sizes were 767 bp in the absence of an IS element and ~2000 bp in the presence.

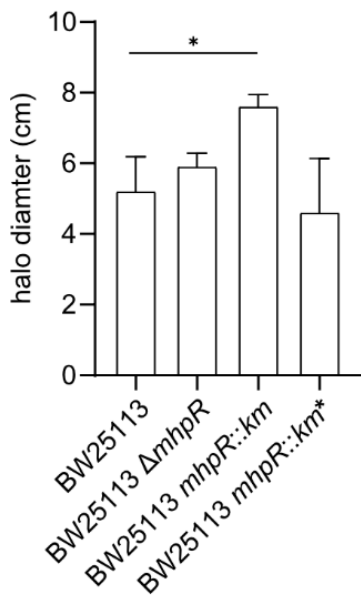


Figure S4: IS element dependent motility of BW25113. Soft agar assay evaluating the motility of BW25113 wild type, Δ mhpR, *mhpR::km*, and, *mhpR::km** strains. Overnight cultures normalized to an OD₆₀₀ of 1 were spotted on LB soft agar [0.3 % (w/v)] and incubated for 16 h. Halo diameters were measured and all experiments were performed in biological replicates (n \geq 4). Error bars represent standard deviations of the mean and significance was evaluated by performing a one-way ANOVA test followed by Bonferroni's multiple comparisons test (* p < 0.05).

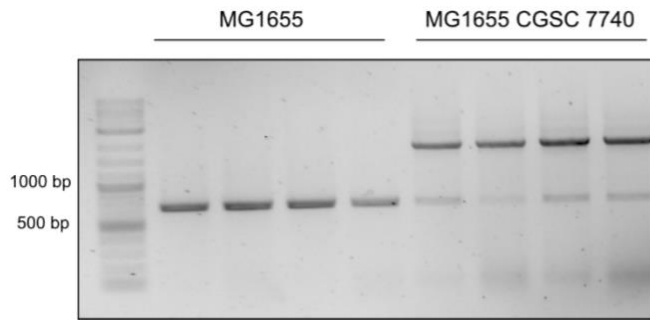


Figure S5: Alterations in the *flhDC* promoter region of two different MG1655 strains. The presence of IS elements in the intergenic region between *flhD* and *uspC* was verified by colony PCR using primers KSO-244 and KSO-245. The expected PCR product sizes were 767 bp in the absence of an IS element and ~2000 bp in the presence.

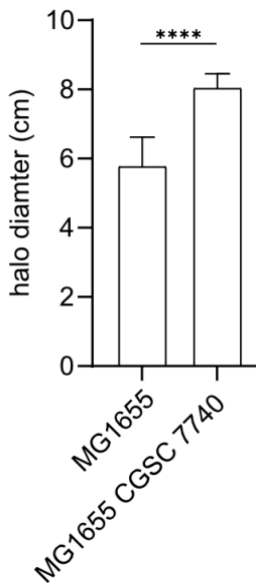


Figure S6: IS element dependent motility of MG1655. Soft agar assay evaluating the motility of MG1655 and MG1655 CGSC7740. Overnight cultures normalized to an OD₆₀₀ of 1 were spotted on LB soft agar [0.3% (w/v)] and incubated for 16 h. Halo diameters were measured and all experiments were performed in biological replicates (n ≥ 4). Error bars represent standard deviations of the mean and significance was evaluated by performing an unpaired t-test (**** p < 0.0001).

Table S1: OD₆₀₀ and pH values determined throughout the experiment conducted for RNA-Seq. pH-shifts were initiated by direct addition of 5 M HCl to growing cultures.

Strain	Replicate I			Replicate II			Replicate III					
	MG1655	MG1655 $\Delta mhpR$	BW25113	BW25113 <i>mhpR::km</i>	MG1655	MG1655 $\Delta mhpR$	BW25113	BW25113 <i>mhpR::km</i>	MG1655	MG1655 $\Delta mhpR$	BW25113	BW25113 <i>mhpR::km</i>
OD600 (0.5)	0.50	0.46	0.47	0.48	0.50	0.50	0.42	0.44	0.45	0.41	0.46	0.49
OD600 (end)	0.88	0.74	0.74	0.91	0.76	0.64	0.62	0.61	0.65	0.78	0.71	0.87
pH (0 min)	7.24	7.24	7.23	7.21	7.26	7.27	7.27	7.27	7.28	7.25	7.23	7.20
pH (15 min)	5.72	5.75	5.71	5.65	5.78	5.78	5.81	5.75	5.83	5.82	5.77	5.79
pH (30 min)	4.38	4.33	4.33	4.27	4.34	4.34	4.32	4.32	4.32	4.33	4.47	4.46

Table S2: *Escherichia coli* strains used in this study.

Strain	Relevant genotype or description	Reference
MG1655	K-12, F-, λ - <i>ilvG</i> -, <i>rfb</i> -50, <i>rph</i> -1	(62)
BW25113	F-, Δ (<i>araD-araB</i>)567, Δ <i>lacZ</i> 4787(:: <i>rrnB</i> -3), λ -, <i>rph</i> -1, Δ (<i>rhaD-rhaB</i>)568, <i>hsdR</i> 514	(63)
ST18	S17 λ <i>pir</i> Δ <i>hemA</i>	(65)
MG1655 Δ <i>mhpR</i>	K-12, F-, λ - <i>ilvG</i> -, <i>rfb</i> -50, <i>rph</i> -1, Δ <i>mhpR</i>	This study
BW25113 <i>mhpR</i> :: <i>km</i>	F-, Δ (<i>araD-araB</i>)567, Δ <i>lacZ</i> 4787(:: <i>rrnB</i> -3), λ -, <i>rph</i> -1, Δ <i>mhpR</i> 786:: <i>kan</i> , Δ (<i>rhaD-rhaB</i>)568, <i>hsdR</i> 514, IS5 insertion 516 bp upstream of <i>flhDC</i>	(29)
BW25113 Δ <i>mhpR</i>	F-, Δ (<i>araD-araB</i>)567, Δ <i>lacZ</i> 4787(:: <i>rrnB</i> -3), λ -, <i>rph</i> -1, Δ (<i>rhaD-rhaB</i>)568, <i>hsdR</i> 514 Δ <i>mhpR</i>	This study
BW25113 <i>mhpR</i> :: <i>km</i> *	F-, Δ (<i>araD-araB</i>)567, Δ <i>lacZ</i> 4787(:: <i>rrnB</i> -3), λ -, <i>rph</i> -1, Δ <i>mhpR</i> 786:: <i>kan</i> , Δ (<i>rhaD-rhaB</i>)568, <i>hsdR</i> 514	This study
MG1655 CGSC 7740	K-12, F-, λ - <i>ilvG</i> -, <i>rfb</i> -50, <i>rph</i> -1, IS insertion upstream of <i>flhDC</i>	(62)
MG1655 Δ <i>flu</i>	K-12, F-, λ - <i>ilvG</i> -, <i>rfb</i> -50, <i>rph</i> -1, Δ <i>flu</i> ::FLP	(37)
MG1655 Δ <i>flu</i> Δ <i>flhC</i>	K-12, F-, λ - <i>ilvG</i> -, <i>rfb</i> -50, <i>rph</i> -1, Δ <i>flu</i> ::FLP, Δ <i>flhC</i> ::FLP	(37)
MG1655 Δ <i>flu</i> <i>P</i> _{tac} - <i>flhDC</i>	K-12, F-, λ - <i>ilvG</i> -, <i>rfb</i> -50, <i>rph</i> -1, Δ <i>flu</i> ::FLP- <i>lacI</i> - <i>P</i> _{tac} - <i>flhDC</i>	(37)

Table S3: Plasmids used in this study.

Name	Reference
pBBR1-MCS5- <i>PmhpR</i> :: <i>lux</i>	This study
pBBR1-MCS5- <i>Pmhp</i> ABCDEFE:: <i>lux</i>	This study
pNPTS-R6KT- Δ <i>mhpR</i>	This study

Table S4: Oligonucleotides used in this study.

Name	Sequence
KSO-0025	CCCGGGCTGCAGGAATTC
KSO-0026	TCTAGAGAATAGGAACTTCGGAAT
KSO-0033	ATCTGGATCCACGAATTCGC
KSO-0034	ATCCTGCAGAGAAGCTTGG
KSO-0041	CAGGAAACAGCTATGACC
KSO-0042	TGTA AACGACGGCCAGT
KSO-0149	AGCCGCTTATCCTTTCACC
KSO-0150	TTCCTTGCGGTCTTGTTCC
KSO-0151	CAGATATTGTGCTCGGTGGTAG
KSO-0152	GACAGGTAGAAACGGGAAGAAC
KSO-0169	CGAAGTTCCTATTCTCTAGATTCAGTACCTCAGACTCGG
KSO-0170	TCGAATTCCTGCAGCCCGGGATTAATTGACATTTCTATAGTTAAACAAC
KSO-0171	CGAAGTTCCTATTCTCTAGAATTAATTGACATTTCTATAGTTAAACAAC
KSO-0172	TCGAATTCCTGCAGCCCGGGTTCAGTACCTCAGACTCGG
KSO-0190	GCCAAGCTTCTCTGCAGGATCCAGCAGGCGAAAATCCTG
KSO-0191	CACCATCGAATGGCGCAAAAC
KSO-0192	TTTTGCGCCATTGATGGTGATTAATTGACATTTCTATAGTTAAACAAC
KSO-0193	GCGAATTCGTGGATCCAGATGGCAGCACTTTGCTTAACAG
KSO-0194	CCCGGTTTTTCGCAGAAAC
KSO-0195	TTCAGTACCTCAGACTCGG
KSO-0214	GCCAAGCTTCTCTGCAGGATGAGTTGCAGCAAGCGGTC
KSO-0224	AGAGATTGAGACGCACGAAAG
KSO-0225	CCATTACAGCCGCAACAATAC
KSO-0226	TATTTGCACCTGGCTTCTCC
KSO-0227	CCGCCATCTTCTGGATATTAC
KSO-0228	TCGCCGTATGTTGCTTACTC
KSO-0229	CCGTCAATGGTCAGGGTATTC
KSO-0230	TGAAGTGGCACAGGCAATAG
KSO-0231	TCGGCAATATCGATCCCTAAAC
KSO-0232	GGAAGCTGGCAATGTCAAAC
KSO-0233	ATAGATCGCGCAGGCTAATG
KSO-0234	GTCATTCCAATGGTGGGATTTG
KSO-0235	GGTCACCTTCGCTTTGTTTG
KSO-0236	ACTGGTTTATGACCTGGGAAC
KSO-0237	CATCGACGCCATTACAAAAC
KSO-0238	GTTAAGCTGGCAGAAACCAATC
KSO-0239	ATCGTCAACGCGGGAATC
KSO-0240	ACCTGAACAACACCACTACC
KSO-0241	GATCTGCGCTTTCGACATATTG
KSO-0242	CGGTACGTCGCTTTGAATTTATG
KSO-0243	GATTAGGCAGCACTTTGCTTAAC
KSO-0244	GTTTCACCGCACCCCGTG
KSO-0245	GGAGAAACGACGCAATCCAAC

Supplemental information – Chapter 2.3

Available online at:

<https://www.pnas.org/doi/full/10.1073/pnas.2118227119>

Supplementary Information for

Eukaryotic catecholamine hormones influence the chemotactic control of *Vibrio campbellii* by binding to the coupling protein CheW

Angela Weigert Muñoz, Elisabeth Hoyer, Kilian Schumacher, Marianne Grognot, Katja M. Taute, Stephan M. Hacker, Stephan A. Sieber*, Kirsten Jung*

*Corresponding authors: Kirsten Jung and Stephan A. Sieber
Email: jung@lmu.de; stephan.sieber@tum.de

This PDF file includes:

Supplementary methods
Figures S1 to S19
Tables S1 to S7
Legends for datasets S1 to S6
SI references

Other supplementary materials for this manuscript include the following:

Datasets S1 to S6

Supplementary methods

Biological methods

Bacterial strains and cultivation

Bacteria were stored as 50% (v/v) glycerol stocks at -80 °C. Overnight cultures for growth assays, photolabeling, and Co-IP experiments were grown from 50% (v/v) glycerol stocks inoculated 1:1000 into 20 mL medium for 15 h at the indicated temperatures and 200 rpm. Overnight cultures were then diluted 1:100 into fresh medium (60 mL) and grown to early stationary phase. For 3D motility and chemotaxis assays, overnight cultures were inoculated from individual *V. campbellii* colonies, grown on 2% (w/v) agar MB plates streaked from a glycerol stock, and grown to saturation in 2 mL MB at 30°C, 200 rpm. Day cultures were inoculated with the overnight cultures at 1:200 dilution in 10 mL MB and grown at 30°C, 250 rpm, until they reached OD₆₀₀ 0.3.

Strain construction

Construction of the $\Delta cheW$ marker-less in-frame deletion in *V. campbellii* ATCC-BAA 1116 was achieved using the suicide plasmid pNPTS138-R6KT-*cheW* as described previously (1). Briefly, 600 bp upstream and downstream of *cheW* were amplified by PCR using *V. campbellii* ATCC-BAA 1116 genomic DNA as template. After PCR product purification, the fragments were fused by overlap PCR. The overlap PCR fragment was cloned into plasmid pNPTS138-R6KT using BamHI and EcoRI as restriction sites. The resulting plasmid pNPTS138-R6KT- $\Delta cheW$ was introduced into *V. campbellii* ATCC-BAA 1116 by conjugative mating using *E. coli* WM3064 as a donor in LB medium containing 2,6-diaminopimelic acid (DAP). Single-crossover integration mutants were selected on LB plates containing kanamycin but lacking DAP. Single colonies were grown over a day without antibiotics and plated onto LB plates containing 10% (w/v) sucrose to select for plasmid excision. Kanamycin-sensitive colonies were checked for targeted deletion by colony PCR using primers bracketing the site of the deletion.

Construction of a plasmid coding for N-terminally His₆-tagged CheW

The *cheW* gene of *V. campbellii* (VIBHAR_RS14640; old locus tag VIBHAR_03137) was cloned into vector pET28a using BamHI and XhoI as restriction sites, resulting in an extension of the sequence by codons for a N-terminal His₆ tag.

Purification of 6His-CheW

To purify CheW of *V. campbellii*, *E. coli* BL21(DE3) carrying the plasmid pET28a-*cheW* was cultivated in LB supplemented with kanamycin (50 mg/mL) at 37 °C. At OD₆₀₀ 0.6, 0.4 mM isopropyl β -D-1-thiogalactopyranoside (IPTG) was added to the culture to induce *cheW* expression at 30 °C for 4 h. Cells were harvested (20 min, 5,000 x g, 4 °C), resuspended, and disrupted by high-

pressure cell disrupter (*Constant Systems Limited*) in ice-cold disruption buffer [20 mM Tris/HCl pH 7.5, 500 mM NaCl, 10 mM imidazole, 3 mg DNase, and 0.5 mM phenazine methosulfate (PMSF) in double-distilled water (ddH₂O)]. After removal of intact cells and cells debris via centrifugation (5,000 x g, 30 min, 4 °C), membrane vesicles were removed by ultracentrifugation (45,000 x g, 60 min, 4°C), and the cell lysate was loaded onto a Ni-nitrilotriacetic acid (NTA) column (*Qiagen*). After a washing step (20 mM Tris/HCl pH 7.5, 500 mM NaCl, 50 mM imidazole), the recombinant protein was eluted with elution buffer (20 mM Tris/HCl pH 7.5, 500 mM NaCl, 250 mM imidazole).

Generation of polyclonal rabbit antibody against 6His-CheW

Customized polyclonal rabbit antibody against 6His-CheW was obtained from *Kaneka Eurogentec*. For this purpose, heterologously produced and purified 6His-CheW was provided as antigen in a Speedy 28-day immunization programme with two rabbits as hosts. 5 mL of rabbit serum was purified after the immunization by affinity purification to separate IgG antibodies from crude serum. Specificity of the polyclonal antibody against CheW was verified by Western blot analyses.

Data acquisition and analysis of 3D trajectories

Phase contrast microscopy recordings were obtained at room temperature (~21 °C) on a Nikon Ti-E inverted microscope using an sCMOS camera (PCO Edge 4.2) and a 40x objective lens (Nikon CFI SPlan Fluor ELWD 40x ADM Ph2, correction collar set to 1.2 mm to induce spherical aberrations) (2). For motility experiments, it was focused 135 µm above the bottom surface of the sample chamber. One to four 1 or 1.5-min long recordings were obtained at 30 fps per condition in motility experiments, alternating between conditions. A typical 1.5-min motility recording yields 1,500 - 2,000 bacterial trajectories. For chemotaxis experiments, it was focused at the center of the 70 µm-tall channel in all three dimensions. Two to three 2 - 2.5-min long recordings were obtained at 30 fps per condition in chemotaxis experiments. Three biological replicates were performed for chemotaxis in a 100 µM/mm **EPI** gradient, one otherwise. Biological replicates used cultures grown from different colonies.

3D trajectories were extracted from phase contrast recordings using a high-throughput 3D tracking method based on image similarity between bacteria and a reference library (2). Trajectories shorter than 5 frames were discarded. Positions were smoothed using 2nd order ADMM-based trend-filtering with regularization parameter $\lambda = 0.3$, and speeds computed as forward differences in positions divided by the time interval between frames. All trajectories with an average speed below a 20 µm/s threshold were considered non-motile and discarded. The range of 3D bacterial trajectories was ~350 µm x 300 µm laterally (x, y) and 200 µm (z) in motility chambers, or the entire 70 µm height (z) of the channel in the chemotaxis device.

For motility experiments, trajectories with a minimum duration of 1 s were analyzed for turn events. The turn event detection was based on the local rate of angular change of direction, computed from

the dot product between the sums of the two consecutive velocity vectors preceding and subsequent to a time point. The threshold for a turn to begin was an α -fold rate relative to the median rate of angular change rate of the run segments, as determined in three iterations of the procedure. We determined by visual inspection of trajectories that a factor $\alpha = 10$ gave satisfactory results. A new run begins with at least two time points (at least 0.066 s) below this threshold.

For chemotaxis experiments, the z position of the top and bottom of the chemotaxis chambers were identified by visual inspection of trajectory data, and all trajectory segments within 10 μm of the top or bottom of the central channel were removed to avoid surface interaction effects. The drift velocity is the average of the x component of all instantaneous 3D speed vectors from all bacteria, x being the gradient direction. We estimate the noise on the drift measurement by a jackknife resampling procedure consisting of dividing the data into subsets of 150 trajectories and computing the standard error of the mean drift obtained for different subsets.

Proteomics methods

General

For proteomics experiments, synthesized probes were stored as DMSO stocks at $-20\text{ }^{\circ}\text{C}$; unmodified parent compounds were dissolved in DMSO on the day of the experiment.

Preparative photolabeling with **EPI-P1**

Preparative scale photolabeling experiments with **EPI-P1** were performed as with **PE-P** with the following exceptions: Labeling was performed in 5 mL culture and **EPI-P1** was added to 7.5 μM (25 μL from a 1.5 mM DMSO stock), the same volume of 5.25 mM acetic acid in DMSO was added as control. Samples were incubated for 30 min at $30\text{ }^{\circ}\text{C}$, 200 rpm and cultures were irradiated for 5 min in 6 cm dishes. Bacteria were lysed in 450 μL PBS + protease inhibitor with sonication (2 x 15 s, 60% intensity), then TX100 was added to 1% (v/v) and sonicated (1 x 10 s, 10% intensity) and samples were incubated for 30 min on ice. Insoluble debris was removed by centrifugation (16,060 x g, 20 min, $4\text{ }^{\circ}\text{C}$).

In situ analytical scale photolabeling

Analytical scale photolabeling experiments were performed as preparative scale experiments with the following exceptions: Probe concentration was 50 μM (0.5% (v/v) DMSO). Irradiation of 1 mL labeled bacteria was performed in a 12-well dish. Lysis and fractionation into soluble and insoluble proteins was performed as for preparative experiments with **PE-P** (in 200 μL).

Analytical photolabeling in lysate in presence of radical scavengers

Lysate (in PBS) was adjusted to a protein concentration of 1 mg/mL and DMSO or **PE-P** was added to 50 μ M (0.1% (v/v) DMSO) in 60-100 μ L lysate in a 96-well plate. Samples were incubated for 1 h at 30 °C, 200 rpm and radical scavengers were added to 1 mM or 10 mM as indicated (11 μ L from a freshly made 10 mM or 100 mM stock in water), mixed thoroughly, and irradiated for 10 min. Proteins were precipitated in acetone and washed with methanol to remove the radical scavengers (as described above), resuspended in 1% (w/v) SDS/PBS (with vortexing and sonication) to the same protein concentration, and subjected to CuAAC with TAMRA-azide.

CuAAC, analytical scale photolabeling

CuAAC for analytical labeling experiments was performed with rhodamine-azide (tetramethylrhodamine 5-carboxamido-(6-azidohexanyl), 5-isomer, *Base Click*). Click reaction was quenched by addition of the same volume of 2 x sample loading buffer (63 mM Tris/HCl, 10% (v/v) glycerol, 2% (w/v) SDS, 0.0025% (w/v) bromophenol blue, 5% (v/v) 2-mercaptoethanol).

SDS-PAGE

Stacking gels consisted of 4% (w/v) acrylamide (in 50 mM Tris, pH 6.8) and resolving gels of 12.5% (w/v) acrylamide (in 300 mM Tris, pH 8.8) and were run in a Tris-glycine buffer (25 mM Tris, 192 mM glycine, 0.1% (w/v) SDS, pH 8.3). Typically, 30 μ L sample (~15 μ g protein), 8 μ L fluorescent marker (BenchMark™ Fluorescent Protein Standard, *Thermo Fisher*), and 12 μ L protein marker (Roti®-Mark Standard, *Carl Roth*) were loaded and gels were run at 150-300 V (depending on gel size) on a EV265 Consort power supply (*Hofer*). Fluorescence was scanned in a LAS-4000 imaging system equipped with a Fujinon VRF43LMD3 lens and a 575DF20 filter (*Fujifilm*). Gels were stained in Coomassie staining solution (0.25% (w/v) Coomassie Brilliant Blue R-250, 9.2% (v/v) concentrated acetic acid, 45.4% (v/v) ethanol) overnight and destained in 10% (v/v) acetic acid, 40% (v/v) ethanol).

Co-IP

Bacteria from an overnight culture were diluted in LB35 medium and grown until early stationary phase, pelleted, washed with PBS, and resuspended in PBS to OD₆₀₀ 4.0 as for preparative photolabeling experiments with **PE-P**. Four replicates were used starting from independent overnight cultures. Next, 10 mL of the suspension in a 50 mL falcon was treated with 100 μ M **EPI** (from 100 mM stock in DMSO) or DMSO and incubated 30 min, 30 °C, 200 rpm. Bacteria were harvested (6,000 x g, 5 min, RT) and resuspended in 2 mL PBS containing 100 μ M **EPI** or the equivalent volume of DMSO. The DSSO crosslinker was added to 2 mM (from a 100 mM stock in DMSO, DSSO synthesized as described previously (3)), and samples were incubated at 30 °C, 200 rpm for 30 min. Bacteria were pelleted (6,000 x g, 10 min, 4 °C), washed with 2 x 1 mL cold 50

mM Tris/HCl, pH 8.0 to quench the DSSO, and the pellet was flash-frozen and stored at -80 °C. The pellet was resuspended in 1 mL lysis buffer (50 mM Tris/HCl, pH 7.4, 150 mM NaCl, 5% (v/v) glycerol, 0.1% (v/v) NP-40) and sonicated 3 x 15 s, 60% intensity, on ice. The lysate was cleared by centrifugation (21,000 x g, 30 min, 4 °C) and the supernatant was sterile filtered (0.2 µm). Protein amount was adjusted to 1 mg (1 µg/µL). Per sample, 30 µL protein A/G bead slurry (*Pierce Biotechnology, Thermo Fisher Scientific*) in LoBind microcentrifuge tubes was equilibrated with 1 x 1 mL cold wash buffer (50 mM Tris/HCl, pH 7.4, 150 mM NaCl, 5% (v/v) glycerol, 0.05% (v/v) NP-40) and centrifuged (1,000 x g, 1 min, 4 °C). The supernatant was discarded and the lysate was added to the beads. Next, 2.5 µg antibody (167 µL from a 0.015 µg/µL stock in 50% (v/v) glycerol) or a rabbit mAb IgG XP® isotype control (1 µL, 2.5 µg/µL, *Cell Signaling Technology*) was added and incubated overnight at 4 °C under constant rotation. Samples were centrifuged (30 s, 500 x g, 4 °C), the supernatant discarded, and the beads washed with 2 x 1 mL cold wash buffer and 3 x 1 mL cold basic buffer (50 mM Tris/HCl, pH 7.4, 150 mM NaCl, 5% (v/v) glycerol). Proteins were reduced and digested by the addition of 25 µL IP elution buffer I (50 mM Tris/HCl, pH 8.0, 5 ng/µL trypsin, 2 M urea, 1 mM DTT) at 25 °C, 1,000 rpm for 30 min. To alkylate cysteines, 100 µL IP elution buffer II (50 mM Tris/HCl, pH 8.0, 2 M urea, 5 mM iodoacetamide) was added, and the samples were incubated overnight (~16 h) at 37 °C, 1,000 rpm. Formic acid was added to 1% (v/v) (pH 2-3) to quench the digestion and samples were desalted on stage tips. Desalting was performed as for photolabeling experiments with slight modifications: two layers of C-18 material was used, and stage tips were equilibrated with 1 x 80 µL methanol, then 1 x 80 µL 80% (v/v) acetonitrile, 0.5% (v/v) formic acid, and with 3 x 70 µL 0.5% (v/v) formic acid. Samples were centrifuged (16,249 x g, 2 min) and loaded, the beads were washed with 2 x 150 µL 0.5% (v/v) formic acid and washes were loaded too. Peptides were desalted with 3 x 70 µL 0.5% (v/v) formic acid and eluted with 2 x 30 µL 80% (v/v) acetonitrile, 0.5% (v/v) formic acid. Solvents were removed in a speed-vac and dry samples were stored at -80 °C.

LC-MS/MS measurements

Co-IP peptide samples were analyzed on an UltiMate 3000 nano HPLC system (*Dionex*) equipped with an Acclaim C18 PepMap100 (75 µm ID x 2 cm) trap column and an Aurora Series Emitter Column with Gen2 nanoZero fitting (75 µm ID x 25 cm, 1.6 µm FSC C18) separation column (column oven heated to 40 °C) coupled to an Orbitrap Fusion (*Thermo Fisher*) in EASY-spray setting. Peptides were loaded on the trap column and washed with 0.1% (v/v) TFA before being transferred to the analytical column and separated using a 152 min gradient (buffer A: 0.1% (v/v) formic acid in water, buffer B: 0.1% (v/v) formic acid in acetonitrile, gradient: 5-22% (v/v) buffer B in 112 min, then to 32% (v/v) buffer B in 10 min, then to 90% (v/v) buffer B in 10 min and hold 90% (v/v) buffer B for 10 min, then to 5% (v/v) buffer B in 0.1 min and hold 5% (v/v) buffer B for 9.9 min) with a flow rate of 400 nL/min. The Orbitrap Fusion was operated in a TOP10 data dependent mode

and full scan acquisition in the orbitrap was performed with a resolution of 120,000 and an AGC target of 2×10^5 (maximum injection time of 50 ms) in a scan range of 300–1,500 m/z. Monoisotopic precursor selection as well as dynamic exclusion (exclusion duration: 60 s) was enabled. Most intense precursors with charge states of 2–7 and intensities greater than 5×10^3 were selected for fragmentation. Isolation was performed in the quadrupole using a window of 1.6 m/z. Precursor ions were collected to an AGC target of 1×10^4 (maximum injection time of 100 ms). Fragments were generated using higher-energy collisional dissociation (HCD, normalized collision energy: 30%) and detected in the ion trap operating at a rapid scan rate.

Photoaffinity labeling peptide samples were analyzed on an UltiMate 3000 nano HPLC system (Dionex) equipped with an Acclaim C18 PepMap100 (75 μm ID \times 2 cm) trap column and a 25 cm Aurora Series emitter column (25 cm \times 75 μm ID, 1.6 μm FSC C18) (Ionoptics) separation column (column oven heated to 40 °C) coupled to a Q Exactive Plus (Thermo Fisher) in EASY-spray setting. Peptides were loaded on the trap column and washed with 0.1% (v/v) TFA before being transferred to the analytical column and separated using a 152 min gradient (buffer A: 0.1% (v/v) formic acid in water, buffer B: 0.1% (v/v) formic acid in acetonitrile. Gradient of buffer B: 5% (v/v) for 7 min, increase to 22% (v/v) in 105 min, then to 32% (v/v) in 10 min, then to 90% (v/v) in 10 min, hold at 90% (v/v) for 10 min, decrease to 5% (v/v) in 0.1 min and hold at 5% (v/v) for 9.9 min) with a flow rate of 400 nL/min. The Q Exactive Plus was operated in a TOP10 data dependent mode full scan acquisition in the orbitrap was performed with a resolution of 140 000 and an AGC target of 3×10^6 (maximum injection time of 80 ms) in a scan range of 300–1,500 m/z. Most intense precursors with charge states of > 1 , a minimum AGC target of 1×10^3 , and intensities greater than 1×10^4 were selected for fragmentation. Peptide fragments were generated using higher-energy collisional dissociation (HCD, normalized collision energy: 27%) and detected in the orbitrap with a resolution of 17 500 m/z. The AGC target was set to 1×10^5 (maximum injection time 100 ms) and the dynamic exclusion duration to 60 s. Isolation in the quadrupole was performed with a window of 1.6 m/z.

Differential isotopic labeling samples were measured on a Q Exactive Plus spectrometer with a different gradient (buffer B: 5% (v/v) for 7 min, increase to 40% (v/v) in 105 min, then to 60% (v/v) B in 10 min, and to 90% (v/v) B in 10 min, hold at 90% (v/v) for 10 min, then decrease to 5% (v/v) in 0.1 min and hold at 5% (v/v) for another 9.9 min) at the same flow rate. All parameters were the same as for photoaffinity labeling experiments except full MS scans were collected at a resolution of 70 000.

Analysis of MS data from photoaffinity labeling and Co-IP experiments

MS data were analyzed using MaxQuant (4, 5) version 1.6.5.0 and peptides were searched against the UniProt database for *Vibrio campbellii* ATCC BAA-1116 / BB120 (taxon identifier 338187,

downloaded on 17.02.2020). Cysteine carbamidomethylation was set as fixed modification and methionine oxidation and N-terminal acetylation as variable modifications. Trypsin (without N-terminal cleavage to proline) was set as proteolytic enzyme with a maximum of two allowed missed cleavages. Label-free quantification (LFQ) mode (6) was performed with a minimum ratio count of 2. The “match between runs” (0.7 min match and 20 min alignment time window) and second peptide identification options were activated. All other parameters were used as pre-set in the software. LFQ intensities were further processed with Perseus (7) version 1.6.1.1. Peptides of the categories “only identified by site”, “reverse”, or “potential contaminant” were removed and LFQ intensities were \log_2 -transformed. Data were filtered to retain only protein groups identified in at least 3/4 valid values (experiments: competitive labeling **PE-P** vs. **EPI**; competitive labeling **PE-P** vs. **PRO/LAB**; Co-IP), 4/5 valid values (competitive labeling **PE-P** vs. **PE**), or 3/3 valid values (labeling with **EPI-P1**) in at least one group and missing values were imputed (width 0.3, downshift 1.8, total matrix). A two-sample Student’s t-test with permutation-based FDR (FDR 0.05) was performed and the significance cut-off was set at p -value = 0.05 ($-\log_{10}(p\text{-value}) = 1.3$) and an enrichment factor of 2 ($\log_2(x) = 1$) or 4 ($\log_2(x) = 2$) as indicated in the plots. Protein IDs were matched to annotations downloaded from annotations.perseus-framework.org on 18.02.2020. Proteins with the annotation “chemotaxis” in the GOBP or KEGG database were highlighted in the Co-IP plots.

Analysis of isoDTB data

Analysis software was set up as previously described (8) using the MSconvert tool (version: 3.0.19172-57d620127) of the ProteoWizard software (version: 3.0.19172 64bit) (9), the FragPipe interface (version: 14.0) (10, 11), MSFragger (version: 3.1.1) (10, 11), Philosopher (version: 3.3.10) (12), IonQuant (version 1.4.6) (13), and Python (version: 3.7.3). The FASTA file (*Vibrio campbellii* ATCC BAA-11116/BB120; taxon identifier 338187, downloaded on 17.02.2020) was modified by adding the reverse sequences manually. Modifications were analyzed as previously described (8). Amino acid selectivity was analyzed and data were evaluated and filtered as previously published (8) performing an Offset Search in MSFragger (10, 11) with mass offsets set as 740.3974 or 746.4040. Run MS1 quant was enabled with Labeling based quant with masses set as 740.3974 or 746.4040. Specific amino acids were quantified and data were evaluated and filtered as previously published (8) performing a Closed Search in MSFragger with variable modifications set to 740.3974 or 746.4040 on Tyr. Run MS1 quant was enabled with Labeling based quant with masses set as 740.3974 or 746.4040.

AlphaFold structure prediction

The sequence of CheW was retrieved from UniProt (Uniprot Code: A7MS42) and used as basis for the AlphaFold prediction on a local installation of the AlphaFold algorithm as released by Jumper *et*

al. (14). Visualization and alignment with the CheW structure from *E. coli* (PDB:2HO9, solution NMR) was done using the open source version of PyMOL 2.4 (15).

Chemical synthesis

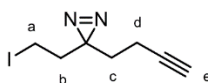
General

Chemicals with reagent or higher grade as well as dry solvents were purchased from *Sigma Aldrich*, *Acros Organics*, or *Alfa Aesar*. 2-(3-But-3-ynyl-3H-diazirin-3-yl)-ethanol was purchased from *Ark Pharm Inc.*

Analytical thin layer chromatography was performed on aluminum-coated TLC silica gel plates (silica gel 60, F254, *Merck KGaA*) with visualization by UV light ($\lambda = 254$ nm) or KMnO_4 -stain (3.0 g KMnO_4 , 20.0 g K_2CO_3 and 5 mL 5% (w/v) NaOH in 300 mL ddH_2O). Column chromatography was carried out using silica gel (40-63 μm (Si 60), *Merck KGaA*). High-resolution mass spectra (HRMS) were measured on a LTQ-FT Ultra (*Thermo Fisher*) equipped with an ESI ion source.

NMR spectra were measured at room temperature on Avance-III HD NMR systems with 300, 400, or 500 MHz (*Bruker Co.*). Chemical shifts are reported in parts per million (ppm) and residual proton signals of deuterated solvents were used as internal reference (^1H NMR: CDCl_3 $\delta = 7.26$ ppm, $\text{DMSO}-d_6$ $\delta = 2.50$ ppm, 0.04% (v/v) DCI in D_2O referenced to D_2O $\delta = 4.79$ ppm. ^{13}C -NMR: CDCl_3 $\delta = 77.16$ ppm, $\text{DMSO}-d_6$ $\delta = 39.52$ ppm, 50% (v/v) AcOD in D_2O referenced to AcOD $\delta = 178.990$ ppm). Coupling constants (J) are reported in Hertz (Hz). Signal multiplicities are denoted with the following abbreviations: s – singlet, d – doublet, dd – doublet of doublets, ddd – doublet of doublet of doublets, t – triplet, td – triplet of doublets, p – pentet, and m – multiplet. NMR data were analyzed using MestReNova (*Mestrelab Research*).

3-(But-3-yn-1-yl)-3-(2-iodoethyl)-3H-diazirine (PCL-I)



PCL-I
 $\text{C}_7\text{H}_{11}\text{N}_2$
248.07 g/mol

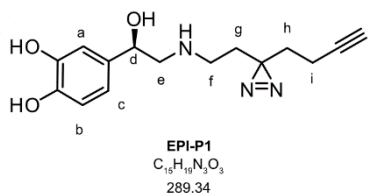
The reaction was performed following a published protocol (16). A solution of imidazole (74 mg, 1.08 mmol, 3.0 eq.) and triphenylphosphine (104 mg, 0.398 mmol, 1.1 eq.) in anhydrous DCM (2 mL) was cooled to 0 °C. Pestled iodine (110 mg, 0.434 mmol, 1.2 eq.) was added and the solution was stirred at 0 °C for 5 min. 2-(3-(But-3-ynyl)-3H-diazirin-3-yl)ethanol (50 mg, 0.361 mmol, 1.0 eq.) was added in DCM (~1 mL) and the reaction mixture was stirred 7 h under exclusion of light. The reaction was quenched with saturated aqueous $\text{Na}_2\text{S}_2\text{O}_3$ (2 mL) and the aqueous layer was extracted with EtOAc (2 x 5 mL). Combined organic layers were washed with brine (1 x 5 mL) and dried over Na_2SO_4 . Solvents were removed under reduced pressure (≥ 50 mbar) and the residue

was purified by column chromatography (EtOAc/n-hexane 1:20). Solvents were removed under reduced pressure (≥ 50 mbar) and the product was obtained as a colorless liquid (55 mg, 0.222 mmol, 62%).

TLC: $R_f = 0.53$ (EtOAc/n-hexane 1:20) [UV/KMnO₄]. **¹H-NMR** (500 MHz, CDCl₃) δ [ppm]: 2.89 (t, $J = 7.6$ Hz, 2H, H-a), 2.12 (t, $J = 7.6$ Hz, 2H, H-d), 2.06-2.00 (m, 3H, H-b, H-e), 1.69 (t, $J = 7.2$ Hz, 2H, H-c). **¹³C-NMR** (75 MHz, CDCl₃) δ [ppm]: 82.56, 69.57, 37.66, 31.96, 28.73, 13.39, -3.88. Analytical data are in accordance with literature reports (16).

(R)-4-(2-((2-(3-(But-3-yn-1-yl)-3H-diazirin-3-yl)ethyl)amino)-1-hydroxyethyl)-benzene-1,2-diol

(EPI-P1)



NE (105 mg, 0.621 mmol, 3.5 eq.) was added to a solution of **PCL-I** (44 mg, 0.177 mmol, 1.0 eq.) in anhydrous DMF (6 mL) and it was stirred at 70 °C (with reflux) under argon for 17 h. Solvents were removed under reduced pressure and the residue was purified by column chromatography (MeOH/AcOH/DCM 1:3:10) and solvents were removed under reduced pressure with toluene co-evaporation. The product **EPI-P1** was obtained as a mixture with acetic acid (**EPI-P1**:AcOH 1:3.5) as a brown solid (53 mg, 0.106 mmol, 62%).

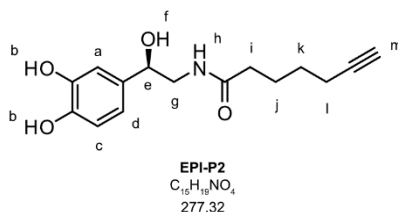
TLC: $R_f = 0.43$ (MeOH/AcOH/DCM 1:3:7) [UV/KMnO₄]. **¹H-NMR** (500 MHz, DCl/D₂O 38:962) δ [ppm]: 6.66 – 6.63 (m, 2H, H-a and H-b), 6.57 (dd, $J = 8.2, 2.1$ Hz, 1H, H-c), 4.63 (dd, $J = 7.9, 5.2$ Hz, 1H, H-d), 3.01 – 2.95 (m, 2H, H-e), 2.78 (td, $J = 8.7, 2.1$ Hz, 2H, H-f), 2.10 (t, $J = 2.7$ Hz, 1H, H-j), 1.80 – 1.74 (m, 13H, AcOH + H-i), 1.59 (ddd, $J = 10.6, 6.4, 2.7$ Hz, 2H, H-g), 1.42 (t, $J = 7.1$ Hz, 2H, H-h). **¹³C-NMR** (101 MHz, AcOD/D₂O 1:1) δ [ppm]: 147.11, 147.04, 134.59, 120.99, 118.78, 116.23, 86.08, 72.85, 71.27, 56.17, 45.43, 33.56, 32.06, 29.07, 15.19. **HRMS:** (ESI) $C_{15}H_{20}N_3O_3^+$ [M+H]⁺ calculated: 290.1499; found: 290.1499.

Amide coupling general protocol

To a solution of 6-heptynoic acid (127 μ L, 0.950 mmol, 1.0 eq.) in DMF (10 mL), EDC•HCl (182 mg, 0.95 mmol, 1.0 eq.) and HOBt (128 mg, 0.95 mmol, 1.0 eq.) was added. The clear solution was stirred at 0 °C for 30 min and then at room temperature for 4 h. Anhydrous TEA (395 μ L, 2.85 mmol, 3.0 eq.; or 4 eq. if amine was HCl salt) was added followed by the amine (0.95 mmol, 1.0 eq.). The mixture was stirred overnight. Water (100 mL) was added, extracted with 3 x EtOAc (30 mL), and combined organic phases were washed with brine (30 mL) and dried over Na₂SO₄. Solvents were

removed under reduced pressure and the crude mixture was purified by SiO₂ chromatography (MeOH/DCM 8:92).

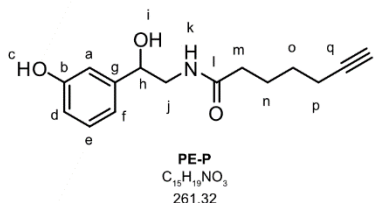
(R)-N-(2-(3,4-Dihydroxyphenyl)-2-hydroxyethyl)hept-6-ynamide (EPI-P2)



The reaction was performed with L-norepinephrine (161 mg, 0.950 mmol, 1.0 eq.) and the product was obtained as a pale orange amorphous solid (86 mg, 0.310 mmol, 16%).

TLC: $R_f = 0.37$ (MeOH/DCM 8:92) [UV/KMnO₄]. **¹H-NMR:** (500 MHz, DMSO-d₆) δ [ppm]: 8.78 (s, 1H, H-b), 8.68 (s, 1H, H-b), 7.77 (t, $J = 5.6$ Hz, 1H, H-h), 6.71 (d, $J = 1.7$ Hz, 1H, H-a), 6.65 (d, $J = 8.0$ Hz, 1H, H-c), 6.54 (dd, $J = 8.0, 1.7$ Hz, 1H, H-d), 5.18 (d, $J = 4.1$ Hz, 1H, H-f), 4.39 (dt, $J = 8.3, 4.4$ Hz, 1H, H-e), 3.23 – 3.17 (m, 1H, H-g), 3.00 (ddd, $J = 13.1, 7.9, 5.1$ Hz, 1H, H-g), 2.74 (t, $J = 2.6$ Hz, 1H, H-m), 2.13 (td, $J = 7.0, 2.6$ Hz, 2H, H-l), 2.08 – 2.04 (m, 2H, H-i), 1.54 (p, $J = 7.4$ Hz, 2H, H-j), 1.39 (p, $J = 7.1$ Hz, 2H, H-k). **¹³C-NMR:** (101 MHz, DMSO-d₆) δ [ppm]: 172.10, 144.83, 144.19, 134.87, 116.88, 115.05, 113.46, 84.43, 71.29, 71.20, 46.96, 34.69, 27.52, 24.42, 17.48. **HRMS:** (ESI) C₁₅H₂₀NO₄⁺ [M+H]⁺ calculated: 278.1387, found: 278.1388.

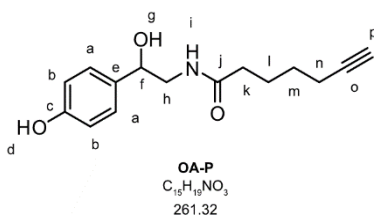
N-(2-Hydroxy-2-(3-hydroxyphenyl)ethyl)hept-6-ynamide (PE-P)



The reaction was performed with DL-norphenylephrine•HCl (180 mg, 1.00 mmol, 1.0 eq.) and the product was obtained as a white powder (169 mg, 0.648 mmol, 65%).

TLC: $R_f = 0.63$ (MeOH/DCM 8:92) [UV/KMnO₄]. **¹H-NMR:** (500 MHz, DMSO-d₆) δ [ppm]: 9.27 (s, 1H, H-c), 7.83 (t, $J = 5.8$ Hz, 1H, H-k), 7.09 (t, $J = 7.8$ Hz, 1H, H-e), 6.74 (s, 1H, H-a), 6.71 (d, $J = 7.6$ Hz, 1H, H-f), 6.61 (dd, $J = 8.0, 2.5$ Hz, 1H, H-d), 5.35 (d, $J = 4.3$ Hz, 1H, H-i), 4.48 (dt, $J = 8.5, 4.5$ Hz, 1H, H-h), 3.28 – 3.22 (m, 1H, H-j), 3.06 – 3.00 (m, 1H, H-j), 2.75 (t, $J = 2.6$ Hz, 1H, H-r), 2.13 (td, $J = 7.0, 2.6$ Hz, 2H, H-p), 2.07 (t, $J = 7.4$ Hz, 2H, H-m), 1.55 (p, $J = 7.4$ Hz, 2H, H-n), 1.38 (p, $J = 7.1$ Hz, 2H, H-o). **¹³C-NMR:** (101 MHz, DMSO-d₆) δ [ppm]: 172.56, 157.62, 145.83, 129.35, 117.08, 114.35, 113.29, 84.86, 71.90, 71.68, 47.31, 35.12, 27.97, 24.85, 17.93. **HRMS:** (ESI) C₁₅H₁₂NO₃⁺ [M+H]⁺ calculated: 262.1438, found: 262.1438.

N-(2-Hydroxy-2-(4-hydroxyphenyl)ethyl)hept-6-ynamide (OA-P)



The reaction was performed with DL-octopamine•HCl (241 mg, 1.27 mmol, 1.0 eq.) and the product was obtained as a white powder (189 mg, 0.723 mmol, 54%).

TLC: R_f = 0.47 (MeOH/DCM 9:1) [UV/KMnO₄]. **¹H-NMR:** (300 MHz, DMSO-d₆) δ [ppm]: 9.22 (s, 1H, H-d), 7.76 (t, J = 5.7 Hz, 1H, H-i), 7.15 – 7.04 (m, 2H, H-a), 6.75 – 6.64 (m, 2H, H-b), 5.22 (d, J = 4.2 Hz, 1H, H-g), 4.47 (dt, J = 8.6, 4.6 Hz, 1H, H-f), 3.26 – 3.01 (m, 2H, H-h), 2.74 (t, J = 2.7 Hz, 1H, H-p), 2.13 (td, J = 7.0, 2.7 Hz, 2H, H-n), 2.06 (t, J = 7.3 Hz, 2H, H-k), 1.60 – 1.48 (m, 2H, H-l), 1.44 – 1.32 (m, 2H, H-m). **¹³C-NMR:** (75 MHz, DMSO-d₆) δ [ppm]: 172.01, 156.34, 134.06, 127.10, 114.68, 84.37, 71.18, 71.14, 46.81, 34.63, 27.48, 24.38, 17.43. **HRMS:** (ESI) C₁₅H₁₈NO₃⁻ [M-H]⁻ calculated: 260.1292; found: 260.1292.

Supplementary figures

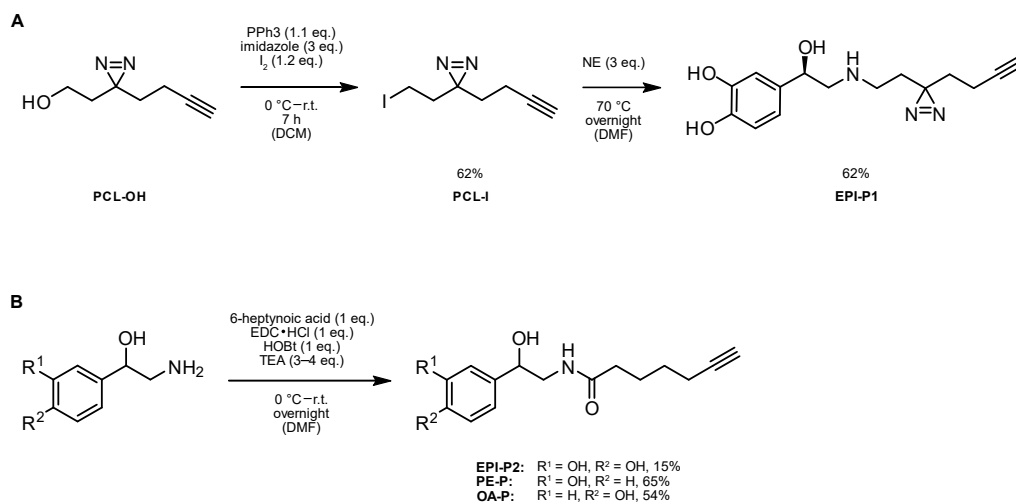


Fig. S1. Synthesis of photoprobes. (A) Probe **EPI-P1** was synthesized via alkylation of **NE**. (B) Probes **EPI-P2**, **PE-P**, and **OA-P** were obtained by acylation of **NE**, **PE**, and **OA**, respectively using amide coupling.

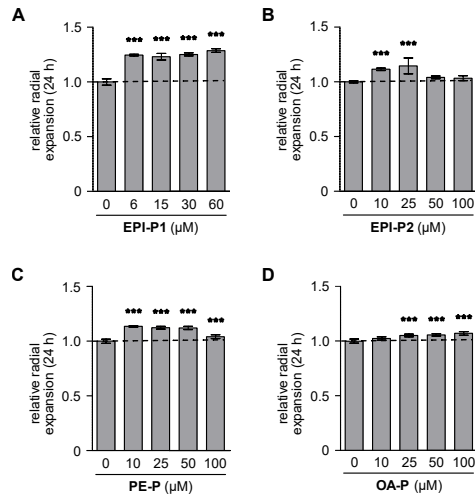


Fig. S2. Soft agar colony expansion assays with (A) **EPI-P1** (diameter of control: 5.68 cm), (B) **EPI-P2** (diameter of control: 4.28 cm), (C) **PE-P** (diameter of control: 6.15 cm), and (D) **OA-P** (diameter of control: 6.15 cm) at different concentrations as indicated. Radial expansions were normalized to an untreated control. Error bars represent the standard deviation from six independent experiments. Significance was determined performing a one-way ANOVA with Tukey's post hoc test (***) = $p < 0.001$).

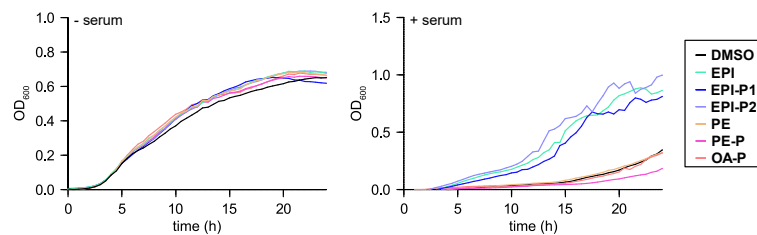


Fig. S3. Bacterial growth in LB35 (left plot) or in LB35 supplemented with 30% (v/v) adult bovine serum to generate iron limitation (right plot) in a 96-well microtiter plate with shaking for 20 s every 5 min at 30 °C. Compounds were added at 50 μ M. Data show the mean of triplicates; standard deviations between replicates account for not more than 15% in all growth experiments.

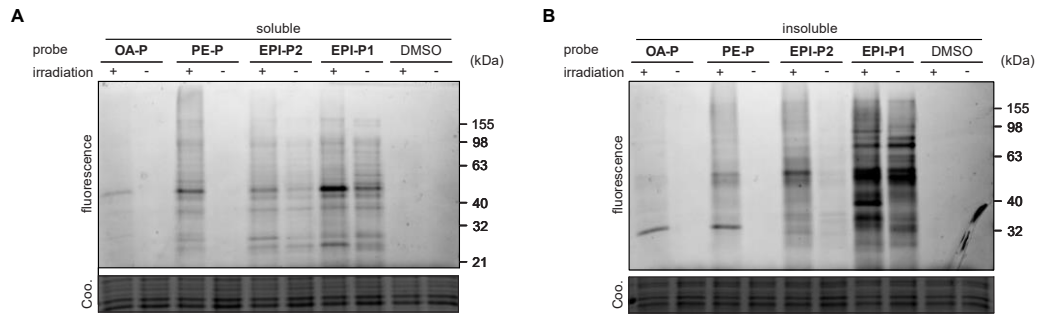


Fig. S4. Comparison of soluble and insoluble fractions from *in situ* photoaffinity labeling. Treatment of live bacteria with the probes (50 μ M) or DMSO was followed by UV-irradiation, lysis, and CuAAC to rhodamine azide. Proteins were separated by SDS-PAGE and scanned for fluorescence. Total protein loading (15 μ g per lane) was visualized by Coomassie staining (Coo.) (A) Soluble (PBS) fraction and (B) insoluble fraction.

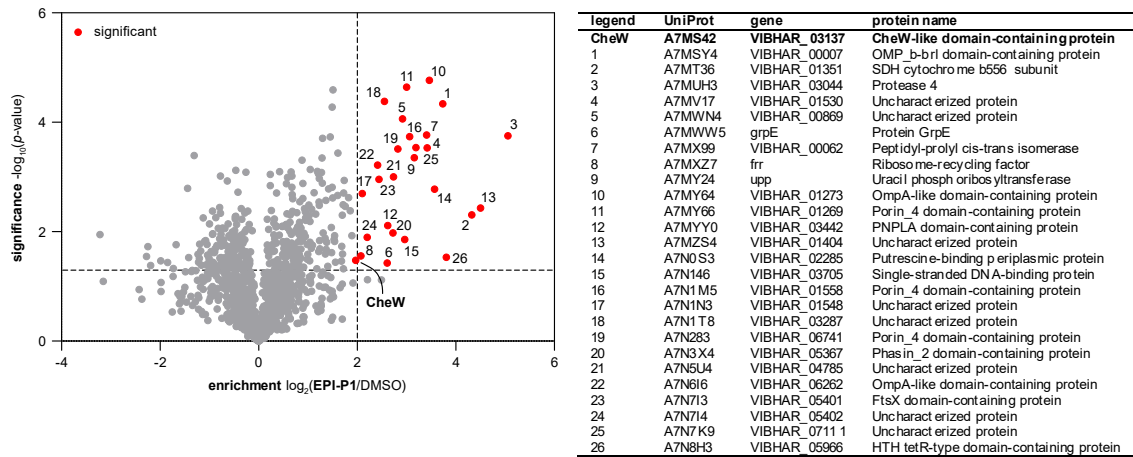


Fig. S5. Volcano plot of photolabeling with **EPI-P1**. Bacteria were labeled with 7.5 μM **EPI-P1**, irradiated, and lysed in 1% (v/v) TX100 (without fractionation). The plot shows proteins enriched by **EPI-P1** compared to the solvent-treated control. The experiment was performed in three independent replicates. Proteins enriched above the cut-off ($-\log_{10}(p\text{-value}) > 1.3$, $\log_2(\text{enrichment}) > 2$) are highlighted in red and listed in the table.

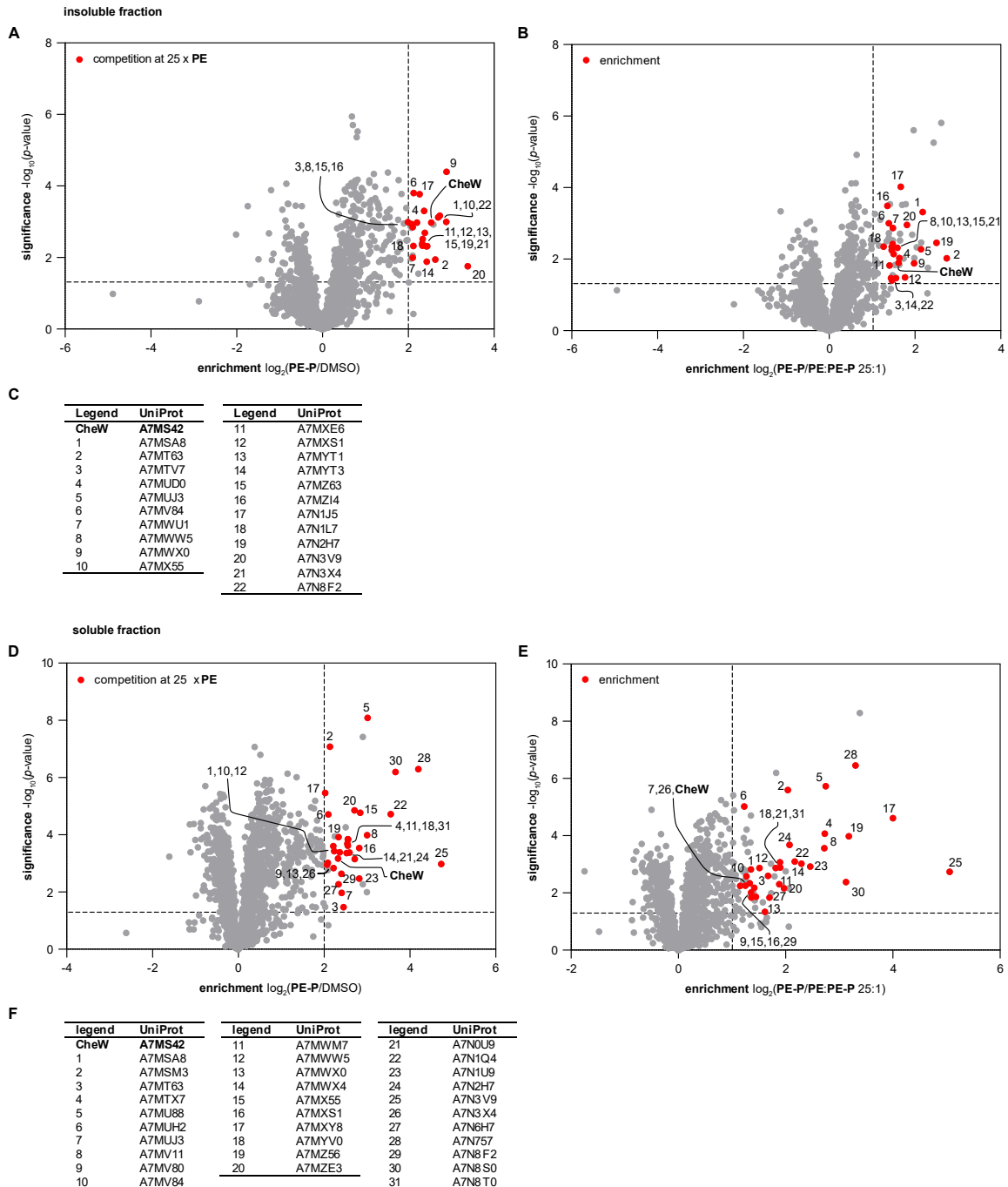


Fig. S6. Volcano plots of competitive labeling experiments with **PE-P** and **PE**. (A) Proteins enriched by **PE-P** compared to the DMSO-treated control. Proteins also outcompeted by a 25-fold excess of **PE** are highlighted in red. Insoluble fraction. (B) Proteins enriched by **PE-P** compared to samples treated with **PE-P** plus a 25-fold excess of **PE**. Proteins also found in the enrichment over DMSO are highlighted in red. Insoluble fraction. (C) UniProt identifiers of proteins enriched by **PE-P** over DMSO and outcompeted by a 25-fold excess of **PE**. Insoluble fraction. (D) Proteins enriched by **PE-P**, soluble fraction. (E) Proteins enriched by **PE-P** and outcompeted by **PE**, soluble fraction. (F) UniProt identifiers of proteins enriched by **PE-P** and outcompeted by **PE**, soluble fraction. All experiments were performed with 10 μ M **PE-P** in five independent replicates.

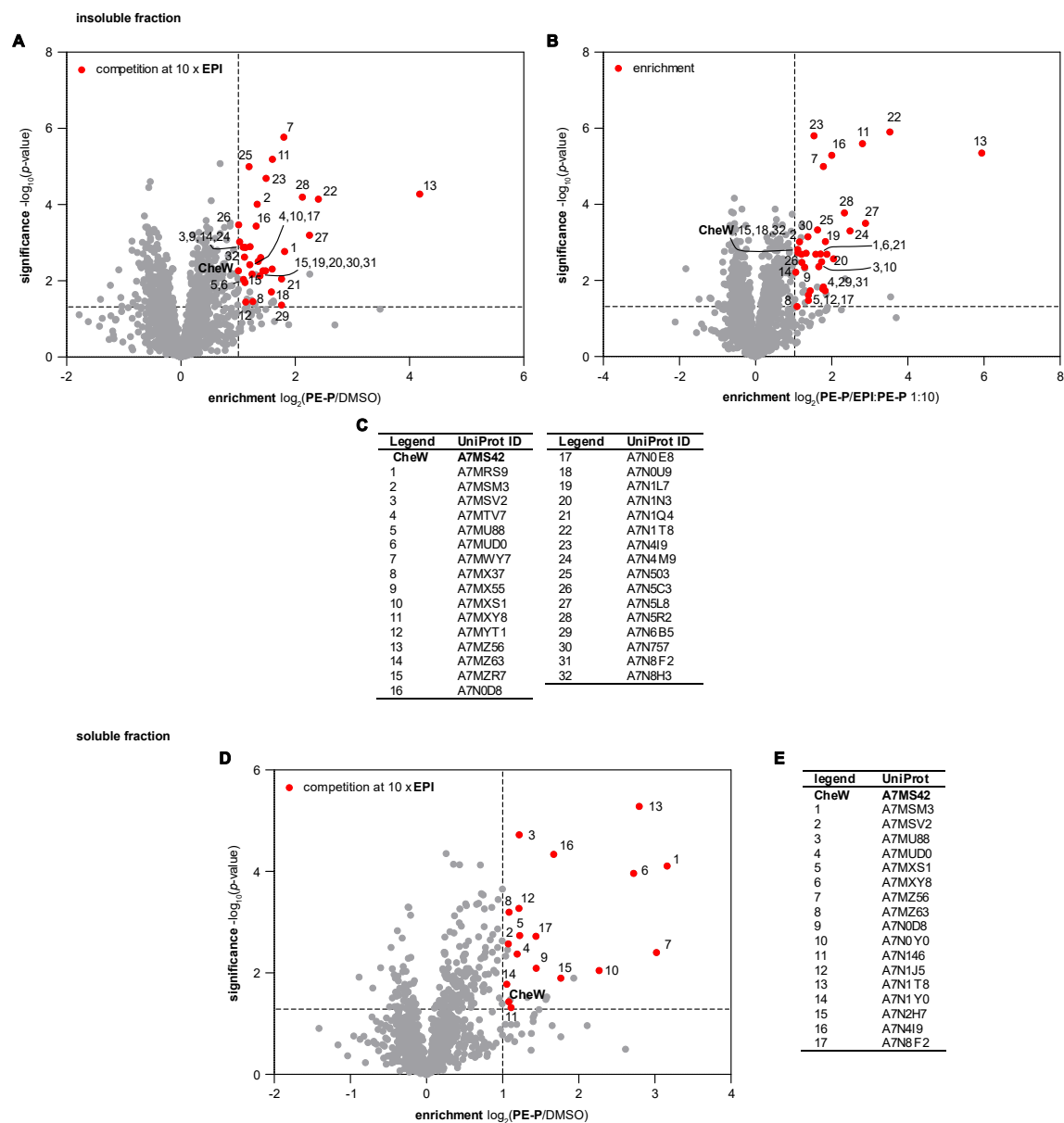


Fig. S7. Volcano plots of competitive labeling experiments with **PE-P** and **EPI**. (A) Proteins enriched by **PE-P** compared to the DMSO-treated control. Proteins also outcompeted by a 10-fold excess of **EPI** are highlighted in red. Insoluble fraction. (B) Proteins enriched by **PE-P** compared to samples treated with **PE-P** plus a 10-fold excess of **EPI**. Proteins also found in the enrichment over DMSO are highlighted in red. Insoluble fraction. (C) UniProt identifiers of proteins enriched by **PE-P** over DMSO and outcompeted by **EPI**. Insoluble fraction. (D) Proteins enriched by **PE-P**, soluble fraction (E) UniProt identifiers of proteins enriched by **PE-P** and outcompeted by **EPI**, soluble fraction. All experiments were performed with 10 μ M **PE-P** in four independent replicates.

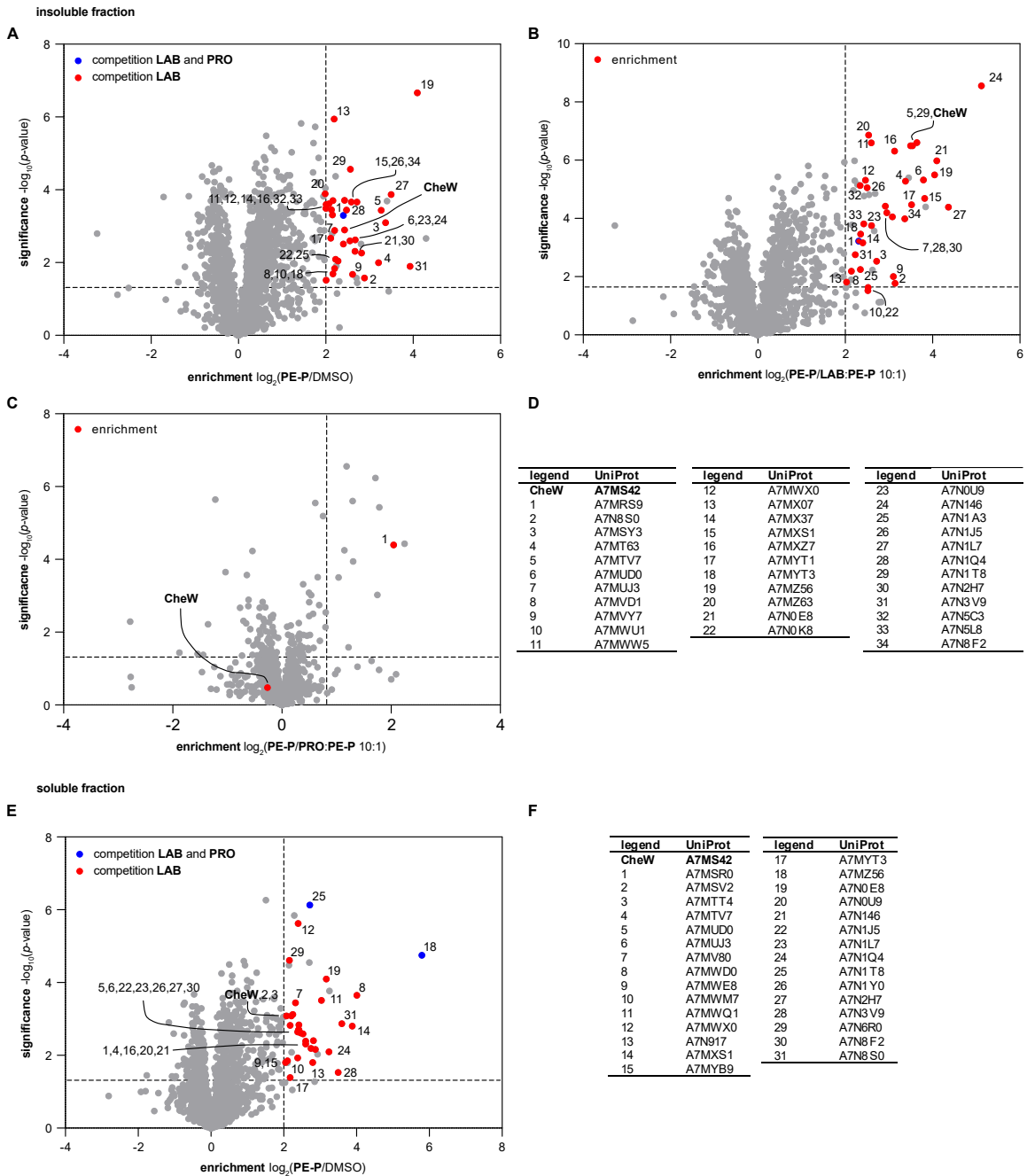


Fig. S8. Volcano plots of competitive labeling experiments with **PE-P** and adrenergic antagonists. (A) Proteins enriched by **PE-P** compared to the DMSO-treated control. Proteins also outcompeted by a 10-fold excess of **LAB** are highlighted in red, proteins outcompeted by both 10-fold **LAB** and **PRO** are highlighted in blue. Insoluble fraction. (B) Proteins enriched by **PE-P** compared to samples treated with **PE-P** plus a 10-fold excess of **LAB**. Proteins also found in the enrichment over DMSO are highlighted in red. Insoluble fraction. (C) Proteins enriched by **PE-P** compared to samples treated with **PE-P** plus a 10-fold excess of **PRO**. Proteins also found in the enrichment over DMSO and CheW are highlighted in red. Insoluble fraction. (D) UniProt identifiers of proteins outcompeted by **LAB** or **PRO**. Insoluble fraction. (E) Proteins enriched by **PE-P** compared to the DMSO-treated control. Proteins also outcompeted by a 10-fold excess of **LAB** are highlighted in red, proteins outcompeted by both 10-fold **LAB** and **PRO** are highlighted in blue. Soluble fraction. (F) UniProt

identifiers of proteins outcompeted by **LAB** or **PRO**. Soluble fraction. All experiments were performed with 10 μM **PE-P** in four independent replicates.

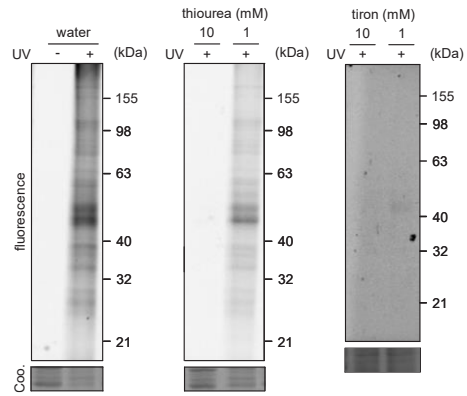


Fig. S9. Photoaffinity labeling in *V. campbellii* lysate with 50 μ M **PE-P** in the presence of radical scavengers. (A) Labeling in the presence of different concentrations of thiourea. (B) Labeling in the presence of tiron at different concentrations. In all experiments, labeled proteins were clicked to rhodamine azide, separated by SDS-PAGE, and visualized for fluorescence. Total protein loading (15 μ g protein per lane) was visualized by Coomassie staining (Coo.).

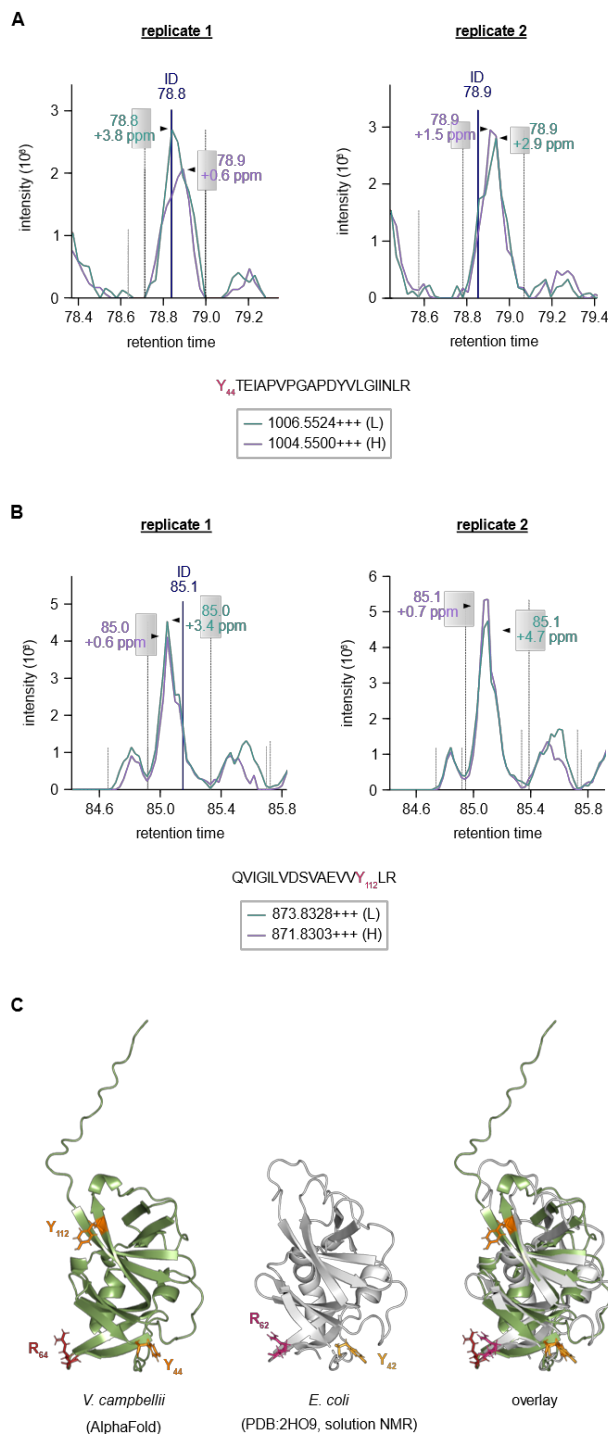


Fig. S10 Binding sites of **PE-P** in CheW. (A) Extracted MS1 ion chromatograms of **PE-P**-labeled peptides. The heavy- and light-labeled peptide containing the Y₄₄ binding site are shown in purple and in cyan, respectively; charge state = 3. (B) Chromatograms of the heavy- (purple) and light-labeled (cyan) peptide containing the Y₁₁₂ binding site; charge state = 3. Both replicates are shown. (C) Structure prediction of CheW from *V. campbellii* (green) generated with AlphaFold (14) and visualized with PyMOL (15). Binding sites Y₄₄ and Y₁₁₂ are highlighted in orange, the conserved arginine R₆₄ is shown in red. The structure of CheW from *E. coli* (gray) was retrieved from PDB (PDB:2HO9, solution NMR) and the alignment was performed in PyMOL; RMSD =

2.217 (1448 to 1448 atoms of 1771 total). In the *E. coli* structure, Y₄₂ (orange) and R₆₂ (red) are conserved.

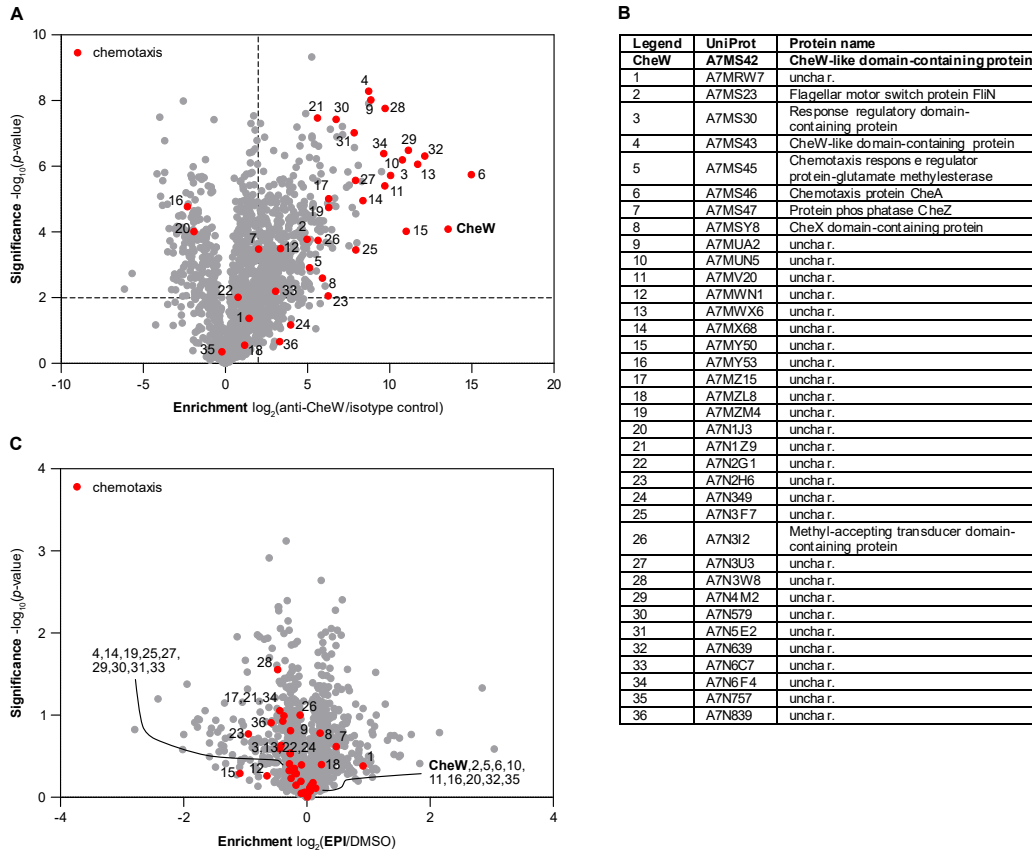


Fig. S11. Volcano plots of Co-IP of CheW binding partners in live *V. campbellii*. Bacteria were treated with 100 μ M **EPI** or DMSO for 30 min and proteins were chemically crosslinked with 2 mM DSSO. Bacteria were lysed and proteins were pulled down using an anti-CheW antibody or an isotype control in the DMSO-treated samples. (A) Proteins enriched by the anti-CheW antibody compared to the isotype control in the DMSO-treated samples. (B) UniProt identifiers of proteins involved in chemotaxis. Listed are proteins with the annotation “chemotaxis” in the GOBP or KEGG database. (C) Proteins enriched by the anti-CheW antibody in samples treated with 100 μ M **EPI** compared to DMSO-treated controls. The abundance of chemotaxis proteins did not change significantly (cut-off criteria: $0.5 \leq \log_2 \text{enrichment} \leq 2$; $-\log_{10}(p\text{-value}) \geq 1.3$). Volcano plot represents t-test results of four independent replicates. Chemotaxis proteins are highlighted in red.

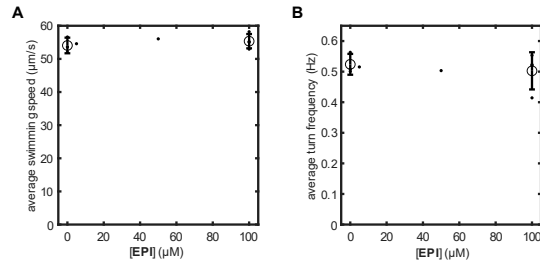


Fig. S12. Motility of *V. campbellii* after 30 min in the absence and presence of **EPI** assessed by 3D tracking. (A) Average motile swimming speed as a function of **EPI** concentration. Motile bacteria were defined as those with an average swimming speed of at least 20 µm/s. (B) Average turning frequency as a function of **EPI** concentration. Technical replicates are shown as points. Open circles with error bars denote average and standard deviation across technical replicates, when at least three replicates are available. The analysis was performed for motile bacteria with a minimum trajectory duration of 1s.

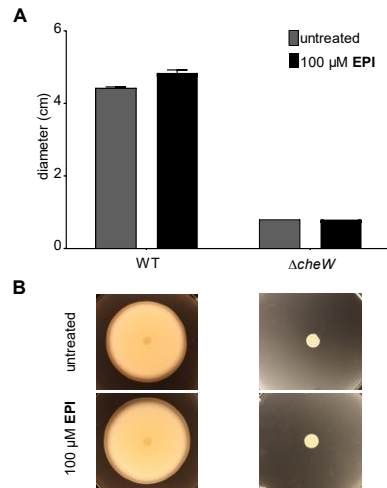


Fig. S13. Soft agar colony expansion assay with the *V. campbellii* $\Delta cheW$ mutant. (A) Plot shows means of expansion of the wild-type (WT) and the $\Delta cheW$ mutant on soft agar in the absence and presence of 100 μ M **EPI** after 24 h. Error bars represent the standard deviation (wild-type n = 7 and mutant n = 6 independent replicates, *** = p < 0.001). (B) Appearance of *V. campbellii* WT and $\Delta cheW$ mutant on soft agar plates with and without **EPI** after 24 h incubation.

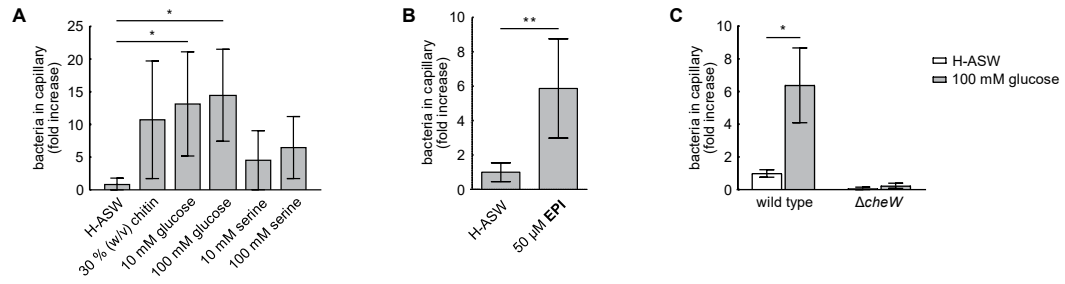


Fig. S14. Capillary assay to determine chemotactic movement of *V. campbellii*. (A) Relative increase of bacterial cell numbers in the capillary containing chitin, glucose, or serine, after 60 min. (B) Relative increase of bacterial cell numbers in the capillary containing EPI after 60 min. Values were normalized to their respective control (HEPES-buffered artificial sea water, H-ASW). (C) Relative increase of *V. campbellii* wild type and $\Delta cheW$ cell numbers in the capillaries filled with H-ASW or 100 mM glucose. Error bars indicate standard deviations; n = 4 replicates. Statistical significance was determined using an unpaired two-tailed *t*-test (* = $p < 0.05$, ** = $p < 0.01$).

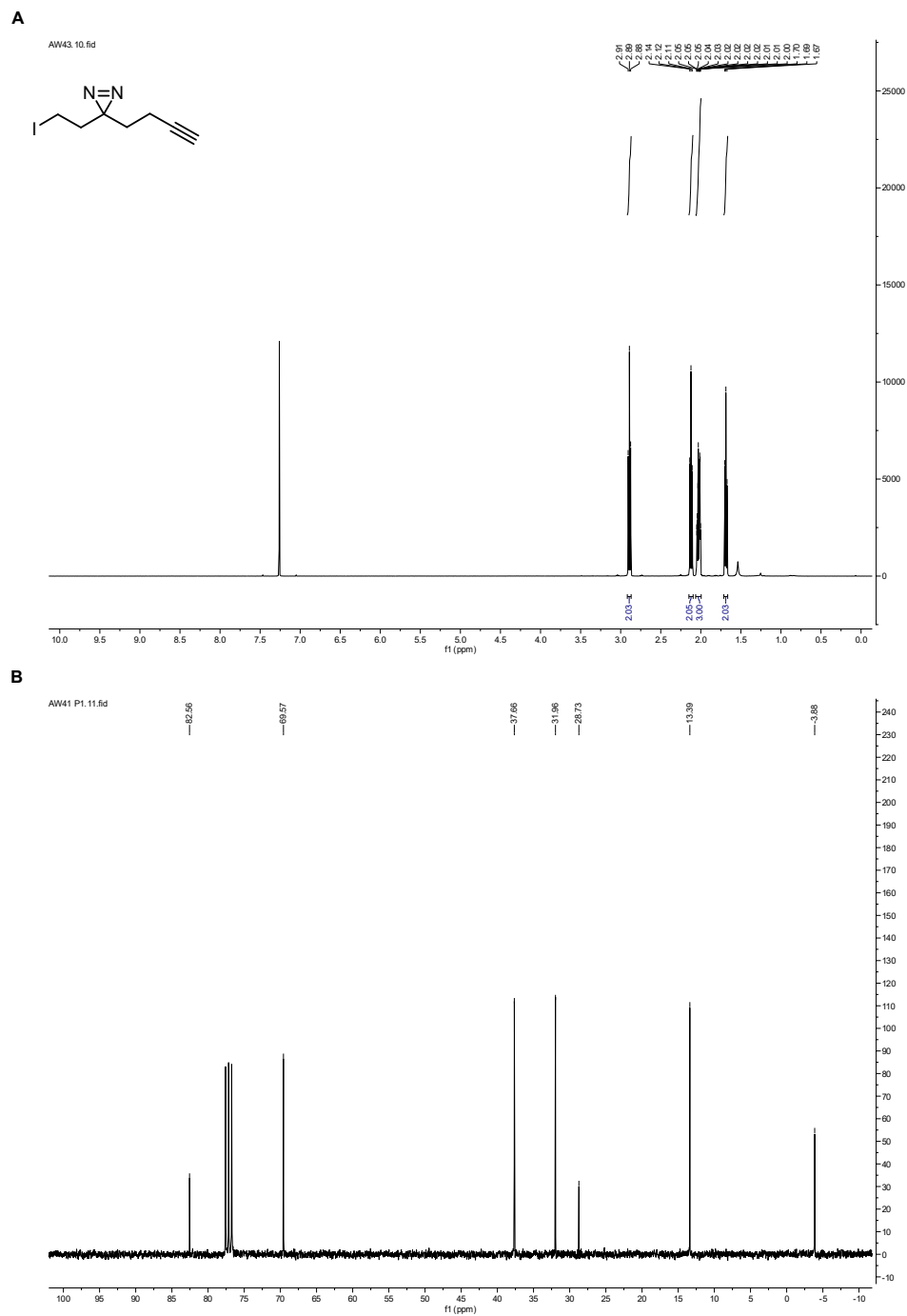


Fig. S15. NMR spectra of 3-(but-3-yn-1-yl)-3-(2-iodoethyl)-3H-diazirine (**PCL-I**) in CDCl₃. (A) ¹H-NMR (500 MHz). (B) ¹³C-NMR (75 MHz).

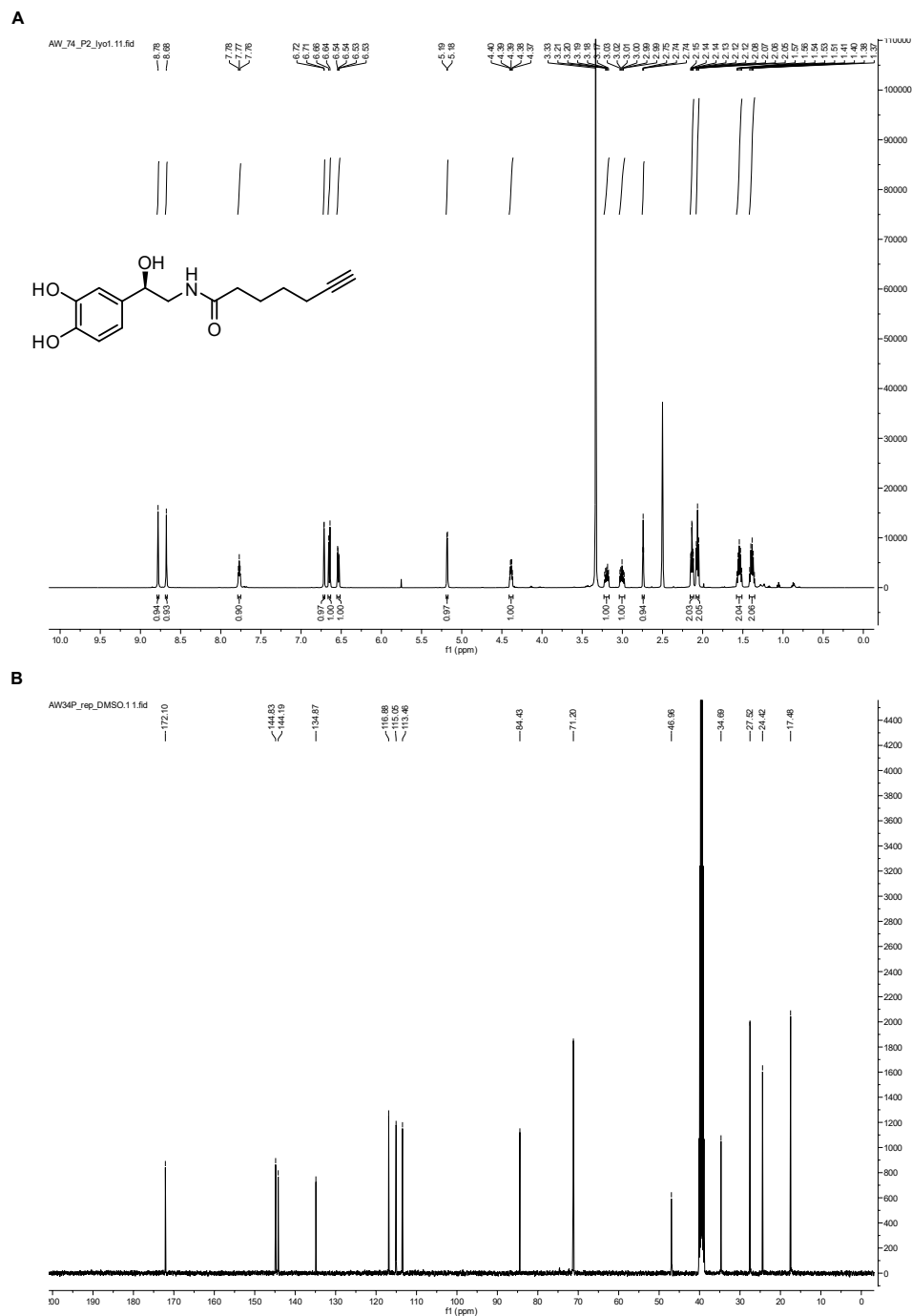


Fig. S17. NMR spectra of *(R)*-N-(2-(3,4-Dihydroxyphenyl)-2-hydroxyethyl)hept-6-ynamide (**EPI-P2**) in DMSO- d_6 . (A) ^1H -NMR (500 MHz). (B) ^{13}C -NMR (101 MHz).

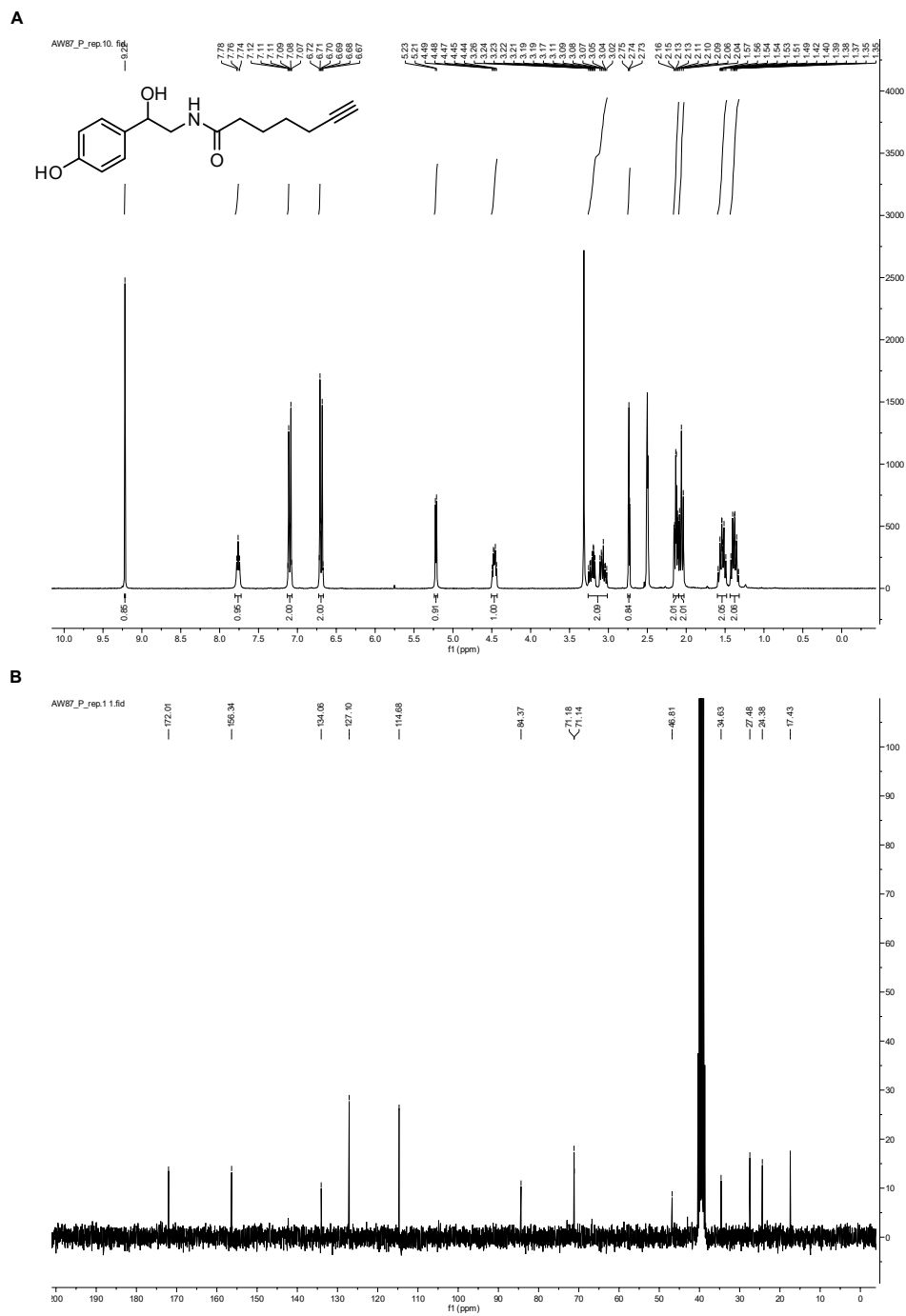


Fig. S18. NMR spectra of *N*-(2-hydroxy-2-(4-hydroxyphenyl)ethyl)hept-6-ynamide (**OA-P**) in DMSO- d_6 . (A) ^1H -NMR (300 MHz). (B) ^{13}C -NMR (75 MHz).

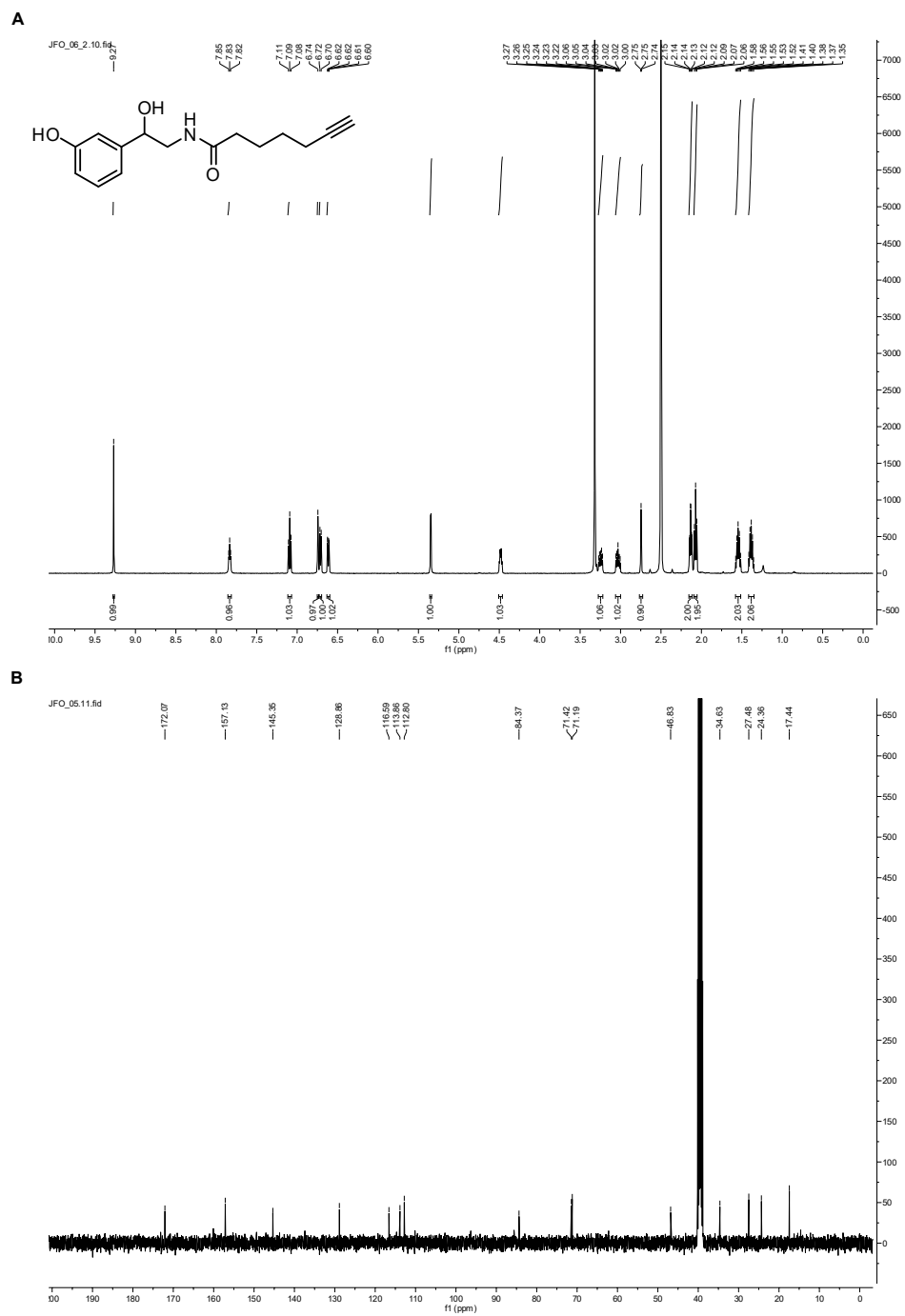


Fig. S19. NMR spectra of *N*-(2-hydroxy-2-(3-hydroxyphenyl)ethyl)hept-6-ynamide (**PE-P**) in DMSO- d_6 . (A) ^1H -NMR (500 MHz). (B) ^{13}C -NMR (101 MHz).

Supplementary tables

Table S1: Doubling times (t_d) of *V. campbellii* cultured in KE minimal medium under iron-limited and non-limited conditions in the presence of the indicated compounds (50 μ M).

compound	t_d (min)	
	iron limitation (+ human apo-transferrin)	no iron limitation
EPI	150	95
EPI-P1	102	100
EPI-P2	184	98
PE	No growth	93
PE-P	No growth	97
OA-P	No growth	96
DMSO	No growth	93

Table S2: Proteins at which **PE-P** was outcompeted by **EPI**, **PE**, and **LAB** but not by **PRO**.

UniProt ID	gene name	protein name
soluble fraction		
A7MXS1	VIBHAR_00356	Uncharacterized protein
A7N2H7	VIBHAR_05151	Uncharacterized protein
A7N8F2	VIBHAR_06507	Uncharacterized protein
A7MS42	VIBHAR_03137	CheW-like domain-containing protein
insoluble fraction		
A7MYT1	VIBHAR_01892	Uncharacterized protein
A7MXS1	VIBHAR_00356	Uncharacterized protein
A7MTV7	yihI	Der GTPase-activating protein YihI
A7MZ63	rpsG	30S ribosomal protein S7
A7N8F2	VIBHAR_06507	Uncharacterized protein
A7MUD0	VIBHAR_02658	Uncharacterized protein
A7N1L7	infA	Translation initiation factor IF-1
A7MS42	VIBHAR_03137	CheW-like domain-containing protein

Table S3. Compounds used in this study.

abbreviation	substance	supplier
EPI	DL-Epinephrine hydrochloride	<i>TCI Chemicals</i>
NE	L-Norepinephrine	<i>Alfa Aesar</i>
PE	(<i>R</i>)-(-)-Phenylephrine hydrochloride	<i>Sigma</i>
LAB	Labetalol hydrochloride	<i>Sigma</i>
PRO	DL-Propranolol hydrochloride	<i>Sigma</i>

Table S4. Bacterial culture conditions.

strain	medium	temperature
<i>Vibrio campbellii</i> (all strains)	LB35, MB, KE	30 °C
<i>Escherichia coli</i> (all strains)	LB	37 °C

Table S5. Media used in this study.

medium	ingredients
KE	100 mM K ₂ HPO ₄ /KH ₂ PO ₄ , 0.058% (w/v) trisodium citrate dihydrate, 0.106% (w/v) (NH ₄) ₂ SO ₄ , 400 μM MgSO ₄ , 0.2% (w/v) glucose, 2% (w/v) NaCl, pH 7.6
LB	1% (w/v) peptone, 0.5% (w/v) NaCl, 0.5% (w/v) yeast extract, pH 7.5
LB35	LB with 3.5% (w/v) NaCl
MB	Difco Marine Broth 2216
TMN	50 mM Tris-HCl, 300 mM NaCl, 5 mM MgCl ₂ , 5 mM glucose, pH 7.5

Table S6. Strains and plasmids used in this study.

strain or plasmid	relevant genotype or description	reference
<i>E. coli</i>		
DH5_αpir	<i>endA1 hsdR17 glnV44 (= supE44) thi-1 recA1 gyrA96 relA1</i> (17) φ80' <i>lacΔ(lacZ)M15 Δ(lacZYA-argF)U169 zdg-232::Tn10 uidA::pir+</i>	
WM3064	<i>thrB1004 pro thi rpsL hsdS lacZΔM15 RP4-1360 Δ(araBAD)567</i> <i>ΔdapA1341::[erm pir]</i>	W. Metcalf, Univ. of Illinois, Urbana
BL21(DE3)	F ⁻ <i>ompT gal dcm lon hsdSB(rB⁻ mB⁻) λ(DE3)</i>	(18)
<i>V. campbellii</i>		
<i>V. campbellii</i> ATCC BAA- 1116	wild type	(19)
<i>V. campbellii</i> <i>ΔcheW</i>	clean deletion of <i>cheW</i>	This work
plasmids		
pET28a	Vector for expression of N-terminally 6xHis-tagged proteins with a thrombin site, Km ^R	<i>Novagen</i>
pET28a- <i>cheW</i>	<i>cheW</i> cloned in the BamHI and XhoI sites of pET28a, Km ^R	This work
pNTPS138- R6KT	<i>mobRP4⁺ ori-R6K sacB</i> ; suicide plasmid for in-frame deletions, Km ^R	(20)
pNPTS138- R6KT- <i>cheW</i>	pNPTS-138-R6KT-derived suicide plasmid for clean deletion of <i>cheW</i> in <i>V. campbellii</i> , Km ^R	This work

Table S7. Oligonucleotides used in this study.

name	sequence (restriction enzyme cutting site in blue)	description
fwd_BamHI_up_cheW	TAGCCGGATCCTTGAACAGCACACTGAGACAGC	
rev_EcoRI_down_cheW	GCGTAGAATTCGCGAGAGGAATATGTCGGGTC	Generation of the pNPTS138-R6KT cheW plasmid for clean deletion of <i>cheW</i> in <i>V. campbellii</i>
rev_start cheW_up	TGAGCCATAAAAGCTTGAGACATAGTTAATCCTCGT TAATG	
fwd_start cheW_down	AAGCTTTTATGGCTCACCTGTAATTGGCTGATGAAT CATGG	
fwd_BamHI_cheW	TAGCCGGATCCATGTCTCAAGCTTTTGAAG	Generation of the overexpression plasmid pET28a-cheW
rev_cheW_Stop_XhoI	TAGCCCTCGAGTTACAGGTGAGCCATCTCATC	coding for N-terminal His ₆ -tagged <i>cheW</i>

Legends for supplementary datasets (separate files)

Dataset S1. Proteomics data of **EPI-P1** photolabeling containing detailed protein annotation, MS data, statistics, and LFQ intensities.

Dataset S2. Proteomics data of **PE-P** photolabeling in competition with **PE** containing detailed protein annotation, MS data, statistics, and LFQ intensities

Dataset S3. Proteomics data of **PE-P** photolabeling in competition with **EPI** containing detailed protein annotation, MS data, statistics, and LFQ intensities

Dataset S4. Proteomics data of **PE-P** photolabeling in competition with **LAB** or **PRO** containing detailed protein annotation, MS data, statistics, and LFQ intensities

Dataset S5. Proteomics data of isoDTB labeling experiment containing amino acid modification, selectivity, and quantification results.

Dataset S6. Proteomics data of Co-IP containing detailed protein annotation, MS data, statistics, and LFQ intensities

SI References

1. S. Brameyer *et al.*, Molecular design of a signaling system influences noise in protein abundance under acid stress in different gammaproteobacteria. *J. Bacteriol. Res.* **202**, e00121-00120 (2020).
2. K. M. Taute, S. Gude, S. J. Tans, T. S. Shimizu, High-throughput 3D tracking of bacteria on a standard phase contrast microscope. *Nat. Commun.* **6**, 8776-8784 (2015).
3. A. Fux, V. S. Korotkov, M. Schneider, I. Antes, S. A. Sieber, Chemical cross-linking enables drafting ClpXP proximity maps and taking snapshots of *in situ* interaction networks. *Cell Chem. Biol.* **26**, 48-59.e47 (2019).
4. J. Cox, M. Mann, MaxQuant enables high peptide identification rates, individualized p.p.b.-range mass accuracies and proteome-wide protein quantification. *Nat. Biotechnol.* **26**, 1367-1372 (2008).
5. S. Tyanova, T. Temu, J. Cox, The MaxQuant computational platform for mass spectrometry-based shotgun proteomics. *Nat. Protoc.* **11**, 2301-2319 (2016).
6. J. Cox *et al.*, Accurate proteome-wide label-free quantification by delayed normalization and maximal peptide ratio extraction, termed MaxLFQ. *Mol. Cell. Proteomics* **13**, 2513-2526 (2014).
7. S. Tyanova *et al.*, The Perseus computational platform for comprehensive analysis of (prote)omics data. *Nat. Methods* **13**, 731-740 (2016).
8. P. R. A. Zanon *et al.*, Profiling the proteome-wide selectivity of diverse electrophiles. *ChemRxiv* <https://doi.org/10.26434/chemrxiv.14186561.v1> (2021).
9. D. Kessner, M. Chambers, R. Burke, D. Agus, P. Mallick, ProteoWizard: open source software for rapid proteomics tools development. *Bioinformatics (Oxford, England)* **24**, 2534-2536 (2008).
10. A. T. Kong, F. V. Leprevost, D. M. Avtonomov, D. Mellacheruvu, A. I. Nesvizhskii, MSFragger: ultrafast and comprehensive peptide identification in mass spectrometry-based proteomics. *Nat. Methods* **14**, 513-520 (2017).
11. F. Yu *et al.*, Identification of modified peptides using localization-aware open search. *Nat. Commun.* **11**, 4065-4073 (2020).
12. F. da Veiga Leprevost *et al.*, Philosopher: a versatile toolkit for shotgun proteomics data analysis. *Nat. Methods* **17**, 869-870 (2020).
13. F. Yu *et al.*, Fast quantitative analysis of timsTOF PASEF data with MSFragger and IonQuant. *Mol. Cell. Proteom.* **19**, 1575-1585 (2020).
14. J. Jumper *et al.*, Highly accurate protein structure prediction with AlphaFold. *Nature* **596**, 583-589 (2021).
15. L. Schrödinger, W. DeLano (2020) PyMOL. Retrieved from <http://www.pymol.org/pymol>.
16. Z. Li *et al.*, Design and synthesis of minimalist terminal alkyne-containing diazirine photocrosslinkers and their incorporation into kinase inhibitors for cell- and tissue-based proteome profiling. *Angew. Chem. Int. Ed.* **52**, 8551-8556 (2013).
17. D. R. Macinga, M. M. Parojcic, P. N. Rather, Identification and analysis of aarP, a transcriptional activator of the 2'-N-acetyltransferase in *Providencia stuartii*. *J. Bacteriol. Res.* **177**, 3407-3413 (1995).
18. F. W. Studier, B. A. Moffatt, Use of bacteriophage T7 RNA polymerase to direct selective high-level expression of cloned genes. *J. Mol. Biol.* **189**, 113-130 (1986).
19. B. Lin *et al.*, Comparative genomic analyses identify the *Vibrio harveyi* genome sequenced strains BAA-1116 and HY01 as *Vibrio campbellii*. *Environ. Microbiol. Rep.* **2**, 81-89 (2010).
20. J. Lassak, A. L. Henche, L. Binnenkade, K. M. Thormann, ArcS, the cognate sensor kinase in an atypical Arc system of *Shewanella oneidensis* MR-1. *Appl. Environ. Microbiol.* **76**, 3263-3274 (2010).

Supplemental information – Chapter 2.4

Available online at:

<https://www.nature.com/articles/s42003-022-03281-4>

Supplementary information

Division of labor and collective functionality in *Escherichia coli* under acid stress

Sophie Brameyer, Kilian Schumacher, Sonja Kuppermann, and Kirsten Jung*

Department of Biology, Microbiology, Ludwig-Maximilians-Universität München, Martinsried, Germany

*Corresponding author:

Prof. Dr. Kirsten Jung

Ludwig-Maximilians-Universität München

Microbiology

Großhaderner Str. 2-4

82152 Martinsried

Phone: + 49 89/2180-74500

Fax: + 49 89/2180-74520

E-Mail: jung@lmu.de

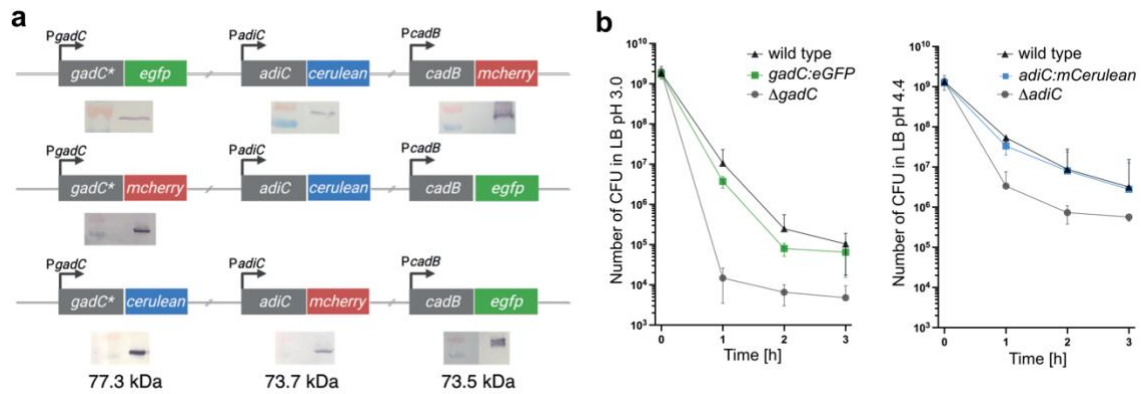
Supplementary Table 1: Quantification of fluorescent microscopic images of different *E. coli* strains during acidic conditions. Quantified noise and mean of relative fluorescence intensity (RF) were calculated for 1,000 cells per condition and time point. Cells were cultivated as described in Fig. 2a. Single-cell fluorescence intensity was acquired by microscopy and the use of the MicrobeJ plugin of the ImageJ software. Relative fluorescence intensity (RF) is the first value. Noise, standard deviation/mean of log-transformed values in the second value. Cells cultivated in KE medium pH 5.8 are always supplemented with 10mM lysine. Copy numbers of *AdiY* (+ *adiY*), *CadC* (+ *cadC*) or *CsiR* (+ *csiR*) were elevated by placing the corresponding genes under control of the arabinose (0.1%)-inducible promoter in plasmid pBAD24. All source data is summarized in Supplementary data 2.

<i>gadC:eGFP-adiC:mCerulean-cadB:mCherry</i>			
	pH 7.6	pH 5.8 + lysine	pH 4.4
t_0	GadC:eGFP 735 RF - 0.10 AdiC:mCerulean 35 RF - 0.04 CadB:mCherry 14 RF - 0.03		
t_{150}	GadC:eGFP 265 RF - 0.11 AdiC:mCerulean 42 RF - 0.05 CadB:mCherry 17 RF - 0.05	GadC:eGFP 1512RF - 0.04 AdiC:mCerulean 39 RF - 0.03 CadB:mCherry 386 RF - 0.37	
t_{300}	GadC:eGFP 836 RF - 0.11 AdiC:mCerulean 40 RF - 0.03 CadB:mCherry 15 RF - 0.04	GadC:eGFP 1734 RF - 0.08 AdiC:mCerulean 34 RF - 0.03 CadB:mCherry 246 RF - 0.26	GadC:eGFP 1401 RF - 0.05 AdiC:mCerulean 164 RF - 0.12 CadB:mCherry 547RF - 0.26
<i>E. coli</i> MG1655 wildtype			
LB pH 4.4 t_{300}			
	eGFP channel	mCerulean channel	mCherry channel
	25 RF - 0.07	37 RF - 0.05	12 RF - 0.09
<u>$\Delta cadA$</u> <i>gadC:eGFP-adiC:mCerulean-cadB:mCherry</i> LB pH 4.4 t_{300}			
	GadC:eGFP 1848 RU - 0.06	AdiC:mCerulean 306 RU - 0.07	CadB:mCherry 1979 RU - 0.23
+ <u><i>csiR</i></u> <i>gadC:mCerulean-cadB:mCherry</i> LB pH 4.4 t_{300}			
	GadC:mCerulean 1636 RF - 0.12		CadB:mCherry 495 RF - 0.29
+ <u><i>csiR</i></u> <i>adiC:mCerulean-cadB:mCherry</i> LB pH 4.4 t_{300}			

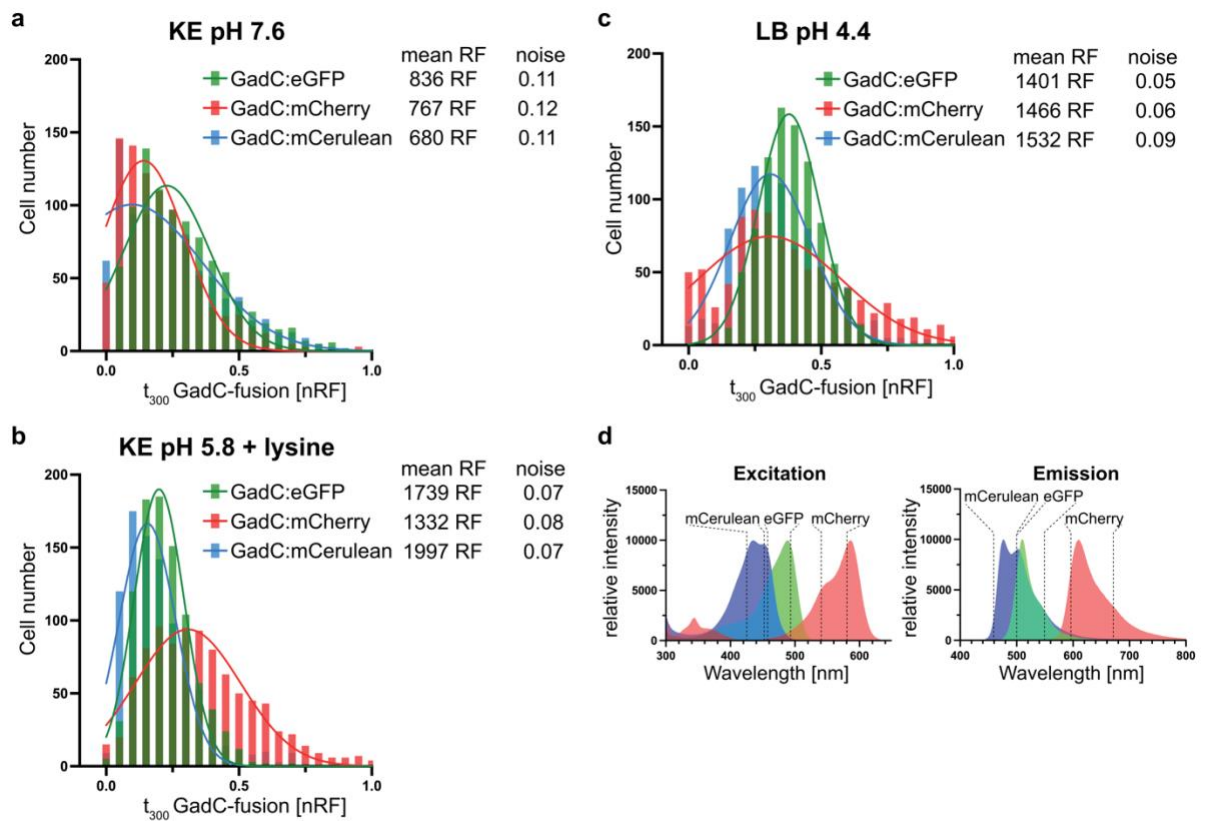
AdiC:mCerulean 92 RF - 0.10		CadB:mCherry 509 RF - 0.31			
+ <u>cadC</u> <u>gadC:mCerulean-cadB:mCherry</u> KE pH 5.8 t₃₀₀					
GadC:mCerulean 856 RF - 0.05		CadB:mCherry 1164 RF - 0.08			
+ <u>cadC</u> <u>adiC:mCherry-cadB:eGFP</u> LB pH 4.4 t₃₀₀					
AdiC:mCherry 30 RF - 0.08		CadB:eGFP 1026 RF - 0.07			
+ <u>adiY</u> <u>adiC:mCerulean-cadB:mCherry</u> LB pH 4.4 t₃₀₀					
AdiC:mCerulean 333 RF - 0.06		CadB: mCherry 396 RF - 0.29			
<u>gadC:mCherry-adiC:mCerulean-cadB:eGFP</u>					
KE pH 7.6 t ₃₀₀		KE pH 5.8 t ₃₀₀		LB pH 4.4 t ₃₀₀	
GadC:mCherry 767 RF - 0.12		GadC:mCherry 1332 RF - 0.08		GadC:mCherry 1466 RF - 0.06	
<u>gadC:mCerulean-adiC:mCherry-cadB:eGFP</u>					
KE pH 7.6 t ₃₀₀		KE pH 5.8 t ₃₀₀		LB pH 4.4 t ₃₀₀	
GadC:mCerulean 680RF - 0.11		GadC:mCerulean 1997 RF - 0.07		GadC:mCerulean 1532 RF - 0.09	

Supplementary Table 2: Occurrence of the main components of the Gad, Adi and Cad system within selected species of the proteobacteria and firmicutes. Phylogenetic distribution is presented in Fig. 4 and sequences are summarized in Supplementary data 1. x, indicates present of a homolog of the protein GadA/B, GadC, CsiR, EvgS, GadE, GadW, GadX, GadY, YdeO, AdiA, AdiC, AdiY, CadA, CadB, CadC and LysP.

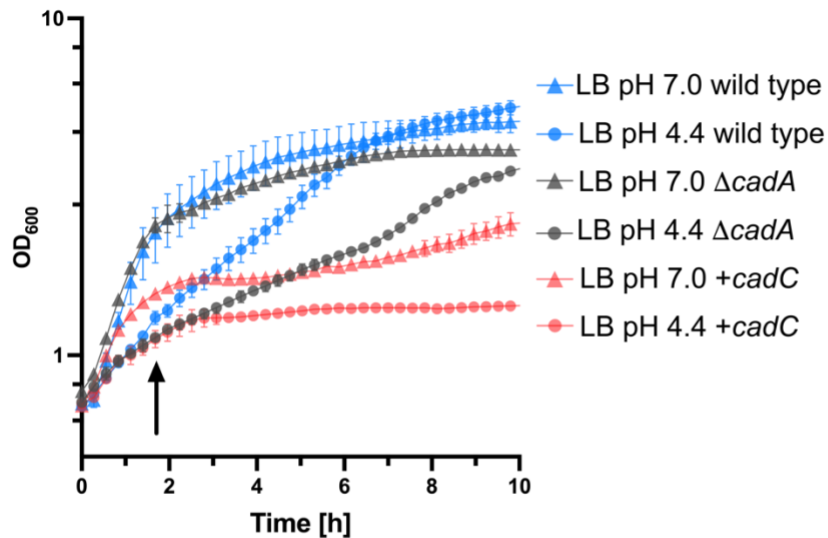
		Gad system								Adi system			Cad system					
		GadA/B	GadC	CsiR	EvgS	GadE	GadW	GadX	GadY	YdeO	AdiA	AdiC	AdiY	CadA	CadB	CadC	LysP	
Proteobacteria	<i>Escherichia coli</i>	x	x	x	x	x	x	x	x	x	x	x	x	x	x	x	x	
	<i>Escherichia albertii</i>	x	x	x		x	x	x	x		x	x	x	x	x	x	x	
	<i>Shigella boydii</i>	x	x	x	x	x	x	x	x	x	x	x	x	x	x		x	
	<i>Shigella flexneri</i>	x	x	x	x	x	x	x	x	x	x	x	x					
	<i>Salmonella enterica</i>			x							x	x	x	x	x	x	x	
	<i>Citrobacter freundii</i>	x	x	x		x					x	x	x	x	x		x	
	<i>Hafnia alvei</i>	x	x	x	x						x	x		x	x	x	x	
	<i>Serratia fonticola</i>	x	x		x						x	x		x	x	x	x	
	<i>Xenorhabdus bovienii</i>										x	x						x
	<i>Stenotrophomonas maltophilia</i>										x	x						
	<i>Vibrio parahaemolyticus</i>													x	x	x		
	<i>Vibrio campbellii</i>													x	x	x		
Firmicutes	<i>Clostridium perfringens</i>	x	x															x
	<i>Lactococcus lactis</i>	x	x															x
	<i>Lactobacillus reuteri</i>	x	x															x
	<i>Listeria monocytogenes</i>	x	x															x
	<i>Enterococcus faecium</i>	x	x															



Supplementary Figure 1: Fluorescently-tagged antiporter hybrid proteins are functional in *E. coli*. (a) Schematic overview of the genomic organization of the different combinations of the three-color reporter strains: *gadC::eGFP-adiC::mCerulean-cadB::mCherry*, *gadC::mCherry-adiC::eGFP-cadB::mCerulean* and *gadC::mCerulean-adiC::mCherry-cadB::eGFP*. To verify the location of the different fluorescent hybrid proteins, the different three-color *E. coli* strains were pelleted at an $OD_{600} = 1$ at t_{300} in LB pH 4.4, fractionated and separated in a 12.5 % SDS-PAGE that was then transferred to nitrocellulose membrane. The different fluorescent hybrid proteins were labeled with either the primary polyclonal α -GFP antibody, α -mCerulean antibody or α -mCherry antibody and the α -rabbit alkaline phosphatase-conjugated antibody was used as secondary antibody. As ladder the PageRuler Prestained Protein Ladder (10 to 180 kDa) was used and only the membrane fraction is shown. The red band of the PageRuler Prestained Protein Ladder corresponds to 70 kDa. The molecular weight of each fluorescent hybrid protein is indicated below the Western blot. (b) Acid survival assay to test functionality of *GadC::eGFP* in LB medium pH 3.0 (left panel) and *AdiC::mCerulean* in LB medium pH 4.4 (right panel) via colony forming units during incubation for 3 h. The three-color strain *gadC::eGFP-adiC::mCerulean-cadB::mCherry* was cultivated and as control *E. coli* MG1655 cells and a deletion of either *gadC* or *adiC* were used. Functionality of the *CadB::eGFP* fusion was already assed via an liquid-based colorimetric assay using a pH indicator ¹.



Supplementary Figure 2: Comparison of the production and distribution of the different fluorescent fusions with GadC at different acidic conditions. Histogram presentation of the normalized relative fluorescence intensity (nRF) quantified for 1,000 cells per fluorescent fusion, GadC:eGFP, GadC:mCherry or GadC:mCerulean, at t_{300} in (a) KE pH 7.6, (b) KE pH 5.8 supplemented with lysine and (c) LB pH 4.4. Calculated mean RF and noise values are summarized in Table S1. nRF, normalized RF values. (d) Comparison of the excitation (left panel) and emission (right panel) wavelength of the fluorophores mCerulean, eGFP and mCherry. Dashed lines indicate the ranges of the fluorescence filter cubes for the three fluorophores of the used Leica DMI8 inverted microscope. Spectra were obtained from the FPbase² and visualized using GraphPad Prism 9.1.0.



Supplementary Figure 3: High CadC copy number and *cadA* deletion slows down growth of *E. coli* at low pH. The *E. coli* strains, MG1655 Δ *cadC* containing plasmid pBAD-*cadC*, and *E. coli* MG1655 wild type containing the empty plasmid pBAD24, were cultivated in KE medium pH 7.6 until exponential phase, then shifted to KE medium pH 5.8 + 10 mM lysine and finally shifted to LB medium at pH 7.0 or pH 4.4 (each supplemented with 0.1% (w/v) arabinose). Cultures were aerobically cultivated in 96-well plates at 37 °C in a Tecan Infinite F500 system (Tecan, Crailsheim, Germany) and growth (OD₆₀₀) was measured every 10 min at 37 °C. In strain MG1655 Δ *cadC* + pBAD-*cadC*, the copy number of CadC is elevated to about 100 CadC molecules per cell, whereas the *E. coli* MG1655 pBAD24 strain produces only ≤ 4 CadC molecules per cell as reported previously³. The black arrow indicates the time point of the values displayed as a bar graph in Fig. 6b.

Supplementary References

1. Brameyer, S. *et al.* Molecular design of a signaling system influences noise in protein abundance under acid stress in different gammaproteobacteria. *J. Bacteriol.* 202, 95–15 (2020).
2. Lambert, T. J. FPbase: a community-editable fluorescent protein database. *Nat. Methods* 16, 277–278 (2019).
3. Ude, S. *et al.* Translation elongation factor EF-P alleviates ribosome stalling at polyproline stretches. *Science* 82–85 (2013).

Acknowledgements

In this section, I would like to thank all people who directly or indirectly contributed to the work mentioned in this thesis.

First, I want to thank Prof. Kirsten Jung for the admission to her group, the opportunity and trust to work on these exciting research projects, and the continuous support throughout the years. I also want to thank Prof. Thomas Nägele for the valuable feedback during the TAC meetings and for being the second examiner of this thesis. Along this line, I acknowledge Dr. Jürgen Lassak for his helpful experimental suggestions, and for being part of the TAC committee as well. I also want to thank Prof. Simon Heilbronner, Prof. Wolfgang Enard, and Prof. Christof Osman for making the effort to read this thesis and being part of the examination committee.

I also want to express gratitude for the opportunity to supervise several Bachelor- and Master students during my PhD thesis. Thank you Pol, Annika, and Djanna. Next, I want to acknowledge all collaboration partners, especially those responsible for bioinformatic data analysis. I want to thank Rick Gelhausen from Prof. Rolf Backofens group who developed the HRIBO analysis pipeline which proved to be essential for the Ribo-Seq project. Thank you Rick for your support, expertise, and the effort invested in the hundreds of emails we exchanged during the project. I also want to acknowledge Willow Kion-Crosby from Lars Barquists group for his contributions in terms of autoencoder-based machine learning. Moreover, I thank Dr. Stefan Krebs for Illumina sequencing, Dr. Karin Kleigrew for LC-MS analysis, Irina Lisevich and Prof. Dr. Victor Sourjik for providing motility mutants, and Dr. Angela Weigert Muñoz, Prof. Stefan Sieber, Dr. Marianne Grognot, and Prof. Katja Taute for the CheW-project collaboration. I also want to thank Dr. Lydia Hadjeras for her expertise and guidance regarding sORF detection.

The LSM graduate school also played a major role throughout my PhD. It provided an ideal framework for finding new friends and allowed me to participate in excellent method and soft skill courses. Thank you Korbinian and Nadine for your support and for answering all my questions. Further, I want to send a special acknowledgement to Prof. Thorsten Waldminghaus, who gave me valuable career suggestions during the VAAM mentoring program.

My special thanks also go to the people from the LMU Munich team: Dr. Sophie Brameyer for introducing me to the lab and the teamwork throughout writing the two reviews. Julia and Elli for the time spent in the first two years of my PhD during the Covid-era. My office members who became my friends: Lingyun, Sophia, Bibakhya, and Leo, who I consider a member of the office as well. Thank you, Nathalie, Sophia, Sabine, and Sophie, as members of Lab G01.001.

Importantly, I thank everyone who was part of the daily coffee break: Julia, Elli, Sophie, Sophia, Alina, and Elena. Special thanks also to all further fellow and former members of the AGs K. Jung, H. Jung, and Lassak: Giovanni, Erica, Jin, Ingrid, Frank, Agata, Dimitar, Ralph, Dan, Nicola, Tania, Steffi, Michelle, Urte, Dania, Siobhan, Sebastian, Ana, Tess, Fabienne, and Korinna. Moreover, I want to thank Grazyna for guiding me through all the problems I encountered with the LMU administration over the years.

A very special acknowledgement also goes to several family members and to my friends (some of which I first met at the LMU biocentre), Björn, Alex, Yannik, Lubna, Lulu, Sophia, Bibakhya, Leo, Sabrina, Laura, Raphaela, Jessy, Merlin, Sara, Lucas, Niko, and Leon. In addition, I also want to thank my friends from team Spetses: Nazgul, Alessio, and Arthur. I also thank Dandan for her continuous support.

Last, I want to thank my family, especially my parents. Without you, none of this would have been possible.

Curriculum Vitae

**Kilian
Schumacher**

Contact

Address:

Phone:

E-mail:

Date of birth:

Nationality:

Languages

German – native speaker
English – C1
French – B2
Swedish – A1

Courses

NGS data analysis
Machine learning in Python
Python for beginners
Python intermediate level
Good manufacturing practice (GMP)
Scientific writing
Affinity Designer
Presenting posters successfully

Memberships

Graduate school Life Science Munich (LSM) student council:

- Web content manager
- Social media committee member

VAAM (Vereinigung für allgemeine und angewandte Mikrobiologie)

Work experience

04/2024 – now	Illumina Solution Center Berlin Inside Sales Account Manager
06/2020 – 03/2024	K. Jung group - LMU Munich PhD Student – Microbiology
10/2017 - 02/2020	Teaching assistant - LMU Munich Organization and supervision of microbiology courses for Bachelor and Medical students
04/2017 – 09/2019	Papenfort group - LMU Munich Master Thesis, Lehre @ LMU program, Bachelor Thesis
04/2019 – 06/2019	J. Larson group – Center of Antibiotic Resistance Research (CARE) University of Gothenburg, Sweden Research project: The potential of wastewater streams and their contaminants to select for antibiotic resistance in <i>E. coli</i>
01/2019 – 06/2019	ERASMUS+ mobility program University of Gothenburg, Sweden

Education

03/2021 – now	Graduate school Life Science Munich (LSM) PhD Student K. Jung group
10/2017 - 03/2020	Master of Science Microbiology LMU Munich & University of Gothenburg Master Thesis: DPO-mediated gene expression control in <i>Vibrio cholerae</i> (Grade: 1,00) Final Grade: 1,06
10/2014 - 09/2017	Bachelor of Science Biology LMU Munich Bachelor Thesis: DPO controlled toxin production in <i>Vibrio cholerae</i> (Grade: 1,30) Final Grade: 1,87

Awards

Lehre@LMU research award 2017
Poster prize - LSM graduate school retreat 2021
Talk prize - LSM graduate school retreat 2022
Poster prize - SPP 2002 conference 2023

List of publications:

- Schumacher K**, Braun D, Kleigrew K, Jung, K. 2024. Motility-activating mutations upstream of *flhDC* reduce acid shock survival of *Escherichia coli*. *Microbiol Spectr.* 12:e0054424.
- Schumacher K**, Gelhausen R, Kion-Crosby W, Barquist L, Backofen R, Jung K. 2023. Ribosome profiling reveals the fine-tuned response of *Escherichia coli* to mild and severe acid stress. *mSystems* <https://doi.org/10.1128/msystems.01037-23>.
- Schumacher K**, Brameyer S, Jung K. 2023. Bacterial acid stress response: from cellular changes to antibiotic tolerance and phenotypic heterogeneity. *Curr Opin Microbiol* 75:102367.
- Schwarz J*, **Schumacher K***, Brameyer S, Jung K. 2022. Bacterial battle against acidity. *FEMS Microbiol Rev* 46.
- Brameyer S, **Schumacher K**, Kuppermann S, Jung K. 2022. Division of labor and collective functionality in *Escherichia coli* under acid stress. *Commun Biol* 5:1–14.
- Muñoz AW, Hoyer E, **Schumacher K**, Grognot M, Taute KM, Hacker SM, Sieber SA, Jung K. 2022. Eukaryotic catecholamine hormones influence the chemotactic control of *Vibrio campbellii* by binding to the coupling protein CheW. *Proc Natl Acad Sci U S A* 119.
- Kraupner N, Hutinel M, **Schumacher K**, Gray DA, Genheden M, Fick J, Flach CF, Larsson DGJ. 2021. Evidence for selection of multi-resistant *E. coli* by hospital effluent. *Environ Int* 150:106436.
- Herzog R, Peschek N, Fröhlich KS, **Schumacher K**, Papenfort K. 2019. Three autoinducer molecules act in concert to control virulence gene expression in *Vibrio cholerae*. *Nucleic Acids Res* 47:3171–3183.

* These authors contributed equally

Participation in conferences and retreats:

Talks:

Schumacher K, Gelhausen R, Kion-Crosby W, Barquist L, Backofen R, Jung K. Ribosome profiling reveals novel small proteins and adaptations to mild and severe acid stress in *Escherichia coli*. In: **VAAM annual meeting**. Göttingen. 2023.

Schumacher K, Gelhausen R, Backofen R, Jung K. Ribosome profiling reveals novel adaptations of *Escherichia coli* to acidic environments. In: **Graduate school Life Science Munich retreat**. Schliersee-Josefstal. 2022.

Posters:

Schumacher K, Gelhausen R, Kion-Crosby W, Barquist L, Backofen R, Jung K. Ribosome profiling reveals novel sORFs and adaptations to acid stress in *Escherichia coli*. In: **SPP 2002 conference: small proteins in prokaryotes, an unexplored world**. Berlin. 2023.

Schumacher K, Gelhausen R, Kion-Crosby W, Barquist L, Backofen R, Jung K. Ribosome profiling reveals novel acid resistance mechanisms and small proteins in *Escherichia coli*. In: **EMBO/EMBL symposium: New approaches and concepts in Microbiology**. Heidelberg. 2023.

Schumacher K, Gelhausen R, Backofen R, Jung K. Expanding the regulatory network of acid resistance in *Escherichia coli* using ribosome profiling. In: **EMBO FEBS Lecture course: The New Microbiology**. Spetses, Greece. 2022.

Schumacher K & Schwarz J, Brameyer S, Brachman A, Jung K. New insights into acid stress adaptation in γ -proteobacteria using various next-generation sequencing (NGS) techniques. In: **VAAM annual meeting**. 2022. virtual.

Schumacher K, Brameyer S, Jung K. Identification of novel acid stress counteracting proteins in *Escherichia coli* using ribosome profiling. In: **Graduate school Life Science Munich retreat**. 2021. virtual.

Brameyer S, **Schumacher K**, Jung K. Heterogeneous activation of three inducible acid resistance systems leads to division of labor in the *Escherichia coli* population. In: **BLAST XVI virtual conference**. 2021. virtual.